CARBAZOLE-BASED ORGANIC DYES FOR DYE-SENSITIZED SOLAR CELLS

Ph.D. THESIS

by
Addanki Venkateswararao

DEPARMENT OF CHEMISTRY
INDIAN INSTITUTE OF TECHNOLOGY ROORKEE
ROORKEE - 247 667 (INDIA)
DECEMBER, 2014

CARBAZOLE-BASED ORGANIC DYES FOR DYE-SENSITIZED SOLAR CELLS

A THESIS

Submitted in partial fulfilment of the requirements for the award of the degree of

DOCTOR OF PHILOSOPHY

in

Chemistry

by
ADDANKI VENKATESWARARAO

DEPARMENT OF CHEMISTRY
INDIAN INSTITUTE OF TECHNOLOGY ROORKEE
ROORKEE-247 667 (INDIA)
DECEMBER, 2014

INDIAN INSTITUTE OF TECHNOLOGY ROORKEE
ROORKEE

CANDIDATE'S DECLARATION

I hereby certify that the work which is being presented in the thesis entitled **CARBAZOLE-BASED ORGANIC DYES FOR DYE-SENSITIZED SOLAR CELLS** in partial fulfilment of the requirements for the award of the Degree of Doctor of Philosophy and submitted in the Department of Chemistry of the Indian Institute of Technology Roorkee is an authentic record of my own work carried out during a period from December, 2010 to December, 2014 under the supervision of Dr. K. R. Justin Thomas, Associate Professor, Department of Chemistry, Indian Institute of Technology Roorkee, Roorkee.

The matter presented in the thesis has not been submitted by me for the award of any other degree of this or any other Institute.

(ADDANKI VENKATESWARARAO)

This is to certify that the above statement made by the candidate is correct to the best of my knowledge.

Dated: _____ **(Dr. K. R. Justin Thomas)**

Supervisor

ACKNOWLEDGEMENTS

I would never have been able to finish my dissertation without the guidance of my supervisor, help from lab mates, friends, and support from my family and wife.

*I would like to express my deepest gratitude to my supervisor, **Dr. K. R. Justin Thomas**, for his excellent guidance, caring, patience, and providing me with an excellent atmosphere for doing research. He has been supportive since the day I began working in the lab and he teach me how to build research ability on my own, literature survey, writing, analyzing results critically, synthetic skills and what not. He is the only person who wants me to see as perfectionist in both education and life. It is an honor to be a student of you in doctoral program. Though, I made several mistakes while pursuing my doctoral program, you corrected and put me in a good path with lot of patience. I tried to learn all the qualities form you sir, but still I have to develop and learn so many things from you because you are library of reference to me in all aspects. He helped a lot for making this thesis via number of times correction and giving suggestions to improve the language skills and output of the thesis. Not only research skills he builds up caliber to creat better future on my own.*

*There are no proper words to convey my deep gratitude and respect for my well-wisher **Mrs. Jeyaseeli Justin**. She was always with me by giving great support. She invited so many times for lunch and dinner and makes my home away from home. I never met a person like you before and I will remember throughout my life. I must sincerely thank to her for caring and love like my mom. Also, she helped a lot to shape the thesis by checking typing and formatting errors.*

I am thankful to Head, Department of Chemistry, IIT Roorkee for all the necessary official support and for all the facilities in the department.

*I thank my SRC (Student Research Committee) members, **Dr. A. K. Singh** (Professor, Department of Chemistry, IIT Roorkee), **Dr. R. K. Peddinti** (Associate Professor, Department of Chemistry, IIT Roorkee) and **Dr. B. S. S. Daniel** (Professor, Department of Metallurgical & Materials Engineering, IIT Roorkee) for their helpful suggestions and constant support and encouragement.*

*I take this opportunity to sincerely acknowledge the University Grants Commissions (**UGC**), Government of India, New Delhi, for providing financial assistance in the form of Junior Research Fellow ship and Senior Research Fellowship which make my work contentedly.*

*Most of the results described in this thesis would not have been obtained without a close collaboration with few laboratories. I owe a great deal of appreciation and gratitude to **Prof. Kuo-Chuan Ho**, Dr. Chuan-Pei Lee and Chun-Ting Li (Department of Chemical Engineering, National Taiwan University, Taipei, Taiwan), Dr. Babu Varghese (Sophisticated Analytical Instrument Facility (SAIF), Indian Institute of Technology, Madras), I expend my thanks to **Dr. Ritu Barthwal** (Professor, Department of Biotechnolgy, IIT Roorkee) for extending the NMR facility. I sincerely acknowledge the funding from Department of Science and Technology (DST, FIST) for procuring high resolution mass spectrometer in the Department.*

My gratitude is also extended to my seniors who taught me research skills such as synthetic and analytical techniques: ***Dr. Payal Tyagi****,* ***Dr. Prachi Singh****,* ***Dr. Neha Kapoor****,* ***Dr. Sushil Kumar****,* ***Dr. Dhiredra Kumar****, and* ***B. M. N. K. Prasad****.* I cannot forget friend and *colleague,* ***Abhishek****,* who went through hard times together, cheered me on, and celebrated each accomplishment. Thank you for continues support. I cannot forget those days of sitting together with research discussions and ideas refining, etc. *I like to thank my colleagues (****Goverdhan, Karthik, Rajendra, Vijayesh, Sonu, Sunil, Ankita, Joseph, Ambika, Tina, Kamesh*** *and* ***Gopinath****) for their support and help for completing my thesis. Finally, I thank all my lab members.*

I specially acknowledge two people ***U. Rajesh*** *and* ***V. Rajesh*** *for providing literature from a distance on one message. Thank you both of you people for knowledge sharing with me all the time.*

Three other friends I must mention are ***Venkatababu, Deepika*** *and* ***Chandrasekhar****. These three constantly asked me "are you done yet?" and affectionately referred to me as their friend the 'professional student'. Thank you for your encouragement, support and most of all your humor. You both kept things light and me smiling. Some more friends I must mention for their support and help: Shesireddy, Thilak, Naveen, Srinivas, Syam, Naresh, Santhosh and Balu.*

I would not have contemplated this road if not for my parents, ***Subbamma*** *and* ***Pedakataiah****, who instilled within me a love of creative pursuits, science and language, all of which finds a place in this thesis. To my parents, thank you. I must acknowledge with tremendous and deep thanks to my partner,* ***Vasanthi Devi*** *for nice understanding, sacrificing her time, encouragement and love. My sister Parvathi and my nephews, Ankammarao and Varshitha, have also been the best of friends along this journey. This thesis would also not be possible without the love and support of my friend* ***Subbarao****, who inspire me about doctoral program, suggested good supervisor for me to join and gave me a home away from home.*

Finally I thank my God, for letting me through all the difficulties. I have experienced your guidance day by day. You are the one who let me finish my degree. I will keep on trusting you for my future. Thank you, Lord.

Addanki Venkateswararao

Abstract

Organic materials suitable for application in electronic devices such as dye-sensitized solar cells (DSSCs) and organic solar cells (OSCs) have received immense attention in recent years due to the demand for alternate energy harnessing technologies. Particularly, DSSC using organic and inorganic sensitizers have attracted huge research focus due to favorable efficiency to cost trade-off. Efficiency of the device containing organic dye is largely dependent on its electronic and structural characteristics. Till to date, power conversion efficiencies greater than 11% have been achieved with ruthenium-based sensitizers. However, rarity, high cost and environmental concern may limit the extensive usage of ruthenium-based dyes. Porphyrins have unique properties such as fast electron injection, good photophysical and thermal stability which make them ideal candidates for photovoltaic applications. But, organic sensitizers have drawn the attention due to their advantages such as high molar absorption coefficients, facile molecular tailoring and cost-effectiveness. Most of the organic sensitizers have a common architecture of donor-π bridge-acceptor (D-π-A). Generally the dyes are constructed using triarylamine donors, oligoarene or oligoheteroarene π-linkers and cyanoacrylic acid acceptor/anchor. Besides triarylamines nitrogen heterocyclic moieties such as indoline, phenothiazine and carbazole also have been used as donors. Carbazole is unique core unit due to its good charge transporting property and it offers many nuclear sites for chromophore incorporation which can be used to fine-tune the functional properties of the materials. For instance, many carbazole derivatives with functional chromophores attached via C-2, C-3, C-6, C-7, and N-9 have been reported for application in organic light emitting diodes and photovoltaic devices. In this thesis, organic dyes featuring carbazole as donor or 2,7-disubstituted carbazole as π-linker have studied in detail. In brief, the effect of conjugation and electron richness of donor on the optical, electrochemical and photovoltaic properties were elucidated carefully with appropriate molecular designs.

The thesis is divided into seven chapters. A survey of carbazole-based organic dyes reported in the literature is presented in Chapter 1. The carbazole-based materials are conveniently classified into various classes based on the nuclear substitution. It is found that the position of attachment of carbazole significantly affects the functional properties of the materials. The electro-optical and photovoltaic properties were discussed thoroughly for better understanding. The structure property relationship of the dyes are critically analyzed and discussed in detail.

Chapter 2 describes the aim and scope of the work. Carbazole is an electron rich heterocyclic compound and offer many nuclear sites at various positions and linear conjugation can be obtained by 2,7-disubstitution.

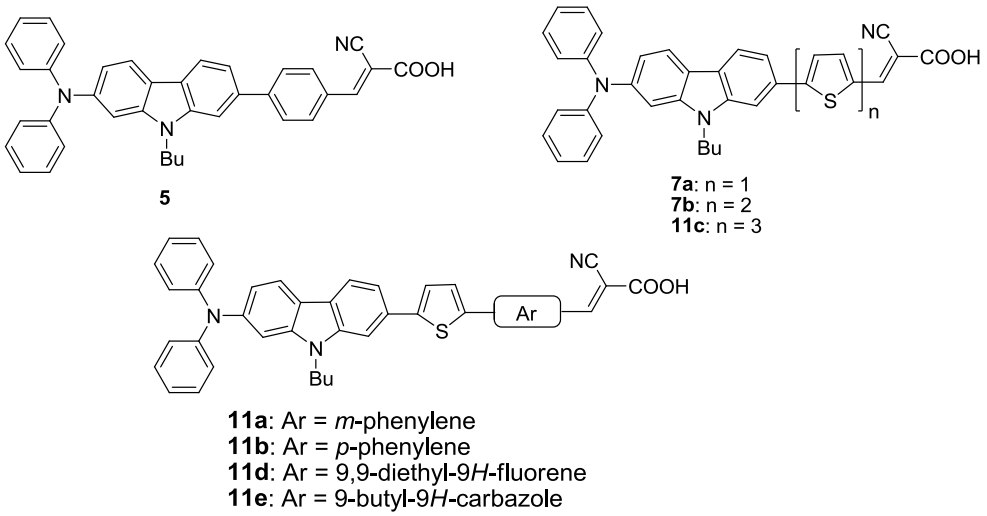

Chart 1 Structure of the dyes containing 2,7-disubstituted carbazole π-linker.

In Chapter 3, carbazole dyes (Chart 1) containing diphenylamine donor, 2,7-carbazole and thiophene in the conjugation pathway and cyanoacrylic acid acceptor are described. They possess red-shifted absorption with high molar extinction coefficient when compared to the corresponding dyes with fluorene or phenyl units in the conjugation. The dyes with oligothiophene conjugation shows bathochromically shifted absorption when compared to the dye containing phenyl linker attributable to the electron richness of the former one. The *para*-conjugation of phenyl linker red shifted absorption compared to *meta*-congener due to delinking of donor and acceptor interactions for the later one. The introduction of fluorene (**11d**) and carbazole (**11e**) linker enhances the molar extinction coefficients while terthiophene (**11c**) red-shifted the absorption when compared to the dye (**7a**) with a thiophene linkage. The DSSC fabricated using the dyes **7b** as sensitizer exhibited power conversion efficiency of 6.8% which increased to 7.2% when chenodexoycholic acid (CDCA) is used to impede dye aggregation. The DSSCs with ionic liquid electrolytes displayed marked stability over 1000 h for the dye **7b**. For dye **11d**, two ethyl chains of fluorene linker helps to minimize the intermolecular interactions and resulted in higher open circuit voltage (V_{OC}) compared to phenyl and carbazole containing

dyes. Electrochemical impedance spectroscopy was used to characterize the interfacial charge transfer and electron recombination kinetics.

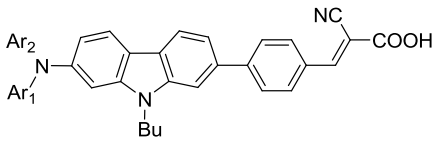

15a: Ar_1 = Phenyl; Ar_2 = 9,9-dipropyl-2-fluorenyl
15b: Ar_1 = Ar_2 = 9,9-diethyl-2-fluorenyl

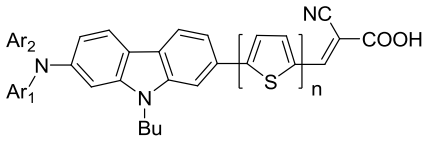

18a: Ar_1 = Phenyl; Ar_2 = 9,9-dipropyl-2-fluorenyl; n = 1
18b: Ar_1 = Ar_2 = 9,9-diethyl-2-fluorenyl; n = 1
19a: Ar_1 = Phenyl; Ar_2 = 9,9-dipropyl-2-fluorenyl; n = 2
19b: Ar_1 = Ar_2 = 9,9-diethyl-2-fluorenyl; n = 2

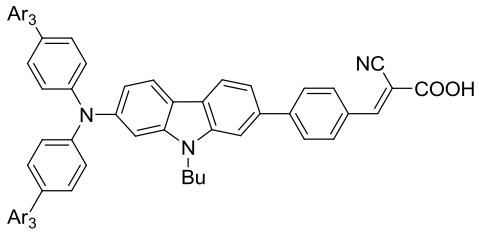

24: Ar_3 = 9,9-diethyl-2-fluorenyl

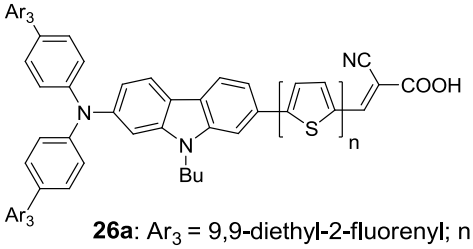

26a: Ar_3 = 9,9-diethyl-2-fluorenyl; n = 1
26b: Ar_3 = 9,9-diethyl-2-fluorenyl; n = 2

Chart 2 Structure of the dyes featuring donor structure modifications.

In Chapter 4, we study the effect of the alternations in the structure of the donor segment. Substitution of phenyl groups with fluorene in the donor unit of carbazole dyes (**5**, **7a** and **7b**) produced several dyes. The structures of the dyes are shown in Chart 2. Replacement of phenyl unit with the fluorene shifts the charge transfer transition peak to the longer wavelength region progressively which reflects changes in the donor unit. The dyes containing bithiophene displayed red shifted absorption compared to the thiophene containing dyes due to elongation of conjugation and electron richness of thiophene units. Moreover, the introduction of fluorene decorated donor raises the HOMO due to facile oxidation which helps to increase the V_{OC}. Also due to the extensive accumulation of electrons in the conduction band of TiO_2 due to the favorable LUMO level which inject electrons efficiently led to negative shift in the Fermi level of TiO_2. Among these dyes **18b** showed the highest efficiency (6.4%). The factors affecting the efficiency of the devices and the manifestations of the molecular structure on it are critically analyzed and discussed at the end. Generally, the fluorene containing dyes improved light-harvesting ability and electron life time (τ).

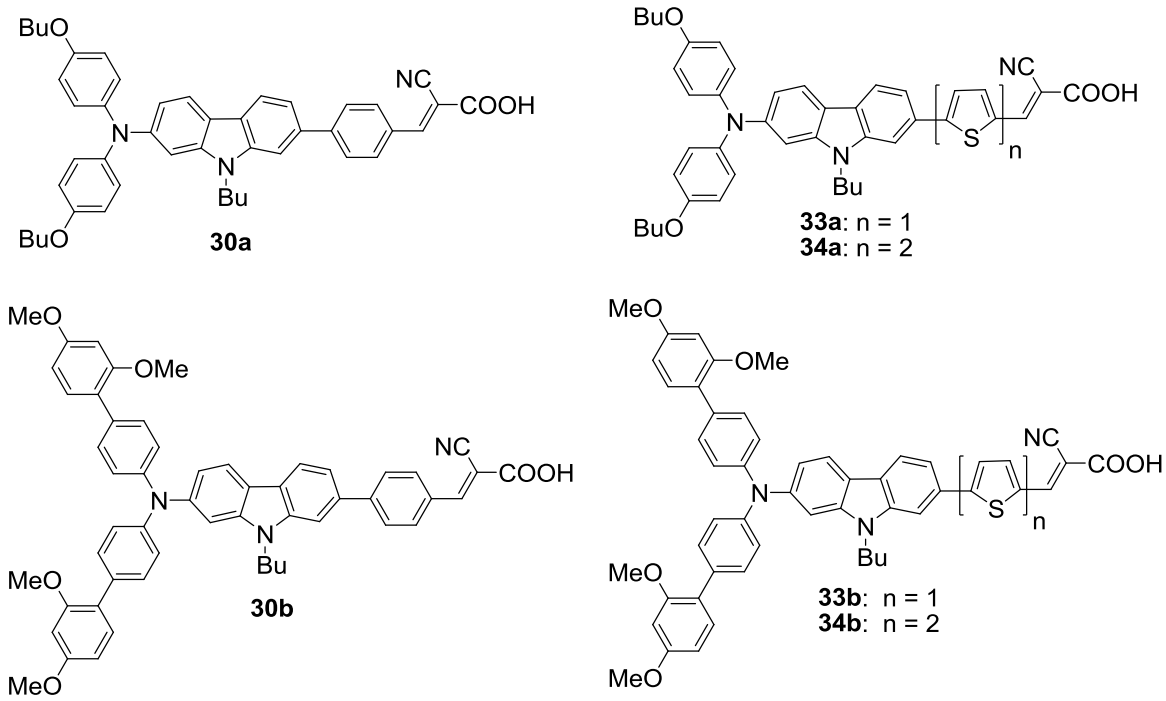

Chart 3 Structures of the alkoxy substituted carbazole based dyes.

In Chapter 5, the organic dyes (Chart 3) containing alkoxy substitution on the donor unit are described. We have used both butoxy and 2,4-dimethophenyl substituents on the diphenylamine donor to maximize the donor strength and retard the intermolecular interactions by providing hydrophobic environment on the donor side. When compared to the parent dyes (**5**, **7a** and **7b**), all these dyes showed red-shifted absorption owing to the introduction of peripheral units which increases the donor strength and facilitate strong donor-acceptor interactions. The oxidation potentials of the dyes are reflective of the electron releasing effect of the peripheral units (4-butoxy > 2,4-dimethoxyphenyl). The excitation energies of the dyes are calculated by TDDFT with two different models B3LYP and MPW1K and the best correlations obtained from later one. Introduction of alkoxy units raised the HOMO and lowered the LUMO. This resulted in the poor dye regeneration and low electron injection efficiency. Among this class of dyes, a dye with 2,4-dimethoxyphenyl peripheral unit and bithiophene in conjugation (**34b**) showed relatively high power conversion efficiency attributable to the favorable electron injection from the excited dye into the conduction band of TiO_2. The suitable LUMO levels of the dyes hike the efficiency while the mismatch of the levels produces inferior efficiency. The charge transport properties of the devices are scrutinized by electrochemical impedance spectroscopy.

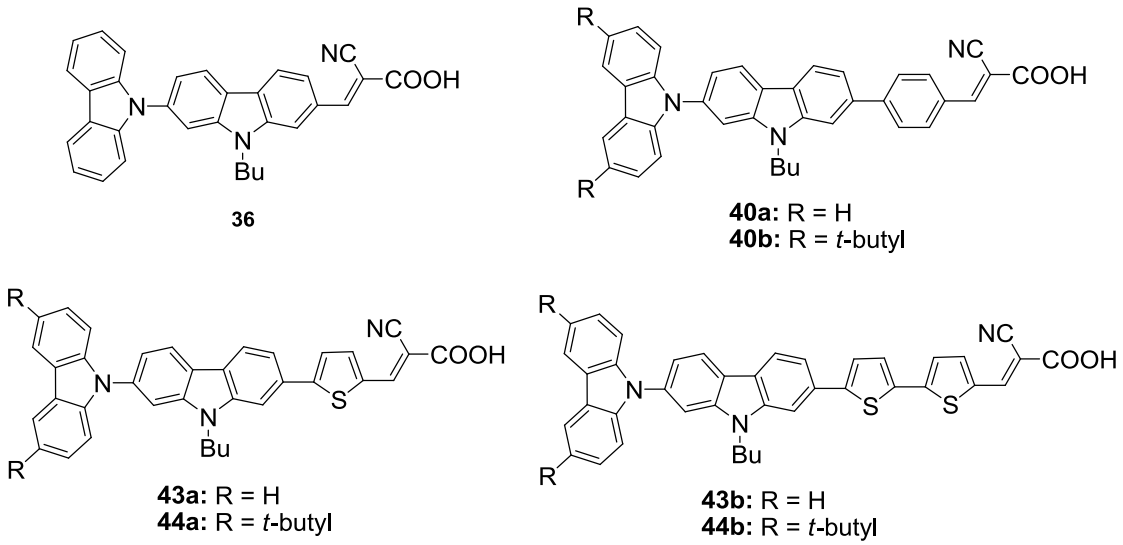

Chart 4 Structure of the organic dyes containing carbazole as donor and π-linker.

In Chapter 6, a set of dyes (Chart 4) using carbazole as donor and π-linker have been synthesized and characterized as effective sensitizers for TiO_2-based DSSCs. The donor properties of the dyes increased on introduction of *tert*-butyl groups at C3 and C6 of carbazole and insertion of thiophene moiety in the conjugation pathway. These structural modifications fine-tuned the optical and electrochemical properties of the dyes. Additionally, the presence of *tert*-butyl groups on the carbazole nucleus minimized the intermolecular interactions. The dyes served as efficient sensitizers in dye-sensitized solar cells and the efficiency ranged from 4.2-6.0%. The *tert*-butyl groups are found to suppress the recombination of injected electrons which contributed to the increment in the photocurrent generation and V_{OC}. A dye (**44a**) with *tert*-butyl groups on the carbazole nucleus and the conjugation bridge composed of carbazole and thiophene fragments exhibited high V_{OC} value. Overall the dye **43b** showed high efficiency of 6.0% with J_{SC} of 15.78 mA cm^{-2}. We unraveled the structural modifications required on the carbazole nucleus on using it as a donor and linker for the optimization of the performance of the DSSCs.

In Chapter 7, the salient features of the work are summarized and the future prospects also addressed. The unique outcome of the work is discussed and a comparative evaluation of optical, electrochemical and photovoltaic properties with those of the known compounds is presented.

Table of Contents

List of Figures

List of Tables

List of Charts

List of Schemes

List of Publications

1. J.-H. Joua, S. Kumar, P.-H. Fang, **A. Venkateswararao**, K. R. J. Thomas, J.-J. Shyue, Y.-C. Wang, T.-H. Lia, H.-H.-Yu, Highly Efficient Ultra-Deep Blue Organic Light-Emitting Diodes with a Wet- and Dry-Process Feasible Cyanofluorene Acetylene Based Emitter. (submitted)
2. **A. Venkateswararao**, K. R. J. Thomas, C.-T. Li, K.-C. Ho, Functional Tuning of Organic Dyes Containing 2,7-Carbazole Linkers by Elongation of Conjugation Pathway with Electron-rich Segments. *RSC Adv.* **2014**, (submitted)
3. **A. Venkateswararao**, K. R. J. Thomas, C.-P. Lee, C.-T. Li, K.-C. Ho, Effect of Auxiliary Chromophores on the Optical, Electrochemical and Photovoltaic Properties of Carbazole-Based Dyes. *Asian J. Org. Chem.,* **2014**, DOI: 10.1002/ajoc.201402235. (**IF**: 2.292)
4. **A. Venkateswararao**, K. R. J. Thomas, C.-P. Lee, C.-T. Li, K.-C. Ho, Organic Dyes Containing Carbazole as Donor and π-Linker: Optical, Electrochemical, and Photovoltaic Properties. *ACS Appl. Mater. Interfaces*, **2014**, *6*, 2528-2539. (**IF**: 5.900)
5. **A. Venkateswararao**, P. Tyagi, K. R. J. Thomas, P.-W. Chen, K.-C. Ho, Organic Dyes Containing Indolo[2,3-*b*]quinoxaline as a Donor: Synthesis, Optical and Photovoltaic Properties. *Tetrahedron*, **2014**, *70*, 6318-6327. (**IF**: 2.817)
6. **A. Venkateswararao**, K. R. J. Thomas, C.-P. Lee, K.-C. Ho, Synthesis and Characterization of Organic Dyes Containing 2,7-Disubstituted Carbazole π-Linker. *Tetrahedron Lett.*, 2013, *54*, 3985-3989. (IF: 2.391)
7. P. Tyagi, **A. Venkateswararao**, K. R. J. Thomas, Solution Processable Indoloquinoxaline Derivatives Containing Bulky Polyaromatic Hydrocarbons: Synthesis, Optical Spectra, and Electroluminescence. *J. Org. Chem.,* 2011, *76*, 4571-4581. (IF: 4.638)

Book Chapter

1. **A. Venkateswararao**, K. R. J. Thomas, Carbazole-Based Organic Dyes for Dye-Sensitized Solar Cells: Role of Carbazole as Donor, Auxiliary Donor and π-Linker. In Solar Cell Nanotechnology; A. Tiwari, R. Boukherroub, M. Sharon, Eds.; Wiley-Scrivener: Beverly, MA, 2014; Chapter 2, pp 41-96.

CHAPTER 1

Carbazole-Based Organic Dyes for Dye-Sensitized Solar Cells: Introduction and Literature Survey

1.1 Introduction

Growing demand for clean energy production from renewable energy sources in the last few decades has led to newer technological breakthroughs such as photovoltaics. Among the photovoltaic methods those have been developed to harvest the solar energy, hetero junction solar cells (HJ), bulk hetero junction solar cells (BHJ) [1] and dye-sensitized solar cells (DSSC) [2] are notable due to their promising characteristics and unlimited practical applications. Though the silicon-based solar cells are commercially available, DSSCs have received immense attention due to their potential advantages like low production cost, transparency, multi-color options, flexibility, light weight and short energy payback time [3]. On the contrary, the bulk hetero junction solar cells have not been demonstrated with reasonable efficiency suitable for practical device manufacturing. They suffer largely due to the limited number of *n*-type organic semiconductors available.

DSSC is typically composed of five major components (Figure 1.1), namely, (i) transparent conducting oxide (TCO), (ii) a mesoporous semiconductor metal oxide (such as TiO_2 or ZnO) film, (iii) a sensitizer, (iv) an electrolyte layer (I_2/I^- couple, Co(II)/Co(III) couple or Fc/Fc^+ couple), (v) counter electrode (platinum or carbon coated glass substrate).

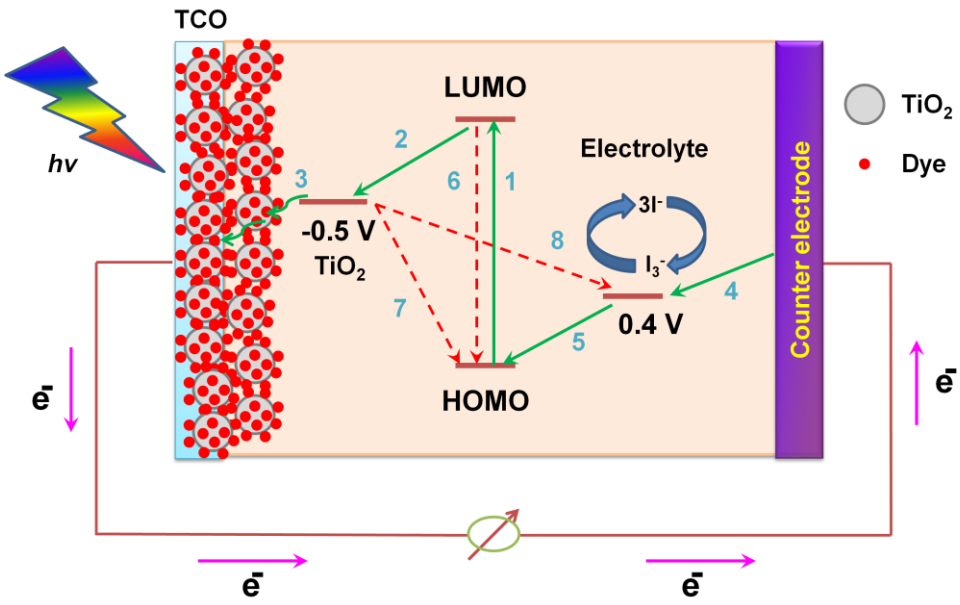

Figure 1.1 Schematic representation of DSSC showing different components and the processes involved during the operation.

Five basic processes which occur during the operation of the DSSC are instrumental in governing the efficiency of the device. They are, (1) absorption of solar light by the dye anchored on TiO_2, (2) injection of electrons into the conduction band (CB) of TiO_2, (3) charge collection at the anode, (4) regeneration of redox couple by electron injection from cathode, (5) reduction/regeneration of the oxidized dye by redox couple, (6) relaxation of the excited dye in to ground state by non-radiative processes such as internal conversion, aggregation-induced quenching, etc., (7) recombination of electrons from the CB of TiO_2 with the oxidized dye, (8) recombination of electrons in CB of TiO_2 with the electrolyte (dark current). The first five processes complete the cyclic flow of electrons and leads to the generation of electricity. The last three processes are detrimental for the efficiency of the DSSC. In order to avoid such undesirable processes the properties of dyes must be fine tuned to possess favorable highest occupied molecular orbital (HOMO) and lowest unoccupied molecular orbital (LUMO) levels [4-6] and structural features to impede unwanted electron passage between the components in DSSC. So the structure-property relationship evaluation for the organic dyes is utmost important to further research outcome in this frontier area to the application level [5].

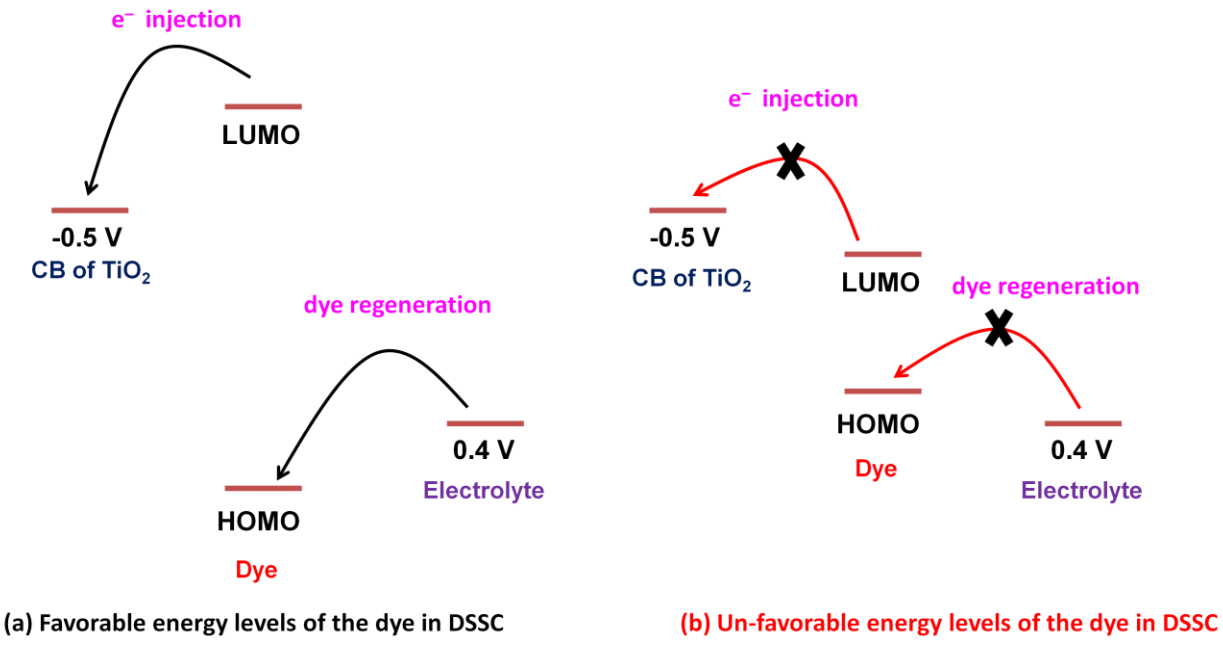

Figure 1.2 Energy level diagram of the dye in DSSC for (a) favorable and (b) un-favorable processes.

The key component of DSSC is dye sensitizer which is essential for efficient light harvesting and electron generation/transfer. The ideal sensitizer should fulfill the following characteristics to achieve better conversion efficiency: (1) The absorption spectra of the dye sensitizer should be broad and cover absorption from visible to NIR region with high molar extinction coefficient to enable the efficient light harvesting with thinner TiO_2 film (2) The dye sensitizer should have suitable anchoring groups such as carboxylates and phosphates for strong binding with semiconductor (3) The dyes should have better charge separation for efficient photo-induced electron transfer from donor to acceptor (4) The suitable energy levels of the dye sensitizer compared to energy level of the components of cell i.e., the LUMO of dye should be more negative than CB of TiO_2 for efficient electron injection from excited dye and HOMO should be more positive than the redox potential of electrolyte for better regeneration of dye. (5) The dye sensitizer should posses steric structural properties to suppress the charge recombination at the interface of TiO_2/dye and aggregation of dyes on TiO_2 film, which are rate determining steps for photocurrent and photo voltage (6) dye sensitizer should posses high thermal and photo stability characteristics [5]. Dye sensitizer with proper alignment of HOMO and LUMO energy levels (Figure 1.2 (a)) are suitable for DSSC applications due to the favorable electron injection and dye regeneration process. But dyes with improper alignment of energy levels (Figure 1.2 (b)) are not suitable for DSSC applications due to the unfavorable electron injection and dye regeneration process.

Dye sensitizer is responsible for the light harvesting of solar flux which inject electron in to semiconductor on relaxation from excited state. In 1991, O'Regan and Grätzel reported the utility of the Ru-based sensitizers (shown in Chart 1.1), [5] cis-(thiocyanato)$_2$bis(2,2′-bipyridyl-4,4′-dicarboxylate)ruthenium(II) coded as **N3**, ditetrabutylammonium salt of **N3** salt coded as **N719**, tris-di(thiocyanato)(4,4',4''-tricarboxy-2,2',6,2''-terpyridine)-ruthenium(II) coded as **N749** (black dye) and cis-di(thiocyanato)(2,2'-bipyridyl-4,4'-dicarboxylate)-(2,2'-bipyridyl-4,4'-dinonyl)-ruthenium(II) coded as **Z907** were developed (shown in Chart 1.1) [7]. All the dyes achieved certified efficiencies greater than (> 10%) with high IPCE values (> 80%) despite possessing poorest absorption in the lower energy region. However the efficiencies of the dyes there suffered from disadvantages such as shorter wavelength, absorption with low molar extinction coefficient, non-availability, purity and cost of the ruthenium metal.

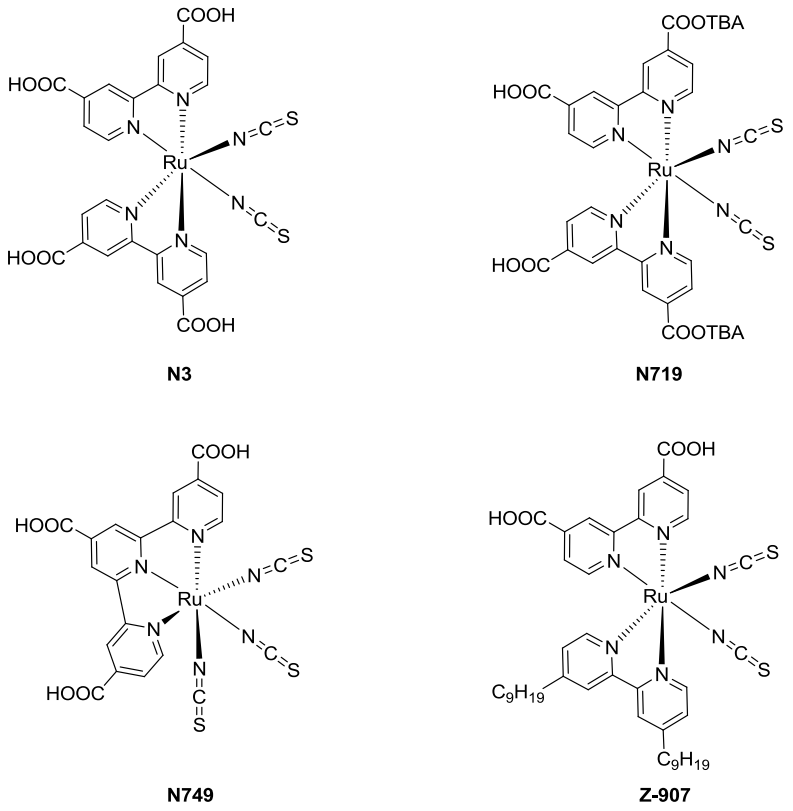

Chart 1.1 Structures of the dye sensitizers (**N3**, **N719**, **N749** and **Z-907**) based on Ruthenium metal complexes.

Metal-free organic dyes have evolved as alternatives to inorganic metal containing sensitizers due to the advantages such as easy synthesis via facile chemical modification, lower production cost, higher molar extinction coefficient and flexible functional tuning. In general, organic dyes possesses donor-π-bridge-acceptor (D-π-A) molecular configuration and most of them possess rod shape structure. With the help of this design we can extend the absorption spectra and tune the HOMO and LUMO energy levels. Till-to-date hundrends of chromophores such as triarylamine, [8] fluorene, [9-11] coumarin, [12-14], dibenzo[*b*,*d*]thiophene, [15] dibenzo[*b*,*d*]furan, [15] pyrene, [16, 17] thieno[3,2-*b*]thiophene, [18, 19] dithienothiophene, [20] cyclopentadithiophene (CPDT), [21, 22] dithieno[3,2-*b*:2′,3′-*d]*pyrrole (DTP), [23, 24] phenothiazine, [25, 26] phenoxazine, [27, 28] indoline, [29, 30] imidazole [31] and pyrenoimidazoles [32] etc. have been used in the assembly of organic dyes. Some of the representative examples of organic dyes are collected in Chart 1.2.

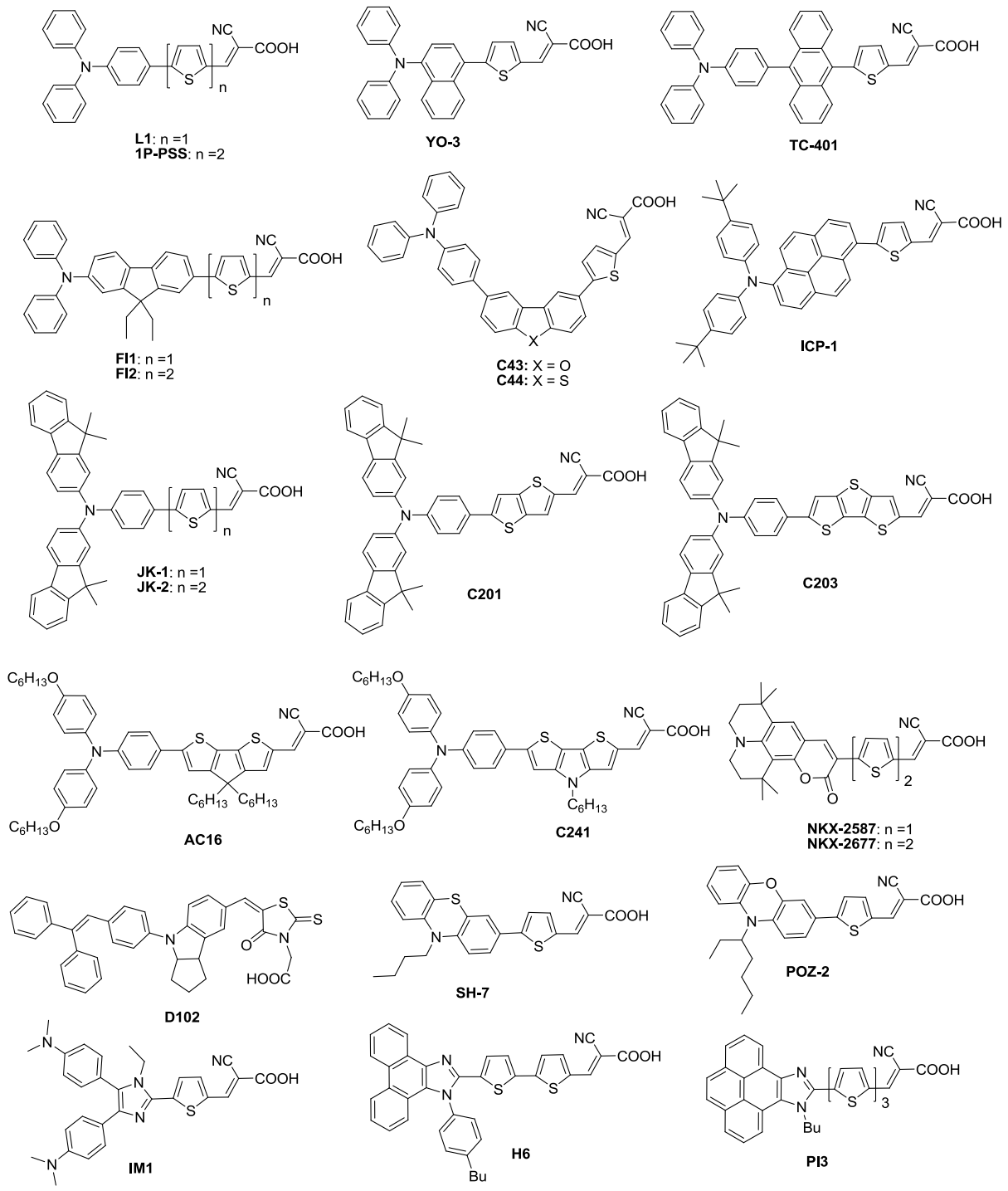

Chart 1.2 Structures of the organic dye sensitizers.

One of the efficient approaches to expand the absorption spectra of the organic dyes is the incorporation of an auxiliary acceptor in the structure D-π-A to increase the donor-acceptor interactions [33]. Acceptors such as benzo[*c*][1,2,5]thiadiazole (BTZ), [34, 35] 2*H*-

benzo[*d*][1,2,3]triazole, [36, 37] diketopyrrolopyrrole (DPP), [38] isoindigo, [39] phthalimide [36] pyrazine, [40] quinoxaline [41, 42] and thieno[3,4-*c*]pyrrole-4,6-dione [43] have been used in the construction of organic dyes and representative examples are presented in Chart 1.3.

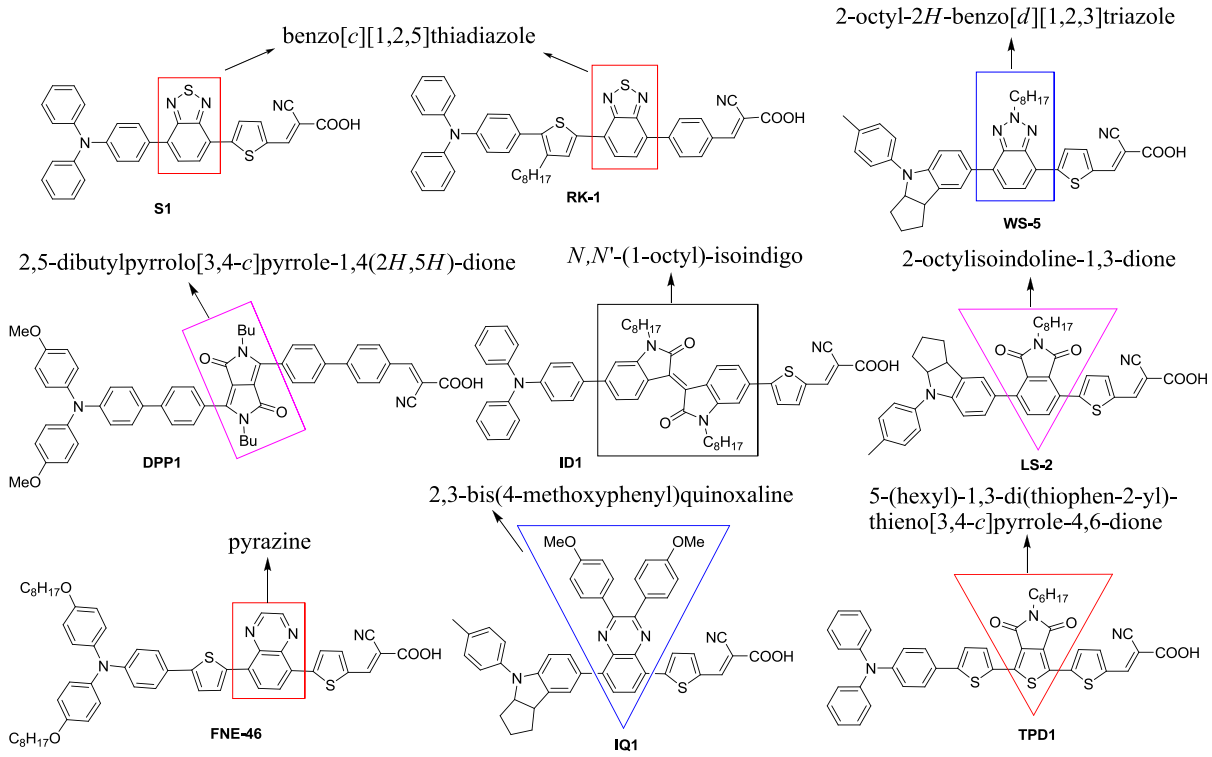

Chart 1.3 Structures of the organic dye sensitizers containing auxiliary acceptor.

Carbazole-based organic materials are exceptionally interesting due to their promising properties such as relatively low oxidation potentials, thermal and photo-stability and hole-conducting capabilities [44, 45]. Moreover, a variety of nuclear positions available for functionalization expand the scope and utility of carbazole-derived materials. Carbazole-containing molecular materials have been successfully demonstrated for application as hole-transporting emitters in organic light-emitting diodes (OLED), [46-48] organic semiconductor in thin-film transistors (TFT) [49-51] and electron donors in photovoltaics [52-54]. The first report on the use of carbazole-based organic dyes came in 2006, authored by Hara and co-workers. Several dyes featuring carbazole as either donor or π-linker have been synthesized and demonstrated as sensitizers in DSSC [9]. In this review, we collect the information available on this emerging class of dyes featuring carbazole either as donor or bridging unit and try to evolve design principles one may adopt to arrive at promising materials.

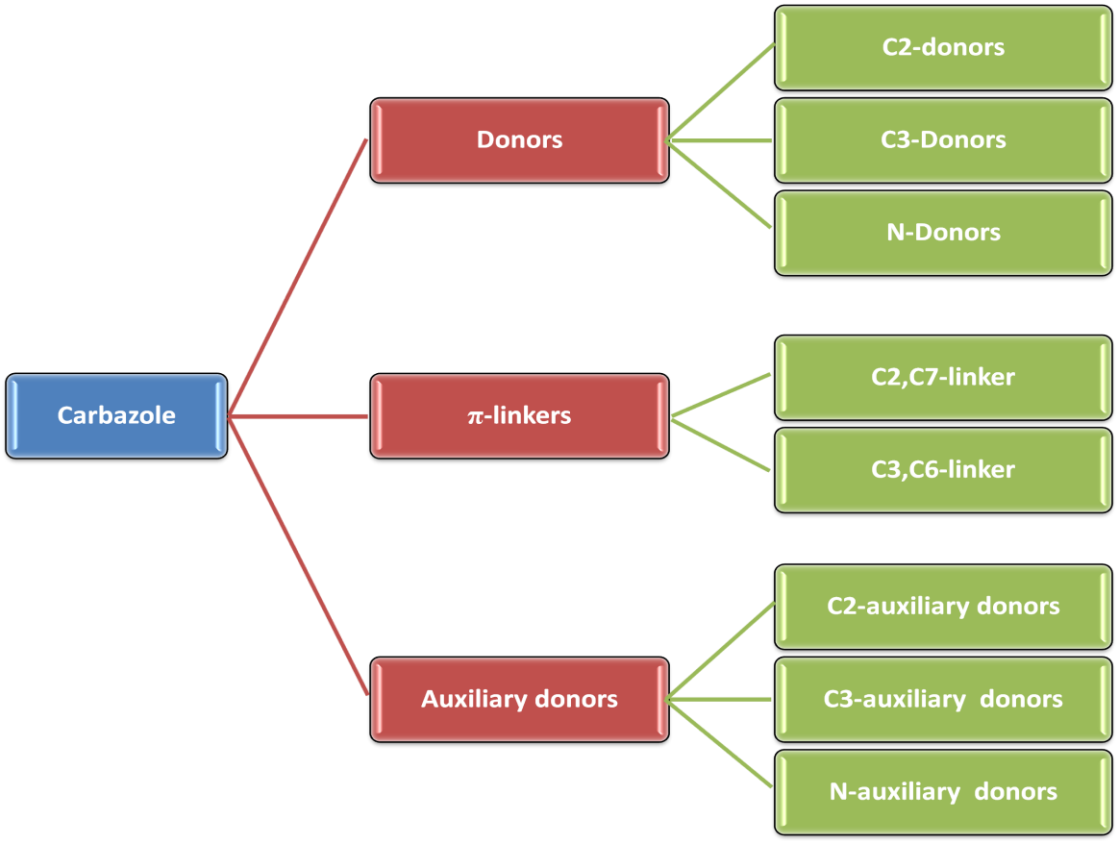

Figure 1.3 Categorization based on the functional role of carbazole in organic dyes suitable for DSSC.

Due to the electron richness of the carbazole unit it has been used as a donor in organic dyes for DSSC. Selective mono functionalization at both C3 and *N*9 have been used to tether the carbazole as donor while difunctionalization at C2 and C7 or C3 and C6 for exploiting it as π-bridging segment. Electron donating character of carbazole normally strengthens the donor-acceptor interaction in dipolar compounds and benefits the optical properties such as absorption wavelength and molar extinction coefficient [55]. It is interesting to examine the effect of structural differences arising due to functionalization at various nuclear positions of carbazole on the vital properties such as absorption and oxidation propensity which play major role in determining the performance of DSSCs. Depending on the role of carbazole in an organic dye, we classify such organic dyes into three categories: donors, auxiliary donors, π-linkers. Further within a group, they are further classified, for convenience of treatment, according to their nuclear substitution pattern (Figure 1.3).

1.2 Carbazole as a donor for dye sensitized solar cells

Electron-donating ability of carbazole is well established though it is less basic than most of the analogous triarylmines [56]. Due to this carbazole-based materials are used as hole-transporting emitters in organic light-emitting diodes [46-48]. Additionally most of the carbazole derivatives inherit high-lying triplet state (T_1) and wide band gap. They are beneficial for them to serve as hosts for deep blue-emitting singlet as well as triplet emitters [57]. Though there is a tradeoff in the absorption properties of carbazole-based dyes, when compared to the analogous triarylamine-based dyes, the former dyes due to rigidity inhibit non-radiative relaxation pathways in the excited state and planarity ensures facile charge migration toward acceptor due to favorable orbital overlap across the conjugation. Carbazole can be functionalized at several nuclear positions but substitutions at C3 and *N*9 have been found to be successful in extracting the electrons from carbazole [8].

1.2.1 Carbazole as donor via C2-position

The general configuration of the dyes where carbazole acts as donor via C2-position showed in Figure 1.4. The functionalization of carbazole at second position is not possible by direct methods (bromine and N-bromosuccinimide (NBS)) and the preparation of 2-bromo carbazole started with reductive cyclization of 4'-bromo-2-nitrobiphenyl with triphenylphosphine or tritheyl phosphate [58]. The functionalization at *N*9-position by simple alkylation or arylation offer good solubility and electron donating strength [59].

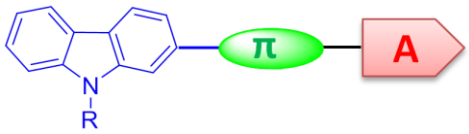

Figure 1.4 Configuration of the organic dyes with carbazole as donor *via* C2-position.

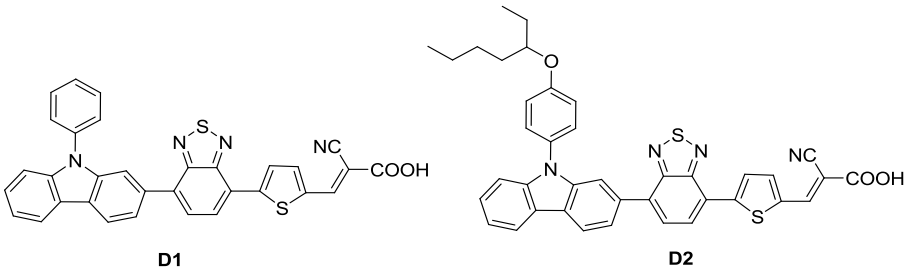

Chart 1.4 Structures of the dyes containing carbazole donor and BTZ auxiliary acceptor.

Valiyaveettil and co-workers reported a set of dyes (Chart 1.4) with configuration of D-A-π-A for DSSC composed of carbazole as donor at C2-position and cyanoacrylic acid as an acceptor bridged by BTZ (auxiliary acceptor) [60]. The synthetic scheme of the dyes is outlined in Scheme 1.1 and it starts with Ullmann-type coupling [61] of 2-bromo-9*H*-carbazole with iodobenzene gave 2-bromo-9-phenyl-9*H*-carbazole and it subsequently converted to 9-phenyl-2-(4,4,5,5-tetramethyl-1,3,2-dioxaborolan-2-yl)-9*H*-carbazole by treatment with *n*-BuLi and 2-isopropoxy-4,4,5,5-tetramethyl-1,3,2-dioxaborolane. Suzuki coupling [62] of carbazole borolane derivative with 4,7-dibromobenzo[*c*][1,2,5]thiadiazole followed by Suzuki coupling with 5-formylthiophen-2-ylboronic acid resulted aldehyde derivatives. These aldehydes converted in to corresponding cyanoacrylic acid dyes (**D1** and **D2**) by Knoevenagel condensation [63] with cyanoacetic acid.

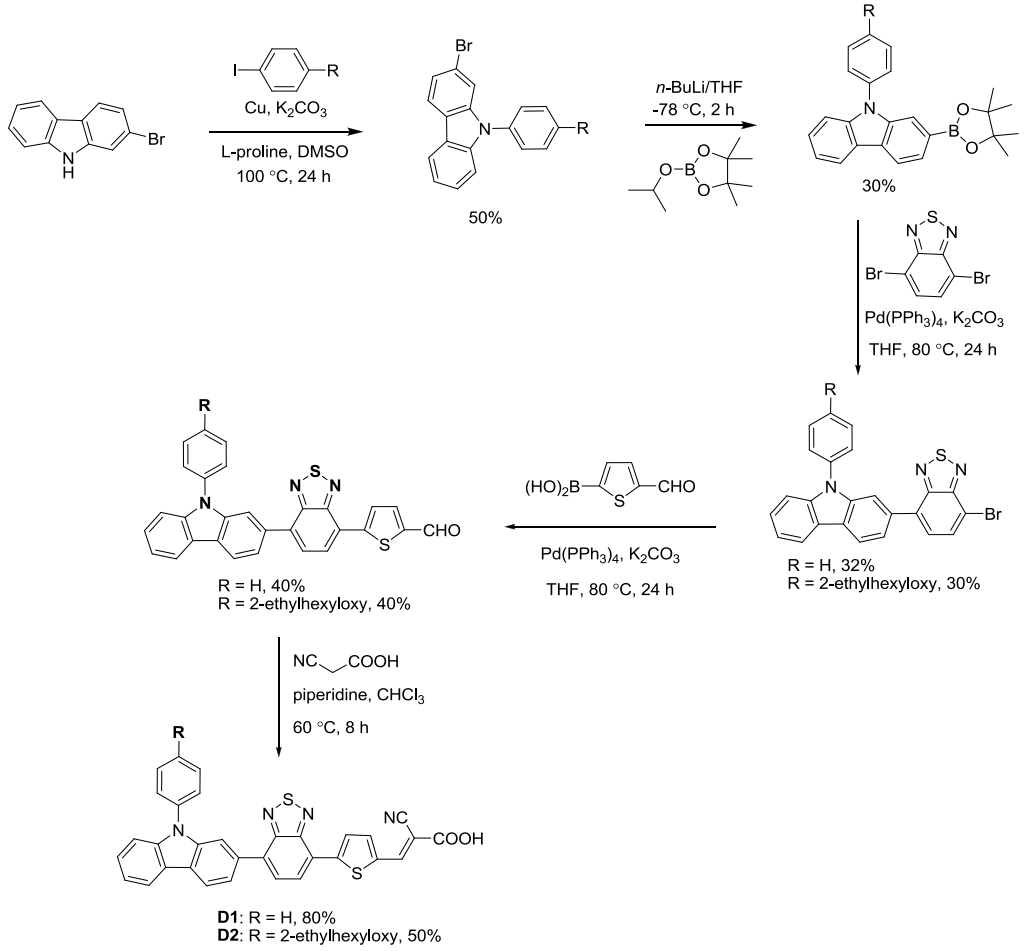

Scheme 1.1 Synthetic scheme of the dyes **D1** and **D2**.

They have compared the optical and photovoltaic properties with same donor connected at C3-position without BTZ unit in conjugation. The dyes (**D1** and **D2)** showed the absorption at 459 nm, 461 nm with molar extinction coefficients of 10239 M^{-1} cm^{-1} and 11021 M^{-1} cm^{-1} respectively and this absorption corresponds to the charge transfer transition from carbazole donor to cyanoacrylic acid acceptor. The dye **D1** showed photovoltaic conversion efficiency of 1.53% with short circuit current density (J_{SC}) of 3.22 mA cm^{-2} and **D2** achieved an efficiency of and 1.20% with J_{SC} of 2.43 mA cm^{-2}. The superior performance of dye **D1** is due to its superior J_{SC} compared to dye **D2** owing to higher dye loading of the former dye.

Table 1.1 Optical, electrochemical and photovoltaic performance parameters of dyes containing carbazole as donor

Dye	$\lambda_{max,}$ nm (ε_{max}, M^{-1} cm^{-1})	E_{ox} , V (*vs* NHE)	E_{ox}^{*}, V (*vs* NHE)	J_{SC} (mA cm^{-2})	V_{OC} (mV)	*ff*	η (%)	*Ref*
D1	459 (10239)	1.27	−0.56	3.22	640	0.73	1.53	[60]
D2	461 (11021)	1.38	−0.59	2.43	670	0.71	1.20	[60]

1.2.2 Carbazole as donor via C3-position

The general molecular configuration of the dyes belonging to this category is displayed in Figure 1.5. The substitution of carbazole at C3-position was often accomplished *via* the bromination of carbazole by using *N*-bromosuccinimide in suitable solvents such as dimethylformamide (DMF), tetrahydrofuran (THF) or dichloromethane (DCM) [64-66]. *N*-alkylation or *N*-arylation is useful to promote the solubility or enhance the donor strength. *N*-alkylation on carbazole is achieved by simple nucleophilic substitution with alkyl halide in the presence of a base aided by a phase transfer catalyst [67]. Though, the *N*-arylation can be achieved by simple nucleophilic substitution with aryl fluorides [68] and harsh conditions required for less activated aryl substrates involving Ullmann protocol [61] or Palladium-catalyzed C-N coupling reaction strategies [70].

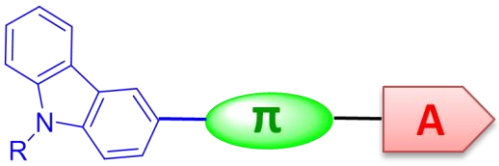

Figure 1.5 Molecular compositions of organic dyes with carbazole as donor *via* C3-position.

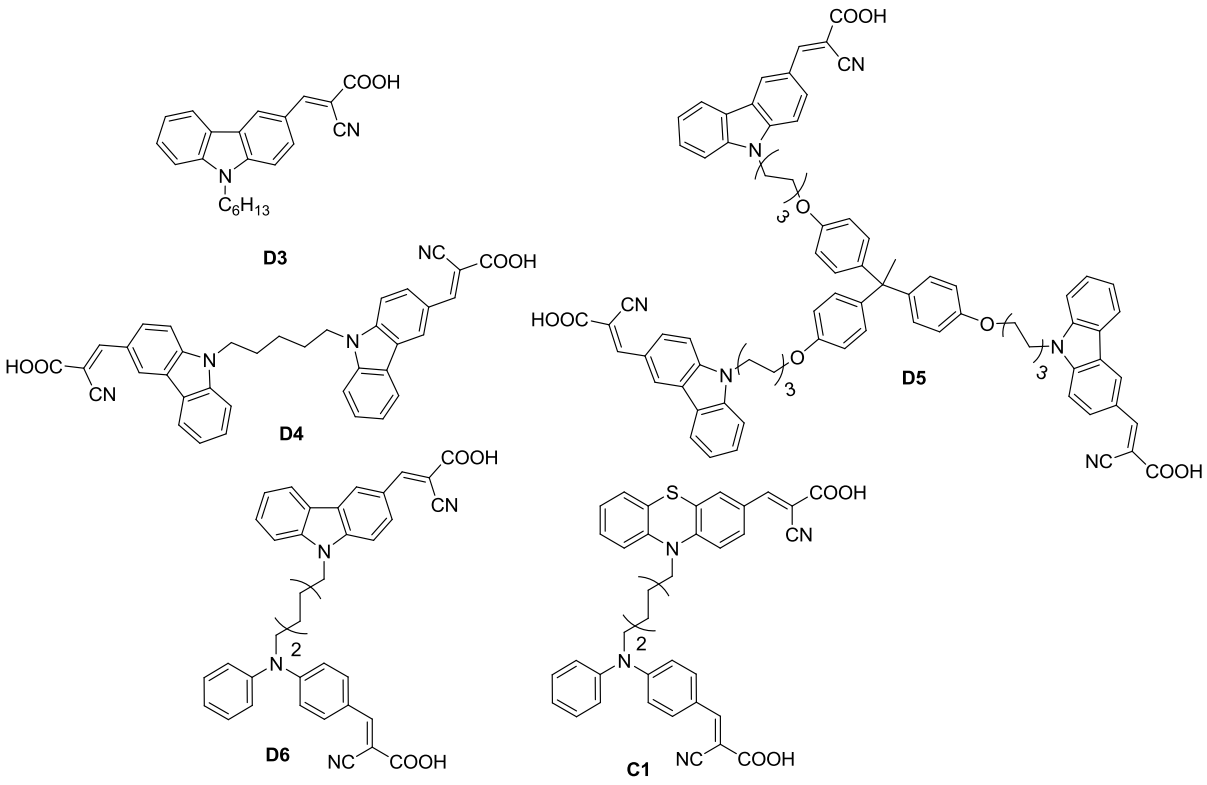

Chart 1.5 Structures of the carbazole dyes having multiple light-harvesting chromophores.

Simple carbazole-based dyes (**D3**-**D5**; Chart 1.5) containing carbazole as donor and cyanoacrylic acid as acceptor was reported by Kim and co-workers [71]. The synthetic scheme of the dyes is shown in Scheme 1.2. Carbazole and diphenylamine were alkylated by reaction with 1-bromohexane or 1,6-dibromohexane gave 9-hexyl-9*H*-carbazole, 9-(2-bromohexyl)-9*H*-carbazole and for selective akylation of carbazole and diphenylamine, 1,6-di(9*H*-carbazol-9-yl)hexane and *N*-(5-bromopentyl)-*N*-phenylaniline obtained, respectively. They converted to the corresponding aldehyde *via* Vilsmeier-Haack reaction [72] in the presence of DMF and $POCl_3$. Alkylation of 9-(5-bromopentyl)-9*H*-carbazole-3-carbaldehyde with hydroxy phenyl ethane in presence of basic medium gave tri-carbazole aldehyde derivative. *N*-(5-bromopentyl)-*N*-phenylaniline alkylated with carbazole in the presence of basic medium afford compound *N*-(5-(9*H*-carbazol-9-yl)pentyl)-*N*-phenylaniline. This was converted to aldehyde derivative by Vilsmeier-Haack reaction. Finally, all the aldehydes were condensed with cyanoacetic acid to yield the target dyes (**D3**-**D6**) by the Knoevenagel reaction.

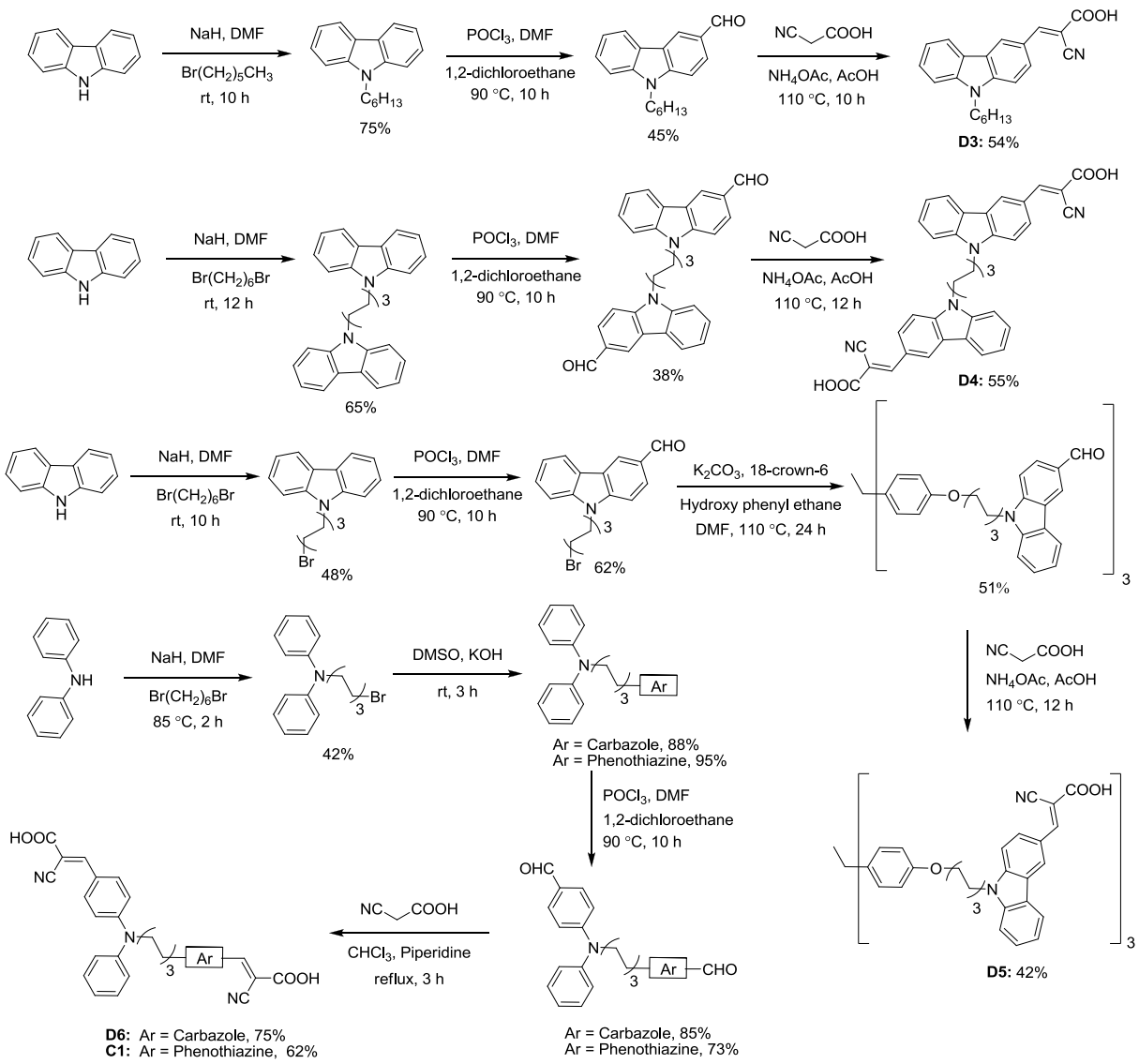

Scheme 1.2 Synthetic scheme of the dyes **D3**-**D6**.

They investigated systematically the effect of number of chromophores on the performance of the DSSCs. The J_{SC} of the dyes increased from **D3** (1.29 mA cm^{-2}) to **D4** (2.31 mA cm^{-2}) due to the increase of molar extinction coefficient with increasing the number of carbazole units there by increasing the light harvesting efficiency. The first excited state potential increased with increasing the number of chromophore units which facilitated the facile electron injection into CB of TiO_2. The open circuit voltage (V_{OC}) of the devices increased monotonously from 540 mV (**D3**) to 715 mV (**D5**) due to the suppression of charge recombination on introduction of a bulky structure and negative shift in Fermi level of TiO_2 caused by the accumulation of electron density in the CB of TiO_2 by efficient electron injection. Cao and co-workers demonstrated

superior performance for the dye **D6** and **C1** (Chart 1.5) constructed by asymmetric double donor-π-acceptor chains over a parent dye **D3** containing one donor-acceptor axis [73]. The dye **D6** showed an efficiency of 2.82% compared to the dye **D3** (0.42%). The overlap of complimentary absorptions of two independent donor-π-acceptor units results in a broader absorption for the dye **D6** which improves the J_{SC}. The facile regeneration facilitated by suitable HOMO improves V_{OC}. The inferior efficiency of **D6** compared to the phenothiazine analog **D7** (η = 4.66%) is attributed to the strong donating nature of phenothiazine.

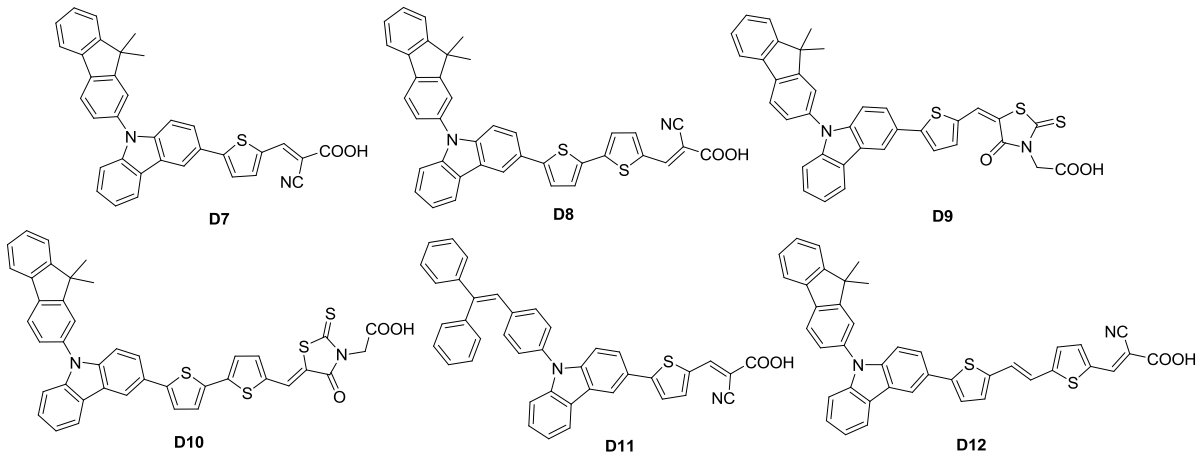

Chart 1.6 Dyes containing carbazole donor with various *N*9-substituents.

Oligothiophene units have been found to act as an effective conjugation pathway in the organic dyes possessing donor-acceptor architecture. Ko and co-workers synthesized dyes (**D7**–**D12** in Chart 1.6) by combining carbazole with oligothiophene bridges and they showed interesting optical and electrochemical trends [74]. The synthetic scheme of the dyes is displayed in Scheme 1.3. The 3-iodo-9*H*-carbazole was synthesized by iodination of 9*H*-carbazole with periodic acid dihydrate and iodine. Stile coupling of 3-iodocarbazole with stannyl oligothiophene gave carbazole oligothiophene derivatives. They were subsequently treated with iodofluorene by Ullmann coupling to obtain fluorene substituted carbazole derivatives. This on lithiation with *n*-*n*-BuLi and quenching with dimethylformamide gave corresponding aldehyde derivatives. *N*-Arylation of 3-(thiophen-2-yl)carbazole with 1-(2-(4-bromophenyl)-1-phenylvinyl)benzene by Ullmann coupling produced the new carbazolyl thiophene followed by treatment with *n*-BuLi and dimethylformamide gave the corresponding aldehyde. Horner-Emmons-Wittig coupling reaction [75] of 5-(9-(9,9-dimethyl-9*H*-fluoren-2-yl)-9*H*-carbazol-3-yl)thiophene-2-carbaldehyde

with (2-thienylmethyl)triphenylphosphonium bromide led to 9-(9,9-dimethyl-9*H*-fluoren-2-yl)-3-(5-(2-(thiophen-2-yl)vinyl)thiophen-2-yl)-9*H*-carbazole and subsequently converted to aldehyde by lithiation with *n*-BuLi and dimethylformamide. The dyes (**D7**-**D12**) were prepared by reaction of corresponding carbazole containing aldehyde derivatives and cyanoacetic acid via Knoevenagel condensation.

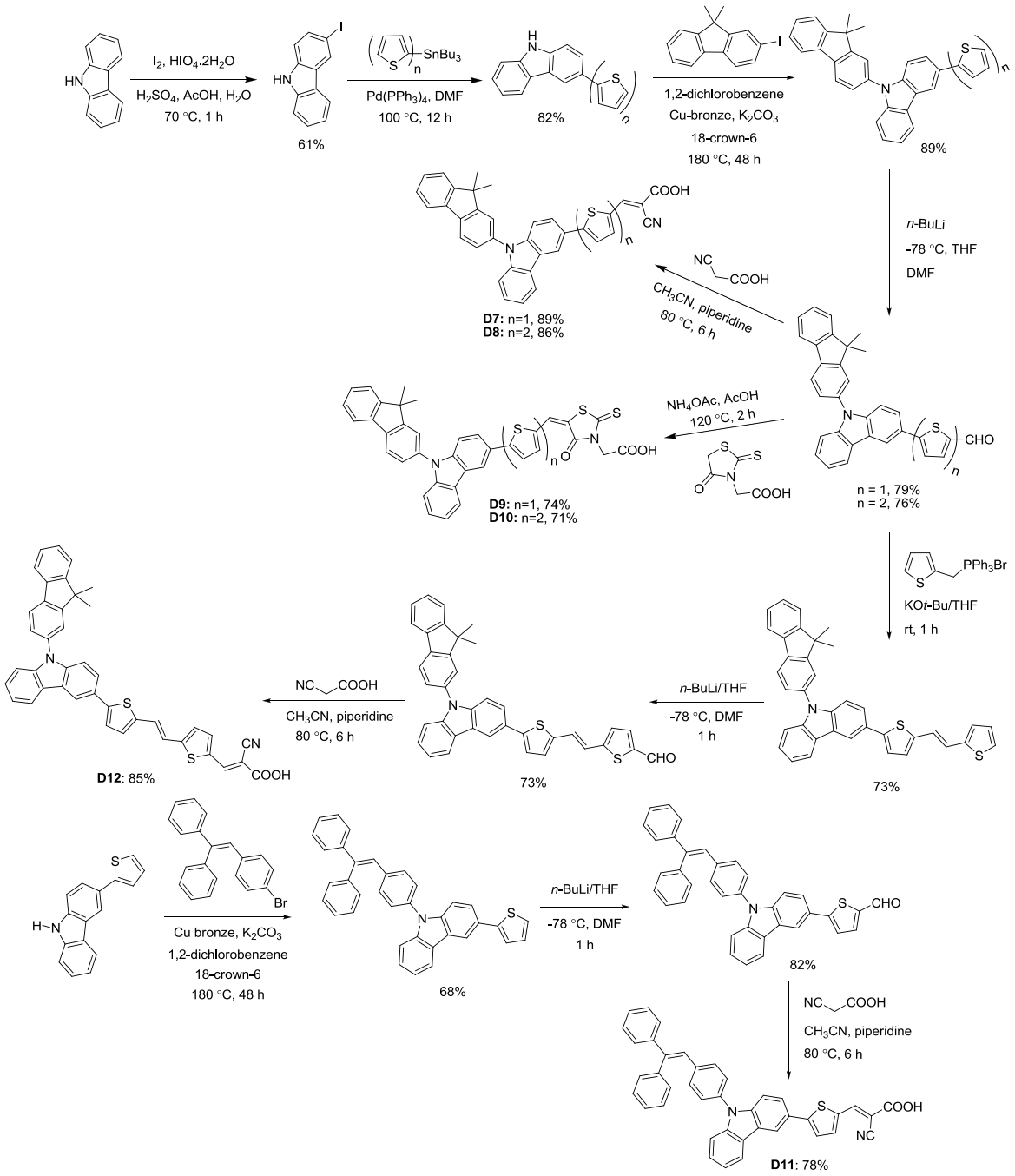

Scheme 1.3 Synthetic scheme of the dyes **D7**-**D12**.

They showed variations in *N*-substituent, conjugation pathway and acceptor unit. Firstly, *N*-substituents such as 9,9-dimethylfluoren-2-yl or 4-(2,2-diphenylvinyl)phenyl group does not affect the nature of the frontier orbitals significantly. The HOMO of the dyes is mainly located on the carbazole and thiophene segments. However, electron-rich *N*-substituents lowered the HOMO energy level and facilitated the regeneration of the oxidized dyes. In addition, the absorption of the dyes was red shifted when compared to the simple dyes without thiophene in the conjugation (**D3** and **D4**). All these favorable properties contributed to the enhancement of device parameters. It is also interesting to note that the substitution of cyanoacrylic acid unit (**D7** and **D8**) with rhodanine group (**D9** and **D10**), though improved the absorption characteristics, did not produce good photocurrent because of less favored electron injection from dye to CB of TiO_2. The dyes **D11** and **D12** generated lower photocurrent than **D7** and **D8**, probably arising due to the lowered LUMO of former compounds which reduce the electron injection efficiency. Slightly better device efficiency realized for **D11** when compared to **D12** may be attributed to the competing *cis-trans* isomerization pathways present for the dyes containing vinylene linkers.

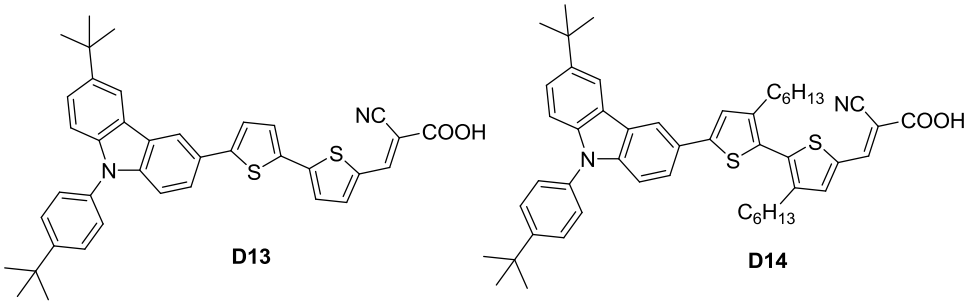

Chart 1.7 Carbazole dyes with bithiophene and hexyl bithiophene conjugation-bridge.

Chen and co-workers designed and synthesized two dyes **D13** and **D14** (Chart 1.7) based on *N*9-(*tert*-butyl) phenyl functionalized 3-*tert*-butylcarbazole [76]. They designed these molecules to unravel the structural elements required to suppress the intermolecular interactions at the surface of TiO_2 which would retard the aggregation propensity. The synthesis of the dyes is showed in Scheme 1.4. It starts with the synthesis of 3-*tert*-butyl-9*H*-carbazole via a photo stimulated reaction in two steps with Buchwald-Hartwig C-N coupling was adopted to synthesize the *tert*-butyl-capped N-arylcarbazole. After bromination, the monobrominated *N*-arylcarbazole was treated with *n*-BuLi and 2-isopropoxy-4,4,5,5-tetramethyl-1,3,2-dioxaborolane was added to yield the corresponding borolane derivative. Then the carbazole borolane derivative was reacted

with monobromo-bithiophene aldehyde by Suzuki coupling to produce the corresponding aldehyde derivatives. Finally, cyanoacrylic acid dyes (**D13** and **D14**) were prepared from carbazole aldehyde derivatives with cyanoaceticacid via Knoevenagel condensation.

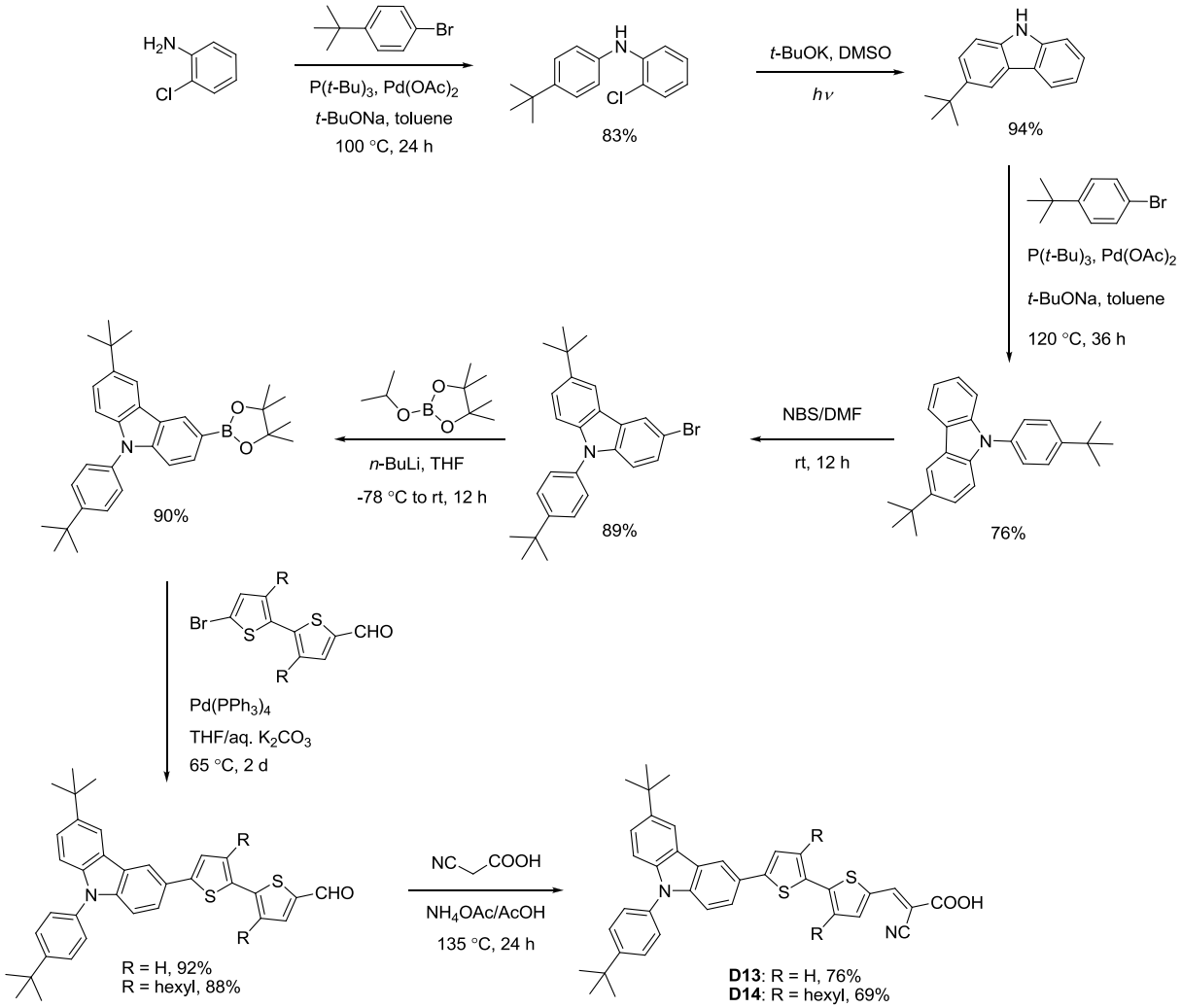

Scheme 1.4 Synthetic scheme of the dyes **D13** and **D14**.

The efficiency of **D14** (3.75%) was slightly higher than **D13** (3.62%) due to the presence of hexyl chains on thiophene in **D14**. This suppresses the electron transfer from TiO_2 to redox electrolyte and results in the increase of V_{OC} from 570 to 660 mV. However, the marginal increase in efficiency is due to the poor absorption characteristics of **D14** triggered by the non-planar conjugation pathway which led to small photocurrent generation. So it appears that structural tweaking for the suppression of electron recombination as demonstrated for **D14** may not be ideal. Also, the efficiency of **D13** is less than that observed for **D8** due to the presence of

low lying LUMO in **D13** which shrinks the gap between the CB of TiO_2 and LUMO of the dye and results in poor thermodynamic driving force for the electron injection.

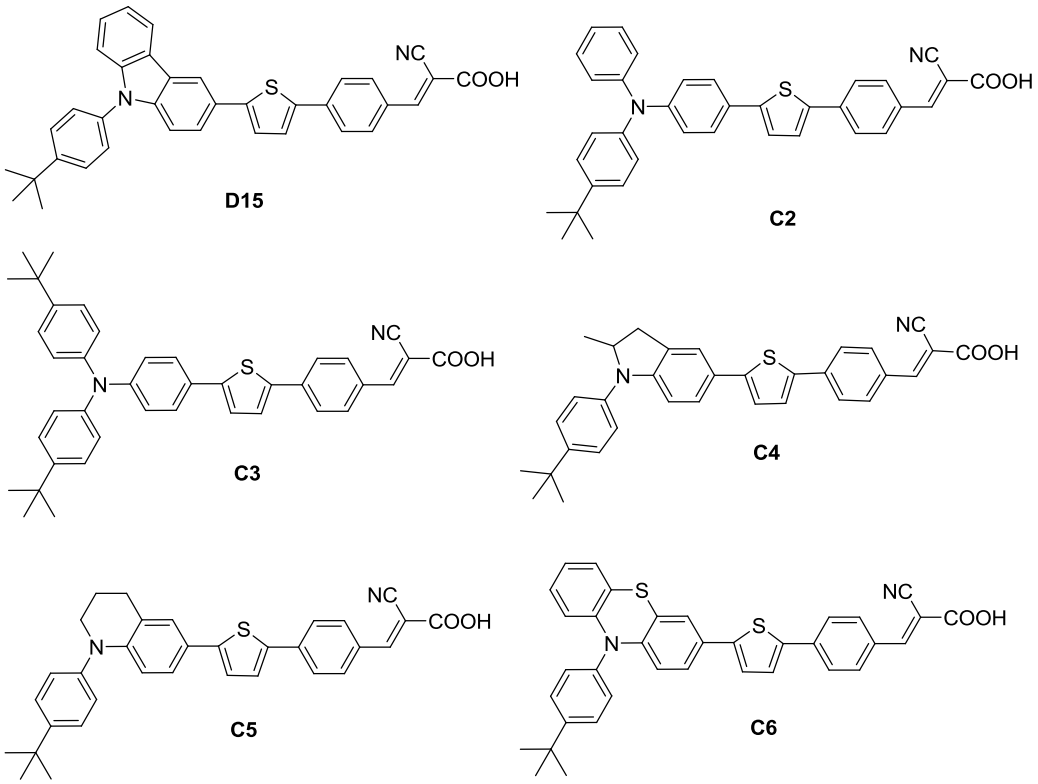

Chart 1.8 Organic dyes containing carbazole, phenothiazine, triphenylamine, indoline or tetrahydroquinoline donor.

Peng and co-workers reported a series of dyes featuring different donors such as triphenylamine, indoline, tetrahydroquinoline, carbazole and phenothiazine (Chart 1.8) [77]. All the dyes possess 4-*tert*-butylphenyl unit as a common group. The synthesis of the dyes showed in Scheme 1.5. The intermediate 9-(4-*tert*-butylphenyl)-3-(thiophen-2-yl)-9*H*-carbazole synthesized by Stille coupling reaction [78] with stannylthiophene and 3-bromo-9-(4-*tert*-butylphenyl)-9*H*-carbazole. It converted to stannyl derivative and followed by Stille coupling with *p*-bromo benzaldehyde led to 4-(5-(9-(4-*tert*-butylphenyl)-9*H*-carbazol-3-yl)thiophen-2-yl)benzaldehyde. Finally it reacted with cyanoacetic acid to produce **D15** by Knoevenagel condensation. Synthesis of the analogous dyes (**C2-C6**) is similar to the procedure described in Scheme 1.5.

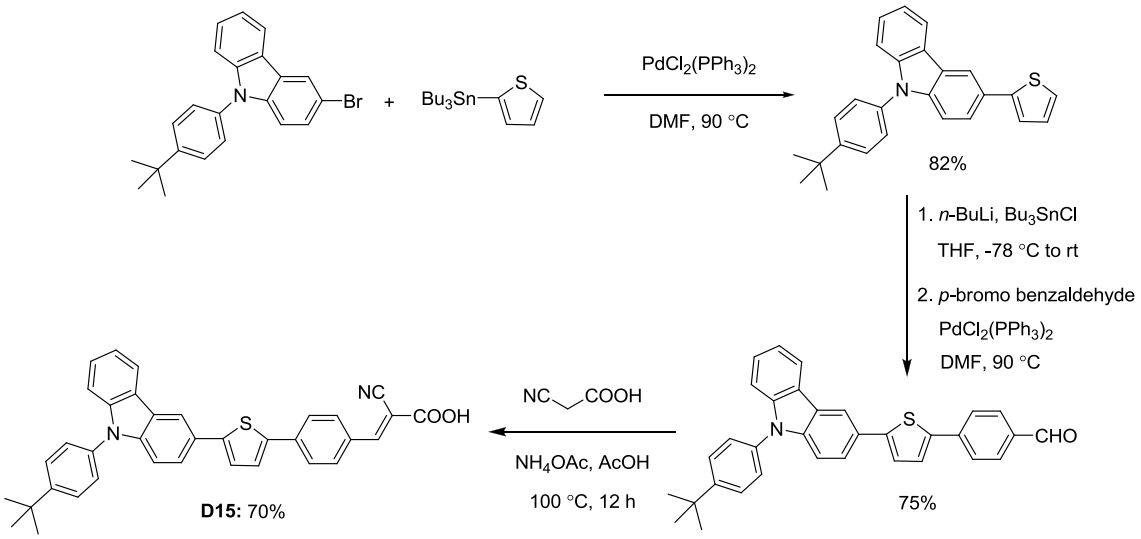

Scheme 1.5 Synthetic scheme of the dye **D15**.

The dye, **D15** with a carbazole unit as a donor displayed better photon-to-electron conversion efficiency (6.72%) among all dyes. The success of the dye **D15** in DSSC is attributed to the red-shifted absorption displayed by the dye on adsorption on TiO_2. It is worthy to note here that **D15** displayed the blue shifted absorption when compared to other dyes in solution. Addition of CDCA as a co-adsorbent did not improve the device performance. All these observations indicate the absence of aggregation at the surface of TiO_2. On comparing with **D8**, irrespective of the variation in *N*-substitution, the replacement of thiophene in **D8** with phenyl unit in **D15** produced higher device efficiency. This is probably due to the higher LUMO level of **D15** which benefits electron injection and leads to accumulation of electrons at CB of TiO_2.

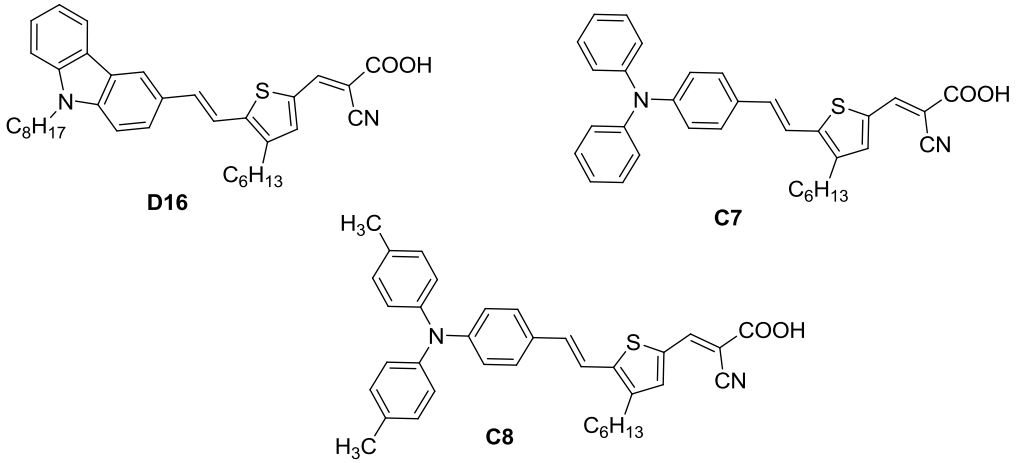

Chart 1.9 Dyes containing 3-vinylcarbazole unit and other comparable donor systems.

Bin and co-workers synthesized dyes (**D16, C7** and **C8;** Chart 1.9) featuring carbazole/triphenylamine as donor, vinylene 3-hexylthiophene as spacer and cyanoacrylic acid as an acceptor [79]. The synthetic strategy of the dyes is illustrated in Scheme 1.6. The intermediate diethyl(3-hexylthiophen-2-yl)methylphosphonate was synthesized by treating 3-hexylthiophene with formaldehyde and hydrochloric acid and then reacted with triethyl phosphite. The intermediate diethyl(3-hexylthiophen-2-yl)methylphosphonate was reacted with triphenylamine and carbazole aldehyde by Wittig-Horner reaction [80] to obtain the corresponding vinylderivatives which formylated by lithiation with *n*-BuLi followed by addition of DMF. The triphenylamine and carbazole aldehyde were converted to dyes (**D16, C7** and **C8**) by Knoevenagel condensation with cyanoacetic acid.

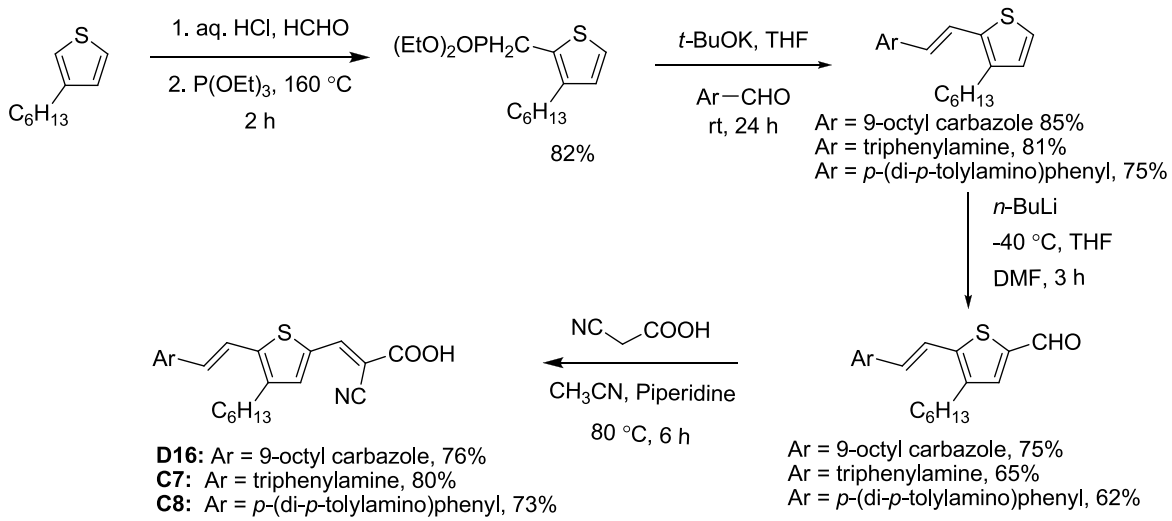

Scheme 1.6 Synthetic scheme of the dyes **D16**, **C7** and **C8**.

The dye **D16** possessing carbazole framework as donor showed exceptional efficiency in DSSC (6.33%) due to its high V_{OC} (700 mV). The hexyl group on thiophene helps to suppress the molecular interactions and keeps the electrolyte away from the TiO_2 layer. The **D16** showed higher efficiency (η = 6.33%) than the similar compound with triphenylamine donor (**C7**; η = 5.48%). However, **D16** showed inferior efficiency than (*E*)-2-cyano-3-(5-(4-(di-*p*-tolylamino)styryl)-4-hexylthiophen-2-yl)acrylic acid (**C8**; η = 6.72%). The higher efficiency observed for **C8** is attributed to the red shifted absorption which leads to improved IPCE at longer wavelength region. The methyl groups in **C8** increases the electron-richness of the donor and facilitates the donor-acceptor interaction in the dye. The benefit of vinyl group in these dyes

is understandable on comparing the optical properties of these dyes with **D7**. Introduction of vinyl bridge elongated the conjugation and produced much intense and red-shifted absorption profile for **D16** (Table 1.2).

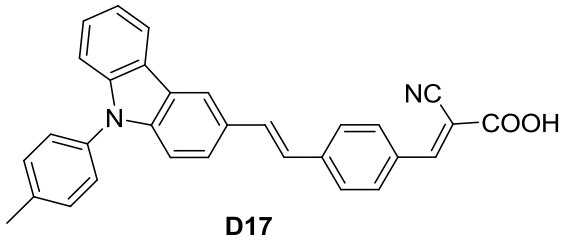

D17

Chart 1.10 Structure of the dye containing carbazole donor.

Soni and coworkers synthesized carbazole based dye (**D17**; Chart 1.10) [81]. The synthetic procedure of the dye is displayed in Scheme 1.7 and it starts with reduction of 9-*p*-tolyl-9*H*-carbazole-3-carbaldehyde with sodium borohydride to leave alcohol derivative which subsequently converted to wittig salt by treating with triphenylphosphinehydrobromide. This wittig salt was condensed with terephthalaldehyde in presence of sodium ethoxide produced (*E*)-4-(2-(9-*p*-tolyl-9*H*-carbazol-3-yl)vinyl)benzaldehyde. This aldehyde was converted into corresponding cyanoacrylic acid by treating with cyanoacetic acid via Knoevenagel condensation.

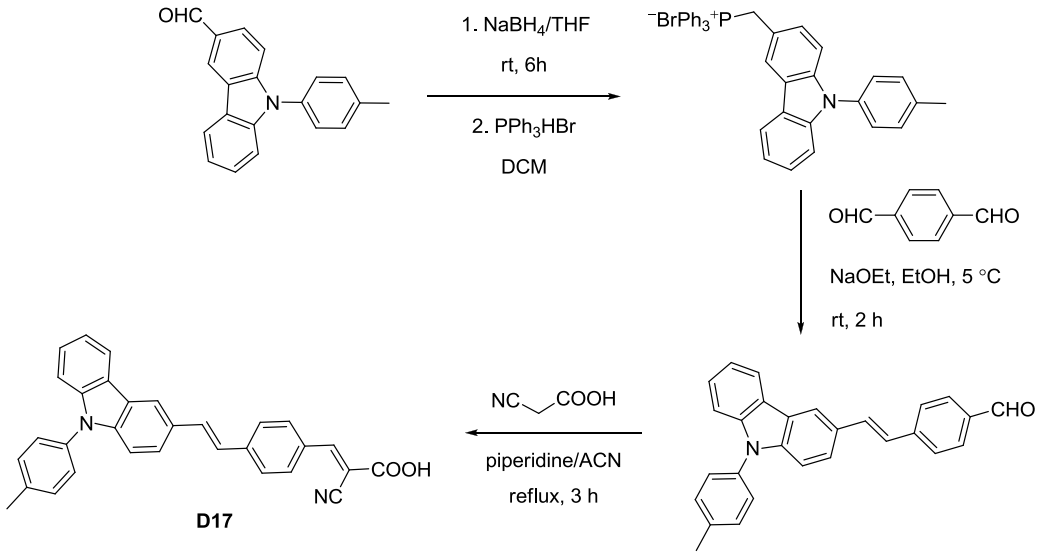

D17

Scheme 1.7 Synthetic scheme of dye **D17**.

The dye **D17** was applied for DSSC application as sensitizers for one dimensional ZnO nanowire (NW) and ZnO nano-particles (NP) semiconductors and achieved power conversion efficiency of 3.6% and 5.7%, respectively, with cobalt tris(2,2′-bipyridyl) redox electrolyte. The enhanced rate of photogenerated electron injection and transport through the one dimensional ZnO NWs resulted in a maximum IPCE of ~62% when compared to ZnO NPs produced only ~48%. While the identical device with iodine redox electrolyte exhibited power conversion efficiency of 4.7%. The significant quenching of the photoluminance and excitation lifetime decay of sensitizer when anchored on ZnO nanowires and nanoparticles is evident from the interactions of sensitizer and ZnO semiconductor.

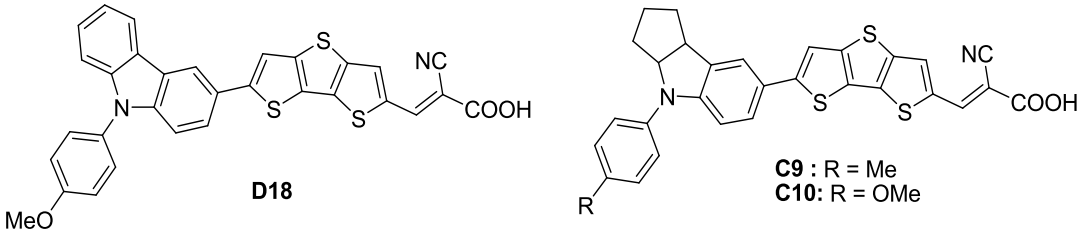

Chart 1.11 Carbazole and indoline dyes containing dithienothiophene linkers.

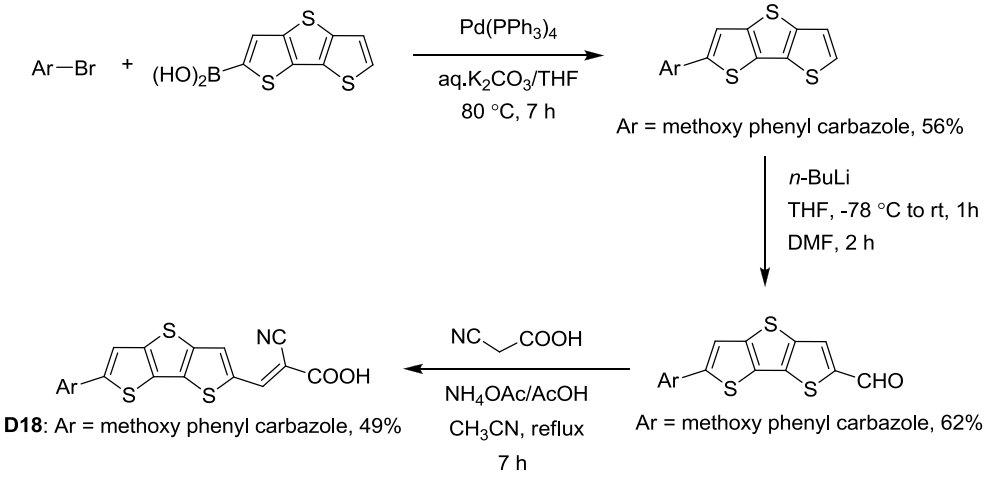

Scheme 1.8 Synthetic scheme of dye **D18**.

Yamamoto and co-workers reported a set of dyes (Chart 1.11) with carbazole or indoline derivative as donor and cyanoacrylic acid acceptor connected by dithienothiophene linker [82]. The synthesis of the dyes showed in Scheme 1.8. Suzuki coupling of bromo derivatives of carbazole with boronic acid derivative of dithienothiophene followed by lithiation with *n*-Buli

and addition of DMF led to aldehyde derivatives. The carbazole aldehydes were converted to respective dyes by Knoevenagel condensation with cyanoacetic acid. On contradiction to the previously mentioned observations, the carbazole-based dyes showed relatively less efficiency in DSSC (Table 1.2). The band gap of the carbazole dyes are high when compared to the related indoline dyes (Chart 1.11) which led to poor absorption in the longer wavelength region.

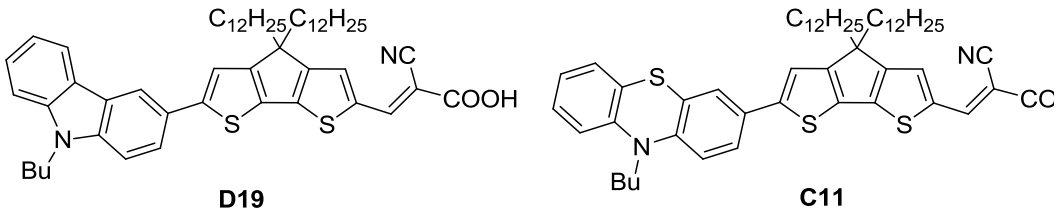

Chart 1.12 Carbazole and phenothiazine dyes containing cyclopenta[1,2-*b*:5,4-*b*′]dithiophene linker.

Grätzel and co-workers reported dyes containing carbazole/phenothiazine donors (**D19** and **C11**; Chart 1.12) [83]. The synthesis of the dyes is showed in Scheme 1.9. Suzuki coupling of bromo derivative of cyclopenta[1,2-*b*:5,4-*b*′]dithiophene with carbazole boronic acid afford aldehyde derivative, which converted to target dye by Knoevenagel condensation with cyanoacetic acid. A dye, **D19** having 4,4-didodecyl-4*H*-cyclopenta[1,2-*b*:5,4-*b*′]dithiophene as a linker displayed longer wavelength absorption peaking at 532 nm with a very high molar extinction coefficient (57500 M^{-1} cm^{-1}). The carbazole dye, **D19** exhibited higher efficiency (7.50%) than similar dye (7.00%) containing phenothiazine as a donor (**C11**). This discrepancy is attributed to the higher molar absorption coefficient realized for the former (**D19**) which led to larger photocurrent. When compared with **D18**, the performance of **D19** is better due to the presence of high lying HOMO in the later which facilitates the dye regeneration.

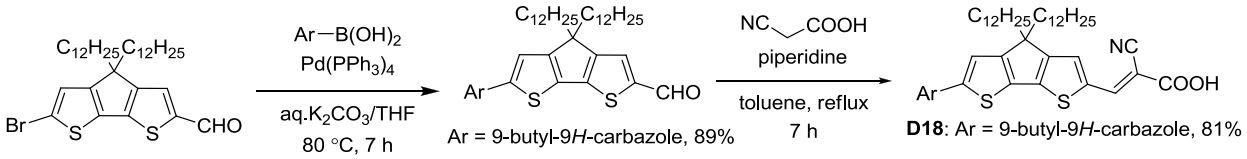

Scheme 1.9 Synthetic scheme of dyes **D19**.

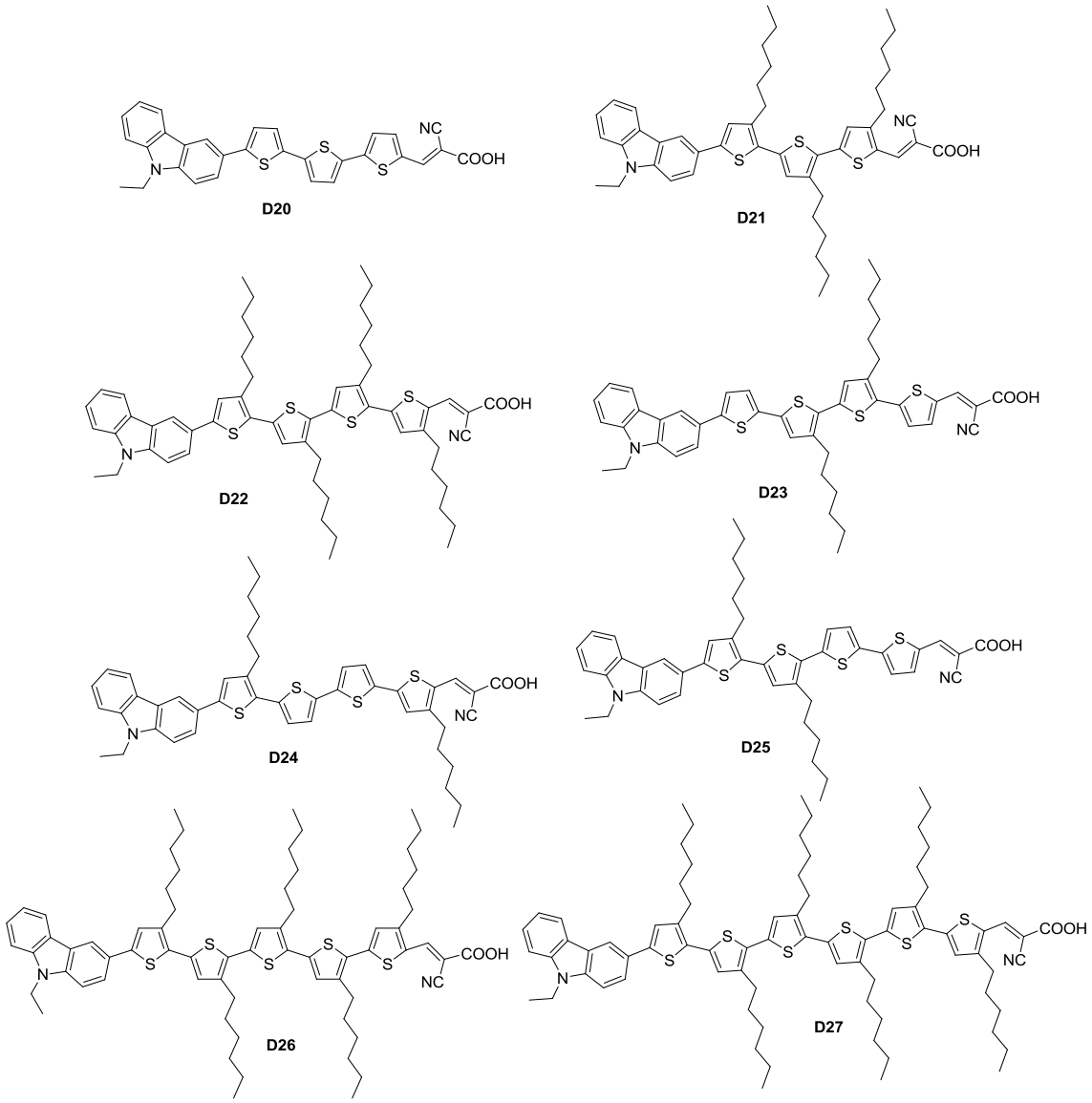

Chart 1.13 Carbazole-based dyes possessing oligothiophene in the conjugation pathway.

Role of alkyl chains present in the conjugation pathway in retarding the recombination of the injected electrons in the CB of TiO_2 with the electrolyte has been investigated by Hara and co-workers by designing some interesting organic dyes (**D20-D22**; Chart 1.13) [9]. They have synthesized organic dyes featuring carbazole donor, terthiophene to hexithiophene segments in the conjugation and cyanoacrylic acid acceptor. The synthetic scheme of the dyes is showed in Scheme 1.10. It starts with Sandmeyer reaction [84] of 9-ethyl-9*H*-carbazol-3-amine gave 9-ethyl-3-iodo-9*H*-carbazole and followed by Kumada coupling [85] with 2-bromo-3-hexylthiophene gave thiophenecarbazole. Then bromination of thienocarbazole with NBS in THF gave mono bromo derivative of thiophenecarbazole and then it coupled with 2-(3-

hexylthiophen-2-yl)-5,5-dimethyl-1,3,2-dioxaborinane followed by Suzuki coupling gave oligothiophenecarbazole. Then Vilsmeier-Haack reaction of oligothiophenecarbazole derivatives with $POCl_3$/DMF gave the corresponding aldehyde derivatives depending on number of thiophene units. Knoevenagel condensation of aldehyde derivatives with cyanoacetic acid gave target dyes (**D20**-**D22**) and synthesis of the dyes **D23**-**D27** was similar to the Scheme 1.10.

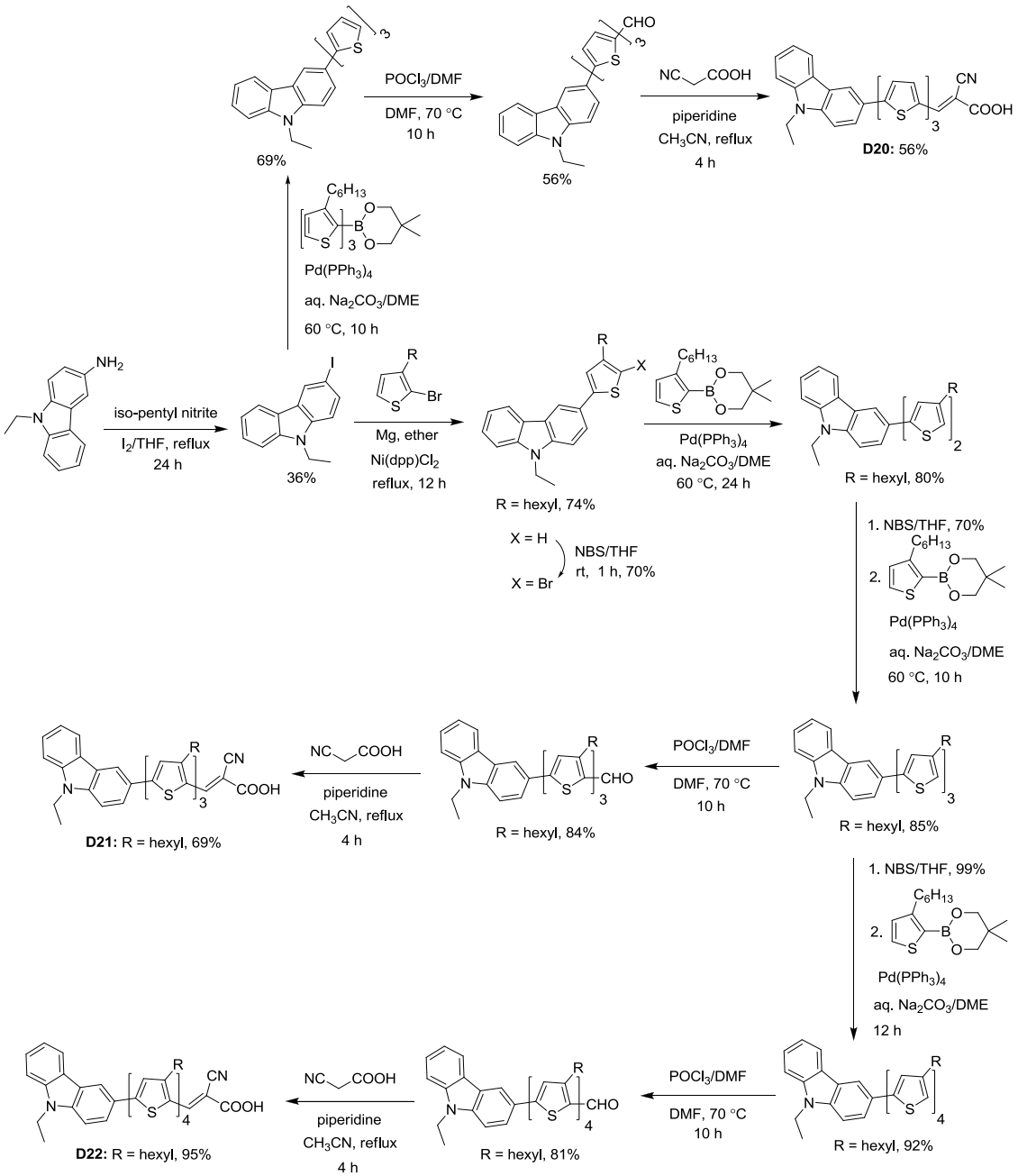

Scheme 1.10 Synthetic scheme of the dyes **D20**-**D22**.

It was found that incorporation of hexyl chains on the thiophene suppress the aggregation and stops from I_3^- reaching TiO_2 layer. This led to an enhancement in the electron lifetime and charge collection efficiency. For instance, the V_{OC} realized for **D21** is significantly larger than that observed for the device based on **D20**. The dye containing four 3-hexylthiophene units (**D22**) exhibited higher efficiency (6.3%) in the series. Studies on interfacial electron transfer kinetics revealed that the larger molecular size of dye and two adsorption sites (wider distribution of charges which control I_3^- concentration at TiO_2 layer and packing density of dyes to block the approaches of I_3^- are essential) lowered the reorganizing energy of dye [86]. The device based on **D22** while using ionic liquid electrolytes showed good long term stability under visible light irradiation at 60 °C [87].

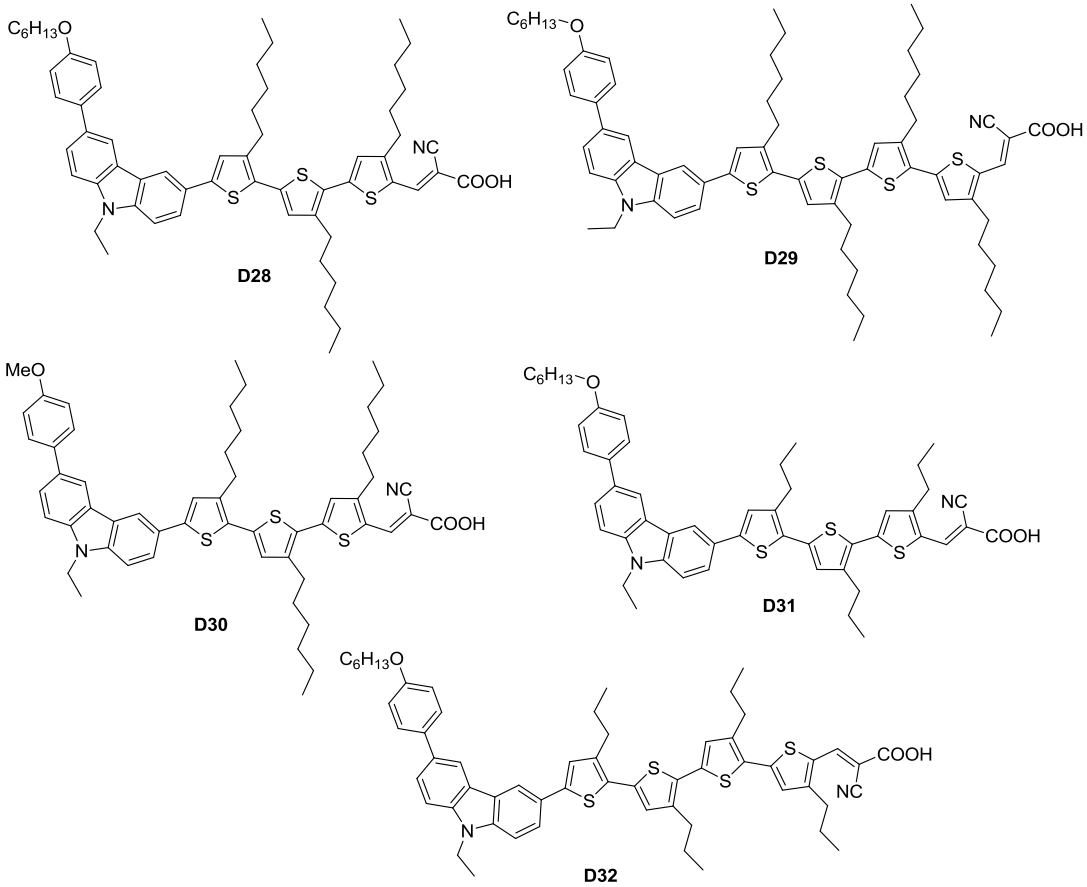

Chart 1.14 Organic dyes designed to unravel the importance of alkyl chain length.

Later, they observed that the number of thiophene units in the oligothiophene conjugation pathway and the position of the hexyl functionalization influence the dye loading and aggregate

thickness [54]. The dyes **D23**–**D25** (Chart 1.13) possess two hexyl chains at different positions and forms thick 3D aggregates on TiO_2 film while **D21** and **D22** which contain three and four hexyl chains forms 2D dense packing. This reveals that dye loading and thickness of aggregates can be easily optimized by appropriate alkyl group introduction. Interestingly, the dyes **D26** and **D27** which possess five and six hexyl substituted thiophenes produced inferior efficiency in the devices than the dyes **D21** and **D22**.

Mori and co-workers found that alkyl chains present on the thiophene unit and the nature of alkoxyphenyl fragment attached to the carbazole nucleus via C3 position (**D28** and **D29;** Chart 1.14) significantly altered the V_{OC} of the devices [88]. The dyes were synthesized similar to the synthetic Scheme1.10 and it start with 3-bromo-9-ethyl-6-(4-(hexyloxy)phenyl)-9*H*-carbazole. Incorporation of alkoxy groups improved the sphericity of the dyes, facilitated the wider distribution of charged atoms and provided good packing at the surface of TiO_2 were efficient to block I_3^- ions from approaching the dyes. This minimized the dark current and increased the V_{OC} significantly. Thus the dyes analogous to **D21** and **D22** but possessing additional hexyloxyphenyl group on carbazole, **D28** and **D29** contributed to the increase in electron life time and V_{OC} (Table 1.2) due to the negatively charged oxygen atoms repelling the approach of I_3^- ions. Supporting this hypothesis, reducing the alkyl chains to propyl on thiophene and methyl in alkoxyphenyl unit produced a counter effect. Due to the optimized structural components in **D28**, it exhibited very high efficiency (8.10%) in DSSC.

Mori and co-workers further improved the efficiency of the devices based on dyes **D21**–**D22** and **D30**–**D32** (Chart 1.14) by using cobalt complex as redox couple [89]. The synthesis of dyes is similar to the procedure described in Scheme1.10. When cobalt complexes were used as redox partner in DSSC a significant enhancement in V_{OC} was observed attributable to the retardation of recombination of electrons. Since the oxidation potential of cobalt redox couple is lower than that of iodide couple, the gap between the CB of TiO_2 and oxidation potential of cobalt complex increases which results in higher V_{OC}. On using cobalt complex, the V_{OC} of **D21** and **D22** increased (720 mV to 790 mV) significantly than those observed while using iodide couple. Among the dyes, **D32** showed promising efficiency (7.90%).

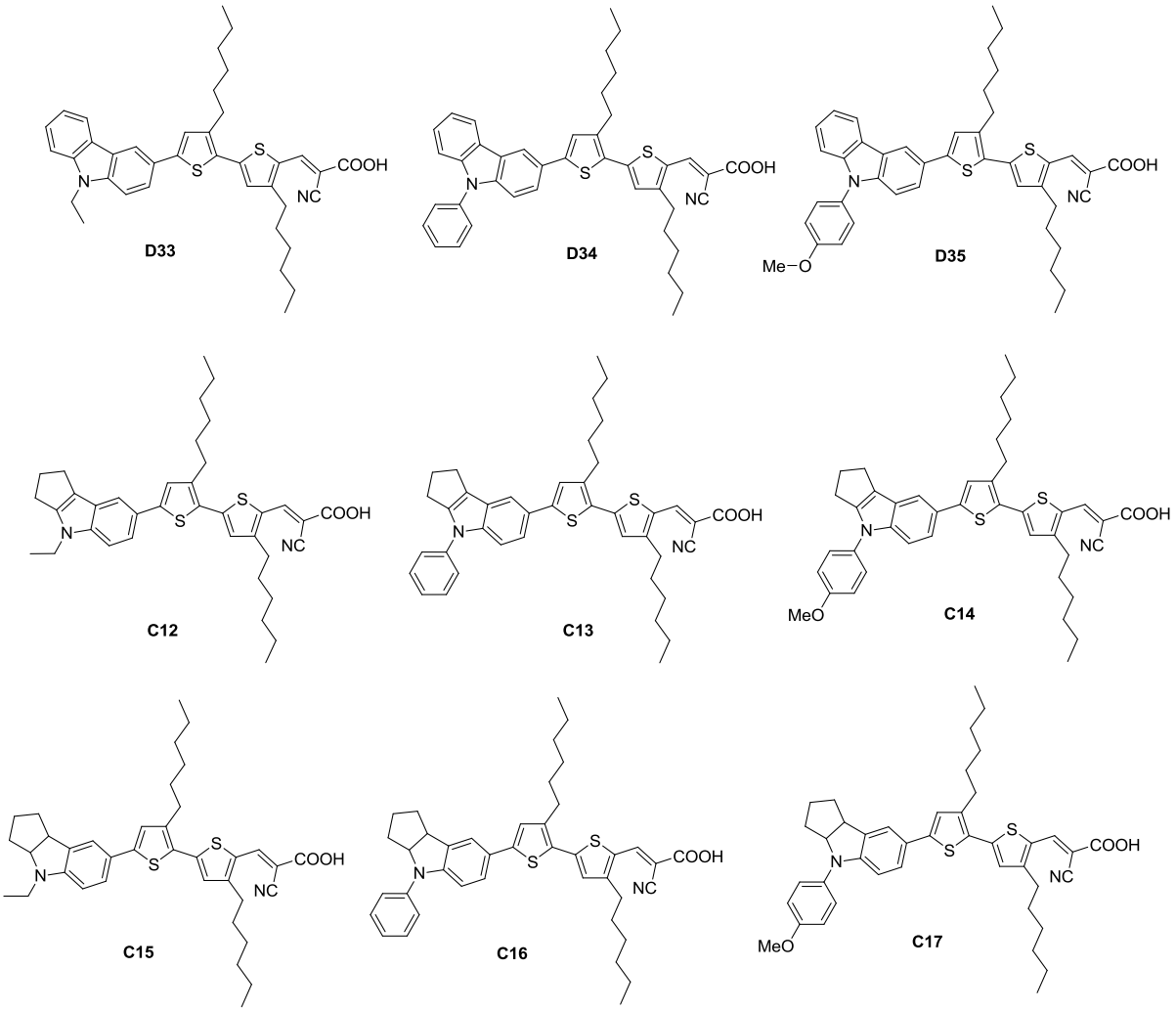

Chart 1.15 Dyes containing carbazole donor and showing difference in *N*-substitution.

Nature of the *N*9-substituent on carbazole has been found to significantly influence the optical and dye loading efficacy of the dyes. Koumura and co-workers prepared three dyes (Chart 1.15) with different *N*-substituents such as ethyl (**D33**), phenyl (**D34**), *p*-methoxyphenyl (**D35**) groups [90]. The synthesis of dyes is similar to the procedure described in Scheme1.10. The dye **D33** possessed higher molar extinction coefficient among the dyes attributable to the phenyl group present on nitrogen. This combined with the superior dye loading characteristics led to larger photocurrent in the DSSC of **D34**. Interestingly, the analogous dyes derived from indole and indoline showed inferior performance when compared to the carbazole dyes due to the less dye loading and poor blocking effect which results in shorter electron lifetimes. The carbazole-based dyes have a special property of surface coverage on TiO_2 electrode which helps in improving the dye loading.

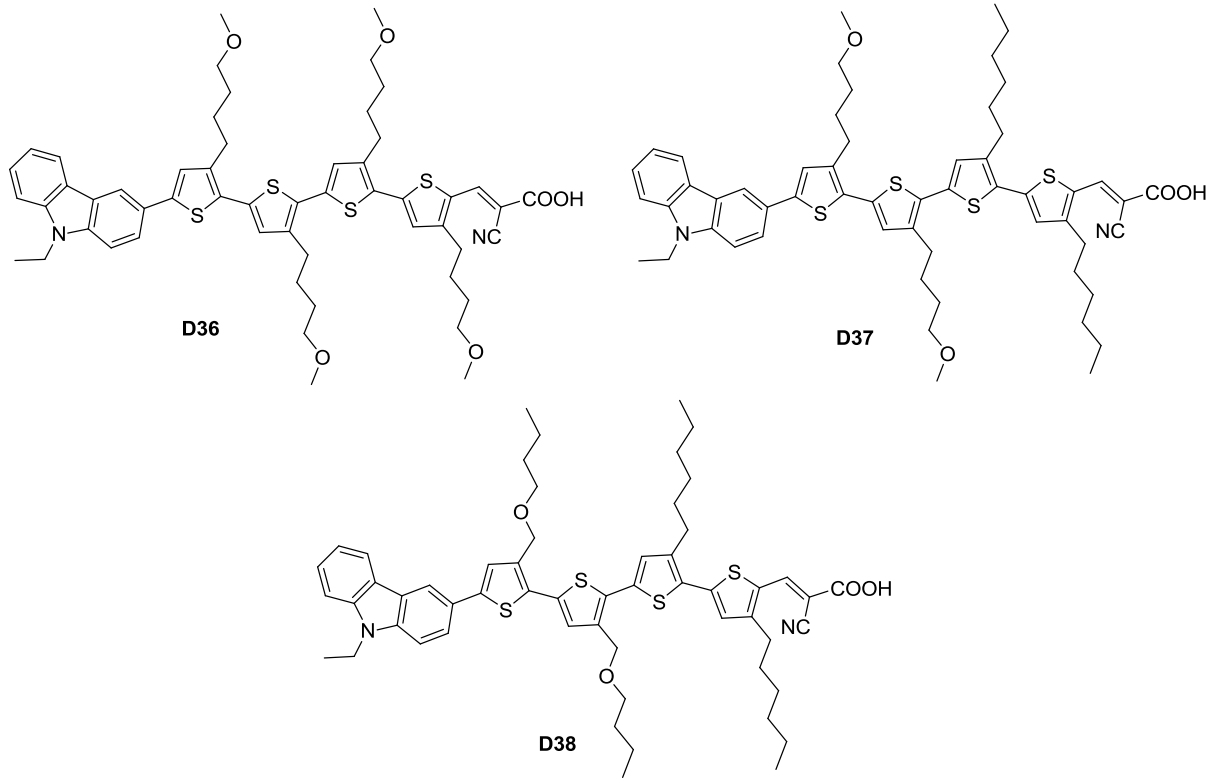

Chart 1.16 Dyes showing influence of ether linkage on carbazole.

Mori and co-workers examined the effect of negative charges on the dye molecules on electron lifetime and performance of dyes by adding ether side groups to the oligothiophene units [91]. The dyes **D36**–**D38** (Chart 1.16) are modified dyes from the parent dye **D22** where alkyl chains contain extra ether groups. The synthesis of dyes is similar to the procedure described in Scheme1.10 and it involves alkoxy thiophene units. The inferior performance of these dyes (**D36**–**D38**) compared to parent dye **D22** due to low V_{OC} (710-770 mV) which originated from the increased concentration of I_3^- ions near to the surface of TiO_2. Also, facilitated by the ether groups position and number of oxygen atoms in dye molecule control the distance between the Li^+ and I_3^- ions on TiO_2 surface. The dye **D37** containing two oxygen atoms showed higher performance when compared to **D36** which contain four oxygen atoms. This clearly proved that partial charges of oxygen atoms on dye molecules decreased the electron lifetime and led to inferior performance.

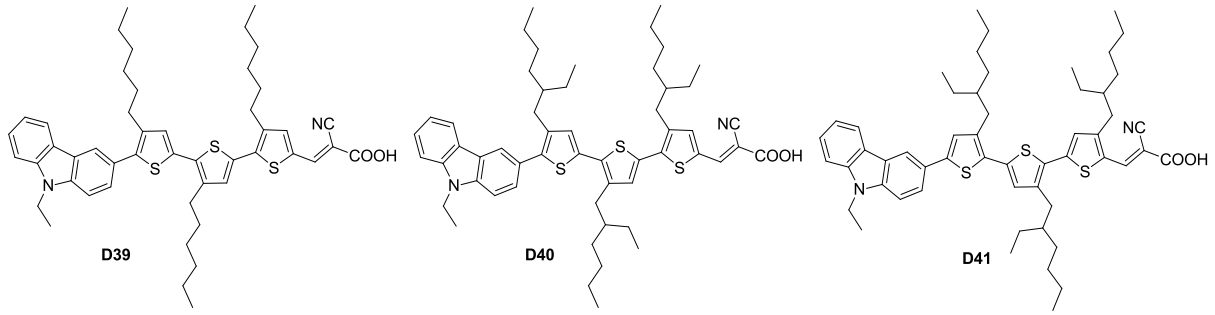

Chart 1.17 Dyes containing various alkyl at different positions on oligothiophene.

Wang and co-workers reveal the effect of branched alkyl chain, position of alkyl chain by introducing *n*-hexyl and 2-ethylhexyl chains at different positions on oligothiophene [92]. The dye **D39** was the isomer of **D21** while **D40** and **D41** (Chart 1.17) were substituted by branched 2-ethyl hexyl chain. The synthesis of dyes is similar to the procedure described in Scheme1.10 and it involves various alkyl substituted thiophene units. The alkyl groups substituted near to the aromatic donor moiety render more steric hindrance; it causes remarkable twist in the molecular skeleton and decreases the donor acceptor interactions. However reduction of intermolecular interactions helped to increase V_{OC}. In contrast, substitution of alkyl groups near to the acceptor makes more planar π-conjugation and it increases the donor acceptor interactions which results in bathochromic shift. The dye **D41** showed higher efficiency in DSSC when compared to **D40** (7.17%). The dye **D41** showed an efficiency of 7.10% and excellent stability over 1000 h for quasi solid state DSSC under AM 1.5 M conditions and it remained 98% of the initial value at the end of 1000 h light soaking.

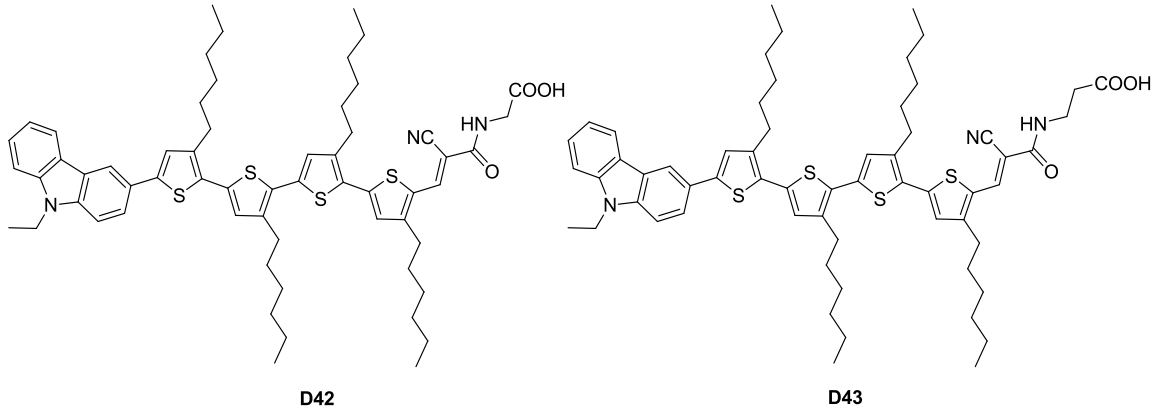

Chart 1.18 Structures of the dyes (**D42** and **D43**) containing cyanoacrylamide acceptor.

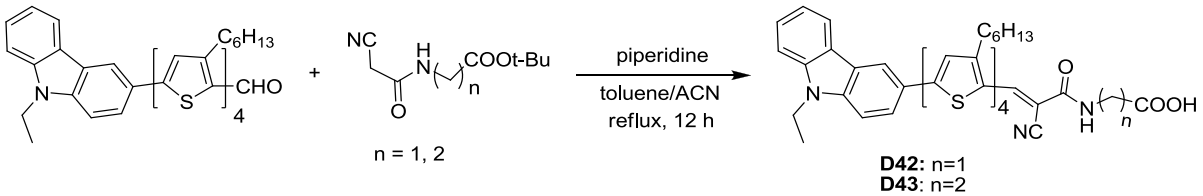

Scheme 1.11 Synthetic scheme of the dyes **D42** and **D43**.

Mori and co-workers examined the influence of non-conjugated bridge between the donor framework and anchoring group by applying it to a previously successful dye, **D22** [93]. Thus the newly synthesized dyes, **D42** and **D43** (Chart 1.18) contain glycine and *β*-alanine as anchoring group. The synthetic scheme of the dyes is outlined in Scheme 1.11. The condensation of carbazole oligothiophene aldehydes (shown in Scheme 1.10) with *N*-(cyanoacetyl)glycine or *N*-(cyanoacetyl)alanine in acetonitrile and toluene in the presence of piperidine gave dyes (**D42** and **D43**). Photocurrent density of **D42** and **D43** is much lesser than the original dye **D21**. The increase in the length of non-conjugating segment decreases the short-circuit current due to low electron injection efficiency (J_{SC} of **D42** is 8.7 mA cm^{-2} and of **D43** is 7.30 mA cm^{-2}). Despite low J_{SC} observed for the dyes, the V_{OC} of **D42** (750 mV) is slightly larger due to less dispersion force with similar blocking effect of dye on comparison with **D22** (690 mV) and **D43** (740 mV) under same conditions.

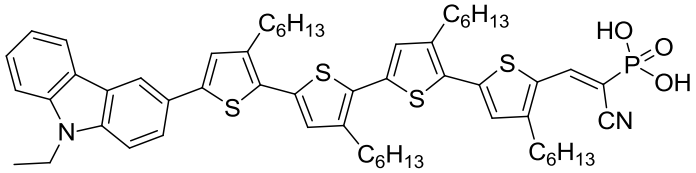

Chart 1.19 Structure of the carbazole dye with phosphonic acid anchoring group.

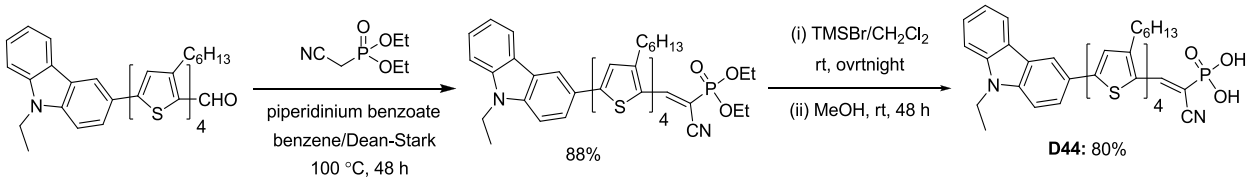

Scheme 1.12 Synthetic scheme of the dye **D44**.

Koumura and co-workers [94] introduced new anchoring unit such as phosphonic acid (**D44**; Chart 1.19) instead of cyanoacrylic acid due to its more stable bonding to a TiO_2 surface because

of its tridentate binding capability. The synthesis of the dyes is displayed in Scheme 1.12. Knoevenagel condensation of 5'''-(9-ethyl-9*H*-carbazol-3-yl)-3',3'',3''',4-tetra-n-hexyl-[2,2',5',2'',5'',2''']quaterthiophenyl-5-carbaldehyde with diethyl cyanomethylphosphonate in the presence of piperidinium benzoate using a Dean-Stark apparatus offered diethyl(1-cyano-2-(5'''-(9-ethyl-9*H*-carbazol-3-yl)-3',3'',3''',4-tetrahexyl-[2,2',5',2'',5'',2'''-quaterthiophen]-5-yl)vinyl)phosphonate. Finally, it was treated with bromotrimethylsilane followed by methanol to produce target dye **D44**. But the dye **D44** with the phosphonic acid anchor unit showed blue-shifted absorption spectra than cyanoacrylic acid dye because of the lower electron-accepting ability of the phosphonic acid than the carboxylic acid. The lower absorption of the dye **D44** led to poor light harvesting and inferior J_{SC} values which resulted in inferior efficiency of the device. After 504 h, the device based on dye **D44** limited the loss of PCE to within 6%, but the device based on the dye **D22** exhibited a loss of 27% in PCE. The difference is mainly due to the desorption of **D22** is three times larger than the dye **D44** which clearly indicates the strong adsorption of phosphonic acid unit with TiO_2 surface, but unfortunately it showed inferior power conversion compared to its congener dye.

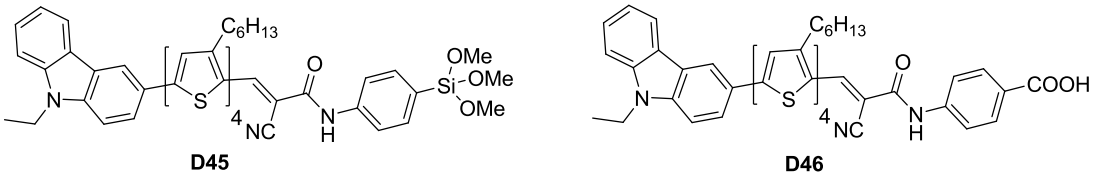

Chart 1.20 Structures of the dyes with anchoring unit of organosilyl and carboxylic acid.

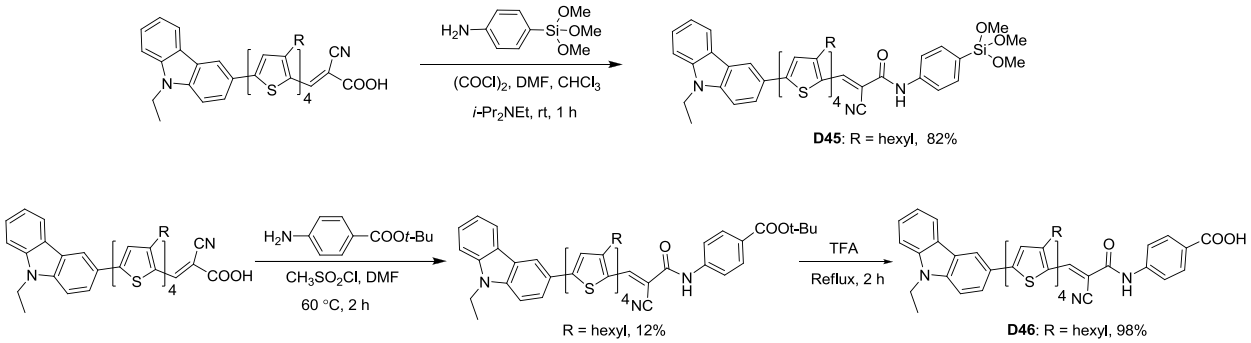

Scheme 1.13 Synthetic scheme of the dyes **D43** and **D44**.

Yano and coworkers designed alkoxysilyl-based anchoring units and modified **D22** dye with this anchoring unit to obtain **D45** and **D46** (Chart 1.20) [95]. The synthesis of the dyes is

outlined in Scheme 1.13. Reaction of **D22** with oxalyl chloride in chloroform and *N,N′*-dimethylformamide followed by the addition of ethyldiisopropylamine and 4-(trimethoxysilyl)aniline gave the dye **D45**. Reaction of **D22** with mesyl chloride and *tert*-butyl 4-aminobenzoate gave the ester and then it was converted to carboxylic acid (**D46**) by addition of trifluoroacetic acid under reflux conditions. The modified dyes showed high photovoltage in DSSC upto 1 V with cobalt (III/II) redox electrolyte and achieved the highest efficiency of 12%. This newly invented organosilyl anchor unit might be a good choice to increase the efficiency of the promising dyes.

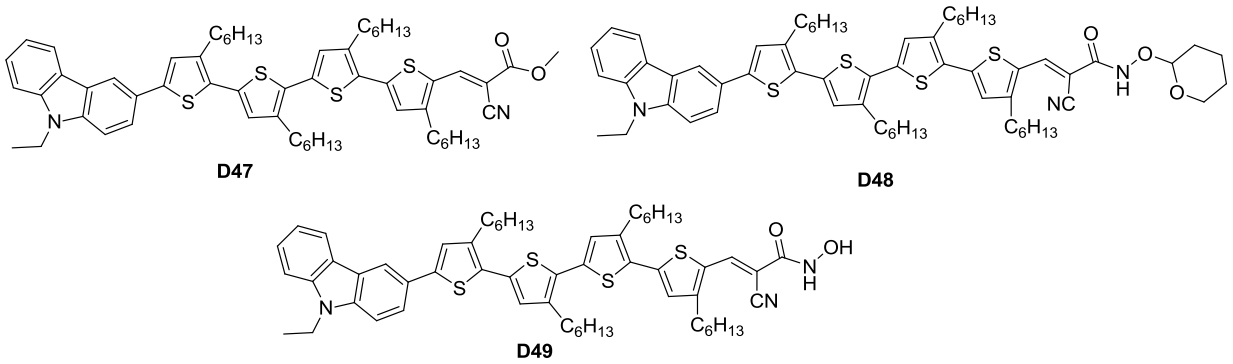

Chart 1.21 Structures of the dyes with bithiazole linker contain different donors.

Crabtree and co-workers [96] modify conventional cyanoacrylic acid moiety of the **D22** organic dye with a highly water stable hydroxamic acid anchoring group and employed for DSSC and extensively studied the optical and photovoltaic properties. The device made with **D49** showed a higher efficiency of 6.9% than its parent **D22** dye (η = 6.6%). The enhanced recombination resistance of the injected electrons improved the device efficiency. Desorption studies of these water soluble dyes demonstrated that the hydroxamate anchoring group led to essentially no loss in device efficiency over the course of the eight days and the commercial dye **D22** decline the efficiency up to 50% of the initial value. The synthetic scheme of the dyes is shown in Scheme 1.14. The commercial dye **D22** is treated with O-(tetrahydro-2*H*-pyran-2-yl)hydroxylamine in presence of *N,N,N′,N′*-tetramethyl-O-(1*H*-benzotriazol-1-yl)uronium hexafluorophosphate produced **D48** dye. The dye **D48** dissolved in mixture of tetrahydrofuran (THF)/water/acetic acid (*v/v*; 7:2:1) and heated at 60 °C resulted **D49**. The dye **D47** prepared from alkylation of **D22** with iodomethane in presence of K_2CO_3 as base.

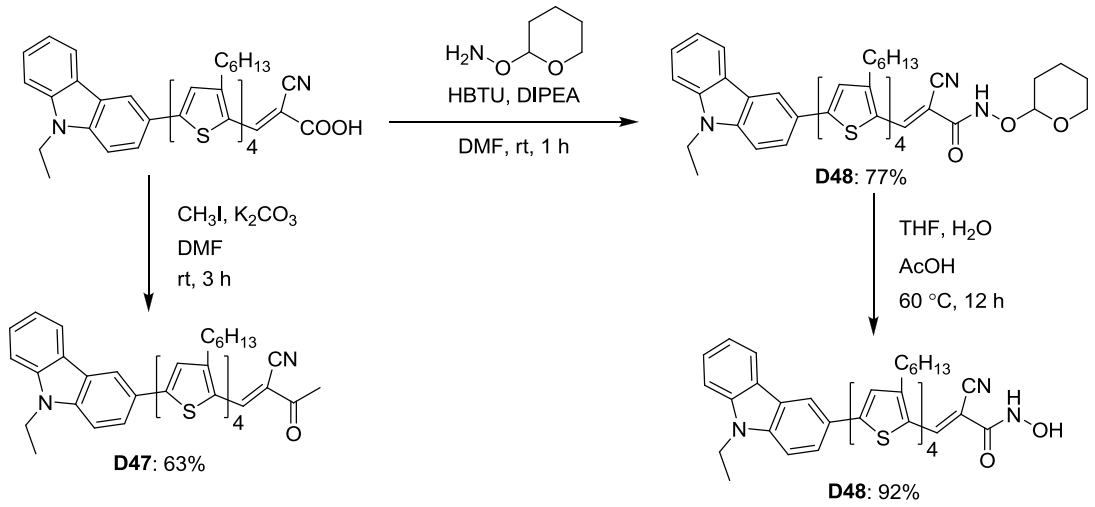

Scheme 1.14 Synthetic scheme of the dyes **D47-D48**.

Koumura and co-workers [97] synthesized crown ether-substituted carbazole dye (**D50** shown in Chart 1.22) to examine the partial charge effect on the donor moiety. Incorporation of crown ether on carbazole core shows its impact on the absorption spectra and led to red shifted absorption. The photovoltaic performance of **D50** is 4.80 % which is comparable to **D41** of efficiency (4.9%) under same conditions. While the electron lifetime of dye **D50** in the presence of a high Li^+ concentration in the electrolyte was lower than **D41** because of the partial charge effect and it is due to the Li^+ localized near the crown ethers attracted surplus I_3^- by electrostatic interactions. The aging behavior in the DSSCs after 24 h reflected in the negative shifts of their E_{CB} levels and blue shifts in their absorption spectra caused by the cancellation of the positive charges of Li^+ on the TiO_2 surface by the approach of I^-/I_3^- ions to that surface. However, the concept of crown ether is useful to design ion concentration-controllable TiO_2/dye/electrolyte interfaces for efficient and stable DSSCs.

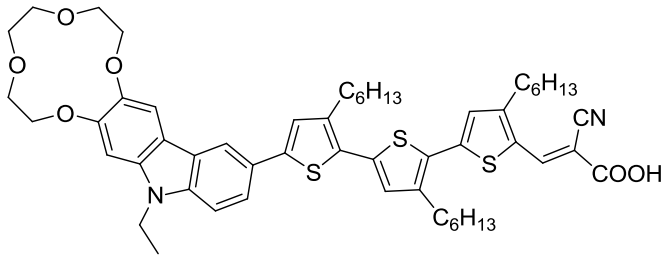

Chart 1.22 Structure of the crown ether-substituted carbazole dye.

The synthetic protocol of the dye **D50** is outlined in Scheme 1.15. It starts with bromination of benzo-12-crown-4-ether with NBS in CCl_4 and followed by nitration gave 2-nitro-3-bromo-benzo-12-crown-4-ether. Then it treated with phenylboronic acid *via* Suzuki coupling afforded 2-nitro-3-phenyl-benzo-12-crown-4-ether which further undergo reductive cyclization with triethyl phosphate gave 2,3-12-crown-4-ether-9*H*-carbazole. It alkylated with ethylbromide in presence of phase transfer catalyst and followed by bromination with NBS in THF produced 6-bromo-9-ethyl-9*H*-carbazole-2,3-12-crown-4-ether. It treated with 2-(4-hexylthiophene) boronic acid neopentyl ester via Suzuki coupling and followed by bromination with NBS in a series to get 9-ethyl-6-(3,4',4"-trihexyl-[2,2',5',2"]terthiophen-5-yl)-9*H*-carbazole-2,3-12-crown-4-ether. It was converted to aldehyde derivative by Vilsmeier-Haack reaction. Finally, dye **D50** obtained by Knoevengel condensation of aldehyde derivative with cyanoacetic acid.

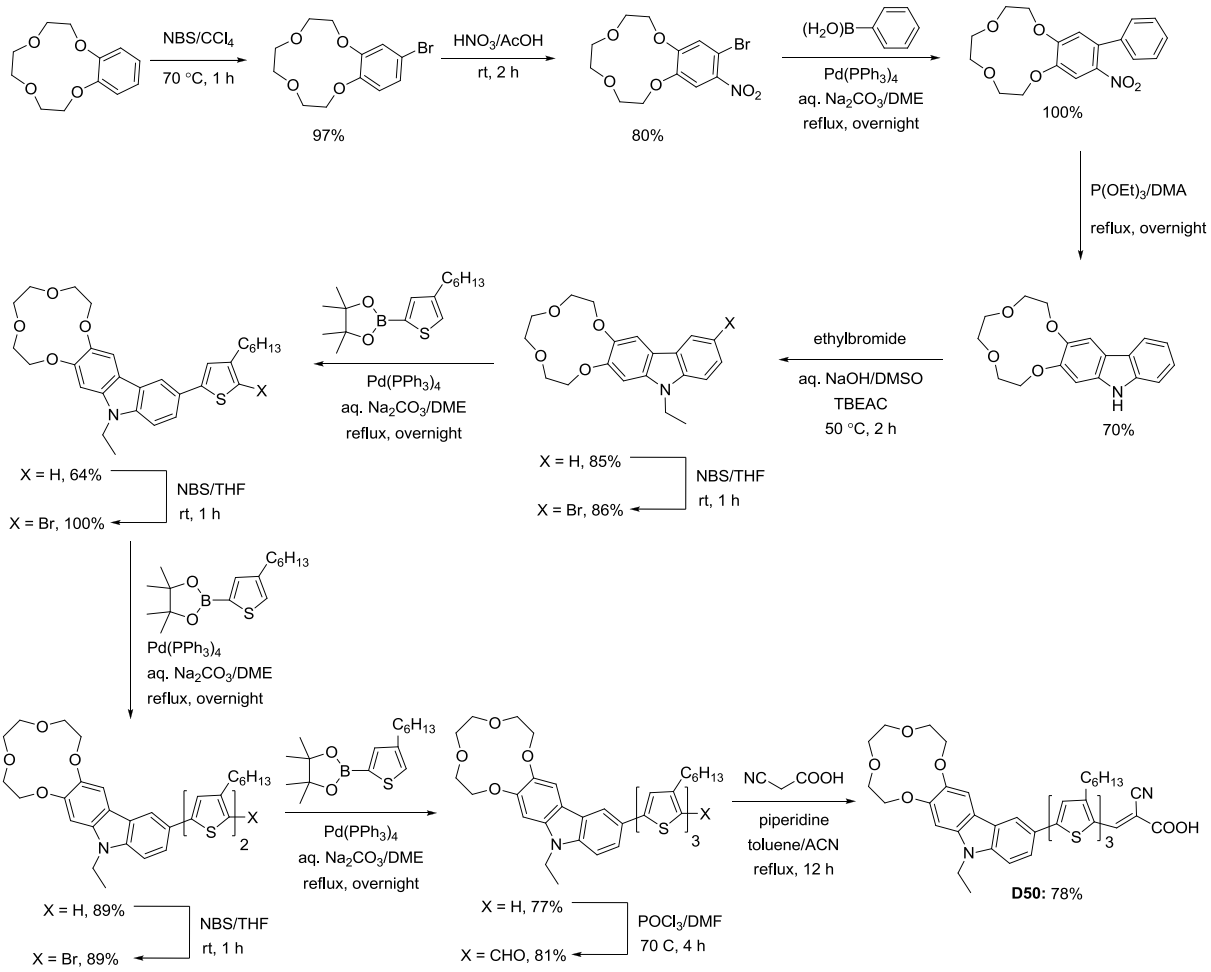

Scheme 1.15 Synthetic scheme of the dye **D50**.

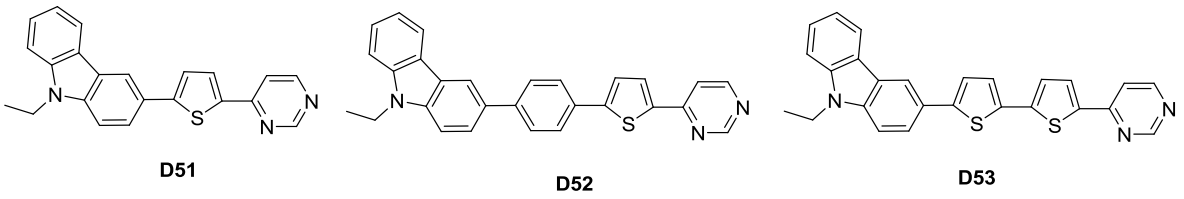

Chart 1.23 Structures of the dyes with pyrimidine acceptor/anchoring unit.

Verbitskiy and co-workers [98] synthesized a set of carbazole based dyes with pyrimidine as acceptor/anchoring unit (**D51-D53**; Chart 1.23). The synthesis of the dyes is displayed in Scheme 1.16 by using microwave mediated Suzuki coupling reaction of bromo-aromatic compounds resulted in target dyes (**D51-D53**). All dyes are displaying the absorption maxima more than 400 nm with high molar extinction coefficients. The ground and excited state potential of the dyes are suitable for photo injection of electron from excited of the dye to CB of the TiO_2 and favorable dye regeneration from redox mediator. These results suggested that these dyes are suitable for DSSC application as sensitizers.

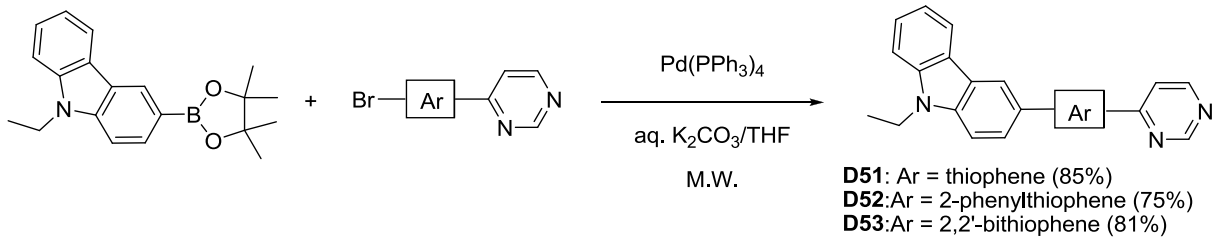

Scheme 1.16 Synthetic scheme of the dyes **D51-D53**.

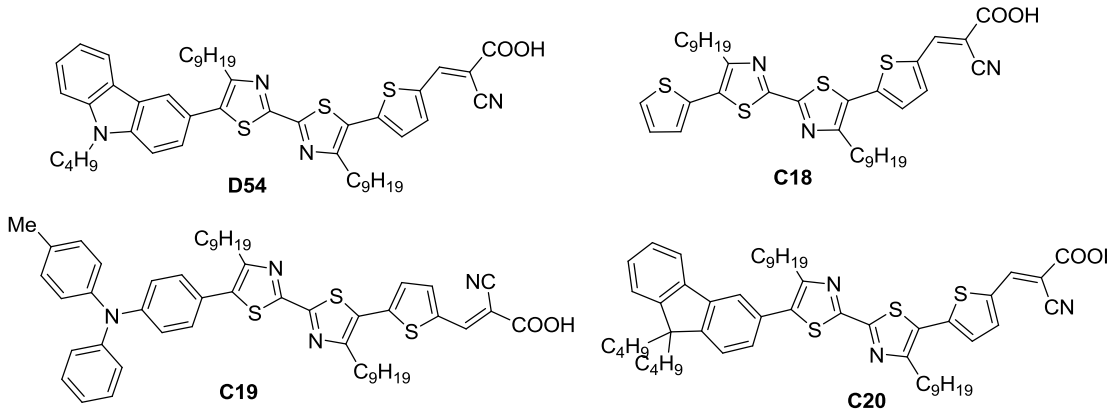

Chart 1.24 Structures of the carbazole dye with bithiazole linker containing different donors and related dyes with different donor units.

Wong and co-workers synthesized a set of dyes based on bithiazole linker containing different donors such as thiophene (**C18**), fluorene (**C19**), triaylamine (**C20**) and carbazole (**D54**) (Chart 1.24) [99]. The synthesis of the dyes is displayed below (shown in Scheme 1.17). The key intermediate 4,4'-dinonyl-2,2'-bithiazole was obtained by bromination of 2-undecanone with bromine to form 1-bromo-undecan-2-one, which undergoes cycloaddition with dithiooxamide by the Hantzsch thiazole synthesis [100]. Subsequently, this compound was monobrominated by *N*-bromosuccinimide (NBS) to give 5-bromo-4,4'-dinonyl-2,2'-bithiazole. Then it is treated with 9-butyl-9*H*-carbazol-3-ylboronic acid by Suzuki coupling to get corresponding carbazole aldehyde derivative. Then this aldehyde was converted to dye (**D54**) via Knoevenagel condensation with cyanoacetic acid. The synthesis of the dyes (**C18-C20**) is prepared according to the Scheme 1.17 by using appropriate boronic acid derivatives. All the dyes displayed strong charge transfer bands due to bithiazole linker but the dye **D54** possessed highest molar extinction coefficients than the other dyes (**C18**–**C20**). **D54** exhibited superior performance of 4.65% with J_{SC} of 9.61 mA cm^{-2}, V_{OC} of 700 mV and *ff* of 0.70 than compared to other dyes (**C18**–**C20**).

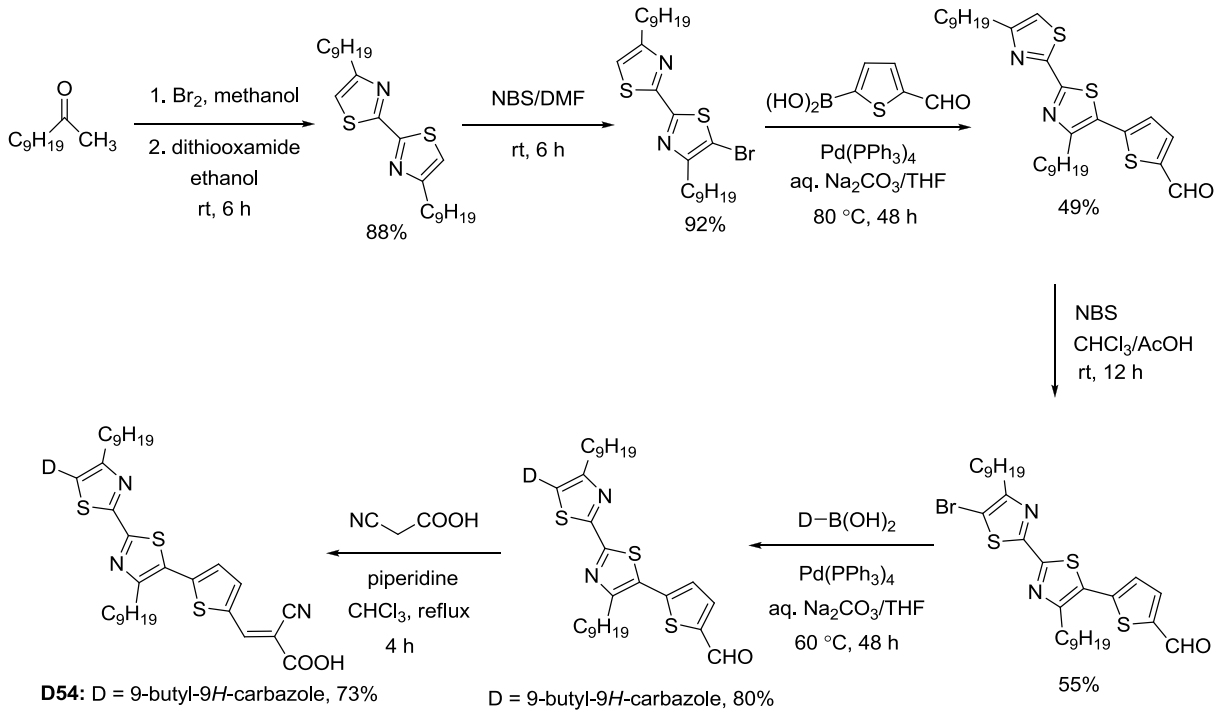

Scheme 1.17 Synthetic scheme of the dye **D54**.

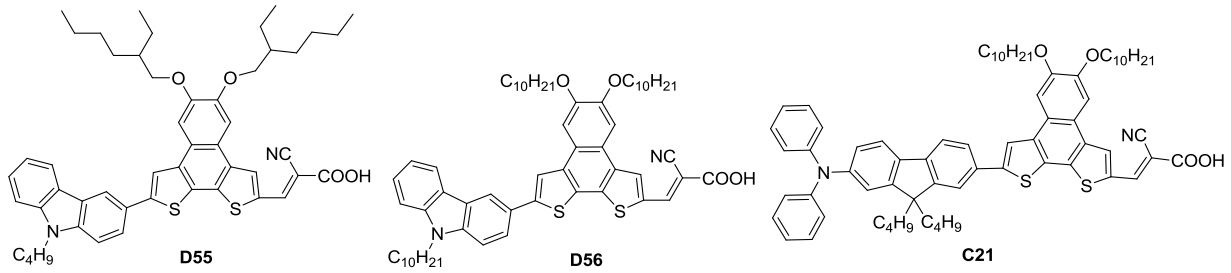

Chart 1.25 Structures of the dyes with naphtho[2,1-*b*:3,4-*b*']dithiophene linker.

Zhu and co-workers introduced first time used naphtho[2,1-*b*:3,4-*b*']dithiophene as linker for the construction of dyes suitable for DSSC along with carbazole or fluorene containing triarylamine as donor [101]. The synthesis of the dyes is outlined in Scheme 1.18. Lithiation of 5,6-bis(ethylhexyloxy)naphtho[2,1-*b*:3,4-*b*′]-dithiophene, with *n*-BuLi followed by reaction with morpholine-4-carbaldehyde afforded mono-carbaldehyde, which subsequently underwent iodination with N-iodosuccinimide (NIS) to give the iodo-product. Palladium catalyzed Suzuki cross-coupling of iodo naphtho[2,1-*b*:3,4-*b*′]-dithiophene with carbazole boronic acid gave carbazole containing aldehyde. Condensation of aldehyde with cyanoacetic acid using Knoevenagel protocol gave the dye **D55**. The synthesis of **D56** and **C21** are similar to the Scheme 1.18.

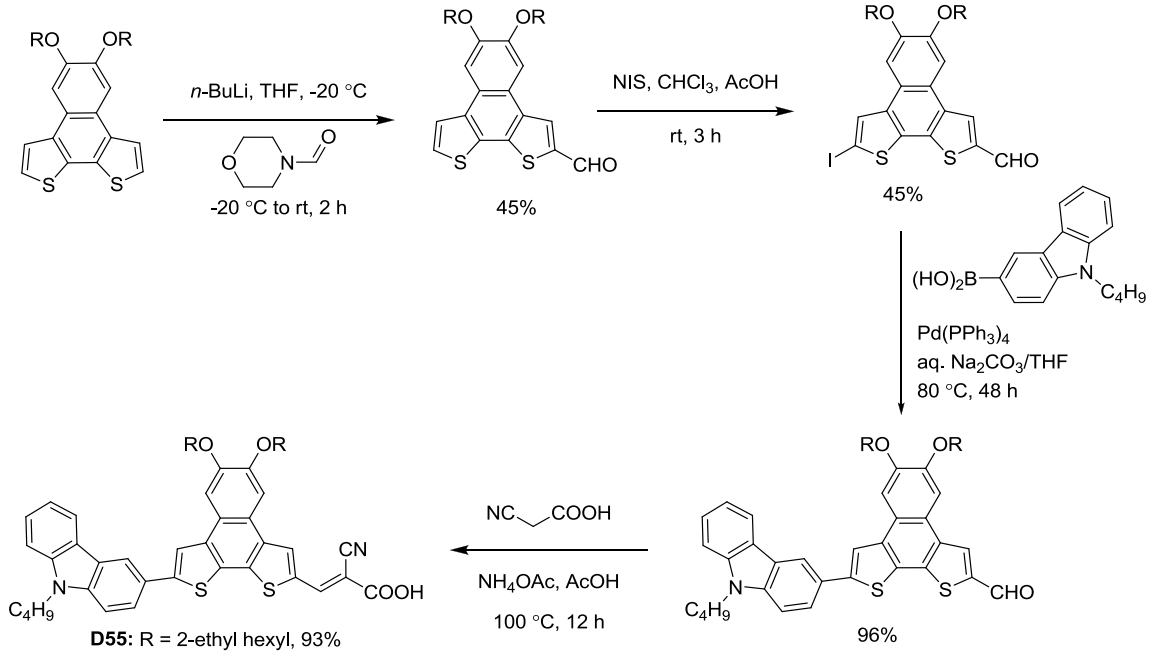

Scheme 1.18 Synthetic scheme of the dye **D55**.

The dye containing carbazole donor (**D55**) shows higher efficiency due to higher J_{SC}. The high photocurrent is attributed to the compact packing of the dye on TiO_2 film and broader IPCE of the device. The dye **D55** containing branched alkoxy chain has achieved higher efficiency of 4.60% when compared to the dye **D56.** The superior performance of **D55** is due to the high molar extinction coefficient and prolonged electron life time of the former dye and efficient regeneration due to its low lying HOMO.

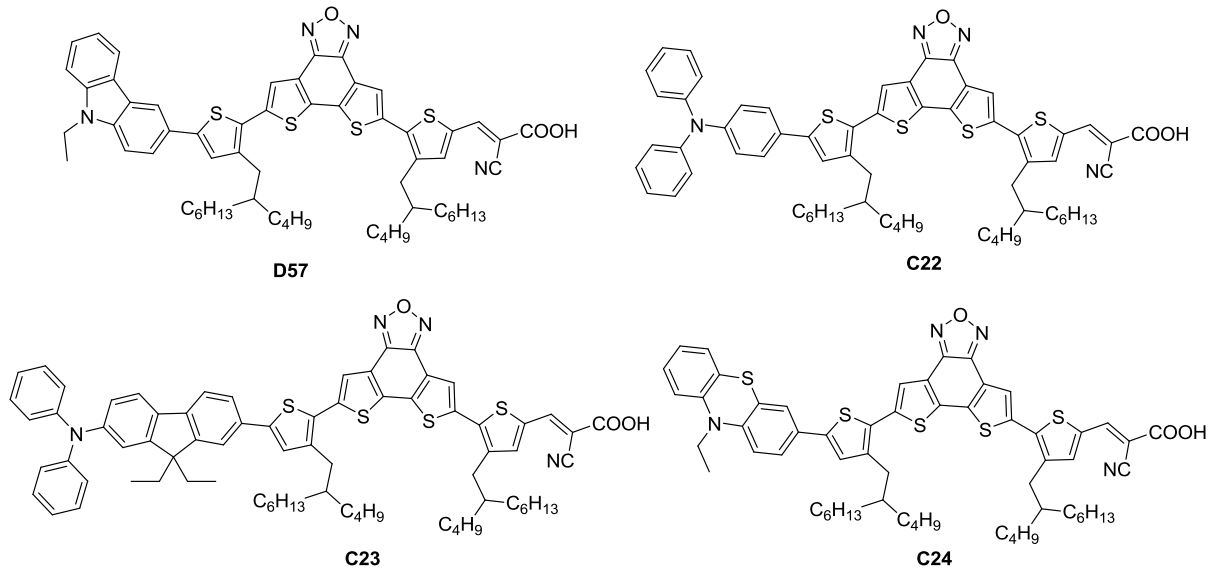

Chart 1.26 Structures of the dyes with dithieno[3',2':3,4;2",3":5,6]benzo[1,2-*c*]furazan linker.

Lin and co-workers [102] synthesized D-π-A'-π-A type sensitizers (**D57** and **C22-C24**; Chart 1.26) by using dithieno[3',2':3,4;2",3":5,6]benzo[1,2-*c*]furazan as linker, cyanoacrylic acid as acceptor and donors composed of carbazole, triphenylamine, diphenylaminofluorene and phenothiazine linkers. All dyes displayed broad absorption spectra covering the wavelength range 350 to 600 nm with the promising molar extinction coefficients (> 40000 M^{-1} cm^{-1}). The dye **D57** achieved higher power conversion efficiency of 5.98% with J_{SC} of 12.43 mA cm^{-2} when compared to the dyes **C23** and **C24** due to good light harvesting property of the carbazole containing dye. But, the dye **C22** exhibited better efficiency of 6.18% due to higher J_{SC} of 12.60 mA cm^{-2} and higher V_{OC} of 700 mV.

Synthesis of the dyes is outlined in Scheme 1.19. The Pd-catalyzed Stille cross-coupling of 5,8-bis(3-(2-butyloctyl)thiophen-2-yl)dithieno[3',2':3,4;2",3":5,6]benzo[1,2-*c*][1,2,5]oxadiazole with 2-butyloctyl-thiophen-2-yl stannane in DMF under reflux condition afforded 5,8-bis(3-(2-

butyloctyl)thiophen-2-yl)dithieno[3',2':3,4;2",3":5,6]benzo[1,2-*c*][1,2,5]oxadiazole. Subsequent formylation using Vilsmeier-Haack reagent and bromination using NBS to produce 5-(8-(5-bromo-3-(2-butyloctyl)thiophen-2-yl)dithieno[3',2':3,4;2",3":5,6]benzo[1,2-*c*][1,2,5]oxadiazol-5-yl)-4-(2-butyloctyl)thiophene-2-carbaldehyde. Then, it reacted with 9-ethyl-9*H*-carbazol-3-ylboronic acid by Stille coupling to give the aldehyde derivative. Finally, **D57** was prepared via Knoevenagel condensation of carbazole containing aldehyde derivative with cyanoacetic acid. The synthesis of other dyes (**C22-C24**) was performed by following a similar procedure.

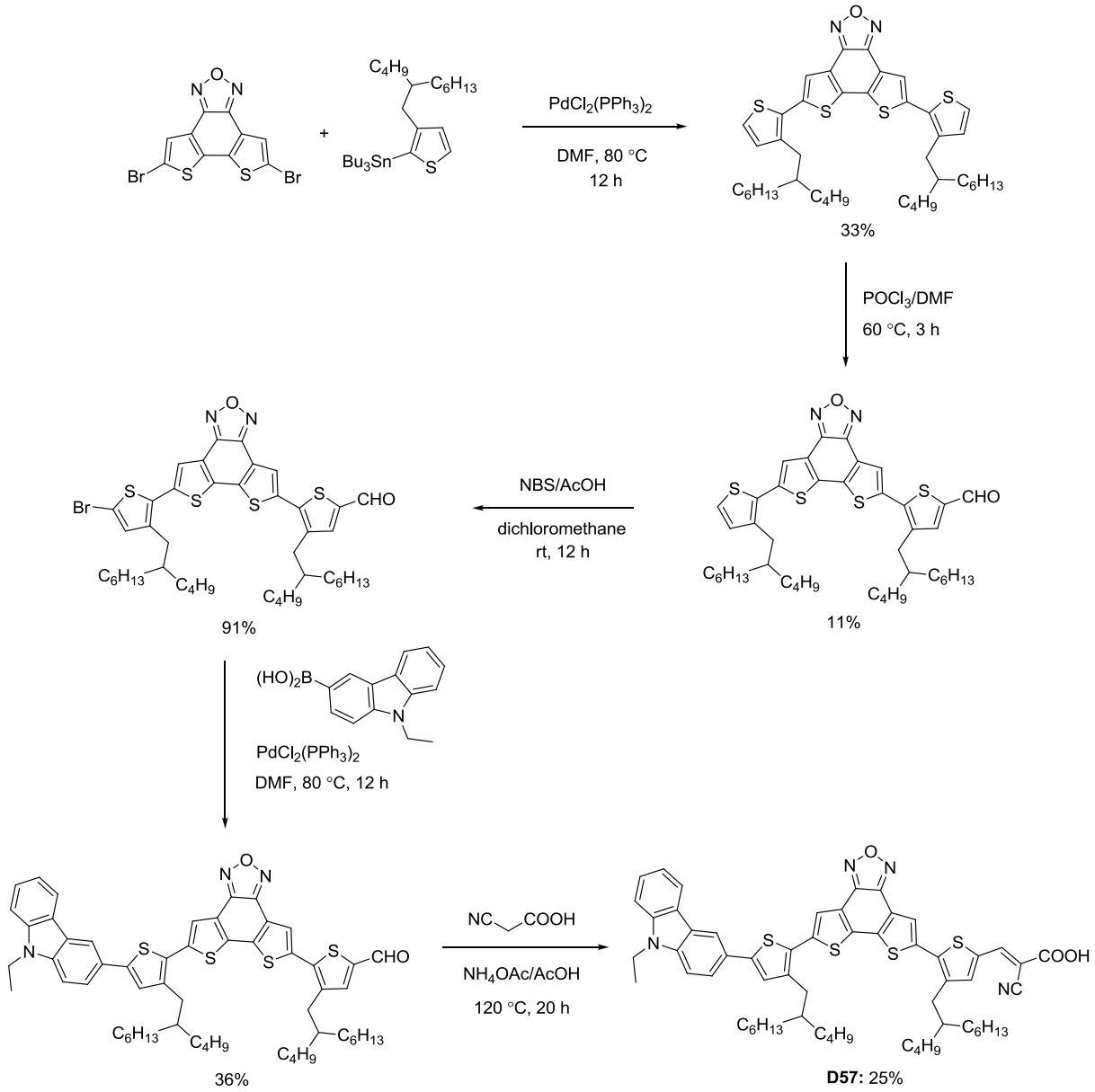

Scheme 1.19 Synthetic scheme of the dye **D57**.

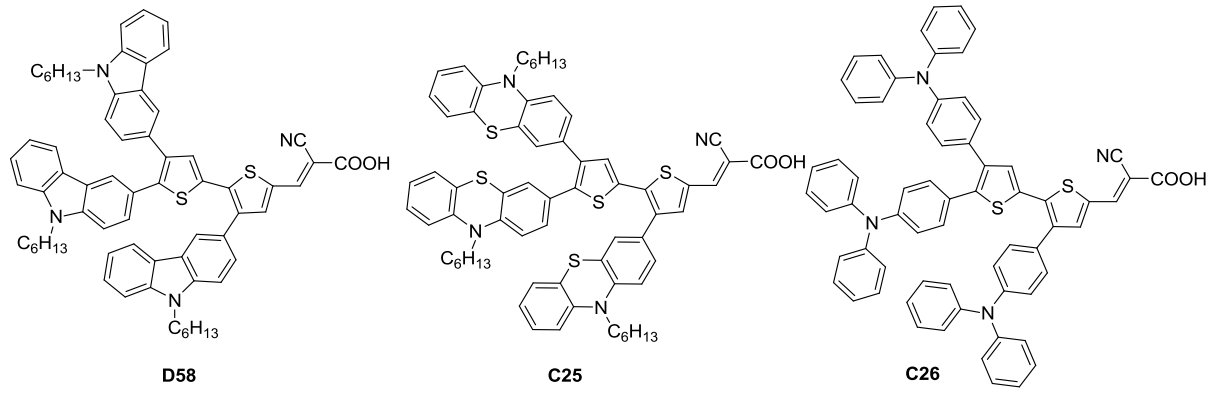

Chart 1.27 Organic dyes based on 2,2'-bithiophene linker with multiple donors.

Chen and co-workers reported three dyes (**D58**, **C25** and **C26;** Chart 1.27) based on 2,2'-bithiophene linker with carbazole, phenothiazine and triphenylamine as donors respectively [103]. The synthetic scheme of the dyes is outlined in Scheme 1.20. Synthesis started with brominated of 2,2'-bithiophene-5-carbaldehyde with NBS in DMF to produce 3,4',5'-tribromo-2,2'-bithiophene-5-carbaldehyde. Then, it reacted with 9-hexyl-3-(4,4,5,5-tetramethyl-1,3,2-dioxaborolan-2-yl)-9*H*-carbazole to give the 3,4',5'-tris(9-hexyl-9*H*-carbazol-3-yl)-2,2'-bithiophene-5-carbaldehyde via Suzuki coupling. Finally, the dye **D58** was obtained through the Knoevenagel condensation of 3,4',5'-tris(9-hexyl-9*H*-carbazol-3-yl)-2,2'-bithiophene-5-carbaldehyde with cyanoacetic acid. The synthesis of **C25** and **C26** is also similar to the Scheme 1.20.

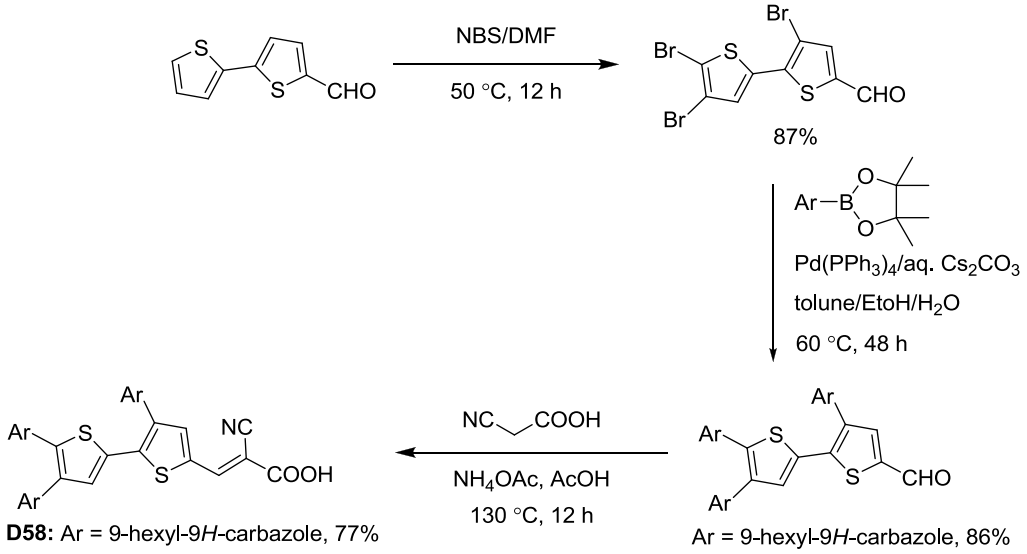

Scheme 1.20 Synthetic scheme of the dye **D58**.

The introduction of bulky (**D58**) donor twists the planarity of the molecule and result in a better charge separation and effective suppression of back electron transfer with blue shifted absorption. The dye **D58** with carbazole donor showed better conversion efficiency of 4.24% due to its larger photocurrent generation (J_{SC} = 9.32 mA cm^{-2}) compared to other dyes.

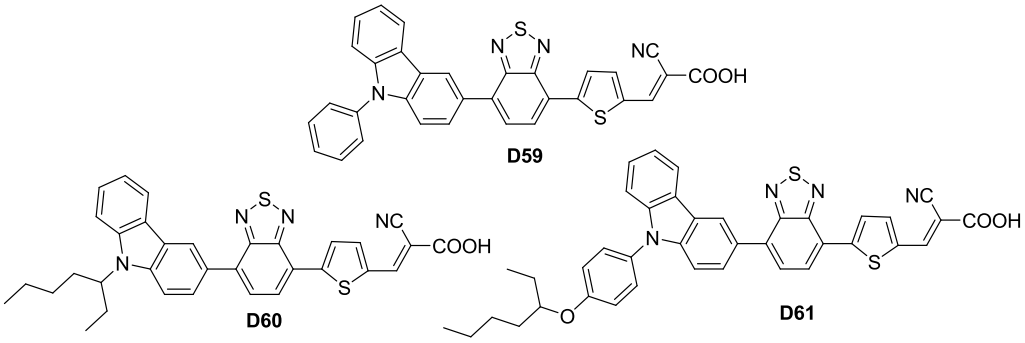

Chart 1.28 Structures of the carbazole dyes contain benzothiadiazole as auxiliary acceptor.

Valiyaveettil and co-workers synthesized a set of dyes (**D59**–**D61;** Chart 1.28) with carbazole as donor connected at C3-position and varied the substitution at *N*9-position with phenyl, alkyl and alkoxy phenyl units [60]. These dyes were synthesized according to Scheme 1.1. The dyes **D59**–**D61** showed red shifted absorption with high molar extinction coefficients when compared to the dyes **D1** and **D2** where carbazole was connected at C2-position.This clearly indicates the presence of strong donor acceptor interactions due to the effective conjugation of carbazole via C3-linkage. The stronger donor acceptor interaction of the dyes (**D59**–**D61**) resulted higher molar extinction coefficients (23993 M^{-1} cm^{-1} to 26206 M^{-1} cm^{-1}) and enhanced J_{SC}. **D61** achieved highest efficiency of 3.80% with J_{SC} of 8.30 mA cm^{-2} among the series due to introduction of electron rich alkoxy phenyl unit at *N*9-position of carbazole.

Gao and coworkers synthesized a set of dyes (**D62-D65**; Chart 1.29) and compared optical properties by various π-bridge and acceptors [104]. The synthesis of the dyes is showed in Scheme 1.21. Carbazole containing aldehyde derivatives were synthesized according to the Scheme 1.1. New carbazole dyes (**D62-D65**) were prepared through Knoevenagel condensation of aldehyde derivatives with cyanoacetic acid or rhodanine acetic acid in the presence of piperidine. The dye with phenyl spacer claimed better efficiency when compared to the thiophene spacer containing dyes due to the better IPCE values of the phenyl spacer containing dye. The dyes which have cyanoacetic acid acceptor display superior photovoltaic properties

even with shorter wavelength and lower molar absorption coefficient compared with dyes having rhodanine acetic acid acceptor. Among all the dyes, **D64** containing phenyl spacer and cyanoacrylic acid acceptor achieved higher efficiency of 5.40% under AM 1.5 irradiation.

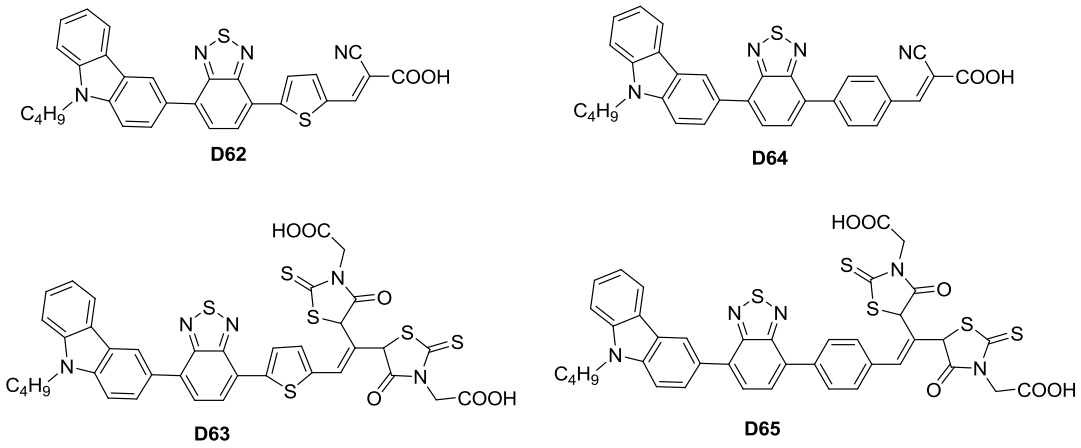

Chart 1.29 Structures of the carbazole dyes with benzothiadiazole as auxiliary acceptor.

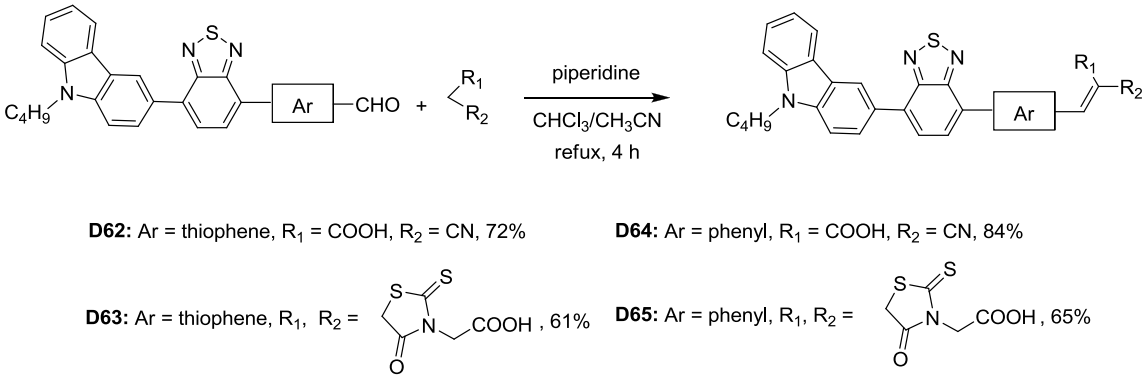

Scheme 1.21 Synthetic scheme of the dyes **D62-D65**.

Li and co-workers [105] synthesized carbazole-based dyes (**D66** and **D67**; Chart 1.30) by incorporating benzothiadiazole as auxiliary chromophore. The dye **D67** (405 nm) contains thiophene linker showed red shifted absorption compared to **D66** (359 nm) due to the extension of conjugation of **D67** dye. The dye **D67** showed better conversion efficiency compared to dye **D66** due to higher J_{SC} of former dye. However, the poor light harvesting property of the dyes resulted in poor photovoltaic performance.

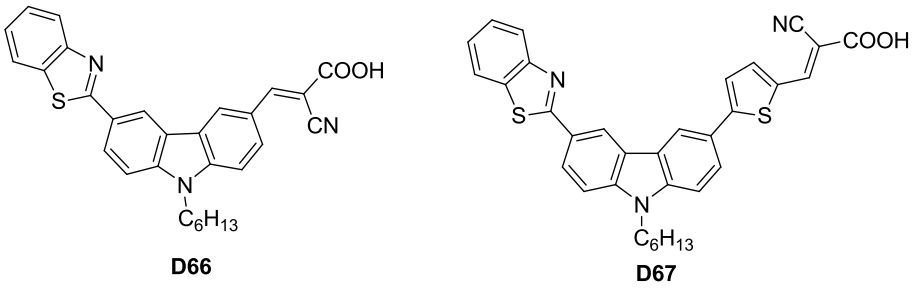

Chart 1.30 Structures of the organic dyes containing carbazole π-linking donor and benzo[*d*]thiazole auxiliary donor.

The synthetic scheme of the dyes, **D66** and **D67** is outlined in Scheme 1.22. It starts with reaction of 9-hexyl-9*H*-carbazole-3-carbaldehyde and thiophenol to obtain 2-(9-hexyl-9*H*-carbazol-3-yl)benzo[*d*]thiazole [106]. Subsequently it formylated by Vilsmeier-Haack reaction with DMF and $POCl_3$ and followed by Knoevengel condensation with cyanoacetic acid led to dye **D66**. Iodination of 9-hexyl-9*H*-carbazole-3-carbaldehyde with KI and KIO_3 in acetic acid and followed by treatment with thiophenol gave 2-(9-hexyl-6-iodo-9*H*-carbazol-3-yl)benzo[*d*]thiazole. Then it treated with 5-formylthiophen-2-ylboronic acid via Suzuki coupling afforded 5-(6-(benzo[*d*]thiazol-2-yl)-9-hexyl-9*H*-carbazol-3-yl)thiophene-2-carbaldehyde and it subsequently converted to dye **D67** by Knoevengel condensation with cyanoacetic acid in presence of piperidine as a catalyst.

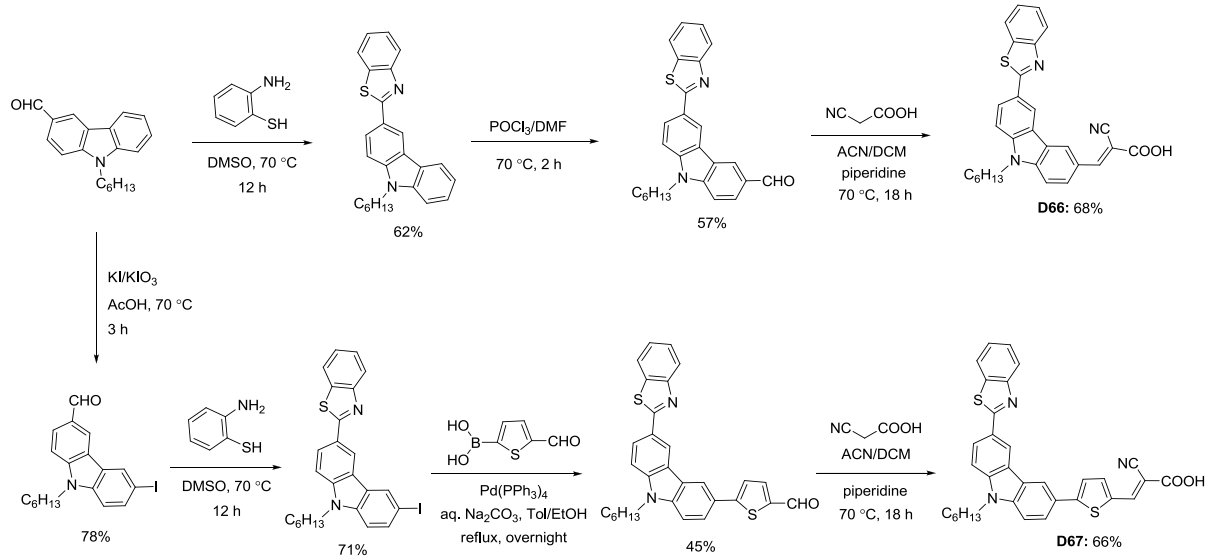

Scheme 1.22 Synthetic scheme of the dyes **D66** and **D67**.

Table 1.2 Optical, electrochemical and photovoltaic performance parameters of dyes containing carbazole as donor.

Dye	$\lambda_{max,}$ nm (ε_{max}, M^{-1} cm^{-1})	E_{ox} , V (*vs* NHE)	E_{ox}^{*}, V (*vs* NHE)	J_{SC} (mA cm^{-2})	V_{OC} (mV)	*ff*	η (%)	*Ref*
D3	349 (21406)	1.44	−1.44	1.29	540	0.60	0.42	[71]
D4	352 (38344)	1.40	−1.45	1.97	565	0.62	0.69	[71]
D5	350 (63902)	1.33	−1.53	2.31	715	0.65	1.07	[71]
D6	403 (38289)	0.92	−1.87	5.73	715	0.69	2.82	[73]
C1	422 (39823)	0.99	−1.45	8.98	756	0.69	4.66	[73]
D7	411 (27000)	1.52[a]	−1.13[a]	9.83	740	0.70	5.02	[74]
D8	435 (30060)	1.29[a]	−1.13[a]	11.50	680	0.66	5.15	[74]
D9	469 (12300)	1.54[a]	−0.79[a]	3.76	620	0.77	1.79	[74]
D10	489 (6012)	1.64[a]	−0.71[a]	1.39	550	0.73	0.55	[74]
D11	406 (21500)	1.58[a]	−1.05[a]	7.85	690	0.71	3.87	[74]
D12	451 (29500)	1.54[a]	−0.90[a]	9.11	610	0.68	3.76	[74]
D13	465 (47900)	1.33	−0.74	10.02	570	0.64	3.62	[76]
D14	417 (18500)	1.35	−0.77	9.44	660	0.63	3.75	[76]
D15	428 (40000)	0.91	−1.55	14.63	685	0.67	6.70	[77]
C2	433 (32600)	0.73	−1.76	13.32	660	0.61	5.43	[77]
C3	439 (34000)	0.69	−1.77	13.96	670	0.66	6.14	[77]
C4	460 (28900)	0.51	−1.77	12.60	630	0.61	4.87	[77]
C5	454 (26400)	0.54	−1.72	8.48	570	0.65	3.14	[77]
C6	446 (33900)	0.56	−1.83	14.12	680	0.64	6.32	[77]
D16	474 (32000)	0.89	−1.33	12.73	700	0.71	6.33	[79]
C7	507 (26000)	1.02	−1.07	11.69	680	0.69	5.48	[79]
C8	512 (29000)	0.95	−1.11	13.93	710	0.68	6.72	[79]
D17	565	1.37	−0.88	12.22	629	0.61	4.70	[81]
D18	428 (35000)	0.59[b]	−1.35[b]	13.45	618	0.68	5.64	[82]
C9	481 (40000)	0.51[b]	−1.37[b]	15.85	589	0.67	6.11	[82]

[a] TiO_2 film; [b]photo emission yield spectrometer

Table 1.2 (cont.)

Dye	$\lambda_{max,}$ nm (ε_{max}, M^{-1} cm^{-1})	E_{ox} , V (*vs* NHE)	E_{ox}^{*}, V (*vs* NHE)	J_{SC} (mA cm^{-2})	V_{OC} (mV)	*ff*	η (%)	*Ref*
C10	485 (41000)	0.46[b]	−1.40[b]	16.17	595	0.66	6.38	[82]
D19	532 (57500)	1.15	−0.96	13.10	770	0.73	7.50	[83]
C11	532 (46500)	0.97	−1.23	12.90	774	0.70	7.00	[83]
D20	485 (40100)	0.99	−0.78	10.56	670	0.63	4.46	[54]
D21	480 (38800)	1.07	−0.83	9.90	750	0.67	4.97	[54], [86]
D21	480 (38800)	0.98	−0.97	10.50	748	0.70	5.50	[86]
D22	473 (35800)	na	na	12.40	720	0.71	6.30	[87]
D22	480 (38400)	0.96	−0.89	10.67	690	0.68	5.01	[54]
D23	474 (33100)	0.86	−0.85	5.72	740	0.48	2.03	[54]
D24	473 (38600)	0.83	−0.87	6.40	730	0.47	2.20	[54]
D25	478 (39300)	0.98	−0.74	10.41	740	0.46	3.54	[54]
D26	na	na	na	11.90	707	0.67	5.61	[75]
D27	471 (46900)	1.09	−0.61	11.38	700	0.60	4.78	[54]
D28	483 (36200)	na	na	14.50	760	0.71	7.80	[88]
D29	480 (38500)	na	na	14.50	730	0.69	7.30	[88]
D30	480 (35200)	0.96	−0.93	10.80	785	0.71	6.00	[89]
D31	481 (35200)	0.95	−1.01	11.70	825	0.69	6.60	[89]
D32	473 (39700)	0.90	−0.99	11.50	826	0.67	6.40	[89]
D33	474 (35900)	0.92	−1.02	8.15	720	0.72	4.20	[89]
D33	474 (35900)	0.92	−1.02	10.20	770	0.65	5.10	[90]
D34	473 (38900)	0.97	−1.12	9.71	760	0.72	5.30	[90]
D35	472 (33900)	1.08	−1.00	9.73	770	0.72	5.40	[90]
C12	472 (28200)	1.12	−0.95	7.63	640	0.72	3.50	[90]
C13	471 (35600)	1.01	−1.06	6.89	690	0.75	3.60	[90]
C14	474 (39100)	0.95	−1.15	8.00	670	0.72	3.90	[90]
C15	513 (31800)	0.66	−1.26	8.74	570	0.74	3.70	[90]

[b]photo emission yield spectrometer; na = not available

Table 1.2 (cont.)

Dye	$\lambda_{max,}$ nm (ε_{max}, M^{-1} cm^{-1})	E_{ox} , V (*vs* NHE)	E_{ox}^{*} , V (*vs* NHE)	J_{SC} (mA cm^{-2})	V_{OC} (mV)	*ff*	η (%)	*Ref*
C16	498 (34000)	0.75	−1.17	7.82	650	0.66	3.40	[90]
C17	509 (34100)	0.67	−1.21	6.22	690	0.70	3.00	[90]
D36	469 (36000)	na	na	5.65	710	0.72	2.90	[91]
D37	485 (38000)	na	na	7.11	770	0.73	4.00	[91]
D38	477 (41000)	na	na	7.06	770	0.74	4.00	[91]
D39	453 (28600)	1.08	−1.07	11.40	835	0.67	6.38	[92]
D40	471 (31900)	1.00	−1.08	12.30	799	0.73	7.17	[92]
D41	470 (28500)	1.03	−1.00	14.98	814	0.71	8.66	[92]
D42	485 (43900)	0.93	−0.94	8.70	750	0.65	4.30	[93]
D43	480 (41500)	0.94	−0.94	7.30	720	0.69	3.60	[93]
D44	450	na	na	6.90	755	0.64	3.40	[94]
D45	498 (43200)	0.99	−0.86	16.10	840	0.76	10.40	[95]
D46	504 (42700)	1.01	na	15.10	821	0.75	9.32	[95]
D47	493	1.01	−1.15	na	na	na	na	[96]
D48	489	1.03	−1.15	na	na	na	na	[96]
D49	489	na	na	19.60	680	0.49	6.50	[96]
D50	484 (35700)	0.90	−1.00	11.20	630	0.67	4.80	[97]
D51	382/41.8	1.39	−1.86	na	na	na	na	[98]
D52	373/56.25	1.39	−1.93	na	na	na	na	[98]
D53	410/45.7	1.24	−1.78	na	na	na	na	[98]
D54	428 (36788)	0.99	−1.23	9.61	695	0.70	4.65	[99]
C18	413 (5140)	1.45	−1.16	2.57	605	0.76	1.18	[99]
C19	432 (25820)	0.90	−1.22	6.85	625	0.70	2.98	[99]
C20	427 (28560)	1.07	−1.17	7.08	655	0.67	3.12	[99]
D55	491 (45300)	0.72	−1.64	10.80	663	0.64	4.60	[101]
D56	483 (40000)	0.71	−1.46	10.60	657	0.65	4.49	[101]

na = not available

Table 1.2 (cont.)

Dye	λ_{max}, nm (ε_{max}, M^{-1} cm^{-1})	E_{ox} , V (*vs* NHE)	E_{ox}^{*}, V (*vs* NHE)	J_{SC} (mA cm^{-2})	V_{OC} (mV)	*ff*	η (%)	*Ref*
C21	493 (42200)	0.65	−1.57	10.30	663	0.64	4.38	[101]
D57	462 (17000)	1.27	−1.07	12.43	680	0.72	5.98	[102]
C22	462 (21700)	1.24	−1.14	12.60	700	0.71	6.18	[102]
C23	464 (31400)	0.99	−1.36	3.23	600	0.72	1.42	[102]
C24	462 (43700)	1.17	−1.17	10.92	690	0.70	5.27	[102]
D58	478 (79200)	1.47	−0.54	9.32	650	0.70	4.24	[103]
C25	425 (66500)	1.35	−0.62	5.73	640	0.66	2.43	[103]
C26	341 (72300)	1.46	−0.48	6.40	640	0.72	2.93	[103]
D59	474 (25712)	1.26	−0.57	7.37	650	0.69	3.29	[60]
D60	484 (26206)	1.21	−0.49	8.30	640	0.74	3.80	[60]
D61	476 (26107)	1.44	−0.58	4.85	650	0.74	2.36	[60]
D62	486 (30633)	1.27	−0.96	12.08	610	0.69	5.07	[104]
D63	507 (45367)	1.34	−0.96	4.12	560	0.71	1.65	[104]
D64	441 (21667)	1.54	−1.10	10.99	710	0.69	5.40	[104]
D65	446 (34667)	1.48	−1.06	6.98	630	0.87	3.81	[104]
D66	359	2.06	−1.39	1.33	660	0.51	0.45	[105]
D67	400	1.73	−1.33	2.10	540	0.44	0.50	[105]

1.2.3 Carbazole as donor linked through *N*9-position

Large number of organic dyes has been reported where carbazole donor is attached to the π-linker through *N*9-position (see Figure 1.6 for a schematic representation). Carbazole can be easily functionalized at *N*9-position either by *N*-arylation or alkylation. *N*-arylation on carbazole can be either achieved by Ullmann coupling reaction involving a copper catalyst and aryl halide preferably an iodide in the presence of a base in polar solvent. This method is cheap and convenient when compared to the palladium catalyzed protocols. This class of dyes has the following advantages: (1) The cation radical formed on removal of electron is easily stabilized by chromophores present at C3 and C6 positions. (2) These dyes normally aggregate at the

surface of TiO_2 but increase the dye loading due to the presence of compact planar structural elements. [8] They can be compared to diphenylamine end capped organic dyes which normally possess a non planar arrangement around the amine nitrogen.

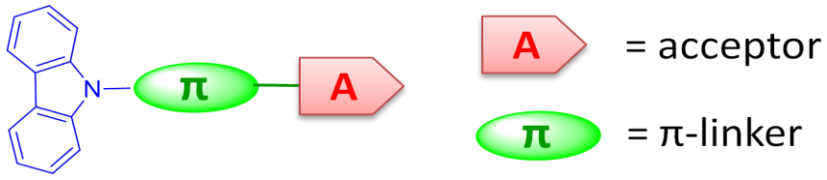

Figure 1.6 Structural configuration of organic dyes with *N*9-linked carbazole donor.

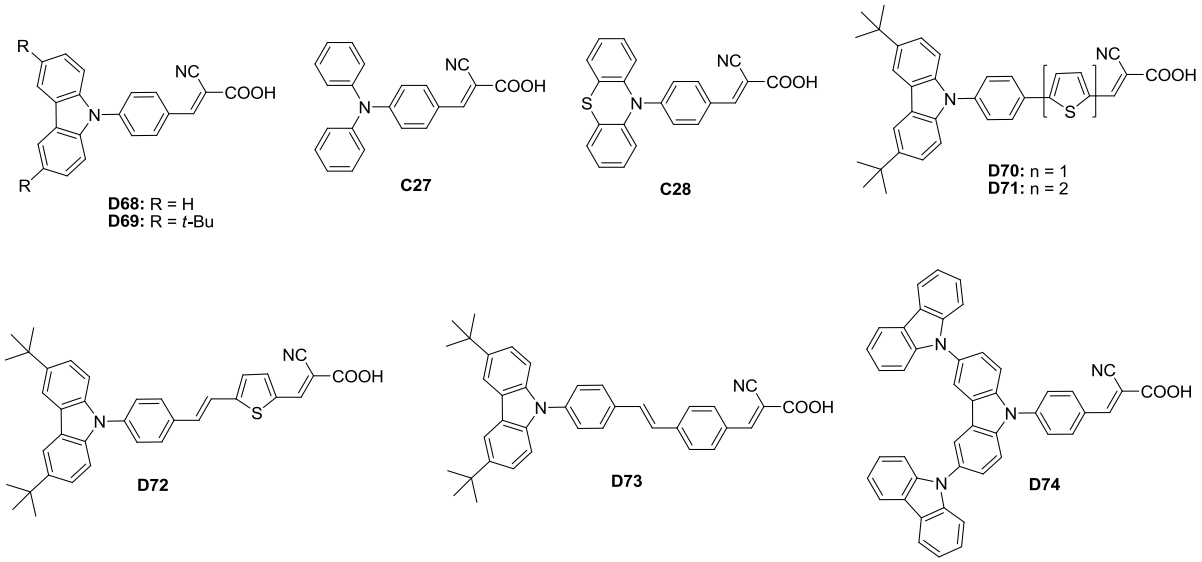

Chart 1.31 Organic dyes with *N*-substituted carbazole as donor and varied conjugation pathway.

Sun and co-workers synthesized dyes the dyes **D68** and **D72** (Chart 1.31) and employed as sensitizer in DSSC utilizing Br^-/Br_3^- redox couple [107]. The DSSC using **D68** exhibited higher conversion efficiency (3.68%) than the one containing (*E*)-2-cyano-3-(4-(diphenylamino)phenyl)acrylic acid (η = 2.74%). The absorption of **D72** (429 nm) was red shifted when compared to **D68** (374 nm). This is due to the extension of conjugation by vinylthiophene. The J_{SC} of **D72** is higher because of better absorption parameters which further improved the efficiency (5.22%) [108]. The Br^-/Br_3^- redox couple has been found to improve the V_{OC} of the devices and the device with **D72** has achieved record V_{OC} of 1156 mV, which is highest for DSSCs utilizing organic dyes. Introduction of *tert*-butyl group on the C3 and C6 position of carbazole has been used to fine tune the HOMO and LUMO of the dyes. Thus, the compound **D69** showed a bathochromic shift in the absorption spectrum when compared to the

similar compound **D68** which lacks the *tert*-butyl substituents. However, the molar extinction coefficient took a beating for the *tert*-butylated derivatives. But, the low lying LUMO of **D69** facilitates the injection of electrons in to the CB of TiO_2 thereby increase J_{SC} (4.71 mA cm^{-2}) which result in an overall higher efficiency (4.05%) when compared to **D68**. But replacement of thiophene in **D72** with phenyl group gave a dye **D73** which exhibited inferior performance in DSSC due to less J_{SC} of dye **D73** [108]. Even though the dye **D73** has higher V_{OC} (1033 mV) compared to **D72**, J_{SC} plays a major role in improving the efficiency. Additionally substitution of carbazole for *tert*-butyl groups (**D74**) was found to be futile as the dye showed significantly blue-shifted absorption [108].

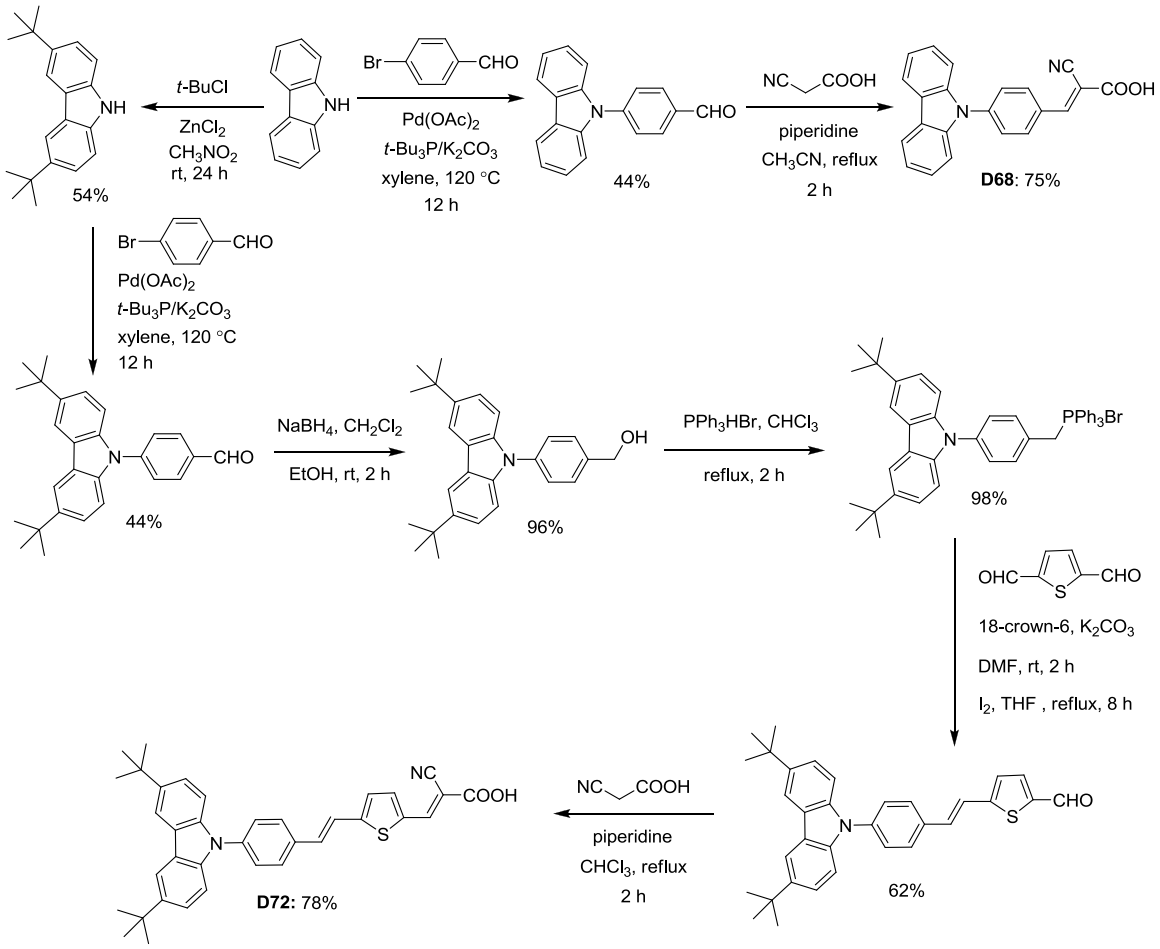

Scheme 1.23 Synthetic scheme of the dyes **D68** and **D72**.

The synthesis of the dyes (**D68** and **D72**) is outlined in Scheme 1.23. It starts with reaction of carbazole with *p*-bromo benzaldehyde via Hartwig-Buchwald C-N coupling to give 4-carbazol-

9-yl-benzaldehyde, which was converted to dye **D68** by Knoevenagel condensation with cyanoacetic acid. Friedal-crafts alkylation [109] of carbazole with *t*-BuCl in presence of $AlCl_3$ afford 3,6-di-*tert*-butyl-9*H*-carbazole, which is treated with *p*-bromo benzaldehyde via Hartwig-Buchwald C-N coupling to give 4-(3,6-di-*tert*-butyl-9*H*-carbazol-9-yl)benzaldehyde. This aldehyde reduced by $NaBH_4$ and subsequently converted to wittig salt by treating with PPh_3HBr. Wittig salt is selectively treated with thiophene-2,5-dicarbaldehyde in presence of basic solvent produced (*E*)-5-(4-(3,6-di-*tert*-butyl-9*H*-carbazol-9-yl)styryl)thiophene-2-carbaldehyde. Finally, it was condensed with cyanoacetic acid via Knoevenagel condensation gave the final dye (**D72**).

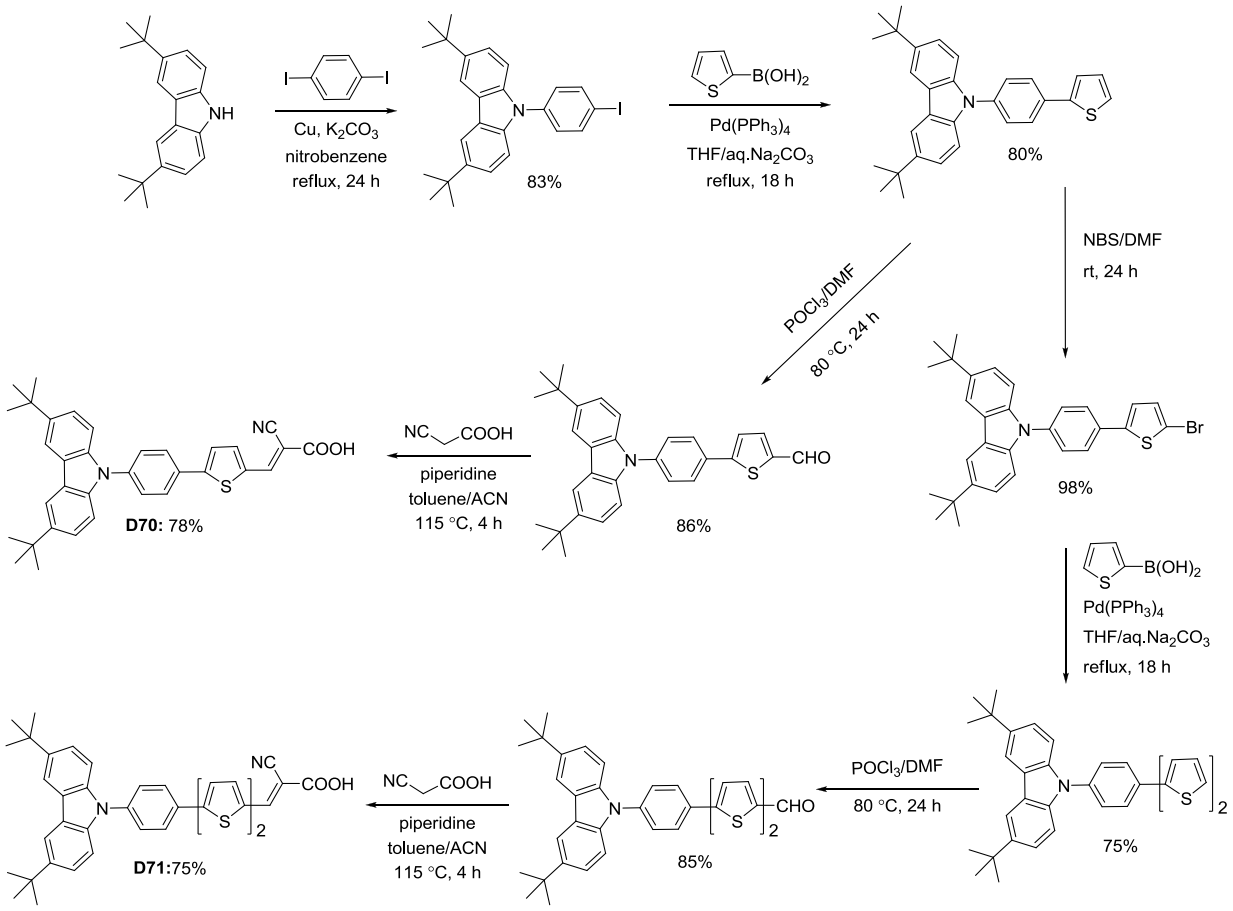

Scheme 1.24 Synthetic scheme of the dyes **D70** and **D71**.

The synthesis of dyes **D70** and **D71** is outlined in Scheme 1.24. The intermediate 3,6-di-*tert*-butyl-9-(4-iodophenyl)-9*H*-carbazole was synthesized via Ullman-type coupling of 3,6-di-*tert*-butyl-9*H*-carbazole and excess amount of 1,4-diiodobenzene in the presence of CuI as a catalyst and K_2CO_3. Then, 3,6-di-*tert*-butyl-9-[4-(2-thienyl)phenyl]-9*H*-carbazole was synthesized by

Suzuki coupling reaction of 3,6-di-*tert*-butyl-9-(4-iodophenyl)-9*H*-carbazole and 2-thiopheneboronic acid. 3,6-di-*tert*-butyl-9-[4-(2-thienyl)phenyl]-9*H*-carbazole was brominated with the NBS and then coupled to the second thiophene unit by using Suzuki coupling. The carbazole-thiophene compounds were formulated by using Vilsmeier-Haack reaction in the presence of the $POCl_3$ and DMF. The Knoevenagel condensation of carbaldehydes with cyanoacetic acid to gave cyanoacrylic acids. Zafer and co-workers found that insertion of thiophene (**D70**) and bithiophene (**D71**) segments in the conjugation pathway of the dye **D68**, is beneficial to red-shift the absorption wavelength [110]. Though the light harvesting property of **D71** increased substantially due to the presence of bithiophene in the conjugation pathway, the device did not yield a favorable efficiency (2.48%) due to low V_{OC} observed for the cell. The diminished V_{OC} may be attributed to the pronounced recombination of electrons with the electrolyte. However, the dye **D71** showed better device efficiency than **D70** due to the broader spectral response which increased its J_{SC}.

Jia and co-workers examined the effect of different donors (diphenylamine, phenothiazine and carbazole) on the performance of dyes (**C27**, **C28** and **D68;** Chart 1.31) [111]. The dye **C27** with triphenylamine showed highest efficiency of 2.03% with J_{SC} of 4.78 mA cm^{-2} and V_{OC} of 608 mV among the other dyes. The inferior efficiency (1.77%) of the dye **D68** is due to the lower light harvesting ability which results in a smaller J_{SC} of 4.25 mA cm^{-2} and V_{OC} of 586 mV.

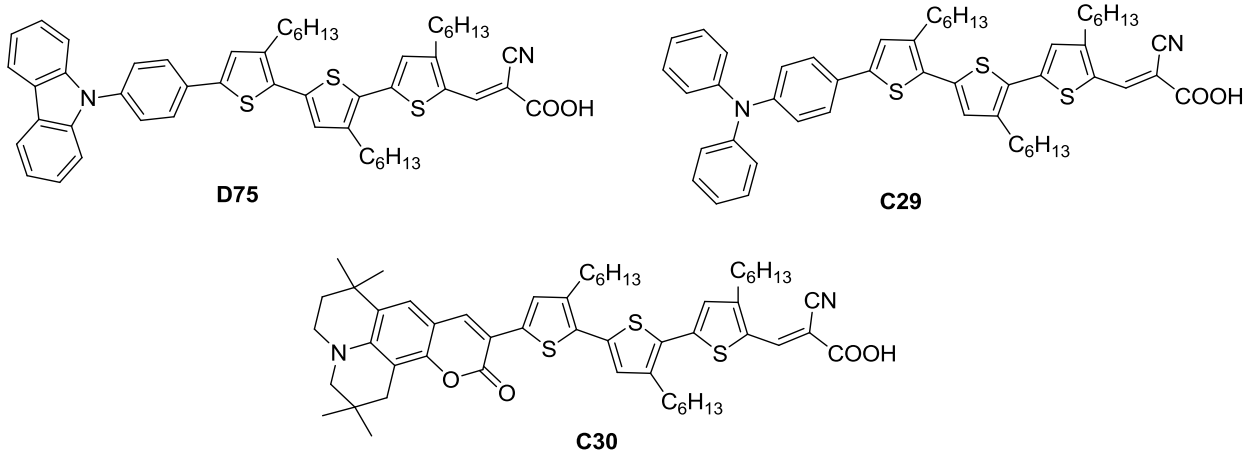

Chart 1.32 Organic dyes containing different donor units.

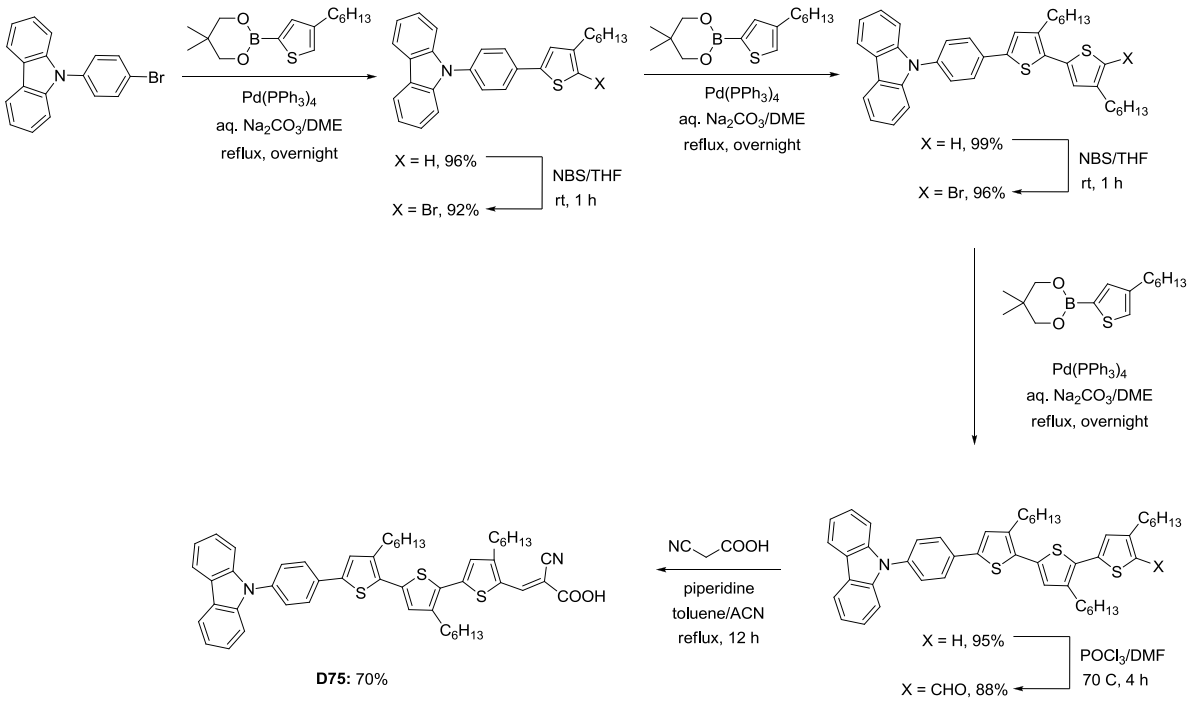

Scheme 1.25 Synthetic scheme of the dye **D75**.

Koumura and co-workers [112] investigated the effect of donor in organic dyes (**D75, C29** and **C30**; Chart 1.32) on recombination in DSSC with cobalt complex electrolyte. Dyes composed of different donors such as carbazole, triphenylamine and coumarin were effectively used in DSSC. The synthetic strategy of the dye **D75** is outlined in Scheme 1.11. It starts with Suzuki coupling of 9-(4-bromophenyl)-9*H*-carbazole with 2-(4-hexylthiophen-2-yl)-5,5-dimethyl-1,3,2-dioxaborinane, followed by bromination with NBS in a series to get 9-[4-(3,4',4''-tri-*n*-hexyl-[2,2',5',2'']terthiophen-5-yl)phenyl]-9*H*-carbazole. It was converted to aldehyde derivative by Vilsmeier-Haack reaction with $POCl_3$/DMF. Finally, dye **D75** obtained by Knoevengel condensation of aldehyde derivative with cyanoacetic acid. The synthesis of **C30** is similar to the scheme described above for **D75**. The dye **C29** which contains triphenylamine as donor unit produced highest V_{OC} of 806 mV and longest electron life time is attributed to the blocking effect by steric hindrance of the nonplanar structure of the donor. While coumarin donor dye **C30** showed lowest V_{OC} and shortest electron lifetime suggesting that the coumarin attracted the cobalt redox couples to the surface of the TiO_2 layer which results increasing the concentration of cobalt complex. The substitution of carbazole raised LUMO level which helps to inject electrons from excited state of the dye to CB of TiO_2. Carbazole donor containing dye **D75** exhibited power conversion efficiency of 6.00% with J_{SC} of 11.00 mA cm^{-2}.

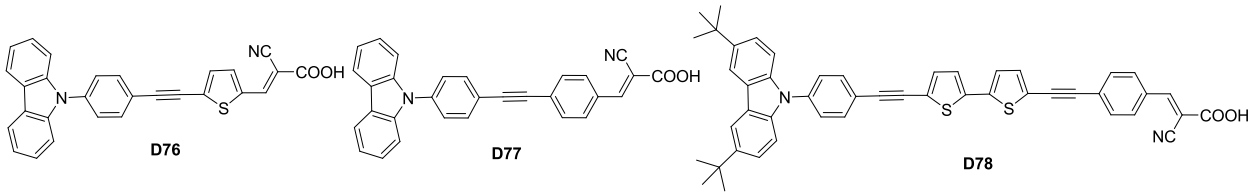

Chart 1.33 Organic dyes with *N*-substituted carbazole donor and acetylene conjugation.

Giribabu and co-workers reported dyes (**D76** and **D77;** Chart 1.33) featuring acetylene extended conjugation between the carbazole donor and cyanoacrylic acid acceptor [113]. The thiophene containing dye **D76** displayed longer wavelength absorption and larger photocurrent when compared to the phenyl linker containing dye **D77**. However, these acetylene linked derivatives are far inferior to the corresponding vinylene derivatives (**D72** and **D73**). Similar trend has been observed earlier for triarylamine-based organic dyes containing fluorenylacetylene linkers [114]. The synthetic route of the dyes is depicted in Scheme 1.26. Reaction of carbazole and 1,4-dibromo benzene by Ullmann type coupling gave 9-(4-bromophenyl)-9*H*-carbazole. It reacted with 2-methyl-3-butyn-2-ol by Sonogashira coupling [115] reaction to afford 4-(4-(9*H*-carbazol-9-yl)phenyl)-2-methylbut-3-yn-2-ol, which deprotected using KOH in toluene to afford 9-(4-ethynylphenyl)-9*H*-carbazole. This alkyne derivative linked with 5-bromothiophene-2-carbaldehyde by Sonogashira reaction to afford 5-((4-(9*H*-carbazol-9-yl)phenyl)ethynyl)thiophene-2-carbaldehyde. Finally, the dye **D76** prepared by reacting either 5-((4-(9*H*-carbazol-9-yl)phenyl)ethynyl)thiophene-2-carbaldehyde with cyanoacetic acid via Knoevenagel condensation. The synthesis of the other dye **D77** also synthesized according same procedure described for **D76**.

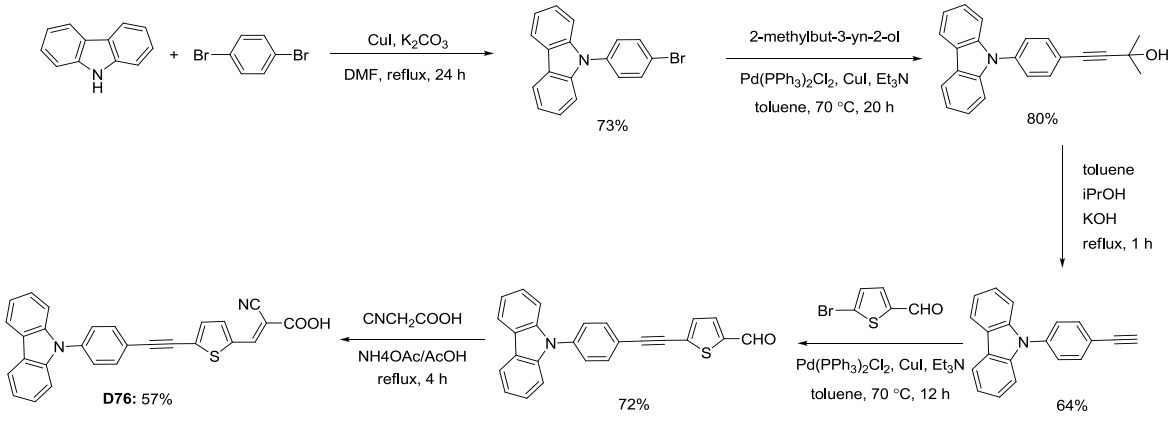

Scheme 1.26 Synthetic scheme of the dye **D76**.

Castellano and co-workers reported an interesting dye (**D78**) with elongated conjugation comprising bithiophene and phenylacetylene segments [116]. The synthetic scheme of the dye **D78** is outlined in Scheme 1.27. 5,5′-dibromo-2,2′-bithiophene reacted with 4-ethynylbenzaldehyde by the Sonogashira coupling gave 4-((5'-bromo-2,2'-bithiophen-5-yl)ethynyl)benzaldehyde which further undergoes Sonogashira coupling with 3,6-di-*tert*-butyl-9-(4-ethynylphenyl)-9*H*-carbazole to obtain 4-((5'-((4-(3,6-di-tert-butyl-9*H*-carbazol-9-yl)phenyl)ethynyl)-2,2'-bithiophen-5-yl)ethynyl)benzaldehyde. It reacted with cyanoacetic acid via Knoevenagel condensation produced the dye **D78**. It exhibited better absorption characteristics when compared to the similar dyes (**D69** and **D70**). This indicated that the bithiophene segment is electron-richer than the carbazole unit. So the bithiophene segment benefits the donor-acceptor interaction. Despite promising absorption qualities, **D78** exhibited poor efficiency when compared to **DL7** and **DL8** (shown in Chart 1.83). The poor performance of **D78** is assigned to low V_{OC} which may originate from the dye aggregation. Dye aggregation may open electron recombination pathways.

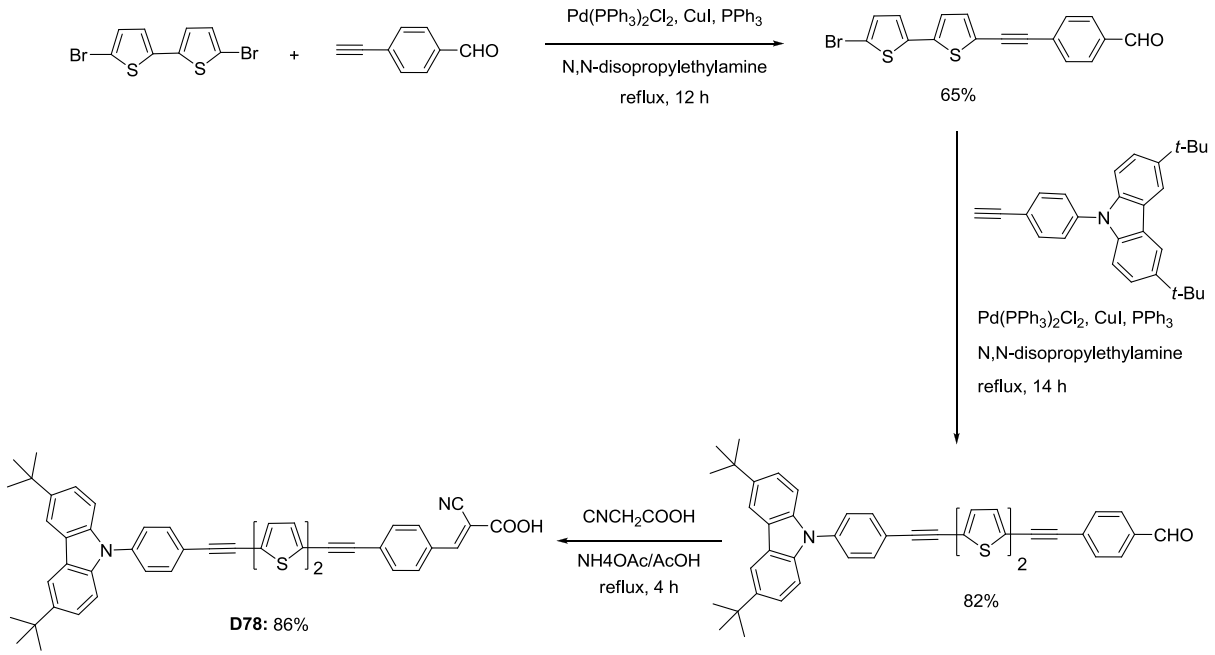

Scheme 1.27 Synthetic scheme of the dye **D78** containing 3,6-di-*tert*-butyl-9*H*-carbazole as donor with acetylene conjugation.

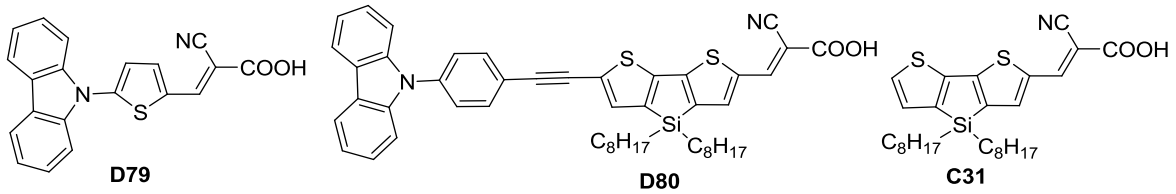

Chart 1.34 Organic dyes contain *N*-substituted carbazole donor and acetylene conjugation.

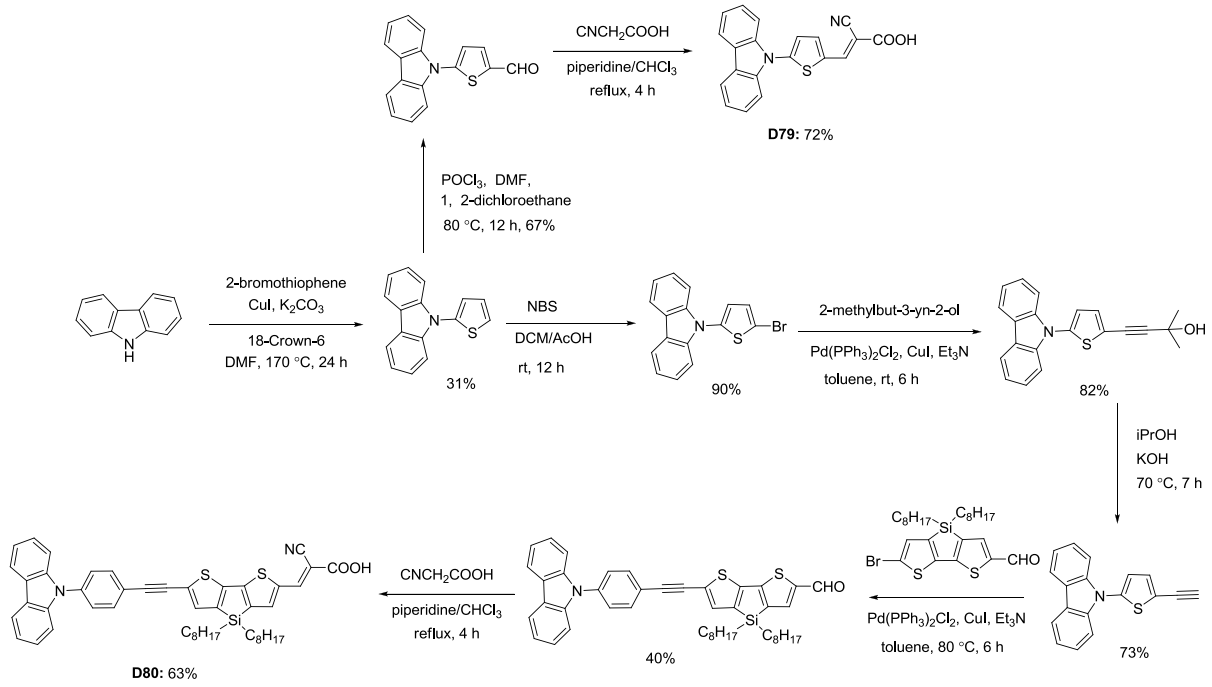

Scheme 1.28 Synthetic scheme of the dyes **D79** and **D80**.

Wang and co-workers [117] synthesized a set of dyes (**D79, D80** and **C31**; Chart 1.34) by using *N*-substituted carbazole donor and thiophene/dithieno[3,2-*b*:2′,3′-*d*]silole as linkers with cyanoacrylic acid acceptor/anchoring unit. The synthesis of the dyes is outlined in Scheme 1.28. Ullmann coupling of carbazole and 2-bromothiophene to afforded 9-(thiophen-2-yl)-9*H*-carbazole. Monobromination of 9-(thiophen-2-yl)-9*H*-carbazole, subsequent reaction with 2-methylbut-3-yn-2-ol under via Sonogashira coupling followed by reaction with potassium hydroxide/isopropanol solution to afford 9-(5-ethynylthiophen-2-yl)-9*H*-carbazole. Sonogashira coupling of 9-(5-ethynylthiophen-2-yl)-9*H*-carbazole with 4,4-dioctyl-6-bromo-dithieno[3,2-*b*:2′,3′-*d*]silole-2-carbaldehyde gave 6-(1-(2-(carbazol-9-yl)-thiophen-5-yl)-ethynyl)-4,4-dioctyl dithieno[3,2-*b*:2′,3′-*d*]silole-2-carbaldehyde. It converted to **D80** via Knoevenagel condensation with cyanoacetic acid. **D79** was obtained by the conversion of 9-(thiophen-2-yl)-9*H*-carbazole to 5-(9*H*-carbazol-9-yl)thiophene-2-carbaldehyde via Vilsmeier-Haack reaction followed by

Knoevenagel condensation. **C31** obtained by Knoevenagel condensation reaction of 4,4′-dioctyl-dithieno[3,2-*b*:2′,3′-*d*]silole-2-carbaldehyde and cyanoacetic acid. The dye **D79** showed red shifted absorption and higher power conversion efficiency (4.80%) compared to dye **D76** due to introduction of dithieno[3,2-*b*:2′,3′-*d*]silole instead of thiophene led to better donor-acceptor interactions. Also it displayed red shifted absorption than compared to **D79** and **C31** due to introduction of dithieno[3,2-*b*:2′,3′-*d*]silole and carbazole unit, respectively. The incorporation of dithieno[3,2-*b*:2′,3′-*d*]silole (**D80**) lowered the LUMO level of the dye which facilitates the electron injection thermodynamically and achieved highest J_{SC} of 10.54 mA cm^{-2} than compared to **C31** (J_{SC} = 6.48 mA cm^{-2}).

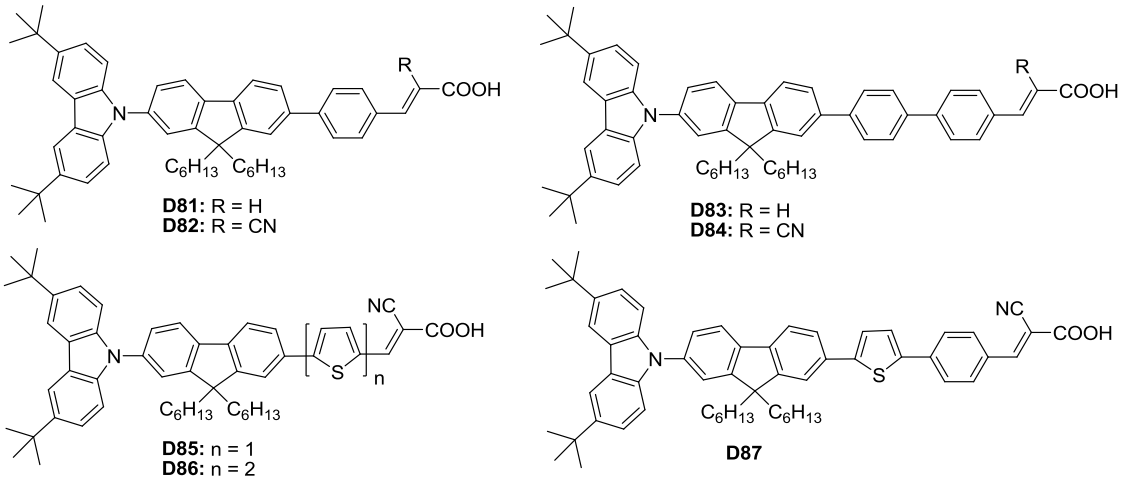

Chart 1.35 Organic dyes containing 3,6-di *tert*-butyl carbazole donor with varied π-conjugated linkers.

Promarak and co-workers [118, 119] theoretically studied the organic dyes (**D81-D84**; Chart 1.35) based on the carbazole donor, fluorene linker, phenyl/thiophene conjugation and acrylic acid/cyanoacrylic acid acceptor by using density functional theory at B3LYP/6-31G (d,p) level [120]. The vertical excitation energies and absorption spectra of the dyes are calculated using time dependent density functional theory. The adsorptions of these dyes on TiO_2 anatase (101) were carried out by using a 38 [TiO_2] cluster model using Perdew-Burke-Ernzerhof functional [121] with the double numerical basis set with polarization. The intra molecular charge transfer from electron donor group to anchoring group of **D82** and **D84** is shown better than the other dyes. The obtained results indicated that the dyes with strong withdrawing CN group have easier injected electron to the CB of semiconductor implying that **D82** and **D84** show better

performance among four dyes. The introduction of thiophene units instead of phenyl linker resulted dyes (**D85-D87**) significantly improved the intra molecular charge transfer transition. In dye **D86** the performance of intra molecular charge transfer significantly affected due to the inter-ring torsion of thiophene-thiophene being decreased compared with phenylene-phenylene spacer of **D83**. It was observed that with increasing the number of π-conjugated unit facilitate the well charge separation between the highest occupied molecular orbital (HOMO) and the lowest unoccupied molecular orbital (LUMO) of these dyes led to a larger photocurrent generation. From the results, the calculated adsorption energies of these dyes on TiO_2 cluster (14 kcal/mol) indicating that these dyes strongly bind to TiO_2 surface. The frontier molecular orbital shapes of the HOMO and LUMO bind to TiO_2 cluster clearly showed that electron injection takes place through intra molecular charge transfer transition.

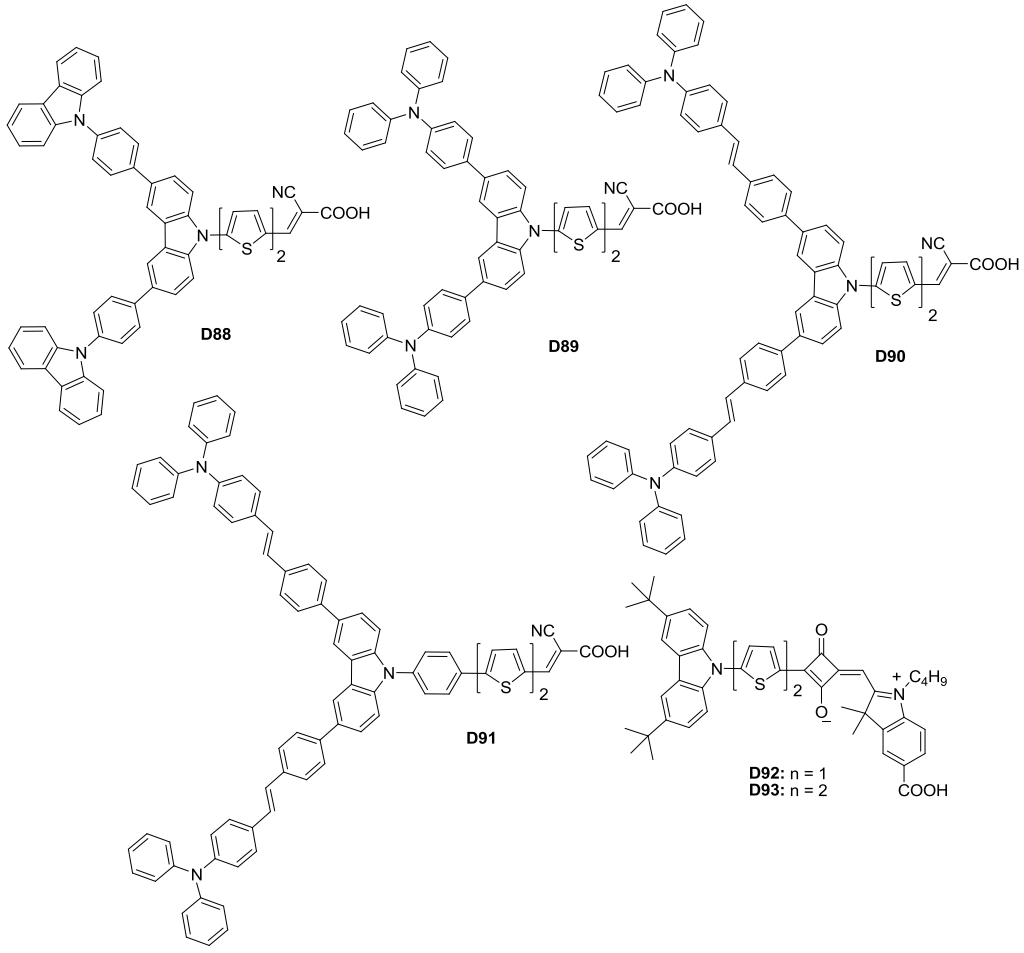

Chart 1.36 Dyes featuring carbazole as donor and auxiliary donor and squaraine-based dyes.

Ko and co-workers [122] synthesized dyes (**D88**–**D91;** Chart 1.36) and shown that the LUMO of the molecules can be fine tuned by proper functionalization at the C3 and C6 positions. The synthesis of the dyes is showed in Scheme 1.29. 3,6 diaryl carbazole derivatives prepared by using Suzuki and Heck coupling reaction [123] and followed by Ullmann coupling with bromo aromatic aldehydes and then subsequently converted to dyes via Knoevenagel condensation. The presence of triphenylamine auxiliary donor in **D89**–**D91** raises the LUMO level when compared to carbazole auxiliary donor (**D88**). The high lying LUMO of **D89**–**D91** provided more thermodynamic driving force for the injection of electron from the excited state of dyes to CB of TiO_2. This resulted in higher J_{SC} for the devices based on these dyes when compared to a dye, **D88**, containing carbazole as auxiliary donor. The dyes containing vinylene linkages (**D90** and **D91**) exhibited high molar extinction coefficients in the absorption spectra. Despite similar absorption properties, the dye **D88** showed very low V_{OC} when compared to **D89**. Probably, the high oxidation potential of **D88** is hampering dye regeneration and reduces the electron density at CB of TiO_2. The longer conjugation pathway present in **D91** led to a red-shifted absorption, which results in comparatively higher J_{SC} (13.70 mA cm^{-2}) and efficiency (6.52%) in the series. The authors found that the DSSC based on the dye **D91** is quite stable up to 1000 h under visible light soaking at 60 °C.

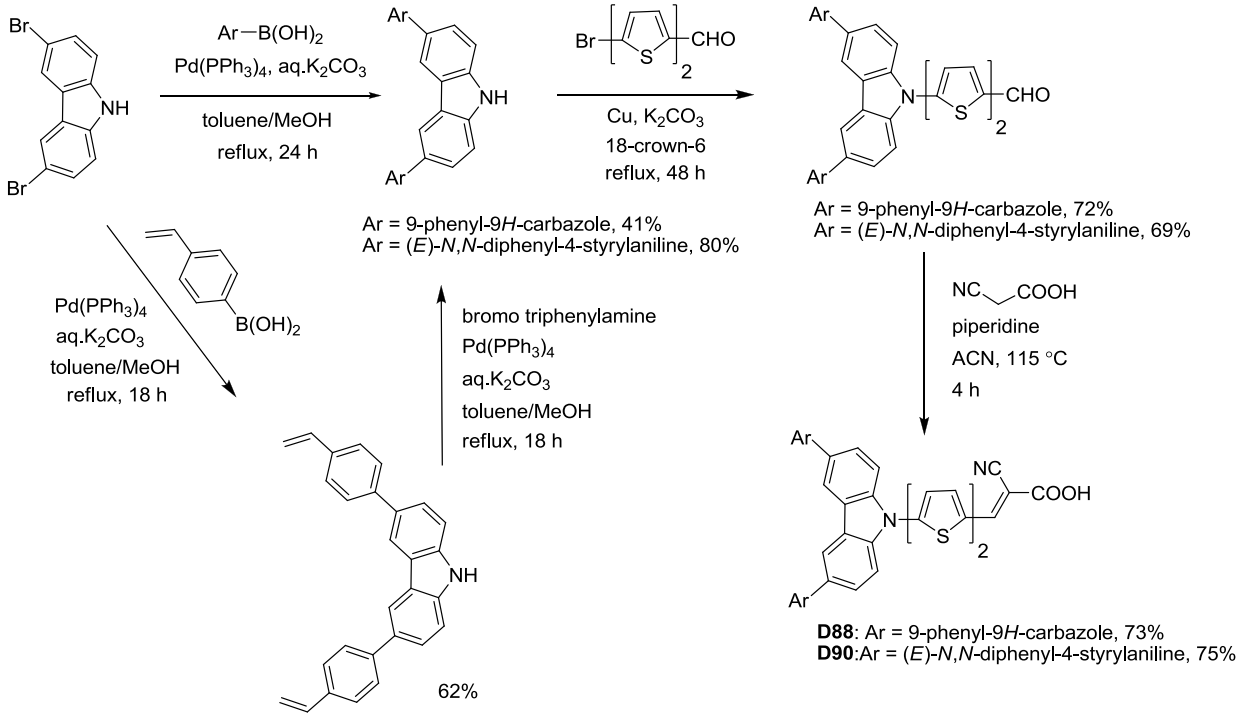

Scheme 1.29 Synthetic scheme of the dyes **D88** and **D90**.

Wu and co-workers first time prepared and characterized another interesting class of organic dyes (Chart 1.36) integrating carbazole and squaraine chromophores to realize panchromatic absorption [124]. In this design, they have used carbazole as donor and thiophene/bithiophene bridged squaraine as acceptor and anchoring unit. The synthesis of the dyes (**D92**, **D93**) is displayed in Scheme 1.30. Friedel-Crafts alkylation of 3,6-di-*tert*-butyl-9-(thiophen-2-yl)-9*H*-carbazole with 3,4-dichlorocyclobut-3-ene-1,2-dione in presence of $AlCl_3$ to afford 3-chloro-4-(5-(3,6-di-*tert*-butyl-9*H*-carbazol-9-yl)thiophen-2-yl)cyclobut-3-ene-1,2-dione, which was subsequently treated with aq. HCl to from hydroxyl substituted derivative. This was condensed with 5-carboxy-2,3,3-trimethyl-1-butyl-3*H*-indolium iodide to gave the final target dye **D92**. The synthesis of **D93** is same as **D92** by starting with 9-(2,2'-bithiophen-5-yl)-3,6-di-*tert*-butyl-9*H*-carbazole.

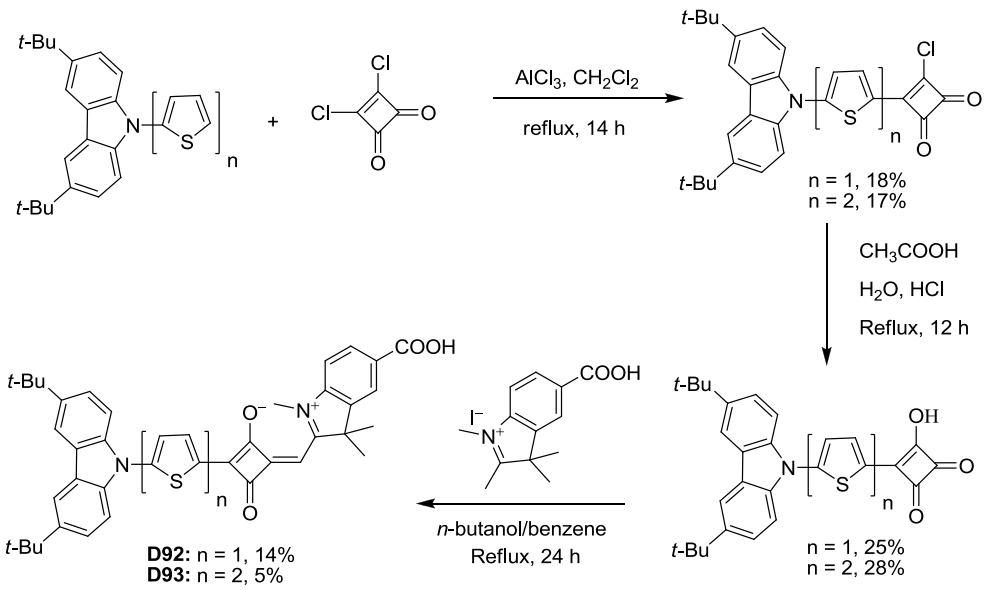

Scheme 1.30 Synthetic scheme of the dyes **D92** and **D93**.

The dyes **D92** and **D93** are showing nice absorption properties covering the range of 500 nm to 700 nm with high molar extinction coefficients. The dye **D93** possessing bithiophene linker showed red shifted absorption with higher molar extinction coefficient than compared to **D92** which contains thiophene linker. The DSSCs of **D92** and **D93** displayed higher J_{SC} and larger V_{OC} when compared to the corresponding dyes without carbazole donor. The dye **D92** achieved high power conversion efficiency of 2.59% than **D93** (η = 2.22%) due to lower V_{OC} of the later dye.

Recently, Su and co-workers synthesized a set of dyes (**D94**–**D97;** Chart 1.37) where carbazole acted as a donor via *N*9-position with various oligothiophene units as linker and cyanoacrylic acid as an acceptor [125]. The dye **D97** has dendritic carbazole donor. The absorption and molar extinction coefficients of the dyes increased with increase in length of conjugation of oligothiophene. The dye **D96** showed most red shifted absorption due to the incorporation of electron rich terthiophene linker. However, the absorption of dye **D97** was blue shifted due to the presence of two carbazole units on the donor unit. The dye **D96** has high conversion efficiency of 4.30% compared to **D94** and **D95** due to higher light harvesting property. Over all the efficiency of **D97** (4.86%) was higher compared to other dyes owing to highest J_{SC} of 14.94 mA cm^{-2}. The dendritic carbazole donor disfavors the aggregation and led to higher V_{OC} of 770 mV. Later they have used donor composed of thiophene substituted at 3 and 6 positions of carbazole and oligothiophene linkers produced **D98-D101 (**Chart 1.37) [126]. They found that the introduction of thiophene increases the electron richness of the carbazole donor and facilitates the donor-acceptor interactions and red shifted absorption than compared to dyes (**D94-D96**). When compared to the parent dye **D95**, the dyes **D99-D101** showed superior J_{SC} due to thiophene substitution favoring better light harvesting properties. Among thiophene substituted carbazole donor dyes, the dye **D101** exhibited highest power conversion efficiency of 5.55% with J_{SC} of 12.14 mA cm^{-2}.

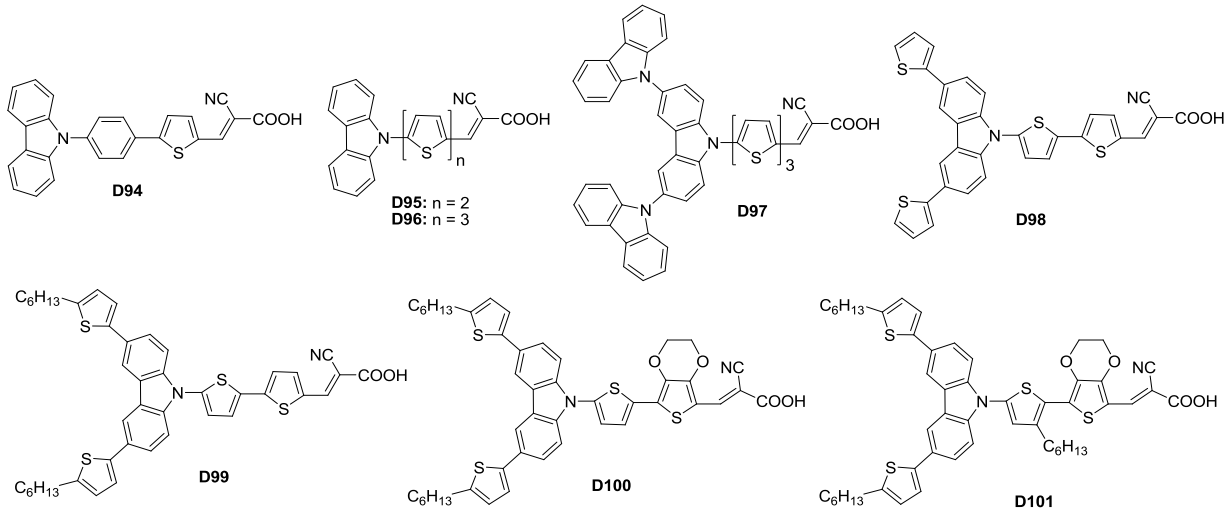

Chart 1.37 Starburst organic dyes containing carbazole/3,6 di-substittuted carbazole donor with thiophene elongated conjugation.

The synthetic scheme of the dyes (**D95**, **D97** and **D99**) is displayed in Scheme 1.31. The key intermediates, 3,6-di(9*H*-carbazol-9-yl)-9*H*-carbazole prepared via Ullmann type coupling of *tert*-butyl 3,6-diiodo-9*H*-carbazole-9-carboxylate with carbazole and 3,6-bis(5-hexylthiophen-2-yl)-9*H*-carbazole prepared via Suzuki coupling of *tert*-butyl 3,6-diiodo-9*H*-carbazole-9-carboxylate with 2-(5-hexylthiophen-2-yl)-4,4,5,5-tetramethyl-1,3,2-dioxaborolane. Ullmann type coupling of carbazole/3,6 disubstituted carbazole derivatives with 5'-bromo-2,2'-bithiophene-5-carbaldehyde gave aromatic carbaxaldehyde derivative which subsequently converted to target dyes (**D95, D97** and **D99**) by reacting with cyanoacetic acid via Knoevengel condensation. Same synthetic strategy used to prepare other dyes (**D98-D101**).

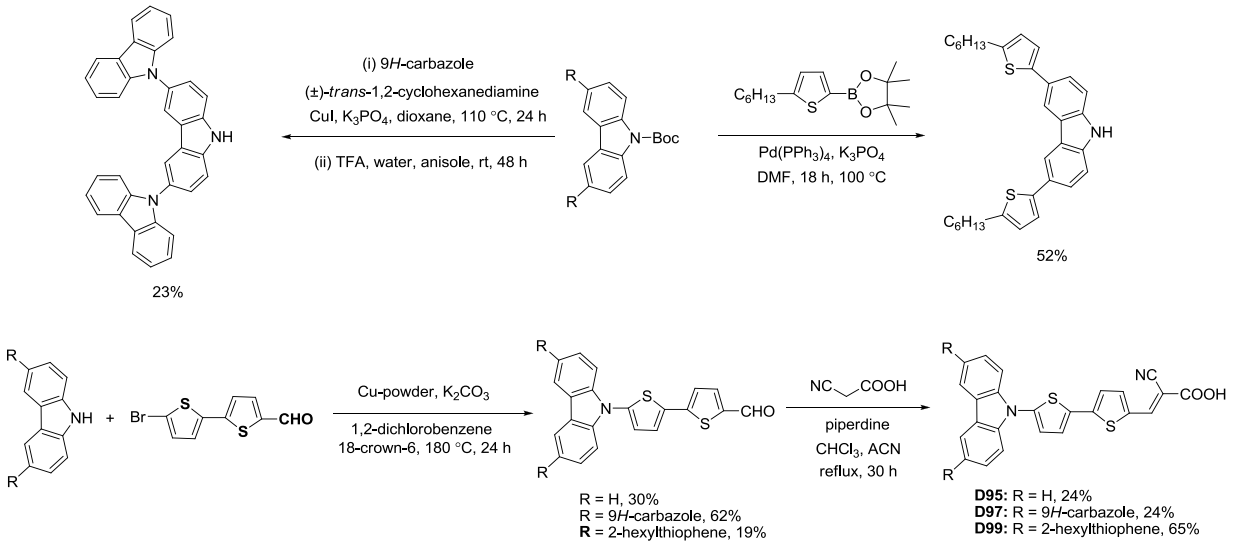

Scheme 1.31 Synthetic scheme of the carbazole dyes.

Wu and co-workers designed and synthesized four dyes with D-π-A configuration and correlated the photophysical and electron transfer mechanism from dye to TiO_2 cluster [127]. The dyes (**D102-D104** and **C32;** Chart 1.38) features 3,6-di-*tert*-butyl-9*H*-carbazole as a donor, cyanoacrylic acid as an acceptor which are connected together by conjugated bridge CPDT and oligothiophenes units. The synthetic scheme of the dyes is outlined in Scheme 1.32. Ullmann coupling of 3,6-di-*tert*-butyl-9*H*-carbazole with 2-bromothiophene afford 3,6-di-*tert*-butyl-9-(thiophen-2-yl)-9*H*-carbazole, which is treated with *n*-BuLi followed by addition tributyltinchloride gave the 3,6-di-*tert*-butyl-9-(5-(tributylstannyl)thiophen-2-yl)-9*H*-carbazole in quantitative yield. This tin reagent underwent Stille reaction with gave the carbazole containing

aldehyde derivative which converted to dye **D102** by Knoevenagel condensation with cyanoacetic acid.

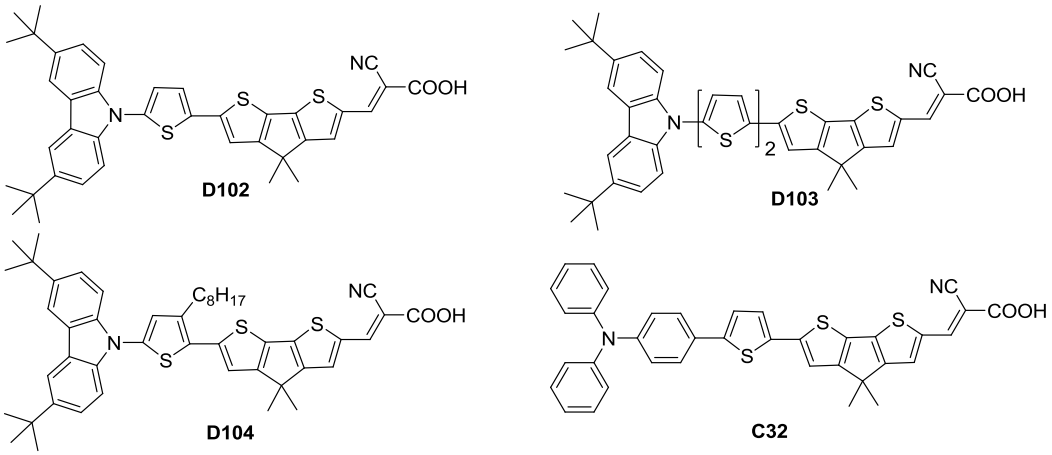

Chart 1.38 Organic dyes with *N*-substituted carbazole as donor and varied conjugation pathways.

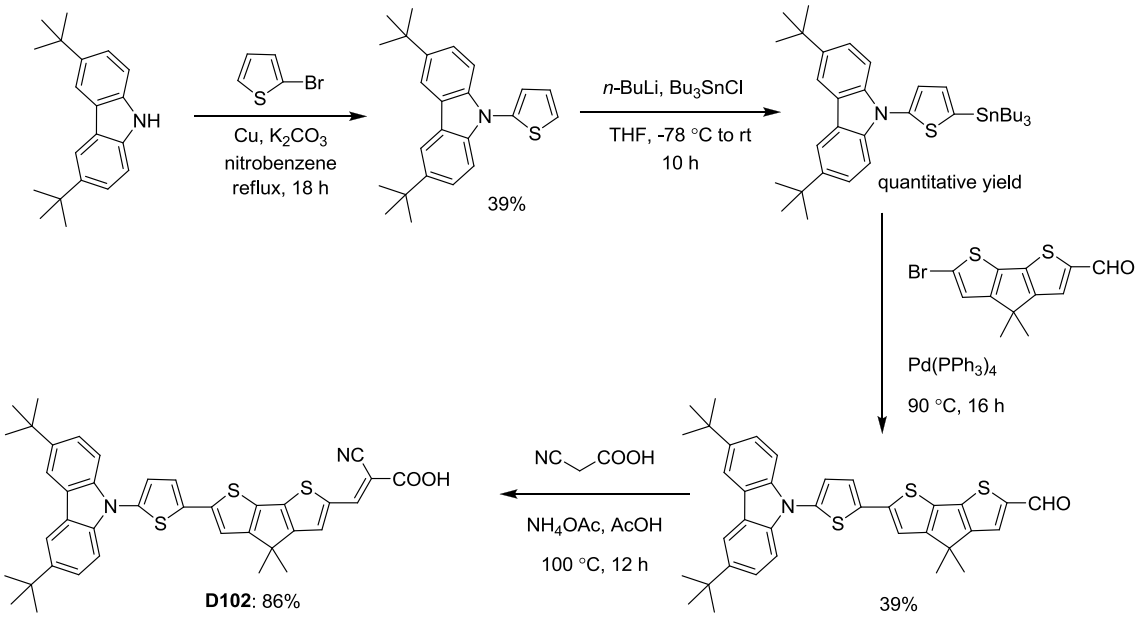

Scheme 1.32 Synthetic scheme of the dye **D102**.

The dye with extending conjugation (**D102-D104**) showed red shifted absorption due to efficient donor-acceptor interactions. The experimental J_{SC} values are in agreement with the theoretical predicated values. The J_{SC} mainly depends on the electron injection and charge transfer of electron from dye to the CB of TiO_2. The dyes follow the direct and indirect electron

injection but, dye **D103** follows mainly indirect mechanism thus led to lower J_{SC}. The dye **D102** gave the highest conversion efficiency of 4.78% among the carbazole donor containing dyes (**D103** and **D104**) due to highest J_{SC} of 10.52 mA cm^{-2}. However, the lower donating strength of carbazole compared to triphenylamine donor (**C32**; η = 5.39%) manifested in the inferior conversion efficiency.

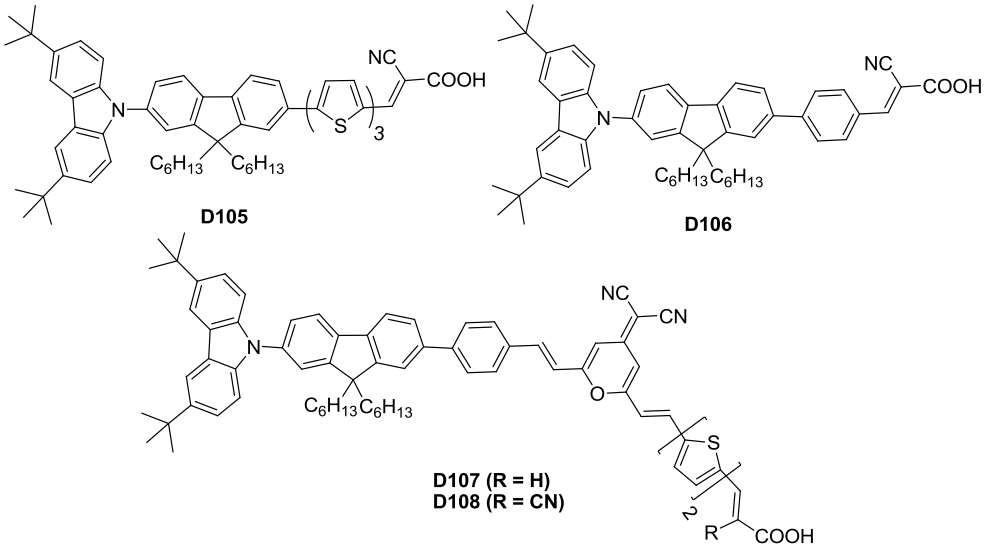

Chart 1.39 Structure of the dyes containing carbazole as donor and fluroene as linker.

Promarak and co-workers designed and synthesized the dyes **D105** and **D106** (Chart 1.39) which contains 3,6-di-*tert*-butylcarbazole as a donor, fluorene as linker and cyanoacrylic acid as acceptor/anchoring unit [128]. Synthesis of dyes is outlined in Scheme 1.33. Key intermediate 9-(7-bromo-9,9-dihexyl-9*H*-fluoren-2-yl)-3,6-di-*tert*-butyl-9*H*-carbazole was synthesized by Ullmann coupling of available 2,7-dibromo-9,9-bishexylfluorene with 3,6-di-*tert*-butylcarbazole. It underwent Suzuki coupling with 2-thiopheneboronic acid and bromination reactions in an iterative manner gave 9-(7-(5'-bromo-2,2'-bithiophen-5-yl)-9,9-dihexyl-9*H*-fluoren-2-yl)-3,6-di-*tert*-butyl-9*H*-carbazole, which further underwent Suzuki coupling with 5-formylthiophene-2-boronic acid gave 5″-[7-(3,6-di-*tert*-butylcarbazol-*N*-yl)-9,9-dihexylfluorene-2-yl]-2,2′:5′,2″-terthiophencarbaldehyde. Knoevenagel condensation of this aldehyde with cyanoacetic acid gave the desired cyanoacrylic acid dye (**D105**). Suzuki coupling of 9-(7-bromo-9,9-dihexyl-9*H*-fluoren-2-yl)-3,6-di-*tert*-butyl-9*H*-carbazole with 4-formylphenylboronic acid gave 4-(7-(3,6-di-*tert*-butyl-9*H*-carbazol-9-yl)-9,9-dihexyl-9*H*-fluoren-2-yl)benzaldehyde. Knoevenagel conden-

sation of this aldehyde with cyanoacetic acid gave the desired cyanoacrylic acid dye (**D106**). Aldol condensation of the 4-(7-(3,6-di-*tert*-butyl-9*H*-carbazol-9-yl)-9,9-dihexyl-9*H*-fluoren-2-yl)benzaldehyde with excess 2-(2,6-dimethylpyran-4-ylidene)malononitrile in the presence of a catalytic amount of piperidine in THF/MeCN afforded the mono-adduct (*E*)-2-(2-(4-(7-(3,6-di-*tert*-butyl-9*H*-carbazol-9-yl)-9,9-dihexyl-9*H*-fluoren-2-yl)styryl)-6-methyl-4*H*-pyran-4-ylidene)malononitrile. It condensed with 5-bromo-2-formylthiophene under the same conditions to give its bromo derivative which on Suzuki coupling with 5-formyl-2-thiopheneboronic acid provided the corresponding aldehyde. The aldehydes were converted to the desired dyes **(D105** and **D107**) *via* Knoevenagel condensation with malonic acid or cyanoacetic acid, respectively.

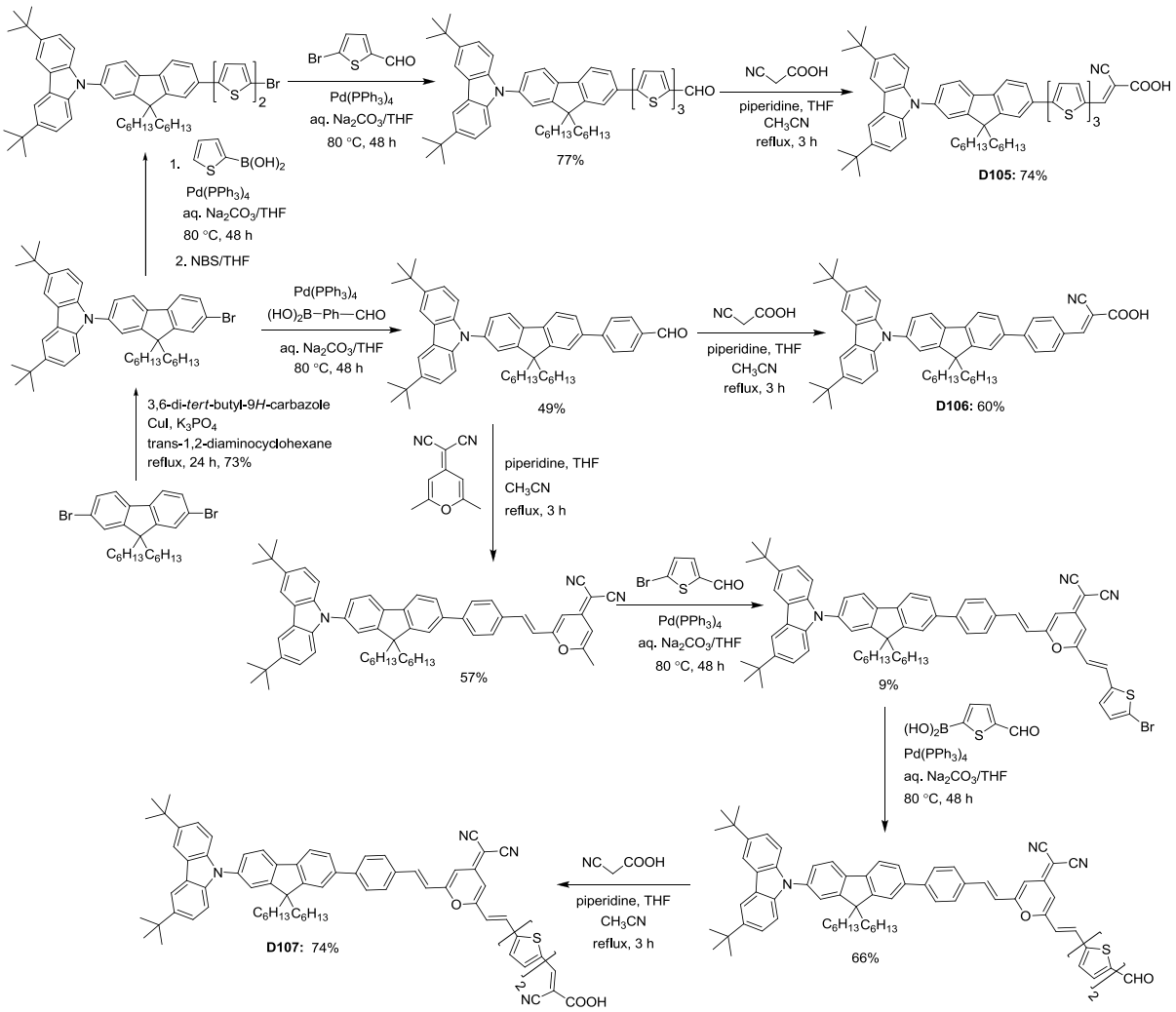

Scheme 1.33 Synthetic scheme of the dyes **D105 –D107**.

The dye **D105** showed power conversion efficiency of 3.64% with J_{SC} of 8.99 mA cm^{-2}, V_{OC} of 620 mV, and *ff* of 0.66. Later they moved from D-π-A to D-π-A-π-A by introducing 2-(4*H*-pyran-4-ylidene)malononitrile as an auxiliary acceptor and synthesized two dyes **D107** and **D108** along with the parent dye **D106** for comparison [129]. The introduction of auxiliary acceptor showed drastic red shifted absorption compared to parent dye **D106**. Overall the dye **D108** has broad absorption and highest efficiency of 3.19% with J_{SC} of 7.14 mA cm^{-2} compared to the dye **D107** due to the absence of cyano group which decreased the *J*sc value (3.70 mA cm^{-2}) resulted in inferior efficiency of 1.64%.

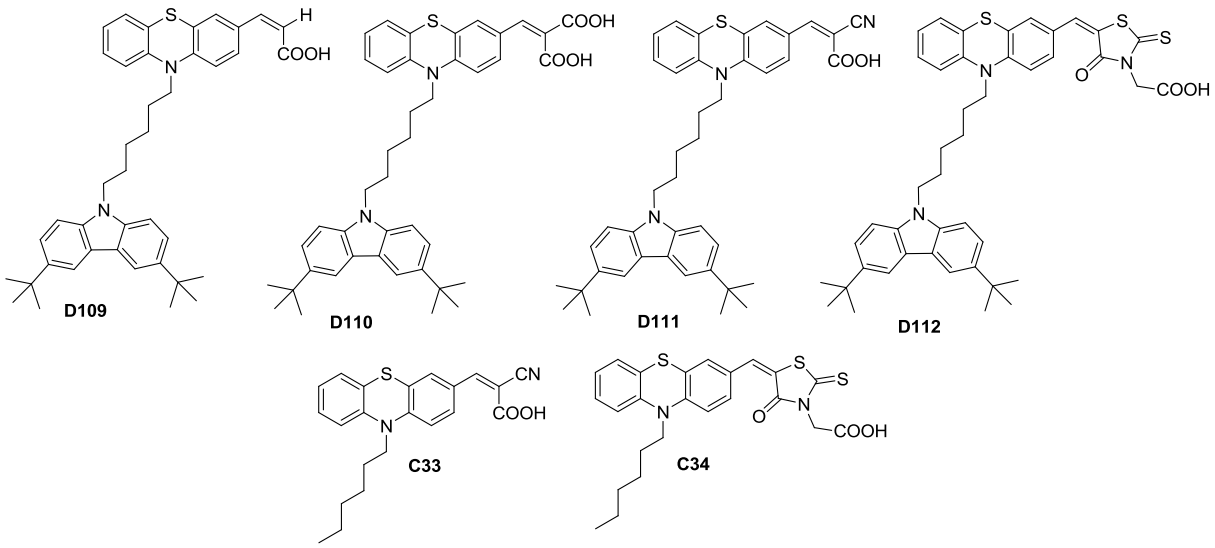

Chart 1.40 Structures of the dyes containing carbazole as antenna connected via alkyl chain and various acceptor units.

Chandrasekaram and coworkers reported a series of dyes (**D109-D112**, **C33** and **C34**; Chart 1.40) based on phenothiazine donor carbazole auxiliary donor and various acceptors such as simple carboxylic acid, malonic acid, cyanoacrylic acid and rhodanine acetic acid [130, 131]. The synthetic scheme of the dyes is displayed in Scheme 1.34. Selective *N*-alkylation of phenothiazine with 1,6-dibromohexane gave 10-(5-bromopentyl)-10*H*-phenothiazine, which is treated with carbazole gave 10-(6-(3,6-di-*tert*-butyl-9*H*-carbazol-9-yl)hexyl)-10*H*-phenothiazine. It was formylated by Vilsmeier-Haack reaction with DMF/$POCl_3$ gave 10-(6-(3,6-di-*tert*-butyl-9*H*-carbazol-9-yl)hexyl)-10*H*-phenothiazine-3-carbaldehyde. Then, the formylated product was subjected to Knoevenagel condensation with malonic acid cyanoacetic acid and rhodanine-3-

acetic acid to afford dyes **D111** and **D112**, respectively. The donors were connected by a non-conjugating alkyl chain. In this system, carbazole has been found to be beneficial for suppressing the back electron transfer, modulate dye aggregation and acts as antenna to harvest photons. The introduction of carbazole unit increases overall efficiency by two folds in the case of rhodanine acetic acid anchoring unit. Among all the dyes, the dye with rhodanine acetic acid showed red shifted absorption while cyanoacrylic acid containing dye exhibited better conversion efficiency (η = 5.8%; J_{SC} = 10.6 mA cm^{-2}). The order of improvement of the photovoltaic performance of dyes with different acceptors followed trend as carboxylic acid < malonic acid < rhodanine acetic acid < cyanoacrylic acid. They also found that the carbazole units closely interact with each other in a face-to-face arrangement and provide an effective blocking layer for the semiconductor surface.

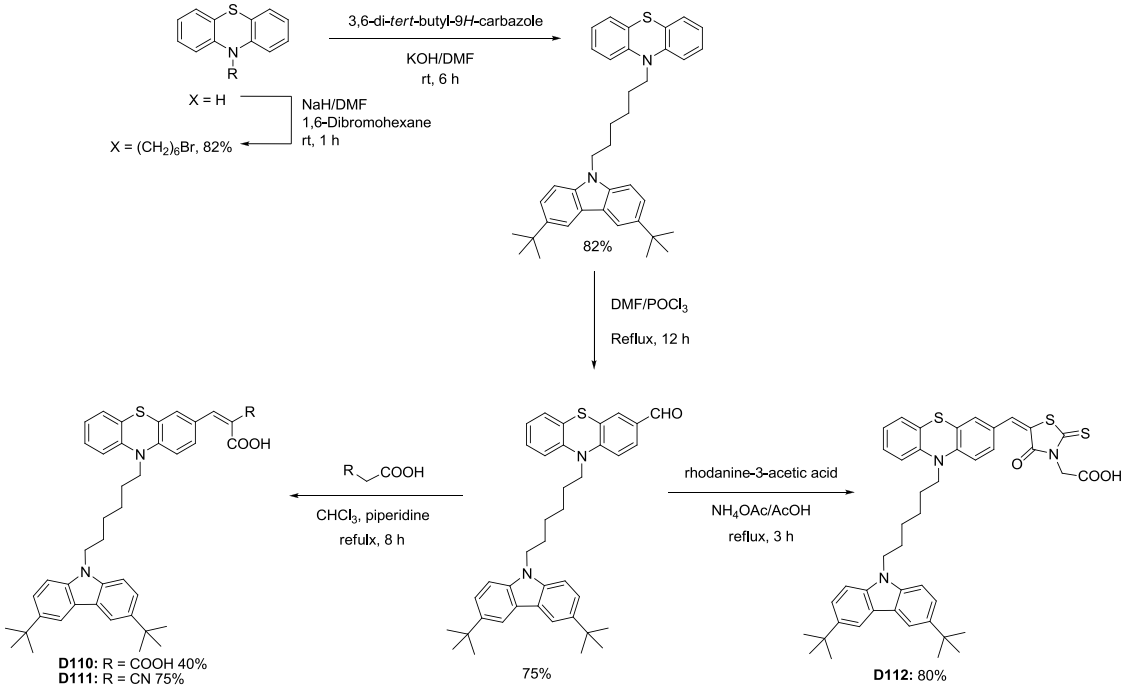

Scheme 1.34 Synthetic scheme of the dyes **D110-D112**.

Carbazole is a weak donor and in most of the dyes designed with carbazole as donor, auxiliary electron-rich chromophores were used to further donor-acceptor interaction and to red-shift the absorption profile. Donor strength in D-π-A architecture can be enhanced by the use of oligomeric carbazoles. Promarak and co-workers designed and synthesized new dyes based on carbazole dendrons as donor [132]. The synthesis of dyes (**D113-D116;** Chart 1.41) is showed in Scheme1.35. First, coupling of each generation of carbazole dendrons (Gn-NH) with 2,5-

dibromothiophene under Ullmann coupling afforded the carbazole dendrons (Gn-NH) thiophenyl bromides. These carbazole containing bromides underwent Suzuki cross-coupling with 5-formylthiophene-2-boronic acid gave the corresponding aldehydes. Finally, these aldehydes were converted to the corresponding cyanoacrylic acids by Knoevenagel condensation with cyanoacetic acid to give the dyes (**D113-D116**). The increase in the size or generation of the carbazole dendritic donor of the dye molecules enhances their total light absorption abilities. Interestingly, fourth generation dye **D116** showed lower conversion efficiency (1.75%) and first generation dye **D113** showed a conversion efficiency of 5.10%. Reason for the poor efficiency of the dendritic dyes is ascribed to their gigantic size which reduces the amount of dye uptake per unit TiO_2.

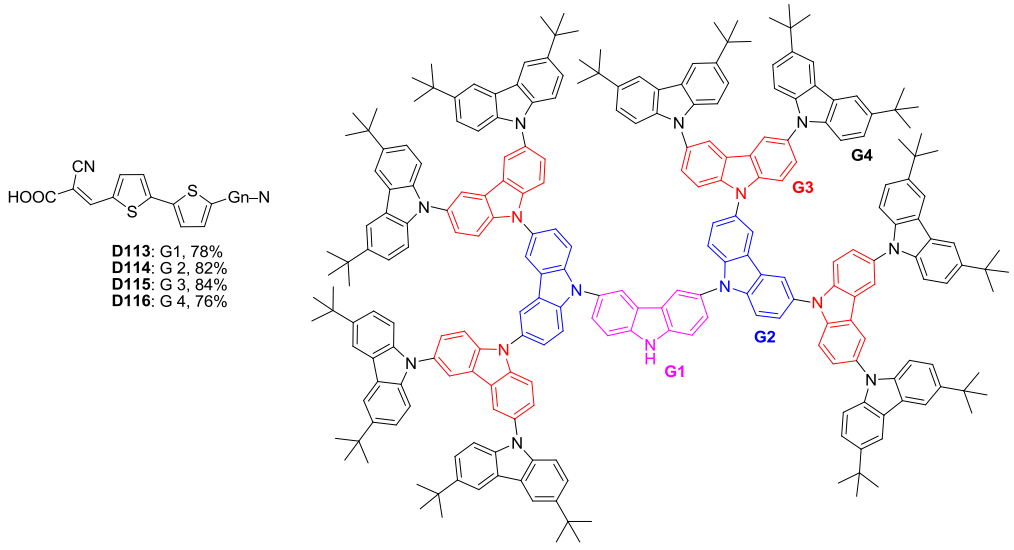

Chart 1.41 Structures of organic dyes containing oligomeric carbazole donor via N-position.

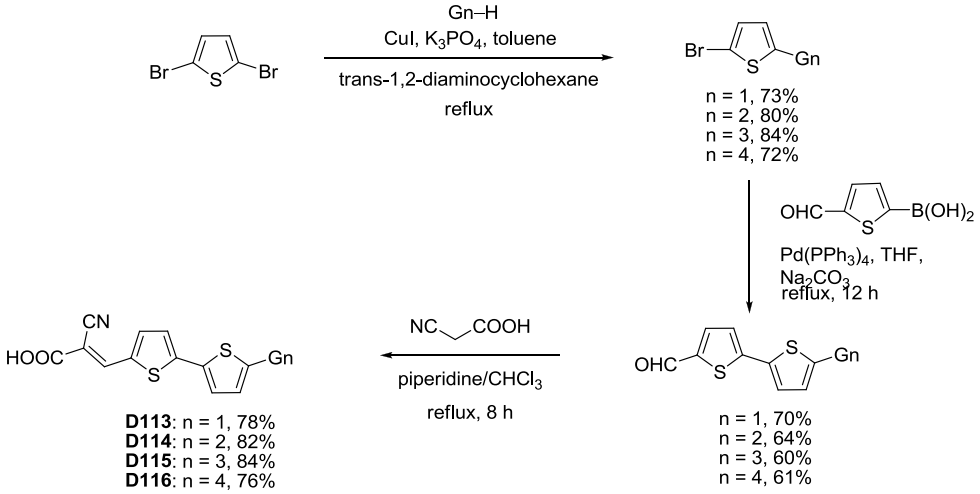

Scheme 1.35 Synthetic scheme of the dyes **D113-D116**.

Liu and coworkers synthesized **D117** which contain carbazole donor [133] and triphenylamine as auxiliary donor with in a D-D-π-π-A configuration (**AD35**-**AD38** shown in Chart 1.77) by using a duplex triphenylamine and carbazole donors for better *V*oc and efficiencies. **D117** showed impressive power conversion efficiency (9.15%). The synthesis of the dye is showed in Scheme 1.36. Suzuki coupling of 7-(5'-bromo-3',4-dihexyl-2,2'-bithiophen-5-yl)-2,3-dihydrothieno[3,4-*b*][1,4]dioxine-5-carbaldehyde with 4-(bis(4-(9*H*-carbazol-9-yl)phenyl)amino)phenylboronic acid gave 7-(5'-(4-(bis(4-(9*H*-carbazol-9-yl)phenyl)amino)phenyl)-3',4-dihexyl-2,2'-bithiophen-5-yl)-2,3-dihydrothieno[3,4-*b*][1,4]dioxine-5-carbaldehyde. It was transformed to **D117** acid via Knoevenagel condensation with cyanoacetic acid.

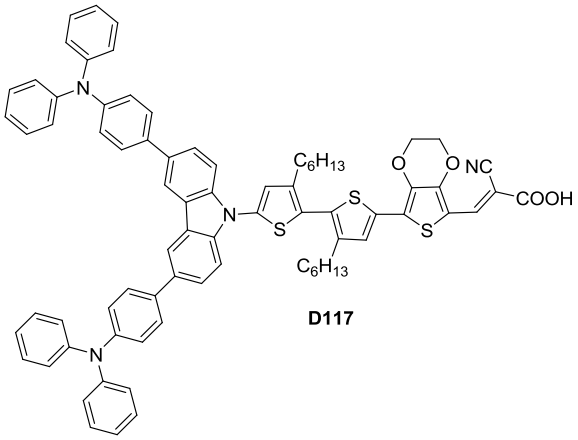

Chart 1.42 Structure of the dye containing main donor and triphenylamine auxiliary donor.

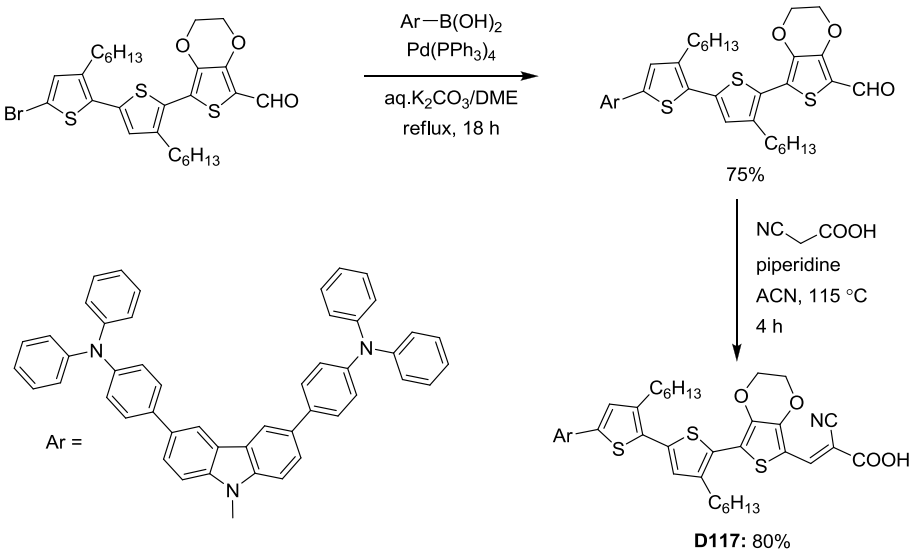

Scheme 1.36 Synthetic scheme of the dye **D117**.

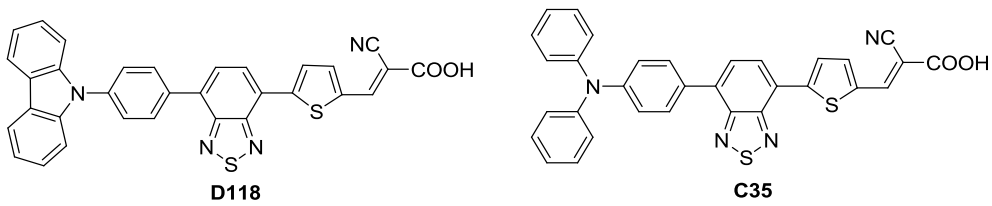

Chart 1.43 Structure of the dye contains carbazole as donor connected at *N*9-position with BTZ as auxiliary acceptor.

Valiyaveettil and co-workers synthesized dyes contiaining carbazole as donor and the dyes with carbazole connected at C2 and C3 position discussed in earlier classification [60]. In this category carbazole served as a donor via *N*9-position and BTZ as auxiliary acceptor. The synthesis of the dyes showed in Scheme 1.1. The dye **D118** showed molar extinction coefficient of higher compared to dyes **D61** and **D1** but lower compared to **D59**–**D61** due to the effect of linkage between the donor and acceptor. The dye **D118** achieved power conversion efficiency of 1.56% with J_{SC} of 3.90 mA cm^{-2}, V_{OC} of 590 mV and *ff* of 0.68. It is clear to say that the carbazole at C3-postion is useful to increase donor-acceptor interactions led to higher efficiency compared to other linkages.

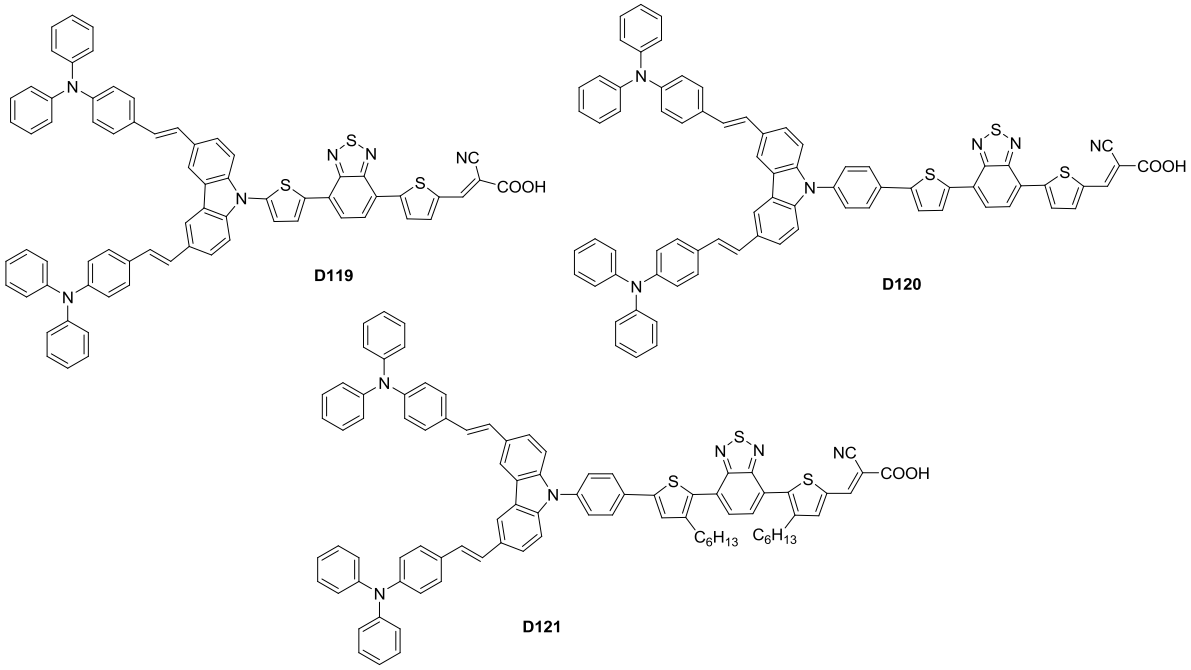

Chart 1.44 Structure of the dye contains duplex triphenylamine and carbazole donors.

Hong and co-workers synthesized three dyes (**D119**-**D121**; Chart 1.44) based on carbazole as donor with substitution at 3 and 6 positions with triphenylamine as auxiliary donor [134]. The synthetic scheme of the dyes (**D119**-**D121**) is outlined in Scheme 1.37. Suzuki coupling of 3,6-bis((*E*)-2-argiovinyl)-9*H*-carbazole with 5-(7-(5-iodothiophen-2-yl)benzo[*c*][1,2,5]thiadiazol-4-yl)thioph-ene-2-carbaldehyde gave the 5-(7-(5-(3,6-bis(4-(diphenylamino)styryl)-9*H*-carbazol-9-yl)thio-phen-2-yl)benzo[*c*][1,2,5]thiadiazol-4-yl)thiophene-2-carbaldehyde. It was condensed with cyanoacetic acid via Knoevenagel condensation to afford dye **D119**. Ullmann coupling of 3,6-bis((*E*)-2-argiovinyl)-9*H*-carbazole with 1-bromo-4-iodobenzene gave 4,4'-(1*E*,1'*E*)-2,2'-(9-(4-bromophenyl)-9*H*-carbazole-3,6-diyl)bis(ethene-2,1-diyl)bis(*N*,*N*-diphenylaniline). Then, this was converted to borolane derivative followed by Suzuki coupling with 5-(7-(5-iodothiophen-2-yl)benzo[*c*][1,2,5]thiadiazol-4-yl)thiophene-2-carbaldehyde gave the corresponding aldehyde derivative which converted to desired dye (**D120**) by Knoevenagel condensation with cyanoacetic acid. The synthesis of dye **D121** is similar to the synthesis of dye **D120**.

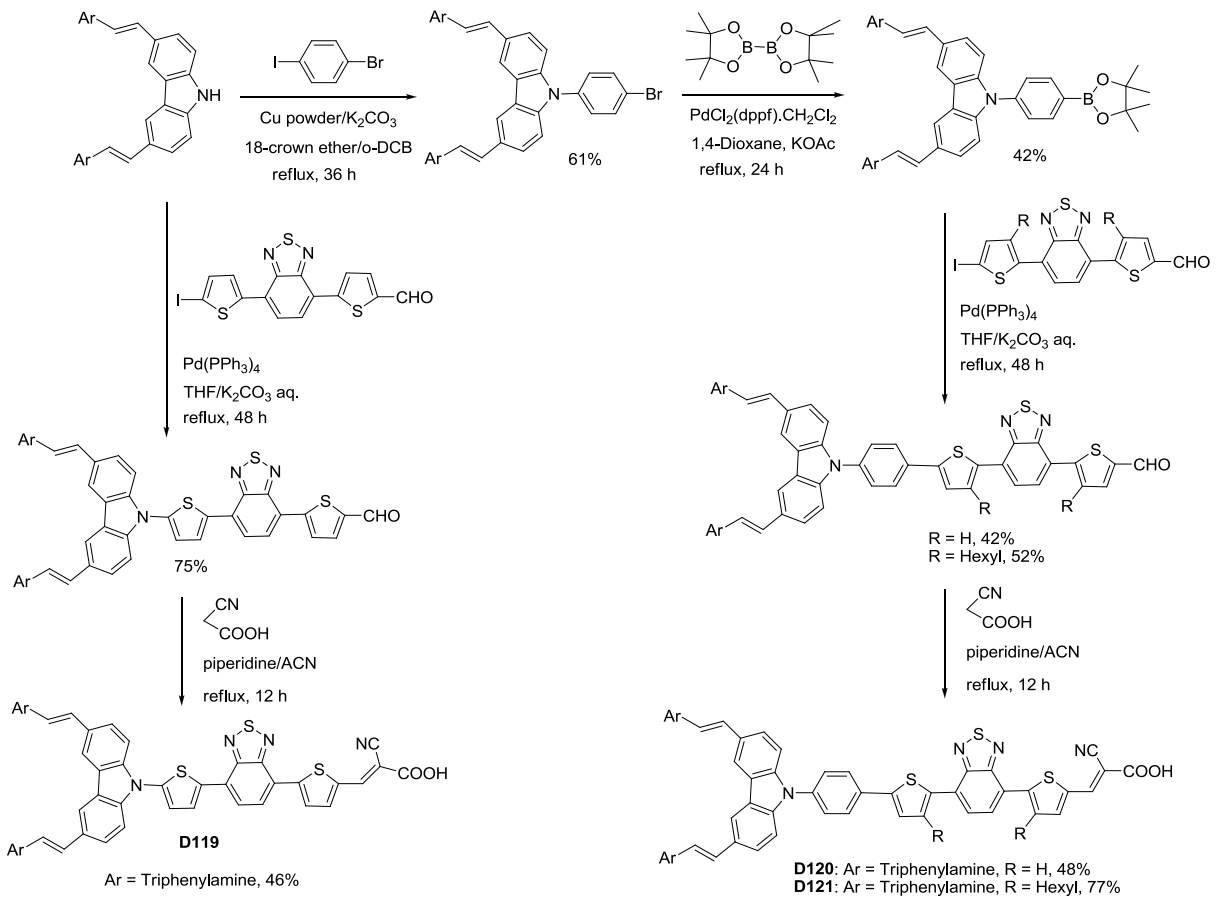

Scheme 1.37 Synthetic scheme of the dyes **D119**-**D121**.

The introduction of auxiliary donor increased the molar extinction coefficient, red shifted the charge transfer transitions and suppression of aggregation on TiO_2 film led to higher *V*oc of devices. The dye **D120** displayed red shifted absorption than **D119** due to the extension of conjugation with phenyl linker. However, blue shift in absorption observed for **D121** due to twisting of conjugation due to alkyl substitution on thiophene unit. The dye **D121** showed an efficiency of 5.11% which is double the conversion efficiency compared to previous dyes (**D1-D2**). The addition of CDCA increases the efficiency up to 6.33% for the dye **D121** and suitable introduction electron rich linkers required to increase the efficiency.

Table 1.3 Optical, electrochemical and photovoltaic performance parameters of dyes containing carbazole as donor

Dye	$\lambda_{max,}$ nm (ε_{max}, M^{-1} cm^{-1})	E_{ox} , V (*vs* NHE)	E_{ox}^{*}, V (*vs* NHE)	J_{SC} (mA cm^{-2})	V_{OC} (mV)	*ff*	η (%)	*Ref*
D68	374 (12300)	1.59	−1.09	4.00	1156	0.80	3.68	[107]
C27	438 (39085)	1.14	−1.46	4.78	608	0.70	2.03	[111]
C28	408 (23083)	1.05	−1.75	4.45	587	0.70	1.83	[111]
D68	401 (17690)	1.06	−1.76	4.25	586	0.71	1.77	[111]
D69	381 (7800)	1.46	−1.35	4.71	1091	0.79	4.05	[108]
D70	438 (71000)	1.55	−0.89	8.47	470	0.60	2.39	[110]
D71	468 (73200)	1.55	−0.78	10.90	400	0.57	2.48	[110]
D72	429 (20900)	1.38	−0.96	7.12	939	0.78	5.22	[108]
D73	416 (27400)	1.48	−1.15	5.83	1033	0.77	4.61	[108]
D74	378 (10800)	1.45	−1.38	3.88	1077	0.78	3.28	[108]
D75	601[a]	1.29	−0.78	11.00	779	0.72	6.00	[112]
C30	669[a]	0.87	−0.99	12.00	758	0.69	6.10	[112]
C29	624[a]	1.05	−0.94	10.00	806	0.70	5.80	[112]
D76	409 (41536)	2.00	−0.59	2.19	601	0.63	0.82	[113]
D77	375 (27038)	1.84	−0.98	1.71	634	0.64	0.70	[113]
D78	420 (16420)	na	na	7.03	523	0.61	2.23	[116]

[a]Absorption edge wavelength; na = not available

Table 1.3 (cont.)

Dye	$\lambda_{max,}$ nm (ε_{max}, M^{-1} cm^{-1})	E_{ox} , V (*vs* NHE)	E_{ox}^{*}, V (*vs* NHE)	J_{SC} (mA cm^{-2})	V_{OC} (mV)	*ff*	η (%)	*Ref*
D79	400	1.10	−1.43	6.48	620	0.71	2.83	[117]
D80	450	0.98	−1.26	10.54	680	0.67	4.80	[117]
C31	409	1.35	−1.11	1.64	520	0.67	0.57	[117]
D88	393 (29000)	1.51	−1.23	6.32	530	0.72	2.41	[122]
D89	393 (28300)	1.11	−1.60	12.20	600	0.77	5.64	[122]
D90	386 (96900)	0.97	−1.80	13.00	630	0.75	6.14	[122]
D91	441 (37500)	1.01	−1.64	13.70	680	0.70	6.52	[122]
D92	603	1.17	−0.75	8.00	473	0.68	2.59	[124]
D93	612 (13400)	0.93	−1.00	8.17	411	0.66	2.22	[124]
D94	416 (8700)	0.74	−1.82	6.17	601	0.74	2.74	[125]
D95	440 (8700)	0.80	−1.58	6.70	589	0.74	2.94	[125]
D96	467 (17300)	0.65	−1.64	9.98	586	0.74	4.30	[125]
D97	465 (34600)	0.67	−1.63	10.65	643	0.71	4.86	[125]
D98	434 (8800)	0.85	−1.61	8.70	574	0.72	3.59	[126]
D99	436 (22400)	0.86	−1.57	10.43	615	0.71	4.54	[126]
D100	461 (37500)	0.90	−1.53	11.30	632	0.72	5.15	[126]
D101	451 (46400)	0.89	−1.55	12.14	652	0.71	5.55	[126]
D102	490 (65157)	0.98	−1.28	10.52	660	0.69	4.78	[127]
D103	501 (71446)	0.90	−1.32	9.74	620	0.71	4.33	[127]
D104	485 (62232)	1.20	−1.12	7.21	660	0.71	3.38	[127]
C32	505 (84006)	0.90	−1.31	11.91	660	0.69	5.39	[127]
D105	460 (23868)	1.07	−1.21	8.99	620	0.66	3.64	[128]
D106	351 (36524)	1.17	−1.64	2.78	620	0.71	1.23	[128]
D107	455 (47311)	1.19	−0.95	3.70	600	0.73	1.64	[128]
D108	467 (60911)	1.19	−0.97	7.14	620	0.72	3.19	[128]
D109	376 (19035)	1.67	−1.71	4.50	722	0.73	2.40	[131]
D110	380 (13566)	1.63	−1.87	6.70	724	0.74	3.60	[131]

Table 1.3 (cont.)

Dye	$\lambda_{max,}$ nm (ε_{max}, M^{-1} cm^{-1})	E_{ox} , V (*vs* NHE)	E_{ox}^{*}, V (*vs* NHE)	J_{SC} (mA cm^{-2})	V_{OC} (mV)	*ff*	η (%)	*Ref*
D111	435 (19000)	na	na	10.80	779	0.75	6.30	[130]
D112	460 (32000)	na	na	6.70	541	0.70	2.50	[130]
C33	440 (14000)	na	na	10.50	719	0.76	5.80	[130]
C34	465 (29000)	na	na	12.70	610	0.72	5.60	[130]
D113	435 (16500)	1.12	−1.54	9.89	720	0.73	5.10	[132]
D114	415 (22900)	1.06	−1.55	7.73	690	0.71	3.81	[132]
D115	413 (24400)	0.99	−1.65	5.70	660	0.68	2.55	[132]
D116	413 (32090)	0.98	−1.69	3.99	630	0.69	1.75	[132]
D117	490 (30700)	1.39	−0.80	18.42	745	0.67	9.15	[133]
D118	445 (23993)	1.25	−0.56	3.90	590	0.68	1.56	[60]
D119	488 (20635)	0.90	−1.46	9.14	540	0.67	3.32	[134]
D120	498 (19680)	0.90	−1.41	10.01	550	0.68	3.70	[134]
D121	376 (116745)	0.94	−1.57	11.11	700	0.66	5.11	[134]

na = not available

1.3 Carbazole as a π-linker

The efficiency of DSSC is mainly affected by two processes, namely, dye aggregation and charge recombination. Since the organic dye structure plays a major role in the above two processes, molecular engineering is an effective way to find the ways to deter them. It has also been generally accepted that altering the nature of the conjugation pathway that bridges the donor and acceptor fragments in an organic dyes is an effective way to fine tune the electronic properties of the dyes. In the construction of organic dyes, scientists have used a wide variety of rigid polyaromatic and heteroaromatic hydrocarbons such as fluorene, [9-11] fluorenone, [135] fluoranthene, [136] pyrene, [16, 17] naphthalene, [137] anthracene, [138] oligophenylene, [139, 140] fused thiophenes, [20-24] dihydrophenanthrene, [141] dibenzothiophene, [15] dibenzofuran, [15] phenothiazine [25, 26] and phenoxazine [27,28] etc. Generally, conjugation pathway comprising electron-rich chromophores have been found to benefit the absorption characteristics. However, very strong electron donors may destabilize the LUMO. So a

chromophore rendering balanced optimization of electronic properties is an ideal bridge. Carbazole, being moderately electron-rich has been widely explored as π-linker in the design of organic dyes. Due to several functionalization possibilities, carbazole has been used as a linker by 2,7-disubstitution or 3,6-disubstitution. Use of 2,7-disubstituted carbazole in the bridge helps to enhance the conjugation and serve as effective charge-delocalizing segment in comparison to the 3,6-disubsituted carbazole. It has been found that 2,7-disubstitution leads to elongation of conjugation pathway and beneficial for absorption properties. Also, 2,7-carbazole-bridged dyes exhibited red-shifted absorptions and lower oxidation potentials than the corresponding fluorene- and phenyl-bridged dyes [55].

1.3.1 Carbazole as a Bridge via C2, C7 Positions

The general molecular design of dyes with 2,7-disubstituted carbazole linker are illustrated schematically in Figure 1.7. The synthesis of the 2,7-dibromo carbazole can be achieved by the reductive cyclization of 4,4'-dibromo-2-nitrobiphenyl [142]. In some cases a central carbazole served as donor for dianchoring bis(acceptor) chromophores.

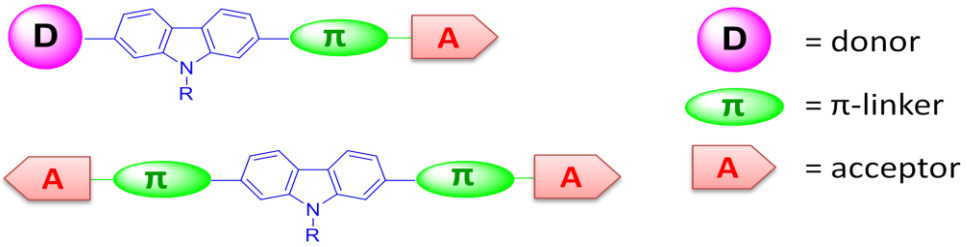

Figure 1.7 Molecular compositions of organic dyes with carbazole as linker via C2, C7-positions.

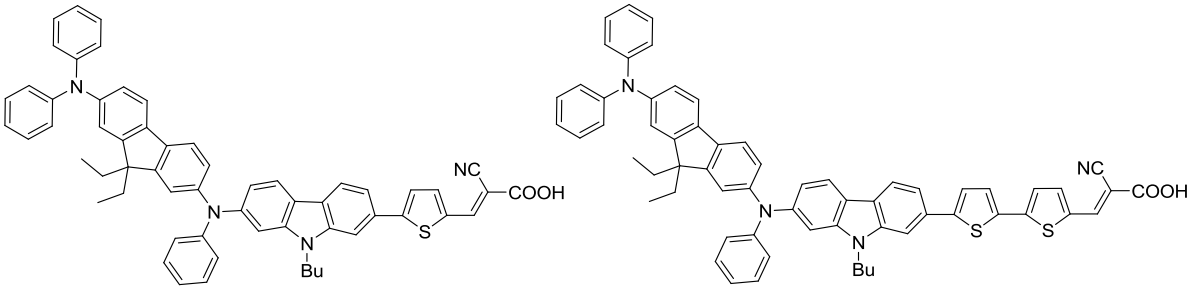

Chart 1.45 Organic dyes featuring 2,7-diaminofluorene donor and 2,7 carbazole linker.

Thomas and co-workers successfully combined the 2,7-diaminofluorene donor and 2,7-disubstituted carbazole linker to obtain two organic dyes **L1** and **L2** (Chart 1.45) [55]. The synthetic scheme of the dyes outlined in Scheme 1.38. It starts with Pd-catalyzed C-N coupling of 9,9-diethyl-*N*,*N*-diphenyl-9*H*-fluoren-2-amine with aniline gave *N*2-(7-bromo-9-butyl-9*H*-carbazol-2-yl)-9,9-diethyl-*N*2,*N*7,*N*7-triphenyl-9*H*-fluorene-2,7-diamine. It underwent C-C coupling via Stille reaction with tin reagent of thiophene protected aldehyde followed by acedic hydrolysis led to corresponding aldehydes. The aldehydes were converted to dyes by Knoevenagel condensation with cyanoacetic acid. They exhibited longer wavelength absorption (Table 1.4) than the corresponding dyes with fluorene and phenylene linkers due to the enhanced electron-richness in the conjugation pathway imparted by the carbazole unit. However, as mentioned earlier, it also had a counter effect in lowering the LUMO energy of the dyes which resulted in poor electron injection efficiency.

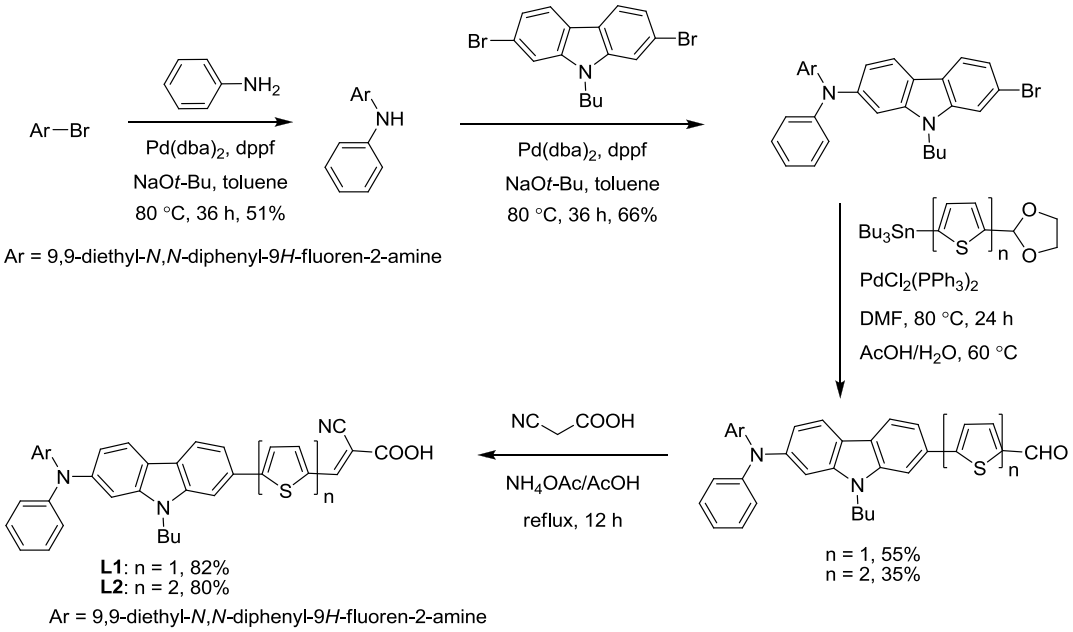

Scheme 1.38 Synthetic scheme of the dyes **L1** and **L2**.

Lin and co-workers reported di-anchoring dyes (Chart 1.46, **L3**–**L5**) with 2,7-disubstituted carbazole as a central donor [143]. The synthetic scheme of the dyes outlined in Scheme 1.39. It starts with Stille coupling of 9-(heptadecan-9-yl)-2,7-bis(4,4,5,5-tetramethyl-1,3-dioxolan-2-yl)-9*H*-carbazole with tin reagents of thiophene protected aldehydes led to corresponding aldehydes. It condensed with cyanoacetic acid by Knoevengel condensation led to desired dyes (**L3** and **L4**)

and synthesis of **L5** also prepared according to the similar method described for **L3**. These rod-shaped molecules (**L3-L5**) showed promising optical properties which could be tuned by altering the oligothiophene spacer length and inserting alkyl chain on the C3-position of thiophene. The dye with extended conjugation (**L4**) exhibited most red-shifted absorption profile while the dye possessing 3-hexylthiophene showed shorter wavelength absorption due to the non-planarity induced to accommodate the hexyl chain. This dye inherited a high lying LUMO which increased the electron injection efficiency and photocurrent density.

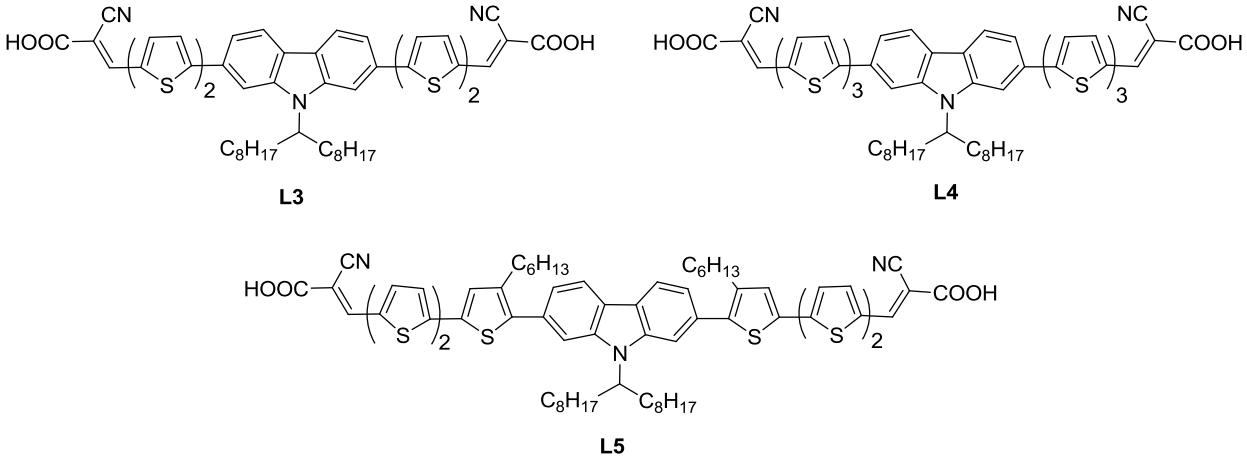

Chart 1.46 Dianchoring organic dyes with 2,7-disubstituted carbazole donor.

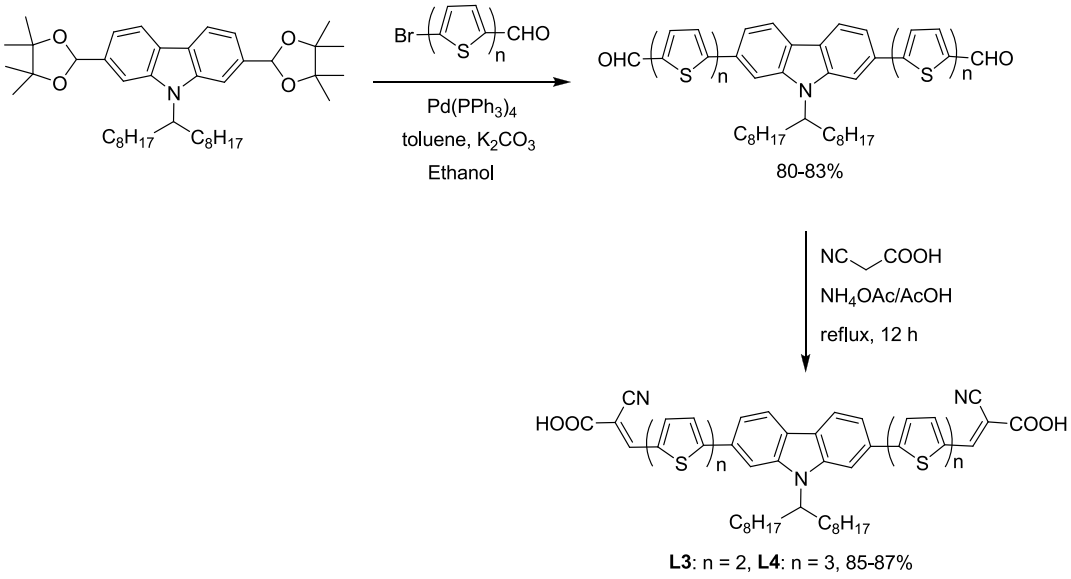

Scheme 1.39 Synthetic scheme of the dyes **L3** and **L4**.

The efficiency of DSSC depends on the nature of the anchoring group present in the dye. A strongly interacting anchoring unit may possess a favorable dipole at the interface between the TiO_2 film and dye facilitates the electron injection into the CB of TiO_2. Though several anchoring units such as hydroxyl, carboxylic acid, cyanoacrylic acid, or rhodanine-3-acetic acid have been tested, cyanoacrylic acid has been found to be more successful. Recently, Harima and co-workers synthesized a series of dyes (**L6**–**L11;** Chart 1.47) featuring diphenylamine donor, 2,7-disubstituted carbazole linker, and pyridine as anchoring unit [144]. They have also prepared for comparison, dyes with the same structural units, but possessing conventional carboxylic acid anchors.

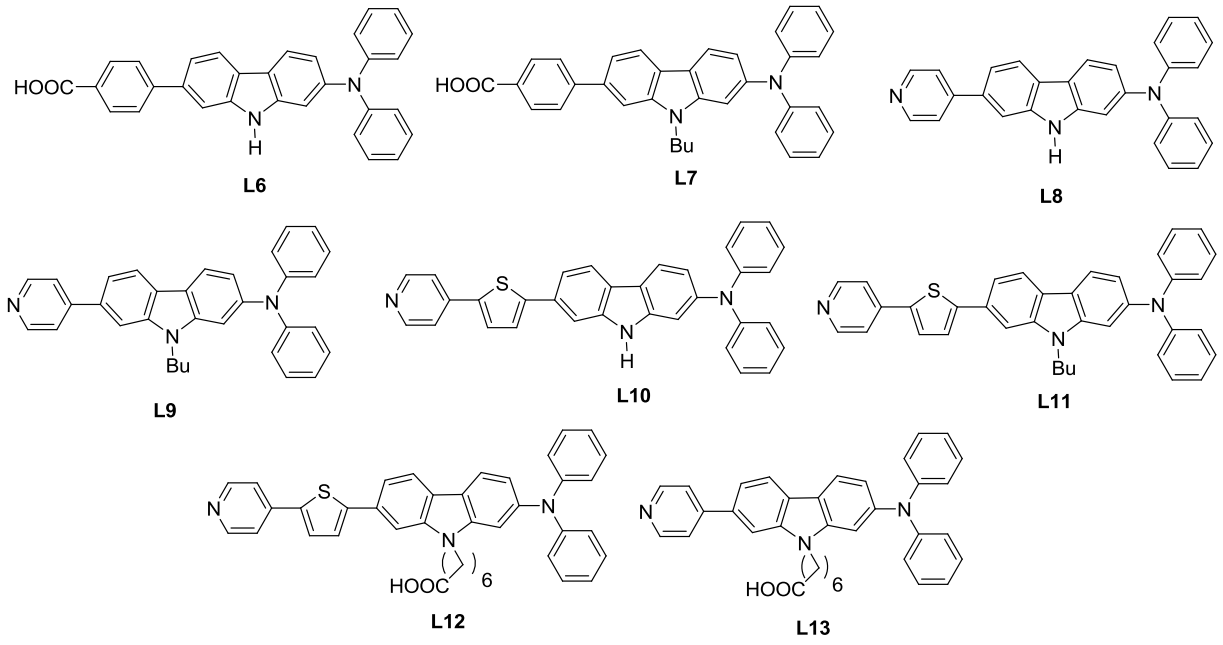

Chart 1.47 Organic dyes featuring 2,7-disubstituted carbazole as a bridge and pyridine anchor.

The synthetic route of the dyes, **L6**-**L9** is displayed in Scheme 1.40. The synthesis begins with Suzuki coupling of 4,4'-dibromo-2-nitrobiphenyl with 4-(ethoxycarbonyl)phenylboronic acid or pyridin-4-ylboronic acid gave mono coupled products which on reductive cyclization gave the ethyl 4-(7-(diphenylamino)-9*H*-carbazol-2-yl)benzoate and *N*,*N*-diphenyl-7-(pyridin-4-yl)-9*H*-carbazol-2-amine (**L8**), respectively. Acidic hydrolysis of ethyl 4-(7-(diphenylamino)-9*H*-carbazol-2-yl)benzoate gave 4-(7-(diphenylamino)-9*H*-carbazol-2-yl)benzoic acid (**L6**). N-alkylation of methyl 4-(7-(diphenylamino)-9*H*-carbazol-2-yl)benzoate or *N*,*N*-diphenyl-7-(pyridin-4-yl)-9*H*-carbazol-2-amine led to ethyl 4-(9-butyl-7-(diphenylamino)-9*H*-carbazol-2-

yl)benzoate and 9-butyl-*N*,*N*-diphenyl-7-(pyridin-4-yl)-9*H*-carbazol-2-amine (**L9**), respectively. Acidic hydrolysis of ethyl 4-(9-butyl-7-(diphenylamino)-9*H*-carbazol-2-yl)benzoate afforded 4-(9-butyl-7-(diphenylamino)-9*H*-carbazol-2-yl)benzoic acid (**L7**).

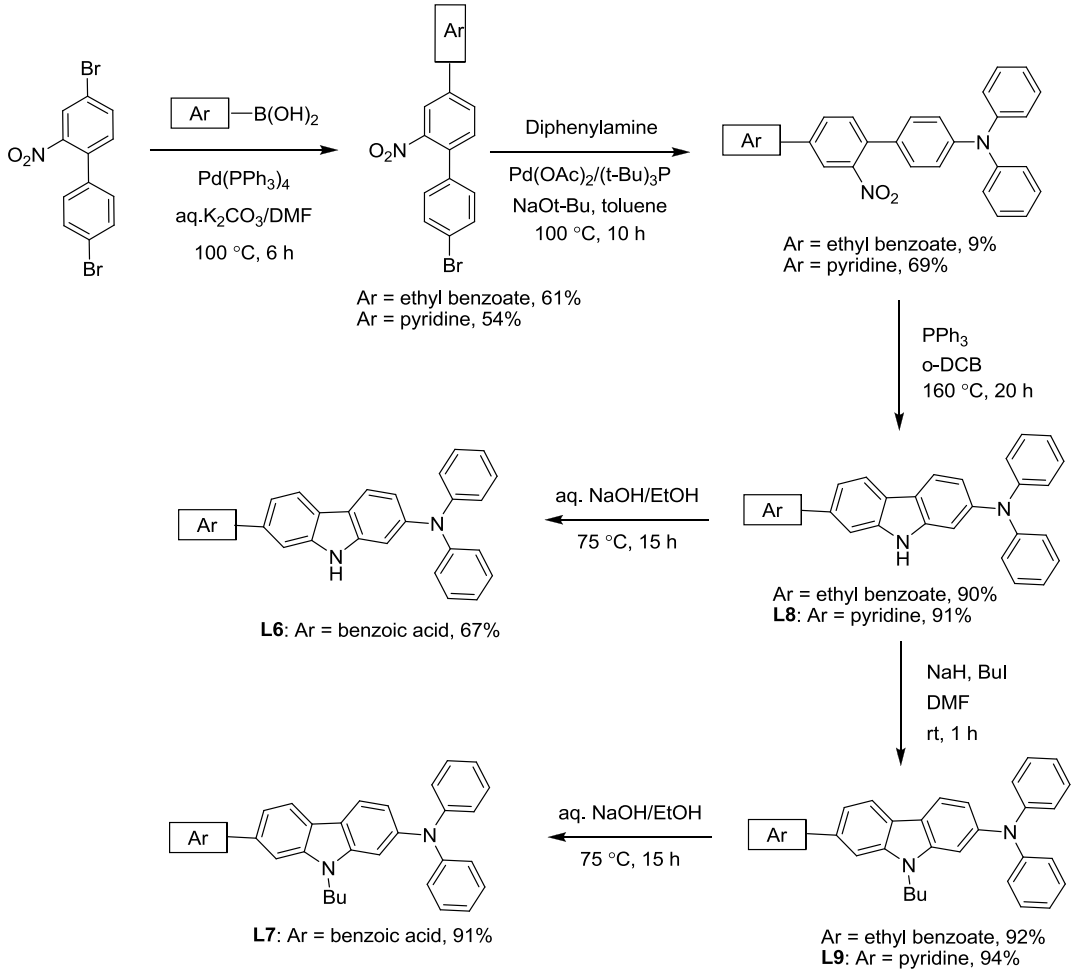

Scheme 1.40 Synthetic scheme of the dyes **L6-L9**.

The efficiency of the pyridine-based dyes **L8** and **L9** (1.04-1.15%) are reasonably higher than those (0.91-0.97%) of the dyes (**L6** and **L7**) with carboxylic acid anchor. Also, insertion of thiophene in the conjugation pathway (**L10** and **L11**) increased the light harvesting property and led to larger J_{SC} (> 5.63 mA cm^{-2}) and efficiencies (> 1.84%). A slight increase in the power conversion efficiency (η = 1.81-2.35%) was observed on incorporation of additional carboxylic acid anchoring group to the above mentioned architecture (**L12** and **L13** in Chart 1.47) [145]. These dyes exhibited higher J_{SC} (5.16-7.04 mA cm^{-2}) when compared to **L6-L11** showing that carboxylic acid anchoring units provide stronger interaction with TiO_2.

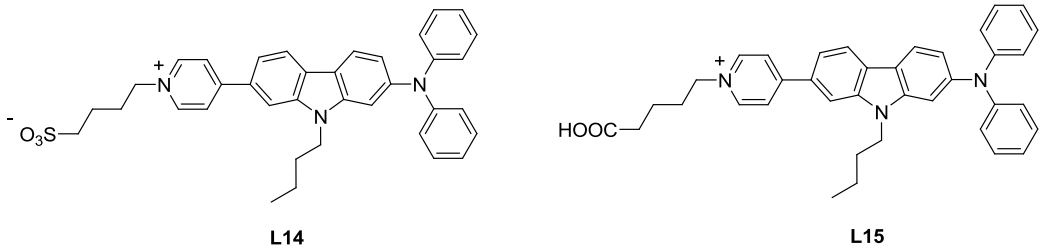

Chart 1.48 Organic dyes based on carbazole with pyridinium cationic anchoring unit.

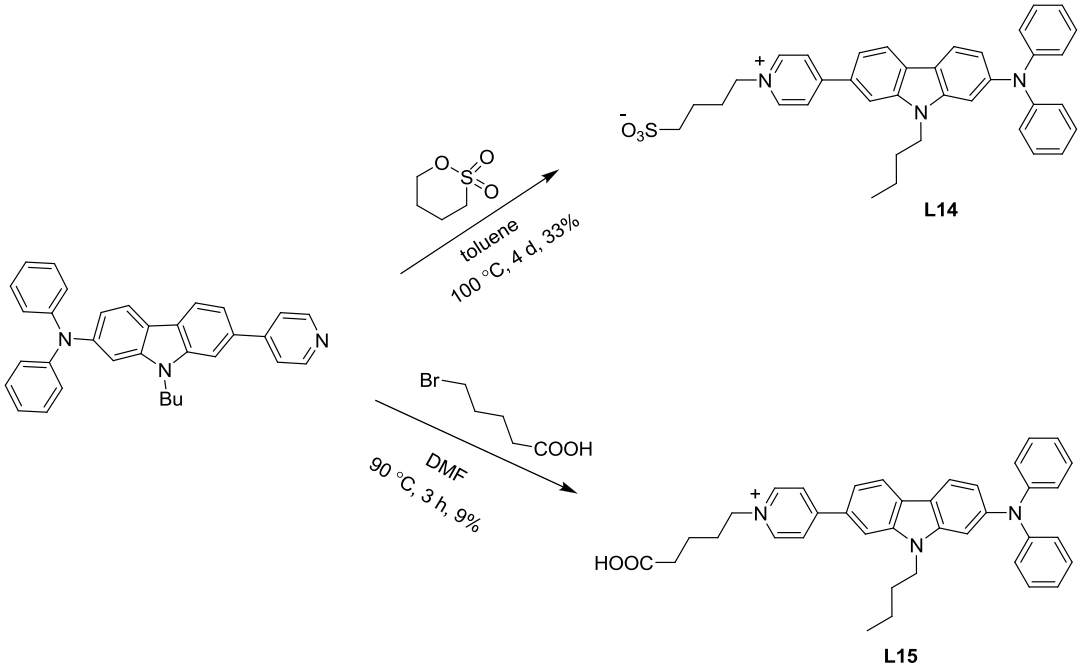

Scheme 1.41 Synthetic scheme of the dyes **L14** and **L15**.

Ooyama and co-workers used specific solvatochromic dyes (**L14** and **L15**; Chart 1.48) with pyridinium anchoring group [146]. The synthesis of the dyes (**L14** and **L15**) is outlined in Scheme 1.41. The reaction of 9-butyl-*N*,*N*-diphenyl-7-(pyridin-4-yl)-9*H*-carbazol-2-amine with 1,4-butanesultone or 5-bromopentanoic acid in heating condition afforded the dyes **L11** and **L12** respectively. The dye **L14** contains sulphonic acid group showed higher efficiency of 1.93% with J_{SC} of 5.52 mA cm^{-2} compared to the dye **L15** of efficiency (1.41%). The reason may be due to the good electronic coupling of **L14** and appropriate combination of dye with electrolyte solution and effective interaction of solvatochromic dye with surface of TiO_2 leads to improvement of light harvesting property of the dye.

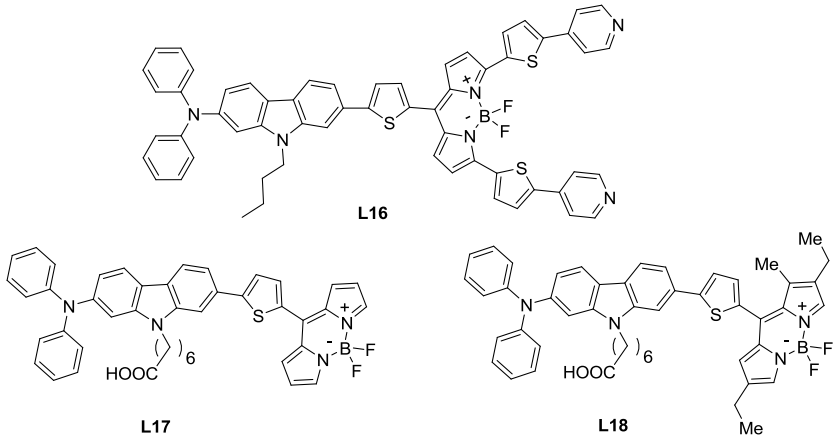

Chart 1.49 Organic dyes featuring diphenyl amino-carbazole substituted BODIPY dyes.

Ooyama and co-workers developed BODIPY based dye (**L16**) with two pyridine arms as electron withdrawing anchoring groups [147]. The synthesis of the dye **L16** is outlined in Scheme 1.42. The condensation of 5-(9-butyl-7-(diphenylamino)-9*H*-carbazol-2-yl)thiophene-2-carbaldehyde with pyrrole in presence of TFA as a catalyst led to dipyrromethane derivative. It chlorinated with N-chlorosuccinimide (NSC) followed by oxidation with DDQ gave the dichlorinated dipyrromethane derivative. It was reacted with NEt_3 and treated with BF_3-OEt_2 to afford the dichloro BODIPY derivative. The BODIPY dye **L16** was prepared by Stille coupling of dichloro BODIPY derivative with 2-(4-pyridyl)-5-tributylstannanylthiophene.

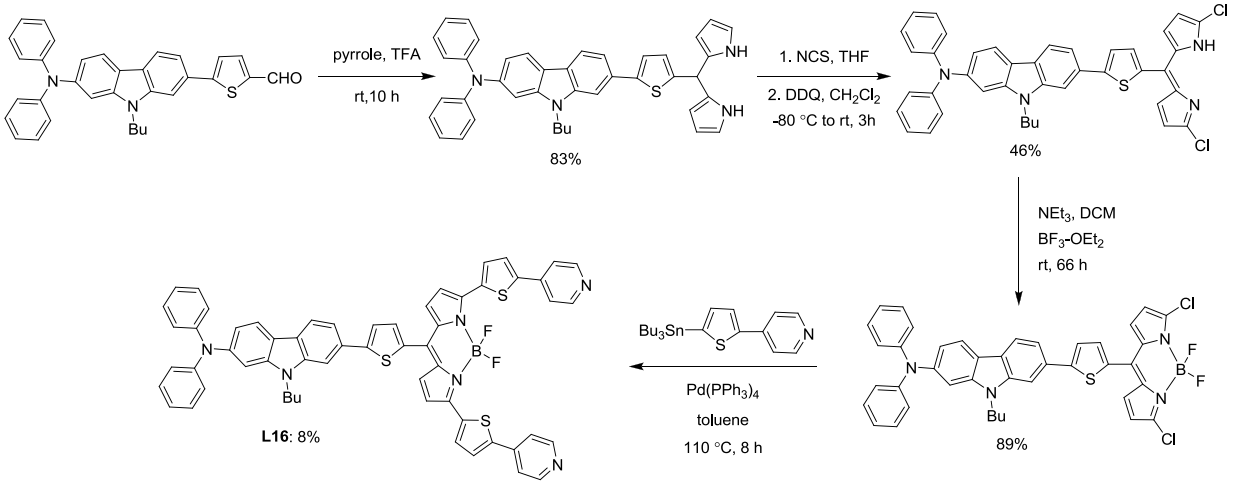

Scheme 1.42 Synthetic scheme of the dye **L16**.

The dye **L16** has good light harvesting capability in the red/near IR region. The expansion of π-conjugation with BODIPY core led to red shifted absorption and the incident power

conversion efficiency of 10% over a range of 500 nm to 700 nm. To achieve higher performance the carboxylic acid anchoring groups was introduced on carbazole to obtain dyes **L17**–**L18** [148]. They showed higher conversion efficiency due to good electronic coupling with TiO_2 compared to pyridine anchoring group. The dye **L18** with alkyl group showed higher power conversion efficiency of 0.65% due to the higher fluorescence quantum yield of (Φ_f = 0.62) compared with dye **L17** with 0.34% (Φ_f = 0.06) lacks alkyl group. Probablly, alkylation at BODIPY nucleus reduces deactivation process.

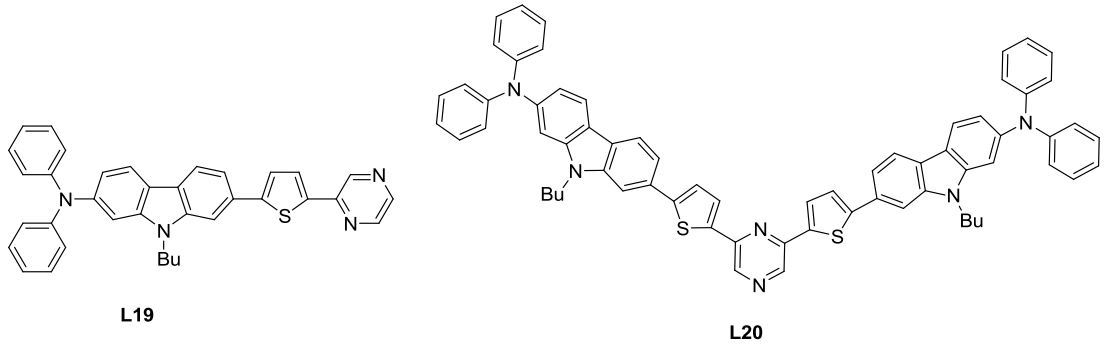

Chart 1.50 Organic dyes featuring diphenylaminocarbazole donor and pyrazine anchoring unit.

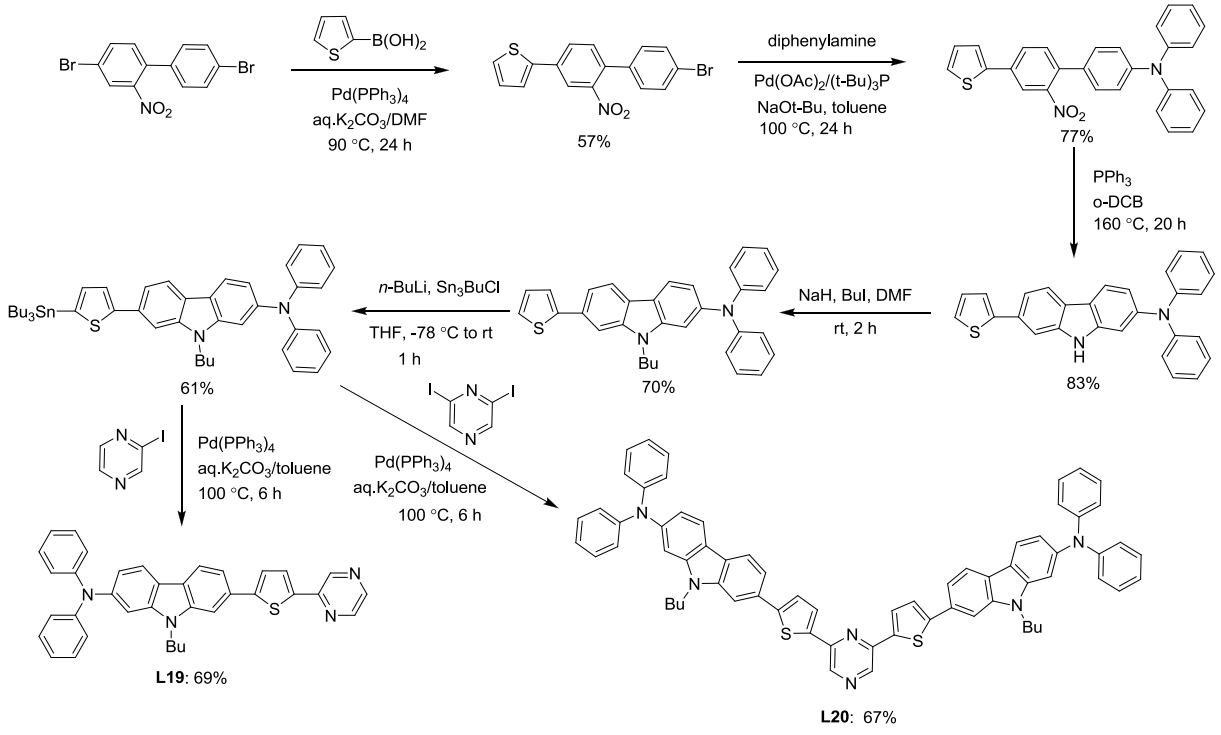

Scheme 1.43 Synthetic scheme of the dyes **L19** and **L20**.

Oyama and co-workers [149] incorporated the pyrazine as electron withdrawing anchoring group based on the 9-butyl-*N*,*N*-diphenyl-9*H*-carbazol-2-amine unit gave **L19** and **L20** (Chart 1.50). The synthesis of the dyes is shown in Scheme 1.43. The synthesis began with selective Suzuki coupling of the 4,4'-dibromo-2-nitrobiphenyl with thiophen-2-ylboronic acid, followed by Hartwig-Buchwald C-N coupling reaction with diphenylamine and subsequently converted to cylcized product by reductive cycliaztion with triphenylphosphine. Then it is subjected to alkylation at N9-position in presence of NaH as base and then treated with butyl lithium and tributyltinchloride resulted in 9-butyl-*N*,*N*-diphenyl-7-(5-(tributylstannyl)thiophen-2-yl)-9*H*-carbazol-2-amine. This can be converted to target dyes **L19** and **L20** by Suzuki coupling of 2-iodopyrazine and 2,6-diiodopyrazine, respectively. These dyes adsorbed on TiO_2 through the formation of the pyrazinium ion or hydrogen bonds at the brØnsted acid sites of TiO_2. This type of linkage with TiO_2 also provides relatively efficient electron injection. **L20** achieved an efficiency of 1.26% due to the longer wavelength absorption led to larger photocurrent compared to the **L19** dye which has only one linking on the pyrazine unit.

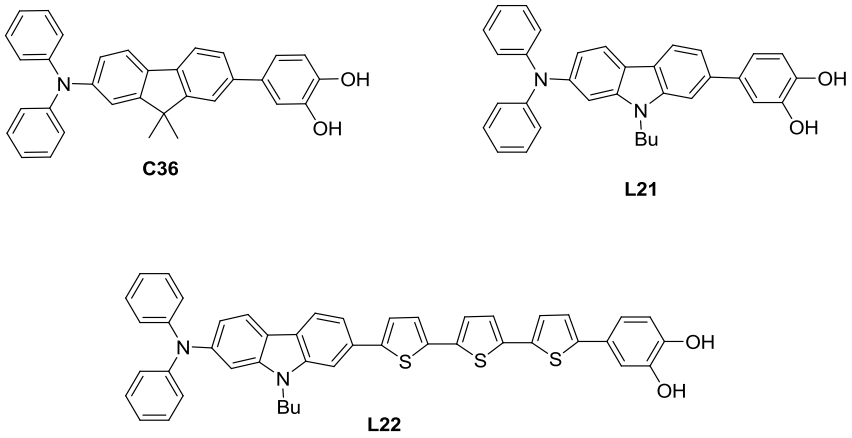

Chart 1.51 Organic dyes based on carbazole with catechol as anchoring group.

Ooyama and co-workers successfully developed new anchoring groups for efficient binding with TiO_2 due to the formation of chelate complex and successfully introduced in DSSC design [150]. Three dyes were synthesized (**C36**, **L21** and **L22**; Chart 1.51) which consist of fluorene, carbazole and carbazole-terthiophene units as linkers, diphenylamine as donor and catechol as anchoring group. The synthesis of the dyes is showed in Scheme 1.44. The Buchwald-Hartwig C-N coupling of 2,7-dibromo-9-butyl-9*H*-carbazole and diphenylamine gave 7-bromo-9-butyl-

N,*N*-diphenyl-9*H*-carbazol-2-amine, which coupled with 2-(3,4-bis(methoxymethoxy)phenyl)-4,4,5,5-tetramethyl-1,3,2-dioxaborolane through Suzuki coupling and followed by acidic hydrolysis led to dye **L21**. The conversion of 7-bromo-9-butyl-*N*,*N*-diphenyl-9*H*-carbazol-2-amine to its borolane derivative and followed by Suzuki coupling with 5-(3,4-Bis(methoxymethoxy)phenyl)-5″-bromo-2,2′:5′,2″-terthiophene and acedic hydrolysis led to dye the **L22**.

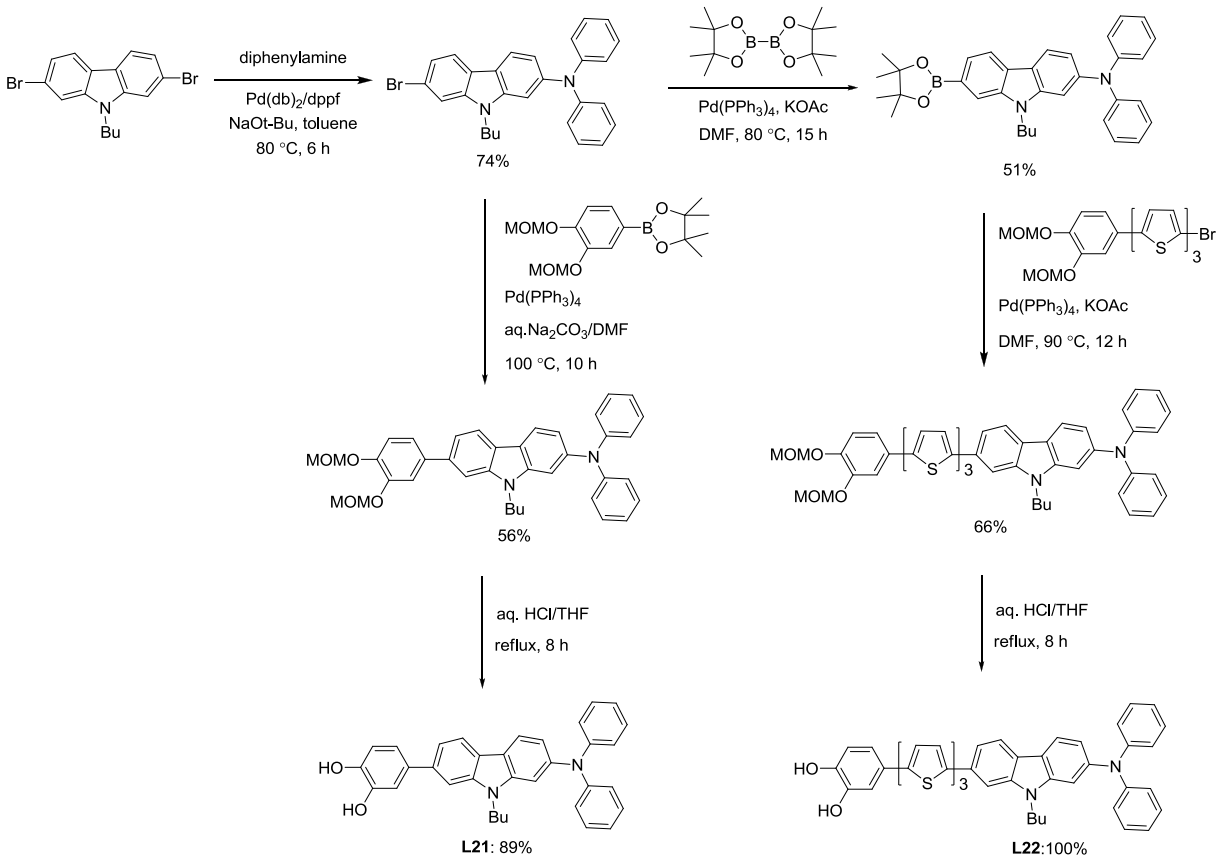

Scheme 1.44 Synthetic scheme of the dyes **L21** and **L22**.

All the dyes posses good light harvesting property corresponding to charge transfer band and IPCE is mainly from the dye to TiO_2 charge transfer band. The introduction of terthiophene increases the ICT from donor to acceptor based on π-π* transition which decreases the DTCT and increases the indirect electron injection pathway from dye to the CB of TiO_2 by photoexcitation of the local band of the adsorbed dye on TiO_2. Finally, the dye **L21** showed the highest efficiency of 0.31% compared to other dyes and further studies with this anchoring group might give fruitful results.

Table 1.4 Optical, electrochemical and photovoltaic performance parameters of dyes containing carbazole as linker

Dye	$\lambda_{max,}$ nm (ε_{max}, M^{-1} cm^{-1})	E_{ox} , V (*vs* NHE)	E_{ox}^{*}, V (*vs* NHE)	J_{SC} (mA cm^{-2})	V_{OC} (mV)	*ff*	η (%)	*Ref*
L1	492 (31000)	0.91	−1.09	12.60	634	0.58	4.62	[55]
L2	493 (33200)	0.90	−1.05	11.80	636	0.56	4.20	[55]
L3	480 (79600)	0.92	−1.26	10.12	620	0.68	4.26	[143]
L4	484 (97900)	0.74	−1.34	11.74	600	0.63	4.41	[143]
L5	470 (82500)	0.89	−1.28	7.44	570	0.67	2.82	[143]
L6	374 (34900)	0.93	−2.12	2.96	503	0.61	0.91	[144]
L7	376 (34300)	1.00	−2.03	3.07	520	0.61	0.97	[144], [145]
L8	372 (30200)	0.97	−2.15	3.16	524	0.63	1.04	[144], [145]
L9	375 (33000)	1.02	−2.07	3.35	522	0.62	1.15	[144], [145]
L10	394 (48100)	0.93	−1.93	5.80	540	0.60	1.89	[144], [145]
L11	396 (49600)	0.97	−1.87	5.63	548	0.60	1.84	[144], [145]
L12	375 (33000)	1.01	−2.08	5.16	568	0.62	1.81	[145]
L13	396 (48700)	0.97	−1.87	7.04	568	0.59	2.35	[145]
L14	437 (27100)	1.09	–1.25	5.52	552	0.63	1.93	[146]
L15	440 (22700)	1.13	–1.21	4.54	468	0.66	1.41	[146]
L16	673 (80900)	1.22	−0.58	0.66	352	0.53	0.12	[147]
L17	501 (54 800)	1.25	−1.15	1.24	408	0.67	0.34	[148]
L18	524 (50 600)	1.27	−1.07	2.33	428	0.65	0.65	[148]
L19	402 (45 400)	1.11	−1.68	0.84	416	0.62	0.22	[149]
L20	397 (65600)	1.11	−1.60	3.49	508	0.57	1.01	[149]
C36	362 (43100)	0.98	−2.27	1.56	416	0.51	0.29	[150]
L21	364 (33800)	0.98	−2.27	1.51	416	0.50	0.31	[150]
L22	429 (81300)	0.97	−1.62	0.75	316	0.47	0.11	[150]

1.3.2 Carbazole as a linker via C3, C6 positions

Organic dyes featuring 3,6-disubstituted carbazole as π-linker are easily achieved by dibromination followed by palladium catalyzed cross-coupling reactions [151]. Most of the organic dyes in this category either used carbazole as linker and donor or as electron-rich conjugating segment (Figure 1.8). 3,6-Disubstitution on carbazole cannot be treated as ideal conjugation as the direct electronic delocalization between the substituent's present on C3 and C6 positions may be limited.

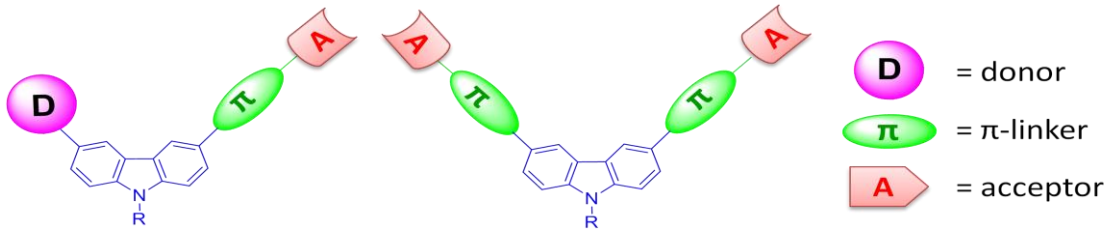

Figure 1.8 Molecular architecture of dyes containing 3,6-disubstituted carbazole as π-linker.

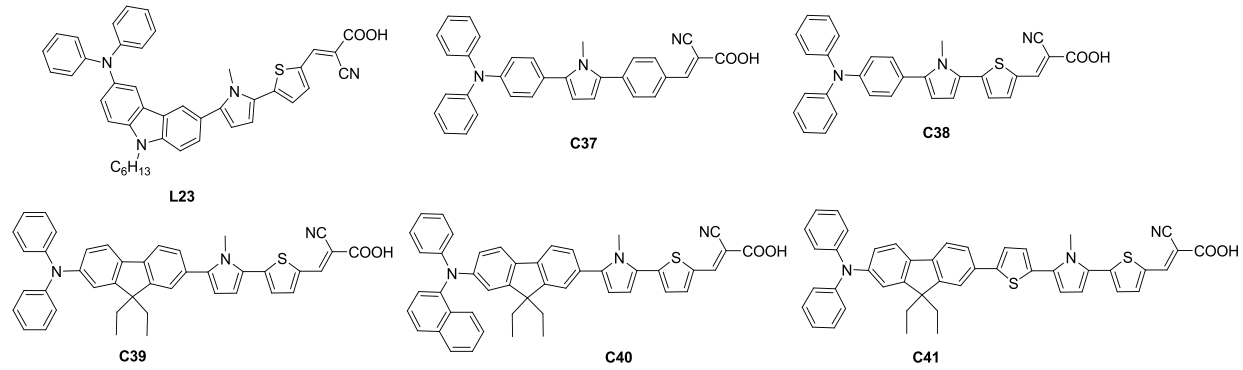

Chart 1.52 Organic dyes contained 3,6-disubstituted carbazole as π-linker and related linkers.

Organic dyes containing pyrrole units in the conjugation are scarce. Lin and co-workers synthesized several dyes in which the conjugation bridge is composed of pyrrole, thiophene and carbazole or other aromatic segments [152]. Diphenylamine end-cap served as a donor while cyanoacrylic acid acted as acceptor. The synthesis of the dyes is showed in Scheme 1.45 and it involve the Stille coupling reaction of 1-methyl-2-tributylstannyl-1*H*-pyrrole with 3,6-dibromo-9-hexyl-9*H*-carbazole and followed by palladium-catalyzed aromatic C-N coupling reaction with diphenylamine gave 9-hexyl-6-(1-methyl-1*H*-pyrrol-2-yl)-*N*,*N*-diphenyl-9*H*-carbazol-3-amine. It is treated with *n*-BuLi and addition of tributyltin-chloride gave its ting reagent which

coupled with 5-bromothiophene-2-carbaldehyde gave the corresponding aldehyde derivative. Condensation of this aldehyde with cyanoacetic acid by Knoevenagel condensation gave the desired dye **L23** and the dyes **C37-C41** also synthesized similar to the synthesis of dye **L23**.

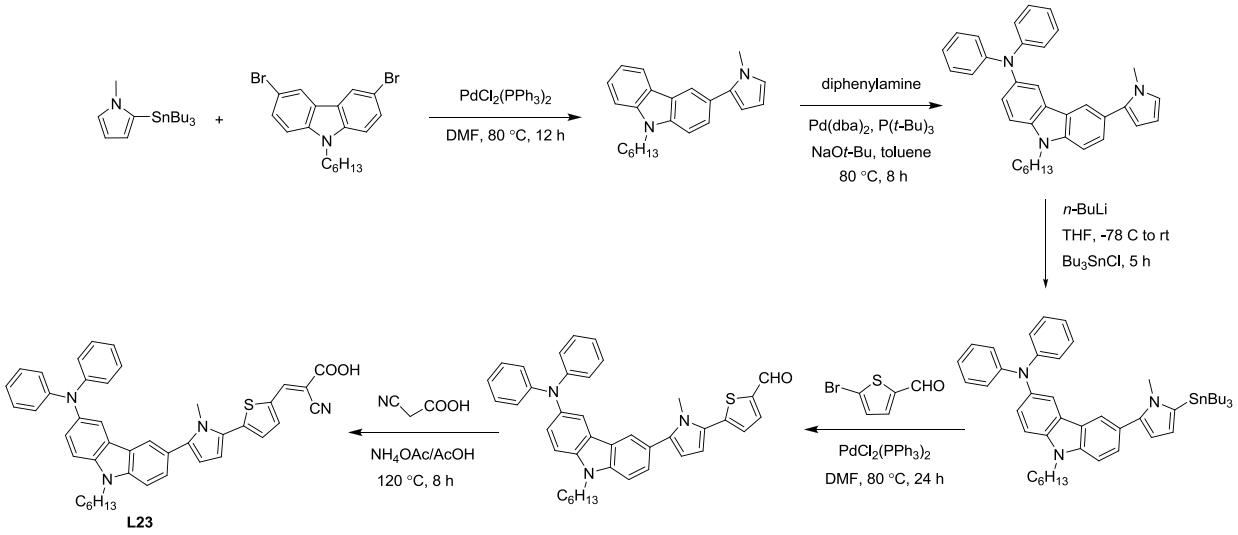

Scheme 1.45 Synthetic scheme of the dye **L23**.

It is interesting to note that the carbazole-based dye (**L23**) exhibited the most red-shifted absorption in the series. However, the molar extinction coefficient realized for the charge transfer transition is significantly low. Though the electron-richness of carbazole increases the donor-acceptor interaction, the broken conjugation because of 3,6-disubstitution on carbazole diminishes the electronic transition probability. **L23** showed an overall efficiency of 4.8% with J_{SC} = 12.93 mA cm^{-2}, V_{OC} = 580 mV and *ff* = 0.64. The comparatively low J_{SC} observed for **L23** is attributed to the less light harvesting capability and low lying LUMO level.

Kuang and co-workers reported a dye (**L24;** Chart 1.53) with triphenylethylene chromophore bearing phenothiazine as donor, 3,6-disubstituted carbazole linker and cyanoacrylic acid acceptor [153]. The synthetic scheme of the dyes is showed in Scheme 1.46. Reaction of bis(4-fluorophenyl)methanone with phenothiazine gave bis(4-(10*H*-phenothiazin-10-yl)phenyl)methanone [154]. Compound 10,10'-(4,4'-(2-(4-bromophenyl)ethene-1,1-diyl)bis(4,1-phenylene))bis(10*H*-phenothiazine) was synthesized via the Wittig-Horner reaction of intermediate1and 1,4-bis(diethoxyphosphinylmethyl)benzene. Reaction of 10,10'-(4,4'-(2-(4-bromophenyl)ethene-1,1-diyl)bis(4,1-phenylene))bis(10*H*-phenothiazine) with 4,4,4',4',5,5,5',5'-octamethyl-2,2'-bi(1,3,2-dioxaborolane) gave the borolane derivative by Suzuki coupling. It

reacted with 6-bromo-9-hexyl-9*H*-carbazole-3-carbaldehyde via Suzuki coupling to give the aldehyde derivative which converted to dye **L24** by Knoevenagel condensation reaction with cyanoacetic acid. The dye achieved an efficiency of 2.69% in the DSSC. This is higher than that reported for the dye, **D3** which lacks the auxiliary donor and exemplifies the requirement of electron rich donors for carbazole-based organic dyes.

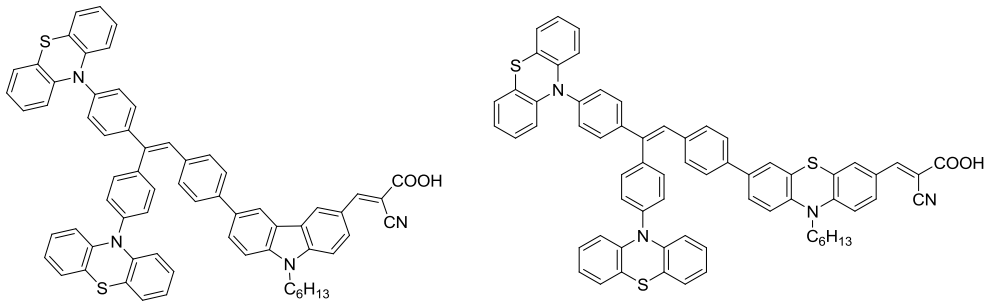

Chart 1.53 Organic dyes containing phenothiazine auxiliary donors and carbazole π-linker.

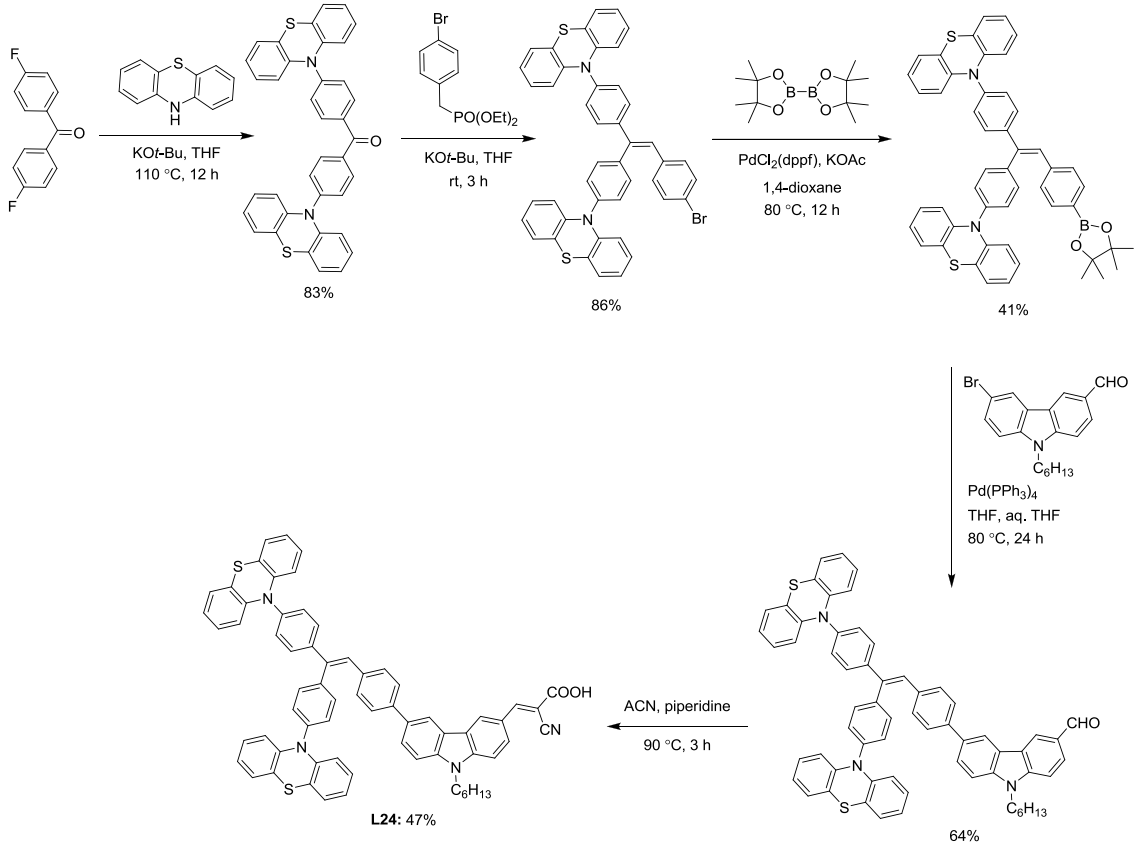

Scheme 1.46 Synthetic scheme of the dye **L24**.

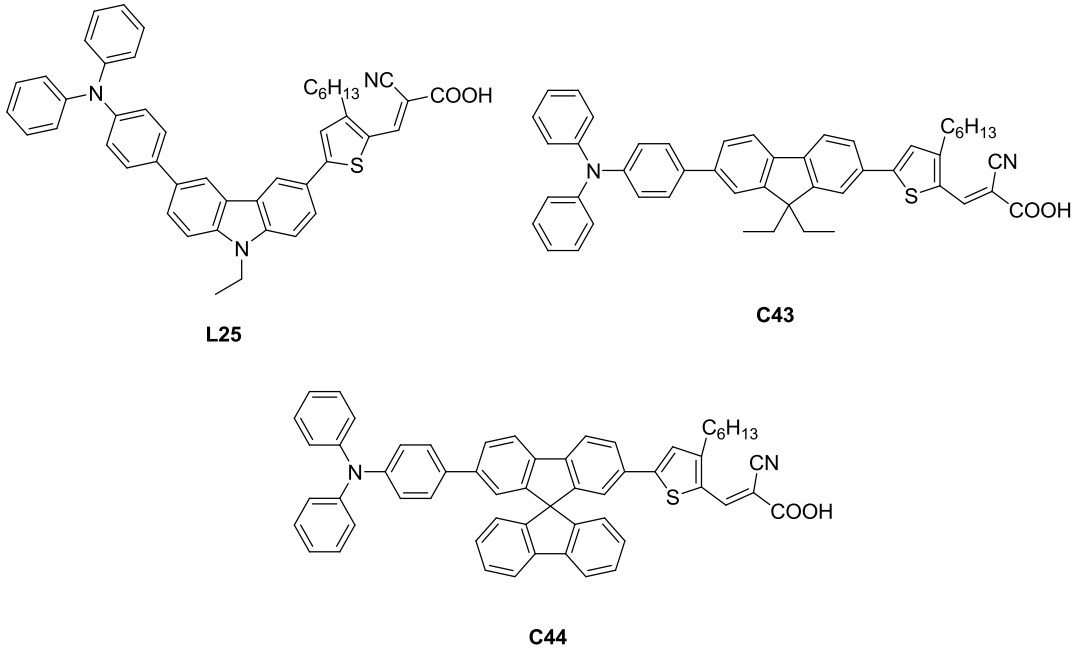

Chart 1.54 Organic dyes containing different π-linker and alkylated thiophene units.

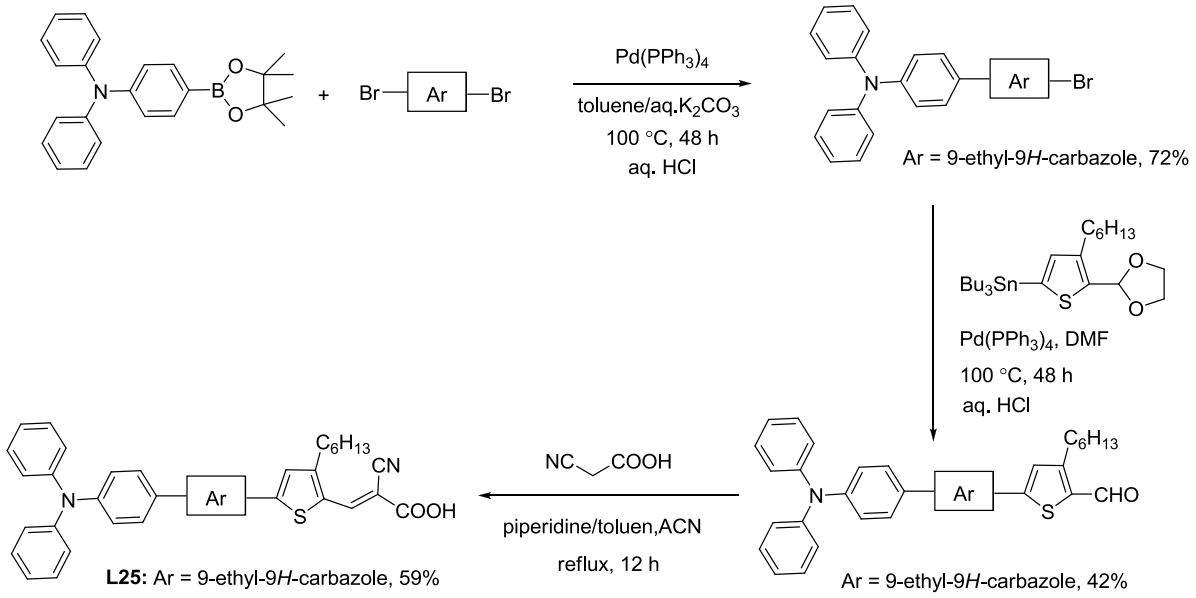

Scheme 1.47 Synthetic scheme of the dye **L25**.

Tan and co-workers synthesized set of dyes (**C43**, **C44** and **L25;** Chart 1.54) containing diarylamine as donor with different linkers (fluorene, spirofluorene and carbazole) and cyanoacrylic acid as an acceptor [155]. The synthesis of the dyes is showed in Scheme 1.47. Firstly, the Suzuki coupling reaction between triphenylamine-based boric ester and 3,6-dibromo-

9-ethyl-9*H*-carbazole gave 4-(6-bromo-9-ethyl-9*H*-carbazol-3-yl)-*N*,*N*-diphenylaniline. Then it reacted with via the Stille coupling reactions of (5-(1,3-dioxolan-2-yl)-4-hexylthiophen-2-yl)tributylstannane gave the corresponding aldehyde derivative. Finally, the Knoevenagel condensation reactions of aldehyde derivative with cyanoacetic acid afforded the target dyes **L25** in the presence of piperidine. The other dyes are also synthesized according to the Scheme 1.47. The dye **L25** showed superior performance of 6.51% with V_{OC} of 660 mV compared to **C44** due to the higher J_{SC} (14.79 mA cm^{-2}) of former dye compared to J_{SC} (9.12 mA cm^{-2}) of **C44**. But **L25** showed inferior performance compared to the **C43** of efficiency (η = 7.03%) due to low lying HOMO of latter dye facilitates the dye regeneration of dye results in a higher V_{OC} of 700 mV.

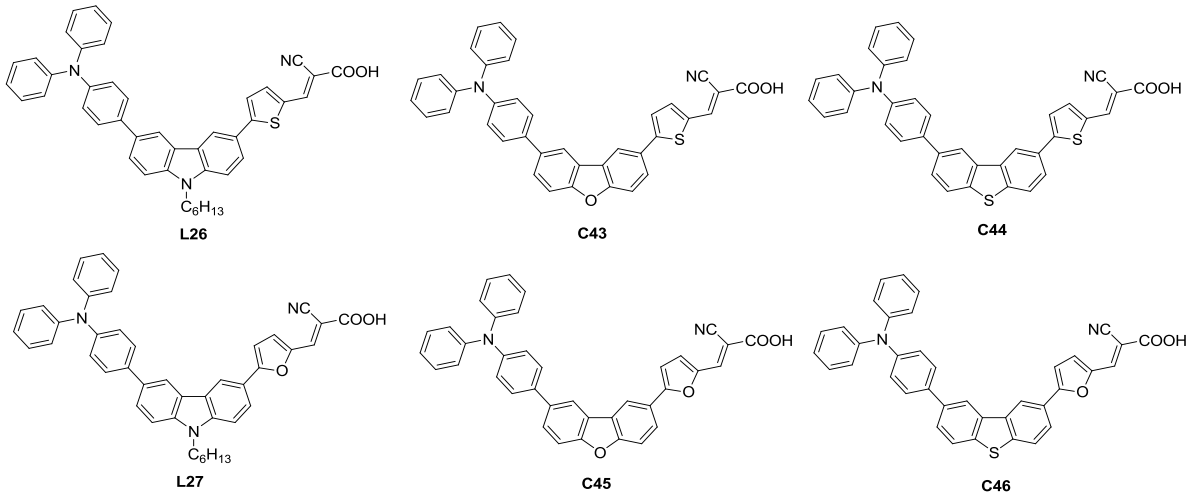

Chart 1.55 Dyes contained carbazole linker and triphenylamine donor and its related dyes.

Recently, Su and co-workers reported a series of D-π-A dyes featuring different linkers such as carbazole, dibenzofuran and dibenzothiphene [15]. Triphenylamine served as donor and cyanoacrylic acid as acceptor. Carbazole dyes (**L26** and **L27**; Chart 1.55) showed red shifted absorption when compared to other dyes (**C43**-**C46**) due to strong electron donating nature of carbazole. The broader IPCE of carbazole dyes manifested in higher J_{SC} (9.36-11.20 mA cm^{-2}), further shifted to high J_{SC} of (11.09-13.89 mA cm^{-2}) in optimized dye bath solvent of acetonitrile. The substitution of hexyl chain on carbazole strongly hampers the intermolecular charge recombination and raises the V_{OC} (730-769 mV). **L27** showed best conversion efficiency (7.09%) with J_{SC} = 13.89 mA cm^{-2}, V_{OC} = 769 mV and *ff* = 0.66 in acetonitrile solvent bath.

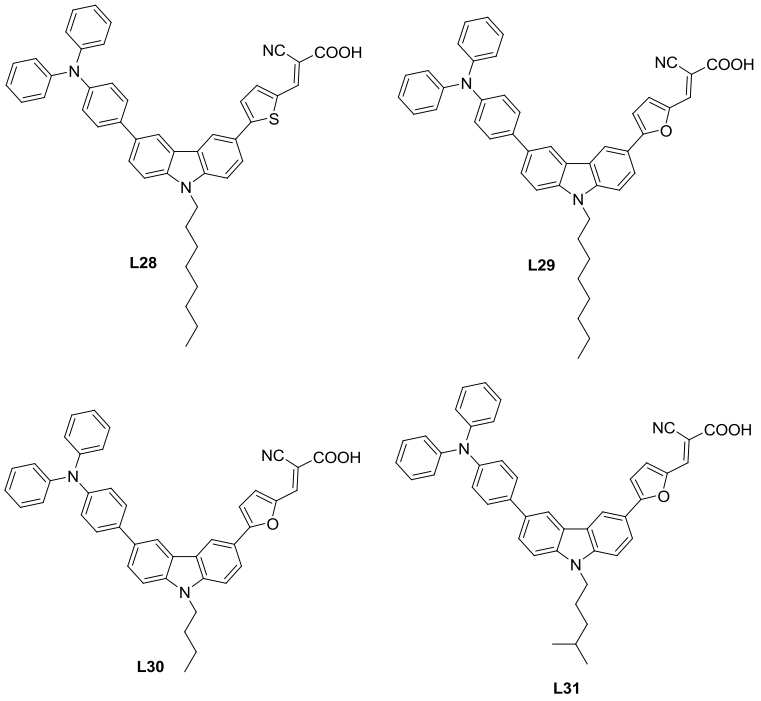

Chart 1.56 Dyes featuring carbazole linker and triphenylamine auxiliary donor.

Li and co-workers synthesized four dyes (**L28**-**L31;** Chart 1.56) with triphenylamine as a donor, carbazole in conjugation with thiophene or furan as linker with cyanoacrylic acid as an acceptor [156]. The introduction of thiophene and furan units increased the molar extinction coefficient in the absorption and results in larger photocurrent generation. The introduction of longer alky chain hampers the electron recombination which led to higher V_{OC} values in the range of 720 to 830 mV. Among all the dyes, **L29** achieved best conversion efficiency of 6.68% with J_{SC} of 13.26 mA cm^{-2}.

Zhou and co-workers reported novel dyes (**L32** and **L33**, Chart 1.57) with carbazole linker and triarylamine donor [157]. The dyes featured different anchoring units such as cyanoacrylic acid (**L32**) and pyridine (**L33**). Synthetic route to the dyes (**L32**-**L35**) is depicted in Scheme 1.48. Suzuki coupling of tris(4-bromophenyl)amine with thiophen-2-ylboronic acid gave 4-bromo-*N*,*N*-bis(4-(thiophen-2-yl)phenyl)aniline which reacted with bis(pinacolato)diboron by Suzuki coupling led to 4-(4,4,5,5-tetramethyl-1,3,2-dioxaborolan-2-yl)-*N*,*N*-bis(4-(thiophen-2-yl)phenyl)aniline. 9-ethyl-3,6-di(2-thiophenyl)carbazole was prepared from 3,6-dibromo-9-ethylcarbazole with thiophen-2-ylboronic acid by Suzuki coupling reaction. It is formylated with $POCl_3$/DMF by Vilsmeier-Haack formylation and followed by by bromination of gave 5-(6-(5-

bromothiophen-2-yl)-9-ethyl-9*H*-carbazol-3-yl)thiophene-2-carbaldehyde. It reacted with 4-(bis(4-(thiophen-2-yl)phenyl)amino)phenylboronic acid via Suzuki coupling gave the corresponding aldehyde derivative. Subsequently Knoevenagel condensations of this aldehyde and cyanoacetic acid led to target dye **L32**. Dibromination of compound 9-ethyl-3,6-di(2-thiophenyl)carbazole resulted intermediate 3,6-bis(5-bromothiophen-2-yl)-9-ethyl-9*H*-carbazole. It reacted with 4-(bis(4-(thiophen-2-yl)phenyl)amino)phenylboronic acid and followed by Suzuki coupling with pyridin-4-ylboronic acid led to dye **L33**. Dyes **L34** and **L35** were synthesized by Suzuki coupling of 3,6-dibromo-9-ethyl-9*H*-carbazole with pyridin-4-ylboronic acid and 4-(bis(4-(thiophen-2-yl)phenyl)amino)phenylboronic acid, respectively.

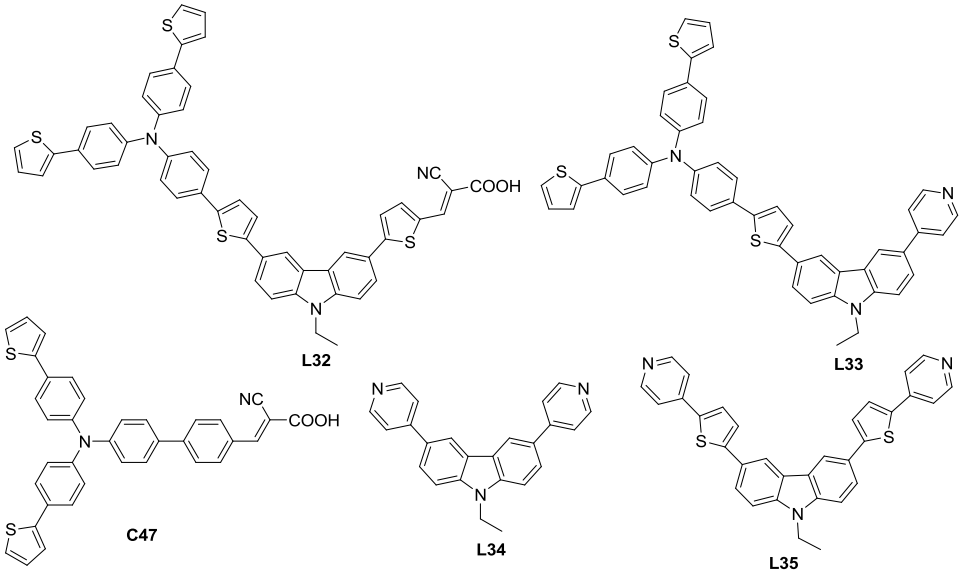

Chart 1.57 Organic dyes based on carbazole acting as π-linker.

Compared to **C47** (η = 5.24%) where biphenyl bridging unit was there in place of carbazole, **L32** showed higher J_{SC} (14.12 mA cm^{-2}) and better conversion efficiency (6.37%). Pyridine-based dye, **L33** displayed significantly low conversion efficiency (η = 1.88%) due to less dye loading, huge dark current and pronounced charge recombination. This again points that pyridine unit cannot serve as a good anchoring unit. Structural modifications are required to tune its anchoring properties. Harima and co-workers thought that dianchoring pyridine dye may solve this problem. They have prepared two dyes (**L34** and **L35**) with chelating-like pyridine units [158]. **L35** displayed red-shifted absorption due to elongated conjugation. However, the efficiency of the devices made use of these dyes is below mark.

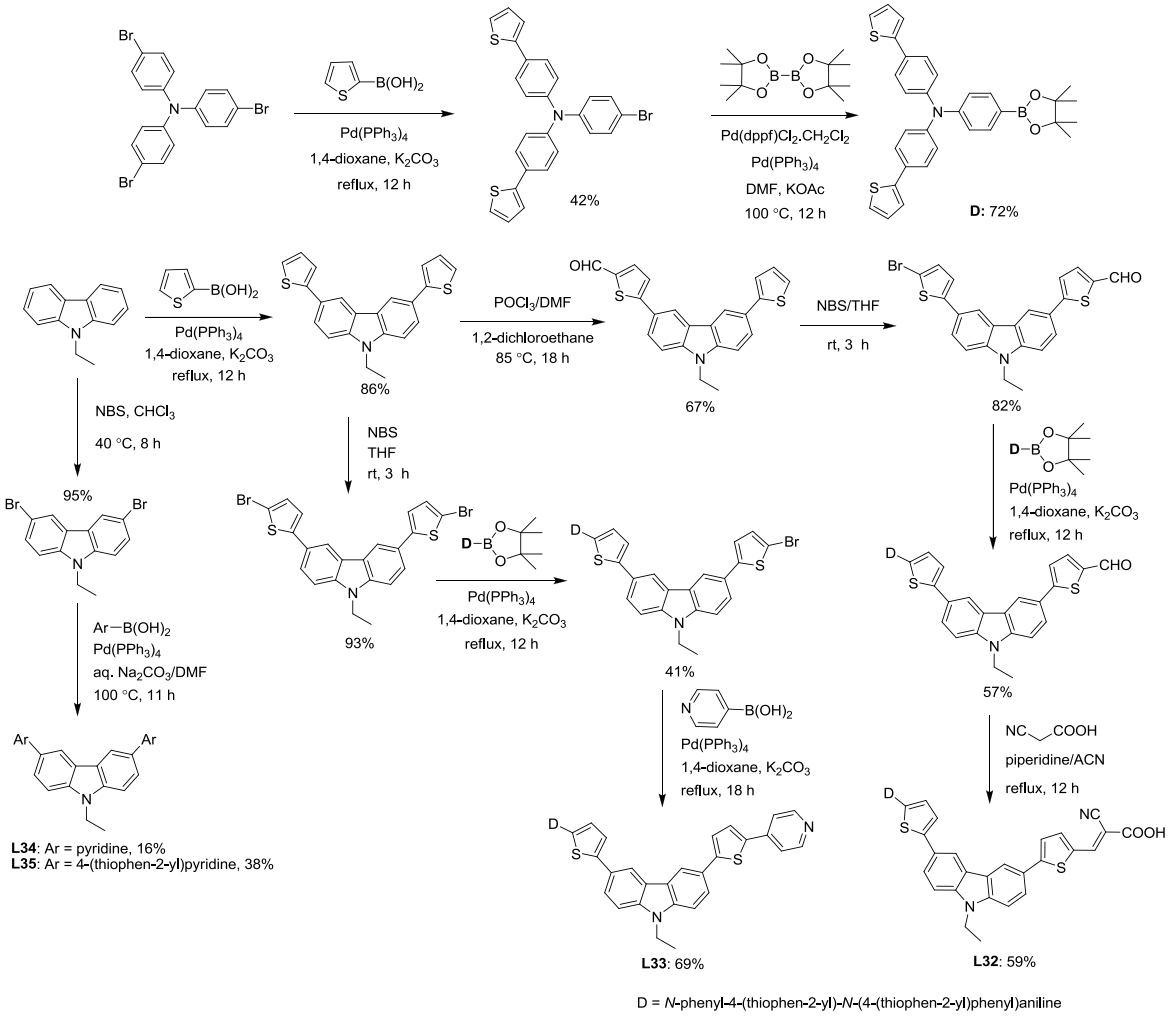

Scheme 1.48 Synthetic scheme of the dyes **L32-L35**.

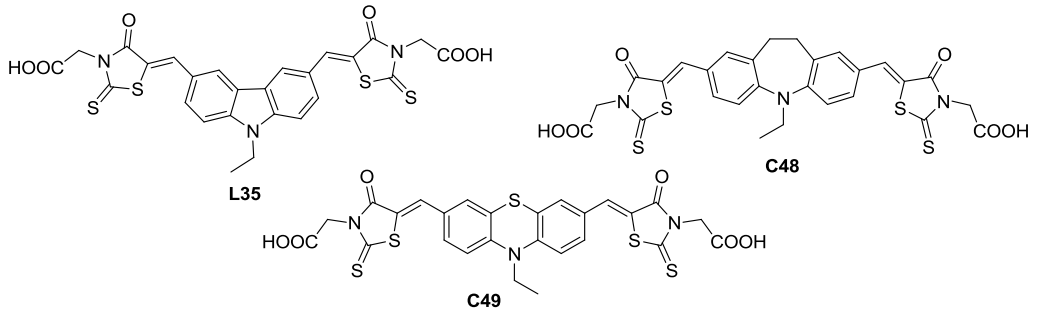

Chart 1.58 Organic dyes containing electron-rich heteroaromatics as π-linker and donor.

Sun and co-workers reported a series of dianchoring dyes (Chart 1.58) with rhodanine as an acceptor and several bridging units such as carbazole, iminodibenzyl and phenothiazine [159]. The synthesis of the dye **L35** is displayed in Scheme 1.49. *N*-hexylcarbazole first treated with a

reagent of imidazole and trifluoroacetic anhydride and followed by hydrolysis led to 9-hexyl-9*H*-carbazole-3,6-dicarbaldehyde. The dye **L35** obtained by the condensation of the 9-hexyl-9*H*-carbazole-3,6-dicarbaldehyde with cyanoacetic acid by Knoevenagel condensation. The synthesis of the dyes (**C48** and **C32**) was also synthesized according to procedure described in Scheme 1.49 by starting with *N*-ethyliminodibenzyl and *N*-ethylphenothiazine. The efficiency of the devices assumed the order according to the linker as: iminodibenzyl (**C48**) < carbazole (**L35**) < phenothiazine (**C49**). The light-harvesting ability of the dye containing phenothiazine dye is marginally better due to improved absorption characteristics and balanced HOMO/LUMO energy levels.

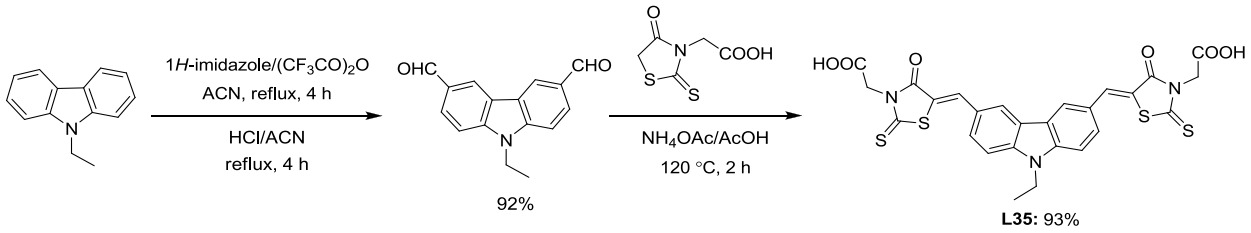

Scheme 1.49 Synthetic scheme of the dyes **L35**.

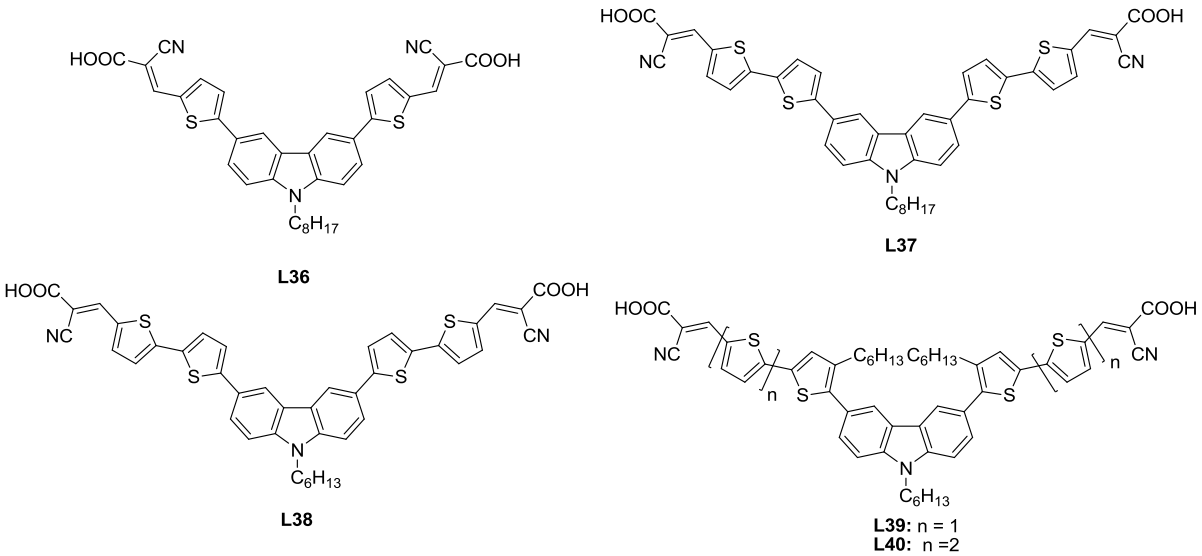

Chart 1.59 Bianchoring organic dyes containing carbazole as π-linking donor and oligothiophene spacers.

The stability and adsorption of dyes on TiO_2 were essential for practical applications. In order to improve affinity of the dyes towards TiO_2, Suranna and co-workers designed a new series of di-anchoring dyes (**L36** and **L37;** Chart 1.59) based on carbazole linker and oligothiophene

spacers [160]. The synthesis of the dyes is outlined in Scheme 1.50.The conversion of 3,6-dibromo-*N*-octyl-carbazole into the corresponding boronic ester by lithiation with *n*-BuLi and subsequent reaction with 2-isopropoxy-4,4,5,5-tetramethyl-1,3,2-dioxaborolane. It coupled with 5-bromothiophene-2-carbaldehyde led to 5,5'-(9-octyl-9*H*-carbazole-3,6-diyl)dithiophene-2-carbaldehyde, which subsequently converted to cyanoacrylic acid dye **L36** by Knoevenagel condensation with cyanoacetic acid. The synthesis of dye **L37** also prepared similar to the dye **L36**.

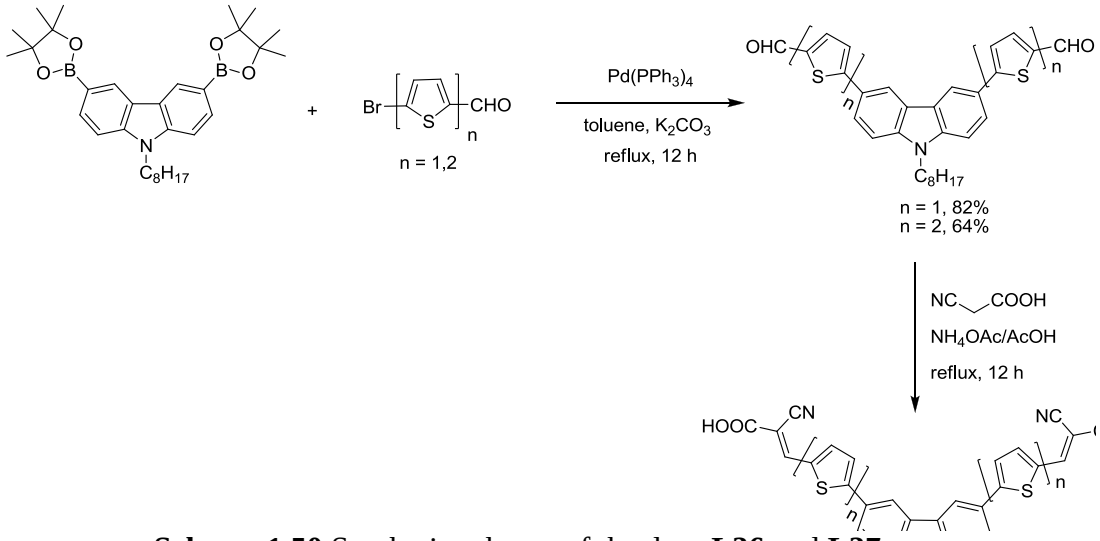

Scheme 1.50 Synthetic scheme of the dyes **L36** and **L37**.

The dye **L37** showed red shifted absorption ($\Delta\lambda$ = 17 nm) and high molar extinction coefficient when compared to **L36** due to the elongated conjugation. The higher IPCE plateau of **L37** (> 60%) in the 400-550 nm region produced J_{SC} of 10.52 mA cm^{-2} and led to high efficiency (5.01%) in DSSC. Lin and co-workers extended this concept and synthesized a series of dyes with carbazole linker (**L38**-**L40**) [143]. They have studied the effect of planarity on the performance of DSSC by introducing hexyl chains on thiophene units. It is interesting to note that the 3,6-disubstituted dyes (**L38**-**L40**) showed red shifted absorption than the corresponding 2,7-disubstituted analogs (**L3**-**L5**). It is probably due to direct conjugation with nitrogen of carbazole in former case, which acts as auxiliary donor. The hexyl chain substitution in **L39**

lowered the absorption wavelength due to the non-planarity. But this is helpful in hampering the intra molecular charge recombination and leads to increase in V_{OC} (640 mV).

Kim and co-workers [161] synthesized a set of 3,6 di-subsituted carbazole dyes (**L41-L46**; Chart 1.60) with various acceptor/anchoring units such as cyanoacrylic acid, rhodanine acetic acid and 5-oxo-1-phenyl-4,5-dihydro-1*H*-pyrazole-3-carboxylic acid and varied the π-conjugation with thiophene units. The increasing order of absorption maxima of the dyes containing different acceptors followed as cyanoacrylic acid < rhodanine acetic acid < 5-oxo-1-phenyl-4,5-dihydro-1*H*-pyrazole-3-carboxylic acid. The extension of π-conjugation with thiophene units (**L44-L46**) causes red shifted absorption due to better donor-acceptor interactions. However, among all the dyes, the dye (**L44**) exhibited highest power conversion efficiency of 3.0% with higher J_{SC} of 7.7 mA cm^{-2}.

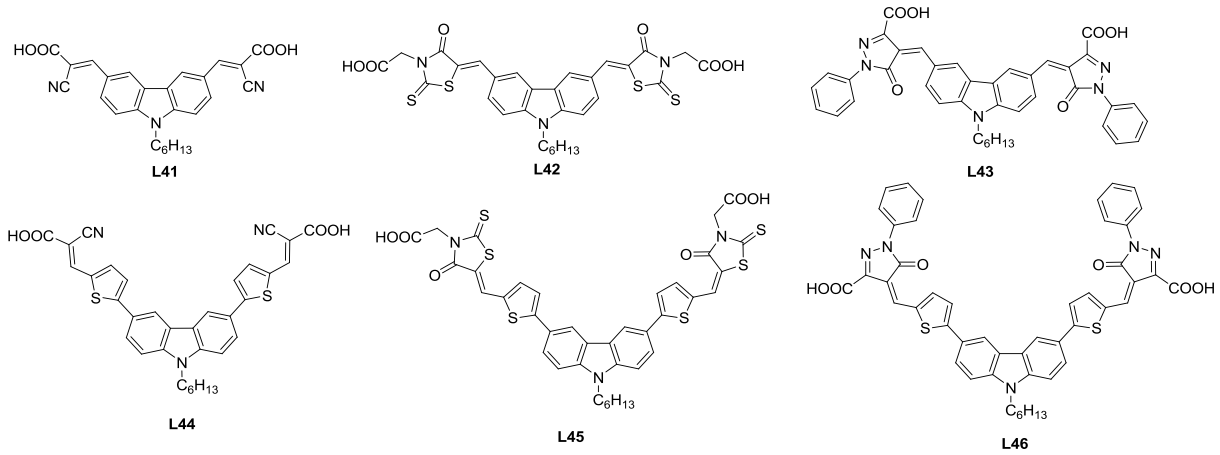

Chart 1.60 Organic dyes containing carbazole π-linking donor and various anchoring units.

The synthetic scheme of the dyes (**L42** and **L43**) is outlined in Scheme 1.51. It involves Knoevengel condensation of 9-hexyl-9*H*-carbazole-3,6-dicarbaldehyde with rhodanine acetic acid and 5-oxo-1-phenyl-4,5-dihydro-1*H*-pyrazole-3-carboxylic acid led to dyes **L42** and **L43** respectively. The synthesis of dyes **L44** is similar to the Scheme 1.50 and other dyes **L45** and **L46** are prepared according to Scheme 1.51.

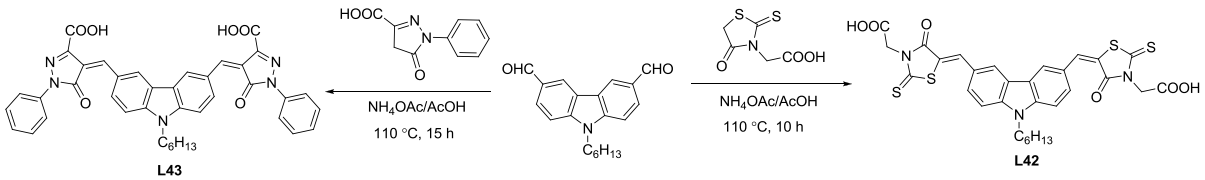

Scheme 1.51 Synthetic scheme of the dyes **L42** and **L43**.

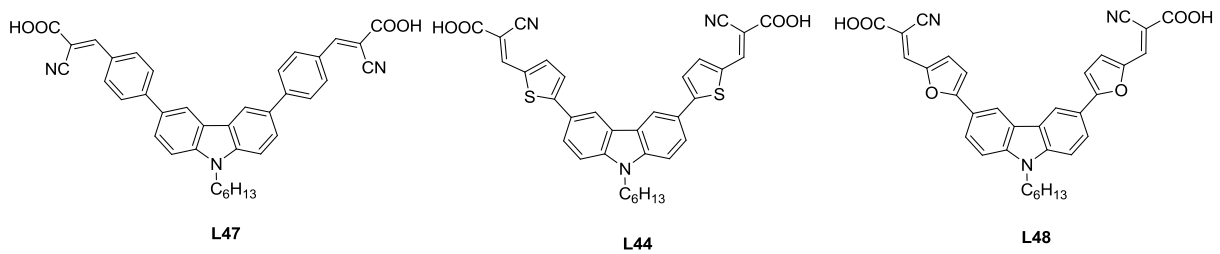

Chart 1.61 Organic dyes containing carbazole as π-linking donor with variation in π-spacers.

Chandrasekharam and co-workers designed and synthesized dyes with bi-anchoring sites at 3 and 6 positions of carbazole by varying linkers of phenyl, thiophene and furan results **L44**, **L47** and **L48** dyes (Chart 1.61) [162]. The synthesis of the dyes is outlined in Scheme 1.52. Suzuki coupling of 3,6-dibromo-9-hexyl-9*H*-carbazole with (4-formylphenyl)-, (5-formylthiophen-2-yl)-, or (5-formylfuran-2-yl)-boronic acid afforded carbazole bis-aldehyde derivatives. These aldehyde derivatives subsequently converted to the dyes (**L44**, **L47** and **L48**) via Knoevenagel condensation reaction with cyanoacetic acid. They studied systematically the effect of linker on the performance of bi-anchoring dyes. The absorption of the dyes with different linker is in the order of phenyl (362 nm) < thiophene (415 nm) < furan (427 nm) and this order follows the electron richness of the linker units. The superior absorption of **L44** led to higher J_{SC} of 8.90 mA cm^{-2} and caused better conversion efficiency of 3.8% with V_{OC} of 580 mV. The dye **L47** obtained efficiency of 3.4% with higher V_{OC} of 700 mV due to the low lying HOMO which favors the regeneration of the dye and reduces strong coupling of dye with TiO_2 film and inject electrons efficiently. The dye **L48** achieved efficiency of 3.2% with J_{SC} of 7.61 mA cm^{-2}, V_{OC} of 580 mV and *ff* of 0.73.

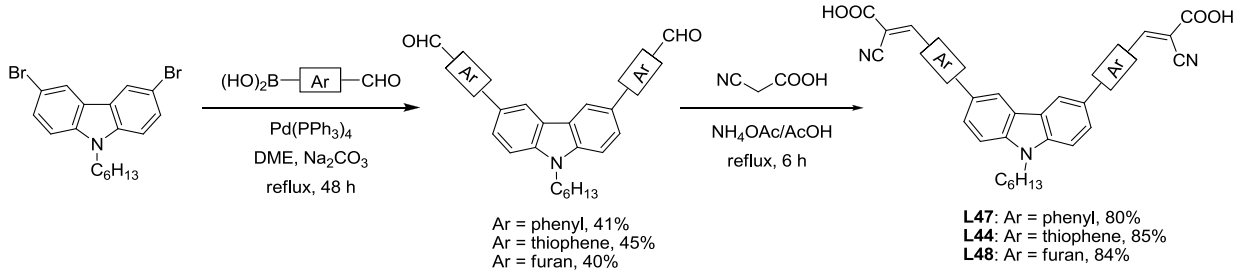

Scheme 1.52 Synthetic scheme of the dyes **L44**, **L47** and **L48**.

Anandan and co-workers extended the conjugation of **L36** by incorporation of cyanovinlylene between thiophene and carbazole produced **L49** dye [163]. The synthesis of the dyes is displayed

in Scheme 1.53. It started with reaction of 9-hexyl-9*H*-carbazole-3,6-dicarbaldehyde with 2-(thiophen-2-yl)acetonitrile by Knoevenagel condensation followed by VilsmeiereHaack formylation resulted in (2*E*,2'*Z*)-3,3'-(9-hexyl-9*H*-carbazole-3,6-diyl)bis(2-(5-formylthiophen-2-yl)acrylonitrile). 9-Hexyl-9*H*-carbazole-3,6-dicarbaldehyde was treated with 4-bromophenylacetonitrile and followed by Suzuki coupling with 4-formylphenylboronic acid resulted in di-aldehyde derivative. The aldehyde derivatives were converted to target dyes by reaction with cyanoacrylic acid under Knoevenagel condensation conditions.

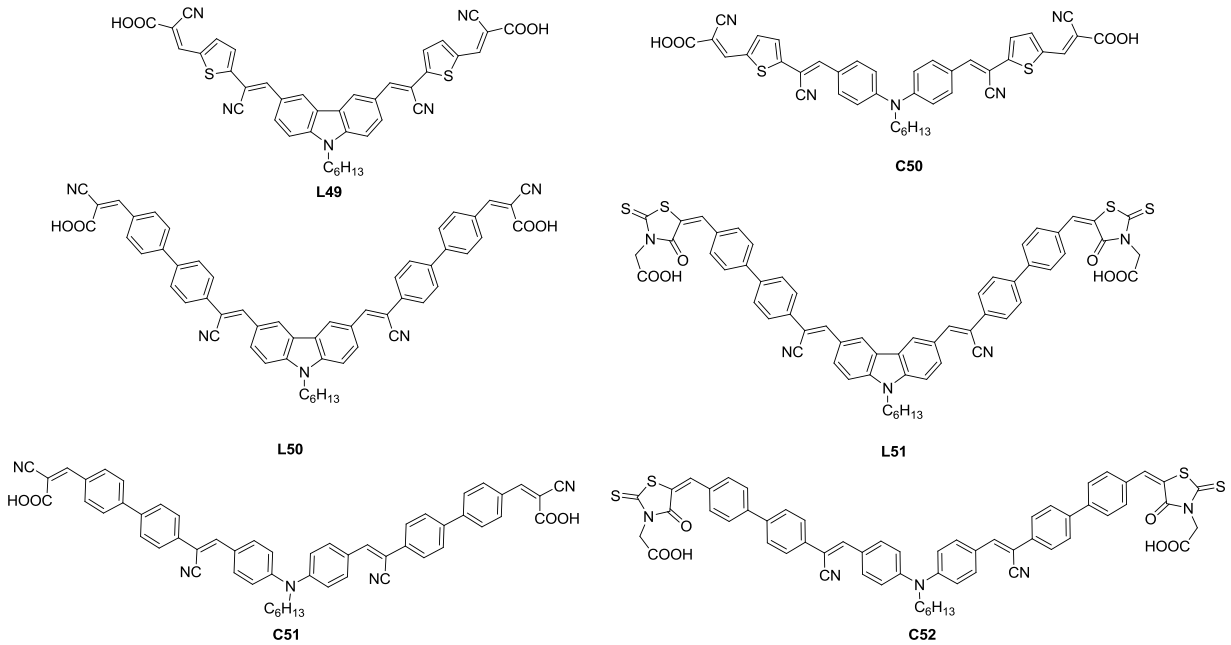

Chart 1.62 Compounds containing carbazole linker and triphenylamine auxiliary donor and related compounds.

The cyanovinylene substitution in **L49** lowered the LUMO level when compared to **L36**. This contributed to the reduction in photovoltage (V_{OC} = 660 mV) and lower conversion efficiency (4.04%). However, the dye **L49** displayed higher efficiency in DSSC when compared to the corresponding diphenylamine dye (**C50**, η = 3.16%) owing to higher dye loading for **L49** facilitated by planar carbazole and higher electron lifetime (~ 4 times). Later they have the extended the conjugation by replacing the thiophene unit with biphenyl unit resulted in new dyes (**L50**) with cyanoacrylic acid and rhodanine 3-acetic acid as acceptor [164]. When compared to the parent dyes (**L49**) these dyes displayed blue shifted absorption due to the twisting of the biphenyl unit, resulted in inferior conversion efficiency. The dye **L50** exhibited highest conversion efficiency of 2.37% than **L51** of efficiency 2.17% due to lower injection of the later

dye. Even though the diphenylamine dyes exhibited red shifted absorption than carbazole based dyes, they displayed inferior conversion efficiency due to the low lying LUMO level which produces poor injection efficiency.

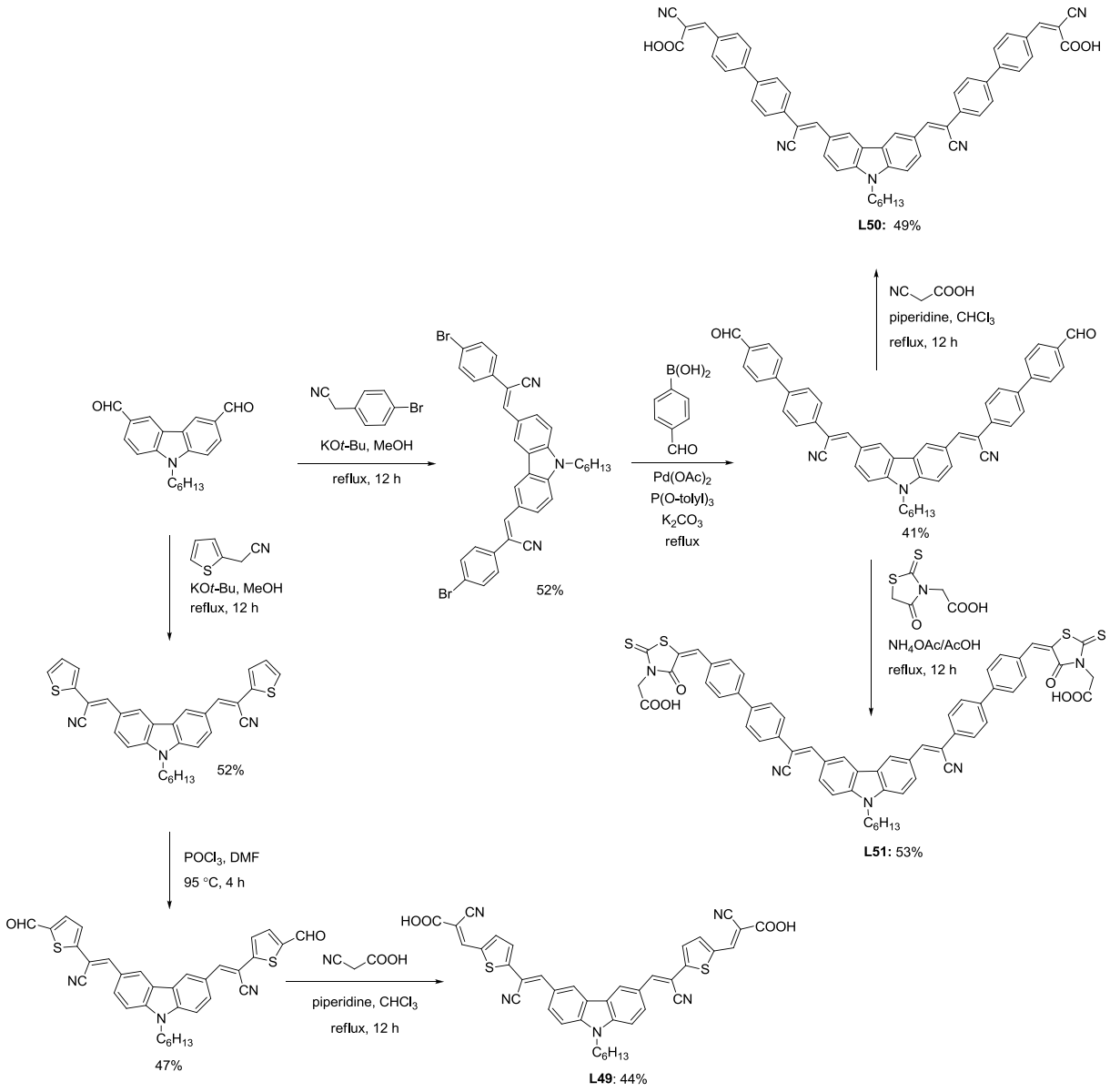

Scheme 1.53 Synthetic scheme of the dyes **L49-L51**.

Table 1.5 Optical, electrochemical and photovoltaic performance parameters of dyes containing carbazole as linker

Dye	$\lambda_{max,}$ nm (ε_{max}, M^{-1} cm^{-1})	E_{ox} , V (*vs* NHE)	E_{ox}^{*}, V (*vs* NHE)	J_{SC} (mA cm^{-2})	V_{OC} (mV)	*ff*	η (%)	*Ref*
L23	497 (7050)	1.07	−0.99	12.93	580	0.64	4.80	[152]
C37	437 (35600)	1.05	−1.29	13.47	600	0.59	4.77	[152]
C38	472 (38400)	1.08	−0.93	14.20	570	0.60	4.79	[152]
C39	475 (52700)	1.11	−1.09	18.14	610	0.56	6.16	[152]
C40	475 (51000)	1.12	−1.08	16.79	640	0.58	6.18	[152]
C41	462 (53800)	1.08	−1.02	13.54	600	0.64	5.25	[152]
L24	412 (21000)	1.11	−1.28	5.27	711	0.72	2.69	[153]
C42	466 (14000)	1.13	−2.20	12.18	826	0.65	6.55	[153]
L25	469 (22000)	1.03	−1.38	14.79	660	0.67	6.51	[155]
C43	457 (37000)	1.13	−1.21	14.25	700	0.71	7.03	[155]
C44	450 (33000)	1.13	−1.25	9.12	630	0.72	4.12	[155]
L26	422 (21400)	0.89	−1.49	9.36	786	0.72	5.29	[15]
C43	406 (28600)	1.00	−1.60	6.02	669	0.75	3.03	[15]
C44	414 (28000)	0.91	−1.57	7.50	704	0.72	3.84	[15]
L27	442 (27000)	0.88	−1.48	11.20	757	0.70	5.91	[15]
C45	384 (23000)	0.98	−1.72	6.83	666	0.74	3.36	[15]
C46	407 (20200)	0.89	−1.63	7.59	745	0.75	4.21	[15]
L28	442 (30000)	0.96	−1.38	11.12	741	0.68	5.59	[156]
L29	468 (36700)	0.95	−1.36	13.26	724	0.66	6.68	[156]
L30	468 (36400)	0.97	−1.34	12.31	737	0.67	6.35	[156]
L31	468 (33500)	0.95	−1.36	12.14	722	0.66	6.04	[156]
L32	379 (50800)	1.22	−1.14	14.12	774	0.58	6.37	[157]
L33	372 (30000)	1.21	−1.57	4.20	674	0.67	1.88	[157]
C47	425 (27100)	1.22	−1.19	12.00	776	0.56	5.24	[157]
L34	327 (21900)	1.54	−1.95	1.84	492	0.63	0.57	[158]
L35	378 (46100)	1.22	−1.75	4.72	556	0.61	1.61	[158]

Table 1.5 (Cont.)

Dye	$\lambda_{max,}$ nm (ε_{max}, $M^{-1}\,cm^{-1}$)	E_{ox} , V (*vs* NHE)	E_{ox}^{*}, V (*vs* NHE)	J_{SC} (mA cm^{-2})	V_{OC} (mV)	*ff*	η (%)	*Ref*
L35	450 (26360)	0.64	−1.92	7.61	589	0.63	2.81	[159]
C48	445 (24040)	0.62	−1.85	9.95	597	0.61	3.59	[159]
C49	489 (25480)	0.55	−1.63	10.60	658	0.70	4.91	[159]
L36	453 (33900)	1.37	−1.13	9.36	712	0.67	4.47	[160]
L37	470 (54000)	1.17	−1.13	10.52	701	0.68	5.01	[160]
L38	470 (58500)	0.80	−1.35	12.66	610	0.62	4.82	[143]
L39	455 (89200)	0.77	−1.50	10.63	640	0.67	4.55	[143]
L40	468 (102400)	0.78	−1.41	9.99	550	0.66	3.64	[143]
L41	389 (30580)	1.53	−1.49	4.10	620	0.68	1.70	[161]
L42	458 (62309)	1.47	−1.02	2.90	530	0.70	1.10	[161]
L43	464 (23569)	1.44	−0.84	2.10	560	0.69	0.80	[161]
L44	406 (43243)	1.32	−1.08	7.70	580	0.66	3.00	[161]
L45	474 (64658)	1.29	−0.92	4.90	540	0.67	1.80	[161]
L46	507 (64009)	1.30	−0.74	7.20	580	0.67	2.80	[161]
L47	362(34300)	1.35	−1.42	6.36	699	0.76	3.40	[162]
L44	415(32700)	1.27	−1.39	8.90	584	0.74	3.80	[162]
L48	427(39200)	1.25	−1.41	7.61	579	0.73	3.20	[162]
L49	438 (35526)	1.76	−0.78	7.64	656	0.68	4.04	[163]
C50	458 (38578)	1.57	−0.79	7.01	612	0.63	3.16	[163]
L50	419 (25000)	1.62	−1.06	5.18	766	0.51	2.37	[164]
C51	446 (32579)	1.39	−1.07	1.67	832	0.62	1.02	[164]
L51	421 (22313)	1.35	−1.26	5.56	709	0.47	2.17	[164]
C52	458 (28617)	1.47	−0.94	2.15	545	0.41	0.56	[164]

1.4 Carbazole as auxiliary donor for DSSC

The auxiliary donor (AD) concept has been widely used to improve the donor-acceptor interaction and consequently the charge migration efficiency from donor to acceptor. Particularly, the auxiliary donor when it is in conjugation with the donor can help to stabilize the cation radical formed on removal of electron by delocalizing the charge. Suitably selected auxiliary donor has been found to enrich the optical and electrochemical properties and led to improvement in the DSSC efficiency [4]. The advantages of using carbazole as AD in DSSC dyes are: (a) elongation in conjugation leads to red shifted absorption, (b) transition probability of charge transfer transition is increased due to push-push donor architecture, (c) hydrophobic nature of carbazole and bulkiness of the overall dye helps to stop the back electron transfer, and (d) the delocalization/stabilization of cation radical increases [8]. Carbazole can be deployed as auxiliary donor by C2, C3, or *N*9-substitution.

1.4.1 Carbazole as auxiliary donor via C2-position

The generally adopted structural composition of the organic dyes with carbazole as auxiliary donor via C2-substitution is illustrated in Figure 1.9. Since the conjugation of the donor is extended to carbazole nitrogen, the donor strength may not experience uplift, but due to extended π-conjugation, delocalization of charge is favorable.

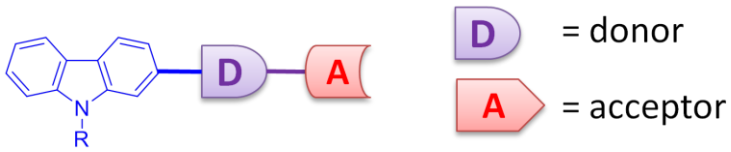

Figure 1.9 Molecular configuration of organic dyes using C2-carbazole as auxiliary donor.

The effect of carbazole as auxiliary donor on simple triphenylamine-based metal free organic dyes was studied by Wang and co-workers. They have prepared three new dyes (Chart 1.63, **AD1**–**AD3**) based on triphenylamine framework and featuring one or two carbazole or acceptor units in a dye [165]. The synthesis of the dyes is outlined in Scheme 1.54. The Suzuki coupling of 4-((4-bromophenyl)(phenyl)amino)benzaldehyde, 4-(bis(4-bromophenyl)amino)benzaldehyde and 4,4'-(4-bromophenylazanediyl)dibenzaldehyde with 2-(4,4,5,5-tetramethyl-1,3,2-

dioxaborolan-2-yl)-9*H*-carbazole led to corresponding triphenylamine aldehyde derivatives which converted to dyes (**AD1**-**AD3**) by Knoevenagel condensation.

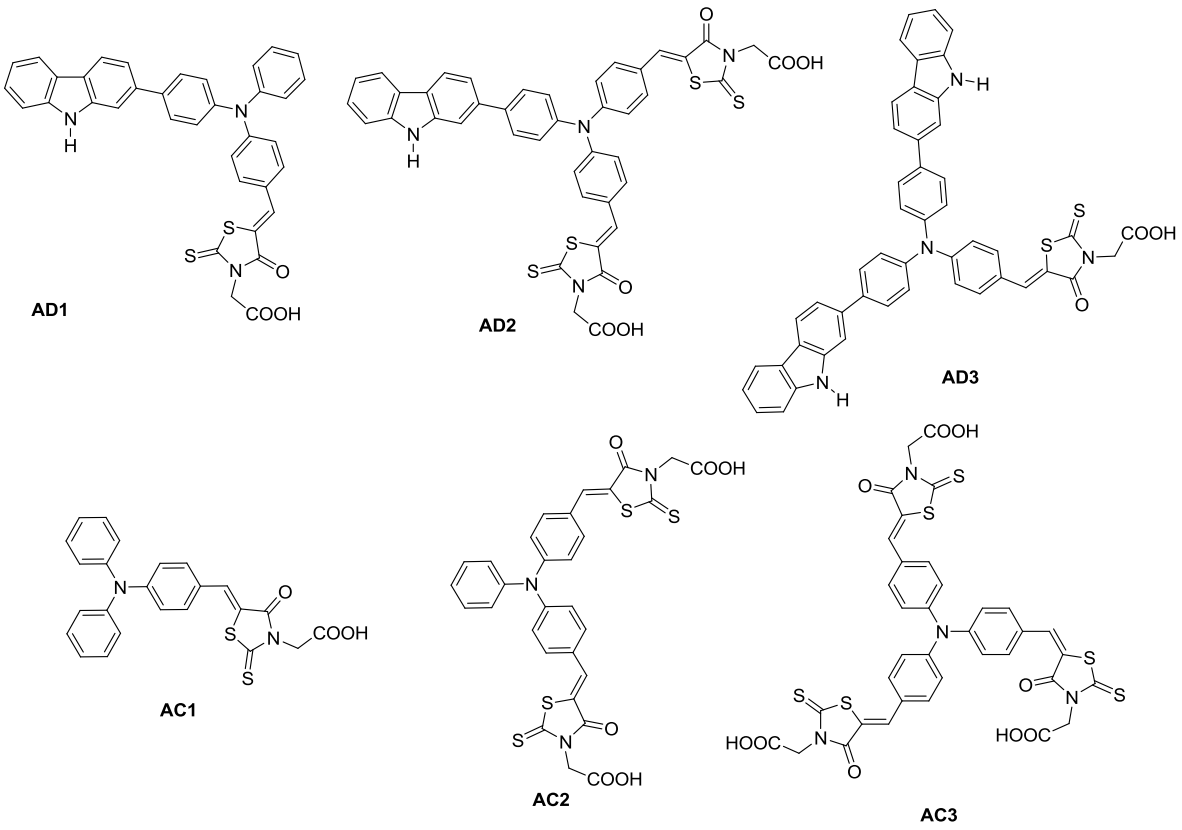

Chart 1.63 Dyes **AD1**−**AD3** with carbazole as auxiliary donor and related parent dyes.

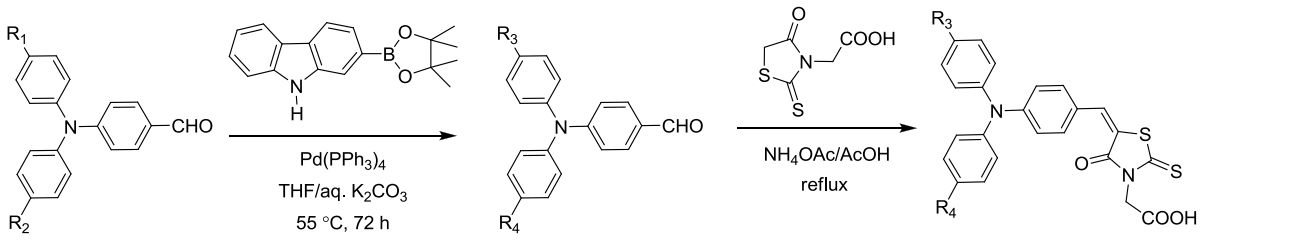

Scheme 1.54 Synthetic scheme of the dyes **AD1**-**AD3**.

The dyes (**AD1**-**AD3**) displayed red-shifted (15-24 nm) absorption when compared to the parent dyes (**AC1**-**AC3**) [166] which established the conjugating effect of carbazole segment. Moreover, introduction of two carbazole units in a dye (**AD3**) benefits the absorption significantly than the dye (**AD2**) containing two acceptor units. Probably in the former dye due

to the presence of two carbazole auxiliary donors the donor-acceptor interaction is enhanced, while in the later dye, it is bifurcated between the two acceptors. Finally, **AD3** displayed higher power conversion efficiency (4.63%) due to larger photocurrents (J_{SC} = 12.70 mA cm^{-2}) when compared to **AD1** and **AD2**.

Table 1.6 Optical, electrochemical and photovoltaic performance parameters of dyes containing carbazole as auxiliary donor

Dye	λ_{max}, nm (ε_{max}, M^{-1} cm^{-1})	E_{ox}, V (*vs* NHE)	E_{ox}^{*}, V (*vs* NHE)	J_{SC} (mA cm^{-2})	V_{OC} (mV)	*ff*	η (%)	*Ref*
AD1	470 (35564)	0.85	−1.27	10.60	579	0.58	3.54	[166]
AD2	491 (28702)	0.88	−1.08	12.70	598	0.61	4.63	[166]
AD3	477 (20170)	0.97	−1.04	5.06	561	0.59	1.67	[166]
AC1	455 (35264)	0.81	−1.53	13.20	562	0.58	4.28	[166]
AC2	467 (44827)	0.81	−1.36	14.20	560	0.60	4.77	[166]
AC3	480 (54656)	0.81	−1.51	11.00	530	0.51	2.97	[166]

1.4.2. Carbazole as auxiliary donor via C3-position

Carbazole has been successfully employed as auxiliary donor via C3-substitution due to facile chemical functionalization possible and vide variety of reactions at this position. Either the carbazole has been used as a part of triarylamine donor or linked *via* an extended conjugation with the amine donor (Figure 1.10). In the former configuration the oxidation potential of the dyes are negatively shifted indicating the donor support of carbazole.

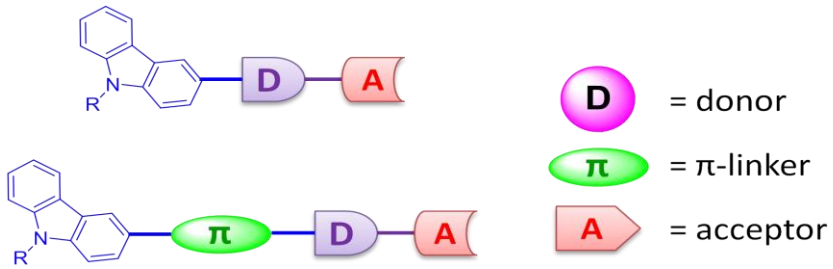

Figure 1.10 Molecular architecture of metal free organic dyes utilizing carbazole as auxiliary donor via C3 linkage.

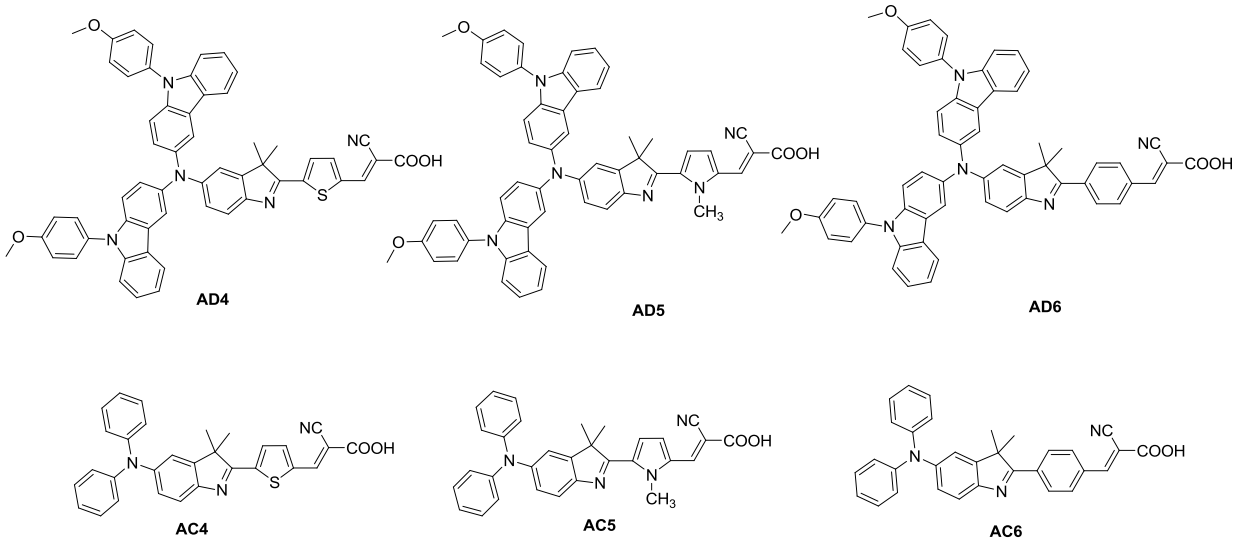

Chart 1.64 Dicarbazolylamine-based organic dyes.

Though the organic dyes featuring trifluorenylamine and 2,7-diaminofluorene donors have been demonstrated as successful sensitizers in DSSC, their carbazole counterparts remained unexplored. Freeman and co-workers synthesized organic materials (Chart 1.64) possessing dicarbazolylamine unit and compared their optical and electronic properties with the corresponding diphenylamine analogs [167]. The synthesis of the dyes showed in Scheme 1.55. Ullmann coupling of carbazole with 1-iodo-4-methoxybenzene gave the 9-(4-methoxyphenyl)-9*H*-carbazole which nitrated with urea nitrate and followed by reduction with tin chloride led to 9-(4-methoxyphenyl)-9*H*-carbazol-3-amine. It reacted with 3-bromo-9-(4-methoxyphenyl)-9*H*-carbazole, which obtained by bromination of 9-(4-methoxyphenyl)-9*H*-carbazole, via Pd-catalyzed C-N coupling afford bis(9-(4-methoxyphenyl)-9*H*-carbazol-3-yl)amine. Pd-catalyzed C-N coupling of 5-bromo-3,3-dimethyl-2-(thiophen-2-yl)-3*H*-indole with bis(9-(4-methoxyphenyl)-9*H*-carbazol-3-yl)amine. It reacted with BuLi followed by addition of DMF led to its aldehyde derivative which converted to the dye (**AD4**) by Knoevenagel condensation with cyanoacetic acid. Iodination of 5-bromo-3,3-dimethyl-2-(1-methyl-1*H*-pyrrol-2-yl)-3*H*-indole with NIS led to its mono iodo derivative which converted aldehyde derivatives by lithiation with *n*-BuLi and followed by addition of DMF. Target dyes (**AD5** and **AD6**) obtained by reacting aldehyde derivatives with cyanoacetic acid via Knoevenagel condensation.

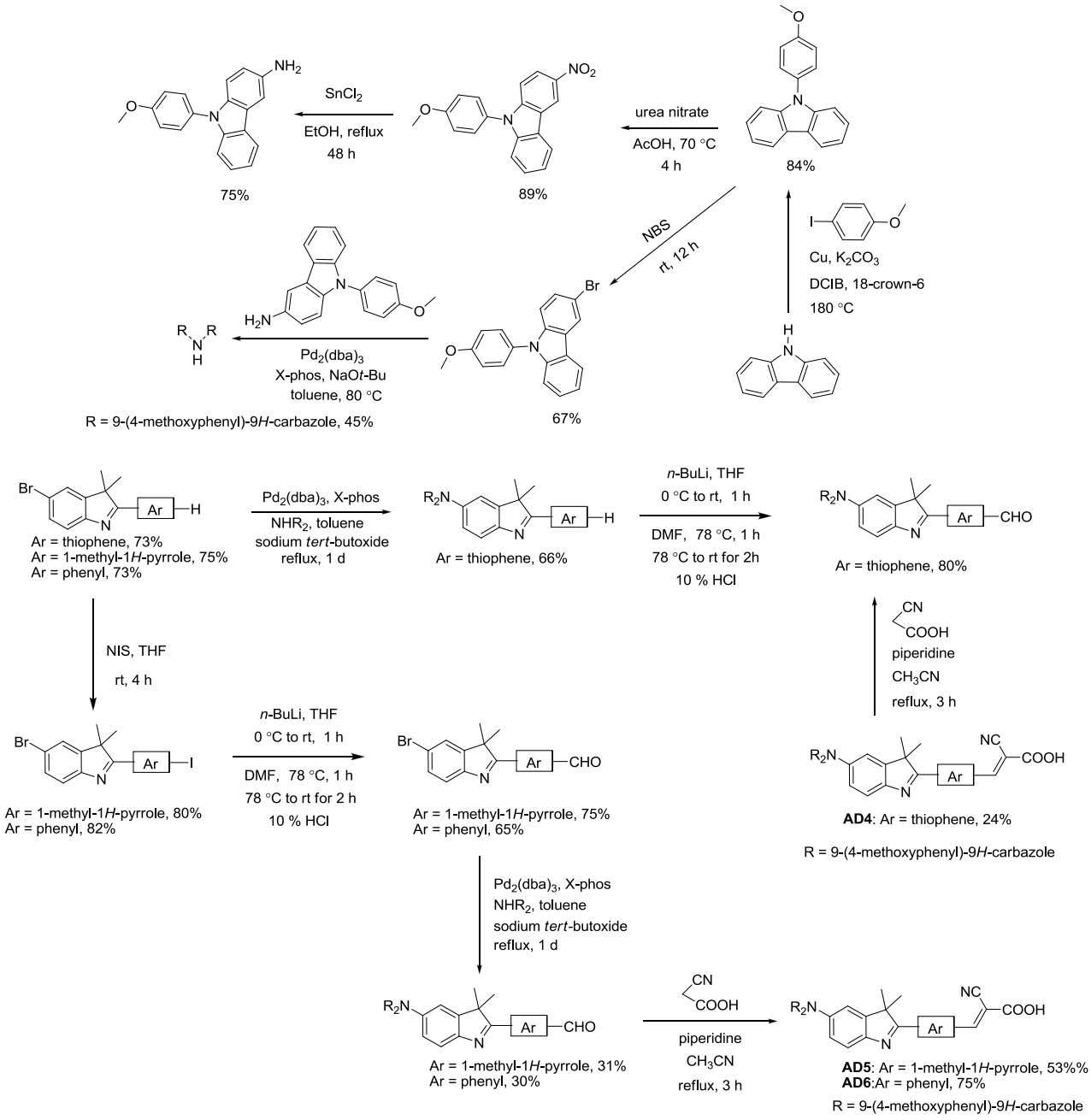

Scheme 1.55 Synthetic scheme of the dyes **AD5-AD6**.

The bis-carbazole dyes (**AD4-AD6**) exhibited red shifted absorption (~ 40 nm) when compared to the diphenylamine analogs (**AC4-AC6**) [168] due to more planar geometry and high donor strength of amine. However their performance in DSSC was affected by their aggregation tendency. The best performance obtained for **AD4** with J_{SC} = 5.35 mA cm^{-2}, V_{OC} = 564 mV, *ff* = 0.68 corresponding an overall conversion efficiency of 2.05%. Addition of CDCA improved the efficiency of the dyes marginally.

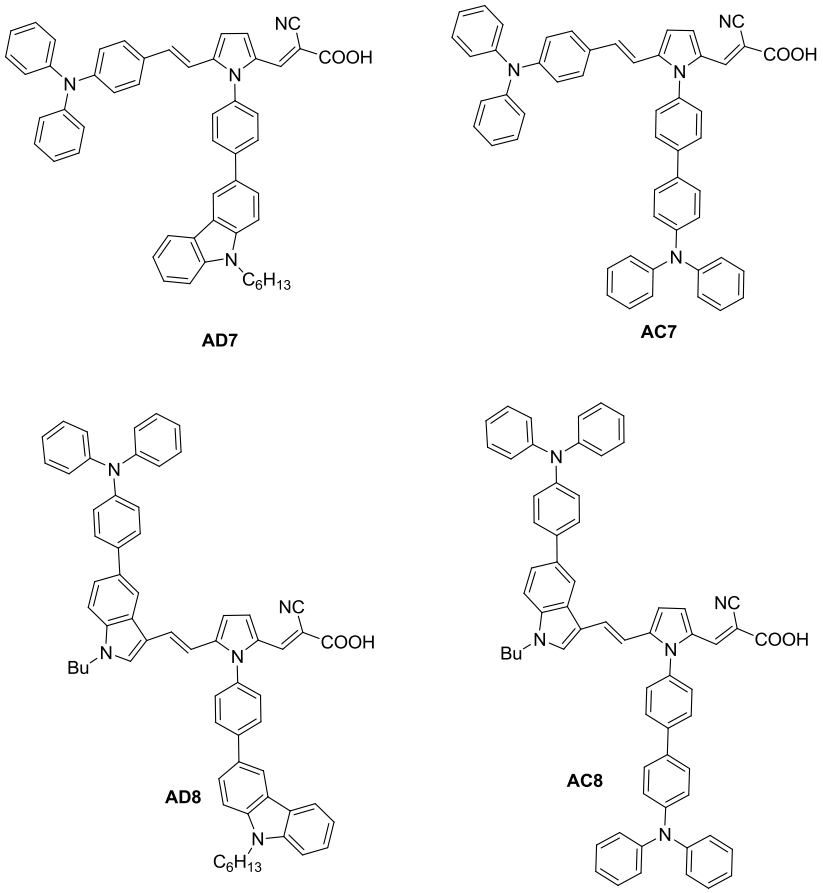

Chart 1.65 Dyes designed to impede dye aggregation based on pyrrole linker.

A novel strategy was adopted by Li and co-workers to suppress the aggregation at the surface of TiO_2 [169]. They have taken a dye with triphenylamine donor, pyrrole linker and cyanoacrylic acid acceptor and functionalized the pyrrole nitrogen with an auxiliary donor of carbazole, triphenylamine donor (Chart 1.65). The synthesis of dyes is showed in Scheme 1.56. Formylation of 1-(4-bromophenyl)-1*H*-pyrrole by Vilsmeier reaction which reacted with diethyl 4-(diphenylamino)benzylphosphonate by Wittig reaction gave (*E*)-4-(2-(1-(4-bromophenyl)-1*H*-pyrrol-2-yl)vinyl)-*N*,*N*-diphenylaniline. It formylated again by Vilsmeier reaction gave (*E*)-1-(4-bromophenyl)-5-(4-(diphenylamino)styryl)-1*H*-pyrrole-2-carbaldehyde which coupled with 9-hexyl-9*H*-carbazol-3-ylboronic acid by Suzuki coupling led to corresponding aldehyde. It reacted with cyanoacetic acid by Knoevenagel condensation gave the dye **AD7**. The synthesis of dye **AD8** is also similar to the dye **AD7**.

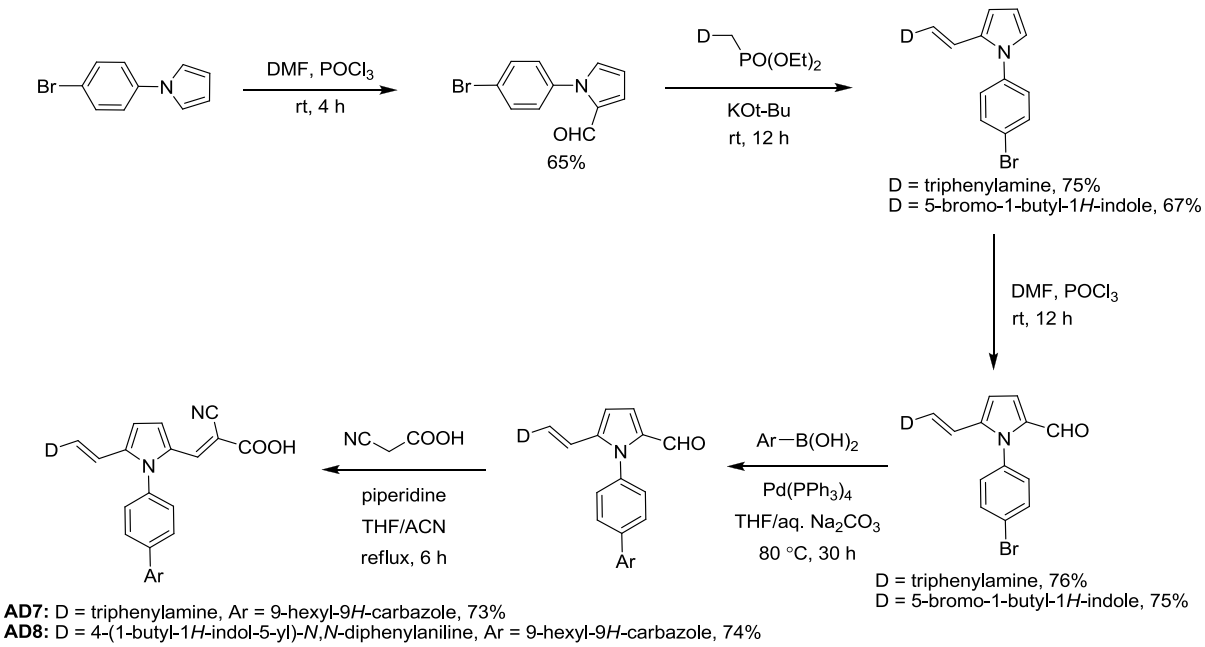

Scheme 1.56 Synthetic scheme of the dyes **AD7** and **AD8**.

The absorption of this exotic dye, **AD7** showed blue shifted absorption profile when compared to the triphenylamine functionalized dye, **AC7**. This resulted in a lower J_{SC} and efficiency (4.62%). However, the dye deploying triphenylamine as auxiliary donor (**AC7**) exhibited high power conversion efficiency (7.21%). The vinyl triphenylamine donor was replaced by indole connected with triphenyl amine result dyes (**AD8** and **AC8**) [170]. The dyes shows poor performance (4.31%) compared to **AD7** and **AC7** due to the low lying LUMO of dyes not favorable for effective injection of electrons into CB of TiO_2.

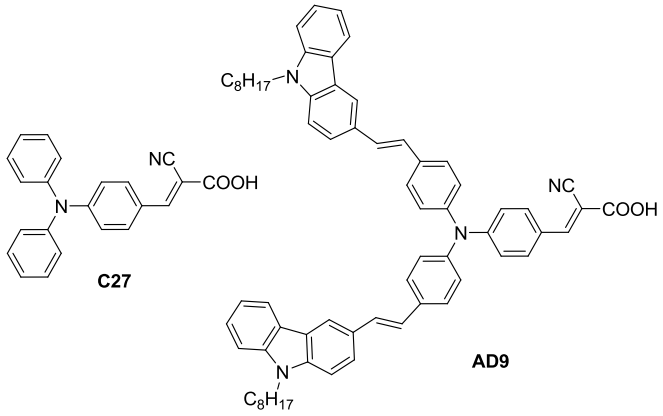

Chart 1.66 Dye possessing 3-vinylcarbazole chromophore and its parent dye.

The performance of the simple triphenylamine-based dye (*E*)-2-cyano-3-(4-(diphenylamino)phenyl)acrylic acid (**C27**) was improved by extending the conjugation with vinylcarbazole chromophore (Chart 1.66). Lu and co-workers successfully made Y shaped dyes based on triphenylamine containing 9-octyl-9*H*-carbazole-vinyl, triphenylamino-vinyl and 10-octyl-10*H*-phenothiazine-vinyl as arms cyanoacrylicacid as acceptor [171]. The synthesis of the dye **AD9** is showed in Scheme 1.57. The Heck reaction between 4-(bis(4-iodophenyl)amino)benzaldehyde and 9-octyl-3-vinyl-9*H*-carbazole catalyzed by afforded 4-(bis(4-((*E*)-2-(9-octyl-9*H*-carbazol-3-yl)vinyl)phenyl)amino)benzaldehyde. It easily transformed into dye **AD9** via Knoevenagel reaction in a yield of 74%. Generally the vinyl conjugated organic dyes show exceptional molar extinction coefficient for the absorption peaks and this increases the generation of photocurrent density. **AD9** showed overall efficiency (3.63%) with J_{SC} = 9.42 mA cm^{-2}, V_{OC} = 730 mV and *ff* = 0.53.

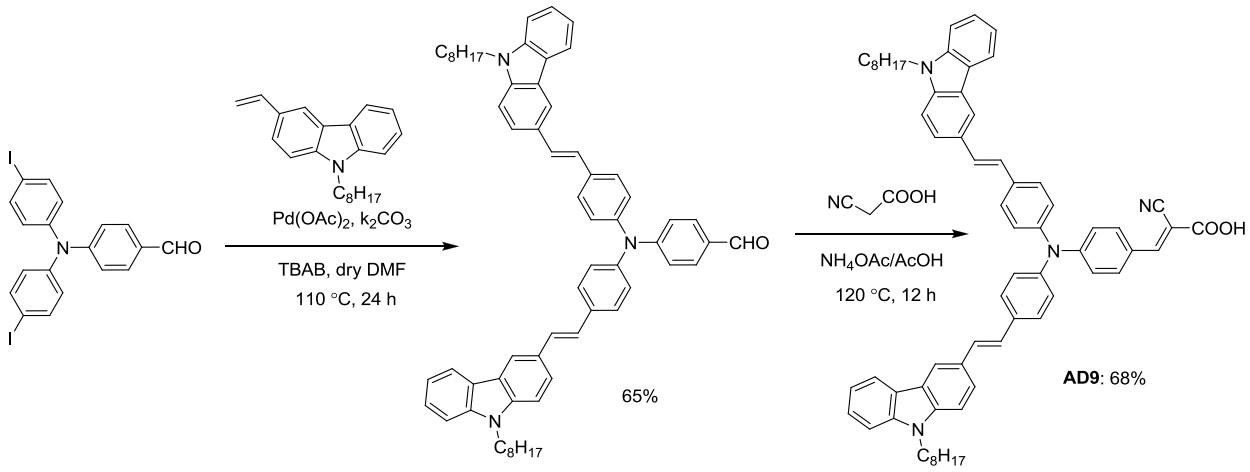

Scheme 1.57 Synthetic scheme of the dye **AD9**.

Zhu and co-workers achieved an excellent stability for DSSC through molecular engineering of indoline dyes (Chart 1.67) [172]. They have introduced 4-tolyl, 2-fluorenyl and 3-carbazolyl units at indoline nitrogen to achieve highly efficient organic dyes. The synthesis of the dyes is displayed in Scheme 1.58. Reaction of 4-(9-pentyl-9*H*-carbazol-3-yl)-1,2,3,3*a*,4,8*b*-hexahydrocyclopenta[*b*]indole-7-carbaldehyde with wittig salt of thiophene gave (*E*)-9-pentyl-3-(7-(2-(thiophen-2-yl)vinyl)-1,2,3,3*a*-tetrahydrocyclopenta[*b*]indol-4(8*bH*)-yl)-9*H*-carbazole. It is lithiated with BuLi followed by the addition of DMF led to its aldehyde derivative which converted to dye (**AD10**) by Knoevenagel condensation. Suzuki coupling of 3-(7-bromo-

1,2,3,3*a*-tetrahydrocyclopenta[*b*]indol-4(8*bH*)-yl)-9-pentyl-9*H*-carbazole with 5-formylthiophen-2-ylboronic acid led to corresponding aldehyde which converted to dye (**AD11**) by Knovevenagel condensation. The synthesis of the dye **AD12** is similar to **AD11** by using 5-formylfuran-2-ylboronic acid.

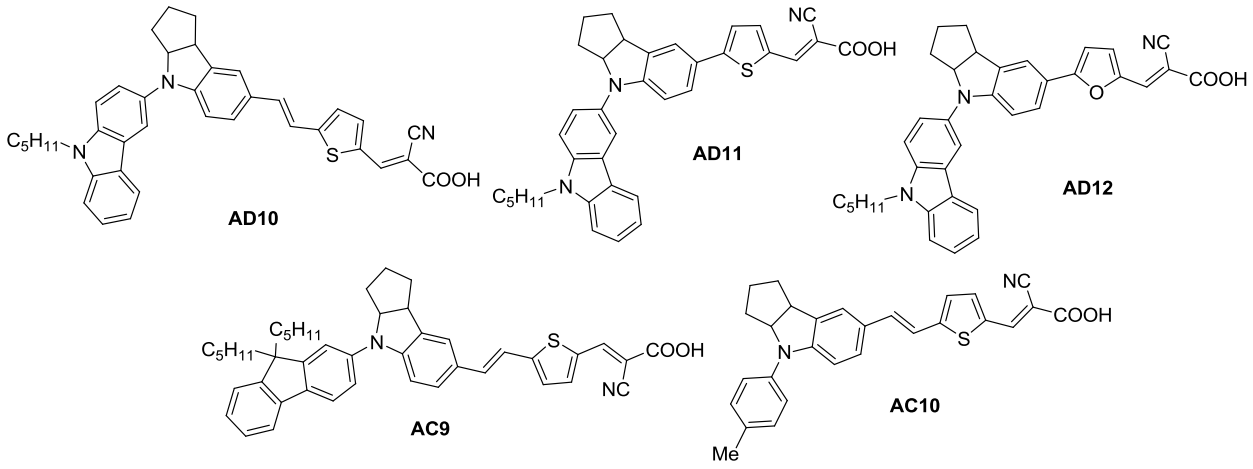

Chart 1.67 Organic dye containing *N*-carbazolylindoline donor and related compounds.

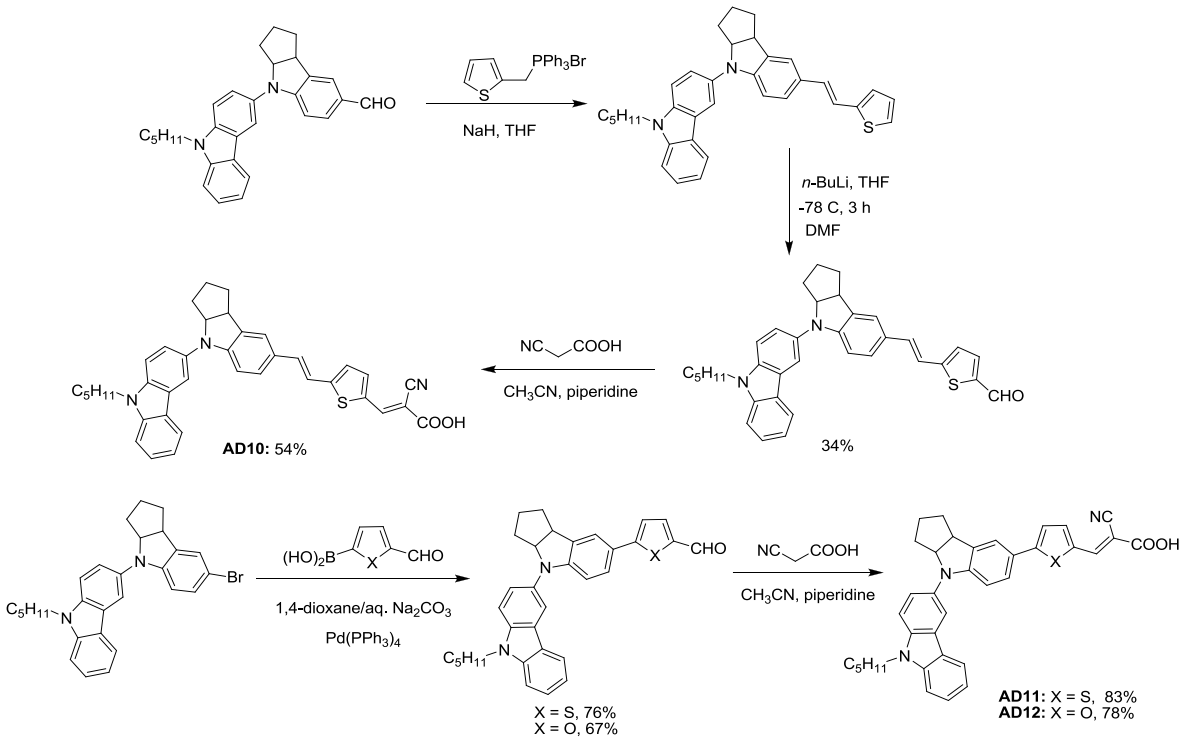

Scheme 1.58 Synthetic scheme of the dyes **AD10**-**AD12**.

The carbazole substituted dye **AD10** showed longer wavelength absorption in the series. This supports the strong electron releasing effect of carbazole. The LUMO of **AD10** is highly negative (–1.95 V) when compared to the CB of TiO_2 which facilitates the injection of electrons to CB of TiO_2. This thermodynamic driving force results in a high J_{SC} of 14.16 mA cm^{-2} and overall efficiency of 5.87%. Despite **AD10** showing broad IPCE spectra in the range of 350-800 nm, low efficiency observed was attributed to aggregation of dyes at the surface of TiO_2. Supporting this hypothesis the addition of CDCA to the dye bath significantly improved the device efficiency (8.49%) with J_{SC} = 18.53 mA cm^{-2}, V_{OC} = 649 mV and *ff* = 0.71. The carbazole substitution increased the donor strength and shifted the LUMO more negatively. Later they have synthesized two dyes (**AD11** and **AD12**) by the introduction of thiophene or furan in place of vinyl thiophene unit of dye **AD10** [173]. The dyes (**AD11** and **AD12**) achieved remarkable efficiencies (9.29% and 9.49%) and photo stability owing to the up shift of CB of TiO_2 resulting in a higher V_{OC} values (756 mV and 779 mV).

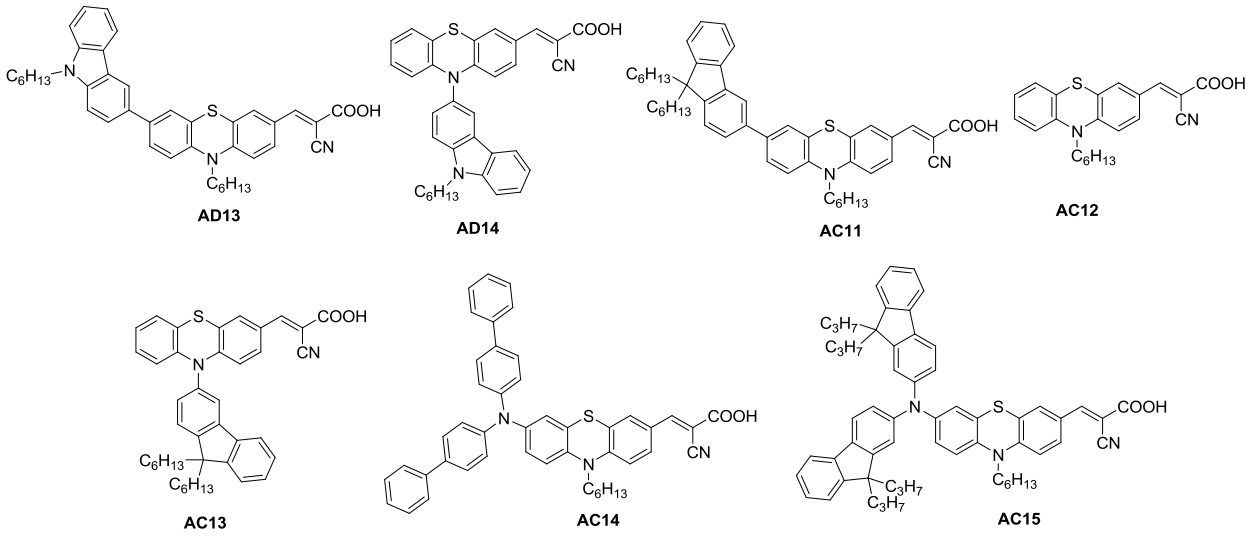

Chart 1.68 Structures of the dyes with phenothiazine linker containing fluorene and carbazole donors.

Wang and Zhu co-workers examined the effect of conjugation on the performance of dyes based on phenothiazine where one set of dyes made by keeping donors (carbazole and flurorene; **AD13** and **AC11**) on C7 position and acceptor at C3-position and another set of dyes made by attaching donors (carbazole and flurorene; **AD14** and **AC13**) at *N*10 position and acceptor at C3-position [174]. The dyes are synthesized according the scheme outlined in Scheme 1.59. N-

alkylation of phenothiazine with hexylbromide in presence of base affords 10-hexyl-10*H*-phenothiazine, which formylated with $POCl_3$ via Vilsmeier-Haack reaction gave 10-hexyl-10*H*-phenothiazine-3-carbaldehyde. It brominated with NBS in THF gave the intermediate 7-bromo-10-hexyl-10*H*-phenothiazine-3-carbaldehyde. It reacted with 9-hexyl-9*H*-carbazol-3-ylboronic acid or dibiphenyl-4-ylamine *via* Suzuki and Ullmann coupling respectively gave the corresponding aldehyde derivatives. These aldehyde derivatives converted to dyes (**AD13** and **AC14**) by Knoevenagel condensation with cyanoacetic acid. Ullmann coupling of phenothiazine with 3-bromo-9-hexyl-9*H*-carbazole gave 10-(9-hexyl-9*H*-carbazol-3-yl)-10*H*-phenothiazine-3-carbaldehyde and it converted to the dye (**AD14**) by reacting with cyanoacetic acid.

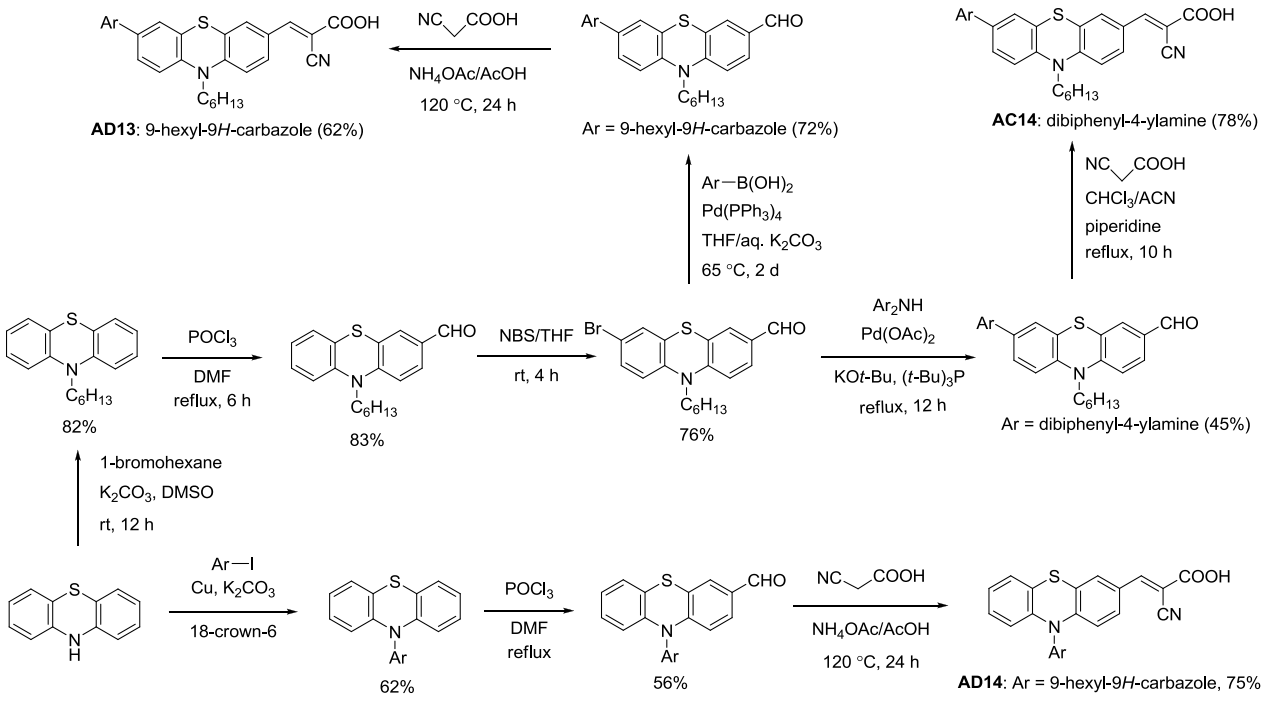

Scheme 1.59 Synthetic scheme of the dyes **AD13** and **AD14**.

The first set of dyes (**AD13** and **AC11**) having long conjugation showed red shifted absorption when compared to second set of dyes (**AD13** and **AC13**) resulted in better light harvesting properties and higher efficiencies for the former set of dyes. The dye containing carbazole as donor, **AD13** shows higher efficiency of 6.72% with J_{SC} of 12.38 mA cm^{-2}, high V_{OC} of 829 mV and *ff* of 0.66 when compared with a dye containing fluorene as donor (**AC11**) efficiency, 6.13% with J_{SC} of 12.43 mA cm^{-2}, high V_{OC} of 767 mV and *ff* of 0.64 due to the high

light harvesting property and recombination resistance of the former dye. Zhu co-workers introduced the different arylamine units instead of the carbazole at the C7-position of phenothiazine in **AD13** dye gave **AC14** and **AC15** dyes [175] (Chart 1.68). The incorporation of arylamine units extends the conjugation and molar extinction coefficient of the charge transfer transition than parent dye. However the absorption wavelength, **AD13** sensitized DSSCs affords a J_{SC} of 14.02 mA cm^{-2}, V_{OC} of 748 mV and a fill factor of 0.68 and overall conversion efficiency of 7.13%. The sterically crowded arylamine donor containing dye (**AC14**) decrease the amount of dye loading on the TiO_2 film which led to decrease in J_{SC} and overall conversion efficiencies of 6.14%. The low lying LUMO of the dye **AC15** gave the poor injection efficiency and lower power conversion efficiency of 6.49%.

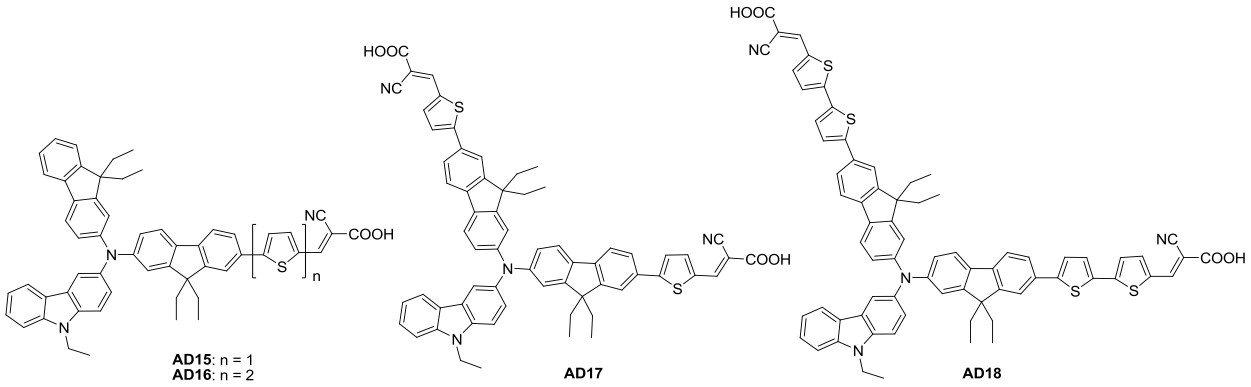

Chart 1.69 Structure of the triarylamine dyes with carbazole donor and mono anchoring and di-anchoring acceptors.

Thomas and coworkers designed and synthesized a set of dyes (**AD15-AD18;** Chart 1.69) with triarylamine donor composed of fluorene and carbazole and compared the photophysical properties and photovoltaic efficiencies of monoanchoring with dianchoring dyes [176]. The introduction of dianchoring unit lowers the LUMO level and diminishes the electron injection. Monoanchoring dyes posses red shifted absorption with two to five fold increments in the molar extinction coefficient and this is responsible for higher efficiency of the monoanchoring dyes (2.71% to 3.73%) compared to dianchoring dyes (0.90 to 1.63%).

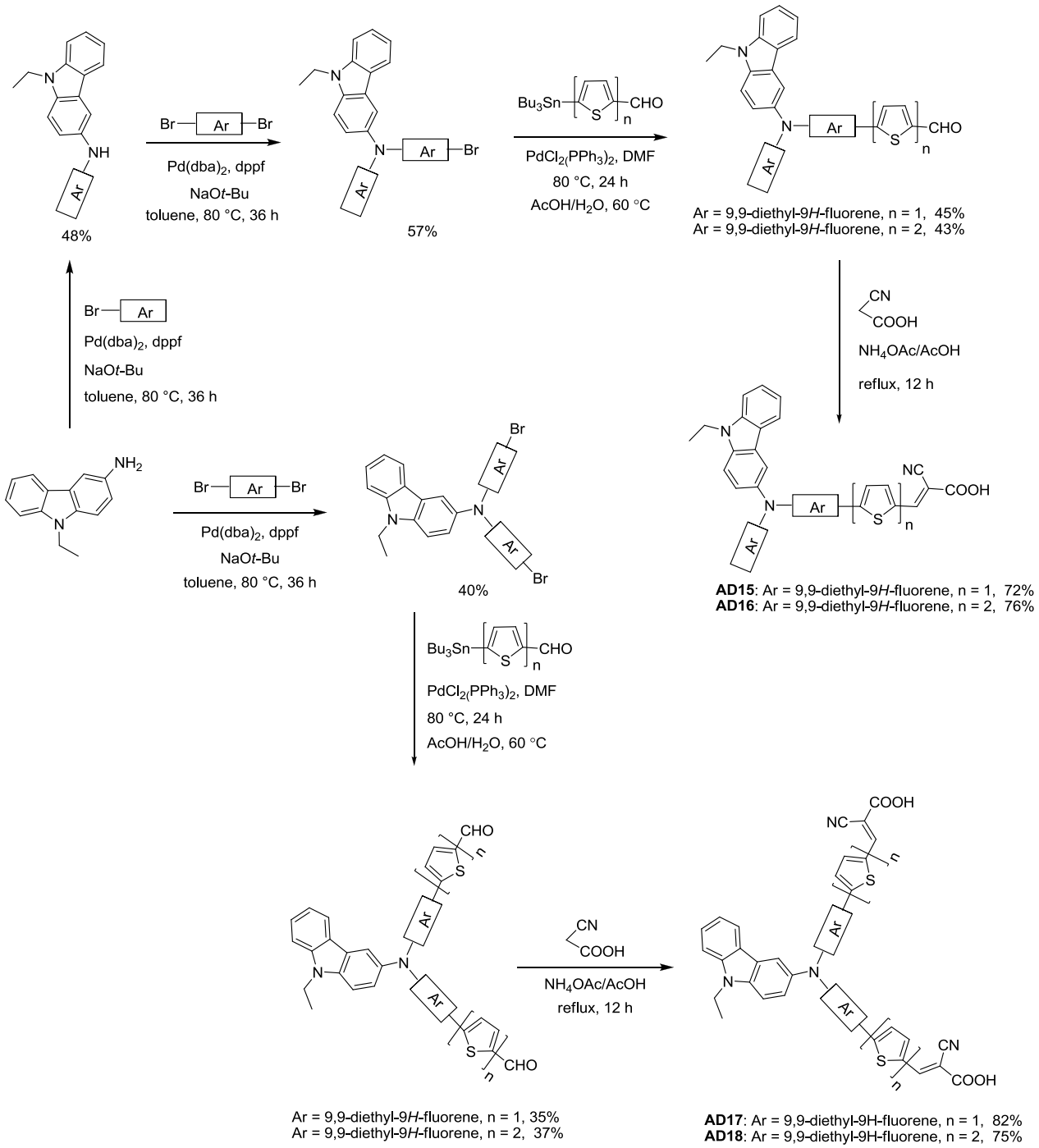

Scheme 1.60 Synthetic scheme of the dyes A**D15-AD18**.

The synthesis of the dyes is outlined in Scheme 1.60. N-(9,9-diethyl-9*H*-fluoren-2-yl)-9-ethyl-9*H*-carbazol-3-amine synthesized via Pd-catalyzed C-N coupling reaction of 2-bromo-9,9-diethyl-9*H*-fluorene with 9-ethyl-9*H*-carbazol-3-amine. It reacted with 2,7-dibromo-9,9-diethyl-9*H*-fluorene under similar conditions to afford *N*-(7-bromo-9,9-diethyl-9*H*-fluoren-2-yl)-*N*-(9,9-

diethyl-9*H* fluoren-2-yl)-9-ethyl-9*H*-carbazol-3-amine which coupled with protected stannylene derivatives of thiophene or bithiophene aldehydes followed by acid hydrolysis. These aldehyde derivatives converted to target dyes (**AD15**, **AD16**) by Knoevenagel condensation with cyanoacetic acid. The reaction of excess 2,7-dibromo-9,9-dibutyl-9*H*-fluorene with 9-ethyl-9*H*-carbazol-3-amine produced the required *N*,*N*-bis(7-bromo-9,9-dibutyl-9*H*-fluoren-2-yl)-9-ethyl-9*H*carbazol-3-amine in reasonable yield and it converted into the desired aldehydes by Stille coupling reactions with the protected stannylene derivatives of thiophene or bithiophene aldehydes followed by acid hydrolysis. Finally, the desired dyes (**AD17**, **AD18**) were obtained by the Knoevenagel condensation of these aldehydes with cyanoacetic acid.

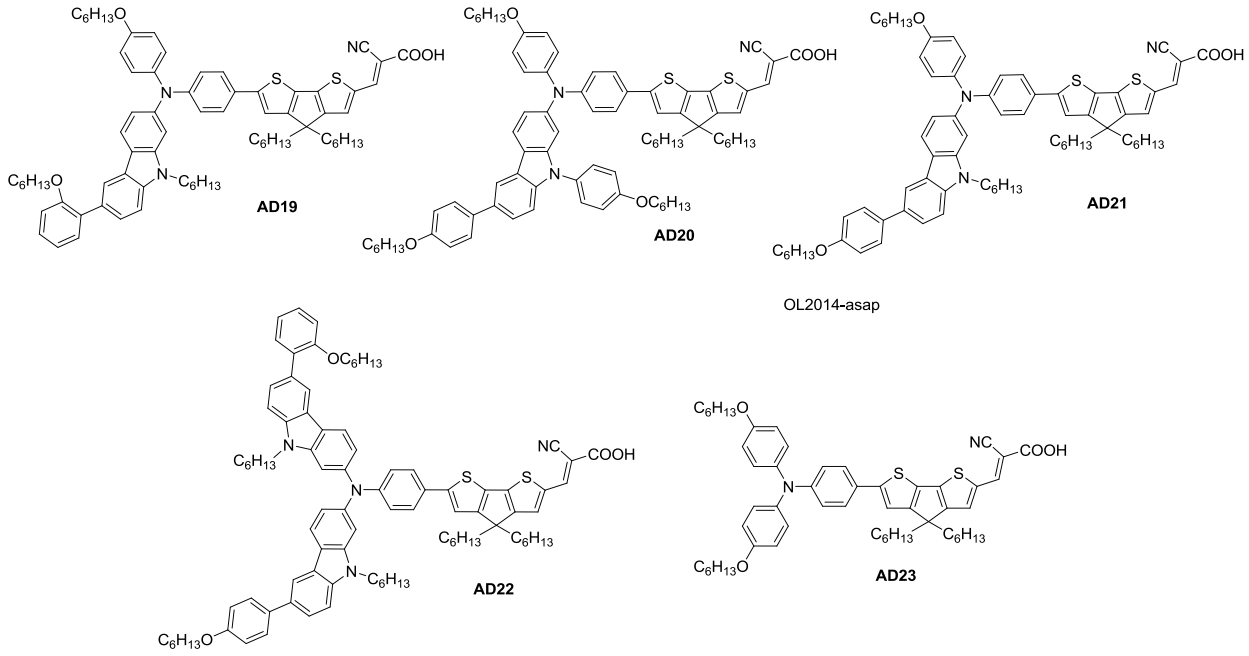

Chart 1.70 Structures of the dyes containing carbazole auxiliary donor via C3-position.

Liang and co-workers [177] synthesized **AD19-AD22** (Chart 1.70) novel triphenylamine donors with carbazole moieties for organic sensitizers and demonstrated asymmetric design of the triphenylamine electron donor containing dyes exhibited superior performance than symmetrical triphenylamine donor containing dyes in DSSC application with cobalt(II/III) redox electrolyte. The synthesis of the dyes is shown in Scheme 1.61. The synthesis of dye **AD20** began with Suzuki coupling of 3-bromo-9-(4-(hexyloxy)phenyl)-6-nitro-9*H*-carbazole with 2-(4-(hexyloxy)phenyl)-4,4,5,5-tetramethyl-1,3,2-dioxaborolane, followed by reduction of the nitro group and subsequent reaction with 1-bromo-4-(hexyloxy)-benzene by Hartwig-Buchwald C-N

coupling reaction. This secondary amine treated with bromo derivative of aromatic compound, followed by Vilsmeier-Haack reaction gave the aldehyde derivative. The target dyes were obtained via Knoevenagel condensation reaction of the aldehydes with cyanoacetic acid in the presence of a catalytic amount of piperidine. Other dyes are also prepared similarly according to the Scheme 1.61.

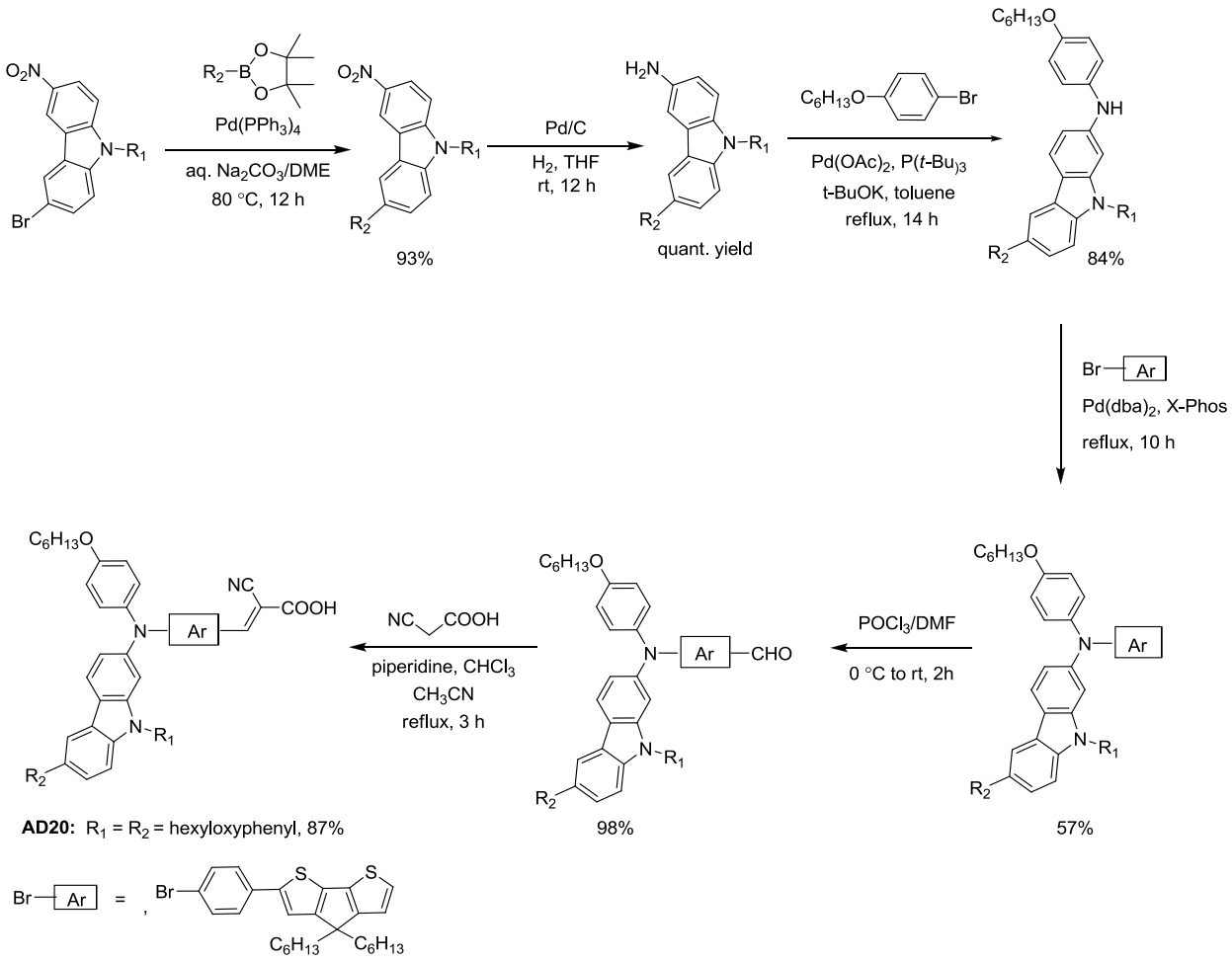

Scheme 1.61 Synthetic scheme of the dye **AD20**.

All these dyes (**AD19-AD22**) displayed red shifted absorption spectra ranging from 539-556 nm than compared to parent dye **AC16** due to strong donor facilitates strong donor-acceptors. Incorporation of carbazole raise the LUMO level of the dyes when compared to **AC16** dye which favors the efficient electron injection in to CB of TiO_2 followed by higher J_{SC}. Over all **AD19** exhibited highest efficiency of 9.18% with highest J_{SC} of 14.6 mA cm^{-2}. This strategy proved asymmetrical donor unit boost the efficiency of DSSC.

Table 1.7 Optical, electrochemical and photovoltaic performance parameters of dyes containing carbazole as auxiliary donor

Dye	$\lambda_{max,}$ nm (ε_{max}, M^{-1} cm^{-1})	E_{ox}, V (*vs* NHE)	E_{ox}^{*}, V (*vs* NHE)	J_{SC} (mA cm^{-2})	V_{OC} (mV)	*ff*	η (%)	*Ref*
AD4	513 (26013)	1.08	−0.99	5.35	560	0.68	2.05	[167]
AD5	417 (19567)	0.86	−1.66	3.86	582	na	1.55	[167]
AD6	477 (26046)	1.10	−1.11	na	na	na	1.49	[167]
AC4	464 (25491)	1.39	−0.92	8.19	618	0.70	3.53	[168]
AC5	395 (17062)	na	na	5.85	664	0.74	2.86	[168]
AC6	435 (22905)	1.37	−1.06	6.89	627	0.72	3.09	[168]
AC7	448	1.01	−1.28	16.34	720	0.61	7.21	[169]
AD7	415	0.82	−1.60	10.50	710	0.62	4.62	[169]
AC8	437 (15800)	0.96	−1.34	9.46	710	0.64	4.31	[170]
AD8	470 (38300)	1.09	−1.18	10.25	690	0.61	4.31	[170]
C27	370 (9400)	0.98	−0.74	6.88	640	0.63	2.79	[171]
AD9	395 (47400)	0.64	−0.87	9.42	730	0.53	3.63	[171]
AD10	523 (27900)	0.83	−1.11	14.16	628	0.66	5.87	[172], [173]
AD11	523 (58200)	0.89	−1.16	16.58	756	0.74	9.29	[173]
AD12	522 (57100)	0.90	−1.17	16.28	779	0.75	9.49	[173]
AC9	504 (27200)	0.98	−1.05	12.28	614	0.68	5.09	[172]
AC10	491 (22300)	1.04	−1.01	9.77	622	0.65	3.99	[172]
AD13	473 (8900)	0.59	−1.53	12.38	829	0.66	6.72	[174]
AC11	465 (15400)	0.64	−1.49	12.43	767	0.64	6.13	[174]
AC12	460 (14300)	0.58	−1.64	9.50	714	0.64	4.37	[174]
AD14	481 (12800)	0.53	−1.58	9.68	742	0.71	5.12	[174]
AC13	478 (10700)	0.57	−1.56	7.62	748	0.70	3.98	[174]
AC14	478 (25800)	0.82	−1.46	12.63	705	0.69	6.14	[175]
AC15	464 (17600)	1.00	−1.36	13.01	734	0.68	6.49	[175]
AD15	474 (31700)	0.95	−1.16	8.30	650	0.69	3.73	[176]

na = not available

Table 1.7 (Cont.)

Dye	$\lambda_{max,}$ nm (ε_{max}, M^{-1} cm^{-1})	E_{ox}, V (*vs* NHE)	E_{ox}^{*}, V (*vs* NHE)	J_{SC} (mA cm^{-2})	V_{OC} (mV)	*ff*	η (%)	*Ref*
AD16	473 (31500)	0.97	−1.12	6.86	571	0.69	2.71	[176]
AD17	492	0.98	−1.17	2.04	497	0.68	0.69	[176]
AD18	506	0.97	−1.15	3.72	512	0.63	1.21	[176]
AD19	556	0.86	−1.16	14.60	925	0.68	9.18	[177]
AD20	550	0.88	−1.15	13.50	937	0.67	8.47	[177]
AD21	539	0.85	−1.19	14.00	913	0.68	8.69	[177]
AD22	553	0.80	−1.24	13.80	901	0.67	8.33	[177]
AC16	546	0.90	−1.16	13.80	865	0.69	8.35	[177]

1.4.3 Carbazole as Auxiliary Donor via *N*9-Position

The general structure of the dyes containing carbazole as auxiliary donor via *N*9-substitution is illustrated in Figure 1.11. This structural arrangement facilitates the delocalization of nitrogen lone pair of electrons in to the conjugation bridge and enrich as the donor strength.

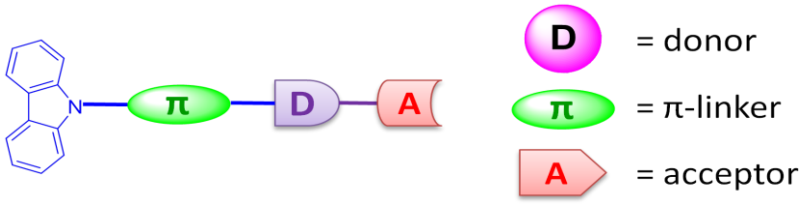

Figure 1.11 Molecular configuration of organic dyes derived using carbazole as auxiliary donor *via N*9-functionalization.

Jungsuttiwong and co-workers [178] theoretically designed and investigated the organic dyes (**AD23-AD25** and **AC17-AC19**) based on triphenylamine and 3,6-di-*t*-butyl carbazole/diphenylamine as auxiliary donor and fluorene as linker. They investigated the molecular structures, frontier molecular orbitals, absorption spectra as well as dye-$(TiO_2)_{38}$ complexes of these dyes were investigated by density functional theory and time-dependent DFT calculations. Among all these dye architectures, the results suggested that the 2D-D-π-A system showed the largest absorption range and diphenylamine auxiliary donor red shifted the

absorption spectra. This diphenylamine provides smaller external dihedral angles which led to wider absorption range with strong charge-transfer character than other dyes and significantly increase HOMO energy while slightly effecting LUMO energy.

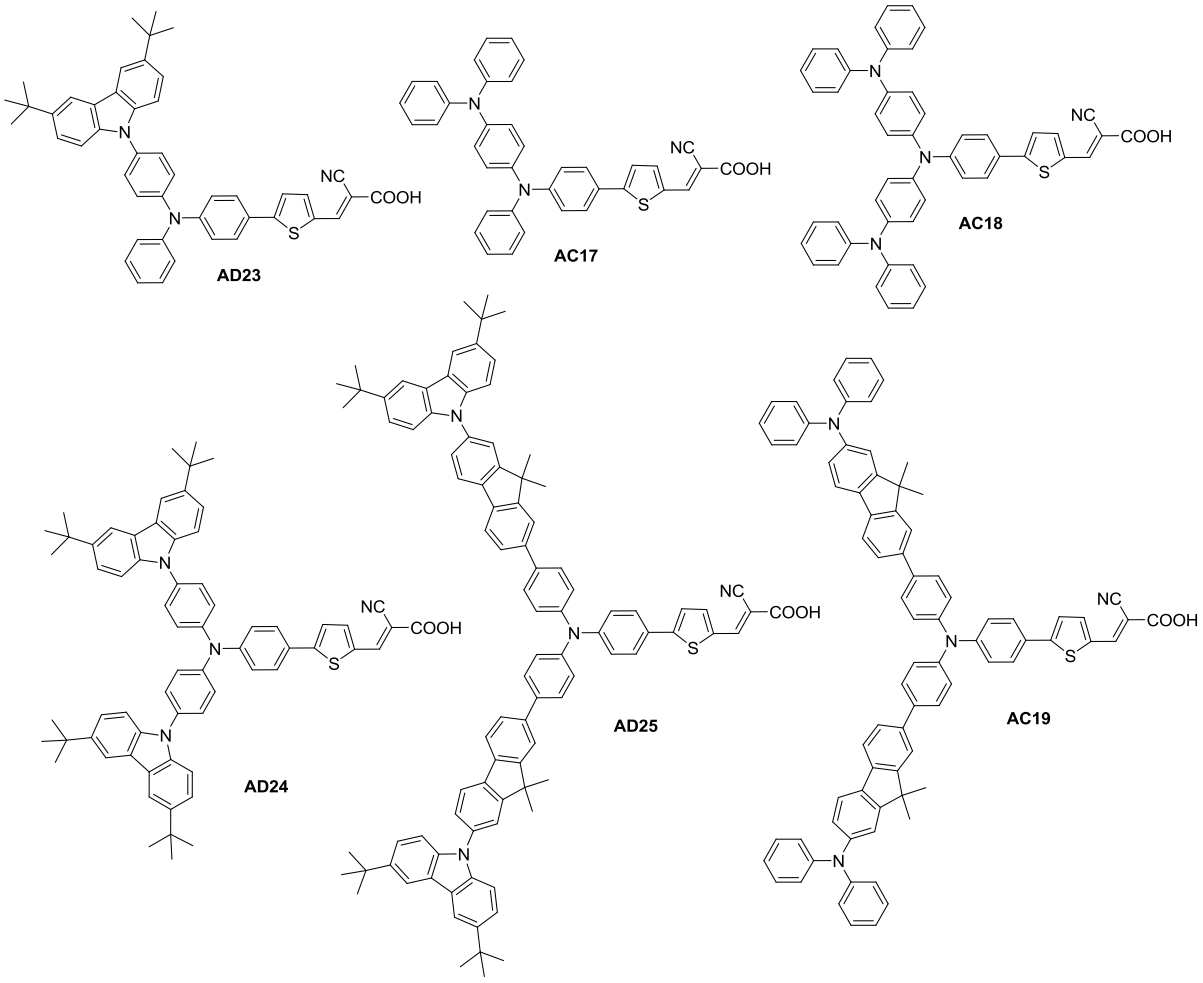

Chart 1.71 Structures of the organic dyes containing 3,6-di-*t*-butyl carbazole as auxiliary donor based on triphenylamine core.

Promarak and co-workers [179] designed organic dyes containing di(thiophen-2-yl)phenylamine as donor, 3,6-di-*t*-butyl carbazole as auxiliary chromophore and cyanoacrylic acid acceptor by using density functional theory and time-dependent density functional theory. The structural results show that the 2D-D-π-A dyes have a non-planar structure and suppress the aggregation of the dyes. The systematic elongation of the dyes (**AD26-AD28**) by increasing the number of thiophenes resulted in longer wavelength absorption and improves their higher light harvesting ability than the dyes (**AC20-AC22**). Among all the dyes, **AD28** would have the best

performance due to its highest predicted light harvesting at the maximum absorption wavelength and the suitable driving force of the electron injection (ΔG_{inj}) from the excited state to the CB of TiO_2.

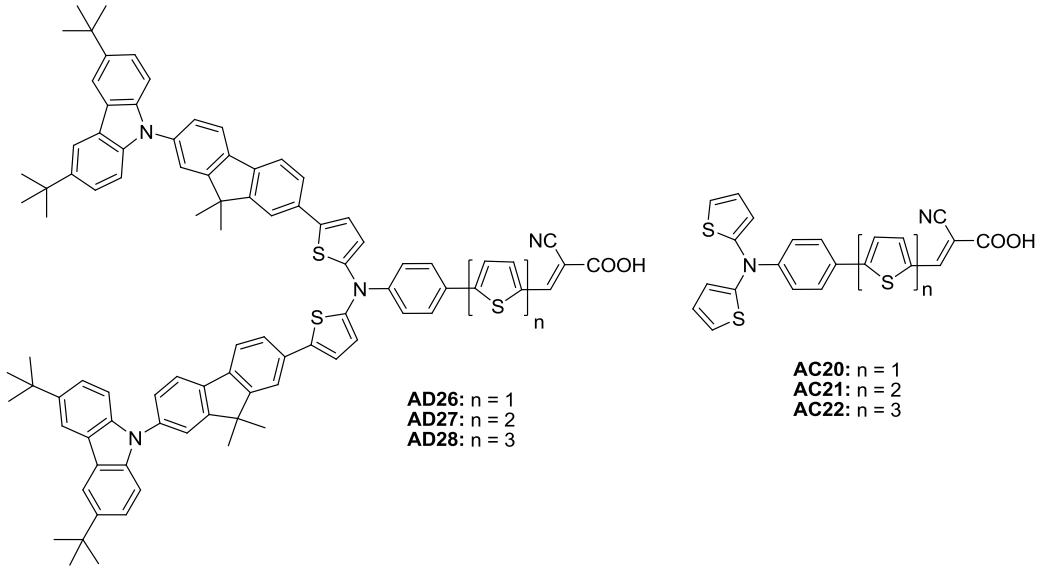

Chart 1.72 Structures of the organic dyes containing 3,6-di-*t*-butyl carbazole as auxiliary donor based on triarylamine core.

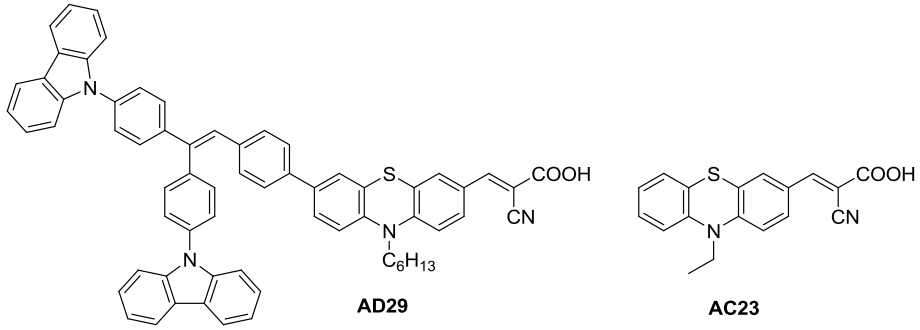

Chart 1.73 Phenothiazine based organic dyes containing carbazole as auxiliary donor.

Kuang and co-workers found that introduction of carbazole functionalized aggregation induced emission (AIE) chromophore to the phenothiazine-based organic dye resulted favorable absorption properties (Chart 1.73 [132]. When compared to (*E)*-2-cyano-3-(10-ethyl-10*H*-phenothiazin-3-yl)acrylic acid (**AC23**), [180] without chromophoric decoration, the absorption spectrum of **AD29** is significantly red-shifted (23 nm). The V_{OC} of **AD29** also improved from

709 mV to 793 mV and J_{SC} increased from 6.13 mA cm^{-2} to 10.76 mA cm^{-2}. The overall efficiency of **AD29** is 5.51%.

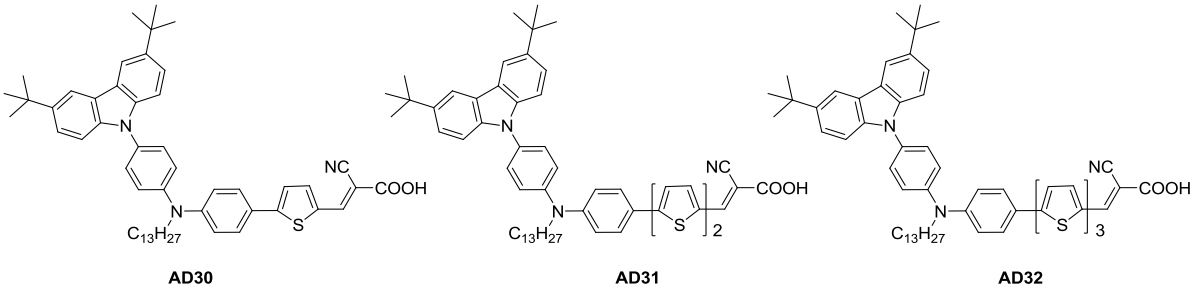

Chart 1.74 Structures of dyes with *N*-functionalized carbazole as auxiliary donor.

Promarak and co-workers utilized 3,6-di(*tert*-butyl)carbazole as an auxiliary donor and obtained three dyes, **AD30**-**AD32** (Chart 1.74) [181]. The dyes showed progressive increase in the absorption wavelength on introducing additional thiophene units in the conjugation pathway between the main donor and the acceptor. Among the dyes, **AD32** displayed good power conversion efficiency owing to its superior light harvesting ability.

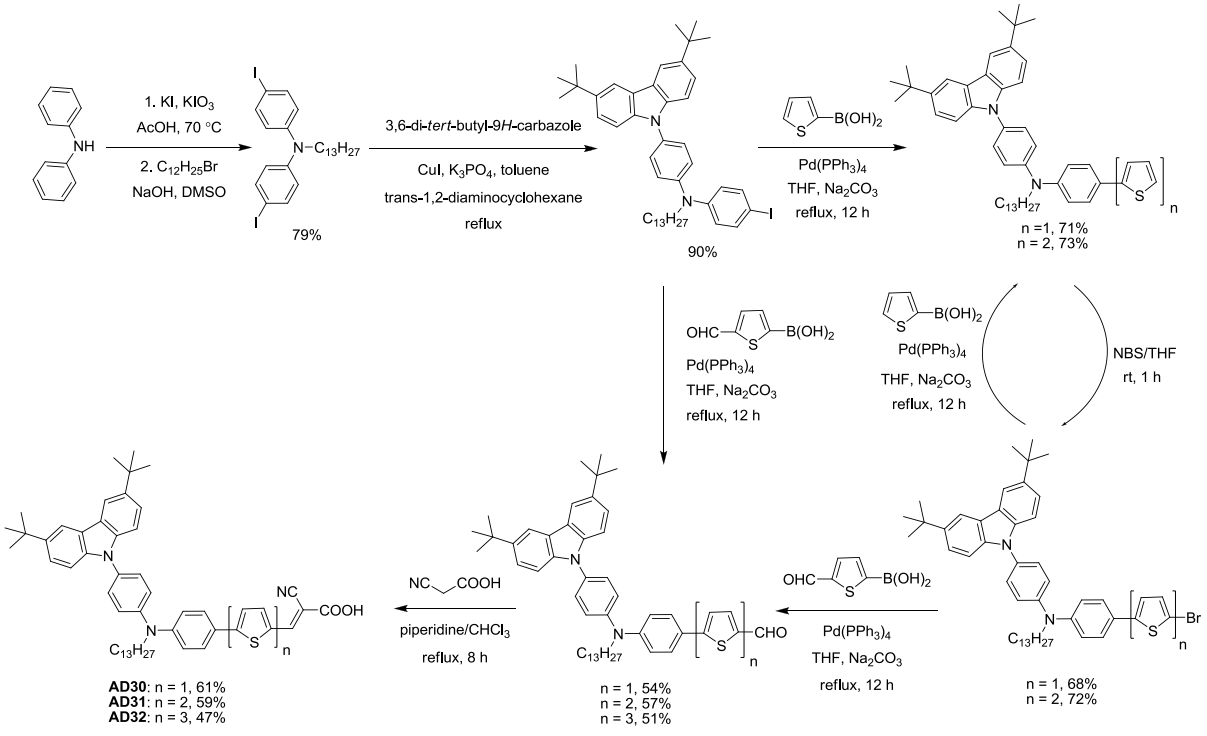

Scheme 1.62 Synthetic scheme of the dyes **AD30**-**AD31**.

The synthesis of the dyes (**AD30-AD32**) is showed in Scheme 1.62. The synthetic scheme starts with iodination of diphenylamine with KI/KIO_3 in acetic acid. *N*-alkylation of bis(4-iodophenyl)amine with alkylbromide in presence of sodium hydroxide led to 4-iodo-*N*-(4-iodophenyl)-*N*-tridecylaniline. Reaction of 4-iodo-*N*-(4-iodophenyl)-*N*-tridecylaniline with 3,6-di-*tert*-butyl-9*H*-carbazole by Ullmann coupling gave 4-(3,6-di-*tert*-butyl-9*H*-carbazol-9-yl)-*N*-(4-iodophenyl)-*N*-tridecylaniline. It reacted with 5-formylthiophen-2-ylboronic acid by Suzuki coupling gave the corresponding aldehyde which converted to cyanoacrylic acid dye **AD30** by reacting with cyanoacetic acid via Knoevenagel condensation. Suzuki coupling of 4-(3,6-di-*tert*-butyl-9*H*-carbazol-9-yl)-*N*-(4-iodophenyl)-*N*-tridecylaniline with thiophen-2-ylboronic acid and iterative brominations and followed by again Suzuki coupling with 5-formylthiophen-2-ylboronic acid by Suzuki coupling gave the corresponding aldehyde which converted to cyanoacrylic acid dye **AD31** and **AD32** by reacting with cyanoacetic acid via Knoevenagel condensation.

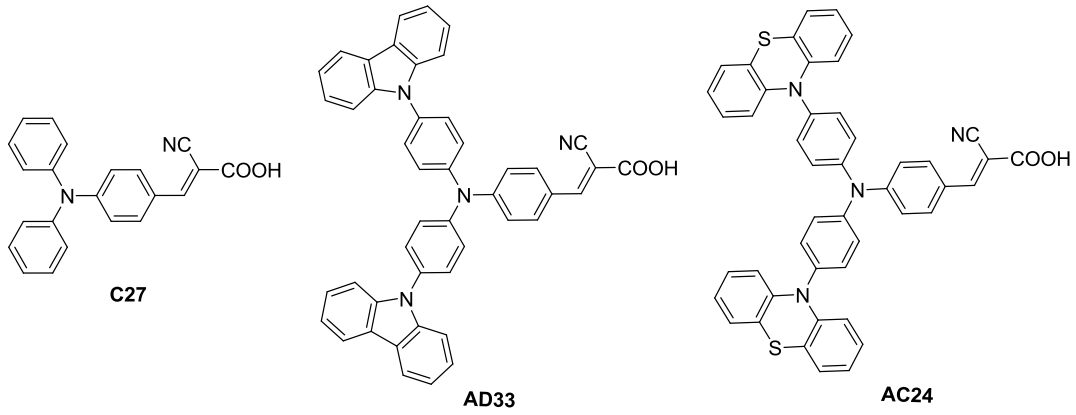

Chart 1.75 Star-burst organic dyes featuring carbazole and phenothiazine as auxiliary donors.

Lin and co-workers studied the influence of the carbazole or phenothiazine containing antennas in starburst triphenylamine-based organic dyes (Chart 1.75) [182]. The synthesis of the dyes (**AD33** and **AC24**) is showed in Scheme 1.63. Iodination of 4-(diphenylamino)benzaldehyde by the reaction of KI/KIO_3 in acetic acid. It reacted with carbazole/phenothiazine by Ullmann coupling gave the corresponding aldehyde derivatives. These reacted with cyanoacetic acid via Knoevenagel condensation gave the dyes (**AD33** and **AC24**). When compared to (*E*)-2-cyano-3-(4-(diphenylamino)phenyl)acrylic acid (**C27**) the absorption peak of **AD33** is bathochromically shifted and LUMO increased to 2.10 eV. This

increased the electron density in the CB of TiO_2 by facilitating the electron harvest and injection efficiencies. Consequently, the efficiency increased to 3.26% from 2.79% observed for **C27**. But the drop in efficiency was observed when compared to phenothiazine auxiliary donor (**AC24**) owing to its low HOMO level not favorable for regeneration of dye led to lower V_{OC}. Later Sun and co-workers improved the efficiency of the DSSC based on **AD33** by using Br^-/Br_3^- redox couple to 3.63% [108]. The hike in efficiency is mainly due to the tremendous increase in V_{OC} (1015 mV) with little sacrifice in J_{SC} (4.41 mA cm^{-2}).

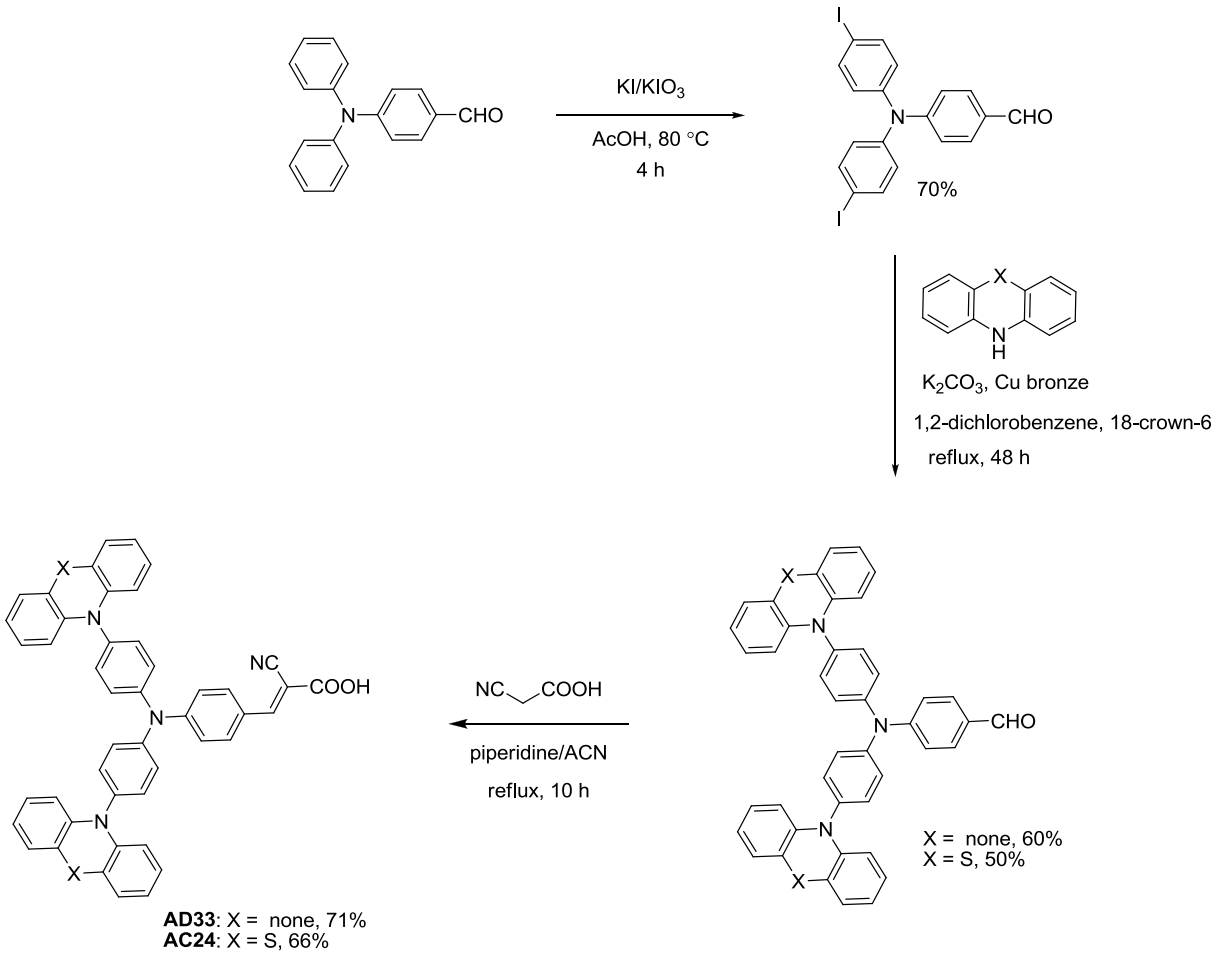

Scheme 1.63 Synthetic scheme of the dyes **AD33** and **AC24**.

Zhang and co-workers reported a series of dyes (Chart 1.76) based on starburst triarylamine dyes for efficient DSSC [4]. The synthesis of the dyes (**AD34**, **AC25-AC27**) is displayed in Scheme 1.64. The triphenylamine containing aldehyde derivatives synthesized according to the Scheme 1.63. The aldehyde derivatives are converted to dyes (**AD34**, **AC25-AC27**) via Knoevengel condensation with cyanoacetic acid. The authors demonstrated the fine-tuning of

HOMO and LUMO energy levels by the modification of auxiliary donors with triphenylamine and carbazole. The LUMO increased on introduction of carbazole in (*Z*)-2-(3-((*E*)-4-(diphenylamino)styryl)-5,5-di-methylcyclohex-2-enylidene)-2-cyanoacetic acid (**AC25**) while swapping it with triphenylamine reduced the LUMO level significantly. Due to the difference in the thermodynamic driving force for the electron injection, the carbazole substituted dye, **AD34** showed higher efficiency (6.02%) than the triphenylamine analog (2.87%). Also when compared to **AD33**, **AD34** showed nearly double device efficiency due to the presence of rigid conjugation bridge in the form of 5,5-dimethyl-3-vinylcyclohex-2-enylidene.

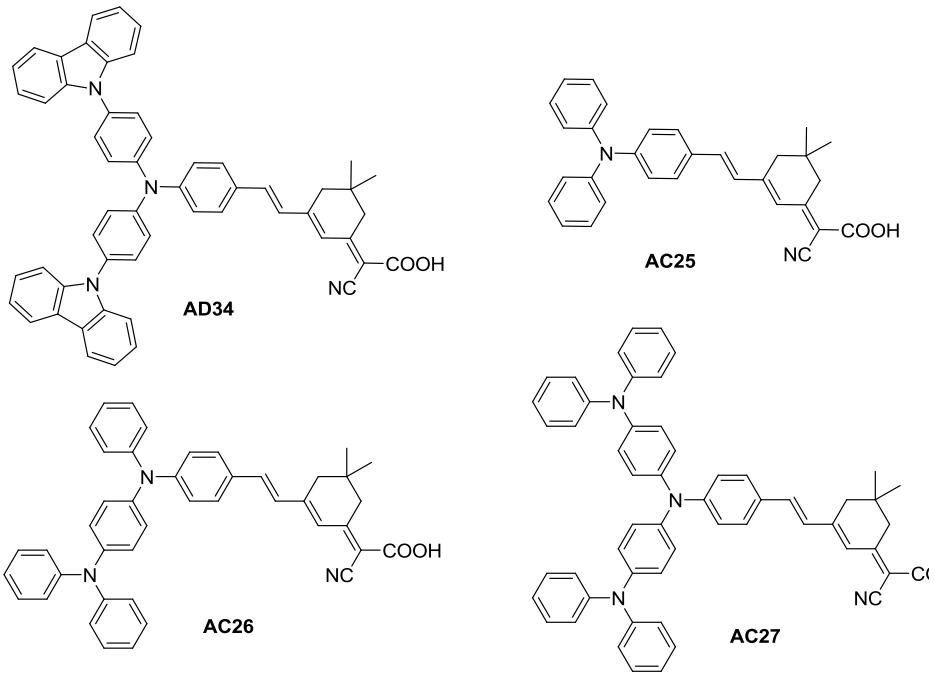

Chart 1.76 Star-burst organic dyes featuring carbazole as auxiliary donors.

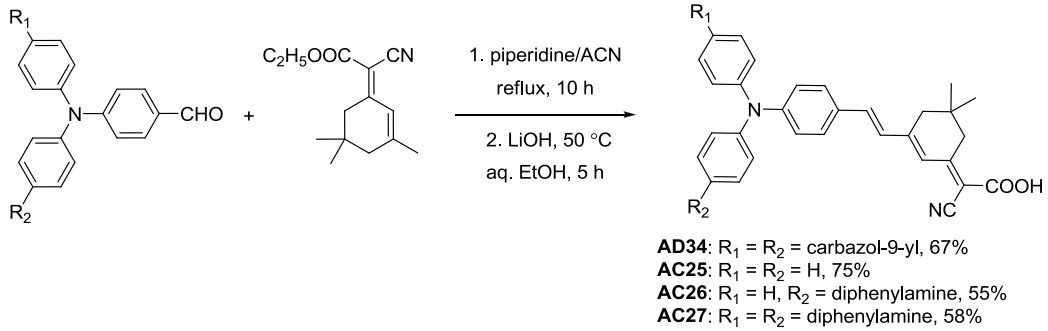

Scheme 1.64 Synthetic scheme of the dyes **AD34** and **AC26-AC27**.

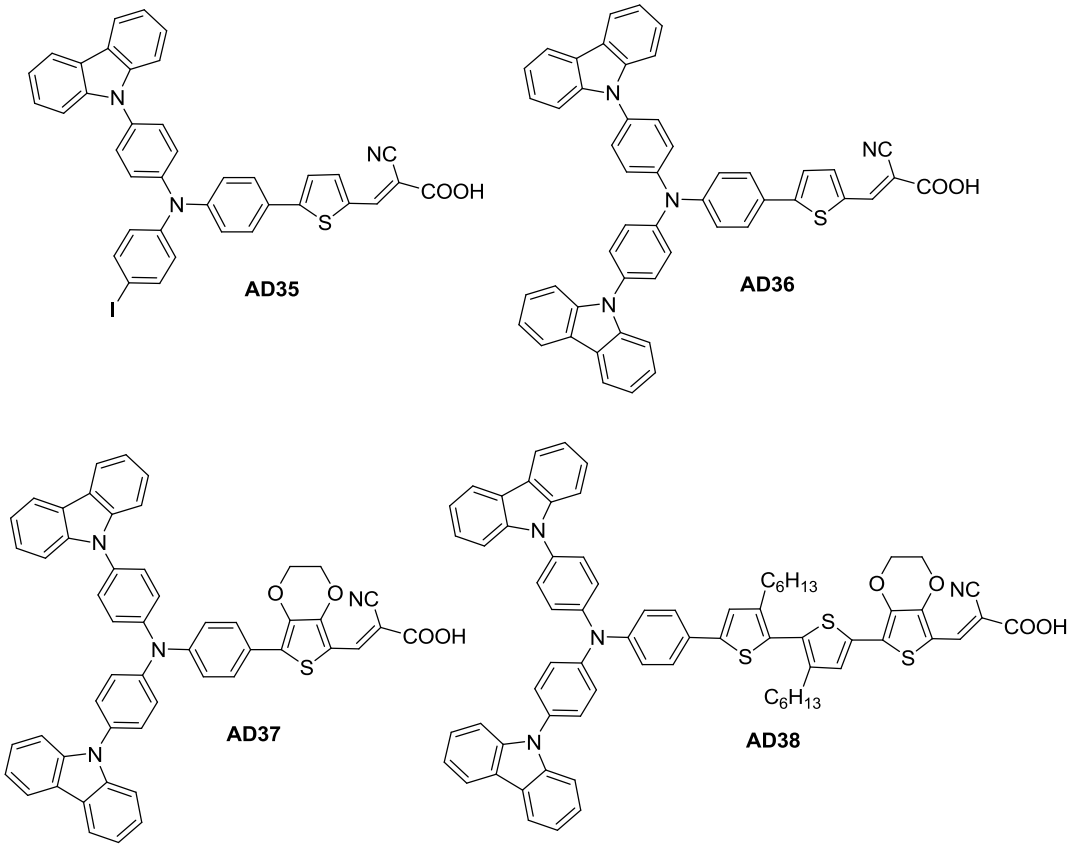

Chart 1.77 Structure of the dyes containing triphenylamine and carbazole-based donors.

Liu and coworkers successfully synthesized triarylamine based organic dyes (**AD35**-**AD37**; Chart 1.77) containing starburst triarylamine group as electron donor and thiophene or 3,4-ethylenedioxythiophene as π-conjugation bridge and cyanoacetic acid as electron acceptor. [183] The synthesis of the dyes (**AD35-AD37**) is depicted in Scheme 1.65. Iodination of triphenylamine with KI/KIO_3 gave the triiodo triphenylamine which is stoichiometrically reacted with carbazole gave the *N*-(4-(9*H*-carbazol-9-yl)phenyl)-4-iodo-*N*-(4-iodophenyl)aniline and *N*,*N*-bis(4-(9*H*-carbazol-9-yl)phenyl)-4-iodoaniline. These iodo-derivatives reacted with 5-formylthiophen-2-ylboronic acid *via* Suzuki coupling gave the corresponding aldehyde derivative which reacted with cyanoacetic acid through Knoevenagel condensation afford dyes **AD35** and **AD36**. The conversion of *N*,*N*-bis(4-(9*H*-carbazol-9-yl)phenyl)-4-iodoaniline to its borolane derivative by lithiation with BuLi followed by addition of 4,4,4',4',5,5,5',5'-octamethyl-2,2'-bi(1,3,2-dioxaborolane). It reacted with 7-bromo-2,3-dihydrothieno[3,4-*b*][1,4]dioxine-5-

carbaldehyde *via* Suzuki coupling gave the corresponding aldehyde which converted to dye **AD37** *via* Knoevenagel condensation with cyanoacetic acid.

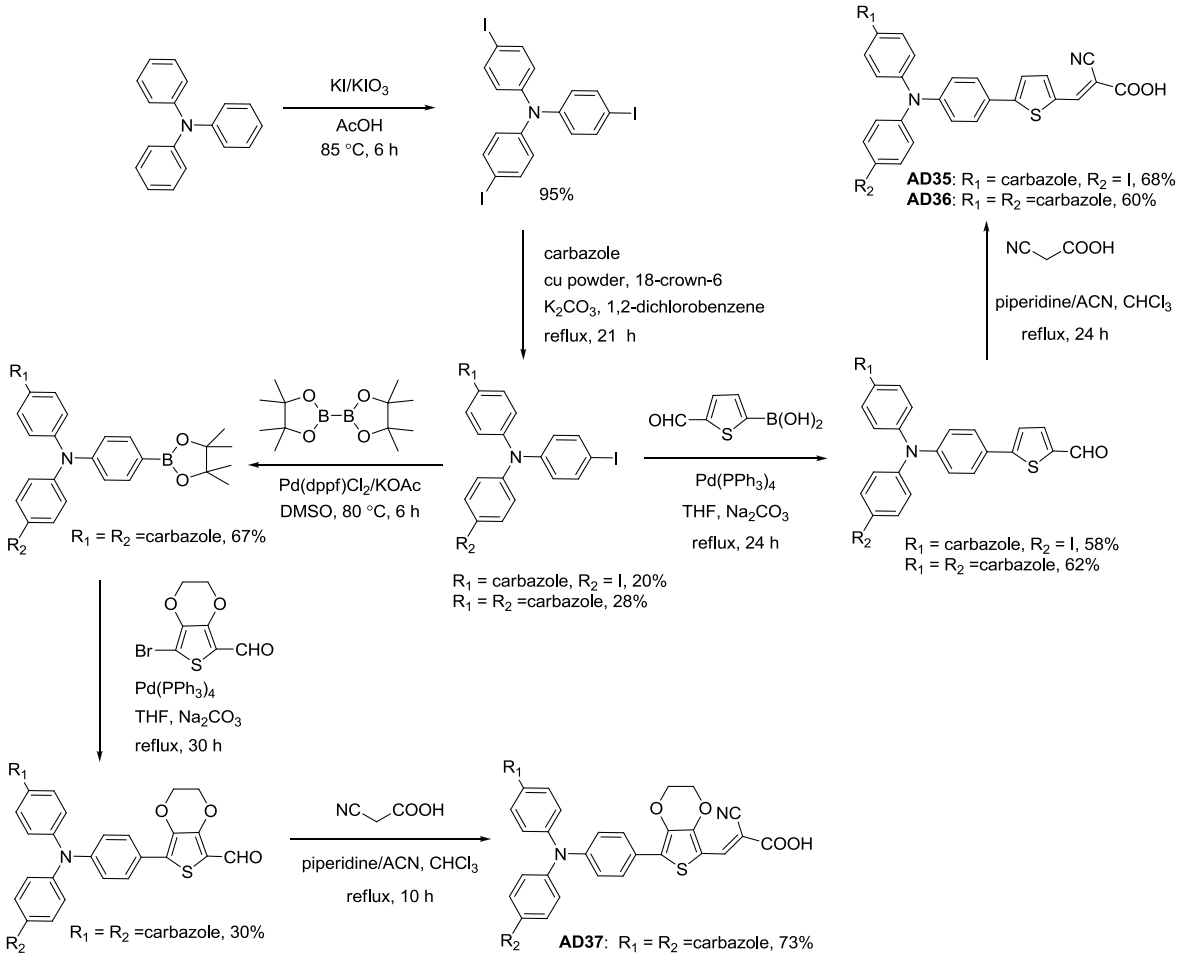

Scheme 1.65 Synthetic scheme of the dyes **AD35-AD37**.

The introduction of the EDOT group in **AD37** red shifted absorption and renders a better degree of charge separation, resulting in a leap in the photovoltaic performance in comparison to **AD36**, and produced efficiency of 6.15% in DSSC. Carbazole incorporation at **AD36** is demonstrated to be useful for retarding the electron transfer from TiO_2 to the oxidized dye or electrolyte and to enhance the charge transfer efficiency in the excited state compared with the related **AD35**. Later, they synthesized **AD38** by introducing two hexyl substituted thiophene units and improved the spectral response. The dye **AD38** has red shifted absorption when compared to **D117** [133] but the LUMO of the **D117** is higher and it facilitates the electron injection from excited state to the CB of TiO_2. The longer wavelength of dye **AD38** responsible

for higher power conversion efficiency of 10.03% in liquid DSSCs and 8.05% in QSS-DSSCs compared to **D117** which exhibited an efficiency of 9.15%.

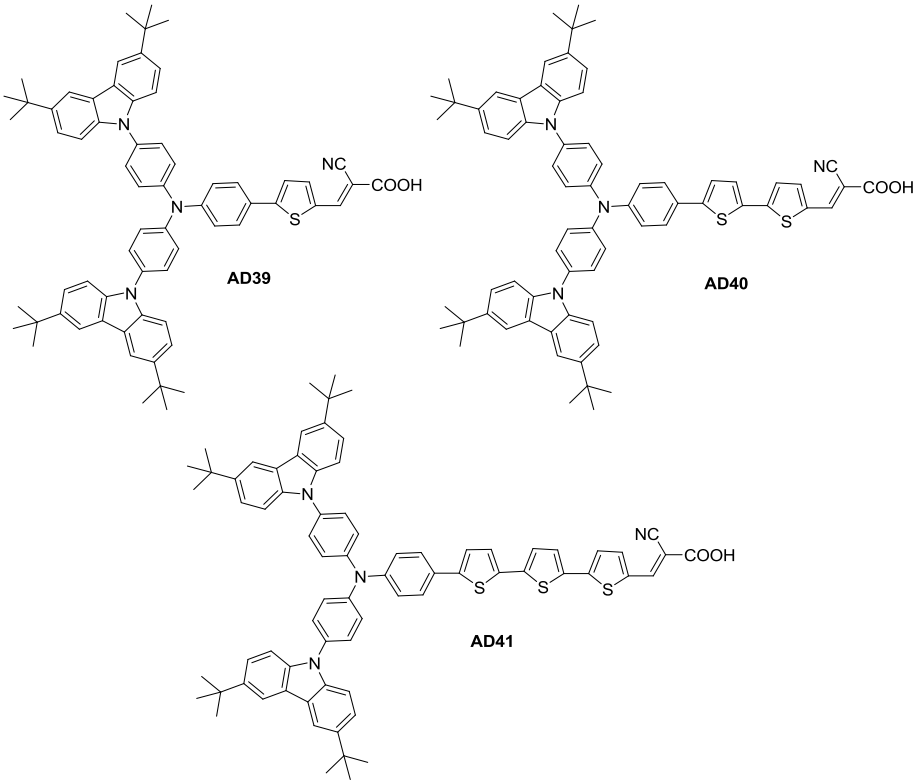

Chart 1.78 Starburst organic dyes with thiophene elongated conjugation.

Promarak and co-workers reported three dyes **AD39**-**AD41** (Chart 1.78) containing 3,6-di-*tert*-butylcarbazole as auxiliary donor [184]. In these dyes, the conjugation extension with thiophene red-shifted the absorption maximum and absorption coefficient increased when compared to the dyes without carbazole auxiliary donors. They exhibited efficiencies in the range of 3.70-4.62%.

Table 1.8 Optical, electrochemical and photovoltaic performance parameters of dyes containing carbazole as auxiliary donor

Dye	$\lambda_{max,}$ nm (ε_{max}, M^{-1} cm^{-1})	E_{ox}, V (*vs* NHE)	E_{ox}^{*}, V (*vs* NHE)	J_{SC} (mA cm^{-2})	V_{OC} (mV)	*ff*	η (%)	*Ref*
AD29	462 (13000)	0.92	−1.00	10.76	793	0.64	5.51	[132]
AD30	457 (25174)	1.07	−1.24	7.19	730	0.67	3.52	[181]

Table 1.8 (cont.)

Dye	$\lambda_{max,}$ nm (ε_{max}, M^{-1} cm^{-1})	E_{ox}, V (*vs* NHE)	E_{ox}^{*}, V (*vs* NHE)	J_{SC} (mA cm^{-2})	V_{OC} (mV)	*ff*	η (%)	*Ref*
AD31	463 (27460)	1.03	−1.23	8.88	700	0.66	4.10	[181]
AD32	472 (30102)	0.98	−1.26	10.89	700	0.67	5.12	[181]
AD33	424 (13834)	0.45	−2.10	7.30	600	0.74	3.26	[182]
AC24	422 (29367)	0.64	−1.99	9.20	625	0.79	4.54	[182]
AD34	480 (25000)	1.68	−0.49	13.80	630	0.69	6.02	[4]
AC25	487 (8850)	1.29	−0.87	13.60	615	0.69	5.77	[4]
AC26	508 (33300)	0.91	−1.26	8.02	543	0.64	2.79	[4]
AC27	522 (19800)	0.68	−1.23	9.05	567	0.56	2.87	[4]
AD35	471 (21400)	0.95	−1.40	10.52	706	0.74	5.48	[183]
AD36	454 (21600)	1.16	−1.16	10.51	728	0.73	5.55	[144]
AD37	486 (22400)	1.07	−1.18	12.21	695	0.72	6.15	[144]
AD38	512 (32800)	1.12	−1.00	19.18	752	0.70	10.03	[133]
AD39	458 (25225)	1.65	−0.60	7.53	720	0.69	3.70	[184]
AD40	455 (29322)	1.60	−0.61	9.02	710	0.68	4.34	[184]
AD41	464 (33926)	1.55	−0.58	9.98	700	0.67	4.62	[184]

1.4.4 Carbazole as auxiliary donor via 3,6-positions

In 2012, Li and co-workers reported new pyrrole-based dyes (**AD42, AC28** and **AC29**; Chart 1.79) with H-shaped molecular architecture [185]. The authors have linked two D-π-A segments via a π-bridge featuring phenyl, fluorene or carbazole units. The synthesis of the dyes is showed in Scheme 1.66. Palladium-catalyzed Suzuki coupling reaction of (*E*)-1-(4-bromophenyl)-5-(4-(diphenylamino)styryl)-1*H*-pyrrole-2-carbaldehyde and 9-hexyl-3,6-bis(4,4,5,5-tetramethyl-1,3,2-dioxaborolan-2-yl)-9*H*-carbazole gave the carzaole containing bis-aldehyde derivative. It condensed with cyanoacetic acid *via* Knoevenagel condensation reaction afford dye **AD42**. The synthesis of the congener dyes (**AC20** and **AC21**) prepared similar to the Scheme 1.66. The carbazole bridged dye **AD42** showed superior performance in the DSSC (η = 5.22%) over the fluorene and phenyl bridged dyes. The efficiency of the devices did not improve on addition of

CDCA which indicated the absence of aggregation at the TiO_2 surface due to nonplanarity of the dye molecule.

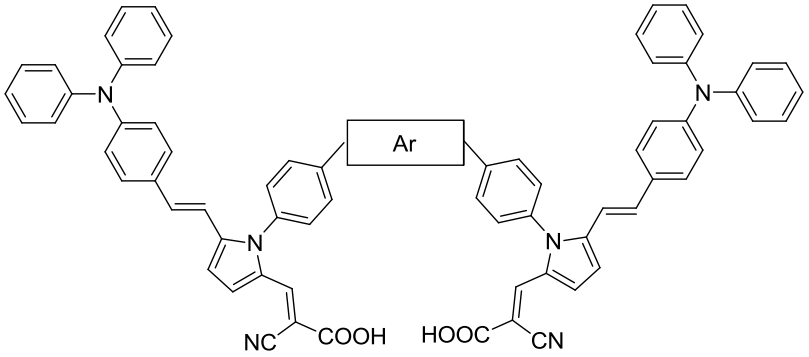

Chart 1.79 H-shaped di-anchoring organic dyes.

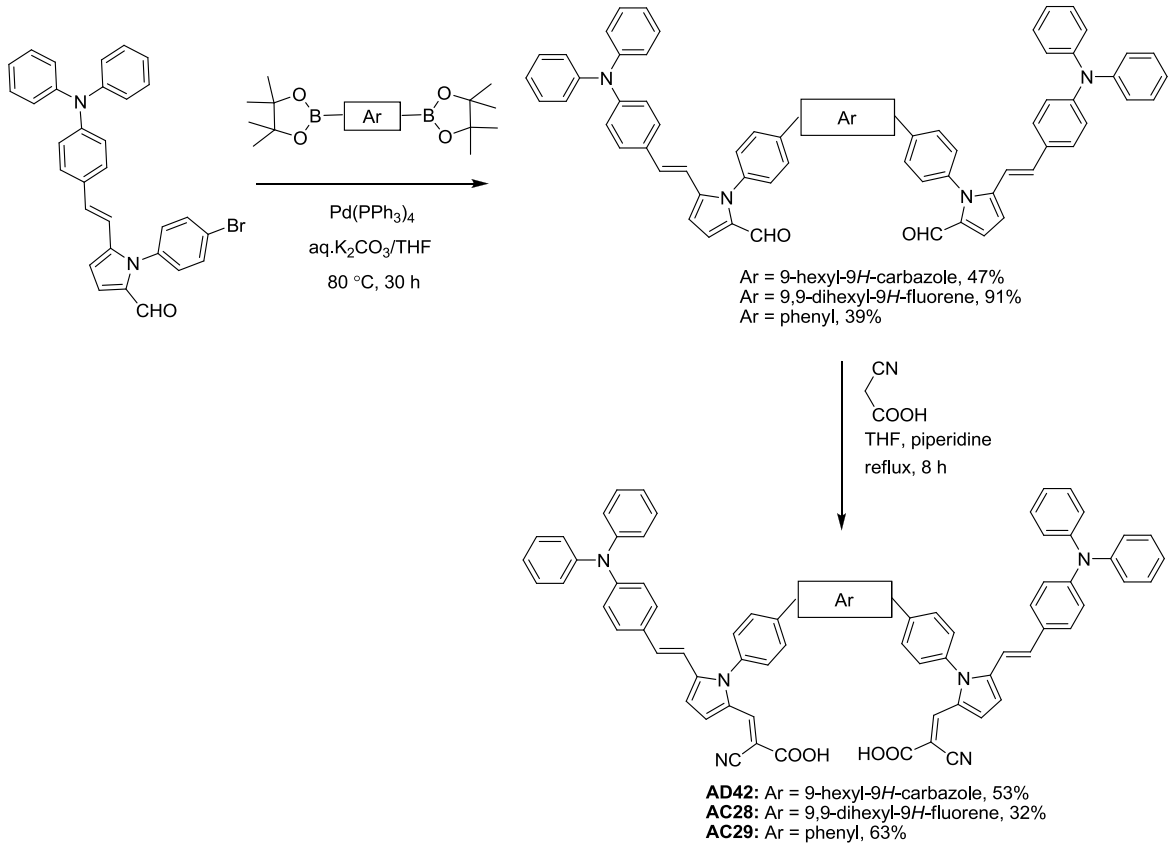

Scheme 1.66 Synthetic scheme of the dyes **AD42, AC28** and **AC29.**

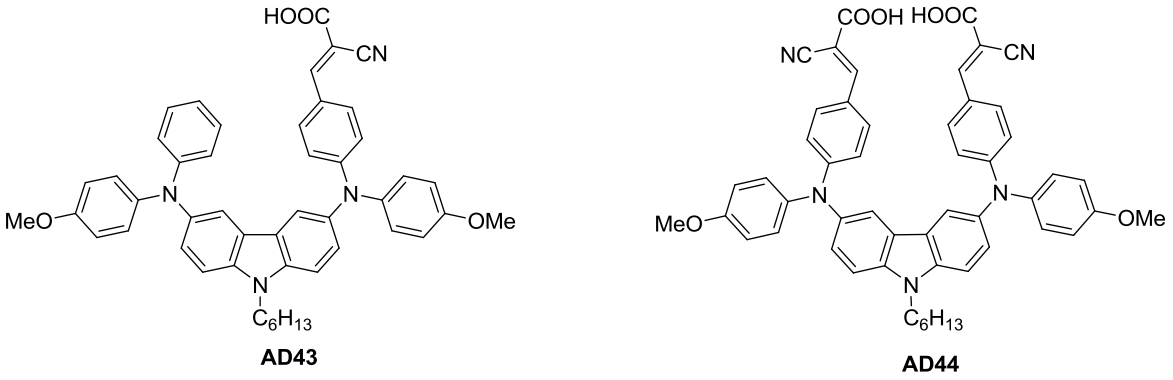

Chart 1.80 H-shaped di-anchoring organic dyes containing carbazole as auxiliary donor.

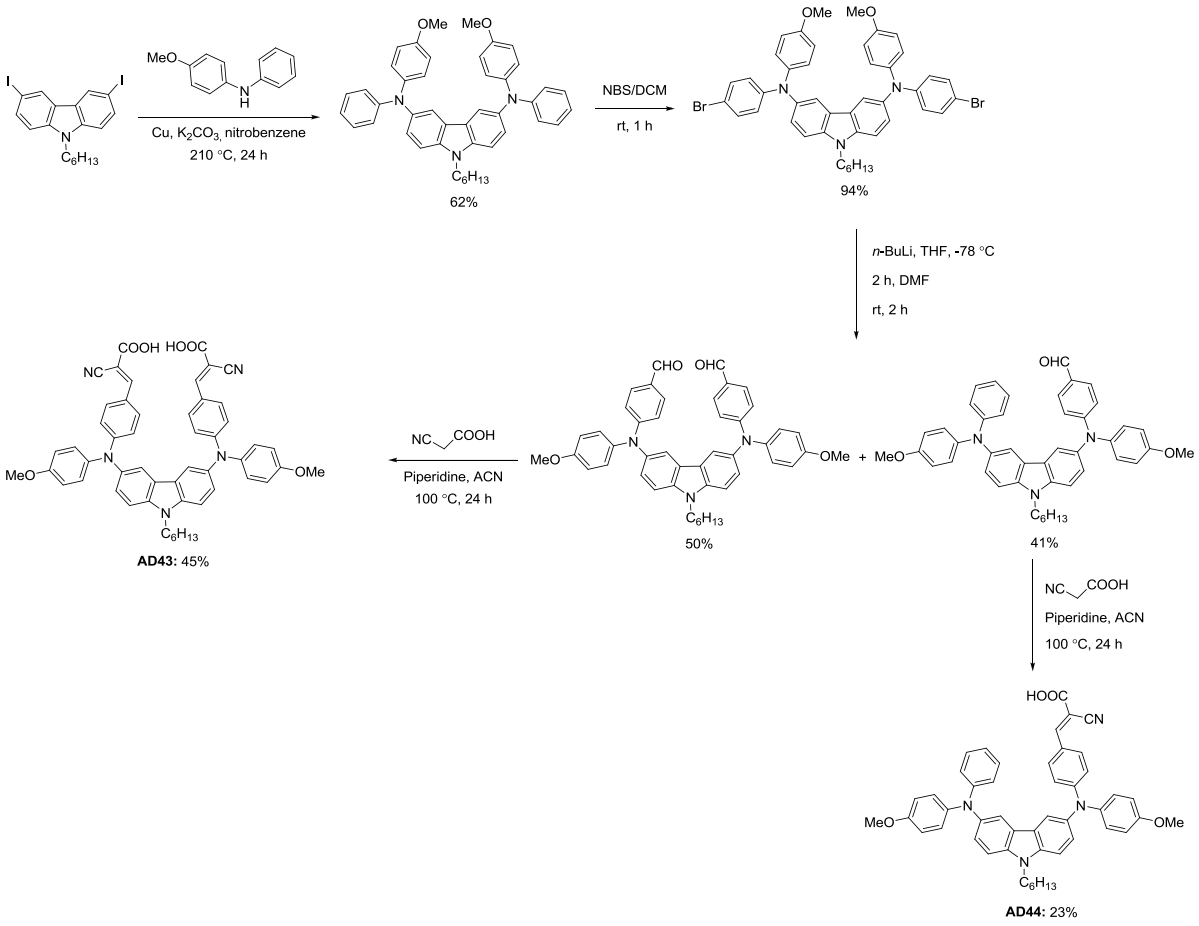

Scheme 1.67 Synthetic scheme of the dyes **AD43** and **AD44**.

Kiatisevi and co-workers [186] designed H shaped organic dyes (**AD43** and **AD44**; Chart 1.80) containing A-π-D-D′-D-π-A molecular design, in which carbazole acts as auxiliary donor and cyanoacrylic acid as acceptor. The synthetic scheme of the dyes is displayed in Scheme 1.67. It started with Ullmann coupling of 9-hexyl-3,6-diiodo-9*H*-carbazole with 4-methoxy-*N*-

phenylaniline gave 9-hexyl-*N*3,*N*6-bis(4-methoxyphenyl)-*N*3,*N*6-diphenyl-9*H*-carbazole-3,6-diamine, which brominated with NBS in dichloromethane led to *N*3,*N*6-bis(4-bromophenyl)-9-hexyl-*N*3,*N*6-bis(4-methoxyphenyl)-9*H*-carbazole-3,6-diamine. It is then treated with butyllithium followed by addition of DMF after two hours afforded a mixture of 4-((9-hexyl-6-((4-methoxyphenyl)(phenyl)amino)-9*H*-carbazol-3-yl)(4-methoxyphenyl)amino)-benzaldehyde and 4,4'-(9-hexyl-9*H*-carbazole-3,6-diyl)bis((4-methoxyphenyl)azanediyl)-dibenzaldehyde. Dyes **L41** and **AD43** obtained by Knoevenagel condensation of mono and dialdehyde derivatives with cyanoacetic acid, respectively. The dyes **AD43** and **AD44** displayed red shifted absorption spectra and photovoltaic properties compared to dye **L41** due to introduction of diphenylamine moiety in between carbazole and cyanoacrylic acid. The mono-anchoring dye **AD43** exhibited inferior performance of 2.54% with J_{SC} of 5.04 mA cm^{-2} than compared to di-anchoring dye **AD44** (3.23%) due to its dianchoring mode provides strong binding and facile injection led to larger J_{SC} of 7.20 mA cm^{-2}.

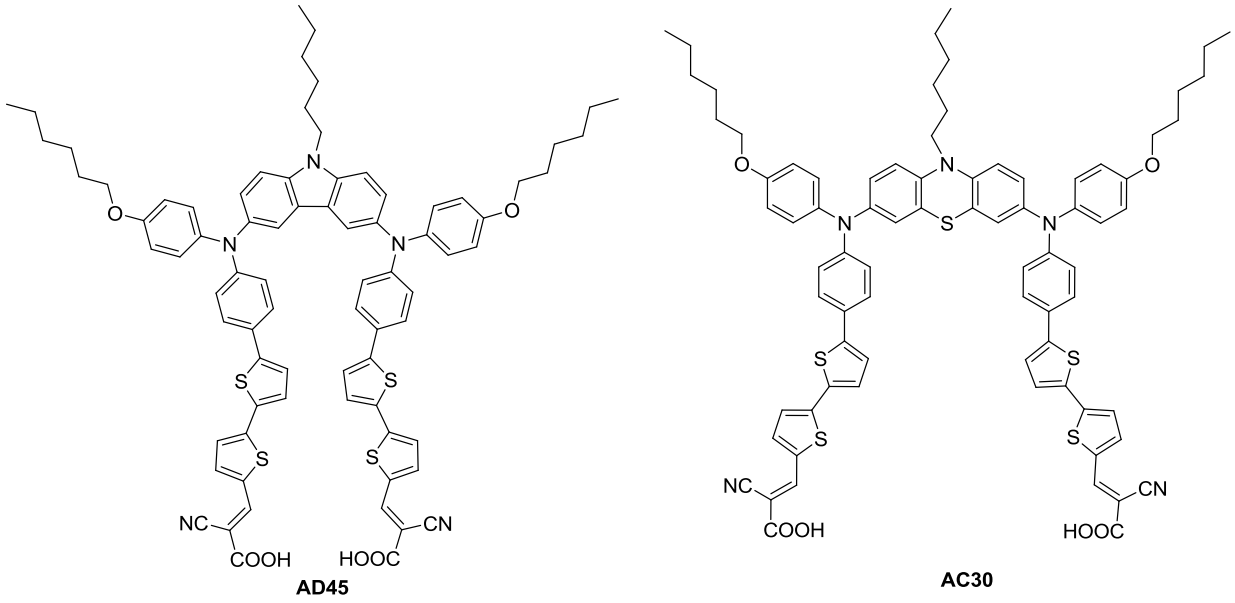

Chart 1.81 H-shaped dianchoring organic dyes containing carbazole or phenothiazine as bridge.

Recently, Kim and co-workers designed dual channel system with carbazole and phenothiazine as core-bridge by adopting configuration of H-shaped dyes (**AD45** and **AC30**; Chart 1.81) reported by Li and co-workers [187]. The dye with carbazole as core-bridge showed red shifted absorption and higher molar extinction coefficient. These dyes showed red shifted

absorption properties than compared to **AD44** dye due to extension of conjugation with oligothiophene units. Carbazole dye shows better charge separation of HOMO and LUMO compared to phenothiazine dye. Consequently **AD45** achieved high conversion efficiency of 3.34% with J_{SC} of 7.92 mA cm^{-2}, V_{OC} of 620 mV and *ff* of 0.68 when compared to **AC30 (**efficiency η = 1.43% with J_{SC} of 3.72 mA cm^{-2}, V_{OC} of 580 mV and *ff* of 0.66).

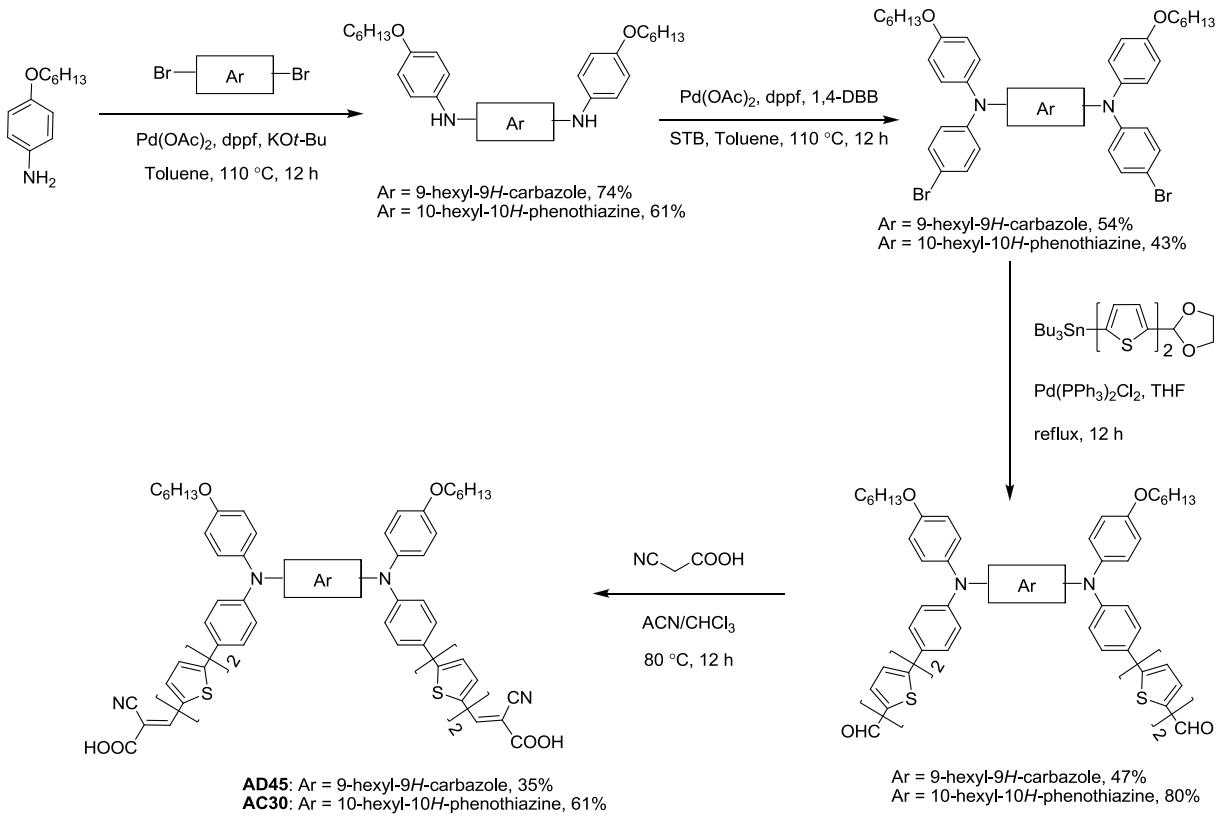

Scheme 1.68 Synthetic scheme of the dyes **AD45** and **AC30**.

The synthesis of the dyes (**AD45** and **AC30**) is outlined in Scheme 1.68. The Pd-catalyzed coupling of 4-(hexyloxy)aniline with 3,6-dibromo-9-hexyl-9*H*-carbazole gave the diamine and followed by again Pd-catalyzed coupling with 1,4-dibromobenzene resulted the carbazole containing dibromo derivative. It coupled with tin reagent of bithiophene protected aldehyde led to bis-aldehyde derivatives which converted to dye **AD45** by Knoevenagel condensation. The synthesis of dye **AC30** is similar to synthesis of **AD45**.

Table 1.9 Optical, electrochemical and photovoltaic performance parameters of dyes containing carbazole as auxiliary donor

Dye	$\lambda_{max,}$ nm (ε_{max}, M^{-1} cm^{-1})	E_{ox}, V (*vs* NHE)	E_{ox}^{*}, V (*vs* NHE)	J_{SC} (mA cm^{-2})	V_{OC} (mV)	*ff*	η (%)	*Ref*
AD42	425	1.00	−1.34	11.29	710	0.65	5.22	[185]
AC28	426	1.02	−1.33	10.75	700	0.67	5.04	[185]
AC29	444	1.02	−1.28	7.95	740	0.70	4.12	[185]
AD43	424 (82400)	0.49	−1.79	5.04	700	0.72	2.54	[186]
AD44	406 (57900)	0.58	−1.81	7.20	600	0.68	3.23	[186]
AD45	497 (54600)	1.03	−1.14	7.92	620	0.68	3.34	[187]
AC30	490 (46500)	0.99	−1.08	3.72	580	0.66	1.43	[187]

1.5 Carbazole as donor as well as linker for DSSC

Different modes of chemical modifications possible for carbazole make it a versatile building block for organic dyes. As described above, carbazole was liberally used as a donor, auxiliary donor or linker in the construction of organic dyes. In some instances, carbazole served as dual function, namely, donor and linker. The structural compositions differ due to the point of attachment at carbazole with the rest of the molecule as shown in Figure 1.12.

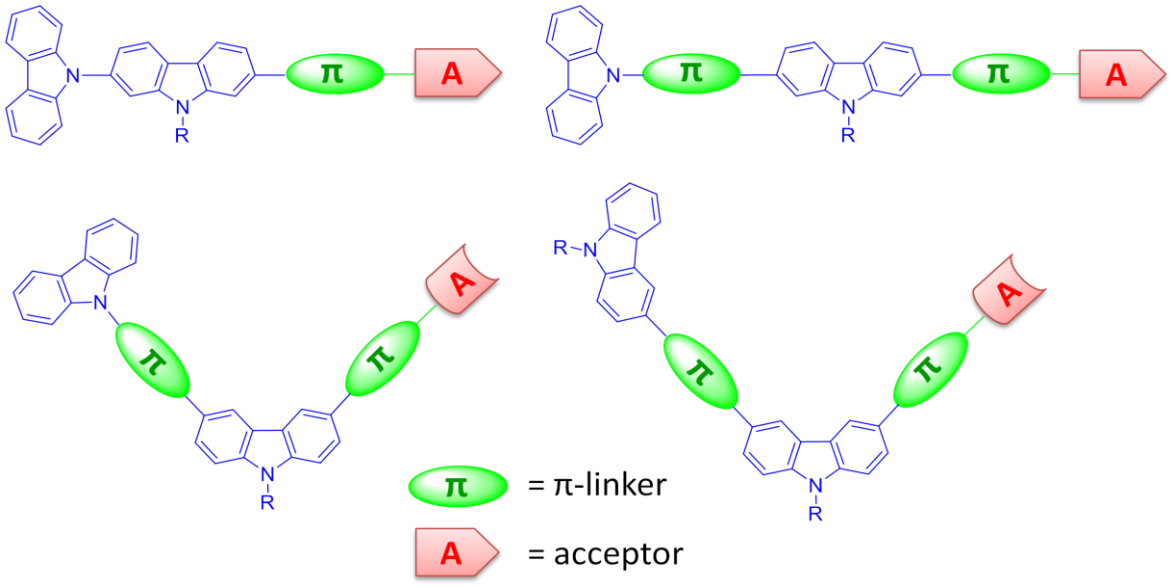

Figure 1.12 Molecular architectures of the dyes possessing carbazole as linker and donor.

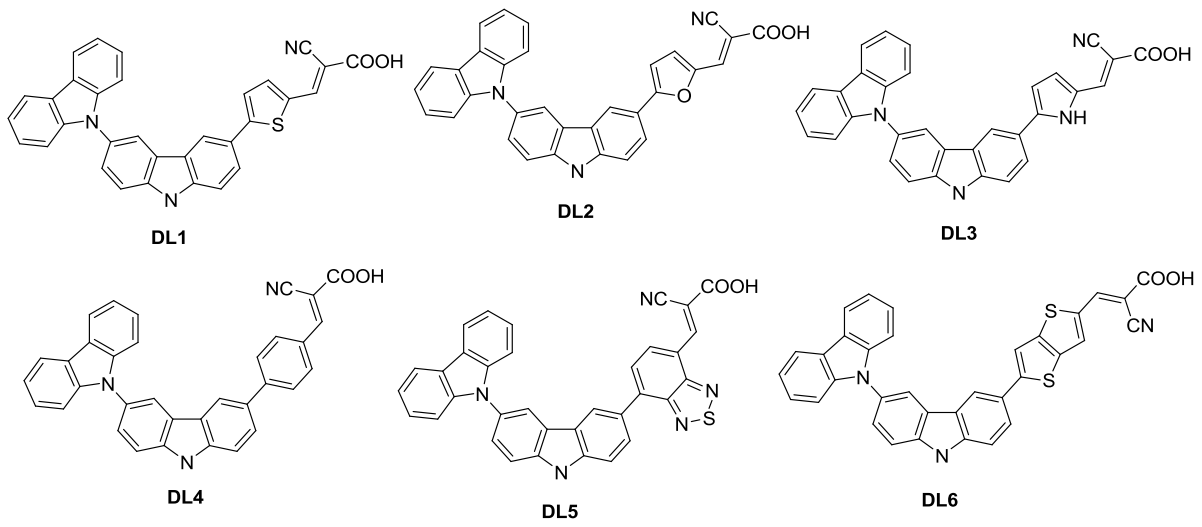

Chart 1.82 Structures of the organic dyes containing carbazole as linker and donor.

Promarak and co-workers [188] designed a set of carbazole based dyes (**DL1**-**DL6;** Chart 1.82) with an assistance from density functional theory (DFT) and time-dependent DFT (TD-DFT). They evaluated these dyes for DSSCs through optimized geometries, charge distributions, electronic structures, simulated absorption spectra, and free energies of electron injection. Based on the previous results they validated the long-range-corrected TD-CAMB3LYP as the best method and results are predicting close to experimental data. They also analyzed the important key parameters such as the HOMO–LUMO energy gap, dipole moment change, distance of charge transfer upon excitation from ground to excited state, free energies of injection, and light-harvesting efficiencies and found that the variation of the linker strongly affects the molecular orbital energy levels. These results suggested that dyes containing benzothiadiazole (**DL5**) and thieno[3,2-*b*]thiophene (**DL6**) as the π-linker exhibit higher efficiencies than the existing carbazole dyes.

Castellano and co-workers reported dyes **DL7** and **DL8** (Chart 1.83) where carbazole served as *N*-donor and 2,7-disubstituted carbazole linker along with cyanoacrylic acid as acceptor [189]. **DL7** and **DL8** showed similar performance in DSSC with efficiency reaching 2.70%. It is interesting to compare with the dye, **D71** (Chart 1.33) which contains bithiophene instead of carbazole linker. **D71** exhibited red-shifted absorption profile (Table 1.3) when compared to **DL8** (Table 1.10). However, the efficiency of **DL8** is better than that realized for **D71**. This

clearly indicates that the carbazole acts as an efficient linker and facilitates charge separation in the molecule. The DSSCs lasted for over 1000 h at 55 °C without much efficiency loss.

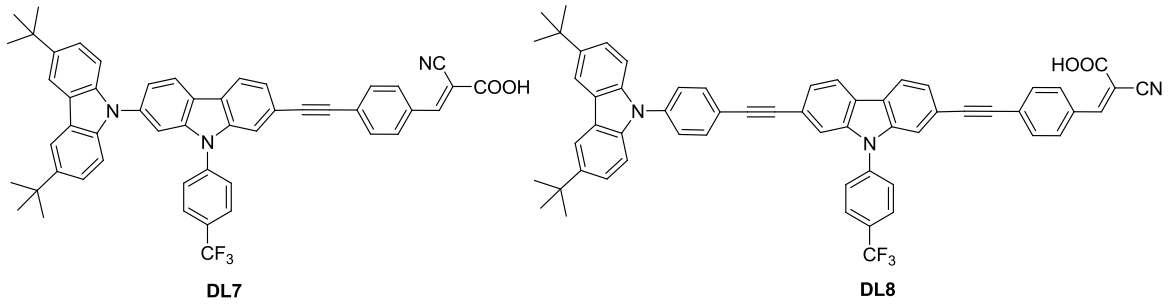

Chart 1.83 Organic dyes containing carbazole as *N*-donor and 2,7-disubstituted linker.

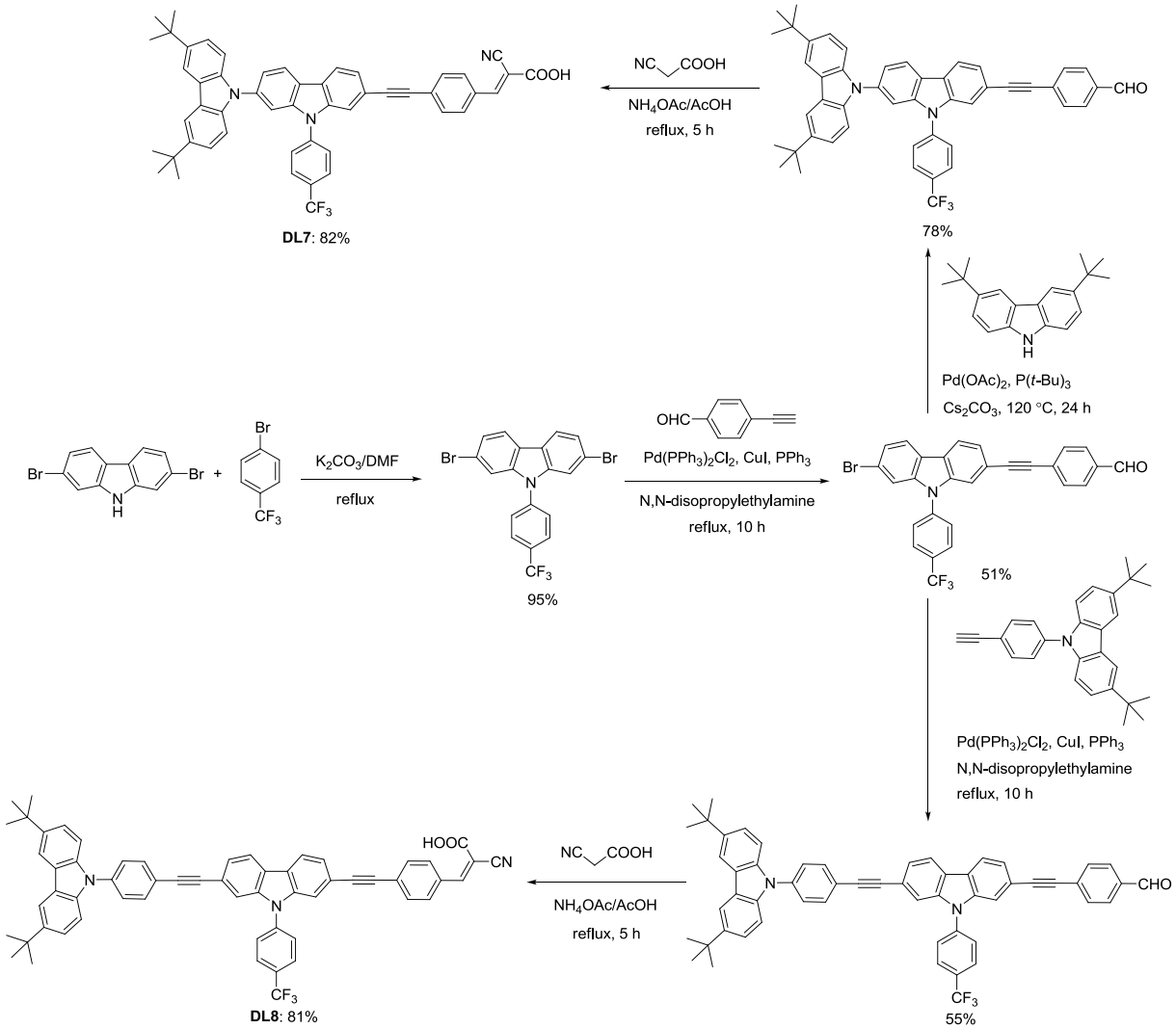

Scheme 1.69 Synthetic scheme of the dyes **DL7** and **DL8**.

The synthesis of the dyes is showed in Scheme 1.69. It starts with *N*-arylation of 2,7-dibromo-9*H*-carbazole was followed by the Sonogashira coupling with 4-ethynylbenzaldehyde to obtain 2,7-dibromo-9-(4-(trifluoromethyl)phenyl)-9*H*-carbazole, which reacted with 4-ethynylbenzaldehyde by Sonogashira coupling gave 4-((7-bromo-9-(4-(trifluoromethyl)phenyl)-9*H*-carbazol-2-yl)ethynyl)benzaldehyde. It reacted with 3,6-di-*tert*-butylcarbazole via Ullmann coupling or 3,6-di-*tert*-butyl-9-(4-ethynylphenyl)-9*H*-carbazole via Sonogashira coupling afforded the carbazole containing aldehydes which further reacted with cyanoacetic acid to give sensitizer **DL7** and **DL8**.

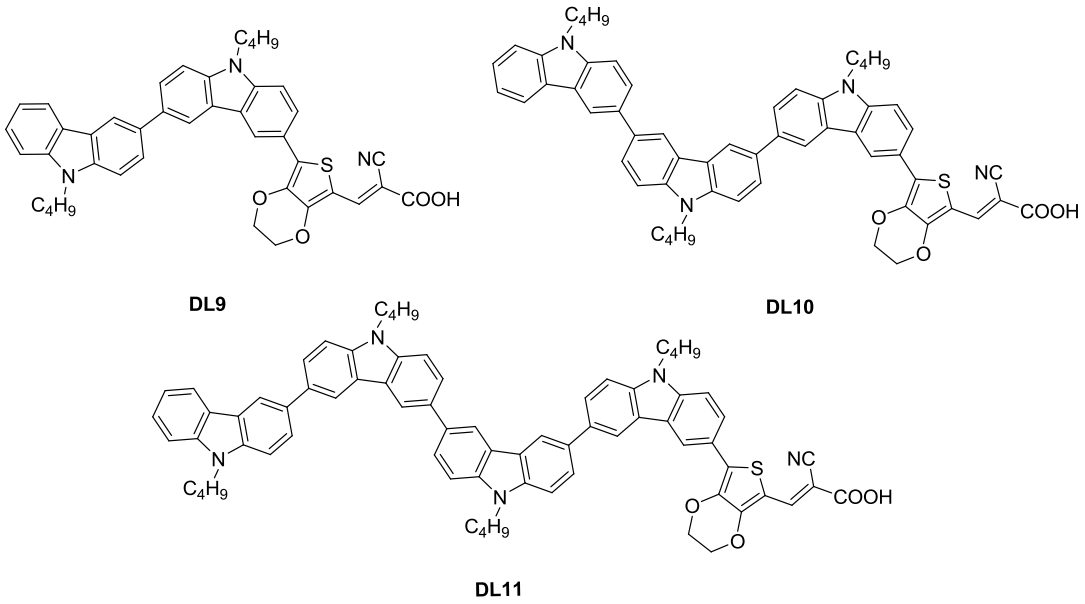

Chart 1.84 Organic dyes containing oligocarbazole units: Carbazole as donor as well as linker.

Fang and co-workers designed three dyes, **DL9**-**DL11** (Chart 1.84) in an attempt to minimize the charge recombination and aggregation at the surface of photoanodes by using oligocarbazole as donor and linker [190]. The number of carbazole units progressively increased from **DL9** to **DL11**. **DL9** possessed two carbazole units while **DL11** contains four. Irrespective of the variation in the number of carbazole units, all the dyes exhibited same absorption wavelength. However, the molar extinction coefficient increased with the number of carbazole units in the chain. Presence of zig-zag structure and alkyl chains played a major role in suppressing the formation of aggregates on TiO_2. The V_{OC} of the devices are high in range of 767-796 mV and is ascribed to the low propensity for charge recombination. Despite the twisted structure, **DL11**

displayed slightly low V_{OC} (792 mV) than **DL10** in DSSC. This is probably due to the loose packing of dye molecules creating voids through which I_3^- ions may diffuse and reach TiO_2 surface and scavenge the electrons. Among the dyes, **DL10** exhibited exceptionally high DSSC efficiency (6.33%). This clearly points that a careful molecular engineering controlling the size and three-dimensional arrangement is necessary to realize efficient DSSCs.

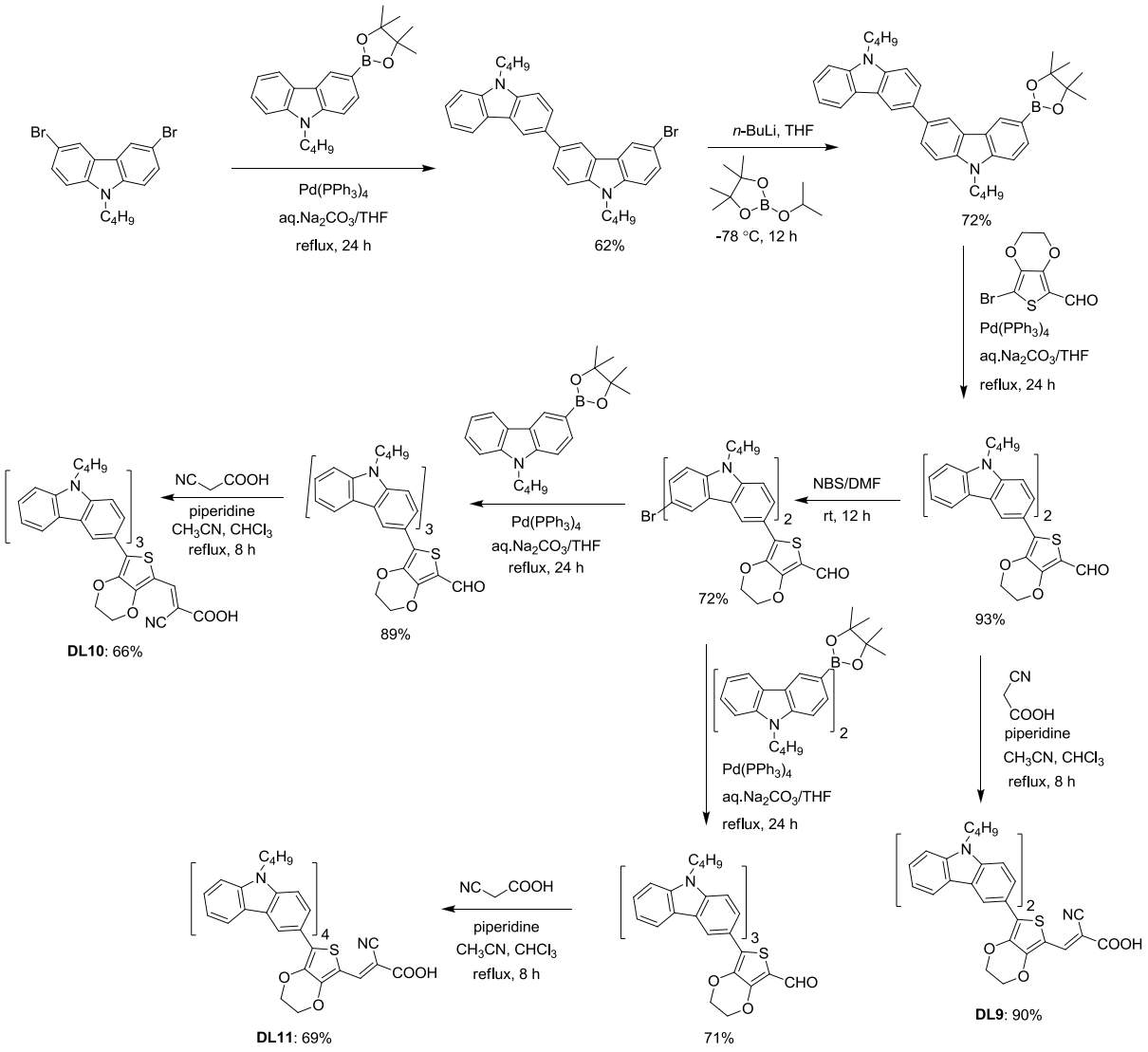

Scheme 1.70 Synthetic scheme of the dyes **DL9-DL11**.

The synthesis of the dyes (**DL9-DL11**) is outlined in Scheme 1.70. Suzuki coupling of 3,6-dibromo-9-butyl-9*H*-carbazole with 9-butyl-3-(4,4,5,5-tetramethyl-1,3,2-dioxaborolan-2-yl)-9*H*-carbazole selectively gave mono-coupled product which converted to the boronic acid derivative

by lithiation followed by addition of 2-isopropoxy-4,4,5,5-tetramethyl-1,3,2-dioxaborolane. It is coupled with 7-bromo-2,3-dihydrothieno[3,4-*b*][1,4]dioxine-5-carbaldehyde by Suzuki coupling gave the corresponding aldehyde which converted to the dye **DL9** by Knoevenagel condensation with cyanoacetic acid. Bromination of 7-(9,9'-dibutyl-9*H*,9'*H*-3,3'-bicarbazol-6-yl)-2,3-dihydrothieno[3,4-*b*][1,4]dioxine-5-carbaldehyde gave monobromproduct by using NBS in DMF solvent. It coupled with oligocarbazole boronic acid derivative via Suzuki coupling led to corresponding aldehydes which converted to the targeted dyes (**DL4**, **DL5**) by Knoevenagel condensation with cyanoacetic acid.

Kuang and co-workers reported a dye (Chart 1.85, **DL12**) containing carbazole substituted triphenylethylene chromophore and 3,6-disubstituted carbazole linker [133]. On comparing with **D3** (Chart 1.5; η = 0.42%), it is obvious that the additional donor increases the efficiency of the DSSC based on **DL12** (2.15%). This is attributed to the red-shifted absorption observed for **DL12** (Table 1.10) when compared to **D3** (Table 1.2). This enhanced light-harvesting capability of **DL12** leads to large photocurrent density.

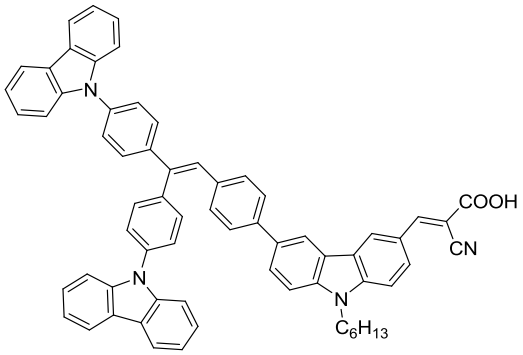

DL12

Chart 1.85 Organic dye featuring 3,6-disubstituted carbazole linker and triphenylethylene-based donor.

Promarak and co-workers designed carbazole based dyes (**DL13-DL15, DL17)** theoretically and demonstrated that these dyes are promising candidates for efficient DSSC [191]. They synthesized a set of dyes (**DL13-DL17;** Chart 1.86) based on carbazole as linker with 3,6-di-*t*-butyl-carbazole as donor and cyanoacrylic acid as acceptor [192]. When compared with the diphenylamine linker dyes (**AD15-AD17**), these dyes displayed higher efficiency. Similarly the efficiencies of **DL14** (4.80%) and **DL15** (5.69%) are higher than the dyes **AD26** (4.34%) and

AD27 (4.62%) which contains triphenylamine as donor and 3,6-di-*t*-butyl-carbazole as auxiliary donor mainly attributable to the light harvesting capability. The dye **DL15** possessing terthiophene linker performed efficiently among all other dyes due to elongated conjugation and electron richness which results in higher J_{SC} of 11.31 mA cm^{-2}. These dyes proved that carbazole is a potential candidate for donor as well as linker for dye sensitizers.

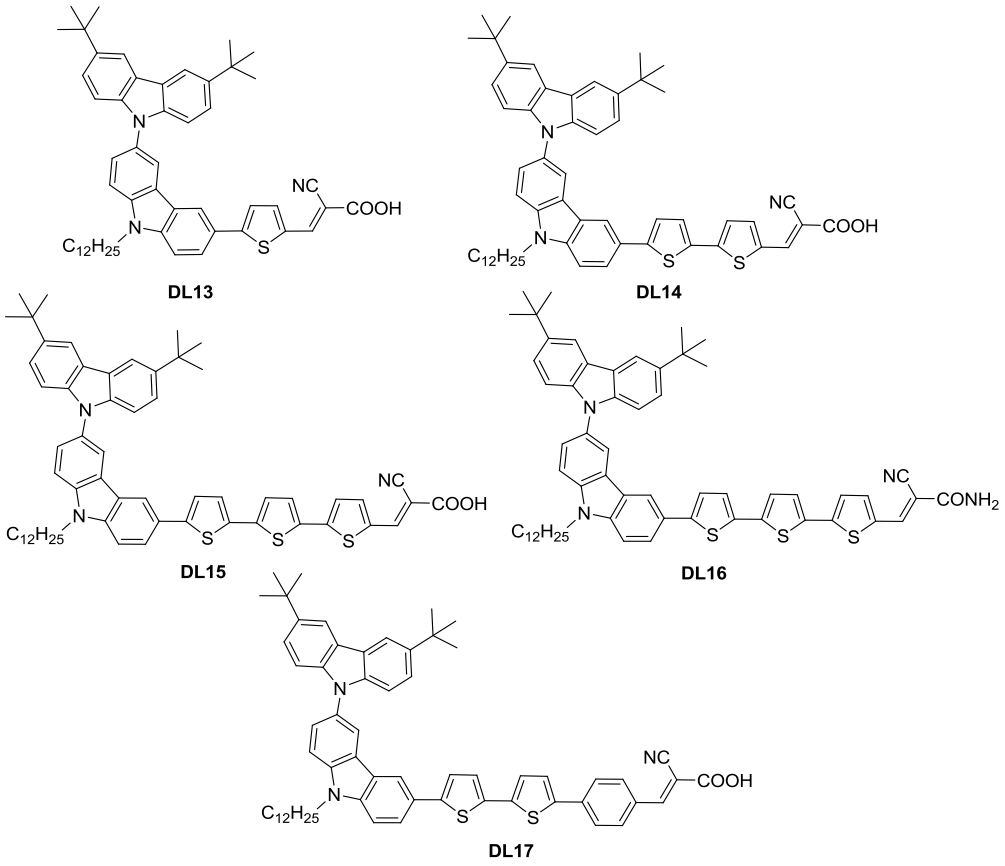

Chart 1.86 Dyes with 3,6-disubstituted carbazole linker and 3,6 di(*t*-butyl)carbazole donor.

Table 1.10 Optical, electrochemical and photovoltaic performance parameters of dyes containing carbazole as donor and linker

Dye	$\lambda_{max,}$ nm (ε_{max}, M^{-1} cm^{-1})	E_{ox}, V (*vs* NHE)	E_{ox}^{*}, V (*vs* NHE)	J_{SC} (mA cm^{-2})	V_{OC} (mV)	*ff*	η (%)	*Ref*
DL7	395 (34120)	1.43	−1.28	6.24	617	0.70	2.70	[189]
DL8	385 (54740)	1.45	−1.18	5.96	642	0.71	2.70	[189]
DL9	448 (35700)	0.99	−1.42	11.47	767	0.67	5.87	[190]
DL10	444 (34400)	0.94	−1.48	11.67	796	0.68	6.33	[190]

Table 1.10 (cont.)

Dye	$\lambda_{max,}$ nm (ε_{max}, M^{-1} cm^{-1})	E_{ox}, V (*vs* NHE)	E_{ox}^{*}, V (*vs* NHE)	J_{SC} (mA cm^{-2})	V_{OC} (mV)	*ff*	η (%)	*Ref*
DL11	456 (38700)	0.94	−1.47	11.46	792	0.68	6.16	[190]
DL12	412 (16000)	1.13	−1.70	4.55	682	0.69	2.14	[133]
DL13	433 (21952)	0.99	−1.42	7.35	740	0.67	3.64	[191]
DL14	457 (23492)	0.95	−1.27	9.70	730	0.68	4.80	[191]
DL15	443 (27938)	0.85	−1.30	11.31	710	0.71	5.69	[191]
DL16	416 (28874)	0.88	−1.48	na	na	na	na	[191]
DL17	487 (21037)	0.88	−0.92	9.98	700	0.67	4.62	[191]

na = not available

1.6 Conclusions

In the past five years, carbazole based organic sensitizers have drawn immense attention of researchers due to the chemical flexibility in the structural modifications and functional tuning. Many carbazole-based dyes have registered impressive power conversion efficiencies in DSSC. Survey of the available dyes showed the use of carbazole as a robust multifunctional building block. It has been demonstrated as donor, auxiliary donor and π-linker in the conventional donor-acceptor molecular architecture. The best efficiency reported for carbazole-based dye is 12.0% by using alkoxysilyl anchoring unit which is very close to the ruthenium dyes. For using the carbazole in organic dyes different connectivity on carbazole have been utilized. It is well established now that the C3 and C6 positions are useful for donor strength alterations and connections through C2 and C7 positions are effective as π-linkers. The C3 and C6 functionalization helps to dissipate the charge and also pushes the electron density towards the acceptor. Among the organic dyes containing carbazole as donor the best efficiency is registered at 8.10% for cyanoacrylic acid acceptor/anchoring unit and 12.0% for alkoxysilyl anchoring unit. By linking the amine donor and cyanoacrylic acid acceptor using a 2,7-disubstituted carbazole a best efficiency of 4.62% has been achieved. Usage of carbazole as auxiliary donor is beneficial to tune the LUMO energy and attain perfect packing at the surface of TiO_2. Where carbazole as auxiliary donor efficiency as high as 8.50% has been reported. Though di-substitution on carbazole has been successfully translated to the design of organic dyes, tetra-substituted

carbazole derivatives have not yet been utilized in the construction of organic dyes. Still there is a window to develop a better sensitizers on 2,7 di-substituted carbazole based dyes by suitable molecular engineering techniques.

1.7 References

1. Y. Liang and L. Yu, A new class of semiconducting polymers for bulk heterojunction solar cells with exceptionally high performance. *Acc. Chem. Res.,* **2010**, *43*, 1227-1236.
2. B. O'Regan and M. Grätzel, A low-cost, high-efficiency solar cell based on dye-sensitized colloidal TiO_2 films. *Nature*, **1991**, *353*, 737-740.
3. A. Hagfeldt, G. Boschloo, L. Sun, L. Kloo and H. Pettersson, Dye-sensitized solar cells. *Chem. Rev.,* **2010**, *110*, 6595-6663.
4. Z. Ning, Q. Zhang, W. Wu, H. Pei, B. Liu and H. Tian, Starburst triarylamine based dyes for efficient dye-sensitized solar cells. *J. Org. Chem.,* **2008**, *73*, 3791-3797.
5. A. Mishra, M. K. R. Fischer and P. Bäuerle, Metal-Free organic dyes for dye-sensitized solar cells: from structure: Property relationships to design rules. *Angew. Chem., Int. Ed.,* **2009**, *48*, 2474-2499.
6. B.-G. Kim, K. Chung and J. Kim, Molecular design principle of all-organic dyes for dye-sensitized solar cells. *Chem. - Eur. J.,* **2013**, *19*, 5220-5230.
7. M. K. Nazeeruddin, A. Kay, I. Rodicio, R. Humphry-Baker, E. Müller, P. Liska, N. Vlachopoulos and M. Grätzel, Conversion of light to electricity by cis-X2bis(2,2′-bipyridyl-4,4′-dicarboxylate)-ruthenium(II) Charge-Transfer Sensitizers (X = Cl^-, Br^-, I^-, CN^-, and SCN^-) on nanocrystalline titanium dioxide electrodes. *J. Am. Chem. Soc.,* **1993**, *115*, 6382-6390.
8. M. Liang and J. Chen, Arylamine organic dyes for dye-sensitized solar cells, *Chem. Soc. Rev.,* **2013**, *42*, 3453-3488.
9. N. Koumura, Z.-S. Wang, S. Mori, M. Miyashita, E. Suzuki and K. Hara, Alkyl-functionalized organic dyes for efficient molecular photovoltaics. *J. Am. Chem. Soc.,* **2006**, *128*, 14256-14257.
10. K. R. J. Thomas and A. Baheti, Fluorene based organic dyes for dye sensitised solar cells: Structure-property relationships. *Mater. Technol.,* **2013**, *28*, 71-87.

11. A. Baheti, K. R. J. Thomas, C.-P. Lee, C.-T. Li and K.-C. Ho, Organic dyes containingfluoren-9-ylidene chromophores for efficient dye-sensitized solar cells. *J. Mater. Chem. A*, **2014**, *2*, 5766-5779.
12. K. Hara, Z.-S. Wang, T. Sato, A. Furube, R. Katoh, H. Sugihara, Y. Dan-oh, C. Kasada, A. Shinpo and S. Suga, Oligothiophene-containing coumarin dyes for efficient dye-sensitized solar cells. *J. Phys. Chem. B*, **2005**, *109*, 15476-15482.
13. Z. S. Wang, Y. Cui, K. Hara, Y. Dan-oh, C. Kasada and A. Shinpo, A high-light-harvesting-efficiency coumarin dye for stable dye-sensitized solar cells. *Adv. Mater.*, **2007**, *19*, 1138-1141.
14. K. Hara, K. Sayama, Y. Ohga, A. Shinpo, S. Suga and H. Arakawa, A coumarin-derivative dye sensitized nanocrystalline TiO_2 solar cell having a high solar-energy conversion efficiency up to 5.6%. *Chem. Comm.*, **2001**, 569-570.
15. S. Cai, X. Hu, J. Han, Z. Zhang, X. Li, C. Wang and J. Su, Efficient organic dyes containing dibenzo heterocycles as conjugated linker part for dye-sensitized solar cells. *Tetrahedron*, **2013**, *69*, 1970-1977.
16. C.-C. Yu, K.-J. Jiang, J.-H. Huang, F. Zhang, X. Bao, F.-W. Wang, L.-M. Yang and Y. Song, Novel pyrene-based donor-acceptor organic dyes for solar cell application. *Org. Electron.*, **2013**, 4445-450.
17. K. R. J. Thomas, N. Kapoor, C.-P. Lee and K.-C. Ho, Organic dyes containing pyrenylamine-based cascade donor systems with different aromatic π linkers for dye-sensitized solar cells: Optical, electrochemical, and device characteristics. *Chem. - Asian J.*, **2012**, *7*, 738-750.
18. M. Wang, M. Xu, D. Shi, R. Li, F. Gao, G. Zhang, Z. Yi, R. Humphry-Baker, P. Wang, S. M. Zakeeruddin and M. Grätzel, High-Performance liquid and solid dye-sensitized solar cells based on a novel metal–free organic sensitizer. *Adv. Mater.*, **2008**, *20*, 4460-4463.
19. G. Zhang, Y. Bai, R. Li, D. Shi, S. Wenger, S. M. Zakeeruddin, M. Grätzel and P. Wang, Employ a bisthienothiophene linker to construct an organic chromophore for efficient and stable dye-sensitized solar cells. *Energy Environ. Sci*., **2009**, *2*, 92-95.
20. H. Qin, S. Wenger, M. Xu, F. Gao, X. Jing, P. Wang, S. M. Zakeeruddin and M. Grätzel, An organic sensitizer with a fused dithienothiophene unit for efficient and stable dye-sensitized solar cells. *J. Am. Chem. Soc.*, **2008**, *130*, 9202-9203.

21. X. Wang, J. Yang, H. Yu, F. Li, L. Fan, W. Sun, Y. Liu, Z. Y. Koh, J. Pan, W.-L. Yim, L. Yan and Q. Wang, A benzothiazole–cyclopentadithiophene bridged D-A-π-A sensitizer with enhanced light absorption for high efficiency dye-sensitized solar cells. *Chem. Commun.*, **2014**, *50*, 3965-3968.
22. X. Cheng, S. Sun, M. Liang, Y. Shi, Z. Sun and S. Xue, Organic dyes incorporating the cyclopentadithiophene moiety for efficient dye-sensitized solar cells. *Dyes Pigm.*, **2012**, *92*, 1292-1299.
23. L. E. Polander, A. Yella, J. Teuscher, R. Humphry-Baker, B. F. E. Curchod, N. A. Astani, P. Gao, J.-E. Moser, I. Tavernelli, U. Rothlisberger, M. Grätzel, M. K. Nazeeruddin and J. Frey, Unravelling the potential for dithienopyrrole sensitizers in dye sensitized solar cells. *Chem. Mater.*, **2013**, *25*, 2642-2648.
24. Z. Wang, M. Liang, L. Wang, Y. Hao, C. Wang, Z. Sun and S. Xue, New triphenylamine organic dyes containing dithieno[3,2-*b*:2',3'-*d*]pyrrole (DTP) units for iodine-free dye-sensitized solar cells. *Chem. Commun.*, **2013**, 49, 5748-5750.
25. H. Tian, X. Yang, R. Chen, Y. Pan, L. Li, A. Hagfeldt and L. Sun, Phenothiazine derivatives for efficient organic dye-sensitized solar cells. *Chem. Comm.*, **2007**, 3741-3743.
26. S. H. Kim, H. W. Kim, C. Sakong, J. Namgoong, S. W. Park, M. J. Ko, C. H. Lee, W. I. Lee and J. P. Kim, Effect of five-membered heteroaromatic linkers to the performance of phenothiazine-based dye-sensitized solar cells. *Org. Lett.*, **2011**, *13*, 5784-5787.
27. H. Tian, X. Yang, J. Cong, R. Chen, J. Liu, Y. Hao, A. Hagfeldt and L. Sun, Tuning of phenoxazine chromophores for efficient organic dye-sensitized solar cells. *Chem. Commun.*, **2009**, 6288-6290.
28. H. Tian, I. Bora, X. Jiang, E. Gabrielsson, K. M. Karlsson, A. Hagfeldt and L. Sun, Modifying organic phenoxazine dyes for efficient dye-sensitized solar cells. *J. Mater. Chem.*, **2011**, *21*, 12462-12472.
29. T. Horiuchi, H. Miura, K. Sumioka and S. Uchida, High efficiency of dye-sensitized solar cells based on metal-free indoline dyes. *J. Am. Chem. Soc.*, **2004**, *126*, 12218-12219.
30. S. Ito, H. Miura, S. Uchida, M. Takata, K. Sumioka, P. Liska, P. Comte, P. Pechy and M. Grätzel, High-conversion-efficiency organic dye-sensitized solar cells with a novel indoline dye. *Chem. Comm.*, **2008**, 5194-5196.

31. M. Velusamy, Y. C. Hsu, J. T. Lin, C. W. Chang and C. P. Hsu, 1-Alkyl-1*H*-imidazole-based dipolar organic compounds for dye-sensitized solar cells. *Chem. -Asian. J.*, **2010**, *5*, 87-96.
32. D. Kumar, K. R. J. Thomas, C.-P. Lee and K.-C. Ho, Novel pyrenoimidazole-based organic dyes for dye-sensitized solar cells. *Org. Lett.*, **2011**, *13*, 2622-2625.
33. Y. Wu and W. Zhu, Organic sensitizers from D-[π]-A to D-A-[π]-A: Effect of the internal electron-withdrawing units on molecular absorption, energy levels and photovoltaic performances. *Chem. Soc. Rev.*, **2013**, *42*, 2039-2058.
34. M. Velusamy, K. R. J. Thomas, J. T. Lin, Y.-C. Hsu and K.-C. Ho, Organic dyes incorporating low-band-gap chromophores for dye-sensitized solar cells. *Org. Lett.*, **2005**, *7*, 1899-1902.
35. H. Zhu, W. Li, Y. Wu, B. Liu, S. Zhu, X. Li, H. Ågren and W. Zhu, Insight into benzothiadiazole acceptor in D-A-π-A configuration on photovoltaic performances of dye-sensitized solar cells. *ACS Sustainable Chem. Eng.*, **2014**, *2*, 1026-1034.
36. W. Li, Y. Wu, Q. Zhang, H. Tian and W. Zhu, D-A-π-A Featured sensitizers bearing phthalimide and benzotriazole as auxiliary acceptor: Effect on absorption and charge recombination dynamics in dye-sensitized solar cells. *ACS Appl. Mater. Interfaces*, **2012**, *4*, 1822-1830.
37. Y. Cui, Y. Wu, X. Lu, Xi Zhang, G. Zhou, F. B. Miapeh, W. Zhu and Z.-S. Wang, Incorporating benzotriazole moiety to construct D-A-π-A organic sensitizers for solar cells: Significant enhancement of open-circuit photovoltage with long alkyl group. *Chem. Mater.*, **2011**, *23*, 4394-4401.
38. S. Qu, B. Wang, F. Guo, J. Li, W. Wu, C. Kong, Y. Long and J. Hua, New diketo-pyrrolo-pyrrole (DPP) sensitizer containing a furan moiety for efficient and stable dye-sensitized solar cells. *Dyes Pigm.*, **2012**, *92*, 1384-1393.
39. W. Ying, F. Guo, J. Li, Q. Zhang, W. Wu, H. Tian and J. Hua, Series of new D-A-π-A organic broadly absorbing sensitizers containing isoindigo unit for highly efficient dye-sensitized solar cells. *ACS Appl. Mater. Interfaces*, **2012**, *4*, 4215-4224.
40. X. Lu, Q. Feng, T. Lan, G. Zhou and Z.-S. Wang, Molecular engineering of quinoxaline-based organic sensitizers for highly efficient and stable dye-sensitized solar cells. *Chem. Mater.*, **2012**, *24*, 3179-3187.

41. K. Pei, Y. Z. Wu, W. J. Wu, Q. Zhang, B. Q. Chen, H. Tian and W. H. Zhu, Constructing organic D-A-π-A-featured sensitizers with a quinoxaline unit for high-efficiency solar cells: the effect of an auxiliary acceptor on the absorption and the energy level alignment. *Chem.-Eur. J.*, **2012**, *18*, 8190-8200.
42. D. W. Chang, H. J. Lee, J. H. Kim, S. Y. Park, S. M. Park, L. Dai and J. B. Baek, Novel quinoxaline-based organic sensitizers for dye-sensitized solar cells. *Org. Lett.*, **2011**, *13*, 3880-3883.
43. Q. Y. Feng, X. F. Lu, G. Zhou and Z. S. Wang, Synthesis and photovoltaic properties of organic sensitizers incorporating a thieno[3,4-*c*]pyrrole-4,6-dione moiety. *Phys. Chem. Chem. Phys.*, **2012**, *14*, 7993-7999.
44. K. R. J. Thomas, J. T. Lin, Y.-T. Tao and C.-W. Ko, Light-emitting carbazole derivatives: Potential electroluminescent materials. *J. Am. Chem. Soc.*, **2001**, *123*, 9404-9411.
45. J. Li, C. Ma, J. Tang, C.-S. Lee and S. Lee, Novel starburst molecule as a hole injecting and transporting material for organic light-emitting devices. *Chem. Mater.*, **2005**, *17*, 615-619.
46. S. L. Lai, Q.X. Tong, M. Y. Chan, T. W. Ng, M. F. Lo, C. C. Ko, S. T. Lee and C. S. Lee, Carbazole–pyrene derivatives for undoped organic light-emitting devices. *Org. Electron.*, **2011**, *12*, 541-546.
47. M. H. Tsai, Y. H. Hong, C. H. Chang, H. C. Su, C. C. Wu, A. Matoliukstyte, J. Simokaitiene, S. Grigalevicius, J. V. Grazulevicius and C. P. Hsu, 3-(9-Carbazolyl)carbazoles and 3,6-di(9-carbazolyl)carbazoles as effective host materials for efficient blue organic electrophosphorescence. *Adv. Mater.*, **2007**, *19*, 862-866.
48. C.-W. Ko, Y.-T. Tao, J. T. Lin and K. R. J. Thomas, Light-Emitting diodes based on a carbazole-derivatized dopant: Origin of dopant excitation as a function of the device structure. *Chem. Mater.*, **2001**, *14*, 357-361.
49. M. Sonntag, K. Kreger, D. Hanft and P. Strohriegl, novel star-shaped triphenylamine-based molecular glasses and their use in OFETs. *Chem. Mater.*, **2005**, *17*, 3031-3039.
50. Y. Wang, L. Hou, K. Yang, J. Chen, F. Wang and Y. Cao, Conjugated silole and carbazole copolymers: Synthesis, characterization, single-layer light-emitting diode, and field effect carrier mobility. *Macromol. Chem. Phys.*, **2005**, *206*, 2190-2198.

51. Y. Song, C.-a. Di, Z. Wei, T. Zhao, W. Xu, Y. Liu, D. Zhang and D. Zhu, Synthesis, characterization, and field-effect transistor properties of carbazolenevinylene oligomers: From linear to cyclic architectures. *Chem.- Eur. J.*, **2008**, *14*, 4731-4740.
52. E. Wang, L. Hou, Z. Wang, Z. Ma, S. Hellström, W. Zhuang, F. Zhang, O. Inganäs and M. R. Andersson, Side-Chain architectures of 2,7-carbazole and quinoxaline-based polymers for efficient polymer solar cells. *Macromolecules,* **2011**, *44*, 2067-2073.
53. J. Li and A. C. Grimsdale, Carbazole-based polymers for organic photovoltaic devices. *Chem. Soc. Rev.* **2010**, *39*, 2399-2410.
54. Z.-S. Wang, N. Koumura, Y. Cui, M. Takahashi, H. Sekiguchi, A. Mori, T. Kubo, A. Furube and K. Hara, Hexylthiophene-functionalized carbazole dyes for efficient molecular photovoltaics: Tuning of solar-cell performance by structural modification. *Chem. Mater.*, **2008**, *20*, 3993-4003.
55. A. Baheti, K. R. J. Thomas, C.-P. Lee and K.-C. Ho, Fine tuning the performance of dsscs by variation of the π-spacers in organic dyes that contain a 2,7-diaminofluorene donor. *Chem. Asian J.*, **2012**, *7*, 2942-2954.
56. P. Singh, A. Baheti and K. R. J. Thomas, Synthesis and optical properties of acidochromic amine-substituted benzo[*a*]phenazines. *J. Org. Chem.*, **2011**, *76*, 6134-6145.
57. H. Sasabe, N. Toyota, H. Nakanishi, T. Ishizaka, Y.-J. Pu and J. Kido, 3,3′-Bicarbazole-based host materials for high-efficiency blue phosphorescent OLEDs with extremely low driving voltage. *Adv. Mater.*, **2012**, *24*, 3212-3217.
58. M. Sonntag and P. Strohriegl, Novel 2,7-Linked carbazole trimers as model compounds for conjugated carbazole polymers. *Chem. Mater.*, **2004**, *16*, 4736-4742.
59. T. Zhao, Z. Liu, Y. Song, W. Xu, D. Zhang and D. Zhu, Novel diethynylcarbazole macrocycles: Synthesis and optoelectronic properties. *J. Org. Chem.*, **2006**, *71*, 7422-7432.
60. A. Keerthi, D. Sriramulu, Y. Liu, C. T. Yuan Timothy, Q. Wang and S. Valiyaveettil, Architectural influence of carbazole push–pull–pull dyes on dye sensitized solar cells. *Dyes Pigm.*, **2013**, *99*, 787-797.
61. F. Monnier and M. Taillefer, Catalytic C-C, C-N, and C-O Ullmann-type coupling reactions. *Angew. Chem., Int. Ed.*, **2009**, *48*, 6954-6971.
62. N. Miyaura and A. Suzuki, Palladium-catalyzed cross-coupling reactions of organoboron compounds. *Chem. Rev.*, **1995**, *95*, 2457-2483.

63. E. Knoevenagel, Ueber eine darstellungsweise des benzylidenacetessigesters. *Chem. Ber.* **1896**, *29*, 172-174.
64. A. Midya, Z. Xie, J.-X. Yang, Z.-K. Chen, D. J. Blackwood, J. Wang, S. Adams and K. P. Loh, A new class of solid state ionic conductors for application in all solid state dye sensitized solar cells. *Chem. Comm.*, **2010**, *46*, 2091-2093.
65. S. Pansay, N. Prachumrak, S. Jungsuttiwong, T. Keawin, T. Sudyoadsuk and V. Promarak, Multibromo-*N*-alkylcarbazoles: synthesis, characterization, and their benzo[*b*]thiophene derivatives. *Tetrahedron Lett.*, **2012**, *53*, 4568-4572.
66. K. Smith, D. M. James, A. G. Mistry, M. R. Bye and D. J. Faulkner, A new method for bromination of carbazoles, β-carbolines and iminodibenzyls by use of *N*-bromosuccinimide and silica gel. *Tetrahedron*, **1992**, *48*, 7479-7488.
67. T. Zhao, Z. Liu, Y. Song, W. Xu, D. Zhang and D. Zhu, Novel diethynylcarbazole macrocycles: Synthesis and optoelectronic properties. *J. Org. Chem.*, **2006**, *71*, 7422-7432.
68. Y. Zheng, A. S. Batsanov, V. Jankus, F. B. Dias, M. R. Bryce and A. P. Monkman, Bipolar molecules with high triplet energies: Synthesis, photophysical, and structural properties. *J. Org. Chem.*, **2011**, *76*, 8300-8310.
69. J. Hassan, M. Sévignon, C. Gozzi, E. Schulz and M. Lemaire, Aryl-Aryl bond formation one century after the discovery of the Ullmann reaction. *Chem. Rev.*, **2002**, *102*, 1359-1470.
70. J. F. Hartwig, Transition metal catalyzed synthesis of arylamines and aryl ethers from aryl halides and triflates: Scope and mechanism. *Angew. Chem., Int. Ed.*, **1998**, *37*, 2047-2067.
71. M. S. Kim, H. S. Yang, D. Y. Jung, Y. S. Han and J. H. Kim, Effects of the number of chromophores and the bulkiness of a nonconjugated spacer in a dye molecule on the performance of dye-sensitized solar cells. *Colloids Surf., A.*, **2013**, *420*, 22-29.
72. A. Vilsmeier and A. Haack, Vilsmeier-Haack reactions in Synthesis of Heterocycles: An Overview, Chapter 2, *Ber. Dtsch. Chem. Ges.*, **1927**, *60*, 119.
73. Y. Hong, J.-Y. Liao, J. Fu, D.-B. Kuang, H. Meier, C.-Y. Su and D. Cao, Performance of dye-sensitized solar cells based on novel sensitizers bearing asymmetric double D-π-A chains with arylamines as donors. *Dyes Pigm.*, **2012**, *94*, 481-489.
74. D. Kim, J. K. Lee, S. O. Kang and J. Ko, Molecular engineering of organic dyes containing *N*-aryl carbazole moiety for solar cell. *Tetrahedron*, **2007**, *63*, 1913-1922.

75. C. Zhang, A. W. Harper and L. R. Dalton, Formylation of diethyl 2-thienylmethylphosphonate for one-pot synthesis of aminothienostilbenecarboxaldehyde. *Synth. Commun.*, **2001**, *31*, 1361-1365.
76. T. Duan, K. Fan, C. Zhong, T. Peng, J. Qin and X. Chen, New organic dyes containing *tert*-Butyl-capped *N*-Arylcarbazole moiety for dye-sensitized solar cells. *RSC Adv.*, **2012**, *2*, 7081-7086.
77. Y. J. Chang, P.-T. Chou, S.-Y. Lin, M. Watanabe, Z.-Q. Liu, J.-L. Lin, K.-Y. Chen, S.-S. Sun, C.-Y. Liu and T. J. Chow, High-Performance organic materials for dye-sensitized solar cells: Triarylene-linked dyads with a 4-*tert*-butylphenylamine donor. *Chem. - Asian J.*, **2012**, *7*, 572-581.
78. J. K. Stille, The palladium-catalyzed cross-coupling reactions of organotin reagents with organic electrophiles. *Angew. Chem. Int. Ed.*, **1986**, *25*, 508-524.
79. D. Liu, B. Zhao, P. Shen, H. Huang, L. Liu and S. Tan, Molecular design of organic dyes based on vinylene hexylthiophene bridge for dye-sensitized solar cells. *Sci. China Ser. B-Chem.*, **2009**, *52*, 1198-1209.
80. A. I. Arkhypchuk, M.-P. Santoni and S. Ott, Revisiting the Phospha-Wittig-Horner reaction. *Organometallics*, **2012**, *31*, 1118-1126.
81. D. Barpuzary, A. S. Patra, J. V. Vaghasiya, B. G. Solanki, S. S. Soni and M. Qureshi, Highly efficient one-dimensional ZnO nanowire-based dye sensitized solar cell using a metal-free, D-π-A-Type, carbazole derivative with more than 5% power conversion. *ACS Appl. Mater. Interfaces*, **2014**, *6*, 12629-12639.
82. M. Akhtaruzzaman, Menggenbateer, A. Islam, A. El-Shafei, N. Asao, T. Jin, L. Han, K. A. Alamry, S. A. Kosa, A. M. Asiri and Y. Yamamoto, Structure-property relationship of different electron donors: Novel organic sensitizers based on fused dithienothiophene π-conjugated linker for high efficiency dye-sensitized solar cells. *Tetrahedron*, **2013**, *69*, 3444-3450.
83. M. Marszalek, S. Nagane, A. Ichake, R. Humphry-Baker, V. Paul, S. M. Zakeeruddin and M. Grätzel, Structural variations of D-[π]-A dyes influence on the photovoltaic performance of dye-sensitized solar cells. *RSC Adv.*, **2013**, *3*, 7921-7927.
84. T. Sandmeyer, Ueber die Ersetzung der Amid-gruppe durch Chlor, Brom und Cyan in den aromatischen Substanzen, *Eur. J. Inorg. Chem.*, **1884**, 17, 2650-2653.

85. Á Molnár, Efficient, Selective, and recyclable palladium catalysts in carbon-carbon coupling reactions. *Chem. Rev.*, **2011**, *111*, 2251-2320.
86. M. Miyashita, K. Sunahara, T. Nishikawa, Y. Uemura, N. Koumura, K. Hara, A. Mori, T. Abe, E. Suzuki and S. Mori, Interfacial electron-transfer kinetics in metal-free organic dye-sensitized solar cells: Combined effects of molecular structure of dyes and electrolytes. *J. Am. Chem. Soc.*, **2008**, *130*, 17874-17881.
87. K. Hara, Z.-S. Wang, Y. Cui, A. Furube and N. Koumura, Long-term stability of organic-dye-sensitized solar cells based on an alkyl-functionalized carbazole dye. *Energy Environ. Sci.*, **2009**, *2*, 1109-1114.
88. N. Koumura, Z.-S. Wang, M. Miyashita, Y. Uemura, H. Sekiguchi, Y. Cui, A. Mori, S. Mori and K. Hara, Substituted carbazole dyes for efficient molecular photovoltaics: Long electron lifetime and high open circuit voltage performance. *J. Mater. Chem.*, **2009**, *19*, 4829-4836.
89. T. N. Murakami, N. Koumura, T. Uchiyama, Y. Uemura, K. Obuchi, N. Masaki, M. Kimura and S. Mori, Recombination inhibitive structure of organic dyes for cobalt complex redox electrolytes in dye-sensitised solar cells. *J. Mater. Chem. A*, **2013**, *1*, 792-798.
90. S. Kajiyama, Y. Uemura, H. Miura, K. Hara and N. Koumura, Organic dyes with oligo-n-hexylthiophene for dye-sensitized solar cells: Relation between chemical structure of donor and photovoltaic performance. *Dyes Pigm.*, **2012**, *92*, 1250-1256.
91. Y. Uemura, S. Mori, K. Hara and N. Koumura, Carbazole dyes with ether groups for dye-sensitized solar cells: Effect of negative charges in dye molecules on electron lifetime. *Jpn. J. Appl. Phys.*, **2012**, *51*, 10NE14.
92. Q. Feng, Q. Zhang, X. Lu, H. Wang, G. Zhou and Z.-S. Wang, Facile and selective synthesis of oligothiophene-based sensitizer isomers: An approach toward efficient dye-sensitized solar cells. *ACS Appl. Mater. Interfaces*, **2013**, *5*, 8982-8990.
93. X.-H. Zhang, J. Ogawa, K. Sunahara, Y. Cui, Y. Uemura, T. Miyasaka, A. Furube, N. Koumura, K. Hara and S. Mori, Alternation of charge injection and recombination in dye-sensitized solar cells by the addition of nonconjugated bridge to organic dyes. *J. Phys. Chem. C*, **2013**, *117*, 2024-2031.

94. T. N. Murakami, E. Yoshida and N. Koumura, Carbazole dye with phosphonic acid anchoring groups for long-term heat stability of dye-sensitized solar cells. *Electrochim. Acta*, **2014**, *131*, 174-183.
95. K. Kakiage, Y. Aoyama, T. Yano, T. Otsuka, T. Kyomen, M. Unno and M. Hanaya, An achievement of over 12 percent efficiency in an organic dye-sensitized solar cell. *Chem. Commun.*, **2014**, *50*, 6379-6381.
96. C. Koenigsmann, T. S. Ripolles, B. J. Brennan, C. F. A. Negre, M. Koepf, A. C. Durrell, R. L. Milot, J. A. Torre, R. H. Crabtree, V. S. Batista, G. W. Brudvig, J. Bisquert and C. A. Schmuttenmaer, Substitution of a hydroxamic acid anchor into the MK-2 dye for enhanced photovoltaic performance and water stability in a DSSC. *Phys. Chem. Chem. Phys.*, **2014**, *16*, 16629-16641.
97. Y. Uemura, Ta. N. Murakami and N. Koumura, Crown ether-substituted carbazole dye for dye-sensitized solar cells: controlling the local ion concentration at the TiO_2/dye/electrolyte interface. *J. Phys. Chem. C*, **2014**, *118*, 16749-16759.
98. E. V. Verbitskiy, E. M. Cheprakova, J. O. Subbotina, A. V. Schepochkin, P. A. Slepukhin, G. L. Rusinov, V. N. Charushin, O. N. Chupakhin, N. I. Makarova, A. V. Metelitsa and V. I. Minkin, Synthesis, spectral and electrochemical properties of pyrimidine containing dyes as photo sensitizers for dye-sensitized solar cells. *Dyes Pigm.*, **2014**, *100*, 201-214.
99. L.-F. Lai, C.-L. Ho, Y.-C. Chen, W.-J. Wu, F.-R. Dai, C.-H. Chui, S.-P. Huang, K.-P. Guo, J.-T. Lin, H. Tian, S.-H. Yang and W.-Y. Wong, New bithiazole-functionalized organic photosensitizers for dye-sensitized solar cells. *Dyes Pigm.*, **2013**, *96*, 516-524.
100. M. Alajarín, J. Cabrera, A. Pastor, P. Sánchez-Andrada and D. Bautista. On the [2 + 2] cycloaddition of 2-aminothiazoles and dimethyl acetylenedicarboxylate. Experimental and computational evidence of a thermal disrotatory ring opening of fused cyclobutenes. *J. Org. Chem.*, **2006**, *14*, 5328-5339.
101. X. Wang, L. Guo, P. F. Xia, F. Zheng, M. S. Wong and Z. Zhu, Dye-Sensitized solar cells based on organic dyes with naphtho[2,1-*b*:3,4-*b*']dithiophene as the conjugated linker. *J. Mater. Chem. A*, **2013**, 13328-13336.
102. J.-S. Ni, J.-H. You, W.-I Hung, W.-S. Kao, H.-H. Chou and J. T. Lin, Organic dyes incorporating the dithieno[3',2':3,4;2",3":5,6]benzo[1,2-*c*]furazan moiety for dye-sensitized solar cells. *ACS Appl. Mater. interface*, **2014**, 6, 22612-22621.

103. T. Duan, K. Fan, C. Zhong, W. Gao, X. Chen, T. Peng and J. Qin, Synthesis and photovoltaic property of new kind of organic dyes containing 2,2'-bithiophene unit with three electron-donors. *J. Photochem. Photobiol., A*, **2014**, *278*, 39-45.

104. L. Han, X. Zu, Y. Cui, H. Wu, Q. Ye and J. Gao, Novel D-A-π-A carbazole dyes containing benzothiadiazole chromophores for dye-sensitized solar cells. *Org. Electron.*, **2014**, *15*, 1536-1544.

105. Q. Zhang, W. Zhu, M. Fang, F. Yin, C. Li, Synthesis, photophysical and electrochemical properties of two novel carbazole-based dye molecules. *Spectrochim. Acta, Part A*, **2015**, *135*, 379-385.

106. N. P. Prajapati, R. H. Vekariya, M.A. Borad and H. D. Patel, Recent advances in the synthesis of 2-substituted benzothiazoles: a review. *RSC Adv.*, **2014**, *4*, 60176-60208.

107. C. Teng, X. Yang, C. Yuan, C. Li, R. Chen, H. Tian, S. Li, A. Hagfeldt and L. Sun, Two novel carbazole dyes for dye-sensitized solar cells with open-circuit voltages up to 1 V based on Br^-/Br_3^- electrolytes. *Org. Lett.*, **2009**, *11*, 5542-5545.

108. C. Teng, X. Yang, S. Li, M. Cheng, A. Hagfeldt, L.-Z. Wu and L. Sun, Tuning the homo energy levels of organic dyes for dye-sensitized solar cells based on Br^-/Br_3^- Electrolytes. *Chem. - Eur. J.*, **2010**, *16*, 13127-13138.

109. R. R. Naredla and D. A. Klumpp, Contemporary carbocation chemistry: Applications in organic synthesis. *Chem. Rev.*, **2013**, *113*, 6905-6948.

110. E. M. Barea, C. Zafer, B. Gultekin, B. Aydin, S. Koyuncu, S. Icli, F. F. Santiago and J. Bisquert, Quantification of the effects of recombination and injection in the performance of dye-sensitized solar cells based on *N*-Substituted carbazole dyes. *J. Phys. Chem. C*, **2010**, *114*, 19840-19848.

111. Z. Wan, C. Jia, L. Zhou, W. Huo, X. Yao and Y. Shi, Influence of different arylamine electron donors in organic sensitizers for dye-sensitized solar cells. *Dyes Pigm.*, **2012**, *95*, 41-46.

112. T. N. Murakami, N. Koumura, M. Kimura and S. Mori, Structural effect of donor in organic dye on recombination in dye sensitized solar cells with cobalt complex electrolyte. *Langmuir*, **2014**, *30*, 2274-2279.

113. K. Srinivas, C. R. Kumar, M. A. Reddy, K. Bhanuprakash, V. J. Rao and L. Giribabu, D-π-A organic dyes with carbazole as donor for dye-sensitized solar cells. *Synth. Met.,* **2011**, *161,* 96-105.

114. P. Singh, A. Baheti, K. R. J. Thomas, C.-P. Lee and K.-C. Ho, Fluorene-based organic dyes containing acetylene linkage for dye-sensitized solar cells. *Dyes Pigm*., **2012**, *95*, 523-533.

115. R. Chinchilla and C. Nájera, The sonogashira reaction: A booming methodology in synthetic organic chemistry. *Chem. Rev.*, **2007**, *107*, 874-922

116. K. Panthi, R. M. Adhikari and T. H. Kinstle, Carbazole donor-carbazole linker-based compounds: Preparation, photophysical properties, and formation of fluorescent nanoparticles. *J. Phys. Chem. A*, **2010**,*114*, 4550-4557.

117. J. Liu, X. Sun, Z. Li, B. Jin, G. Lai, H. Li, C. Wanga, Y. Shen and J. Hua, New D-π-A system dye based on dithienosilole and carbazole: Synthesis, photo-electrochemical properties and dye-sensitized solar cell performance. *J. Photochem. Photobiol., A*, **2014**, *294*, 54-61.

118. T. Yakhanthip, S. Jungsuttiwong, S. Namuangruk, N. Kungwan, V. Promarak, T. Sudyoadsuk, P. Kochpradist, Theoretical investigation of novel carbazole-fluorene based D-π-A conjugated organic dyes as dye-sensitizer in dye-sensitized solar cells (DSCs). *J. Comput. Chem.*, **2011**, *32*, 1568-1576.

119. S. Jungsuttiwong, T. Yakhanthip, Y. Surakhot, J. Khunchalee, T. Sudyoadsuk, V. Promarak, N. Kungwan and S. Namuangruk, The effect of conjugated spacer on novel carbazole derivatives for dye-sensitized solar cells: Density functional theory/time-dependent density functional theory study. *J. Comput. Chem.*, **2012**, *33*, 1517-1523.

120. R. G. Parr and W. Yang, Density-functional theory of the electronic structure of molecules. *Annu. Rev. Phys. Chem.*, **1995**, *46*, 701-728.

121. J. P. Perdew, K. Burke and M. Ernzerhof, Generalized gradient approximation made simple. Phys. Rev. Lett., **1996**, *77*, 3865-3867.

122. W. Lee, N. Cho, J. Kwon, J. Ko and J.-I. Hong, New organic dye based on a 3,6-disubstituted carbazole donor for efficient dye-sensitized solar cells. *Chem. - Asian J.*, **2012**, *7*, 343-350.

123. I. P. Beletskaya and A. V. Cheprakov, The Heck Reaction as a Sharpening Stone of Palladium Catalysis. *Chem. Rev.*, **2000**, *100*, 3009-3066.

124. J.-Y. Li, T.-H. Lin, S.-C. Chen and C.-G. Wu, Unsymmetrical squaraines incorporating cabazole as a donor for dye-sensitized solar cells. *J. Chin. Chem. Soc.*, **2012**, *59*, 1337-1344.
125. L.-L. Tan, L.-J. Xie, Y. Shen, J.-M. Liu, L.-M. Xiao, D.-B. Kuang and C.-Y. Su, Novel organic dyes incorporating a carbazole or dendritic 3,6-diiodocarbazole unit for efficient dye-sensitized solar cells. *Dyes Pigm.*, **2014**, *100*, 269-277.
126. J.-F. Huang, J.-M. Liu, L.-L. Tan, Y.-F. Chen, Y. Shen, L.-M. Xiao, D.-B. Kuang, C.-Y. Su, Novel carbazole based sensitizers for efficient dye-sensitized solar cells: Role of the hexyl chain. *Dyes Pigm.*, **2015**, *114*, 18-23.
127. C.-G. Wu, W.-T. Shieh, C.-S. Yang, C.-J. Tan, C.-H. Chang, S.-C. Chen, C.-Y. Wu and H.-H. G. Tsai, Molecular engineering of cyclopentadithiophene-containing organic dyes for dye-sensitized solar cell: Experimental results vs theoretical calculation. *Dyes Pigm.*, **2013**, *99*, 1091-1100.
128. T. Sudyoadsuk, J. Khunchalee, S. Pansay, P. Tongkasee, S. Morada, T. Kaewin, S. Jungsuttiwong and V. Promarak, An organic dye using *N*-dodecyl-3-(3,6-di-*tert*-butylcarbazol-*N*-yl)carbazol-6-yl as a donor moiety for efficient dye-sensitized solar cells. *Tetrahedron Lett.*, **2013**, *54*, 4903-4907.
129. T. Khanasa, N. Prachumrak, P. Kochapradist, S. Namuangruk, T. Keawin, S. Jungsuttiwong, T. Sudyoadsuk and V. Promarak, The design, synthesis and characterization of D-π-A-π-A type organic dyes as sensitizers for dye-sensitized solar cells (DSSCs). *Tetrahedron Lett.*, **2014**, *55*, 3244-3248.
130. G. Marotta, M. Anil Reddy, S. P. Singh, A. Islam, L. Han, F. D. Angelis, M. Pastore and M. Chandrasekharam, Novel carbazole-phenothiazine dyads for dye-sensitized solar cells: A combined experimental and theoretical study. *ACS Appl. Mater. Interfaces*, **2013**, *5*, 9635-9647.
131. K. S. V. Gupta, J. Zhang, G. Marotta, M. A. Reddy, S. P. Singh, A. Islam, L. Han, F. D. Angelis, M. Chandrasekharama, M. Pastore, Effect of the anchoring group in the performance of carbazolephenothiazine dyads for dye-sensitized solar cells. *Dyes Pigm.*, **2015**, *113*, 536-545.
132. P. Thongkasee, A. Thangthong, N. Janthasing, T. Sudyoadsuk, S. Namuangruk, T. Keawin, S. Jungsuttiwong and V. Promarak, Carbazole-dendrimer-based donor-π-acceptor type

organic dyes for dye-sensitized solar cells: Effect of the size of the carbazole dendritic donor. *ACS Appl. Mater. Interfaces,* **2014**, *6,* 8212-8222.

133. L.-L. Tan, J.-F. Huang, Y. Shen, L.-M. Xiao, J.-M. Liu, D.-B. Kuang and C.-Y. Su, Highly efficient and stable organic sensitizers with duplex starburst triphenylamine and carbazole donors for liquid and quasi-solid-state dye-sensitized solar cells. *J. Mater. Chem. A,* **2014**, *2*, 8988-8994.
134. W. Lee, J. Y. Seng and J.-I. Hong, Metal-free organic dyes with benzothiadiazole as an internal acceptor for dye-sensitized solar cells. *Tetrahedron*, **2013**, *69*, 9175-9182.
135. C. Qin, A. Islam and L. Han, Incorporating a stable fluorenone unit into D-A-π-A organic dyes for dye-sensitized solar cells. *J. Mater. Chem*., **2012**, *22*, 19236-19243.
136. T. Wang, J. Han, Z. Zhang, B. Xu, J. Huang and J. Su, Bistriphenylamine-substitutedfluoranthene derivatives as electroluminescent emitters and dye-sensitized solar cells. *Tetrahedron,* **2012**, *68*, 10372-10377.
137. C. Olivier, F. Sauvage, L. Ducasse, F. Castet, M. Grätzel and T. Toupance, Fine-tuning of triarylamine-based photosensitizers for dye-sensitized solar cells. *ChemSusChem,* **2011**, *4*, 731-736.
138. K. R. J. Thomas, P. Singh, A. Baheti, Y.-C. Hsu, K.-C. Ho and J. T. Lin, Electro-optical properties of new anthracene based organic dyes for dye-sensitized solar cells. *Dyes Pigm.*, **2011**, *91*, 33-43.
139. S. Hwang, J. H. Lee, C. Park, H. Lee, C. Kim, C. Park, M.-H. Lee, W. Lee, J. Park, K. Kim, N.-G. Park and C. Kim, A highly efficient organic sensitizer for dye-sensitized solar cells. *Chem. Comm.,* **2007**, 4887-4889.
140. S.-B. Ko, A.-N. Cho, M.-J. Kim, C.-R. Lee and N.-G. Park, Alkyloxy substituted organic dyes for high voltage dye-sensitized solar cell: Effect of alkyloxy chain length on open-circuit voltage. *Dyes Pigm.,* **2012**, *94*, 88-98.
141. R. Y.-Y. Lin, Y.-S. Yen, Y.-T. Cheng, C.-P. Lee, Y.-C. Hsu, H.-H. Chou, C.-Y. Hsu, Y.-C. Chen, J. T. Lin, K.-C. Ho and C. Tsai, Dihydrophenanthrene-based metal-free dyes for highly efficient cosensitized solar cells. *Org. Lett.*, **2012**, *14*, 3612-3615.
142. A. W. Freeman, M. Urvoy and M. E. Criswell, Triphenylphosphine-mediated reductive cyclization of 2-nitrobiphenyls: A practical and convenient synthesis of carbazoles. *J. Org. Chem.,* **2005**, *70*, 5014-5019.

143. H.-C. Chu, D. Sahu, Y.-C. Hsu, H. Padhy, D. Patra, J.-T. Lin, D. Bhattacharya, K.-L. Lu, K.-H. Wei and H.-C. Lin, Structural planarity and conjugation effects of novel symmetrical acceptor-donor-acceptor organic sensitizers on dye-sensitized solar cells. *Dyes Pigm.,* **2012**, *93*, 1488-1497.

144. Y. Ooyama, S. Inoue, T. Nagano, K. Kushimoto, J. Ohshita, I. Imae, K. Komaguchi and Y. Harima, Dye-sensitized solar cells based on donor-acceptor π-conjugated fluorescent dyes with a pyridine ring as an electron-withdrawing anchoring group. *Angew. Chem., Int. Ed.,* **2011**, 50, 7429-7433.

145. Y. Ooyama, T. Nagano, S. Inoue, I. Imae, K. Komaguchi, J. Ohshita and Y. Harima, Dye-Sensitized solar cells based on donor-π-acceptor fluorescent dyes with a pyridine ring as an electron-withdrawing-injecting anchoring group. *Chem. - Eur. J.,* **2011**, *17*, 14837-14843.

146. Y. Ooyama, Y. Oda, T. Mizumo, Y. Harima and J. Ohshita, Synthesis of specific solvatochromic D-π-A dyes with pyridinium ring as electron-withdrawing group for dye-sensitized solar cells. *Eur. J. Org. Chem.,* **2013**, 4533-4538.

147. Y. Ooyama, Y. Hagiwara, T. Mizumo, Y. Harima and J. Ohshita, Photovoltaic performance of dye-sensitized solar cells based on D-π-A type BODIPY dye with two pyridyl groups. *New J. Chem.*, **2013**, *37*, 2479-2485.

148. Y. Ooyama, Y. Hagiwara, T. Mizumo, Y. Harima and J. Ohshita, Synthesis of diphenylamino-carbazole substituted BODIPY dyes and their photovoltaic performance in dye-sensitized solar cells. *RSC Adv.*, **2013**, *3*, 18099-18106.

149. Y. Ooyama, K. Uenaka, Y. Harima and J. Ohshita, Development of D-π-A dyes with a pyrazine ring as an electron-withdrawing anchoring group for dye-sensitized solar cells, *RSC Adv.*, **2014**, *4*, 30225-30228.

150. Y. Ooyama, T. Yamada, T. Fujita, Y. Harima and J. Ohshita, Development of D-π-Cat fluorescent dyes with a catechol group for dye-sensitized solar cells based on dye-to-TiO_2 charge transfer *J. Mater. Chem. A,* **2014**, *2*, 8500-8511.

151. K. R. J. Thomas, J. T. Lin, Y.-T. Tao and C.-W. Ko, Light-Emitting carbazole derivatives: Potential electroluminescent materials. *J. Am. Chem. Soc.,* **2001**, *123*, 9404-9411.

152. Y.-S. Yen, Y.-C. Hsu, J. T. Lin, C.-W. Chang, C.-P. Hsu and D.-J. Yin, Pyrrole-based organic dyes for dye-sensitized solar cells. *J. Phys. Chem. C,* **2008**, *112*, 12557-12567.

153. C. Chen, J.-Y. Liao, Z. Chi, B. Xu, X. Zhang, D.-B. Kuang, Y. Zhang, S. Liu and J. Xu, Metal-free organic dyes derived from triphenylethylene for dye-sensitized solar cells: Tuning of the performance by phenothiazine and carbazole. *J. Mater. Chem.*, **2012**, *22*, 8994-9005.

154. Z. Yang, Z. Chi, T. Yu, X. Zhang, M. Chen, B. Xu, S. Liu, Y. Zhanga and J. Xu, Triphenylethylene carbazole derivatives as a new class of AIE materials with strong blue light emission and high glass transition temperature. *J. Mater. Chem.*, **2009**, *19*, 5541-5546.

155. P. Shen, Y. Tang, S. Jiang, H. Chen, X. Zheng, X. Wang, B. Zhao and S. Tan, Efficient triphenylamine-based dyes featuring dual-role carbazole, fluorene and spirobifluorene moieties. *Org. Electron.*, **2011**, *12*, 125-135.

156. J. He, J. Hua, G. Hu, X. J. Yin, H. Gong and C. Li, Organic dyes incorporating a thiophene or furan moiety for efficient dye-sensitized solar cells. *Dyes Pigm.*, **2014**, *104*, 75-82.

157. M.-D. Zhang, H.-X. Xie, X.-H. Ju, L. Qin, Q.-X. Yang, H.-G. Zheng and X.-F. Zhou, D-D-π-A organic dyes containing 4,4′-di(2-thienyl)-triphenylamine moiety for efficient dye-sensitized solar cells. *Phys. Chem. Chem. Phys.*, **2013**, *15*, 634-641.

158. Y. Ooyama, N. Yamaguchi, I. Imae, K. Komaguchi, J. Ohshita and Y. Harima, Dye-sensitized solar cells based on D-[π]-A fluorescent dyes with two pyridyl groups as an electron-withdrawing-injecting anchoring group. *Chem.Comm.*, **2013**, *49*, 2548-2550.

159. T.-Y. Wu, M.-H. Tsao, S.-G. Su, H. P. Wang, Y.-C. Lin, F.-L. Chen, C.-W. Chang and I.-W. Sun, Synthesis, characterization and photovoltaic properties of di-anchoring organic dyes. *J. Braz. Chem. Soc.*, **2011**, *22*, 780-789.

160. R. Grisorio, L. De Marco, G. Allegretta, R. Giannuzzi, G. P. Suranna, M. Manca, P. Mastrorilli and G. Gigli, Anchoring stability and photovoltaic properties of new D(-π-A)$_2$ dyes for dye-sensitized solar cell applications. *Dyes Pigm.*, **2013**, *98*, 221-231.

161. S. A. Kim, H. J. Jo, M. R. Jung, Y. C. Choi, D. K. Lee, M. Lee and J. H. Kim, Synthesis and photovoltaic performance of long wavelength absorbing organic dyes for dye-sensitized solar cells. *Mol. Cryst. Liq. Cryst.*, **2011**, *551*, 283-294.

162. K. S. V. Gupta, T. Suresh, S. P. Singh, A. Islam, L. Han and M. Chandrasekharam, Carbazole based A-π-D-π-A dyes with double electron acceptor for dye-sensitized solar cell. *Org. Electron.*, **2014**, *15*, 266-275.

163. S. Ramkumar and S. Anandan, Synthesis of bianchored metal free organic dyes for dye sensitized solar cells. *Dyes Pigm.*, **2013**, *97*, 397-404.

164. S. Ramkumar, S. Manoharan, S. Anandan, Synthesis of D-(π-A)$_2$ organic chromophores for dye-sensitized solar cells, *Dyes Pigm.*, **2012**, *94*, 503-511.

165. C.-H. Yang, S.-H. Liao, Y.-K. Sun, Y.-Y. Chuang, T.-L. Wang, Y.-T. Shieh and W.-C. Lin, Optimization of multiple electron donor and acceptor in carbazole-triphenylamine-based molecules for application of dye-sensitized solar cells. *J. Phys. Chem. C*, **2010**, *114*, 21786-21794.

166. C.-H. Yang, H.-L. Chen, Y.-Y. Chuang, C.-G. Wu, C.-P. Chen, S.-H. Liao and T.-L. Wang, Characteristics of triphenylamine-based dyes with multiple acceptors in application of dye-sensitized solar cells. *J. Power Sources*, **2009**, *188*, 627-634.

167. B. H. Kim and H. S. Freeman, Effects of bis-carbazole based D-[π]-A sensitizers on solar energy capture in DSSCs. *Photochem. Photobiol. Sci.* **2013**, *12*, 421-431.

168. B. H. Kim and H. S. Freeman, Structure-photovoltaic performance relationships for DSSC sensitizers having heterocyclic and benzene spacers. *J. Mater. Chem.*, **2012**, *22*, 20403-20409.

169. Q. Li, L. Lu, C. Zhong, J. Huang, Q. Huang, J. Shi, X. Jin, T. Peng, J. Qin and Z. Li, New pyrrole-based organic dyes for dye-sensitized solar cells: Convenient syntheses and high efficiency. *Chem. - Eur. J.*, **2009**, *15*, 9664-9668.

170. Q. Li, L. Lu, C. Zhong, J. Shi, Q. Huang, X. Jin, T. Peng, J. Qin and Z. Li, New indole-based metal-free organic dyes for dye-sensitized solar cells. *J. Phys. Chem. B*, **2009**, *113*, 14588-14595.

171. J. Jia, K. Cao, P. Xue, Y. Zhang, H. Zhou and R. Lu, Y-shaped dyes based on triphenylamine for efficient dye-sensitized solar cells. *Tetrahedron*, **2012**, *68*, 3626-3632.

172. B. Liu, Q. Liu, D. You, X. Li, Y. Naruta and W. Zhu, Molecular engineering of indoline based organic sensitizers for highly efficient dye-sensitized solar cells *J. Mater. Chem.*, **2012**, *22*, 13348-13356.

173. B. Liu, B. Wang, R. Wang, L. Gao, S. Huo, Q. Liu, X. Li and W. Zhu, Influence of conjugated π-linker in D-D-π-A indoline dyes: towards long-term stable and efficient dye-sensitized solar cells with high photovoltage. *J. Mater. Chem. A*, **2014**, *2*, 804-812.

174. Y. Hua, S. Chang, H. Wang, D. Huang, J. Zhao, T. Chen, W.-Y. Wong, W.-K. Wong and X. Zhu, New phenothiazine-based dyes for efficient dye-sensitized solar cells: Positioning effect of a donor group on the cell performance. *J. Power Sources*, **2013**, *243*, 253-259.
175. S. Wang, H. Wang, J. Guo, H. Tang and J. Zhao, Influence of the terminal electron donor in D-D-π-A phenothiazine dyes for dye-sensitized solar cells, *Dyes Pigm.*, **2014**, *109*, 96-104.
176. A. Baheti, K. R. J. Thomas, L.-C. Lin and K.-M. Lee, Monoanchoring (D-D-π-A) and Dianchoring (D-D-$(\pi\text{-A})_2$) Organic dyes featuring triarylamine donors composed of fluorene and carbazole. *Asian J. Org. Chem.*, **2014**, *3*, 886-898.
177. Y. Tan, M. Liang, Z. Lu, Y. Zheng, X. Tong, Z. Sun and S. Xue, Novel triphenylamine donors with carbazole moieties for organic sensitizers toward cobalt(II/III) redox mediators, *Org. Lett.*, **2014**, *16*, 3978-3981.
178. R. Tarsang, V. Promarak, T. Sudyoadsuk, S. Namuangrukc and S. Jungsuttiwong, Tuning the electron donating ability in the triphenylamine-based D-π-A architecture for highly efficient dye-sensitized solar cells. *J. Photochem. Photobiol., A*, **2014**, *273*, 8-16.
179. S. Namuangruk, J. Meeprasert, S. Jungsuttiwong, V. Promarak and N. Kungwan, Organic sensitizers with modified di(thiophen-2-yl)phenylamine-donor units for dye-sensitized solar cells: a computational study. *Theor. Chem. Acc.*, **2014**, *133*, 1534.
180. D. Cao, J. Peng, Y. Hong, X. Fang, L. Wang and H. Meier, Enhanced performance of the dye-sensitized solar cells with phenothiazine-based dyes containing double D-A branches. *Org. Lett.*, **2011**, *13*, 1610-1613.
181. S. Namuangruk, R. Fukuda, M. Ehara, J. Meeprasert, T. Khanasa, S. Morada, T. Kaewin, S. Jungsuttiwong, T. Sudyoadsuk and V. Promarak, D-D-π-A-Type organic dyes for dye-sensitized solar cells with a potential for direct electron injection and a high extinction coefficient: Synthesis, characterization, and theoretical investigation. *J. Phys. Chem. C*, **2012**, *116*, 25653-25663.
182. Z. Wan, C. Jia, Y. Duan, L. Zhou, J. Zhang, Y. Lin and Y. Shi, Influence of the antennas in starburst triphenylamine-based organic dye sensitized solar cells: phenothiazineversuscarbazole. *RSC Advances*, **2012**, *2*, 4507-4514.
183. L.-L. Tan, H.-Y. Chen, L.-F. Hao, Y. Shen, L.-M. Xiao, J.-M. Liu, D.-B. Kuang and C.-Y. Su, Starburst triarylamine based dyes bearing a 3,4-ethylenedioxythiophene linker for efficient dye-sensitized solar cells. *Phys. Chem. Chem. Phys.*, **2013**, *15*, 11909-11917.

184. T. Khanasa, N. Jantasing, S. Morada, N. Leesakul, R. Tarsang, S. Namuangruk, T. Kaewin, S. Jungsuttiwong, T. Sudyoadsuk and V. Promarak, Synthesis and characterization of D-D-π-A-type organic dyes bearing bis(3,6-di-*tert*-butylcarbazol-9-ylphenyl)aniline as donor moiety for dye-sensitized solar cells. *Eur. J. Org. Chem.*, **2013**, 2608-2620.

185. Q. Li, J. Shi, H. Li, S. Li, C. Zhong, F. Guo, M. Peng, J. Hua, J. Qin and Z. Li, Novel pyrrole-based dyes for dye-sensitized solar cells: From rod-shape to "*H*" type. *J. Mater. Chem.*, **2012**, *22*, 6689-6696.

186. S. Pramjit, U. Eiamprasert, P. Surawatanawong, P. Lertturongchai, S. Kiatisevi, Carbazole-bridged double D-A dye for efficient dye-sensitized solar cell. *J. Photochem. Photobiol., A*, **2015**, *296*, 1-10.

187. K. D. Seo, B. S. You, I. T. Choi, M. J. Ju, M. You, H. S. Kang and H. K. Kim, Dye-sensitized solar cells based on organic dual-channel anchorable dyes with well-defined core bridge structures. *ChemSusChem*, **2013**, *6*, 2069-2073.

188. N. Kungwan, P. Khongpracha, S. Namuangruk, J. Meeprasert, C. Chitpakdee, S. Jungsuttiwong and V. Promarak, Theoretical study of linker-type effect in carbazole-carbazolebased dyes on performances of dye-sensitized solar cells, *Theor. Chem. Acc.*, **2014**, 133, 1523.

189. A. C. Onicha, K. Panthi, T. H. Kinstle and F. N. Castellano, Carbazole donor and carbazole or bithiophene bridged sensitizers for dye-sensitized solar cells. *J. Photochem. Photobiol. A*, **2011**, *223*, 57-64.

190. H. Lai, J. Hong, P. Liu, C. Yuan, Y. Li and Q. Fang, Multi-carbazole derivatives: new dyes for highly efficient dye-sensitized solar cells. *RSC Adv.*, **2012**, *2*, 2427-2432.

191. S. Jungsuttiwong, R. Tarsang, T. Sudyoadsuk, V. Promarak, P. Khongpracha and S. Namuangruk, Theoretical study on novel double donor-based dyes used in high efficient dye-sensitized solar cells: The application of TDDFT study to the electron injection process. *Org. Electron.*, **2013**, *14*, 711-722.

192. T. Sudyoadsuk, S. Pansay, S. Morada, R. Rattanawan, S. Namuangruk, T. Kaewin, S. Jungsuttiwong and V. Promarak, Synthesis and characterization of D-D-π-A-type organic dyes bearing carbazole-carbazole as a donor moiety (D-D) for efficient dye-sensitized solar cells. *Eur. J. Org. Chem.*, **2013**, 5051-5063.

CHAPTER 2

Carbazole-Based Organic Dyes for Dye-Sensitized Solar Cells: Aim and Scope

Organic electronics is the immensely active research field with broad applications such as organic light emitting diodes (OLEDs), [1, 2] thin film transistors (TFT) [3, 4] and dye sensitized solar cells (DSSCs) [5, 6]. Among them, dye-sensitized solar cells are considered as better technology to solve the energy crisis of the world. Since 1991, Grätzel and co-workers [7] developed the DSSC using the organic and organometallic dyes and nanocrystalline titanium dioxide semiconductor have attracted wide attention owing to their cheap production cost, environmental compatibility, structural flexibility and versatile constituents. Dyes used as sensitizers play a key role and generally decide the efficiency of the DSSC. Ruthenium-based organometallic dyes, [8, 9] triarylamine-containing metal free organic dyes, [10] quantum dots [11, 12] and perovskites [13] have been demonstrated as successful sensitizers and the DSSC efficiency have been scaled up to 15%. Despite this progress, the large scale application of the Ru-, quantum dot and perovskite-based devices is hampered due to the associated heavy metal toxicity, efficiency *vs* cost tradeoff, narrow absorption window to the solar spectrum, and compatibility issues with the hole transporter. On the better side the organic dyes offered flexible structural design, high optical density in the visible region and eco-friendly synthetic methods and above all cost effectiveness [4]. Triarylamine-based dyes display relatively red-shifted absorption with high molar extinction coefficient owing to the strong donor strength [10]. Also, the trigonal structural arrangement of the triarylamine segment provided inhibition for the aggregation of the dyes at the surface of TiO_2 [10]. In order to improve the efficiency of the DSSC, we need to explore/study new heterocyclic compounds to unravel structure-property relationship.

Carbazole is a fused hetero aromatic system and it is an attractive building block in electronic applications such as OLEDs and DSSCs due to their unique charge transporting properties, pronounced thermal stability and multiple functionalization possibilities at different positions [14-18]. From thorough review of carbazole-based dyes presented in Chapter 1, it is evident that either carbazole has been used as a peripheral donor or as a π-linker [19-22]. However, the efficiency of the carbazole-based dyes is low due to poor absorption which needs to be improved for commercial exploitations. So far the carbazole has been demonstrated as linker via C3 and C6 positions with moderate efficiency due to weak electronic communication between donor and acceptor through carbazole linkage [21]. Few reports are available on 2,7-disubstituted carbazole linker by using pyridine as an acceptor with very mediocre efficiencies [17, 18]. The dyes

generally suffered due to forming aggregates on surface of TiO_2 and can be minimized by suitable molecular engineering by incorporating bulky donors or alkyl/alkoxy substituted donor [4]. Due to the presence of electron rich amine functionality, carbazole can easily donate electron; however, the cation radical formed after the removal of electron is quite unstable owing to the large structural reorganization associated with the oxidation [23]. Substitution of electron releasing groups on the carbazole nucleus at 3 and 6 positions can enhance the donor strength of the carbazole [20, 24]. Interestingly, 2,7-disubstitution provides better conjugation and offers better delocalization and communication between the donor and acceptor on comparing with 3,6 di-substitution.

In this thesis, we present the design, synthesis and characterization of new carbazole-based organic dyes suitable for DSSC. We also present the theoretical interpretation of experimental photophysical properties and energy levels of the dye sensitizers. Carbazole-based materials have wide absorption, high molar extinction coefficients, good charge transport properties and suitable HOMO and LUMO energy levels which make them pro-material for application in DSSC as sensitizers.

The structure of the bridging unit is very important due to its dual role of light absorbing chromophore and a channel for charge transporting charges [25]. So we have chosen the 2,7-disubstituted carbazole as suitable linker and it satisfies both the fundamental purposes [26, 27]. The π-conjugation changed with oligothiophene and different aromatic linkers to tune the energy levels and absorption of the dyes [28, 29]. The difluorenylamine moiety has been proved as better unit to prevent aggregation due to its bulky non planar structure and possess greater stability when exposed to light [30, 31]. Insulating groups on the donor and linker is essential to increase the efficiency and position of alkyl groups also played a role in governing the efficiency. The alkoxy units are well known for increasing the donor strength, results in red shifted the absorption spectra and provides hydrophobic environment which help to minimize the recombination of the electrons from conduction band of TiO_2 to the electrolyte [32, 33]. *N*-(2',4'-dimethoxybiphenyl-4-yl)-2',4'-dimethoxy-*N*-phenylbiphenyl-4-amine proved as better unit for spectral properties and improvement of open circuit voltage (V_{OC}) resulting a high power conversion efficiency [34]. Carbazole is not only good for linker, but also act as donor and substitution of electron releasing groups on periphery further increases the donor strength and

help to optimize the donor-acceptor interactions [21, 25]. Keeping all the points in mind we have aimed to design and synthesize the carbazole-based organic dyes with various modulations on donor and linker units (Figure 2.1).

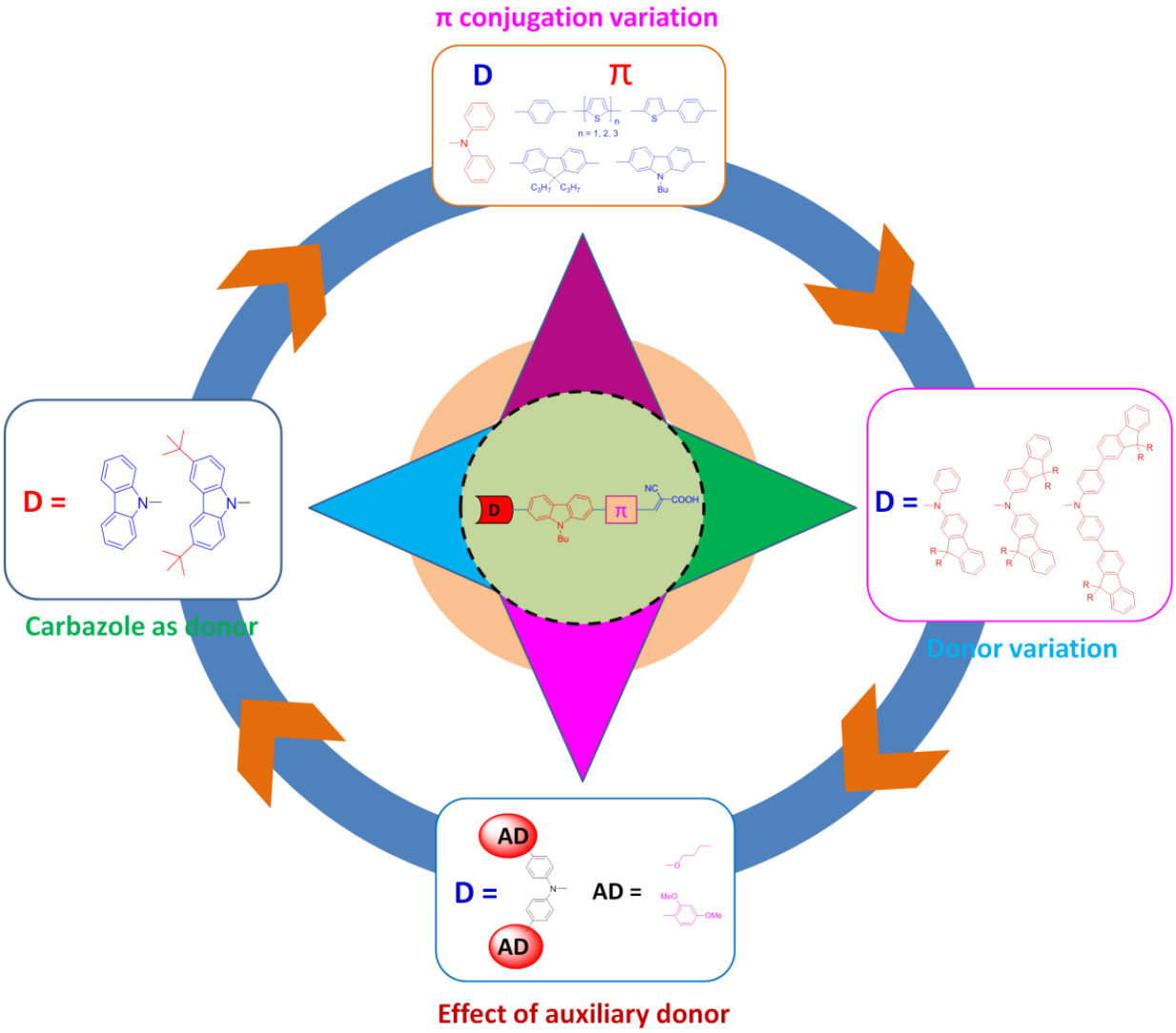

Figure 2.1 Structural engineering of the carbazole based organic dyes for DSSC.

In this thesis, we would like to explore the role 2,7-disubstituted carbazole as a linker for the design of organic dyes featuring simple D-π-A molecular configuration. Donor units will be varied from diphenylamine to fluorenylamines and carbazole. Also we attempt to optimize the donor strength by decorating the diphenylamine segment with electron-rich chromophores such as alkoxy and fluorene units. Besides this, modification of conjugation pathway with additional aromatics such as thiophene and fluorene is also attempted to optimize the optical and photovoltaic performance of the dyes.

References

[1] T. Leijtens, I.-K. Ding, T. Giovenzana, J. T. Bloking, M. D. McGehee and A. Sellinger, Hole transport materials with low glass transition temperatures and high solubility for application in solid-state dye-sensitized solar cells. *ACS Nano,* **2012**, *6*, 1455-1462.

[2] J. Li, D. Liu, Y. Li, C.-S. Lee, H.-L. Kwong and S. A Lee, High Tg Carbazole-based hole-transporting material for organic light-emitting devices. *Chem. Mater.*, **2005**, *17*, 1208-1212.

[3] A. Hagfeldt, G. Boschloo, L. Sun, L. Kloo and H. Pettersson, Dye-sensitized solar cells. *Chem. Rev.*, **2010**, *110*, 6595-6663.

[4] A. Mishra, M. K. R. Fischer and P. Bäuerle, Metal-free organic dyes for dye-sensitized solar cells: From structure: Property relationships to design rules. *Angew. Chem., Int. Ed.*, **2009**, *48*, 2474-2499.

[5] A. R. Murphy and J. M. J. Fréchet, Organic semiconducting oligomers for use in thin film transistors. *Chem. Rev.*, **2007**, *107*, 1066-1096.

[6] J. Zaumseil and H. Sirringhaus, Electron and ambipolar transport in organic field-effect transistors. *Chem. Rev.*, **2007**, *107*, 1296-1323.

[7] B. O'Regan and M. Grätzel, A low-cost, high-efficiency solar cell based on dye-sensitized colloidal TiO_2 films. *Nature*, **1991**, *353*, 737-740.

[8] M. Grätzel, Recent advances in sensitized mesoscopic solar cells. *Acc. Chem. Res.*, **2009**, *42*, 1788-1798.

[9] M. K. Nazeeruddin, A. Kay, I. Rodicio, R. Humphry-Baker, E. Müller, P. Liska, N. Vlachopoulos and M. Grätzel, Conversion of light to electricity by cis-X2bis(2,2′-bipyridyl-4,4′-dicarboxylate)-ruthenium(II) charge-transfer sensitizers (X = Cl^-, Br^-, I^-, CN^-, and SCN^-) on nanocrystalline titanium dioxide electrodes. *J. Am. Chem. Soc.*, **1993**, *115*, 6382-6390.

[10] M. Liang and J. Chen, Arylamine organic dyes for dye-sensitized solar cells, *Chem. Soc. Rev.*, **2013**, *42*, 3453-3488.

[11] P. V. Kamat, Quantum dot solar cells. *The Next Big Thing* in photovoltaics. *J. Phys. Chem. Lett.*, **2013**, *4*, 908-918.

[12] L. Etgar, T. Moehl, S. Gabriel, S. G. Hickey, A. Eychmüller and M. Grätzel, Light energy conversion by mesoscopic PbS quantum dots/TiO_2 heterojunction solar cells. *ACS Nano,* **2012**, *6*, 3092-3099.

[13] N.-G. Park, Organometal perovskite light absorbers toward a 20% efficiency low-cost solid-state mesoscopic solar cell. *J. Phys. Chem. Lett.*, **2013**, *4*, 2423-2429.

[14] P. Kotchapradist, N. Prachumrak, R. Tarsang, S. Jungsuttiwong, T. Keawin, T. Sudyoadsuk and V. Promarak, Pyrene-functionalized carbazole derivatives as non-doped blue emitters for highly efficient blue organic light-emitting diodes. *J. Mater. Chem. C*, **2013**, *1*, 4916-4924.

[15] L.-S. Cui, S.-C. Dong, Y. Liu, Q. Li, Z.-Q. Jiang and L.-Z. Liao, A Simple systematic design of phenylcarbazole derivatives for host materials to high-efficiency phosphorescent organic light-emitting diodes. *J. Mater. Chem. C*, **2013**, *1*, 3967-3975.

[16] K. R. J. Thomas, J. T. Lin, Y.-T. Tao and C.-W. Ko, Light emitting carbazole derivatives: potential electroluminescent materials. *J. Am. Chem. Soc.*, **2001**, *123*, 9404-9411.

[17] Y. Ooyama, S. Inoue, T. Nagano, K. Kushimoto, J. Ohshita, I. Imae, K. Komaguchi and Y. Harima, Dye-sensitized solar cells based on donor-acceptor π-conjugated fluorescent dyes with a pyridine ring as an electron-withdrawing anchoring group. *Angew. Chem., Int. Ed.*, **2011**, *50*, 7429-7433.

[18] Y. Ooyama, T. Nagano, S. Inoue, I. Imae, K. Komaguchi, J. Ohshita and Y. Harima, Dye-sensitized solar cells based on donor-π-acceptor fluorescent dyes with a pyridine ring as an electron withdrawing-injecting anchoring group. *Chem.–Eur. J.*, **2011**, *17*, 14837-14843.

[19] C. Teng, X. Yang, C. Yuan, C. Li, R. Chen, H. Tian, S. Li, A. Hagfeldt and L. Sun, Two novel carbazole dyes for dye-sensitized solar cells with open-circuit voltages up to 1 V based on Br^-/Br_3^- electrolytes. *Org. Lett.*, **2009**, *11*, 5542-5545.

[20] C. Teng, X. Yang, S. Li, M. Cheng, A. Hagfeldt, L.-Z. Wu and L. Sun, Tuning the HOMO energy levels of organic dyes for dye-sensitized solar cells based on Br^-/Br_3^- Electrolytes. *Chem. - Eur. J.*, **2010**, *16*, 13127-13138.

[21] Y.-S. Yen, Y.-C. Hsu, J. T. Lin, C.-W. Chang, C.-P. Hsu and D.-J. Yin, Pyrrole-based organic dyes for dye-sensitized solar cells. *J. Phys. Chem. C*, **2008**, *112*, 12557-12567.

[22] Y. Ooyama, S. Inoue, T. Nagano, K. Kushimoto, J. Ohshita, I. Imae, K. Komaguchi and Y. Harima, Dye-sensitized solar cells based on donor–acceptor π-conjugated fluorescent dyes

with a pyridine ring as an electron-withdrawing anchoring group. *Angew. Chem., Int. Ed.*, **2011**, *50*, 7429-7433.

[23] K. Brunner, A. van Dijken, H. Börner, J. J. A. M. Bastiaansen, N. M. M. Kiggen and B. M. W. Langeveld, Carbazole compounds as host materials for triplet emitters in organic light-emitting diodes: Tuning the HOMO level without influencing the triplet energy in small molecules. *J. Am. Chem. Soc.*, **2004**, *126*, 6035-6042.

[24] W. Lee, N. Cho, J. Kwon, J. Ko and J.-I. Hong, New organic dye based on a 3,6-disubstituted carbazole donor for efficient dye sensitized solar cells. *Chem.–Asian J.*, **2012**, *7*, 343-350.

[25] Y. J. Chang and T. J. Chow, Dye-sensitized solar cell utilizing organic dyads containing triarylene conjugates. *Tetrahedron*, **2009**, *65*, 4726-4734.

[26] A. Baheti, K. R. J. Thomas, C.-P. Lee and K.-C. Ho, Fine tuning the performance of DSSCs by variation of the π-spacers in organic dyes that contain a 2,7-diaminofluorene donor. *Chem. Asian J.*, **2012**, *7*, 2942-2954.

[27] H.-C. Chu, D. Sahu, Y.-C. Hsu, H. Padhy, D. Patra, J.-T. Lin, D. Bhattacharya, K.-L. Lu, K.-H. Wei and H.-C. Lin, Structural planarity and conjugation effects of novel symmetrical acceptor–donor–acceptor organic sensitizers on dye-sensitized solar cells. *Dyes Pigm.*, **2012**, *93*, 1488-1497.

[28] A. Mishra, N. Pootrakulchote, M. Wang, S.-J. Moon, S. M. Zakeeruddin, M. Grätzel and P. Bäuerle, A thiophene-based anchoring ligand and its heteroleptic Ru(II)-Complex for efficient thin-film dye-sensitized solar cells. *Adv. Funct. Mater.*, **2011**, *21*, 963-970.

[29] K. R. J. Thomas, Y.-C. Hsu, J. T. Lin, K.-M. Lee, K.-C. Ho, C.-H. Lai, Y.-M. Cheng and P.-T. Chou, 2,3-Disubstituted thiophene-based organic dyes for solar cells. *Chem. Mater.*, **2008**, *20*, 1830-1840.

[30] S. Kim, J. K. Lee, S. O. Kang, J. Ko, J.-H. Yum, S. Fantacci, F. D. Angelis, D. D. Censo, M. K. Nazeeruddin and M. Grätzel, Molecular engineering of organic sensitizers for solar cell applications. *J. Am. Chem. Soc.*, **2006**, *128*, 16701-16707.

[31] M. Xu, S. Wenger, H. Bala, D. Shi, R. Li, Y. Zhou, S. M. Zakeeruddin, M. Grätzel and P. Wang, Tuning the energy level of organic sensitizers for high-performance dye-sensitized solar cells. *J. Phys. Chem. C*, **2009**, *113*, 2966-2973.

[32] R. Li, J. Liu, N. Cai, M. Zhang and P. Wang, Synchronously reduced surface states, charge recombination, and light absorption length for high-performance organic dye-sensitized solar cells. *J. Phys. Chem. B*, **2010**, *114*, 4461-4464.

[33] W. Wu, J. Yang, J. Hua, J. Tang, L. Zhang, Y. Long and H. Tian, Efficient and stable dye-sensitized solar cells based on phenothiazine sensitizers with thiophene units. *J. Mater. Chem.*, **2010**, *20*, 1772-1779.

[34] D. P. Hagberg, X. Jiang, E. Gabrielsson, M. Linder, T. Marinado, T. Brinck, A. Hagfeldt and L. Sun, Symmetric and unsymmetric donor functionalization. Comparing structural and spectral benefits of chromophores for dye-sensitized solar cells. *J. Mater. Chem.*, **2009**, *19*, 7232-7238.

CHAPTER 3

Functional Tuning of Organic Dyes Containing 2,7-Carbazole and Other Electron-Rich Segments in the Conjugation Pathway

3.1 Introduction

Organic dyes suitable for application as sensitizers for inorganic semiconductors such as titanium dioxide (TiO_2) [1] and zinc oxide (ZnO) [2] in dye-sensitized solar cells (DSSCs) have received immense attention in recent years due to the possibility that these devices could serve as low cost consumer power generation equipment in the near future. Performance of DSSCs fabricated using the organic dyes are largely dependent on the electronic and structural characteristics of organic dyes [3-10]. The absorption properties and the frontier orbital energies affect the charge generation and collection efficiency in the devices. Broader and intense charge transfer absorption of the dyes is beneficial for the charge generation while the LUMO level higher than the conduction band energy of the semiconductor is essential to thermodynamically drive the charge injection [6]. It has been recently found that the recombination of injected electrons with the oxidized dye or the triiodide ions (I_3^-) in electrolyte severely diminishes the photocurrent density [11]. Several structural modifications such as introduction of alkyl chains, [12-15] bridged bi-anchoring architecture, [16-18] etc. have been identified to retard the recombination reactions and contribute to the hike in short-circuit current (J_{SC}) and open-circuit voltage (V_{OC}) of the devices. Despite the sincere efforts by the chemists in the design of new organic dyes, the DSSCs fabricated using the organic dyes are inferior to those derived from organometallic ruthenium complexes [10]. The reason for the poor performance of organic dyes, despite possessing high molar extinction coefficient for the charge transfer transition, is unclear [6]. In order to unravel this puzzle, more studies on the structure-property relationship on metal free organic dyes are necessary.

The performance of the cell mainly depends on the dye which is responsible for absorbing the light of solar spectrum. Ideal design of the dye should result panchromatic absorption with high molar extinction coefficients as well as better injection of the electron into conduction band of TiO_2 and regeneration of the dye. Organic sensitizers containing triarylamine, [9] fluorene, [13, 19, 20] coumarin dyes, [21, 22] phenothiazine, [23, 24] phenoxazine, [25, 26] cyclopentadithiophene, [27, 28] indoline, [29, 30] etc. chromophores have exhibited impressive photovoltaic performance. Typically organic dyes designed with a D-π-A molecular configuration where the nature of linker (π) bridging the donor (D) and acceptor (A) determines the charge separation and so photovoltaic performance. Triarylamines are commonly employed

as donors due to the trigonal geometry to prevent aggregation while cyanoacrylic acid is the proven acceptor/anchoring group. The efficiency can be improved by molecular engineering involving one of the following methods. (a) Amplification of the electron richness of the donor unit by the introduction of additional electron donating units [31-33]. (b) Incorporation of electron-rich or low band gap chromophores in the conjugation pathway [4, 34]. (c) Introduction of auxiliary acceptors in the vicinity of the acceptor end [35, 36]. All these methodologies gave successful results for the dye molecules which ensured a facile charge migration from the donor to the acceptor through the π-spacer. Out of these strategies, suitably introducing the electron rich linker close to donor may impact the efficiency of device. Development of suitable structural architecture for longer wavelength absorption is needed and introduction/increment of linker appears to be the acceptable method to fine tune the electronic properties of the dyes [37]. Dyes composed of aromatic linker assist the interactions between the donor and acceptor units. It was found that the introduction of fluorene and carbazole benefits in electro-optical properties [38]. However the elongated planar conjugation of linker suffers from aggregation which diminishes device efficiency. The peripheral or lateral alkyl groups and twisted geometry of the dye diminish the aggregation on TiO_2 surface [7]. The electron rich oligothiophene units achieve the longer wavelength absorption with strong ICT transition peak [39, 40]. The common problems offered by the organic dyes were back electron transfer and dark current. Bäuerle *et al.* reported that the back electron transfer is effectively blocked by introducing a twisted phenyl spacer. This results in the efficiency hike 6.5 times than the parent dye [4]. The suitable energy levels of the components such as dyes and electrolyte minimized the dark current. Introduction of electron-rich segments in the conjugation pathway raises the HOMO and LUMO energy and facilitate the regeneration of the dye and electron-injection from the photo-excited dye into the conduction band of TiO_2 [7].

Classic example of oligothiophenes as linker was demonstrated by Thomas and co-workers [39]. They have extended the conjugation in **L1** [41] by using oligothiophenes to obtain dyes **1P-PSS** and **TTT** with red-shifted absorption which led to high power conversion efficiencies. Chow and co-workers [37] studied the effect of triarylene-bridge (**1P-PPP**, **1P-PSP** and **1P-PSS**) composed of different aromatic units such as phenyl/thiophene groups and studied the effect of the thiophene position in triaryl conjugation pathway. The thiophene unit provides better delocalization and adjacent phenyl unit causes a twist with large dihedral angle. The overall

configuration helps to retard the charge recombination. A careful structural design is needed to balance the charge separation and charge recombination resulting in better conversion efficiency. Lin and co-workers [42] fused the twisted biphenyl unit of dye **1P-PPP** by ethane chain to obtain 9,10-dihydrophenanthrene based dye (**BP1**) which showed red shifted absorption with high molar extinction coefficient and led to higher power conversion efficiency. Later Thomas and co-workers [20] demonstrated the replacement of biphenyl unit with fluorene to generate the fluorene based dyes (**Fl1** and **Fl2**) red shifted absorption than 9,10-dihydrophenanthrene analogue due to more planar and rigid structure. Again Lin and co-workers [43] inserted pyrrole unit in TPA dyes, **Fl1** and **Fl2,** and formed **C37**, **C38** and **C39**, **C41** dyes. They found that pyrrole rings are useful for effective charge separation and red shifted absorption compared to thiophene analogues due to its large twisting angle and more electron richness respectively. From these it is evident that the incorporation of electron rich heteroaryl segments in the conjugation pathway is beneficial for light harvesting.

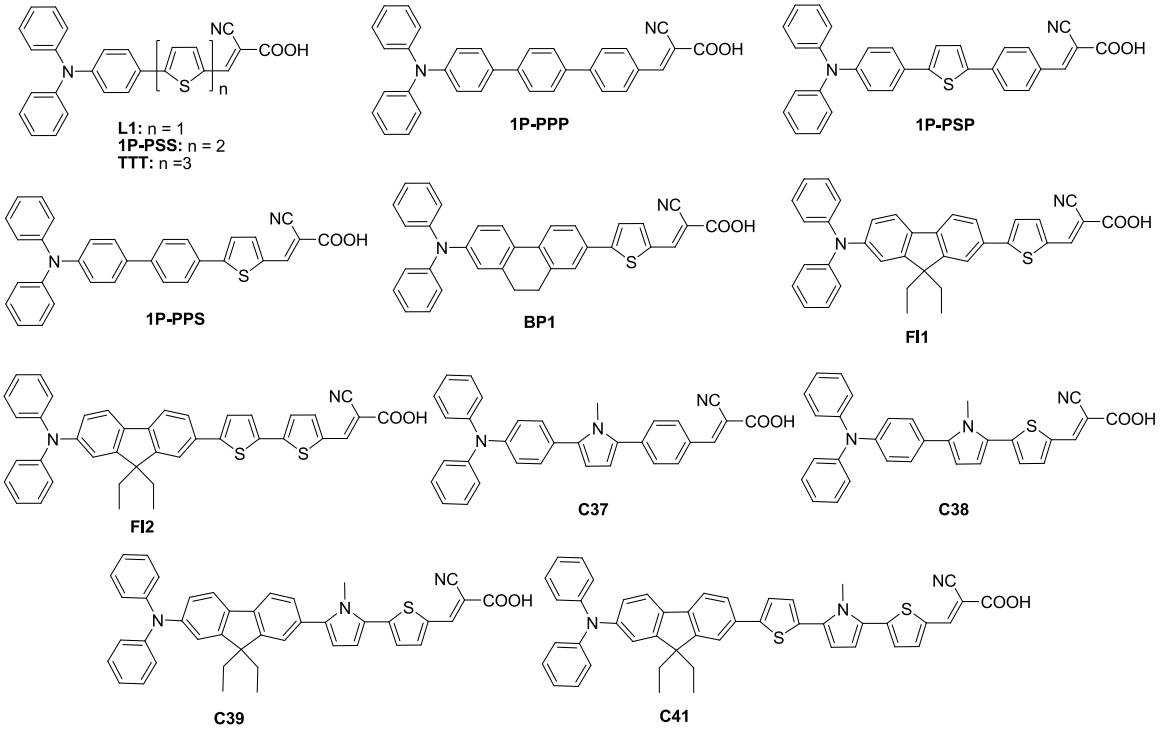

Chart 3.1 Structures of the triarylamine dyes with different conjugation pathway.

Table 3.1 Optical, electrochemical and photovoltaic performance data of the known dyes

Dye	$\lambda_{max,}$ nm (ε_{max}, M^{-1} cm^{-1})	E_{ox} , V (*vs* NHE)	E_{ox}^{*}, V (*vs* NHE)	J_{SC} (mA cm^{-2})	V_{OC} (mV)	*ff*	*η* (%)	*Ref*
L1	404 (25000)	1.21	–1.43	5.42	735	0.69	2.75	[41]
1P-PSS	473 (43500)	1.26	–0.94	16.00	630	0.61	6.15	[39]
TTT	480 (46150)	1.20	–0.97	15.20	610	0.58	5.41	[39]
1P-PPP	380 (30200)	1.62	–1.15	11.43	650	0.62	4.58	[37]
1P-PSP	427 (29000)	1.56	–0.97	15.36	690	0.50	5.25	[37]
1P-PPS	417(23,000)	1.63	–0.91	13.86	650	0.57	5.14	[37]
BP1	441 (40300)	1.28	na	13.61	610	0.64	5.33	[42]
Fl1	469 (34900)	1.18	–0.98	10.56	690	0.65	4.70	[20]
Fl2	487 (40500)	1.08	–1.00	7.52	618	0.65	3.01	[20]
C37	437 (35600)	1.05	–1.29	13.47	600	0.59	4.77	[43]
C38	472 (38400)	1.08	–0.93	14.20	570	0.60	4.79	[43]
C39	475 (52700)	1.11	–1.09	18.14	0.61	0.56	6.16	[43]
C41	462 (53800)	1.13	–1.02	13.54	600	0.64	5.25	[43]

na = not available

Carbazole-based organic materials have been widely employed as active ingredients in electronic devices such as organic light-emitting diodes (OLEDs) [44-46] and DSSCs [47-48] due to their unique charge transporting properties and pronounced thermal stability. Carbazole is an attractive building block as it offers many nuclear sites for functional group incorporation [49, 50]. For instance, carbazole derivatives with functional chromophores attached *via* C-2, C-3, C-6, C-7 and N-9 have been reported for application in organic light-emitting diodes and photovoltaic devices. However, the utility of 2,7-disubstituted carbazole derivatives is limited due to the non-availability of direct methods for chemical modifications at the C-2 and C-7 positions (Chart 3.2) [51]. Particularly, in the dyes serving as sensitizers in DSSCs, carbazole has been utilized as an electron rich π-linker via C3 and C6 difunctionlization [43, 52-56]. Due to the presence of electron rich amine functionality carbazole dye can easily donate electron, however, the cation radical formed after the removal of electron is quite unstable owing to the large structural reorganization associated with the oxidation centered on carbazole [57]. However, an oxidation occurring at a triarylamine may be stabilized by carbazole conjugation.

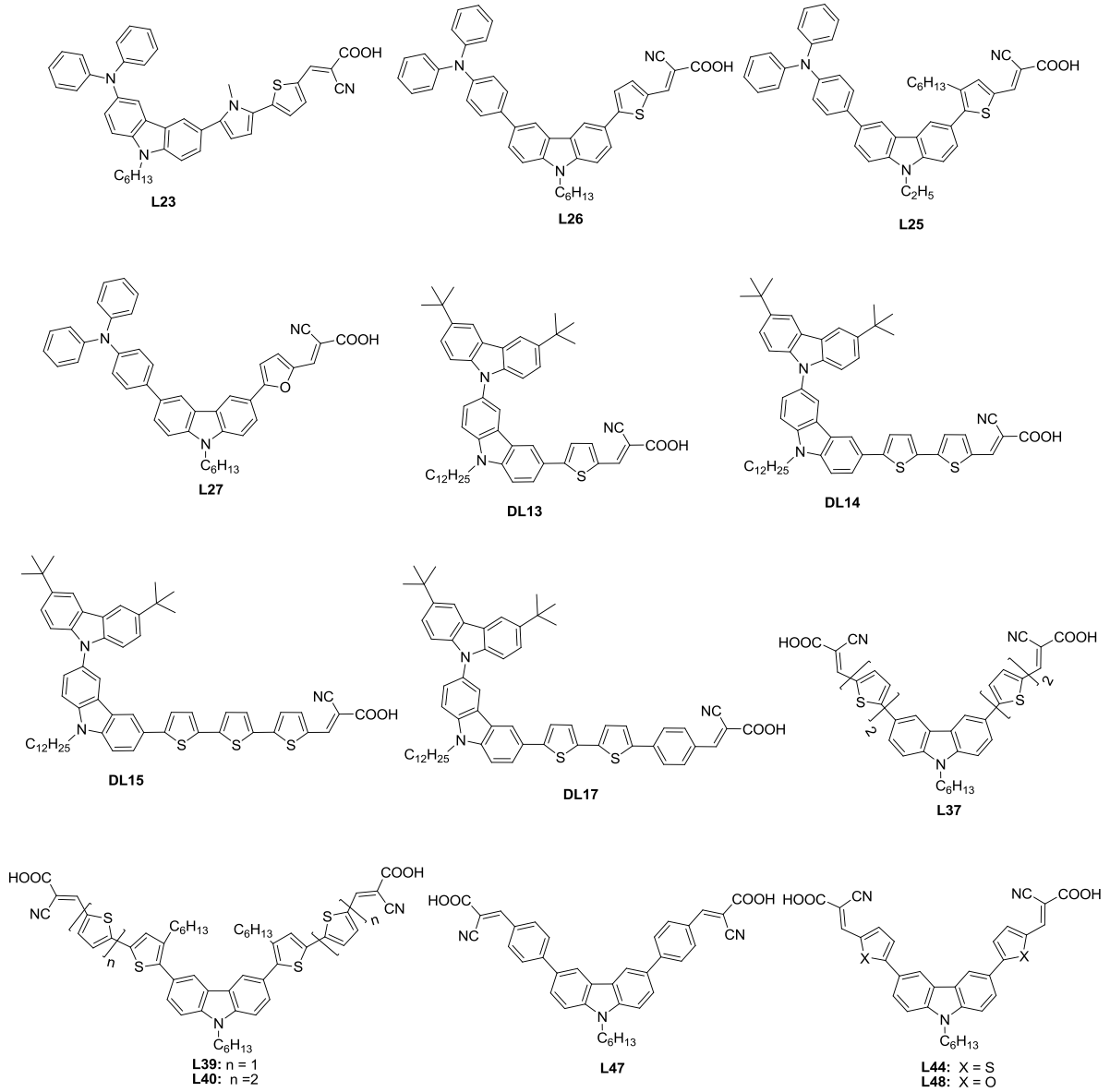

Chart 3.2 Structures of dyes with 3,6-disubstituted carbazole.

Keeping all this in mind, we have designed and synthesized a set of metal-free organic dyes (Chart 3.3) possessing 2,7-carbazolyl bridging unit, diphenylamine donor, and cyanoacrylic acid acceptor, additionally the incorporation of various aromatic π-linkers such as phenyl, oligothiophenes, thienylbenzene, thienylfluorene, thienylcarbazole. The phenyl spacer (**5** and **11b**) helps to retard back electron transfer, while electron rich terthiophene unit (**11c**) ensures red shifted absorption. The fluorene and carbazole units enhance the molar extinction coefficients in the absorption and alkyl chains attached at C9 and N9 positions respectively may impede the aggregation. The structure-property relationships of the dyes are thoroughly examined by

varying linkers. While our work was in progress, Ooyama and co-workers reported 2,7-carbazole bridged dyes with pyridine anchors as best with low efficiency [47]. The dyes reported in this chapter showed excellent light-harvesting properties when used as sensitizer in DSSCs which illustrate the benefits of the cyanoacrylic acid unit as an efficient acceptor and anchoring segment. We found that despite the presence of carbazole, additional electron-rich thiophene units were required to enhance the functional properties such as optical absorption and redox potentials in these dyes.

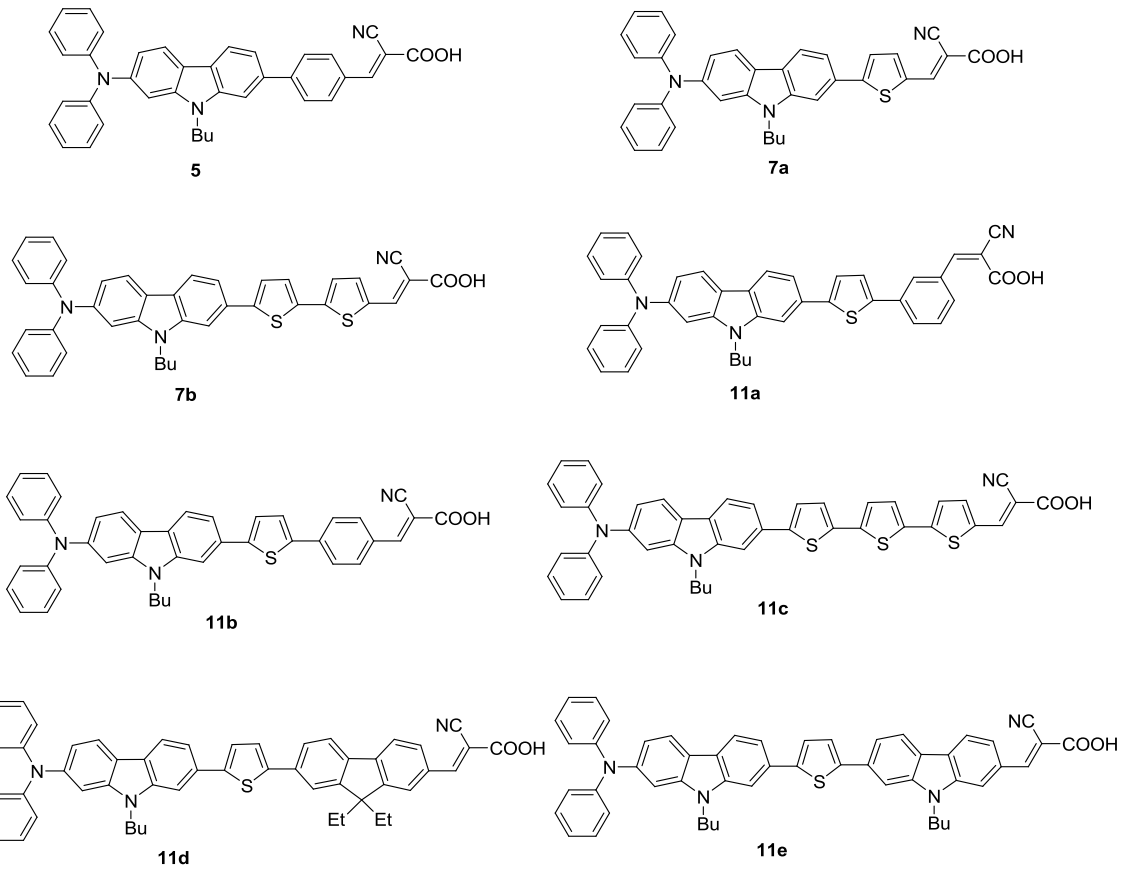

Chart 3.3 Structure of the 2,7-disubstituted carbazole dyes.

3.2 Results and Discussion

3.2.1 Synthesis and Characterization

The dyes (**5**, **7a** and **7b**) were synthesized by following a three-step protocol involving Hartwig–Buchwald C–N coupling reaction, [58] Stille reaction, [59] and Knoevenagel condensation [60] as illustrated in Scheme 3.1. In the first step, diphenylamine was reacted with a slight excess of

2,7-dibromo-9-butyl-9*H*-carbazole [61, 62] to obtain 7-bromo-9-butyl-*N*,*N*-diphenyl-9*H*-carbazol-2-amine (**3**) in good yield (78%). The Suzuki coupling [63] of 4-formylphenylboronic acid with carbazole bromo derivatives (**3**) in presence of $Pd(PPh_3)_4$ led to corresponding carboxaldehyde (**4**) in excellent yield. The bromo compound **3** was subjected to the Stille reaction [59] with the tin reagents of the protected aryl aldehydes and subsequent acid hydrolysis generated the required conjugated aldehydes **6a** and **6b**. The aldehyde derivatives (**4**, **6a** and **6b**) were then easily converted to the desired dyes (**5**, **7a** and **7b**) by condensing with cyanoacetic acid in the presence of ammonium acetate in acetic acid. The required aldehyde, 7-bromo-9-butyl-9*H*-carbazole-2-carbaldehyde (**8**) was prepared from **1** by lithiation with *n*-butyl lithium followed by quenching with DMF and subsequent acidic hydrolysis.

The synthetic scheme to prepare the target dyes (**11a-11e**) is also shown in Scheme 3.1. The synthesis began with Stille coupling [59] of 7-bromo-9-butyl-*N*,*N*-diphenyl-9*H*-carbazol-2-amine (**3**) with tributyl(thiophen-2-yl)stannane in the presence of $PdCl_2(PPh_3)_2$ to produce 9-butyl-*N*,*N*-diphenyl-7-(thiophen-2-yl)-9*H*-carbazol-2-amine (**9**) in good yield. Reaction of **9** with *n*-butyllithium followed by quenching with tri-*n*-butyl-tinchloride gave the 9-butyl-*N*,*N*-diphenyl-7-(5-(tributylstannyl)thiophen-2-yl)-9*H*-carbazol-2-amine in quantitative yield. The Stille coupling reaction [59] of 9-butyl-*N*,*N*-diphenyl-7-(5-(tributylstannyl)thiophen-2-yl)-9*H*-carbazol-2-amine with appropriate aryl caboxaldehydes leads to carbazole substituted aryl carboxaldehyde (**10a-10e**) in excellent yields. They were (**10a-10e**) subsequently converted to the target dyes (**11a-11e**) in good yields by Knoevenagel condensation [60] with cyanoacetic acid. The dyes are brown to black in color. They were thoroughly characterized by IR, NMR and HRMS studies. The spectral parameters are consistent with the proposed structures. All the dyes are reasonably soluble in organic solvents such as cyclohexane (CH), toluene (Tol), tetrahydrofuran (THF), dichloromethane (DCM), *N*,*N*-dimethylformamide (DMF) and acetonitrile (ACN).

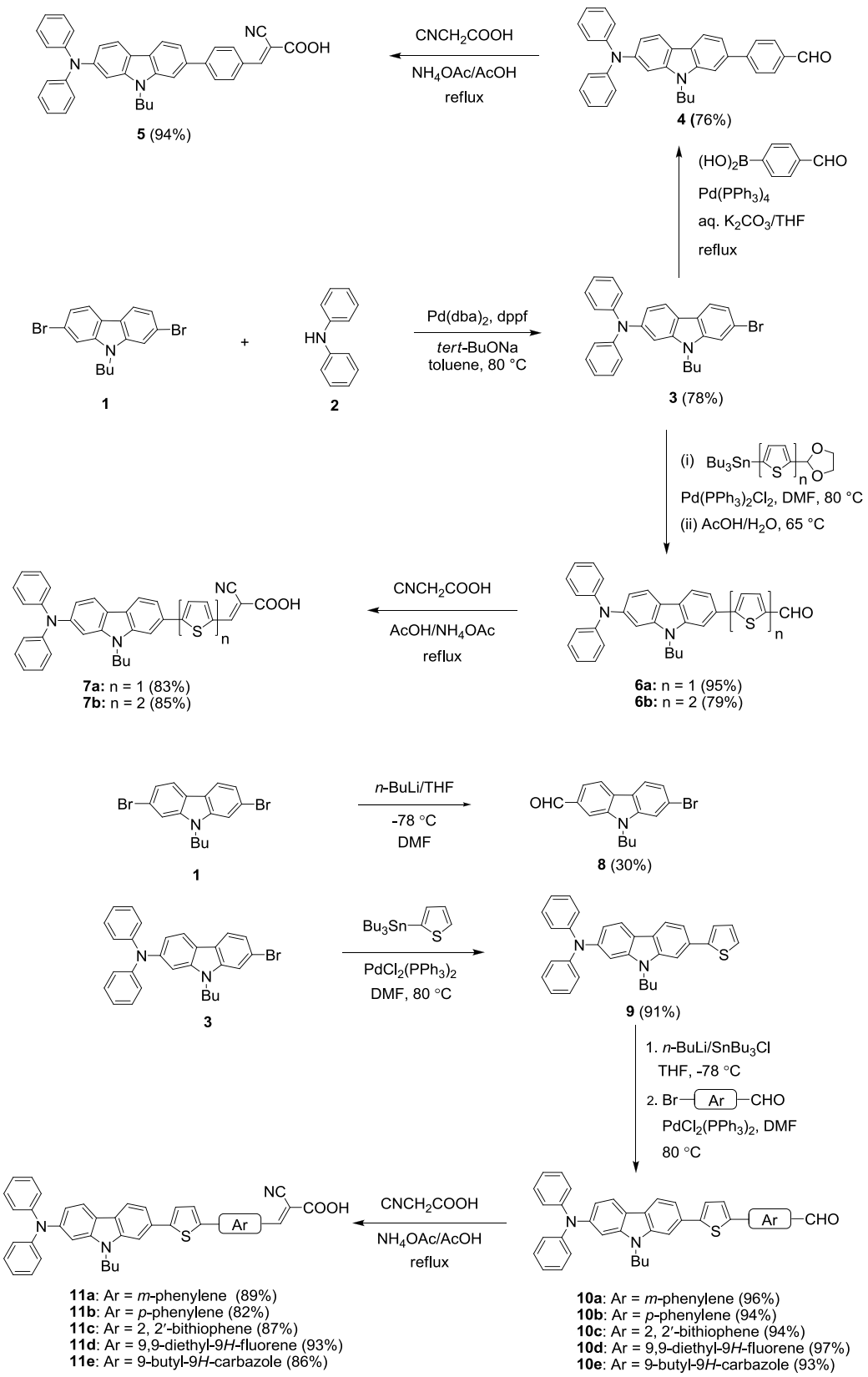

Scheme 3.1 Synthetic scheme for the preparation of 2,7-disubstituted carbazole dyes.

3.2.2 Photophysical Properties

The photophysical properties of the dyes were investigated by measuring the absorption and emission spectra of the dyes in different solvents such as CH, Tol, THF, DCM, DMF and ACN differing in dielectric constants to elucidate the solvatochromism behaviour of the dyes.

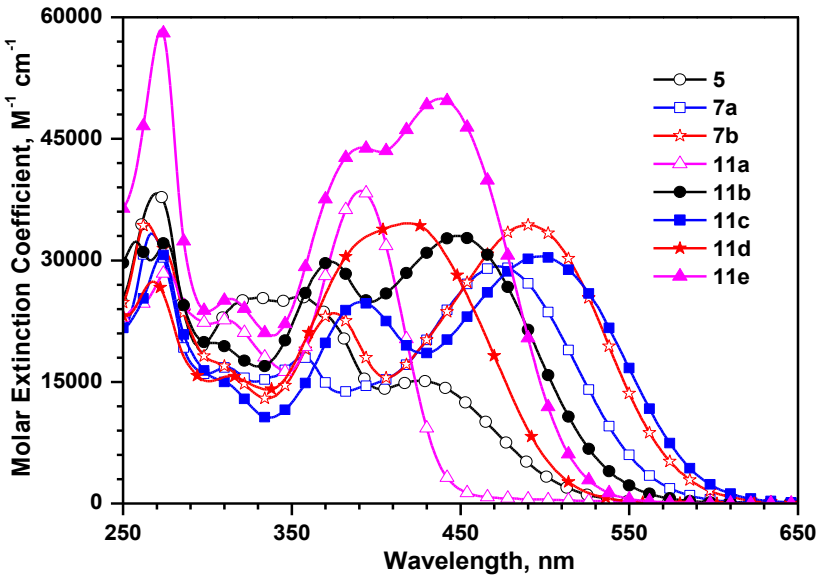

Figure 3.1 Absorption spectra of the dyes (**5, 7** and **11**) recorded in DCM.

The absorption spectra of the dyes recorded in DCM solution are displayed in Figure 3.1 and the pertinent data presented in Table 3.2. All the dyes displayed three or more distinguishable absorption peaks attributable to the carbazole and diphenylamine localized π-π* transitions, electronic excitation between the π-π* orbitals delocalized over the entire conjugation pathway and amine to cyanoacrylic acid charge transfer transition in that order. But, the the absence of charge transfer transition band for the dye **11a** is attributable to the *meta*-substitution of cyanoacrylic acid which delinks the donor-acceptor interaction [64, 65]. Absorption peaks that appeared at around 260 nm and 310 nm are insensitive to the nature of the π-spacer and are similar to those observed for carbazole and diphenylamine localized electronic transitions [66]. The absorption maxima of the charge transfer transition in the dyes red shifted on increasing the conjugation length and electron richness of the linker.

The CT absorption wavelength of the dyes follows the order **11a** (391 nm) < **11d** (420 nm) < **5** (427 nm) < **11e** (439 nm) < **11b** (448 nm) < **7a** (472 nm) < **7b** (489 nm) < **11c** (498 nm). The shorter wavelength absorption of **11a** is due to the *meta*-substitution of cyanoacrylic acid. The absorption maxima at 427 nm for the dye **5** is red shifted to 472 nm for the dye **7a** due to the replacement of phenyl unit with electron rich thiophene unit which causes stronger donor-acceptor interaction. Again, the absorption maxima of the dye **7a** red shifted to 489 nm and 498 nm for bithiophene containing dye **7b** and terthiophene dye containing dye **11c,** respectively. They have also displayed increment in molar extinction coefficients attributable to the elongation of conjugation due to the insertion of additional thiophene units in **7a**. Extension of conjugation by oligothiophene unit has been found to be beneficial to enhance the electron-richness in the conjugation pathway and hike the transition probability of the corresponding transitions [39, 40]. The substitution of phenyl ring instead of thiophene unit near to cyanoacrylic acid in the dye **7b** resulted a blue shift in the absorption of 41 nm for the dye **11b**. The phenyl ring causes significant twisting and reduces the conjugation when compared to thiophene analogue, which diminishes donor-acceptor interaction [65]. The introduction of fluorene instead of phenyl increases the molar extinction coefficient with a blue-shifted absorption (28 nm) when compared to the dye **11b**. The introduction of carbazole shows red shifted absorption (19 nm) with higher molar extinction coefficient when compared to fluorene due to the electron richness of the carbazole [38]. This clearly indicates that the oligothiophene units showed red shifted absorption when compared to phenyl, fluorene and carbazole chromophore due to strong donor-acceptor interactions in the former.

All the dyes possess significantly high molar extinction coefficients when compared with Ru dyes (**N3** and **N719**) [67]. The high molar extinction coefficients of the dyes may be useful to harvest the light and generate high photo current. It is interesting to note that the absorption wavelengths of these dyes (**7a**, **7b** and **11c**) are significantly red-shifted when compared to those containing phenyl, [34, 41] biphenyl, [37] fluorene, [20, 68] or 9,10-dihydrophenanthrene [42] unit substituted for carbazole or dyes with a pyridine acceptor [45, 46] in a similar structural composition. The superiority of the absorption properties of the dyes is due to the electron rich carbazole unit which facilitate conjugation between the donor and acceptor and enhances donor-acceptor interactions.

Table 3.2 Optical properties of the dyes recorded in DCM

Dye	$\lambda_{abs,}$ nm ($\varepsilon_{max} \times 10^3$ M^{-1} cm^{-1})		
	DCM	DCM + TFA	DCM + TEA
5	427 (15.2), 355 (25.5), 331 (25.4), 271 (38.3)	433 (14.8), 356 (26.9), 270 (39.3)	382 (40.2), 349 (36.7)
7a	472 (29.3), 357 (18.0), 311 (16.8)	482 (28.6), 359 (18.3)	426 (36.6), 315 (19.6)
7b	489 (34.3), 375 (23.5), 311 (16.9), 264 (34.6)	495 (35.1), 375 (24.3), 264 (35.8)	443 (46.4), 310 (18.8)
11a	391 (38.6), 311 (22.6), 276 (28.6)	391 (35.9), 313 (22.1), 276 (27.2)	391 (37.0), 276 (30.0)
11b	448 (33.0), 374 (29.8), 276 (32.2)	452 (30.6), 374 (27.7), 276 (30.1)	414 (43.5), 275 (31.1)
11c	498 (30.5), 391 (24.8), 273 (30.7)	505 (31.1), 391 (25.1)	456 (35.8), 387 (21.1), 271 (30.9)
11d	420 (34.6), 314 (15.7), 268 (27.4)	430 (32.9), 397 (31.9), 313 (16.2)	412 (49.2), 307 (18.0)
11e	439 (50.0), 391 (43.9), 314 (25.2), 273 (58.4)	446 (47.9), 389 (44.9), 316 (25.5), 273 (59.3)	417 (69.0), 309 (26.8), 271 (65.1)

The absorption and emission spectra of the bromo and aldehyde derivatives of the corresponding dyes were recorded in DCM solution. The absorption spectra is displayed in Figure 3.2 and pertinent data collected in Table 3.3. All the dyes exhibited longer wavelength absorption when compared to the corresponding bromo- and aldehyde derivatives. The absorption wavelength assumes the order in accordance with the electron-withdrawing effect of the end group (Br < CHO < cyanoacrylic acid). The drastic red shifted absorption of the dyes when compared to the precursor bromo and aldehyde derivatives clearly indicates that the dyes are inheriting intramolecular charge transfer from donor to acceptor. But, the dye **11a** and its corresponding aldehyde (**10a**) displayed same absorption indicating the absence of charge transfer. From these observations, it is evident that the donor and acceptor connected by electron rich conjugation directly are more appropriate for light harvesting applications.

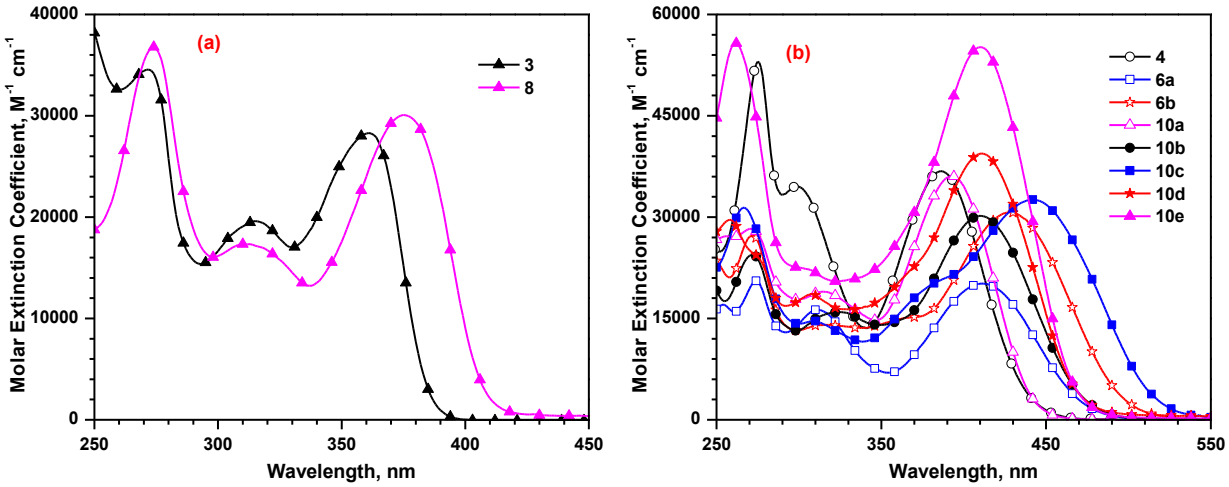

Figure 3.2 Absorption spectra of the precursors (a) bromo and (b) aldehyde derivatives recorded in DCM.

Table 3.3 Optical properties of bromo and aldehyde compounds recorded in DCM

compd.	$\lambda_{abs,}$ nm ($\varepsilon_{max} \times 10^3$ M^{-1} cm^{-1})	$\lambda_{em,}$ nm	Stokes shift, cm^{-1}
3	361 (28.3), 315 (19.6), 272 (34.6)	402	2825
4	386 (36.8), 299 (34.6), 275 (53.0)	555	7888
6a	411 (20.2), 311 (16.3), 274 (20.6)	565	6631
6b	439 (53.4), 372 (67.6), 272 (53.9)	575	5388
8	375 (30.1), 313 (17.3), 274 (36.8)	432	3519
10a	393 (36.1), 317 (18.9), 271 (28.2)	486	4869
10b	410 (30.2), 325 (15.9), 272 (24.4)	569	6816
10c	441 (32.6), 308 (14.6), 267 (31.4)	565	4977
10d	411 (39.4), 308 (18.6), 258 (29.6)	544	5949
10e	410 (55.2), 261 (55.8)	524	5306

To confirm the nature of charge transfer transition, absorption spectra of the dyes were recorded in solvents of different dielectric constants. The absorption spectra of the dyes showed negative solvatochromism for longer wavelength absorption and is attributed to the effective solvation of the dyes [69, 70] but the peaks below 350 nm did not exhibit response to solvent polarity (shown in Figures 3.3-3.5). This clearly indicates that the charge transfer state of the

dyes is effectively solvated in polar solvents. Unusual red-shifted absorption observed for DCM solutions of the dyes attributed to the instant stabilization of the polarizable electrons in excited state and this type of behaviour is well documented for the cationic dyes in chloro-solvents [71, 72]. Similarly, the anomalous blue shift observed for the dyes in THF solution probably originates due to the hydrogen bonding between carboxylic acid unit of the dyes and THF which results in partial deprotonation of the carboxylic acid unit and decreases the donor-acceptor interactions [73]. The basic nature of DMF solvent was well documented in literature, it deprotonates the dyes and produce a blue shift for the dyes [74]. Interestingly, the absorption spectrum of the dye **11a** is insensitive to solvent polarity (shown in Figure 3.4) due to the lack of donor-acceptor interaction in this dye.

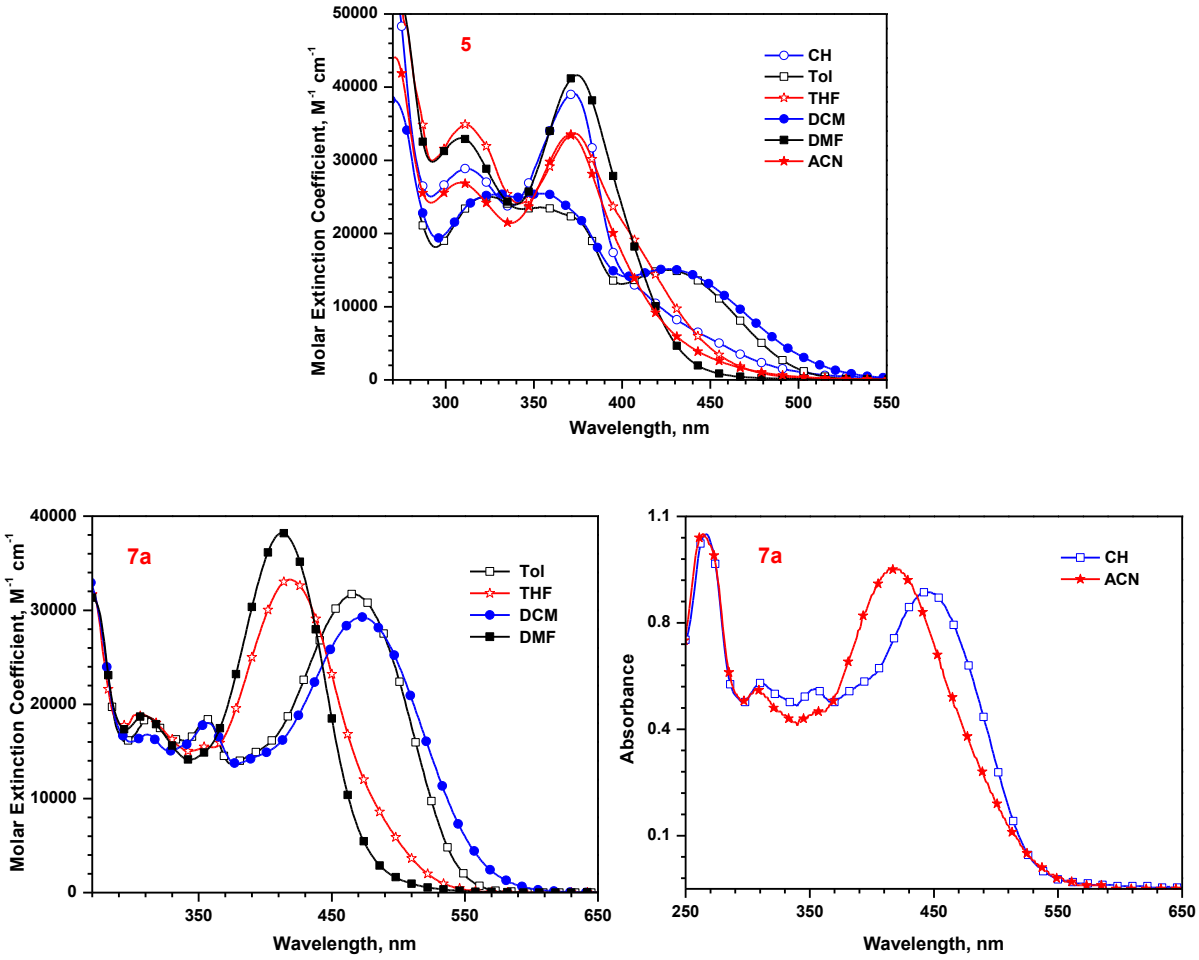

Figure 3.3 Absorption spectra of the dyes (**5** and **7a**) recorded in different solvents.

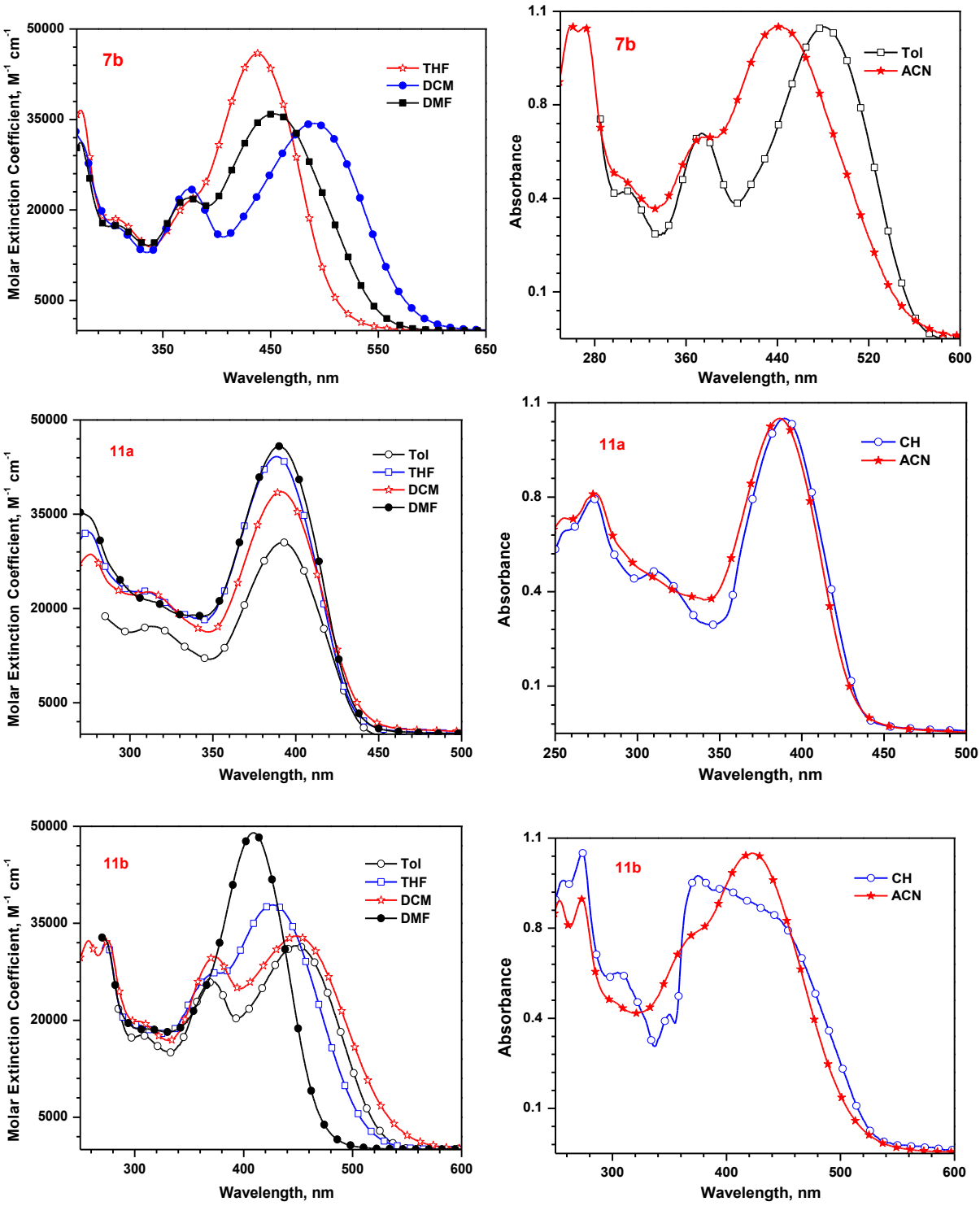

Figure 3.4 Absorption spectra of the dyes (**7b, 11a** and **11b**) recorded in different solvents.

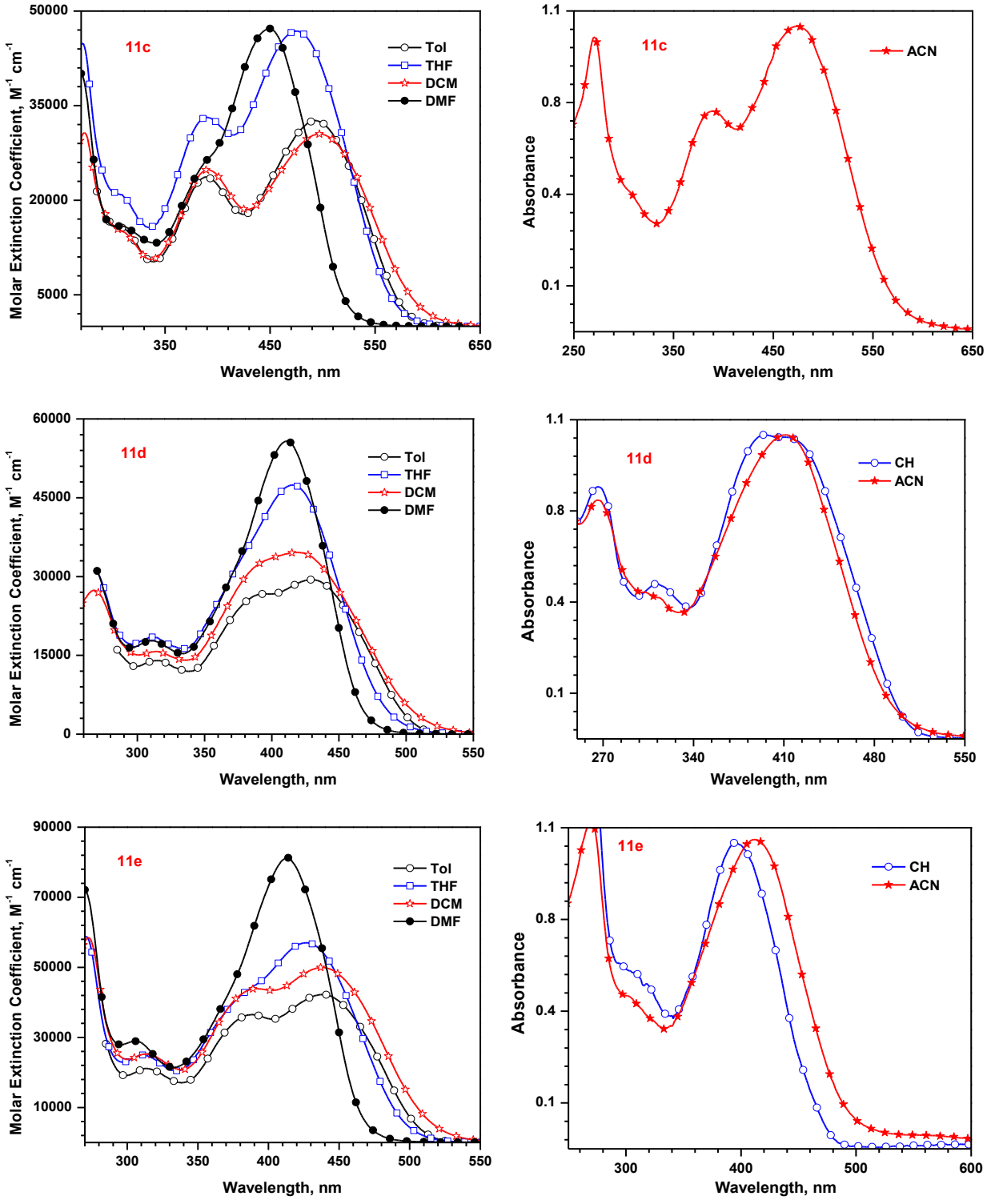

Figure 3.5 Absorption spectra of the dye (**11c, 11d** and **11e**) recorded in different solvents.

Table 3.4 Absorption spectral data of the dyes recorded in different solvents

Dye	$\lambda_{abs,}$ nm ($\varepsilon_{max} \times 10^3\ M^{-1}\ cm^{-1}$)					
	TiO_2 film	CH	Tol	THF	DMF	ACN
5	na	373 (39.1), 312 (28.9)	426 (15.0), 356 (23.5), 325 (25.0), 271 (38.3)	373 (33.7), 311 (34.9)	375 (41.6), 309 (33.0)	371 (33.4), 309 (27.0), 271 (44.1)
7a	451	445, 354, 311, 267	468 (31.7), 356 (18.5), 313 (18.6)	451 (35.3), 351 (17.0), 314 (17.9), 275 (27.1)	412 (38.1), 309 (18.8)	418 (4.51), 264 (5.0)
7b	487	ns	481, 374	453 (35.9), 374 (22.0), 308 (17.4)	438 (45.9), 306 (18.5)	441, 377, 272
11c	525	ns	493 (32.6), 389 (23.7), 312 (15.3)	475 (46.8), 389 (33.1), 309 (20.9)	449 (47.2), 386 (25.6), 310 (15.9)	475, 389, 270
11a	na	390, 311, 274	393 (30.5), 313 (17.1)	388 (44.2), 309 (22.8), 275 (32.2)	390 (45.8)	387, 274
11b	483	397, 375, 350, 305, 274	448 (31.5), 372 (26.0), 307 (17.8)	427 (37.8), 368 (27.0)	409 (49.0)	422, 368, 273, 254
11d	464	397, 351, 304, 267	430 (29.4), 396 (26.7), 315 (14.0)	416 (47.4), 312 (18.5)	412 (55.7), 311 (17.7)	411, 303, 266
11e	470	416, 402, 348, 305, 270	438 (42.2), 388 (36.5), 314 (21.2)	427 (57.0), 312 (25.0)	414 (81.2), 305 (28.9)	412, 303, 269

na = not measured; ns = not soluble

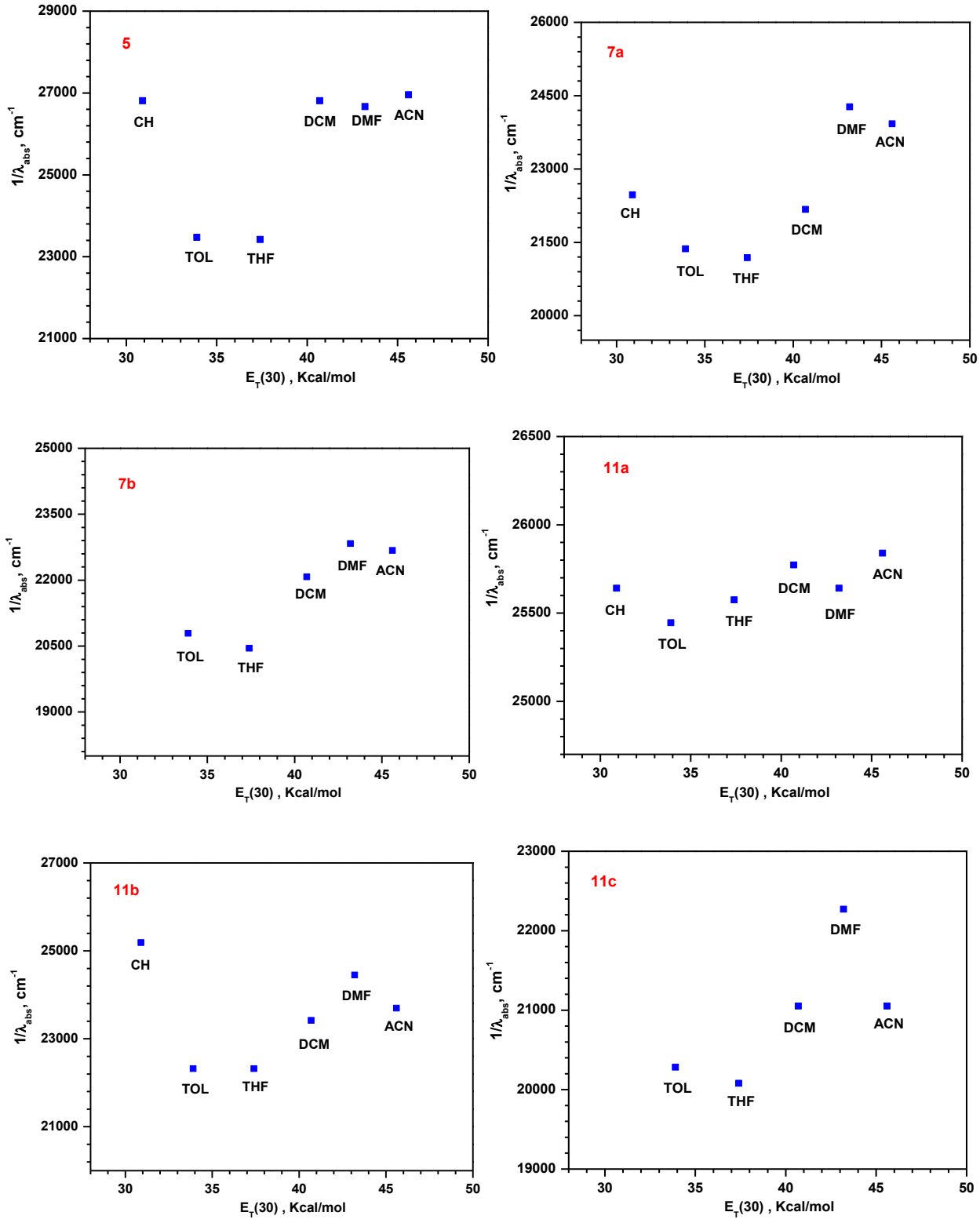

Figure 3.6 Variation of absorption (in cm^{-1}) with the solvents polarity parameter $E_T(30)$.

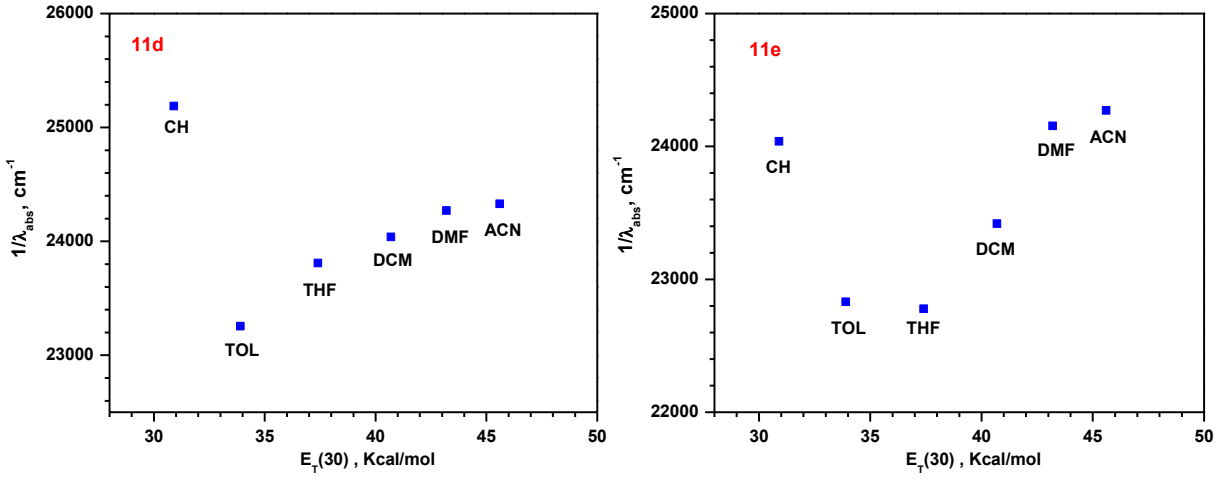

Figure 3.7 Variation of absorption (in cm^{-1}) with the solvents polarity parameter $E_T(30)$.

The solvatochromism data of the dyes were analyzed by correlating with $E_T(30)$ parameter [75] and plots are displayed in Figures 3.6 and 3.7. The dyes exhibited deviation from linearity for the polar solvents such as DCM due to the solvent specific interaction which led to unusual red shift for these dyes. Similar behaviour has been earlier observed for organic dyes and attributed to the instant stabilization due to a fast rearrangement of polarizable electrons during excitation [71, 72].

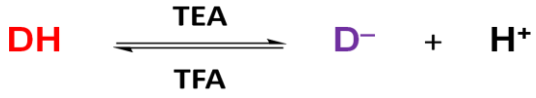

Figure 3.8 The equilibrium of protonated (DH) and deprotonated form (D^-) of the dye solutions for acid-base addition.

The existence of equilibrium between the neutral (D) and deprotonated (D^-) forms of the dyes (Figure 3.8) was confirmed by the trifluoroacetic acid (TFA) and triethylamine (TEA) addition to the dyes in DCM. The addition of TEA deprotonates the dye and shifts the equilibrium towards deprotonated (D^-) form which contain carboxylate ion (COO^-) of less electron withdrawing capability than carboxylic acid (COOH). It results in weak donor-acceptor interaction thus produces blue shifted absorption. However, the addition of TFA pushes the equilibrium towards the protonated form of the dye (D) and this provide strong donor-acceptor interaction and consequently red-shifts the absorption [73, 76].

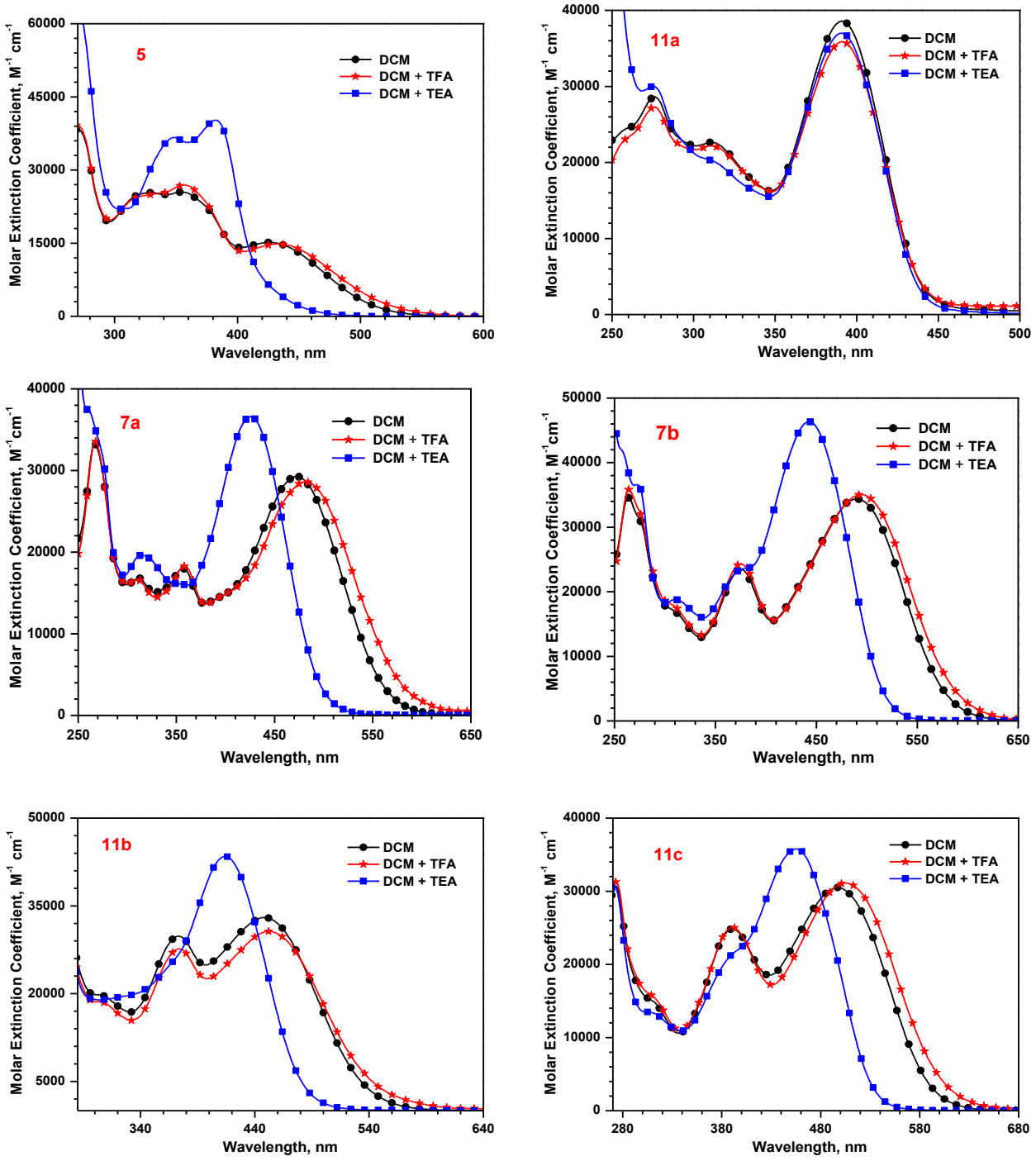

Figure 3.9 Absorption spectra of the dyes (**5, 11a**, **7a-7b** and **11b-11c)** recorded in DCM, after the addition of TFA and TEA.

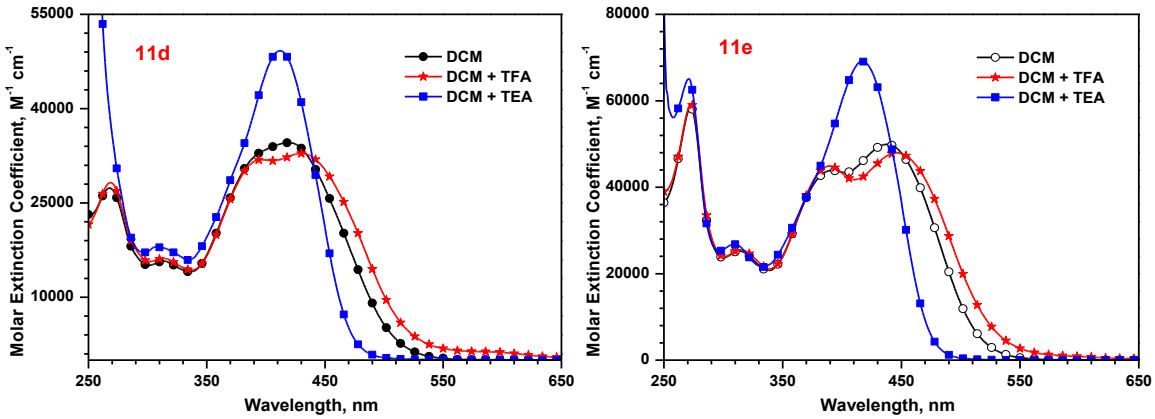

Figure 3.10 Absorption spectra of the dyes (**11d** and **11e)** recorded in DCM, after the addition of TFA and TEA.

Interestingly, the blue shift observed in case of TEA addition is more pronounced than the red shift observed in case of TFA. This may be due to the reason that most of the dye molecules are present in protonated form in DCM solutions. This study confirms the charge transfer nature for the longer wavelength absorption of the dyes. The dye **11a** which has *meta*-substitution of cyanoacrylic acid does not show any change on addition of TFA or TEA, further confirming the absence of charge transfer transition in this molecule [65].

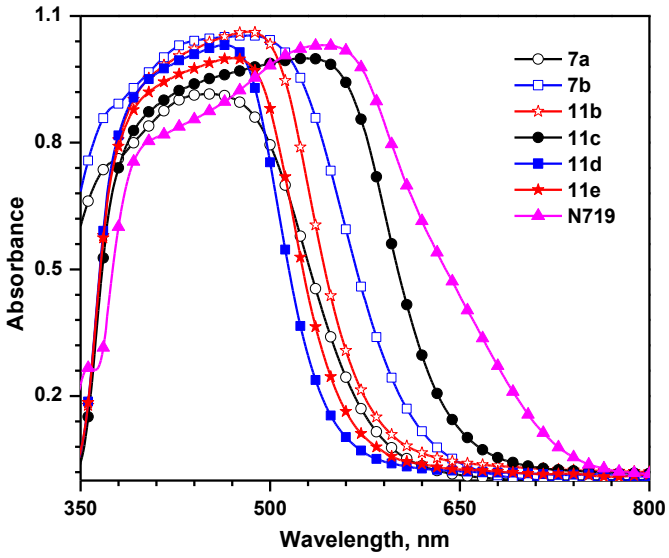

Figure 3.11 Absorption spectra of the dyes (**7a**, **7b** and **11b-11e**) recorded for TiO_2 films.

Absorption spectra recorded for the dyes anchored on transparent nanocrystalline anatase TiO_2 films are displayed in Figure 3.11. Red-shifted absorption indicates *J*-aggregation of the dyes at the surface of TiO_2 or the use of thicker TiO_2 film [77], while

hypsochromic shift results due to the deprotonation of the dyes or formation of *H*-aggregates [78]. All the dyes showed red shifted absorption except monothiophene dye **7a**, indicate that after one thiophene unit introduction of another thiophene or aromatic rings causes stacking interactions due to possible planar conjugation available at the surface of TiO_2 films. It was speculated that the dyes are stacking on TiO_2 film due to intermolecular stacking interactions. The reason for blue shifted absorption maxima of **7a** may be due to the deprotonation of the dye on surface of the TiO_2 film and lack of aggregation.

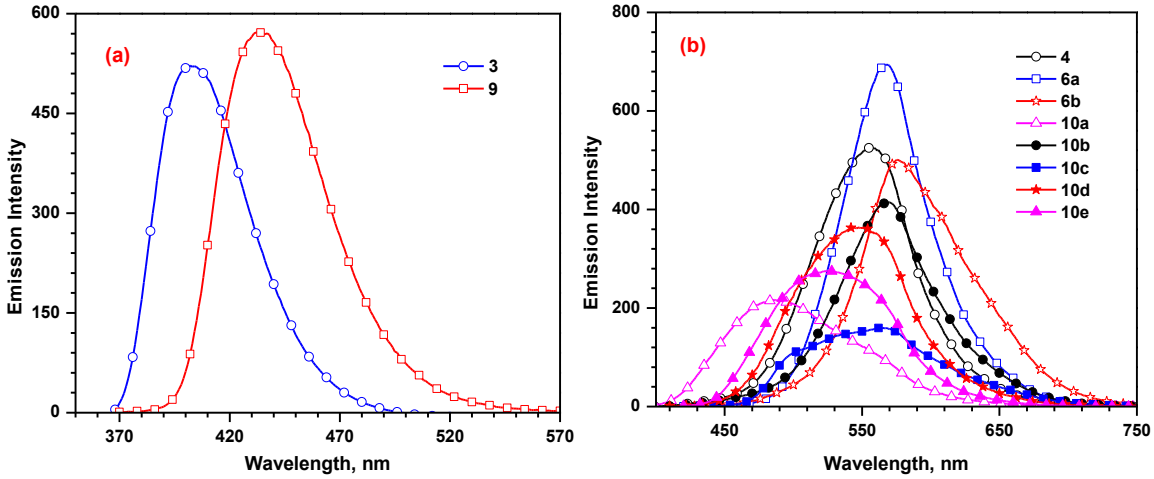

Figure 3.12 Emission spectra of bromo (a) and aldehyde (b) derivatives recorded in DCM.

The dyes are moderately emitting in toluene but weak emission was observed for dichloromethane solutions. This is probably due to the dipolar quenching predominant in the polar solvents. This indicated the excited state is more polar with noticeable dipole which might interact with solvent dipole and relax the excited state of the dye by electron transfer mechanism [79, 80]. The emission spectra of the dyes recorded in DCM are shown in Figure 3.12 and for comparison photoluminescence of precursors (bromo and aldehyde) recorded under identical condition also included. The emission wavelength of the dyes follows the order **11a** (481 nm) < **11b** (500 nm) < **11d** (513 nm) < **11e** (526 nm) < **5** (537 nm) < **11c** (565 nm) < **7a** (572 nm) < **7b** (579 nm). The shortest emission peak observed for **11a** due to the absence of donor-acceptor interaction. The introduction of oligothiophene units produced red shifted emission due to more pronounced donor-acceptor interaction and it allows the migration of electron density from the donor to acceptor and from a polar excited state which facilitates a dipolar relaxation with the solvent dipoles. The phenyl linked dye **11b** emits at shorter wavelength while the fluorene

and carbazole linked dyes (**11d** and **11e)** emit at longer wavelength owing to the reduced donor-acceptor interactions included by the twisting of the phenyl unit. The introduction of electron rich carbazole spacer (**11e**) enhances donor acceptor interactions compared to fluorene spacer (**11d**). It appears that the nature of the linker played a major role in excited state of the dye. Also, the dyes showed red shifted absorption when compared to their precursors (Figure 3.12). Since the excited state is charge transfer in nature, most of the dyes exhibited poor emission in polar solvents. However, **11a** displayed positive solvatochromism. It indicates that in this dye excited state is more polar in nature. Charge transfer via *meta*-conjugation in the excited state has been demonstrated for D-*m*π-A dyads. [81]

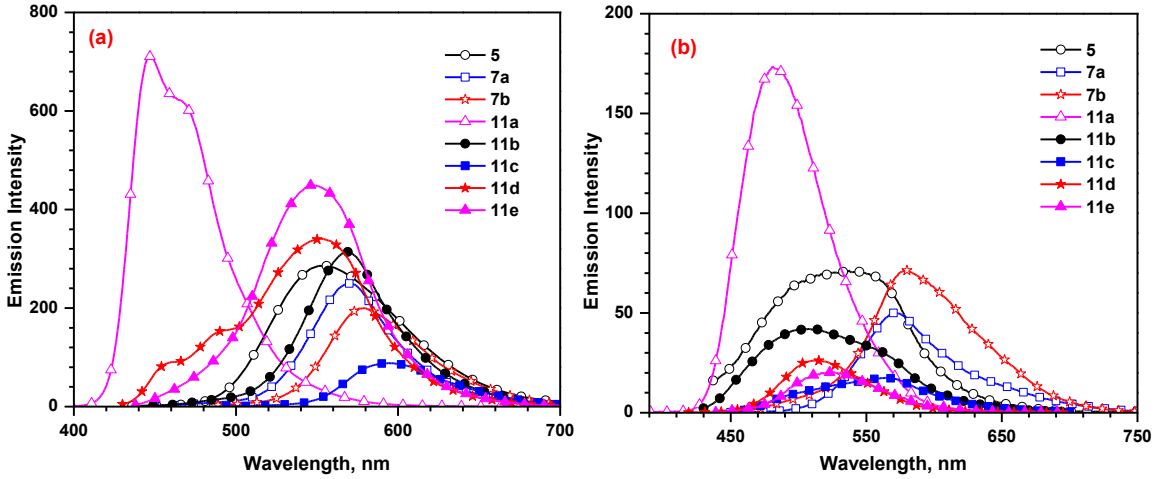

Figure 3.13 Emission spectra of the dyes (**5**, **7** and **11a-11e**) recorded in Tol (a) and DCM (b).

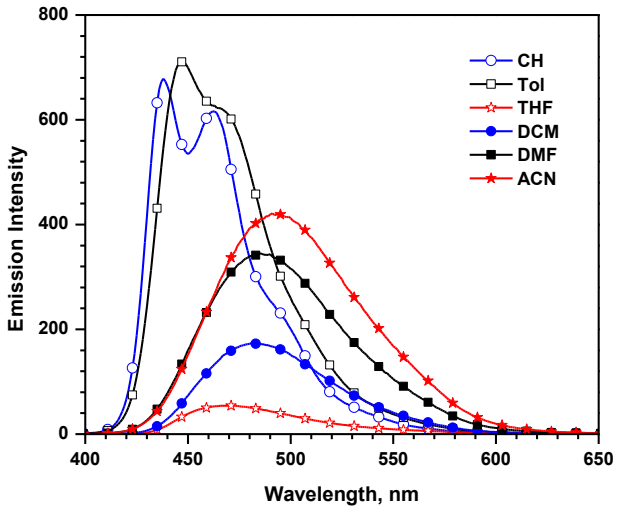

Figure 3.14 Emission spectra of the dye (**11a**) recorded in different solvents.

3.2.3 Theoretical Calculations

To gain further insight into the electronic structure of the compounds the structures of the compounds were optimized by density functional theory (DFT) [82] calculations at the 6-31+G (d, p) level by two different correlation functionals B3LYP [82] and MPW1K [83]. The vertical energies were computed using the time dependent density functional theory in the same level. The vertical excitations and their orbital contribution are listed in Tables 3.5 and 3.6.

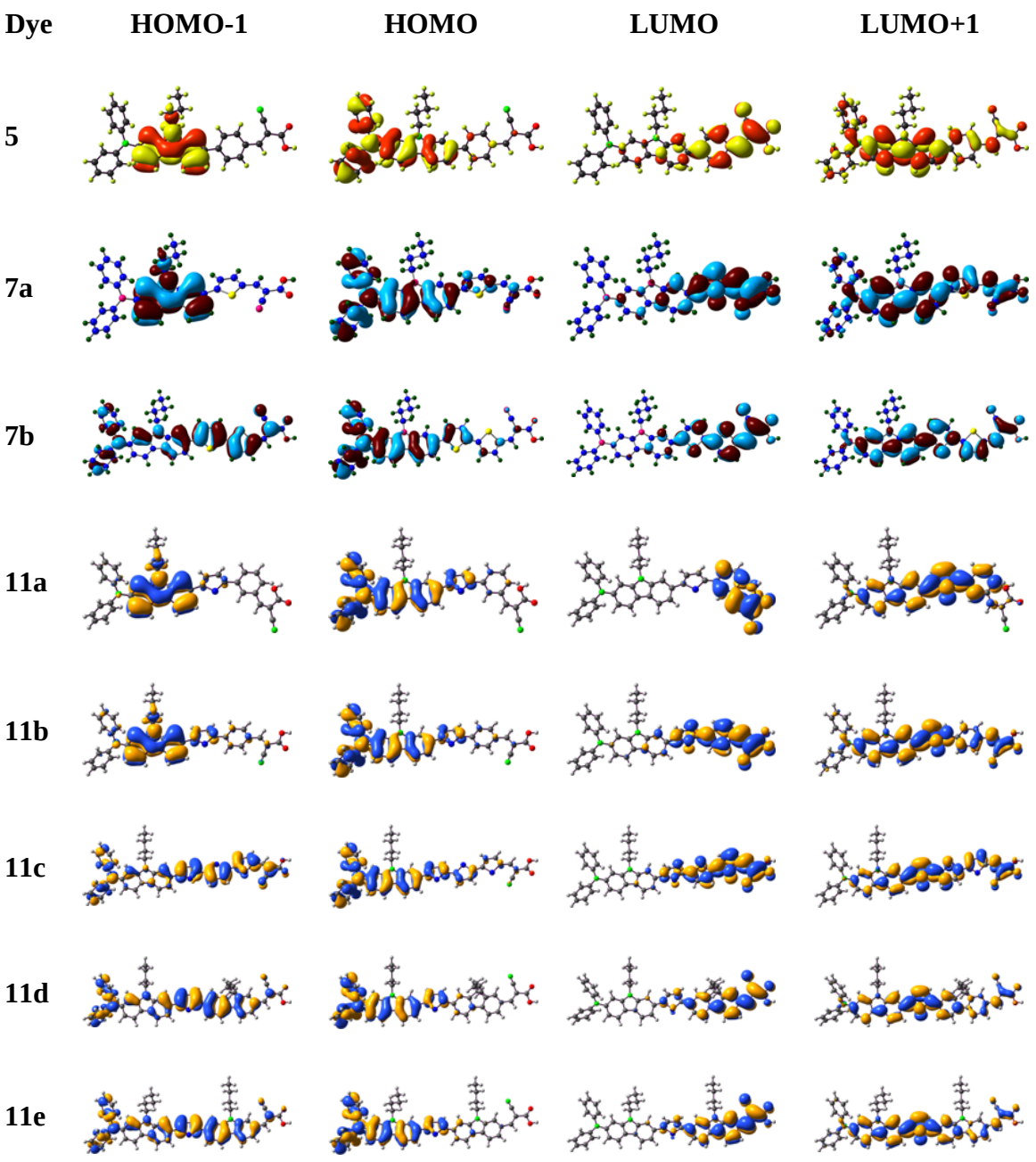

Figure 3.15 Frontier molecular orbitals of the dyes.

HOMO of the dyes is mainly located on the amine donor unit and spread up to the carbazole and thiophene units. The LUMO of the dyes is predominantly contributed by the cyanoacrylic acid and the thiophene units. But, for the dye **11a** the LUMO is located only on the cyanoacrylic acid unit. For the dyes **11d** and **11e**, the LUMO is mainly distributed on cyanoacrylic acid and carbazole/fluorene unit near to it and these dyes has good charge separation. Longer wavelength absorption originates from the transfer of electron from HOMO to LUMO with high oscillator strength. Absence of significant overlap between the HOMO and LUMO indicates facile charge separation on photo-excitation and beneficial injection of electron into the conduction band of TiO_2.

HOMO-1 in the dyes **11c-11e** is mainly located on carbazole thiophene near the acceptor and this serve as donor and injects an electron into LUMO on shorter wavelength photoexcitation. MPW1K theory shows HOMO-1 to LUMO has considerable contribution in longer wavelength transition along with HOMO to LUMO transition contribution. This clearly indicates that the longer wavelength absorption for the dyes may have contribution from both charge transfer and π-π* transitions. The two theories clearly suggest that the longer wavelength absorption correspond to the transition from HOMO to LUMO and next high energy transition arises from the HOMO-1 to LUMO and HOMO-2 to LUMO. But, in bithiophene dyes the LUMO+1 is spread over the entire molecule. The peak position estimated by B3LYP calculations are over estimated but MPW1K gave more reliable results.

Table 3.5 Computed vertical transition energies and their oscillator strengths, assignments, dipole moments and band gaps for the dyes using B3LYP theory

Dye	λ	*f*	assignments	μ_g (D)	HOMO (eV)	LUMO (eV)	E_g (eV)
5 (vacuum)	560.9	0.36	HOMO → LUMO (100%)	6.40	-4.98	-2.53	2.44
	383.4	0.88	HOMO-2 → LUMO (92%)				
	357.6	0.24	HOMO → LUMO+1 (88%)				
	309.2	0.26	HOMO → LUMO+3 (71%)				
5 (THF)	591.7	0.42	HOMO → LUMO (100%)	7.52	-4.97	-2.63	2.35
	398.7	0.88	HOMO-2 → LUMO (95%)				
	362.4	0.37	HOMO → LUMO+1 (92%)				
	315.8	0.18	HOMO-3 → LUMO (90%)				
	311.8	0.21	HOMO → LUMO+3 (78%)				

Table 3.5 (cont.)

Dye	λ	*f*	assignments	μ_g (D)	HOMO (eV)	LUMO (eV)	E_g (eV)
7a (vacuum)	559.0	0.51	HOMO→LUMO (100%)	9.69	-5.01	-2.56	2.45
	455.1	0.02	HOMO-1→LUMO (98%)				
	397.3	0.95	HOMO-2→LUMO (92%)				
	359.0	0.19	HOMO→LUMO+1 (87%)				
	310.3	0.14	HOMO→LUMO+3 (66%)				
7a (THF)	607.8	0.63	HOMO→LUMO (100%)	12.67	-4.99	-2.70	2.30
	419.4	0.91	HOMO-2→LUMO (96%)				
	365.5	0.29	HOMO→LUMO+1 (91%)				
7b (vacuum)	605.4	0.52	HOMO→LUMO (100%)	7.75	-4.96	-2.70	2.25
	470.5	0.16	HOMO-2→LUMO (69%), HOMO-1→LUMO (30%)				
	457.1	1.01	HOMO-1→LUMO (66%), HOMO-2→LUMO (30%)				
	393.9	0.33	HOMO→LUMO+1 (88%)				
7b (THF)	653.4	0.66	HOMO→LUMO (99%)	9.64	-4.95	-2.82	2.12
	503.4	0.25	HOMO-1→LUMO (78%), HOMO-2→LUMO (21%)				
	485.1	0.89	HOMO-2→LUMO (77%), HOMO-1→LUMO (20%)				
	402.3	0.41	HOMO→LUMO+1 (90%)				
11a (vacuum)	428.0	0.87	HOMO→LUMO+1 (97%)	7.11	-4.90	-2.60	2.30
	342.8	0.65	HOMO-2→LUMO+1 (63%), HOMO-3→LUMO (22%)				
	339.7	0.16	HOMO-3→LUMO (48%), HOMO→LUMO+2 (41%)				
	335.3	0.12	HOMO→LUMO+2 (39%), HOMO-2→LUMO+1 (30%), HOMO-3→LUMO (21%)				
11a (THF)	431.1	1.05	HOMO→LUMO+1 (97%)	8.00	-4.92	-2.65	2.26
	346.1	0.50	HOMO-2→LUMO+1 (55%), HOMO-3→LUMO (40%)				
	342.2	0.40	HOMO-3→LUMO (49%), HOMO-2→LUMO+1 (33%)				

Table 3.5 (cont.)

Dye	λ	*f*	assignments	μ_g (D)	HOMO (eV)	LUMO (eV)	E_g (eV)
11b (vacuum)	591.0	0.42	HOMO→LUMO (100%)	10.03	-4.93	-2.62	2.30
	440.7	1.10	HOMO-2→LUMO (90%)				
	391.8	0.37	HOMO→LUMO+1 (91%)				
	343.2	0.27	HOMO-3→LUMO (81%)				
11b (THF)	619.4	0.50	HOMO→LUMO (99%)	12.29	-4.94	-2.72	2.22
	482.3	0.11	HOMO-1→ LUMO (99%)				
	460.9	1.01	HOMO-2→ LUMO (96%)				
	397.9	0.49	HOMO→LUMO+1 (93%)				
	350.4	0.22	HOMO-3→LUMO (92%)				
	322.8	0.13	HOMO-2→LUMO+1 (62%)				
11c (vacuum)	648.1	0.55	HOMO→LUMO (100%)	7.45	-4.89	-2.79	2.10
	513.9	1.17	HOMO-1→LUMO (97%)				
	437.6	0.44	HOMO→LUMO+1 (88%)				
	396.5	0.17	HOMO-3→LUMO (67%), HOMO-1→LUMO+1 (25%)				
	353.9	0.16	HOMO→LUMO+2 (86%)				
11c (THF)	679.3	0.70	HOMO→LUMO (99%)	9.03	-4.90	-2.87	2.03
	541.7	1.10	HOMO-1→LUMO (97%)				
	442.8	0.54	HOMO→LUMO+1 (90%)				
	405.1	0.14	HOMO-3→LUMO (82%)				
	356.5	0.21	HOMO→LUMO+2 (87%)				
11d (vacuum)	602.3	0.30	HOMO→LUMO (99%)	5.21	-4.83	-2.59	2.25
	472.3	0.83	HOMO-1→LUMO (96%)				
	416.3	0.65	HOMO→LUMO+1 (92%)				
	367.3	0.44	HOMO-4→LUMO (87%)				
	343.5	0.32	HOMO-1→LUMO+1 (67%)				
11d (THF)	612.5	0.37	HOMO→LUMO (99%)	6.40	-4.89	-2.67	2.22
	486.5	0.89	HOMO-1→LUMO (96%)				
	420.5	0.78	HOMO→LUMO+1 (92%)				
	374.9	0.42	HOMO-3→LUMO (90%)				
	347.4	0.29	HOMO-1→LUMO+1 (72%), HOMO-2→LUMO+1 (15%)				
	339.8	0.11	HOMO→LUMO+2 (87%)				

Table 3.5 (cont.)

Dye	λ	*f*	assignments	μ_g, D	HOMO (eV)	LUMO (eV)	$E_{0\text{-}0}$ (eV)
11e (vacuum)	567.1	0.32	HOMO→LUMO (99%)	8.92	-4.86	-2.49	2.38
	454.0	0.90	HOMO-1→LUMO (94%)				
	415.1	0.64	HOMO→LUMO+1 (91%)				
	359.2	0.51	HOMO-4→LUMO (77%), HOMO-1→LUMO+1 (18%)				
	344.1	0.24	HOMO-1→LUMO+1 (61%), HOMO-4→LUMO (16%), HOMO→LUMO+2 (15%)				
11e (THF)	581.7	0.38	HOMO→LUMO (98%)	10.10	-4.89	-2.56	2.33
	469.5	0.92	HOMO-1→LUMO (94%)				
	420.6	0.79	HOMO→LUMO+1 (92%)				
	367.3	0.45	HOMO-4→LUMO (87%)				
	348.9	0.26	HOMO-1→LUMO+1 (70%), HOMO-2→LUMO+1 (16%)				
	341.1	0.11	HOMO →LUMO+2 (88%)				

Table 3.6 Computed vertical transition energies and their oscillator strengths, assignments, dipole moments and band gaps for the dyes using MPW1K theory

Dye	λ	*f*	assignments	μ_g (D)	HOMO (eV)	LUMO (eV)	E_g (eV)
5 (vacuum)	403.7	0.93	HOMO→LUMO (88%)	6.37	-5.88	-2.05	3.83
	316.7	0.80	HOMO-2→LUMO (75%)				
	305.1	0.18	HOMO→LUMO+1 (81%)				
	272.9	0.23	HOMO→LUMO+3 (76%)				
	262.6	0.15	HOMO-3→LUMO (37%), HOMO-4→LUMO (17%)				
5 (THF)	415.9	1.07	HOMO→LUMO (86%)	7.40	-5.92	-2.16	3.76
	324.9	0.70	HOMO-2→LUMO (74%)				
	309.0	0.35	HOMO→LUMO+1 (85%)				
	275.4	0.33	HOMO→LUMO+3 (87%)				
	266.4	0.13	HOMO-5→LUMO (38%), HOMO-3→LUMO (23%)				

Table 3.6 (cont.)

Dye	λ	*f*	assignments	μ_g (D)	HOMO (eV)	LUMO (eV)	E_g (eV)
7a (vacuum)	411.2	1.12	HOMO→LUMO (85%)	9.31	-5.86	-1.99	3.87
	325.8	0.40	HOMO-2→LUMO (82%)				
	303.0	0.29	HOMO→LUMO+1 (84%)				
	272.2	0.22	HOMO→LUMO+3 (59%), HOMO→LUMO+2 (28%)				
7a (THF)	434.9	1.27	HOMO→LUMO (83%)	12.00	-5.89	-2.14	3.75
	338.5	0.34	HOMO-2→LUMO (79%)				
	307.0	0.40	HOMO→LUMO+1 (85%)				
	274.5	0.23	HOMO→LUMO+3 (41%), HOMO→LUMO+2 (37%)				
7b (vacuum)	433.4	1.49	HOMO→LUMO (70%)	6.82	-5.81	-2.16	3.65
	361.3	0.28	HOMO-1→LUMO (66%), HOMO→LUMO (26%)				
	321.9	0.47	HOMO→LUMO+1 (77%)				
	271.9	0.22	HOMO→LUMO+4 (81%)				
7b (THF)	457.8	1.66	HOMO→LUMO (65%), HOMO-1→LUMO (23%)	8.23	-5.84	-2.29	3.56
	375.0	0.18	HOMO-1→LUMO (53%), HOMO→LUMO (30%)				
	327.4	0.59	HOMO→LUMO+1 (77%)				
11a (vacuum)	400.6	0.14	HOMO→LUMO (82%), HOMO-2→LUMO (15%)	7.16	-5.80	-2.07	3.73
	356.9	1.41	HOMO→LUMO+1 (78%)				
	297.1	0.31	HOMO-2→LUMO+1 (59%), HOMO→LUMO+2 (23%)				
	279.7	0.49	HOMO-6→LUMO (64%), HOMO-3→LUMO (10%)				
	274.0	0.26	HOMO→LUMO+4 (70%)				
	271.7	0.16	HOMO→LUMO+3 (32%), HOMO→LUMO+2 (22%) HOMO→LUMO+4 (16%)				

Table 3.6 (cont.)

Dye	λ	*f*	assignments	μ_g (D)	HOMO (eV)	LUMO (eV)	E_g (eV)
11a (THF)	402.9	0.17	HOMO→LUMO (78%), HOMO-2→LUMO (16%)	8.03	-5.86	-2.13	3.73
	360.7	1.58	HOMO→LUMO+1 (76%)				
	301.1	0.44	HOMO-2→LUMO+1 (55%), HOMO→LUMO+2 (22%)				
	287.4	0.50	HOMO-6→LUMO (73%)				
	276.3	0.32	HOMO→LUMO+4 (86%)				
	271.6	0.19	HOMO→LUMO+2 (33%), HOMO→LUMO+3 (87%)				
11b (vacuum)	428.2	1.47	HOMO→LUMO (75%)	6.29	-5.79	-2.20	3.59
	354.0	0.52	HOMO-2→LUMO (37%), HOMO-1→LUMO (32%)				
			HOMO→LUMO (21%)				
	325.8	0.39	HOMO→LUMO+1 (77%)				
	281.7	0.13	HOMO-3→LUMO (73%)				
	273.6	0.25	HOMO→LUMO+5 (67%), HOMO→LUMO+4 (17%)				
11b (THF)	441.6	1.66	HOMO→LUMO (69%), HOMO-2→LUMO (18%)	7.51	-5.86	-2.29	3.57
	362.6	0.36	HOMO-2→LUMO (42%), HOMO→LUMO (25%), HOMO-1→LUMO (23%)				
	330.8	0.55	HOMO→LUMO+1 (77%)				
	286.2	0.15	HOMO-3→LUMO (61%)				
	275.7	0.32	HOMO→LUMO+5 (85%)				
11c (vacuum)	488.4	1.86	HOMO→LUMO (61%), HOMO-1→LUMO (31%)	9.97	-5.82	-2.19	3.63
	398.5	0.18	HOMO-1→LUMO (58%), HOMO→LUMO (34%)				
	354.4	0.55	HOMO→LUMO+1 (73%)				

Table 3.6 (cont.)

Dye	λ	*f*	assignments	μ_g (D)	HOMO (eV)	LUMO (eV)	E_g (eV)
11c (THF)	510.8	2.00	HOMO→LUMO (56%), HOMO-1→LUMO (36%)	12.13	-5.87	-2.28	3.59
	406.0	0.10	HOMO-1→LUMO (52%), HOMO→LUMO (38%)				
	360.7	0.65	HOMO→LUMO+1 (71%)				
	276.1	0.33	HOMO→LUMO+4 (65%), HOMO-1→LUMO+4 (16%)				
11d (vacuum)	425.8	1.43	HOMO→LUMO (65%), HOMO-1→LUMO (22%)	5.24	-5.71	-2.14	3.58
	362.5	0.51	HOMO-1→LUMO (54%), HOMO→LUMO (32%)				
	341.7	0.69	HOMO→LUMO+1 (71%)				
	301.8	0.15	HOMO-3→LUMO (64%)				
11d (THF)	432.8	1.69	HOMO→LUMO (57%), HOMO-1→LUMO (28%)	6.46	-5.82	-2.22	3.60
	365.8	0.37	HOMO-1→LUMO (50%), HOMO→LUMO (35%)				
	347.2	0.90	HOMO→LUMO+1 (71%)				
11e (vacuum)	409.8	1.68	HOMO→LUMO (60%), HOMO-1→LUMO (22%)	8.80	-5.75	-2.03	3.72
	349.2	0.49	HOMO-1→LUMO (51%), HOMO→LUMO (33%)				
	341.1	0.57	HOMO→LUMO+1 (68%)				
	289.4	0.16	HOMO-4→LUMO (38%), HOMO-1→LUMO+1 (25%) HOMO-1→LUMO (16%)				
	274.7	0.24	HOMO→LUMO+4 (58%), HOMO→LUMO+3 (22%)				

Table 3.6 (cont.)

Dye	λ	*f*	assignments	μ_g (D)	HOMO (eV)	LUMO (eV)	E_g (eV)
11e (THF)	417.5	1.92	HOMO→LUMO (54%), HOMO-1→LUMO (27%)	9.82	-5.82	-2.11	3.72
	354.8	0.30	HOMO-1→LUMO (49%), HOMO→LUMO (25%)				
	346.5	0.81	HOMO→LUMO+1 (62%), HOMO→LUMO (20%)				
	291.3	0.17	HOMO-4→LUMO (37%), HOMO-1→LUMO+1 (22%), HOMO-1→LUMO (17%)				
	276.6	0.32	HOMO→LUMO+4 (54%), HOMO→LUMO+3 (27%)				

3.2.4 Electrochemical Properties

The redox propensity of the dyes was estimated in DCM by cyclic voltammetry and differential pulse voltammetry measurements. The cyclic voltammograms of the dyes are displayed in Figure 3.16. All the measurements were performed in the presence of ferrocene which served as internal standard and the oxidation potentials are reported relative to the ferrocene/ferrocenium redox couple. The excited state potential E_{ox}* was calculated by subtracting the value of E_{ox} from $E_{0\text{-}0}$, whereas the band gap $E_{0\text{-}0}$ obtained from the intersection of absorption and emission. ΔG_{inj} was calculated from the difference between the E_{ox}* and conduction band of TiO_2 (E_{CB}).

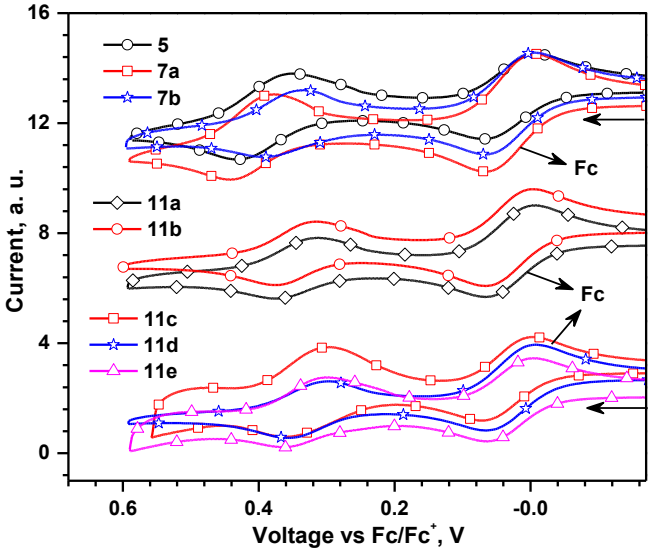

Figure 3.16 Cyclic voltammograms of the dyes (**11a-11e**) recorded in DCM.

Table 3.7 Electrochemical properties of the dyes and precursors recorded in DCM

compd.	E_{ox} (ΔE_P), V	HOMO, eV	LUMO, eV	$E_{0\text{-}0}$, eV	E_{ox}^*, V	ΔG_{inj}, V
3	0.40 (87), 0.92	5.20	1.92	3.28	-2.11	1.61
8	0.33 (73), 0.81	5.13	2.04	3.09	-1.99	1.49
4	0.38 (69), 0.87	5.18	2.54	2.64	-1.49	0.99
6a	0.39 (70), 0.88	5.19	2.64	2.55	-1.39	0.89
6b	0.35 (73), 0.75	5.15	2.67	2.48	-1.36	0.86
10a	0.33 (71), 0.74	5.13	2.31	2.82	-1.72	1.22
10b	0.34 (73), 0.77	5.14	2.59	2.55	-1.44	0.94
10c	0.32 (75), 0.61	5.12	2.67	2.45	-1.36	0.86
10d	0.32 (57), 0.64	5.12	2.52	2.60	-1.51	1.01
10e	0.32 (66), 0.61	5.12	2.48	2.64	-1.55	1.05
5	0.36 (84), 0.76	5.16	2.86	2.30	-1.17	0.67
7a	0.38 (65), 0.86	5.18	2.85	2.33	-1.18	0.68
7b	0.33 (52), 0.71	5.13	2.86	2.27	-1.17	0.67
11a	0.32 (63), 0.72	5.12	2.29	2.83	-1.75	1.25
11b	0.32 (51), 0.72	5.12	2.53	2.59	-1.50	1.00
11c	0.30 (79), 0.62	5.10	2.77	2.33	-1.28	0.78
11d	0.30 (43), 0.64	5.10	2.51	2.59	-1.52	1.02
11e	0.31 (64), 0.60	5.11	2.56	2.55	-1.48	0.98

All the dyes showed one quasi reversible redox couple and one irreversible oxidation wave, corresponding to the removal of electron from the amine unit and conjugation pathway, respectively. The first oxidation potential of the dyes assume an order of **11c** = **11d** (0.30 V) < **11e** (0.31 V) < **11a** = **11b** (0.32 V) < **5** (0.36 V) < **7a** (0.38 V). Even though electron rich thiophene dye **7a** showed difficult oxidation compared to phenyl dye **5** due to its twisting of phenyl linker resulting weak donor-acceptor interaction and led to easy oxidation [4]. The simultaneous introduction of thiophene units increased the electron richness and showed easy oxidation. The incorporation of fluorene and carbazole increased the conjugation length and then decrease the donor-acceptor interaction and oxidation potentials of the dyes. The electron rich fluorene (**11d**) and carbazole (**11e**) linkers containing dyes are easy to oxidise when compared to phenyl containing dye (**11b**). So, the oxidation potentials are influenced by the nature of conjugation pathway and the effectiveness of interaction between donor and acceptor.

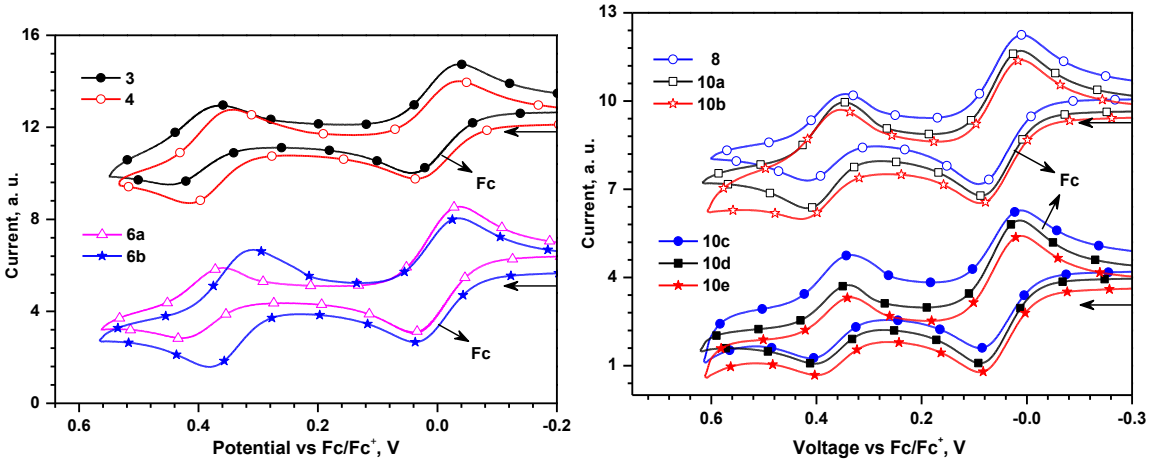

Figure 3.17 Cyclic voltammograms of the carbazole aldehyde derivatives recorded in DCM.

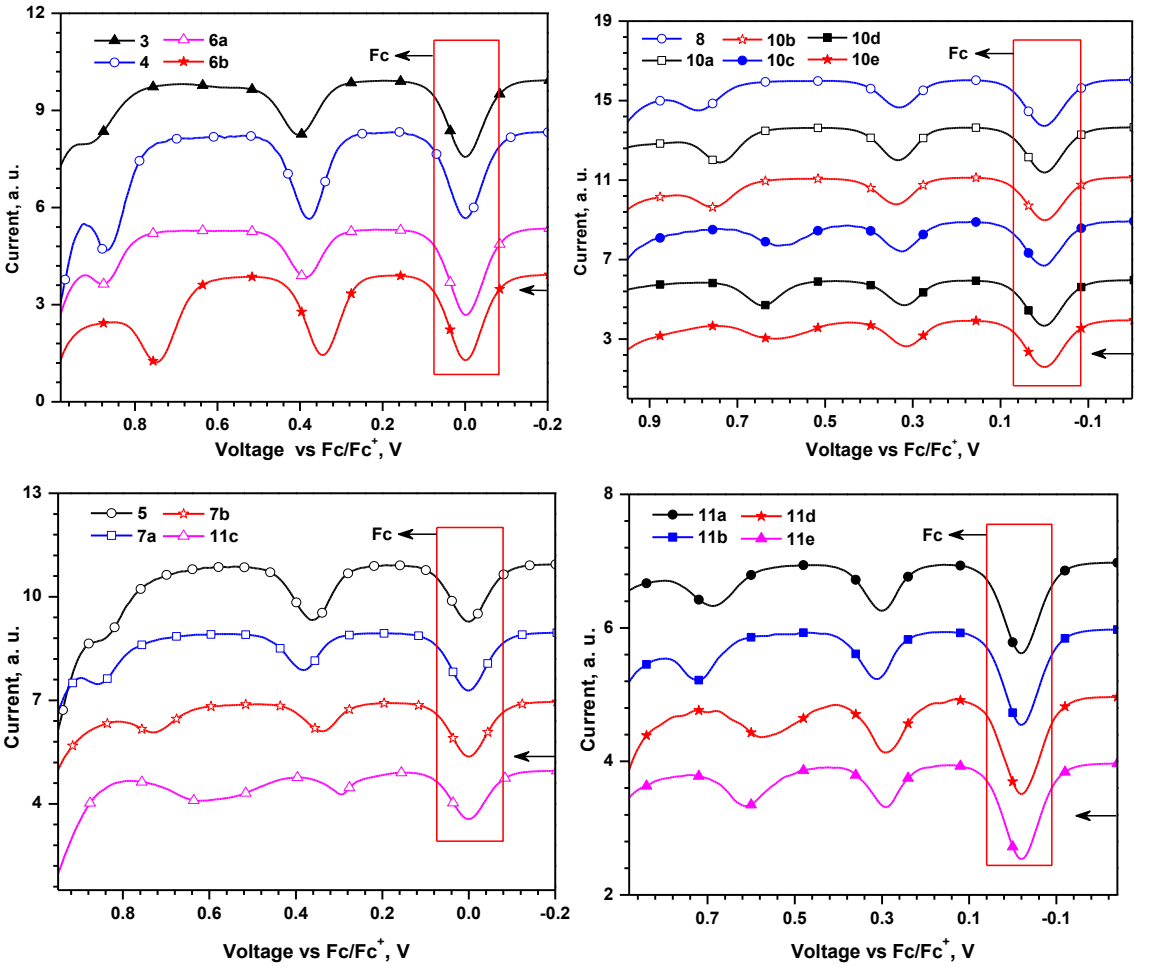

Figure 3.18 Differential pulse voltammograms of the bromo, aldehyde derivatives and dyes recorded in DCM.

For efficient electron injection into the conduction band of the TiO_2, the excited state oxidation potential of the dyes must be more negative than the conduction band of the TiO_2 [7]. The excited-state oxidation potentials (–1.17 V to –1.74 V *vs* NHE) of the

sensitizers are more negative than the conduction band of the TiO_2 (–0.5 V *vs* NHE) [84] which provide the required thermodynamic driving force for the electron injection from the photo-excited dye to the conduction band of TiO_2. The order of ΔG_{inj} for the dyes are following the order **5** = **7b** (0.67 V) < **7a** (0.68 V) < **11c** (0.78 V) < **11e** (0.98 V) < **11b** (1.00 V) < **11a** (1.25 V). Higher ΔG_{inj} facilitate the better thermodynamic driving force for injection of electron from excited state of the dyes. Similarly, the oxidized dyes can be effectively regenerated only if their ground state oxidation potentials are more anodic than the redox potential of the redox electrolyte. The oxidation potentials of the dyes (1.07-1.15 V *vs* NHE) are larger than the redox potential of the I^-/I_3^- redox couple (0.4 V *vs* NHE) [85]. This predicts a facile regeneration of the dyes by the I^-/I_3^- electrolyte after electron injection. These two processes are the important factors to govern the efficiency of the DSSC.

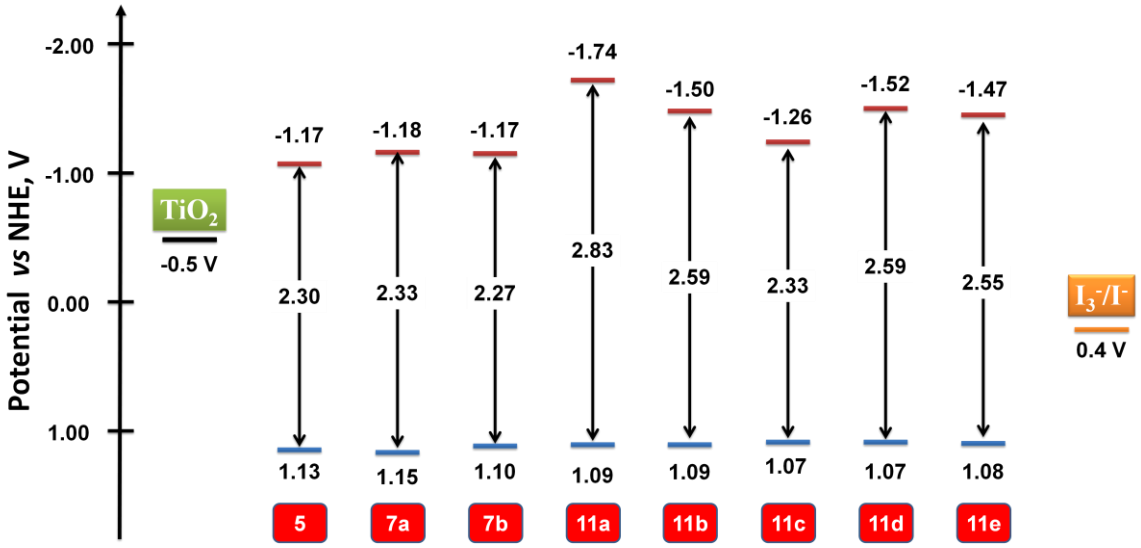

Figure 3.19 Comparison of the energy levels of the dyes (**5**, **7a**, **7b** and **11a-11e**) in the ground and excited states.

3.2.5 DSSC Characteristics

DSSCs were fabricated using the dyes (**7a** and **7b**) as sensitizers, and an electrolyte composed of 0.1 M LiI, 0.6 M 1-propyl-2,3-dimethyl imidazolium iodide (DMPII), 0.05 M I_2, and 0.5 M *tert*-butylpyridine (TBP) in a 1:1 solvent mixture of acetonitrile/3-methoxypropionitrile. The device performance data under AM 1.5, 100 mW cm^{-2} illumination are compiled in Table 3.8.

Table 3.8 Performance parameters of the DSSCs fabricated using the dyes **7a** and **7b**

Dye	J_{SC}, mA cm^{-2}	V_{OC}, mV	*ff*	η (%)	R_{rec}, Ω	R_{ct2}, Ω	f_{max}, Hz	τ_e, ms
7a	15.30	660	0.60	6.05	22.50	17.55	12.74	12.50
7b	18.10	630	0.60	6.83	12.00	14.72	51.05	3.12
7b + A[a]	19.30	628	0.59	7.20	-	13.02	41.88	3.80
7b + B[b]	18.30	620	0.61	6.92	-	13.77	41.88	3.80
7b + C[c]	13.60	616	0.65	5.45	-	18.49	76.03	2.09
N719	19.40	687	0.63	8.36	31.24	9.05	10.42	15.27

[a] 1mM CDCA; [b] 10mM CDCA; [c] 20mM CDCA

The incident photon-to-current conversion efficiencies (IPCE) and the photocurrent-voltage (I-V) curves of the DSSCs are plotted in Figures 3.20 and 3.21, respectively. Both the dyes gave impressive power conversion efficiencies (η = 6.01% and 6.83%) in the DSSCs. The superior performance of the device based on the dye **7b** is originating from the higher short circuit current attributable to the better absorption characteristics of **7b**. The dye **7b** exhibits highest IPCE at shorter wavelength region and the devices produced superior photon conversion up to 520 nm.

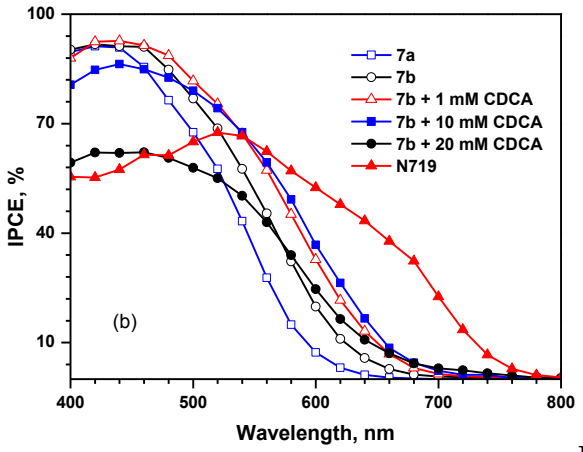

Figure 3.20 IPCE spectra of the devices fabricated using the dyes **7a** and **7b**.

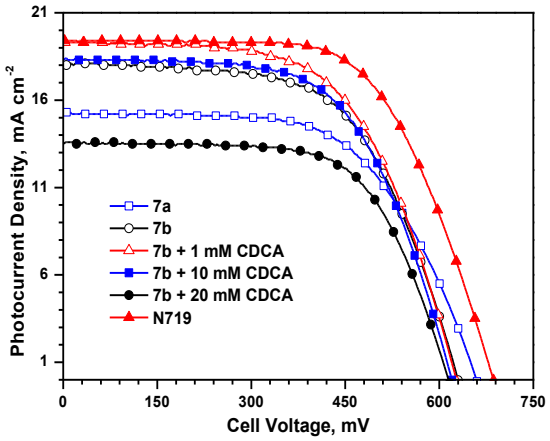

Figure 3.21 I-V Characteristics of the devices fabricated using the dyes **7a** and **7b**.

The devices were studied by electrochemical impedance spectroscopy (EIS) to understand the kinetics of electron transfer at the interfaces. The Nyquist and Bode phase plots observed for the devices under illumination are displayed in Figures 3.22 and 3.23 and the relevant data listed in Table 3.8. They display three semicircles for all DSSCs and each semicircle corresponds to the resistance experienced at a particular interface of the components present in the DSSC device. The bigger semicircle in the Nyquist plot

(Figure 3.22) corresponds to the electron transport resistance (R_{ct2}) at TiO_2/dye/interface and the calculated value is smaller for the device with **7b**. It further lowered on addition of chenodexoycholic acid (CDCA) up to 10 mM. Smaller R_{ct2} indicates a favourable electron collection at the photoanode which results in a high photocurrent. This is attributable to the thermodynamically more favourable LUMO in **7b** (Figure 3.19) [41]. The electron lifetime extracted from the angular frequency (ω_{min}) at the mid-frequency peak in the Bode phase plot (Figure 3.23) using $\tau_e = 1/\omega_{min}$, significantly small for the devices fabricated using **7b** which suggests faster charge recombination and larger dark current leading to comparatively low open circuit voltage. Slight enhancement in the electron lifetime was observed on the addition of CDCA. It probably indicates that the addition of CDCA inhibits the intermolecular dye association at the surface of TiO_2 [86].

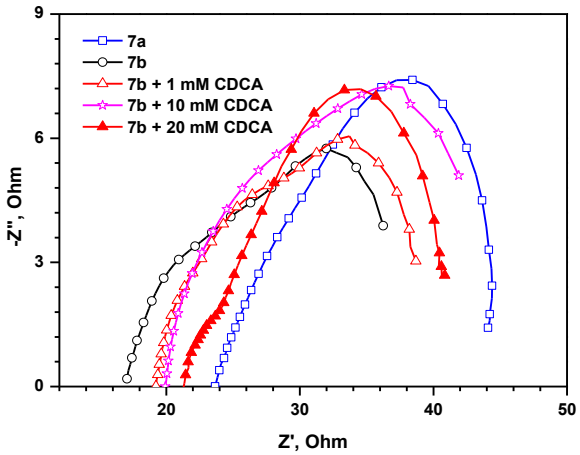

Figure 3.22 Nyquist plots observed for the DSSCs measured under illumination.

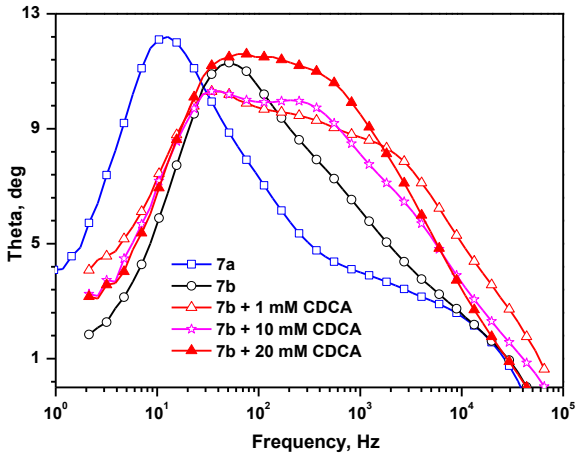

Figure 3.23 Bode-phase plots observed for the DSSCs measured under illumination.

Generally, dye aggregation at the surface of TiO_2 reduces the electron lifetime and facilitates charge recombination in the DSSCs fabricated using organometallic or organic dyes [86]. To examine the possibility of dye aggregation, DSSCs were fabricated with various amounts of CDCA co-adsorbed photoanodes. The photocurrent density and power conversion efficiency increased on addition of 1 mM CDCA to the dye solution. However, on addition of higher amounts (10 mM or 20 mM) of CDCA to the dye solution reduced the V_{OC} and J_{SC} which led to comparatively low power conversion efficiency than that observed for the dye alone (Table 3.8). This outcome can be rationalized by the following explanations: (1) pure dye solution leads to aggregation of the dyes on the TiO_2 electrode which causes inefficient electron injection; (2) an optimum amount of CDCA (1 mM) is sufficient to impede the dye aggregation; (3) the high CDCA concentration

reduces the adsorbed amount of the dye on TiO_2 films and the ability to harvest light. As a consequence, the highest η value of 7.20% has been obtained when 1 mM CDCA was present in the dye solution.

In order to investigate the durability of the photoanodes sensitized with **7b** or **7b**/CDCA, DSSCs were also fabricated using binary-ionic liquid electrolyte composed of 1-methyl-3-propylimidazolium iodide (PMII) and 1-ethyl-3-methylimidazolium tetrafluoroborate (EMIBF4) (65:35) in 0.2 M I_2 and 0.5 M TBP due to their advantages such as negligible vapor pressure, high thermal stability, wide electrochemical window, and high ionic conductivity [87]. Though these DSSCs based on ionic liquid electrolytes and sensitized with **7b** or **7b**/CDCA showed slightly lower power conversion efficiencies (4.06% and 4.59%, respectively) than the liquid DSSCs, they were found to be stable for long term up to the tested 1000 h (Figure 3.25). These results indicate that the photoanodes sensitized with **7b** or **7b**/CDCA can survive for long duration without significant loss in overall conversion efficiency.

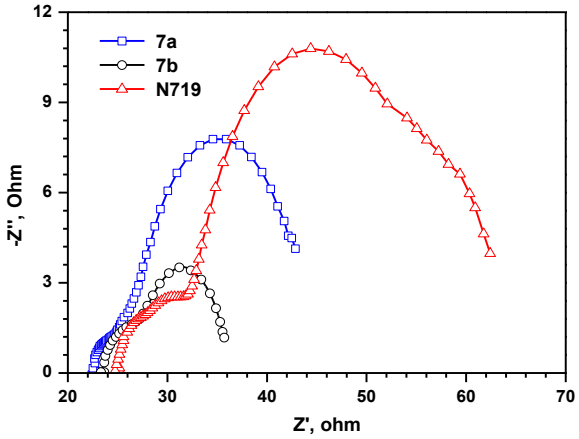

Figure 3.24 Nyquist plots observed for the DSSCs measured under dark conditions.

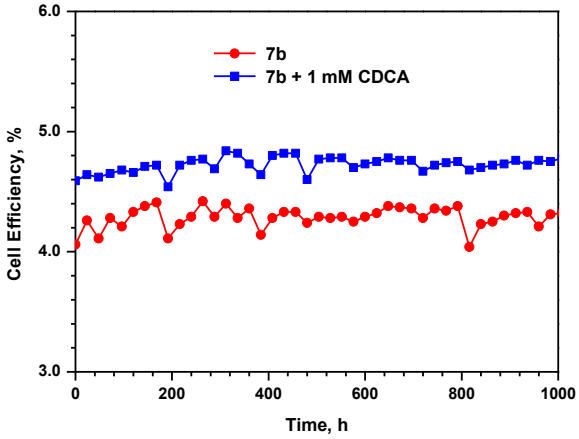

Figure 3.25 Stability data of DSSCs with **7b** and with **7b**/CDCA, obtained at different times for 1,000 h.

The photovoltaic performances of the dyes (**11b-11e**) are listed in Table 3.9. The IPCE action spectra and *J-V* curve of the devices are shown in Figures 3.26 and 3.27. Incident photon current conversion spectrum (IPCE) is the conversion of incident photons to electrons generated in the external circuit. The broader and higher IPCE values are required for higher photocurrent generation and better power conversion efficiency. The dye **11d** showed lower IPCE due to lower molar extinction coefficient. The dyes **11b** and **11c** showed higher conversion efficiencies of 80% and 70% at 420 nm and showed onset at 650 nm. The dye **11c** showed more than 70% IPCE from 400-520 nm and it reaches

maximum (82%) at 440 nm with onset around 710 nm. This indicates that **11c** has better light harvesting property compared to other dyes owing to the red shifted absorption.

Table 3.9 Photovoltaic performance parameters of the DSSCs fabricated using the dyes

Dye	η (%)	V_{OC}, mV	J_{SC}, mA cm^{-2}	*ff*	R_{rec}, ohm	R_{ct2}, ohm	τ_e, ms
11b	3.08	574.6	8.29	0.65	31.97	33.17	1.16
11c	4.88	582.6	13.08	0.64	39.90	23.38	3.12
11d	3.12	632.2	7.35	0.67	42.81	37.78	8.41
11e	2.46	566.7	7.70	0.57	30.34	34.58	1.16
N719	7.88	732.1	16.57	0.65	-	-	-

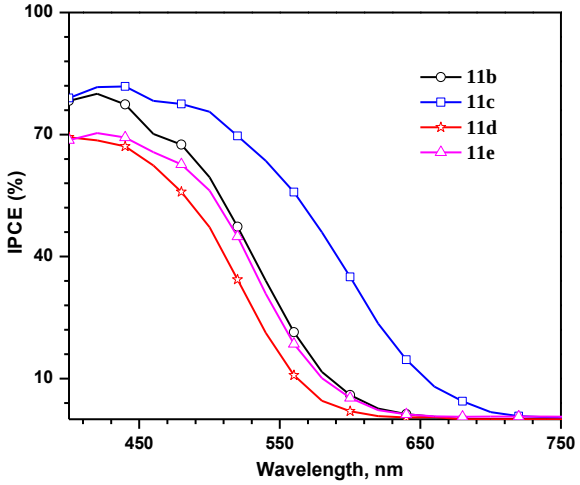

Figure 3.26 IPCE spectra of the devices fabricated using the dyes (**11b-11e**).

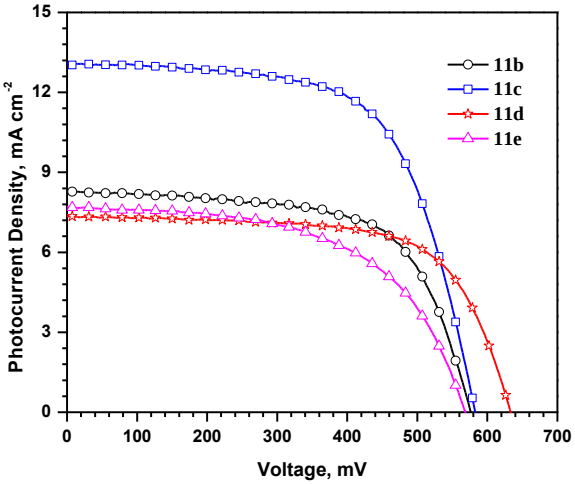

Figure 3.27 I-V characteristics of the devices fabricated using the dyes (**11b-11e**).

Efficiency of the dyes follows the order **11e** < **11d** < **11b** < **11c.** Highest conversion efficiency of 4.88% for **11c** (J_{SC} = 13.08 mA cm^{-2}, V_{OC} = 583 mV and *ff* = 0.64) owing to broad light harvesting property of the dye. The inferior performance of the dye **11e** (η = 2.4%) is due to the poor absorption in the visible region. The dye **11d** which have fluorene linker shows higher conversion efficiency of 3.12% (J_{SC} = 7.35 mA cm^{-2}, V_{OC} = 632 mV) compared to the dye **11e** which contain carbazole (η = 2.46%, J_{SC} = 7.70 mA cm^{-2} and V_{OC} = 567 mV). In case of **11d,** higher V_{OC} obtained due to two alkyl chains present on fluorene which suppress the aggregation of the dyes effectively [88]. The short circuit current density for the dyes follows the order of **11d** < **11e** < **11b** < **11c** and it follows the order of absorption of the dyes. Higher absorption maxima and broad spectral

response of the dye **11c** results highest J_{SC} among other dyes. The J_{SC} and efficiency are following the same order.

The interfacial charge transport resistance greatly governs the efficiency of the device made with dye sensitizer for DSSC. To scrutinize the effect of electron transport resistance, we measured the EIS under forward bias with a frequency range from 10 mHz to 65 KHz and amplitude of 10 mV. Figure 3.28 shows Nyquist plots of dyes under dark conditions. In principle, Nyquist plot shows three semicircles which corresponds the charge transfer resistance at Pt electrode/electrolyte interface, charge recombination resistance (R_{rec}) at TiO_2/dye/electrolyte interface and Warburg diffusion of I^- in the electrolyte interface respectively. Radius of the larger semicircle corresponds to R_{rec} indicates the recombination of injected electrons to conduction band of TiO_2 with oxidized species (I_3^-) of electrolyte, called as dark current. It was found that fluorene has great potential to suppress back electron transfer and good electronic communication compared to phenyl and carbazole linkers [88]. The R_{rec} order of the dyes follows order of **11e** < **11b** < **11c** < **11d**. Probably, the alkyl groups on C9 position of fluorene provides a hydrophobic environment to repel the ionic electrolyte from approaching TiO_2 surface. The dark current of **11e** is more which is not favourable for good performance of DSSC.

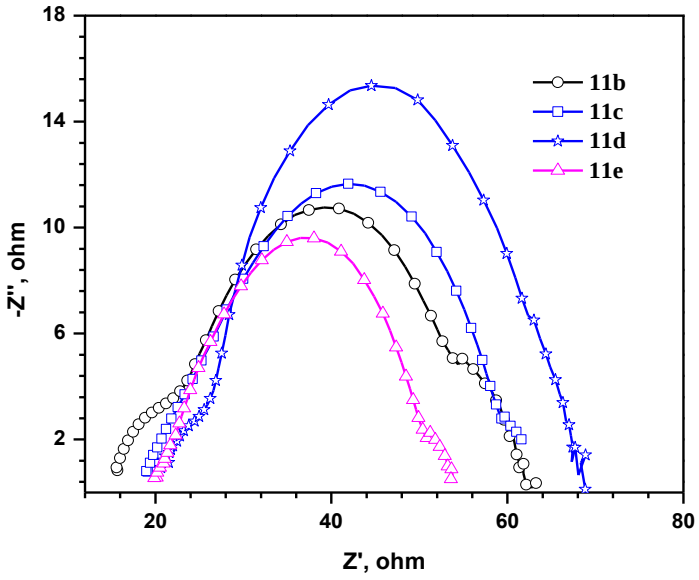

Figure 3.28 Nyquist plots observed for the DSSCs under dark.

Figures 3.29 and 3.30 shows Nyquist and Bode phase plots of the dyes under illumination which are useful to find out the electron transfer resistance (R_{ct2}) at the interface of TiO_2/dye/electrolyte and observed order is **11c** < **131** < **11e** < **11d**. The lower

R_{ct2} of **11c** is due to good electronic coupling of dye with TiO_2, more planarity of linker results good donor-acceptor could certainly inject the electron efficiently to conduction band of TiO_2, considerably increases the efficiency of DSSC. The Bode phase plot shows two peaks and lower frequency corresponds to the larger semicircle observed in Nyquist plot, reciprocal of lower frequency relates to the lifetime of the electron and it can be calculated by $\tau_e = 1/\omega_{min}$. The lifetime (τ_e) order of the dyes follows as order **11b** (1.16 ms) ≈ **11e** (1.16 ms) < **11c** (3.12 ms) < **11d** (8.41 ms), suggesting that the ethyl groups of fluorene forms blocking and its suppress the back electron transfer which help to improve the efficiency of DSSC. The lowest τ_e of carbazole linker dye **11e** compared to its analogous linker of fluorene due to more dark current experienced by device and led to inferior performance of the dye.

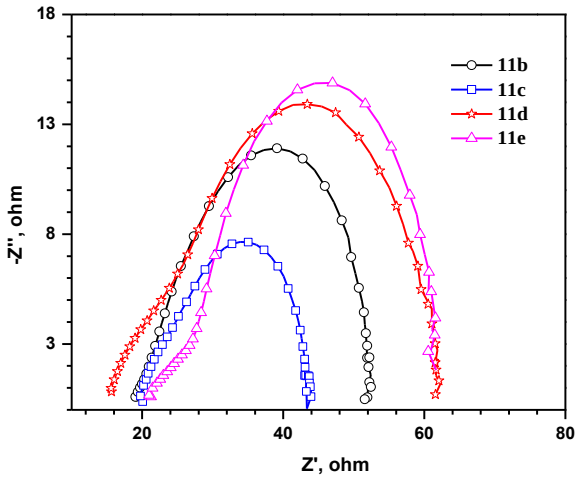

Figure 3.29 Nyquist plots observed for the DSSCs measured under illumination.

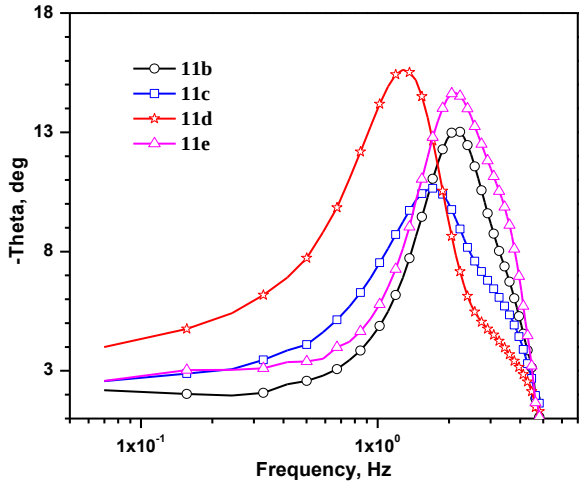

Figure 3.30 Bode-phase plots observed for the DSSCs measured under illumination.

3.3 Conclusions

A series of 2,7-disubstituted carbazole based dyes containing diphenylamine donor, 2,7-carbazole and oligothiophene in the conjugation pathway and cyanoacrylic acid acceptor are described. They possess red-shifted absorption with high molar extinction coefficient when compared to the corresponding dyes with fluorene or phenyl units in the conjugation. The dyes with oligothiophene conjugation shows bathochromically shifted absorption when compared to the dye containing phenyl linker attributable to the electron richness of the former one. The *para*-conjugation of phenyl linker red shifted absorption compared to *meta*-congener due to delinking of donor and acceptor interactions for the later dye. The introduction of fluorene (**10d**) and carbazole (**10e**) linker enhances the

molar extinction coefficients while terthiophene (**10c**) red-shifted the absorption when compared to the dye (**7a**) with a thiophene linkage. The DSSC fabricated using the dye **7b** as sensitizer exhibited power conversion efficiencies of 6.8% which increased to 7.2% when chenodexoycholic acid (CDCA) is used to impede dye aggregation. The DSSCs with ionic liquid electrolytes displayed marked stability over 1000 h for the dye **7b**. For dye **10d**, two ethyl chains of fluorene linker helps to minimize the intermolecular interactions and resulted in higher open circuit voltage (V_{OC}) compared to phenyl and carbazole containing dyes. Electrochemical impedance spectroscopy was used to characterize the interfacial charge transfer and electron recombination kinetics.

3.4 Experimental Section

3.4.1 General Experimental Methods

All the chemicals were purchased from readily available commercial sources and used as such without further purification. All the Solvents were dried by standard procedures prior to use. Column chromatography purifications were performed with the use of silica gel (230-400 mesh) as a stationary phase in a column with 40 cm long and 3.0 cm diameter. The IR spectra were recorded with a NEXUS FT-TR spectrometer (Thermo nicolet) by using KBr pellets. The ^{1}H and ^{13}C NMR spectra were recorded with a Bruker (Bruker Avance 3) spectrometer operating at 500.13 and 125.77 MHz respectively. Deuterated chloroform ($CDCl_3$) and dimethyl sulfoxide (DMSO-d_6) were used as solvent with residual peak at δ 7.26 and 2.52 for ^{1}H; 77.0 and 39.5 for ^{13}C, respectively. UV-Vis spectra were recorded in Tol, DCM, CH, DMF, ACN, THF solvents at room temperature in quartz cuvettes using a Cary spectrophotometer (Cary 100). Emission spectra were recorded using a spectro fluorophotometer at room temperature. The cyclic voltammetry (CV) and differential pulse voltammetry (DPV) performed with epsilon (Basi epsilon) electrochemical analyzer instrument using a glassy carbon working electrode, a non-aqueous $Ag/AgNO_3$ reference electrode. The experiments were performed at room temperature under nitrogen atmosphere in DCM using 0.1 M tetrabutylammonium perchlorate (Bu_4NClO_4) as supporting electrolyte. The $E_{1/2}$ values were determined as ($E_p^a + E_p^c$)/2, where E_p^a and E_p^c are the anodic and cathodic peak potentials, respectively. The high resolution mass spectra were obtained from a Bruker Daltoniks GmBH (micrOTOF-QII) ESI mass spectrometer in the positive ion mode.

3.4.2 Computational Methods

Gaussian 09 program package was used to perform all the computations [89]. The ground-state geometries were fully optimized without any symmetry constraints using DFT employing a Becke's [90] hybrid correlation functional B3LYP [82] with 6-31g (d,p) basis set for all atoms. Vibrational analysis on the optimized structures was performed to confirm the structure. The excitation energies and oscillator strengths for the lowest 10 singlet-singlet transitions at the optimized geometry in the ground state were obtained by TD-DFT calculations using the same basis set with two different kinds of hybrid functionals namely B3LYP [82] and MPW1K [83].

3.4.3 Device Fabrication and Characterization

A fluorine-doped SnO_2 conducting glass (FTO, 7 Ω sq^{-1}, transmittance ~ 80%, NSG America, Inc., New Jersey, USA) was first cleaned with a neutral cleaner, and then washed with deionized water, acetone, and isopropyl alcohol, sequentially. The conducting surface of the FTO was treated with a solution of titanium tetraisopropoxide (1 g) in 2-methoxyethanol (3 g) for obtaining a good mechanical contact between the conducting glass and TiO_2 film, as well as to isolate the conducting glass surface from the electrolyte. TiO_2 paste was coated onto the treated conducting glass by rolling a metal strip over it (doctor blade technique). After coating each TiO_2 layer, the dried TiO_2 film was gradually heated to 450 °C in an oxygen atmosphere, and subsequently sintered at that temperature for 30 min. The TiO_2 photo-anodes of the DSSCs employed in the experiments were composed of a 14 μm thick transparent TiO_2 layer with a scattering layer of 4.5 μm thickness. After sintering at 450 °C and cooling to 80 °C, the TiO_2 film was immersed in a 3×10^{-4} M solution of dye at room temperature for 24 h. **N719** (Solaronix S.A., Aubonne, Switzerland) was dissolved in acetonitrile (ACN) and *tert*-butyl alcohol (volume ratio of 1:1) and used as a standard dye solution for device optimization. The solutions of the dyes were prepared in a mixing solvent containing ACN, *tert*-butyl alcohol and dimethyl sulfoxide (DMSO) (volume ratio of 1:1:3). Then the photoanode (FTO/TiO_2/dye) was placed on a platinum-sputtered conducting glass electrode (ITO, 7 Ω sq^{-1}, Ritek Corporation, Hsinchu, Taiwan), keeping the two electrodes separated by a 25 μm-thick surlyn® (SX1170-25, Solaronix S.A., Aubonne, Switzerland). The two electrodes were then sealed by heating. A mixture of 0.1 M LiI, 0.6 M 1-propyl-2,3-dimethylimidazolium iodide (DMPII), 0.05 M I_2, and 0.5 M *tert*-

butylpyridine (TBP) in 3-methoxypropionitrile (MPN)/CAN (volume ratio of 1:1) was used as the electrolyte. The electrolyte was injected into the gap between the electrodes by capillarity; the electrolyte-injecting hole was previously made in the counter electrode with a drilling machine, and the hole was sealed with hot-melt glue after the injection of the electrolyte. Surface of the DSSC was covered by a mask with a light illuminated area of 0.16 cm^2 and then illuminated by a class-A quality solar simulator (XES-301S, AM 1.5 G, San-Ei Electric Co., Ltd.). Incident light intensity (100 mW cm^{-2}) was calibrated with a standard Si Cell (PECSI01, Peccell Technologies, Inc.). Photocurrentevoltage curves of the DSSCs were obtained with a potentiostat/galvanostat (PGSTAT 30, Autolab, Eco-Chemie, The Netherlands). The thickness of the TiO_2 film was judged by scanning electron microscopic images (SEM, NanoSEM 230, Novat). For UV-absorption spectra, dye molecules were coated on the TiO_2 films and the corresponding spectra were obtained using an UV-visible spectrophotometer (V-570, Jasco, Japan) equipped with a total integrating sphere. Electrochemical impedance spectra (EIS) were obtained by the above-mentioned potentiostat/galvanostat, equipped with an FRA2 module, under a constant light illumination of 100 mW cm^{-2}. The frequency range explored was 10 mHz-65 kHz. The applied bias voltage was set at the open circuit voltage of the DSSC, between the ITO-Pt counter electrode and the FTO-TiO_2-dye working electrode, starting from the short circuit conditions; the corresponding AC amplitude was 10 mV. The impedance spectra were analyzed using an equivalent circuit model. Incident photo-to-current conversion efficiency (IPCE) curves were obtained under short-circuit conditions. The light source was a class A quality solar simulator (PEC-L11, AM 1.5 G, Peccell Technologies, Inc.); light was focused through a monochromator (Oriel Instrument, model 74100) onto the photo-voltaic cell. The monochromator was incremented through the visible spectrum to generate the IPCE (λ) as defined by IPCE (λ) = 1240 ($J_{SC}/\lambda\varphi$), where λ is the wavelength, J_{SC} is short-circuit photocurrent density (mA cm^{-2}) recorded with a potentiostat/galvanostat, and is the incident radiative flux (W m^{-2}) measured with an optical detector (Oriel Instrument, model 71580) and a power meter (Oriel Instrument, model 70310).

3.4.3 Synthesis

2,7-Dibromo-9-butyl-9*H*-carbazole (**1**) [61, 62], 5'-bromo-2,2'-bithiophene-5-carbaldehyde [91] and 7-bromo-9,9-diethyl-9*H*-fluorene-2-carbaldehyde [56] were synthesized according to the reported procedure.

7-Bromo-9-butyl-*N*,*N*-diphenyl-9*H*-carbazol-2-amine, 3. A mixture of 2,7-dibromo-9-butyl-9*H*-carbazole (3.81 g, 10 mmol), diphenylamine (**2**, 0.85 g, 5 mmol), pd(dba)$_2$ (0.03 g, 0.10 mmol), dppf (0.03 g, 0.10 mmol), sodium *tert*-butoxide (1.20 g, 12.5 mmol), and toluene (10 mL) taken in a pressure tube was heated at 80 °C for 48 h under N_2 atmosphere. After completion of the reaction, the volatiles were removed under vacuum, and the resulting solution was extracted with DCM (3 × 50 mL). The combined organic extract washed with brine solution, dried over Na_2SO_4, and concentrated. Further the crude product was purified by column chromatography on silica gel by using hexanes/DCM mixture (5:1) as an eluent. White solid; Yield 1.83 g (78%); mp 86 °C; ^{1}H NMR ($CDCl_3$, 500.13 MHz) 7.91 (d, *J* = 8.5 Hz, 1H), 7.86 (d, *J* = 8.0 Hz, 1H), 7.50 (d, *J* = 1.5 Hz, 1H), 7.32 (d, *J* = 2.0 Hz, 2H), 7.28 (m, 3H), 7.17 (dd, *J* = 7.5 Hz, 1.0 Hz, 4H), 7.10 (d, *J* = 2.0 Hz, 1H), 7.05 (t, *J* = 6.5 Hz, 2H), 7.00 (dd, *J* = 8.5 Hz, 1.5 Hz, 1H), 4.11 (t, *J* = 7.0 Hz, 2H), 1.75 (m, 2H), 1.32 (m, 2H), 0.90 (t, *J* = 7.5 Hz, 3H); ^{13}C NMR ($CDCl_3$, 125.77 MHz) δ 148.22, 146.74, 141.80, 141.71, 129.40, 124.08, 122.68, 122.11, 121.97, 120.97, 120.90, 118.43, 118.09, 117.86, 117.45, 42.83, 31.01, 20.50, 13.92; HRMS calcd for $C_{28}H_{25}BrN_2Na$ $[M + Na]^+$ *m/z* 491.1093, found 491.1109.

4-(9-Butyl-7-(diphenylamino)-9*H*-carbazol-2-yl)benzaldehyde, 4. A two neck RB flask charged with a mixture of **3** (0.47 g, 1 mmol), 4-formylphenylboronic acid (0.18 g, 1.2 mmol), anhydrous K_2CO_3 (0.48 g, 3.5 mmol) and $Pd(PPh_3)_4$ (0.04 g, 0.03 mmol) were dissolved in mixture of THF/H_2O (3:1). The reaction mixture was degassed with N_2 and refluxed for 12 h under nitrogen atmosphere. After cooling to room temperature, the organic layer extracted with DCM and dried with sodium sulfate. The crude product was purified by column chromatography on silica gel by using a hexane/ DCM mixture (2:1) as eluent. Yellow solid; Yield 0.38 g (76%); mp 180 °C; IR (KBr, cm^{-1}) 1692 ($\nu_{C=O}$); ^{1}H NMR ($CDCl_3$, 500.13 MHz) δ 10.07 (s, 1H), 8.06 (d, *J* = 8.0 Hz, 1H), 7.98 (d, *J* = 8.0 Hz, 2H), 7.94 (d, *J* = 8.5 Hz, 1H), 7.87 (d, *J* = 8.5 Hz, 2H), 7.56 (d, *J* = 1.5 Hz, 1H), 7.47 (dd, *J* = 8.0 Hz, 1H), 7.25-7.28 (m, 4H), 7.12-7.17 (m, 4H), 7.11-7.12 (m, 1H), 7.00-7.04 (m, 2H), 6.99-7.00 (m, 1H), 4.19 (t, *J* = 7.0 Hz, 2H), 1.77 (sept, *J* = 8.0 Hz, 2H), 1.31 (sept, *J* = 2.5 Hz, 2H), 0.88 (t, *J* = 7.0 Hz, 3H); ^{13}C NMR ($CDCl_3$, 125.77 MHz) δ 191.98, 148.38, 148.20, 146.80, 142.37, 141.34, 136.46, 134.89, 130.32, 129.21, 128.97, 127.98, 124.09, 123.28, 122.65, 121.14, 120.21, 118.72, 118.11, 117.23, 107.29, 104.80, 42.71, 31.13, 20.50, 13.89; HRMS calcd for $C_{35}H_{30}N_2O$ $[M]^+$ *m/z* 494.2352, found 494.2375.

5-(9-Butyl-7-(diphenylamino)-9*H*-carbazol-2-yl)thiophene-2-carbaldehyde, 6a. A mixture of **3** (0.94 g, 2 mmol) and (5-(1,3-dioxolan-2-yl)thiophen-2-yl)tributylstannane (0.98 g, 2.2 mmol) was dissolved in dry DMF (5 mL) and degassed with nitrogen, and add $Pd(PPh_3)_2Cl_2$ (0.02 g, 0.02 mmol). The reaction mixture was heated at 80 ℃ for 15 h. After cooling the reaction mixture poured into water. The organic compound extracted with DCM (3 × 40 mL). The combined organic extract washed with brine solution, dried over Na_2SO_4, and concentrated to leave yellow solid. The yellow solid dissolved in 5 mL of acetic acid and heated at 65 °C for 2 h. Added 5 mL of water and continued the heating for 2 h. Extracted the organic layer with DCM and dried over Na_2SO_4. Further the crude product was purified by column chromatography on silica gel by using hexane/DCM mixture (1:1) as an eluent: Yellow solid; Yield 0.95 g (95%); mp 125 ℃; IR (KBr, cm^{-1}) 1657 ($\nu_{C=O}$); ^{1}H NMR ($CDCl_3$, 500.13 MHz) δ 9.88 (s, 1H), 7.98 (d, *J* = 7.0 Hz, 1H), 7.90 (d, *J* = 8.5 Hz, 1H), 7.75 (d, *J* = 4.0 Hz, 1H), 7.59 (s, 1H), 7.49 (dd, *J* = 13.0 Hz, 4.0 Hz, 2H), 7.28 (s, 2H), 7.25 (d, *J* = 3.5 Hz, 2H), 7.16 (d, *J* = 8.0 Hz, 4H), 7.09 (s, 1H), 7.03 (t, *J* = 7.5 Hz, 2H), 6.97-6.99 (m, 1H), 4.15 (t, *J* = 7.0 Hz, 2H), 1.72-1.78 (m, 2H), 1.28-1.34 (m, 2H), 0.88 (t, *J* = 7.0 Hz, 3H); ^{13}C NMR ($CDCl_3$, 125.77 MHz) δ 156.09, 148.11, 147.14, 142.59, 141.81, 141.07, 137.67, 129.52, 129.26, 124.23, 124.20, 123.74, 122.81, 121.21, 120.28, 117.96, 117.80, 117.26, 106.38, 104.55, 42.72, 31.09, 20.48, 13.88; HRMS calcd for $C_{33}H_{28}N_2OSNa$ $[M + Na]^+$ *m/z* 523.1814, found 523.1836.

5-(5-(9-Butyl-7-(diphenylamino)-9*H*-carbazol-2-yl)thiophen-2-yl)thiophene-2-carbaldehyde, 6b. Compound **6b** synthesized from **3** (0.47 g, 1 mmol) and (5-(5-(1,3-dioxolan-2-yl)thiophen-2-yl)thiophen-2-yl)tributylstannane (0.58 g, 1.1 mmol) mixture by following a procedure similar to that described above for **6a.** Red solid; Yield 0.46 g (79%); mp 151 °C; IR (KBr, cm^{-1}) 1647 ($\nu_{C=O}$); ^{1}H NMR ($CDCl_3$, 500.13 MHz) δ 9.87 (s, 1H), 7.98 (d, *J* = 7.5 Hz, 1H), 7.91 (d, *J* = 8.5 Hz, 1H), 7.69 (d, *J* = 4.0 Hz, 1H), 7.53 (d, *J* = 1.5 Hz, 1H), 7.47 (dd, *J* = 8.0 Hz, 1H), 7.37 (dd, *J* = 10.5 Hz, 4.0 Hz, 2H), 7.28-7.30 (m, 2H), 7.27 (d, *J* = 1.0 Hz, 2H), 7.25 (d, *J* = 2.0 Hz, 1H), 7.16 (dd, *J* = 8.5 Hz, 1.0 Hz, 4H), 7.09 (d, *J* = 1.5 Hz, 1H), 7.01-7.05 (m, 2H), 6.98 (d, *J* = 8.0 Hz, 1.5 Hz, 1H), 4.18 (t, *J* = 7.0 Hz, 2H), 1.75-1.79 (m, 2H), 1.30-1.34 (m, 2H), 0.89 (t, *J* = 7.0 Hz, 3H); ^{13}C NMR ($CDCl_3$, 125.77 MHz) δ 171.88, 148.16, 147.81, 147.47, 146.75, 142.38, 141.36, 141.19, 137.49, 134.52, 130.14, 129.20, 127.26, 124.09, 123.90, 123.82, 123.22, 122.65, 120.99, 120.22, 118.23, 117.46, 117.27, 105.68, 104.76, 42.68, 31.09, 20.48, 13.88; HRMS calcd for $C_{37}H_{30}N_2OS_2$ $[M]^+$ *m/z* 582.1794, found 582.1772.

(*E*)-3-(4-(9-Butyl-7-(diphenylamino)-9*H*-carbazol-2-yl)phenyl)-2-cyanoacrylic acid, 5. The aldehyde **4** (0.16 g, 0.33 mmol), 2-cyanoacetic acid (0.04 g, 0.5 mmol), ammonium acetate (0.04 g, 0.25 mmol), and acetic acid (5 mL) were mixed and refluxed for 24 h. The resulting red precipitate was filtered and washed several times with water and dried. It was crystallized from hexane/DCM mixture to obtain the analytically pure sample. Yellow solid; Yield 0.55 g (94%); mp 170 °C; IR (KBr, cm^{-1}) 2221 ($\nu_{C\equiv N}$); ^{1}H NMR ($CDCl_3$, 500.13 MHz) δ 8.40 (s, 1H), 8.17-8.21 (m, 2H), 8.01-8.15 (m, 2H), 8.00 (s, 1H), 7.85-7.89 (m, 1H), 7.64 (dd, *J* = 8.5 Hz, 1.5 Hz, 1H), 7.55-7.56 (m, 1H), 7.31 (m, 4H), 7.19 (d, *J* = 2.0 Hz, 1H), 7.04-7.10 (m, 6H), 6.88-6.91 (m, 1H), 4.34 (t, *J* = 6.0 Hz, 2H), 1.67-1.69 (m, 2H), 1.19-1.24 (m, 2H), 0.67-0.83 (m, 3H); ^{13}C NMR ($CDCl_3$, 125.77 MHz) δ 163.41, 152.81, 147.63, 147.57, 146.00, 145.07, 141.88, 141.05, 135.37, 131.20, 130.30, 129.40, 127.96, 127.86, 127.52, 127.37, 122.71, 122.58, 122.41, 121.48, 120.27, 118.11, 117.66, 116.85, 116.57, 107.51, 105.08, 104.84, 41.70, 30.60, 19.70, 13.64; HRMS calcd for $C_{38}H_{31}N_3O_2Na$ $[M + Na]^+$ *m/z* 584.2308, found 584.2301.

(*E*)-3-(5-(9-Butyl-7-(diphenylamino)-9*H*-carbazol-2-yl)thiophen-2-yl)-2-cyanoacrylic acid, 7a. Compound **7a** was obtained from **6a** (0.57 g, 1 mmol) by following a procedure similar to that described above for **5**. Red solid; Yield 0.41 g (83%); mp 240 °C; IR (KBr, cm^{-1}) 2212 ($\nu_{C\equiv N}$); ^{1}H NMR ($CDCl_3$, 500.13 MHz) δ 8.37 (s, 1H), 8.00 (d, *J* = 3.0 Hz, 1H), 7.92 (d, *J* = 8.5 Hz, 1H), 7.82 (d, *J* = 4.0 Hz, 1H), 7.62 (d, *J* = 1.0 Hz, 1H), 7.53-7.57 (m, 2H), 7.28-7.29 (m, 4H), 7.16-7.18 (m, 4H), 7.08 (d, *J* = 1.5 Hz, 1H), 7.04 (t, *J* = 7.5 Hz, 2H), 6.98-7.00 (m, 1H), 4.19 (t, *J* = 8.0 Hz, 2H), 1.77 (quintet, *J* = 7.5 Hz, 2H), 1.25-1.31 (m, 2H), 0.87-0.90 (m, 3H); ^{13}C NMR (DMSO-d_6, 125.77 MHz) δ 147.98, 146.95, 142.65, 141.26, 134.59, 129.93, 129.44, 125.48, 124.22, 123.88, 123.38, 122.10, 121.06, 118.17, 118.00, 117.13, 107.07, 105.07, 42.24, 31.03, 20.16, 14.08; HRMS calcd for $C_{36}H_{29}N_3O_2SNa$ $[M + Na]^+$ *m/z* 590.1872, found 590.1855.

(*E*)-3-(5-(5-(9-Butyl-7-(diphenylamino)-9*H*-carbazol-2-yl)thiophen-2-yl)thiophen-2-yl)-2-cyanoacrylic acid, 7b. Compound **7b** was obtained from **6b** (0.29 g, 0.5 mmol) by following a procedure similar to that described above for **5**. Black solid; Yield 0.28 g (85%); mp 265 °C; IR (KBr, cm^{-1}) 2208 ($\nu_{C\equiv N}$); ^{1}H NMR (DMSO-d_6, 500.13 MHz) δ 8.50 (s, 1H), 8.05-8.11 (m, 2H), 8.00 (d, *J* = 3.5 Hz, 1H), 7.92 (s, 1H), 7.64-7.77 (m, 3H), 7.55 (d, *J* = 7.5 Hz, 1H), 7.31-7.34 (m, 4H), 7.17 (s, 1H), 7.05-7.09 (m, 6H), 6.88 (d, *J* = 8.5 Hz, 1H), 4.31 (m, 3H), 1.67 (t, *J* = 14.0 Hz, 2H), 1.19-1.23 (m, 2H), 0.81 (t, *J* = 7.5 Hz, 3H); ^{13}C NMR (DMSO-d_6, 125.77 MHz) δ 163.65, 147.53, 146.87, 146.27, 145.99,

145.81, 141.89, 141.62, 140.86, 133.69, 133.50, 129.56, 129.39, 128.36, 125.21, 124.67, 123.54, 122.71, 122.35, 121.35, 120.38, 117.75, 117.03, 116.64, 105.82, 104.81, 97.87, 41.68, 30.60, 19.69, 13.65; HRMS calcd for $C_{40}H_{31}N_3O_2S_2$ $[M]^+$ *m/z* 649.1852, found 649.1852.

7-bromo-9-Butyl-9*H*-carbazole-2-carbaldehyde, 8. A solution of 2,7-dibromo-9-butyl-9*H*-carbazole (**1**, 3.78 g, 10 mmol) in dry THF (60 mL) was cooled to -78 °C and a solution of *n*-butyl lithium in hexane (7.0 mL, 1.6 M) was added drop wise over 15 minutes. After the addition was over, it was stirred for additional 1 h and treated with DMF (1.5 mL). The reaction mixture was slowly allowed to attain room temperature and continued to stir overnight. Finally, the volatiles were removed by vacuum evaporation and the residue triturated with aqueous ammonium chloride solution. The organic soluble content was extracted with DCM, dried over anhydrous sodium sulfate and evaporated to yield the crude product. It was purified by column chromatography on silica gel by using hexane/ DCM (2:3) as an eluent. White solid; Yield: 0.99 g (30%); mp 90-92 °C; IR (KBr, cm^{-1}) 1692 ($\nu_{C=O}$) ; ^{1}H NMR ($CDCl_3$, 500.13 MHz) δ 10.16 (s, 1H), 8.17 (d, *J* = 8.0 Hz, 1H), 7.95-8.00 (m, 2H), 7.75-7.76 (m, 1H), 7.60 (s, 1H), 7.38 (dd, *J* = 8.5 Hz, 1.5 Hz, 1H), 4.32 (t, *J* = 7.5 Hz, 2H), 1.86 (quin, *J* = 7.5 Hz, 2H), 1.42 (quin, *J* = 3.0 Hz, 2H), 0.97 (t, *J* = 7.5 Hz, 3H); ^{13}C NMR ($CDCl_3$, 125.77 MHz) δ 192.55, 142.89, 140.28, 134.13, 127.54, 122.90, 122.59, 121.82, 121.54, 120.83, 120.63, 112.34, 109.81, 43.32, 31.10, 20.58, 13.89; HRMS calcd for $C_{17}H_{17}BrNO$ $[M + H]^+$ *m/z* 330.0488, found 330.0487.

9-Butyl-*N*,*N*-diphenyl-7-(thiophen-2-yl)-9*H*-carbazol-2-amine, (9). A mixture of 7-bromo-9-butyl-*N*,*N*-diphenyl-9*H*-carbazol-2-amine (**3**, 1.05 g, 4 mmol), tributyl(thiophen-2-yl)stannane (1.87 g, 4.8 mmol), $Pd(PPh_3)_2Cl_2$ (0.03 g, 0.04 mmol) and DMF (5 mL) were sequentially charged into a two neck flask under N_2 atmosphere and heated at 80 °C for 15 h. After cooling, the reaction mixture poured into water. The organic compound extracted with DCM (3 × 40 mL). The combined organic extract washed with brine solution, dried over Na_2SO_4. Further the crude product was purified by column chromatography on silica gel by using hexane/ DCM mixture (4:1) as an eluent. White solid; Yield 1.71 g (91%); mp 119 °C; ^{1}H NMR ($CDCl_3$, 500.13 MHz) δ 7.96 (d, *J* = 7.5 Hz, 1H), 7.91 (d, *J* = 8.5 Hz, 1H), 7.54 (d, *J* = 1.0 Hz, 1H), 7.47 (dd, *J* = 8.5 Hz, 1.5 Hz, 1H), 7.40 (dd, *J* = 3.5 Hz, 1.0 Hz, 1H), 7.24-7.30 (m, 6H), 7.15-7.17 (m, 4H), 7.01-7.13 (m, 2H), 7.01 (dt, *J* = 7.5 Hz, 1.5 Hz, 2H), 6.97 (dd, *J* = 15 Hz, 1.5 Hz, 1H), 4.17 (t, *J* =

7.0 Hz, 2H), 1.75-1.78 (m, 2H), 1.29-1.34 (m, 2H), 0.89 (t, *J* = 7.5 Hz, 3H); ^{13}C NMR ($CDCl_3$, 125.77 MHz) δ 148.25, 146.37, 145.83, 142.18, 141.28, 131.31, 129.15, 128.04, 124.37, 123.94, 122.84, 122.48, 120.85, 120.07, 118.52, 117.75, 117.26, 105.86, 105.01, 42.64, 31.07, 20.46, 13.85; HRMS calcd for $C_{32}H_{28}N_2S$ $[M]^+$ *m/z* 472.1973, found 472.1976.

3-(5-(9-Butyl-7-(diphenylamino)-9*H*-carbazol-2-yl)thiophen-2-yl)benzaldehyde, 10a. A solution of 9-butyl-*N*,*N*-diphenyl-7-(thiophen-2-yl)-9*H*-carbazol-2-amine (**8**, 4.72 g, 10 mmol) in dry THF (60 mL) was cooled to -78 °C. A solution of *n*-butyl lithium (7.0 mL, 1.6 M) added to it with vigorous stirring over 20 minutes. After the addition was over, the resulting mixture was stirred for another 2 h at this temperature and Bu_3SnCl (3.91 g, 12 mmol) was added and the solution stirred at room temperature overnight. The reaction was quenched by the addition of cooled water and the organic product extracted with chloroform (3 × 30 mL). The combined organic extract dried over anhydrous K_2CO_3, and concentrated to leave compound 9-Butyl-*N*,*N*-diphenyl-7-(5-(tributylstannyl)thiophen-2-yl)-9*H*-carbazol-2-amine in a quantitative yield. A mixture of 9-butyl-*N*,*N*-diphenyl-7-(5-(tributylstannyl)thiophen-2-yl)-9*H*-carbazol-2-amine (1.05 g, 1.2 mmol), 3-bromobenzaldehyde (0.19 g, 1 mmol) was dissolved in dry DMF (5 mL) and degassed with nitrogen, and added $Pd(PPh_3)_2Cl_2$ (0.01 g, 0.01 mmol). The reaction mixture was heated at 80 °C for 15 h. After cooling the reaction mixture poured into water. The organic compound extracted with DCM (3 × 40 mL) and dried over Na_2SO_4. Further the crude product was purified by column chromatography on silica gel by using hexane/DCM mixture (1:2) as an eluent. Yellow solid; Yield 0.55 g (96%); mp 151 °C; IR (KBr, cm^{-1}) 1706 ($\nu_{C=O}$); ^{1}H NMR ($CDCl_3$, 500.13 MHz) δ 10.08 (s, 1H), 8.16 (t, *J* = 1.5 Hz, 1H), 7.98 (d, *J* = 8.0 Hz, 1H), 7.92 (dd, *J* = 8.0 Hz, 2.5 Hz, 2H), 7.78-7.80 (m, 1H), 7.56-7.59 (m, 2H), 7.51 (dd, *J* = 8.0 Hz, 1.5 Hz, 1H), 7.42 (dd, *J* = 11.0 Hz, 3.5 Hz, 2H), 7.27-7.28 (m, 2H), 7.25 (s, 1H), 7.16-7.17 (m, 4H), 7.10 (d, *J* = 2.0 Hz, 1H), 7.01-7.04 (m, 3H), 6.98 (dd, *J* = 8.0 Hz, 1.5 Hz, 1H), 4.19 (t, *J* = 7.0 Hz, 2H), 1.77-1.80 (m, 2H), 1.31-1.35 (m, 2H), 0.90 (m, 3H); ^{13}C NMR ($CDCl_3$, 125.77 MHz) δ 192.31, 148.39, 146.73, 146.41, 142.47, 141.42, 141.32, 137.19, 135.65, 131.29, 130.93, 129.84, 129.37, 128.77, 126.32, 125.22, 124.20, 124.06, 123.02, 122.75, 121.10, 120.34, 118.57, 117.55, 117.45, 105.77, 105.06, 42.86, 31.29, 20.68, 14.09; HRMS calcd for $C_{39}H_{32}N_2OS$ $[M]^+$ *m/z* 576.2229, found 576.2232.

4-(5-(9-Butyl-7-(diphenylamino)-9*H*-carbazol-2-yl)thiophen-2-yl)benzaldehyde, 10b. Compound **10b** was synthesized from 9-Butyl-*N*,*N*-diphenyl-7-(5-(tributylstannyl)thiophen-2-yl)-9*H*-carbazol-2-amine (0.45 g, 0.6 mmol) and 4-bromobenzaldehyde (0.09 g, 0.5 mmol) by following a procedure similar to that described above for **10a**. Yellow solid; Yield 0.27 g (94%); mp 155 °C; IR (KBr, cm^{-1}) 1695 ($\nu_{C=O}$); ^{1}H NMR ($CDCl_3$, 500.13 MHz) δ 10.00 (s, 1H), 7.97 (d, *J* = 8.0 Hz, 1H), 7.89-7.92 (m, 3H), 7.79-7.80 (m, 2H), 7.56 (s, 1H), 7.47-7.48 (m, 2H), 7.41 (d, *J* = 3.5 Hz, 1H), 7.25-7.28 (m, 3H), 7.16 (d, *J* = 8.0 Hz, 4H), 7.10 (s, 1H), 7.02 (t, *J* = 7.0 Hz, 2H), 6.98 (d, *J* = 8.5 Hz, 1H), 4.17 (t, *J* = 7.5 Hz, 2H), 1.76-1.80 (m, 2H), 1.30-1.34 (m, 2H), 0.89 (t, *J* = 7.5 Hz, 3H); ^{13}C NMR ($CDCl_3$, 125.77 MHz) δ 191.43, 148.19, 147.51, 146.66, 142.34, 141.23, 141.10, 140.18, 134.92, 130.54, 129.21, 126.18, 125.57, 124.12, 124.06, 123.04, 122.62, 120.97, 120.19, 118.32, 117.43, 117.28, 105.64, 104.82, 42.69, 31.11, 20.50, 13.90; HRMS calcd for $C_{39}H_{32}N_2OSNa$ $[M + Na]^+$ *m/z* 599.2127, found 599.2125.

5-(5-(5-(9-Butyl-7-(diphenylamino)-9*H*-carbazol-2-yl)thiophen-2-yl)thiophen-2-yl)thiophene-2-carbaldehyde, 10c. Compound **10c** was synthesized from 9-Butyl-*N*,*N*-diphenyl-7-(5-(tributylstannyl)thiophen-2-yl)-9*H*-carbazol-2-amine (0.45 g, 0.6 mmol) and 5'-bromo-2,2'-bithiophene-5-carbaldehyde (0.14 g, 0.5 mmol) by following a procedure similar to that described above for **10a**. Red solid; Yield 0.31 g (94%); mp 182 °C; IR (KBr, cm^{-1}) 1687 ($\nu_{C=O}$); ^{1}H NMR ($CDCl_3$, 500.13 MHz) δ 9.87 (s, 1H), 7.97 (d, *J* = 8.5 Hz, 1H), 7.91 (d, *J* = 8.0 Hz, 1H), 7.68 (d, *J* = 4.0 Hz, 1H), 7.52 (s, 1H), 7.47 (d, *J* = 8.0 Hz, 1H), 7.33-7.34 (m, 2H), 7.26-7.28 (m, 4H), 7.24-7.25 (m, 2H), 7.15-7.18 (m, 5H), 7.10 (s, 1H), 7.02 (t, *J* = 7.5 Hz, 2H), 6.97 (dd, *J* = 8.5 Hz, 2.0 Hz, 1H), 4.18 (t, *J* = 6.5 Hz, 2H), 1.74-1.80 (m, 2H), 1.28-1.34 (m, 2H), 0.89 (t, *J* = 2.0 Hz, 3H); ^{13}C NMR ($CDCl_3$, 125.77 MHz) δ 182.46, 148.19, 146.93, 146.60, 145.84, 142.31, 141.53, 141.22, 139.45, 137.48, 135.05, 134.22, 130.48, 129.20, 127.06, 125.50, 124.32, 124.04, 123.99, 123.67, 122.91, 122.60, 120.93, 120.19, 118.33, 117.37, 117.27, 105.53, 104.84, 42.67, 31.10, 20.50, 13.91; HRMS calcd for $C_{41}H_{32}N_2OS_3$ $[M]^+$ *m/z* 664.1676, found 664.1644.

7-(5-(9-Butyl-7-(diphenylamino)-9*H*-carbazol-2-yl)thiophen-2-yl)-9,9-diethyl-9*H*-fluorene-2-carbaldehyde, 10d. Compound **10d** was synthesized from 9-Butyl-*N*,*N*-diphenyl-7-(5-(tributylstannyl)thiophen-2-yl)-9*H*-carbazol-2-amine (0.45 g, 0.6 mmol) and 7-bromo-9,9-diethyl-9*H*-fluorene-2-carbaldehyde (0.16 g, 0.5 mmol) by following a procedure similar to that described above for **10a**. Orange solid; Yield 0.63 g (97%); mp 160 °C; IR (KBr, cm^{-1}) 1691 ($\nu_{C=O}$); ^{1}H NMR ($CDCl_3$, 500.13 MHz) δ 10.06 (s, 1H), 8.00

(d, *J* = 8.0 Hz, 1H), 7.92 (d, *J* = 8.0 Hz, 1H), 7.87 (dd, *J* = 6.0 Hz, 1.5 Hz, 2H), 7.84 (d, *J* = 8.0 Hz, 1H), 7.80 (d, *J* = 8.0 Hz, 1H), 7.71 (dd, *J* = 8.0 Hz, 1.5 Hz, 1H), 7.64 (d, *J* = 1.5 Hz, 1H), 7.58 (d, *J* = 1.0 Hz, 1H), 7.52 (dd, *J* = 8.5 Hz, 1.5 Hz, 1H), 7.43 (d, *J* = 3.5 Hz, 1H), 7.42 (dd, *J* = 7.0 Hz, 1H), 7.27-7.29 (m, 3H), 7.25 (s, 1H), 7.16 (dd, *J* = 3.5 Hz, 1.0 Hz, 4H), 7.10 (d, *J* = 1.5 Hz, 1H), 7.01-7.04 (m, 2H), 6.98 (dd, *J* = 7.5 Hz, 2.0 Hz, 1H), 4.19 (t, *J* = 7.0 Hz, 2H), 2.12-2.17 (m, 4H), 1.78-1.81 (m, 2H), 1.28-1.36 (m, 2H), 0.87-0.92 (m, 3H), 0.36 (t, *J* = 7.5 Hz, 6H); ^{13}C NMR ($CDCl_3$, 125.77 MHz) δ 192.51, 152.45, 151.04, 148.38, 147.70, 146.65, 145.66, 143.27, 142.44, 141.44, 139.49, 135.44, 135.22, 131.17, 130.94, 129.36, 125.03, 124.70, 124.17, 124.06, 123.29, 122.86, 122.72, 121.64, 121.07, 120.32, 120.10, 120.06, 118.60, 117.55, 117.44, 105.67, 105.08, 56.64, 42.85, 32.88, 31.30, 20.69, 14.10, 8.72; HRMS calcd for $C_{50}H_{44}N_2OS$ $[M]^+$ *m/z* 720.3174, found 720.3163.

9-Butyl-7-(5-(9-butyl-7-(diphenylamino)-9*H*-carbazol-2-yl)thiophen-2-yl)-9*H*-carbazole-2-carbaldehyde, 10e. Compound **10d** was synthesized from 9-Butyl-*N*,*N*-diphenyl-7-(5-(tributylstannyl)thiophen-2-yl)-9*H*-carbazol-2-amine (0.45 g, 0.6 mmol) and 7-bromo-9-butyl-9*H*-carbazole-2-carbaldehyde (0.17 g, 0.5 mmol) by following a procedure similar to that described above for **10a**. Yellow solid; Yield 0.34 g (93%); mp 172 °C; IR (KBr, cm^{-1}) 1691 ($\nu_{C=O}$); ^{1}H NMR ($CDCl_3$, 500.13 MHz) δ 10.16 (s, 1H), 8.13-8.19 (m, 2H), 7.91-8.00 (m, 3H), 7.75 (d, *J* = 7.5 Hz, 1H), 7.67 (s, 1H), 7.53-7.62 (m, 3H), 7.43-7.47 (m, 3H), 7.28 (s, 2H), 7.16 (d, *J* = 6.0 Hz, 4H), 7.11 (s, 2H), 6.98-7.04 (m, 3H), 4.41 (m, 2H), 4.19 (m, 2H), 1.92-1.93 (m, 2H), 1.78-1.79 (m, 2H), 1.44-1.47 (m, 2H), 1.32-1.34 (m, 2H), 0.98-1.00 (m, 3H), 0.89-0.91 (m, 3H); ^{13}C NMR ($CDCl_3$, 125.77 MHz) δ 192.60, 148.23, 146.49, 145.58, 143.66, 142.77, 142.28, 141.29, 140.76, 134.08, 133.81, 131.05, 129.19, 128.01, 124.69, 124.00, 123.92, 122.70, 122.55, 121.91, 121.70, 121.29, 120.90, 120.46, 120.15, 118.45, 118.04, 117.43, 117.29, 109.59, 105.76, 105.49, 104.93, 43.17, 42.68, 31.25, 31.12, 20.63, 20.51, 13.91; HRMS calcd for $C_{49}H_{43}N_3OS$ $[M]^+$ *m/z* 721.3126, found 721.3121.

(*E*)-3-(3-(5-(9-Butyl-7-(diphenylamino)-9*H*-carbazol-2-yl)thiophen-2-yl)phenyl)-2-cyanoacrylic acid, 11a. A mixture of 3-(5-(9-butyl-7-(diphenylamino)-9*H*-carbazol-2-yl)thiophen-2-yl)benzaldehyde (**10a**, 0.19 g, 0.33 mmol), 2-cyanoacetic acid (0.04 g, 0.5 mmol), ammonium acetate (0.04 g, 0.25 mmol), and acetic acid (5 mL) refluxed for 24 h. The resulting yellow precipitate was filtered and washed several times with water and dried. It was crystallized from DCM /hexane mixture to obtain the analytically pure

sample. Brown solid; Yield 0.19 g (89%); mp 125 °C; IR (KBr, cm^{-1}) 2221 ($\nu_{C\equiv N}$); ^1H NMR (DMSO-d_6, 500.13 MHz) δ 8.30 (s, 1H), 8.05-8.11 (m, 2H), 7.88 (s, 2H), 7.59-7.72 (m, 3H), 7.49-7.53 (m, 2H), 7.31-7.34 (m, 4H), 7.20 (s, 1H), 7.04-7.09 (m, 7H), 6.88 (d, *J* = 8.0 Hz, 1H), 4.31 (m, 2H), 1.68 (m, 2H), 1.21-1.23 (m, 2H), 0.82 (t, *J* = 7.0 Hz, 3H); ^{13}C NMR ($CDCl_3$, 125.77 MHz) δ 147.56, 145.83, 144.61, 141.78, 140.90, 130.42, 129.37, 126.57, 124.66, 124.15, 123.48, 122.68, 121.20, 120.33, 118.62, 117.88, 116.91, 116.65, 105.40, 104.88, 41.70, 30.55, 19.68, 13.59; HRMS calcd for $C_{42}H_{33}N_3O_2S$ $[M]^+$ *m/z* 666.2186, found 666.2187.

(*E*)-3-(4-(5-(9-Butyl-7-(diphenylamino)-9*H*-carbazol-2-yl)thiophen-2-yl)phenyl)-2-cyanoacrylic acid, 11b. It was prepared form 4-(5-(9-butyl-7-(diphenylamino)-9*H*-carbazol-2-yl)thiophen-2-yl)benzaldehyde (**10b**, 0.19 g, 0.33 mmol) and 2-cyano acetic acid (0.04 g, 0.5 mmol) by following a procedure described above for **11a**. Red solid; Yield 0.17 g (82%); mp 205 °C; IR (KBr, cm^{-1}) 2216 ($\nu_{C\equiv N}$); ^1H NMR (DMSO-d_6, 500.13 MHz) δ 8.20 (s, 1H), 8.11 (d, *J* = 8.0 Hz, 1H), 8.07 (d, *J* = 8.0 Hz, 3H), 7.92 (t, *J* = 7.0 Hz, 3H), 7.80 (d, *J* = 3.5 Hz, 1H), 7.75 (d, *J* = 4.0 Hz, 1H), 7.55 (d, *J* = 8.5 Hz, 1H), 7.33 (t, *J* = 7.5 Hz, 4H), 7.18 (d, *J* = 1.5 Hz, 1H), 7.05-7.10 (m, 6H), 6.89 (dd, *J* = 8.0 Hz, 1.5 Hz, 1H), 4.31 (t, *J* = 6.5 Hz, 2H), 1.66-1.71 (m, 2H), 1.21-1.25 (m, 2H), 0.83 (t, *J* = 7.0 Hz, 3H); ^{13}C NMR (DMSO-d_6, 125.77 MHz) δ 148.06, 146.64, 146.43, 142.35, 141.38, 140.95, 138.09, 131.98, 130.93, 130.58, 129.88, 127.72, 125.80, 125.66, 124.02, 123.20, 118.32, 117.53, 117.16, 106.13, 105.35, 42.20, 31.05, 20.18, 14.10; HRMS calcd for $C_{42}H_{33}N_3O_2S$ $[M]^+$ *m/z* 643.2287, found 643.2288.

(*E*)-3-(5-(5-(5-(9-Butyl-7-(diphenylamino)-9*H*-carbazol-2-yl)thiophen-2-yl)thiophen-2-yl)thiophen-2-yl)-2-cyanoacrylic acid, 11c. It was prepared form 5-(5-(5-(9-Butyl-7-(diphenylamino)-9*H*-carbazol-2-yl)thiophen-2-yl)thiophen-2-yl)thiophene-2-carbaldehyde (**10c**, 0.33 g, 0.5 mmol) and 2-cyanoacetic acid (0.06 g, 0.7 mmol) by following a procedure described above for **11a**. Black solid. Yield (0.32 g, 87%); mp 212 °C; IR (KBr, cm^{-1}) 2216 ($\nu_{C\equiv N}$); ^1H NMR (DMSO-d_6, 500.13 MHz) δ 8.50 (s, 1H), 8.05-8.10 (m, 2H), 8.00 (d, *J* = 4.0 Hz, 2H), 7.87 (s, 1H), 7.69 (d, *J* = 4.0 Hz, 1H), 7.63 (dd, *J* = 6.5 Hz, 4.0 Hz, 2H), 7.50-7.54 (m, 2H), 7.46 (d, *J* = 4.0 Hz, 1H), 7.33 (t, *J* = 8.5 Hz, 4H), 7.17 (d, *J* = 1.5 Hz, 1H), 7.05-7.09 (m, 6H), 4.30 (t, *J* = 7.0 Hz, 2H), 1.64-1.70 (m, 2H), 1.18-1.25 (m, 2H), 0.78 (t, *J* = 7.5 Hz, 3H); ^{13}C NMR (DMSO-d_6, 125.77 MHz) δ 163.59, 147.61, 146.13, 145.95, 145.14, 144.84, 141.88, 141.38, 140.93, 138.48, 134.17, 134.01, 133.35, 129.94, 129.41, 128.22, 126.42, 125.31, 125.00, 124.83, 123.56, 122.73,

122.12, 121.28, 120.37, 117.88, 116.95, 116.66, 116.62, 105.59, 104.88, 41.74, 30.59, 19.71, 13.65; HRMS calcd for $C_{44}H_{33}N_3O_2S_3$, $[M]^+$ *m/z* 731.1729, found 731.1729.

(*E*)-3-(7-(5-(9-Butyl-7-(diphenylamino)-9*H*-carbazol-2-yl)thiophen-2-yl)-9,9-diethyl-9*H*-fluoren-2-yl)-2-cyanoacrylic acid, 11d. It was prepared form 7-(5-(9-butyl-7-(diphenylamino)-9*H*-carbazol-2-yl)thiophen-2-yl)-9,9-diethyl-9*H*-fluorene-2-carbaldehyde (**10d**, 0.36 g, 0.5 mmol) and 2-cyanoacetic acid (0.06 g, 0.7 mmol) by following a procedure described above for **11a**. Red solid; Yield 0.37 g (93%); mp 138 °C; IR (KBr, cm^{-1}) 2216 ($\nu_{C\equiv N}$); ^{1}H NMR (DMSO-d_6, 500.13 MHz) δ 8.37 (s, 1H), 8.16 (s, 1H), 8.05-8.11 (m, 4H), 8.00-8.01 (m, 1H), 7.88-7.90 (m, 2H), 7.79-7.78 (m, 1H), 7.72-7.76 (m, 2H), 7.55-7.57 (m, 1H), 7.31-7.34 (m, 4H), 7.17 (d, *J* = 1.5 Hz, 1H), 7.05-7.10 (m, 6H), 6.87-6.89 (m, 1H), 4.31 (t, *J* = 6.0 Hz, 2H), 2.08-2.19 (m, 4H), 1.67-1.70 (m, 2H), 1.20-1.26 (m, 2H), 0.81-0.84 (m, 3H), 0.30-0.34 (m, 6H); ^{13}C NMR (DMSO-d_6, 125.77 MHz) δ 152.20, 150.66, 148.09, 146.31, 144.72, 142.69, 142.30, 141.44, 139.62, 134.55, 130.96, 129.88, 126.01, 125.35, 125.23, 125.01, 123.97, 123.16, 122.35, 122.18, 121.72, 120.99, 120.84, 119.91, 118.43, 117.41, 117.18, 105.92, 105.46, 56.43, 42.21, 32.12, 31.11, 20.20, 14.14, 8.93; HRMS calcd for $C_{53}H_{45}N_3O_2S$ $[M]^+$ *m/z* 787.3227, found 787.3224.

(*E*)-3-(9-Butyl-7-(5-(9-butyl-7-(diphenylamino)-9*H*-carbazol-2-yl)thiophen-2-yl)-9*H*-carbazol-2-yl)-2-cyanoacrylic acid, 11e. It was prepared form 9-butyl-7-(5-(9-butyl-7-(diphenylamino)-9*H*-carbazol-2-yl)thiophen-2-yl)-9*H*-carbazole-2-carbaldehyde (**10e**, 0.24 g, 0.5 mmol) and 2-cyanoacetic acid (0.04 g, 0.5 mmol) by following a procedure described above for **11a**. Red solid; Yield 0.34 g (86%); mp 234 °C; IR (KBr, cm^{-1}) 2217 ($\nu_{C\equiv N}$); ^{1}H NMR (DMSO-d_6, 500.13 MHz) δ 8.52 (s, 1H), 8.36 (s, 1H), 8.25-8.32 (m, 2H), 8.00 (m, 3H), 8.00 (d, *J* = 8.0 Hz, 1H), 7.89 (s, 1H), 7.73-7.79 (m, 2H), 7.62 (d, *J* = 8.0 Hz, 1H), 7.53 (d, *J* = 7.5 Hz, 1H), 7.30-7.32 (m, 4H), 7.17 (s, 1H), 7.03-7.08 (m, 6H), 6.86 (d, *J* = 7.5 Hz, 1H), 4.48-4.49 (m, 2H), 4.28-4.30 (m, 2H), 1.82-1.84 (m, 2H), 1.65-1.67 (m, 2H), 1.34-1.37 (m, 2H), 1.20-1.23 (m, 2H), 0.92 (t, *J* = 7.5 Hz, 3H), 0.81-0.82 (m, 3H); ^{13}C NMR (DMSO-d_6, 125.77 MHz) δ 163.71, 155.13, 147.58, 145.78, 144.28, 142.76, 142.27, 141.77, 140.92, 140.16, 133.15, 130.48, 129.36, 128.51, 125.74, 125.63, 124.78, 123.48, 122.65, 122.02, 121.82, 121.17, 121.10, 120.80, 120.70, 120.28, 117.90, 117.45, 116.90, 116.62, 112.75, 105.60, 105.32, 104.89, 42.25, 41.68, 30.65, 30.58, 19.79, 19.70, 13.60; HRMS calcd for $C_{52}H_{44}N_4O_2S$ $[M]^+$ *m/z* 788.3179, found 788.3155.

3.5 References

[1] S. Ahmad, E. Guillén, L. Kavan, M. Grätzel and M. K. Nazeeruddin, Metal free sensitizer and catalyst for dye sensitized solar cells. *Energy Environ. Sci.,* **2013**, *6,* 3439-3466.

[2] Q. G. Zhang, C. S. Dandeneau, X.-Y. Zhou and G.-Z. Cao, ZnO Nanostructures for dye-sensitized solar cells. *Adv. Mater.,* **2009**, *21,* 4087-4108.

[3] Y.-Z. Wu and W.-H. Zhu, Organic sensitizers from D-π-A to D-A-π-A: Effect of the internal electron-withdrawing units on molecular absorption, energy levels and photovoltaic performances. *Chem. Soc. Rev.,* **2013**, *42,* 2039-2058.

[4] S. Haid, M. Marszalek, A. Mishra, M. Wielopolski, T. Joël, J.-E. Moser, R. Humphry-Baker, S. M. Zakeeruddin, M. Grätzel and P. Bäuerle, Significant improvement of dye-sensitized solar cell performance by small structural modification in π-conjugated donor-acceptor dyes. *Adv. Funct. Mater.,* **2012**, *22,* 1291-1302.

[5] Y.-S. Yen, H.-H. Chou, Y.-C. Chen, C.-Y. Hsu and J. T. Lin, Recent developments in molecule-based organic materials for dye sensitized solar cells. *J. Mater. Chem.,* **2012**, *22*, 8734-8747.

[6] B.-G. Kim, K. Chung and J. Kim, Molecular design principle of all organic dyes for dye-sensitized solar cells. *Chem.–Eur. J.,* **2013**, *19,* 5220-5230.

[7] A. Mishra, M. K. R. Fischer and P. Bäuerle, Metal-Free organic dyes for dye-sensitized solar cells: From structure: Property relationships to design rules. *Angew. Chem. Int. Ed.,* **2009**, *48*, 2474-2499.

[8] Y. Ooyama and Y. Harima, Photophysical and electrochemical properties, and molecular structures of organic dyes for dye sensitized solar cells. *ChemPhysChem,* **2012**, *13,* 4032-4080.

[9] M. Liang and J. Chen, Arylamine organic dyes for dye-sensitized solar cells. *Chem. Soc. Rev.,* **2013**, *42,* 3453-3488.

[10] A. Hagfeldt, G. Boschloo, L. Sun, L. Kloo and H. Pettersson, Dye-sensitized solar cells. *Chem. Rev.,* **2010**, *110,* 6595-6663.

[11] E. M. Barea and J. Bisquert, Properties of chromophores determining recombination at the TiO_2-dye-electrolyte interface. *Langmuir,* **2013**, *29,* 8773-8781.

[12] Y. Cui, Y. Wu, X. Lu, X. Zhang, G. Zhou, F. B. Miapeh, W. Zhu and Z.-S. Wang, Incorporating benzotriazole moiety to construct D-A-π-A organic sensitizers for solar cells: Significant enhancement of open-circuit photovoltage with long alkyl group. *Chem. Mater.,* **2011**, *23*, 4394-4401.

[13] N. Koumura, Z.-S. Wang, S. Mori, M. Miyashita, E. Suzuki and K. Hara, Alkyl-functionalized organic dyes for efficient molecular photovoltaics. *J. Am. Chem. Soc.*, **2006**, *128*, 14256-14257.

[14] Z.-S. Wang, N. Koumura, Y. Cui, M. Takahashi, H. Sekiguchi, A. Mori, T. Kubo, A. Furube and K. Hara, Hexylthiophene functionalized carbazole dyes for efficient molecular photovoltaics: Tuning of solar-cell performance by structural modification. *Chem. Mater.,* **2008**, *20*, 3993-4003.

[15] X. Hu, S. Cai, G. Tian, X. Li, J. Su and J. Li, Rigid triarylamine based D-A-π-A structural organic sensitizers for solar cells: The significant enhancement of open-circuit photovoltage with a long alkyl group. *RSC Adv.,* **2013**, *3*, 22544-22553.

[16] X. Ren, S. Jiang, M. Cha, G. Zhou and Z.-S. Wang, Thiophene bridged double D-π-A dye for efficient dye-sensitized solar cell. *Chem. Mater.,* **2012**, *24*, 3493-3499.

[17] D. Cao, J. Peng, Y. Hong, X. Fang, L. Wang and H. Meier, Enhanced performance of the dye-sensitized solar cells with phenothiazine-based dyes containing double D-A branches. *Org. Lett.*, **2011**, *13*, 1610-1613.

[18] A. Baheti, K. R. J. Thomas, C.-P. Lee and K.-C. Ho, Synthesis and characterization of dianchoring organic dyes containing 2,7-diaminofluorene donors as efficient sensitizers for dye-sensitized solar cells. *Org. Electron.,* **2013**, *14*, 3267-3276.

[19] K. R. J. Thomas and A. Baheti, Fluorene based organic dyes for dye sensitised solar cells: Structure-property relationships. *Mater. Technol.,* **2013**, *28*, 71-87.

[20] A. Baheti, K. R. J. Thomas, C.-P. Lee, C.-T. Li and K.-C. Ho, Organic dyes containingfluoren-9-ylidene chromophores for efficient dye-sensitized solar cells. *J. Mater. Chem. A*, **2014**, *2*, 5766-5779.

[21] K. Hara, Z.-S. Wang, T. Sato, A. Furube, R. Katoh, H. Sugihara, Y. Dan-oh, C. Kasada, A. Shinpo and S. Suga, Oligothiophene-containing coumarin dyes for efficient dye-sensitized solar cells. *J. Phys. Chem. B*, **2005**, *109*, 15476-15482.

[22] Z. S. Wang, Y. Cui, K. Hara, Y. Dan-oh, C. Kasada and A. Shinpo, A high-light-harvesting-efficiency coumarin dye for stable dye-sensitized solar cells. *Adv. Mater.*, **2007**, *19*, 1138-1141.

[23] H. Tian, X. Yang, R. Chen, Y. Pan, L. Li, A. Hagfeldt and L. Sun, Phenothiazine derivatives for efficient organic dye-sensitized solar cells. *Chem. Comm.*, **2007**, 3741-3743.

[24] S. H. Kim, H. W. Kim, C. Sakong, J. Namgoong, S. W. Park, M. J. Ko, C. H. Lee, W. I. Lee and J. P. Kim, Effect of five-membered heteroaromatic linkers to the performance of phenothiazine-based dye-sensitized solar cells. *Org. Lett.*, **2011**, *13*, 5784-5787.

[25] H. Tian, X. Yang, J. Cong, R. Chen, J. Liu, Y. Hao, A. Hagfeldt and L. Sun, Tuning of phenoxazine chromophores for efficient organic dye-sensitized solar cells. *Chem. Commun.*, **2009**, 6288-6290.

[26] H. Tian, I. Bora, X. Jiang, E. Gabrielsson, K. M. Karlsson, A. Hagfeldt and L. Sun, Modifying organic phenoxazine dyes for efficient dye-sensitized solar cells. *J. Mater. Chem.*, **2011**, *21*, 12462-12472.

[27] X. Wang, J. Yang, H. Yu, F. Li, L. Fan, W. Sun, Y. Liu, Z. Y. Koh, J. Pan, W.-L. Yim, L. Yan and Q. Wang, A benzothiazole-cyclopentadithiophene bridged D-A-π-A sensitizer with enhanced light absorption for high efficiency dye-sensitized solar cells. *Chem. Commun.*, **2014**, *50*, 3965-3968.

[28] X. Cheng, S. Sun, M. Liang, Y. Shi, Z. Sun and S. Xue, Organic dyes incorporating the cyclopentadithiophene moiety for efficient dye-sensitized solar cells. *Dyes Pigm.*, **2012**, *92*, 1292-1299.

[29] T. Horiuchi, H. Miura, K. Sumioka and S. Uchida, High efficiency of dye-sensitized solar cells based on metal-free indoline dyes. *J. Am. Chem. Soc.*, **2004**, *126*, 12218-12219.

[30] S. Ito, H. Miura, S. Uchida, M. Takata, K. Sumioka, P. Liska, P. Comte, P. Pechy and M. Grätzel, High-conversion-efficiency organic dye-sensitized solar cells with a novel indoline dye. *Chem. Comm.*, **2008**, 5194-5196.

[31] A. Baheti, P. Singh, C.-P. Lee, K. R. J. Thomas and K.-C. Ho, 2,7-Diaminofluorene-based organic dyes for dye-sensitized solar cells: Effect of auxiliary donor on optical and electrochemical properties. *J. Org. Chem.*, **2011**, *76*, 4910-4920.

[32] G. Li, Y.-F. Zhou, X.-B. Cao, P. Bao, K.-J. Jiang, Y. Lina, L.-M. Yang and L.-M. Yang, Novel TPD-based organic D-π-A dyes for dye-sensitized solar cells. *Chem. Commun.*, **2009**, 2201-2203.

[33] K. R. J. Thomas, N. Kapoor, C.-P. Lee and K.-C. Ho, Organic Dyes Containing Pyrenylamine-based cascade donor systems with different aromatic π linkers for dye-sensitized solar cells: Optical, electrochemical, and device characteristics. *Chem. Asian J.*, **2012**, *7*, 738-750.

[34] W. Li, Y. Wu, Q. Zhang, H. Tian and W. Zhu, D-A-π-A featured sensitizers bearing phthalimide and benzotriazole as auxiliary acceptor: Effect on absorption and charge recombination dynamics in dye-sensitized solar cells. *ACS Appl. Mater. Interfaces*, **2012**, *4*, 1822-1830.

[35] B.-S. Chen, D.-Y. Chen, C.-L. Chen, C.-W. Hsu, H.-C. Hsu, K.-L. Wu, S.-H. Liu, P.-T. Chou and Y. Chi, Donor–acceptor dyes with fluorine substituted phenylene spacer for dye-sensitized solar cells. *J. Mater. Chem.*, **2011**, *21*, 1937-1945.

[36] D. W. Chang, H. J. Lee, J. H. Kim, S. Y. Park, S.-M. Park, L. Dai and J.-B. Baek, Novel quinoxaline-based organic sensitizers for dye sensitized solar cells. *Org. Lett.*, **2011**, *13*, 3880-3883.

[37] Y. J. Chang and T. J. Chow, Dye-sensitized solar cell utilizing organic dyads containing triarylene conjugates. *Tetrahedron*, **2009**, *65*, 4726-4734.

[38] A. Baheti, K. R. J. Thomas, C.-P. Lee and K.-C. Ho, Fine tuning the performance of DSSCs by variation of the π-spacers in organic dyes that contain a 2,7-diaminofluorene donor. *Chem. Asian J.*, **2012**, *7*, 2942-2954.

[39] K. R. J. Thomas, Y.-C. Hsu, J. T. Lin, K.-M. Lee, K.-C. Ho, C.-H. Lai, Y.-M. Cheng and P.-T. Chou, 2,3-Disubstituted thiophene-based organic dyes for solar cells. *Chem. Mater.*, **2008**, *20*, 1830-1840.

[40] A. Mishra, N. Pootrakulchote, M. Wang, S.-J. Moon, S. M. Zakeeruddin, M. Grätzel and P. Bäuerle, A thiophene-based anchoring ligand and its heteroleptic Ru(II)-complex for efficient thin-film dye-sensitized solar cells. *Adv. Funct. Mater.*, **2011**, *21*, 963-970.

[41] D. P. Hagberg, T. Marinado, K. M. Karlsson, K. Nonomura, P. Qin, G. Boschloo, T. Brinck, A. Hagfeldt and L. Sun, Tuning the HOMO and LUMO energy levels of organic chromophores for dye sensitized solar cells. *J. Org. Chem.*, **2007**, *72*, 9550-9556.

[42] R. Y.-Y. Lin, Y.-S. Yen, Y.-T. Cheng, C.-P. Lee, Y.-C. Hsu, H.-H. Chou, C.-Y. Hsu, Y.-C. Chen, J. T. Lin, K.-C. Ho and C. Tsai, Dihydrophenanthrene-based metal-free dyes for highly efficient cosensitized solar cells. *Org. Lett.*, **2012**, *14*, 3612-3615.

[43] Y.-S. Yen, Y.-C. Hsu, J. T. Lin, C.-W. Chang, C.-P. Hsu and D.-J. Yin, Pyrrole-based organic dyes for dye-sensitized solar cells. *J. Phys. Chem. C*, **2008**, *112*, 12557-12567.

[44] L.-S. Cui, S.-C. Dong, Y. Liu, Q. Li, Z.-Q. Jiang and L.-Z. Liao, A simple systematic design of phenylcarbazole derivatives for host materials to high-efficiency phosphorescent organic light-emitting diodes. *J. Mater. Chem. C*, **2013**, *1*, 3967-3975.

[45] K. R. J. Thomas, J. T. Lin, Y.-T. Tao and C.-W. Ko, Light emitting carbazole derivatives: Potential electroluminescent materials. *J. Am. Chem. Soc.*, **2001**, *123*, 9404-9411.

[46] P. Kotchapradist, N. Prachumrak, R. Tarsang, S. Jungsuttiwong, T. Keawin, T. Sudyoadsuk and V. Promarak, Pyrene-functionalized carbazole derivatives as non-doped blue emitters for highly efficient blue organic light-emitting diodes. *J. Mater. Chem. C*, **2013**, *1*, 4916-4924.

[47] Y. Ooyama, S. Inoue, T. Nagano, K. Kushimoto, J. Ohshita, I. Imae, K. Komaguchi and Y. Harima, Dye-sensitized solar cells based on donor-acceptor π-conjugated fluorescent dyes with a pyridine ring as an electron-withdrawing anchoring group. *Angew. Chem., Int. Ed*., **2011**, *50*, 7429-7433.

[48] Y. Ooyama, T. Nagano, S. Inoue, I. Imae, K. Komaguchi, J. Ohshita and Y. Harima, Dye-Sensitized solar cells based on donor-π-acceptor fluorescent dyes with a pyridine ring as an electron withdrawing-injecting anchoring group. *Chem.–Eur. J.*, **2011**, *17*, 14837-14843.

[49] H.-Y. Wang, F. Liu, L.-H. Xie, C. Tang, B. Peng, W. Huang and W. Wei, Topological arrangement of fluorenyl-substituted carbazole triads and starbursts: Synthesis and optoelectronic properties. *J. Phys. Chem. C*, **2011**, *115*, 6961-6967.

[50] H. Huang, Q. Fu, B. Pan, S. Zhuang, L. Wang, J. Chen, D. Ma and C. Yang, Butterfly-shaped tetrasubstituted carbazole derivatives as a new class of hosts for highly efficient solution processable green phosphorescent organic light-emitting diodes. *Org. Lett.*, **2012**, *14*, 4786-4789.

[51] N. Blouin and M. Leclerc, Poly(2,7-carbazole)s: Structure-property relationships. *Acc. Chem. Res.*, **2008**, *41*, 1110-1119.

[52] P. Shen, Y. Tang, S. Jiang, H. Chen, X. Zheng, X. Wang, B. Zhao and S. Tan, Efficient triphenylamine-based dyes featuring dual-role carbazole, fluorene and spirobifluorene moieties. *Org. Electron.*, **2011**, *12*, 125-135.

[53] K. S. V. Gupta, T. Suresh, S. P. Singh, A. Islam, L. Han and M. Chandrasekharam, Carbazole based A-π-D-π-A dyes with double electron acceptor for dye-sensitized solar cell. *Org. Electron.*, **2014**, *15*, 266-275.

[54] T. Sudyoadsuk, S. Pansay, S. Morada, R. Rattanawan, S. Namuangruk, T. Kaewin, S. Jungsuttiwong and V. Promarak, Synthesis and characterization of D-D-π-A-type organic dyes bearing carbazole–carbazole as a donor moiety (D–D) for efficient dye-sensitized solar cells. *Eur. J. Org. Chem.*, **2013**, 5051-5063.

[55] S. Cai, X. Hu, J. Han, Z. Zhang, X. Li, C. Wang and J. Su, Efficient organic dyes containing dibenzo heterocycles as conjugated linker part for dye-sensitized solar cells. *Tetrahedron*, **2013**, *69*, 1970-1977.

[56] A. R. Morales, A. Frazer, A. W. Woodward, H.-Y. Ahn-White, A. Fonari, P. Tongwa, T. Timofeeva and K. D. Belfield, Design, Synthesis, and structural and spectroscopic studies of push-pull two-photon absorbing chromophores with acceptor groups of varying strength. *J. Org. Chem*., **2013**, *78*, 1014-1025.

[57] K. Brunner, A. van Dijken, H. Börner, J. J. A. M. Bastiaansen, N. M. M. Kiggen and B. M. W. Langeveld, Carbazole compounds as host materials for triplet emitters in organic light-emitting diodes: Tuning the HOMO level without influencing the triplet energy in small molecules. *J. Am. Chem. Soc.*, **2004**, *126*, 6035-6042.

[58] J. F. Hartwig, Transition metal catalyzed synthesis of arylamines and aryl ethers from aryl halides and triflates: Scope and mechanism. *Angew. Chem., Int. Ed.*, **1998**, *37*, 2047-2067.

[59] J. K. Stille, The Palladium-catalyzed cross-coupling reactions of organotin reagents with organic electrophiles. *Angew. Chem., Int. Ed.*, **1986**, *25*, 508-524.

[60] E. Knoevenagel, Ueber eine darstellungsweise des benzylidenacetessigesters. *Chem. Ber.*, **1896**, *29*, 172-174.

[61] A. W. Freeman, M. Urvoy and M. E. Criswell, Triphenylphosphine-mediated reductive cyclization of 2-nitrobiphenyls: A practical and convenient synthesis of carbazoles. *J. Org. Chem.*, **2005**, *70*, 5014-5019.

[62] Y. Che, D. E. Gross, H. Huang, D. Yang, X. Yang, E. Discekici, Z. Xue, H. Zhao, J. S. Moore and L. Zang, Diffusion-controlled detection of trinitrotoluene: Interior nanoporous structure and low highest occupied molecular orbital level of building blocks enhance selectivity and sensitivity. *J. Am. Chem. Soc.*, **2012**, *134*, 4978-4982.

[63] N. Miyaura and A. Suzuki, Palladium-catalyzed cross-coupling reactions of organoboron compounds. *Chem. Rev.*, **1995**, *95*, 2457.

[64] Y.-D. Lin, C.-T. Chien, S.-Y. Lin, H.-H. Chang, C.-Y. Liu and T. J. Chow, *Meta* versus *para* substituent effect of organic dyes for sensitized solar cells. *J. Photochem. Photobiol., A*, **2011**, *222*, 192-202.

[65] P. Singh, A. Baheti, K. R. J. Thomas, C.-P. Lee and K.-C. Ho, Fluorene-based organic dyes containing acetylene linkage for dye-sensitized solar cells. *Dyes Pigm.*, **2012**, *95*, 523-533.

[66] K. Panthi, P. Z. El-Khoury, A. N. Tarnovsky and T. H. Kinstle, Synthesis and computational studies of diphenylamine donor-carbazole linker-based donor-acceptor compounds. *Tetrahedron*, **2010**, *66*, 9641-9649.

[67] M. K. Nazeeruddin, A. Kay, I. Rodicio, R. Humphry-Baker, E. Müller, P. Liska, N. Vlachopoulos and M. Grätzel, Conversion of light to electricity by cis-X2bis(2,2′-bipyridyl-4,4′-dicarboxylate)-ruthenium(II) charge-transfer sensitizers (X = Cl^-, Br^-, I^-, CN^-, and SCN^-) on nanocrystalline titanium dioxide electrodes. *J. Am. Chem. Soc.*, **1993**, *115*, 6382-6390.

[68] C.-H. Chen, Y.-C. Hsu, H.-H. Chou, K. R. J. Thomas, J. T. Lin and Hsu, C.-P. Dipolar compounds containing fluorene and a heteroaromatic ring as the conjugating bridge for high-performance dye-sensitized solar cells. *Chem. Eur. J.*, **2010**, *16*, 3184-3193.

[69] O.van den Berg, W. F. Jager and S. J. Picken, 7-Dialkylamino-1-alkylquinolinium salts: Highly versatile and stable fluorescent probes. *J. Org. Chem.*, **2006**, *71*, 2666-2676.

[70] A. Granzhan, H. Ihmels and G. Viola, 9-Donor-substituted acridizinium salts: Versatile environment-sensitive fluorophores for the detection of biomacromolecules. *J. Am. Chem. Soc.*, **2007**, *129*, 1254-1267.

[71] Z.-S. Wang, F.-Y. Li and C.-H. Huang, Photocurrent enhancement of hemicyanine dyes containing rso3-group through treating TiO_2 films with hydrochloric acid. *J. Phys. Chem. B*, **2001**, *105*, 9210-9217.

[72] P. Singh, A. Baheti and K. R. J. Thomas, Synthesis and optical properties of acidochromic amine-substituted benzo[*a*]phenazines. *J. Org. Chem.*, **2011**, *76*, 6134-6145

[73] M. K. Nazeeruddin, P. Péchy, T. Renouard, S. M. Zakeeruddin, R. Humphry-Baker, P. Comte, P. Liska, L. Cevey, E. Costa, V. Shklover, L. Spiccia, G. B. Deacon, C. A. Bignozzi and M. Grätzel, Engineering of efficient panchromatic sensitizers for nanocrystalline TiO_2-based solar cells. *J. Am. Chem. Soc.*, **2001**, *123*, 1613-1624.

[74] A. Baheti, P. Tyagi, K. R. J. Thomas, Y.-C. Hsu and J. T. Lin, Simple triarylamine-based dyes containing fluorene and biphenyl linkers for efficient dye-sensitized solar cells. *J. Phys. Chem. Lett.*, **2009**, *113*, 8541-8547.

[75] C. Reichardt, Solvatochromic dyes as solvent polarity indicators. *Chem. Rev.*, **1994**, *94*, 2319-2358.

[76] M. K. Nazeeruddin, S. M. Zakeeruddin, R. Humphry-Baker, M. Jirousek, P. Liska, N. Vlachopoulos, V. hklover, C. H. Fisher and M. Grätzel, Acid-base equilibria of (2,2‘-bipyridyl-4,4‘-dicarboxylic acid)ruthenium(II) complexes and the effect of protonation on charge-transfer sensitization of nanocrystalline titania. *Inorg. Chem.*, **1999**, *38*, 6298-6305.

[77] K. Sayama, S. Tsukagoshi, K. Hara, Y. Ohga, A. Shinpou, Y. Abe, S. Suga and H. Arakawa, Photoelectrochemical properties of J aggregates of benzothiazole merocyanine dyes on a nanostructured TiO_2 film. *J. Phys. Chem. B*, **2002**, *106*, 1363-1371.

[78] C. Teng, X. Yang, C. Yang, H. Tian, S. Li, X. Wang, A. Hagfeldt and L. Sun, Influence of triple bonds as π-Spacer units in metal-free organic dyes for dye-sensitized solar cells. *J. Phys. Chem. C*, **2010**, *114*, 11305-11313.

[79] K. Rurack, J. L. Bricks, G. Reck, R. Radeglia and U. Resch-Genger, Chalcone-analogue dyes emitting in the near-infrared (NIR): Influence of donor-acceptor substitution and cation complexation on their spectroscopic properties and X-ray structure. *J. Phys. Chem. A*, **2000**, *104*, 3087-3109.

[80] J. A. Pollard, D. Zhang, J. A. Downing, F. J. Knorr and J. L. McHale, Solvent effects on interfacial electron transfer from Ru(4,4′-dicarboxylic acid-2,2′-bipyridine)$_2$(NCS)$_2$ to nanoparticulate TiO_2: Spectroscopy and solar photoconversion. *J. Phys. Chem. A*, **2005**, *109*, 11443-11452.

[81] J.-S. Yang, K.-L. Liau, C.-W. Tu and C.-Y. Hwang, Excited-State Behavior ofN-Phenyl-Substitutedtrans-3-Aminostilbenes: Where the "m-Amino Effect" Meets the "Amino-Conjugation Effect". *J. Phys. Chem. A*, **2005**, *109*, 6450-6456.

[82] R. G. Parr and W. Yang, Density-functional theory of the electronic structure of molecules. *Annu. Rev. Phys. Chem.*, **1995**, *46*, 701-728.

[83] B. J. Lynch, P. L. Fast, M. Harris and D. G. Truhlar, Adiabatic connection for kinetics. *J. Phys. Chem. A*, **2000**, *104*, 4811-4815.

[84] P. Wang, S. M. Zakeeruddin, J.-E. Moser and M. Grätzel, A new ionic liquid electrolyte enhances the conversion efficiency of dye-sensitized solar cells. *J. Phys. Chem. B*, **2003**, *107*, 13280-14285.

[85] M. Grätzel, Photoelectrochemical cells. *Nature*, **2001**, *414*, 338-344.

[86] M. Lu, M. Liang, H.-Y. Han, Z. Sun and S. Xue, organic dyes incorporating bis-hexapropyltruxeneamino moiety for efficient dye-sensitized solar cells. *J. Phys. Chem. C*, **2011**, *115*, 274-281.

[87] M. M. Elmahdy, C. Gutsche and F. Kremer, Forces within single pairs of charged colloids in aqueous solutions of ionic liquids as studied by optical tweezers. *J. Phys. Chem. C*, **2010**, *114*, 19452-19458.

[88] B. Liu, Q. Liu, D. You, X. Li, Y. Naruta and W. Zhu, Molecular engineering of indoline based organic sensitizers for highly efficient dye-sensitized solar cells. *J. Mater. Chem.*, **2012**, *22*, 13348-13356.

[89] M. J. Frisch, G. W. Trucks, H. B. Schlegel, G. E. Scuseria, M. A. Robb, J. R. Cheeseman, G. Scalmani, V. Barone, B. Mennucci, G. A. Petersson, H. Nakatsuji, M. Caricato, X. Li, H. P. Hratchian, A. F. Izmaylov, J. Bloino, G. Zheng, J. L. Sonnenberg, M. Hada, M. Ehara, K. Toyota, R. Fukuda, J. Hasegawa, M. Ishida, T. Nakajima, Y. Honda, O. Kitao, H. Nakai, T. Vreven, J. A. Montgomery, J. E. Peralta, F. Ogliaro, M. Bearpark, J. J. Heyd, E. Brothers, K. N. Kudin, V. N. Staroverov, R. Kobayashi, J. Normand, K. Raghavachari, A. Rendell, J. C. Burant, S. S. Iyengar, J. Tomasi, M. Cossi, N. Rega, N. J. Millam, M. Klene, J. E. Knox, J. B. Cross, V. Bakken, C. Adamo, J. Jaramillo, R. Gomperts, R. E. Stratmann, O. Yazyev, A. J. Austin, R. Cammi, C. Pomelli, J. W. Ochterski, R. L. Martin, K. Morokuma, V. G. Zakrzewski, G. A. Voth, P. Salvador, J. J. Dannenberg, S. Dapprich, A. D. Daniels, O. Farkas, J. B. Foresman, J. V. Ortiz, J. Cioslowski, D. J. Fox, Gaussian 09, Revision A.02, Gaussian, Inc.: Wallingford, CT, **2009**.

[90] A. D. Becke, A new mixing of Hartree-Fock and local density-functional theories. *J. Chem. Phys.*, **1993**, *98*, 1372-1377.

[91] H.-C. Chu, D. Sahu, Y.-C. Hsu, H. Padhy, D. Patra, J.-T. Lin, D. Bhattacharya, K.-L. Lu, K.-H. Wei and H.-C. Lin, Structural planarity and conjugation effects of novel symmetrical acceptor-donor-acceptor organic sensitizers on dye-sensitized solar cells. *Dyes Pigm.*, **2012**, *93*, 1488-1497.

CHAPTER 4

Organic Dyes Containing Flourene Amine Donor for Efficient Dye-Sensitized Solar Cells

4.1 Introduction

Organic dyes should possess a strong absorption band ranging from the visible to near IR region and a suitable LUMO energy level should be essential in order to inject electrons effectively to the conduction band of TiO_2 without any recombination of electrons with oxidized dye and electrolyte to achieve highly efficient DSSC [1-3]. The extension of conjugation by incorporation of π-linker units between the donor and acceptor is a feasible strategy to broaden the absorption spectra. Though, large π-conjugated system leads to poor photovoltaic performance due to aggregation of dyes on the surface of TiO_2 and electron losses by recombination [4-7]. To overcome these hurdles and improve the efficiency of DSSC, huge number of organic dyes were developed based on triarylamine donor due to its good electron donating and transporting capability, as well as its special propeller starburst molecular structure [8-10]. However, triarylamine containing dyes are restricted by narrow incident power conversion spectra and low open circuit voltage which led to poor power conversion efficiencies. Systematic molecular engineering on triarylamine donor is needed for achieving better photovoltaic conversion efficiencies. Further, chemical modification of triarylamine units helps to fine-tune the photophysical properties of sensitizer and it facilitates the formation of suitable HOMO and LUMO energy levels [11-17].

Chow and co-workers synthesized a set of dyes containing diphenylamine and naphthylphenylamine donors [5]. Naphthylphenylamine containing dyes (**1N-PPS** and **1N-PSS**; Chart 4.1) exhibited higher V_{OC} values (660 mV and 710 mV) than the corresponding diphenylamine containing dyes (**1P-PPS**; V_{OC} = 650 mV, **1P-PSS**; V_{OC} = 660 mV) attributable to the naphthylphenyl amine which provides the following features: 1) higher absorption wavelength for the charge transfer transition 2) larger size of naphthalene group effectively hinder self-aggregation of the dyes on TiO_2 surface 3) better stabilization of oxidized dye after injection of electron into the conduction band of the TiO_2. Lin and co-workers [18] also demonstrated that naphthylphenlamine containing dye **BP2** (η = 5.95%) performed better than diphenylamine containing dye **BP1** (η = 5.33%). Higher efficiency of **BP2** is due to the higher J_{SC} (14.16 mA cm^{-2}) and V_{OC} (650 mV) than **BP1** (J_{SC} = 13.61 mA cm^{-2} and V_{OC} = 610 mV) and it is ascribed to higher dye loading and stabilization of oxidized **BP2** dye. Thomas and co-workers [19, 20] synthesized fluorene based dyes containing diphenylamine (**FL1** and **FL2**; Chart 4.1), naphthylphenylamine (**FL3**), anthracenylphenylamine (**FL4**) and pyrenylphenylamine (**FL5**) donors and used in DSSC.

They found that the dye **FL3** exhibited higher power conversion efficiency of 5.23% which is better than other dyes (**FL1;** 4.70%, **FL2;** 3.01%, **FL4;** 2.86% and **FL5;** 3.35%). Highest molar extinction coefficients and better charge separation of the dye **FL3** is responsible for its superior power conversion efficiency when compared to their congeners.

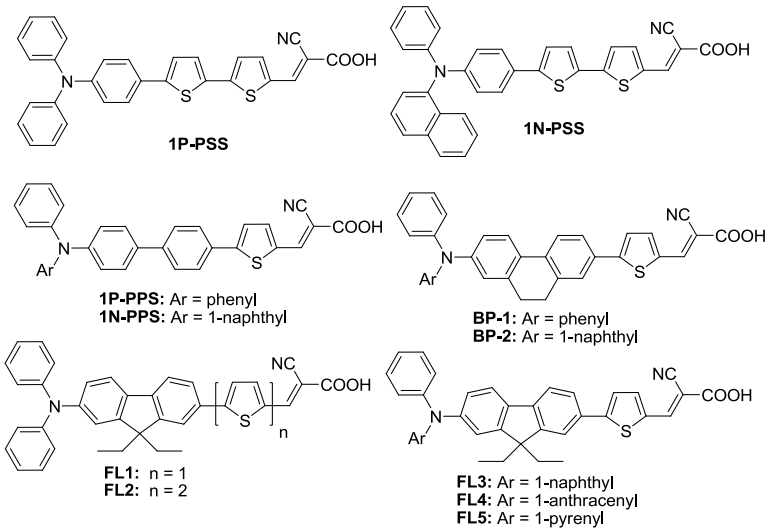

Chart 4.1 Structures of the dyes containing various arylamine donor units.

Fluorene offers methods to incorporate alkyl chains on sp^3 carbon at C9-position which may increase the electron recombination resistance and its stability towards UV-irradiation and heating [11, 21-23]. Incorporation of fluorene units facilitates the efficient electron injection into the conduction band of TiO_2 which led to larger photocurrent density of the dyes. Ko and co-workers synthesized dyes (**JK-1** and **JK-2**; Chart 4.2) containing difuorenylamine donor and effectively used in DSSC [11]. Interestingly, stable devices based on the fluorene was obtained with high conversion efficiency of 7.20% (J_{SC} = 12.20 mA cm^{-2}) which lasted for more than 1200 h.

Grätzel and co-workers utilized electron rich fused heterocycles such as thieno[3,2-*b*]thiophene and dithieno[3,2-*b*;2′,3′-*d*]thiophene linkers instead of thiophene in **JK-1**, to obtain **C201** and **C203** (shown in Chart 4.2), respectively [24, 25]. Both of the dyes **C201** and **C203** exhibited longer wavelength absorptions with high molar extinction coefficient when compared to the parent dye **JK1** due to the elongation of the conjugation and electron richness of the fused heterocyclic units. Thus, the devices using dyes **C201** and **C203** achieved power conversion efficiencies of 7.80% and 8.00%, respectively owing to its larger J_{SC} values (13.35 mA cm^{-2} and 14.33 mA cm^{-2}).

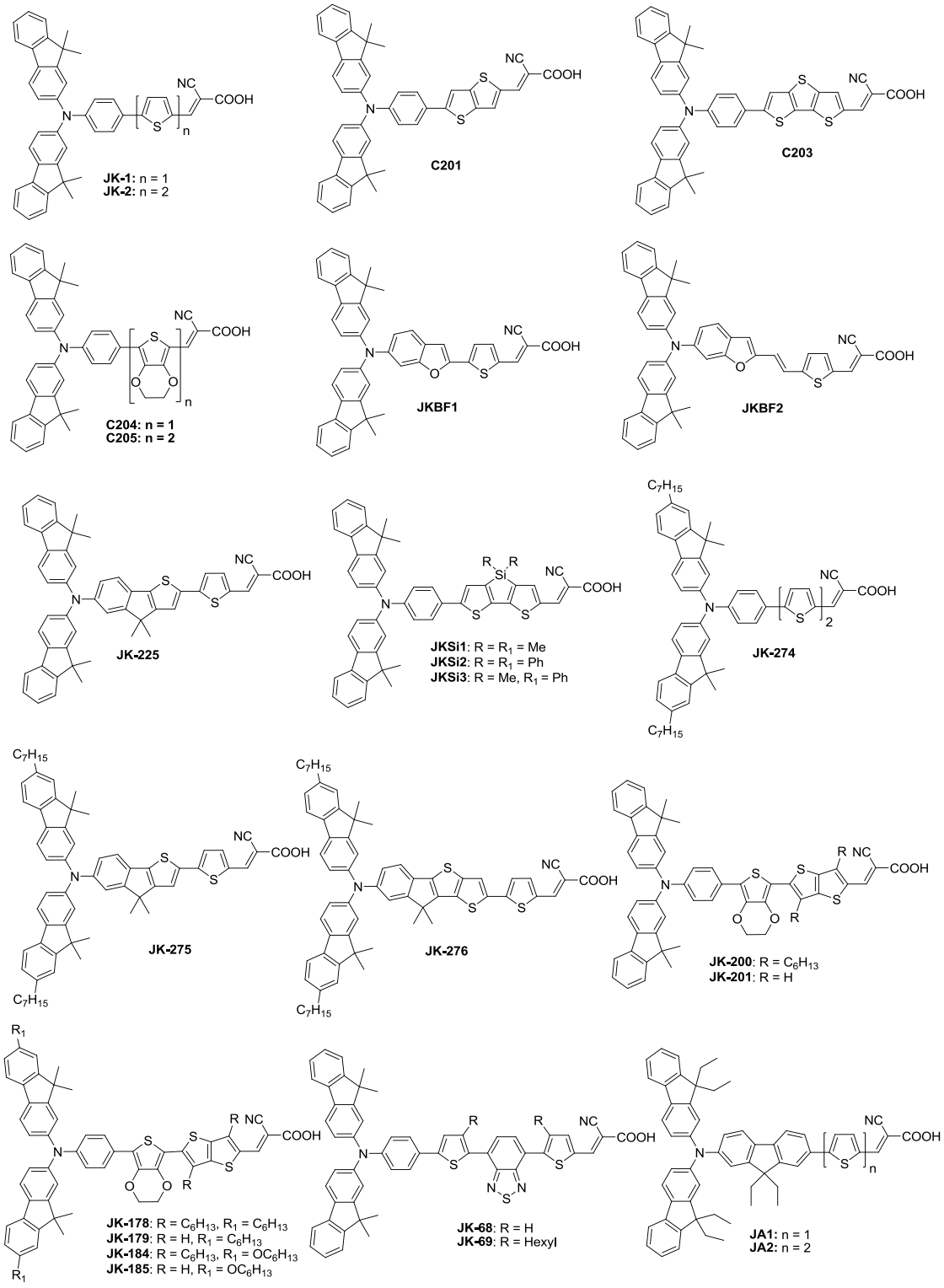

Chart 4.2 Structures of the dyes containing difluorenylamine donor unit.

Consequently, the longer wavelength absorption of the dyes is found to strongly influence the efficiency of the dyes, Grätzel and co-workers incorporated 3,4-ethylenedioxythiophene unit as a linker to obtain red shifted absorption [26]. The dyes (**C204** and **C205**; Chart 4.2) showed longer wavelength absorption and better light harvesting ability than the congeners **JK-1** and **JK-2**. This leads to better power conversion efficiencies for dyes, **C204** (J_{SC} =

13.82 mA cm^{-2}, η = 7.92%) and **C205** (J_{SC} = 15.68 mA cm^{-2}, η = 8.32%). Ko and co-workers synthesized dyes **JKBF1** and **JKBF1** (shown in Chart 4.2) by incorporating benzo[*b*]furan linker and studied the effect of structural modification on the efficiency of the DSSC [27]. Absorption in these dyes was red shifted when compared to the parent dyes (**JK1** and **JK2**). However the molar extinction coefficients drastically decreased which leads to inferior light harvesting capability and J_{SC} values with relatively inferior power conversion efficiencies (**JKBF1**; 6.65% and **JKBF1;** 4.70%).

Ko and co-workers incorporated the planar indeno[1,2-*b*]thiophene bridging group into the **JK2** dye, to obtain **JK-225** which displayed longer wavelength absorption with high molar extinction coefficient [28]. The dye **JK-225** achieved higher power conversion efficiency of 8.20% with J_{SC} = 13.84 mA cm^{-2}, V_{OC} = 790 mV and *ff* = 0.75. Again, they synthesized fused dithienosilole-based dyes (**JKSi1**-**JKSi3**; Chart 4.2) using difluorenylamine donor by variation of the substitution at 3-position of the dithienosilole spacer [29]. The dyes benefited optical properties in terms of the red shifted absorption and molar extinction coefficient. The dye **JKSi2** which contain two phenyl groups on the Si atom showed blue shifted absorption followed by low J_{SC} of 13.90 mA cm^{-2} when compared to other congener **JKSi1** (J_{SC} = 15.10 mA cm^{-2}) which contain two methyl groups and **JKSi3 (**J_{SC} = 14.70 mA cm^{-2}) contain one methyl and one phenyl groups on the Si atom. However, the enhanced electron lifetime of the dye **JKSi2** is favourable to obtain higher efficiency of 7.50% when compared to other dyes **JKSi1** and **JKSi3** (6.73% and 6.81%).

Ko and co-workers incorporated 4,4-dimethyl-4*H*-indeno[1,2-*b*]thiophene or 4,4-dimethyl-4*H*-indeno[1,2-*b*]thienothiophene linker, bis(7-heptyl-9,9-dimethyl-9*H*-fluuoren-2-yl)amine donor and synthesized **JK-274**, **JK-275** and **JK-276** dyes (shown in Chart 4.2) [30]. These dyes exhibited red shifted absorption and high J_{SC} attributable to the elongation of conjugation. They achieved higher power conversion efficiencies (**JK-274;** 7.69%, **JK-275;** 7.54% and **JK-276**; 8.40%) when compared to the prototype dye **JK1**. Ko and co-workers synthesized a set of dyes by using 3,4-ethylenedioxythiophene and thieno[3,2-*b*]thiophene as linker and studied the effect of structural modification on the performance of the dyes [31]. The hexyloxy group on the sensitizer is utilized to improve the efficiency and stability of the dyes. All the dyes showed red shifted absorption and better light harvesting ability when compared to the dye **JK1**. The dye **JK-184** exhibited higher power conversion efficiency of 8.70% (J_{SC} = 17.49 mA cm^{-2}, V_{OC} = 700 mV and *ff* = 0.70) and it has remarkable stability up to 1000 h under light soaking experiments at 60 °C with ionic liquid electrolyte.

Thomas and co-workers designed and synthesized a set of dyes (**JA-1** and **JA-2**) by introducing fluorene as linker instead of phenyl linker in **JK-1** and **JK-2** and demonstrated DSSC application [12]. The dye **JA-2** containing bithiophene showed highest efficiency of 5.80% (J_{SC} = 11.71 mA cm^{-2}, V_{OC} = 709 mV and *ff* = 0.71) than thiophene containing dye **JA1** (η = 4.65%, J_{SC} = 9.69 mA cm^{-2}, V_{OC} = 664 mV and *ff* = 0.70). Elongation of conjugation for **JA2** is responsible for longer wavelength absorption and larger J_{SC} than those of the dye **JA1**. These dyes showed longer wavelength absorption compared to **JK-1** and **JK-2** but they exhibited inferior power conversion efficiencies ascribed to low J_{SC} and low V_{OC} values. The high lying HOMO of these dyes are not favourable for dye regeneration and led to low V_{OC} values when compared to the **JK-1** and **JK-2** dyes.

Table 4.1 Optical, electrochemical and photovoltaic performance parameters of arylamine donor containing dyes

Dye	$\lambda_{max,}$ nm (ε_{max}, M^{-1} cm^{-1})	E_{ox} , V (*vs* NHE)	E_{ox}^{*}, V (*vs* NHE)	J_{SC} (mA cm^{-2})	V_{OC} (mV)	*ff*	η (%)	*Ref*
1P-PPS	417 (23000)	1.63	–0.91	13.86	650	0.57	5.14	[5]
TT	461 (27100)	1.56	–0.74	16.26	660	0.58	6.17	[5]
1N-PPS	422 (36300)	1.59	–0.93	14.20	660	0.60	5.68	[5]
1N-PSS	461 (31300)	1.58	–0.74	14.28	710	0.60	6.12	[5]
BP1	441 (40300)	1.28	na	13.61	610	0.64	5.33	[18]
BP2	430 (36500)	1.29	na	14.16	650	0.65	5.95	[18]
FL1	469 (34900)	1.18	–0.98	10.56	690	0.65	4.70	[19]
FL2	487 (40500)	1.08	–1.00	7.52	618	0.65	3.01	[19]
FL3	421 (52900)	1.28	na	12.47	650	0.65	5.23	[20]
FL4	421 (46300)	1.22	na	7.59	570	0.67	2.86	[20]
FL5	425 (54500	1.23	na	8.38	600	0.67	3.35	[20]
JK-1	436 (30000)	1.06	–1.27	12.20	764	0.77	7.20	[11]

na = not available

Table 4.1 (cont.)

Dye	$\lambda_{max,}$ nm (ε_{max}, M^{-1} cm^{-1})	E_{ox} , V (*vs* NHE)	E_{ox}^{*}, V (*vs* NHE)	J_{SC} (mA cm^{-2})	V_{OC} (mV)	*ff*	η (%)	*Ref*
JK-2	452 (39000)	1.01	–1.36	14.00	753	0.77	8.01	[11]
C201	514 (41200)	1.00	–0.78	13.35	777	0.75	7.80	[24]
C203	525 (50000)	0.98	–0.76	14.33	734	0.76	8.00	[25]
C204	525 (33500)	1.00	–0.87	13.82	762	0.75	7.92	[26]
C205	544 (38500)	0.89	–0.87	15.68	746	0.71	8.32	[26]
JKBF1	463 (25300)	1.23	–1.07	14.39	700	0.66	6.65	[27]
JKBF2	479 (33300)	1.15	–1.04	11.43	670	0.62	4.70	[27]
JK-225	480 (55000)	0.93	–1.26	13.84	790	0.75	8.20	[28]
JKSi1	504 (49000)	1.06	–1.05	15.10	649	0.69	6.73	[29]
JKSi2	459 (24100)	1.07	–1.20	13.90	739	0.73	7.50	[29]
JKSi3	485 (16500)	1.06	–1.26	14.70	640	0.72	6.81	[29]
JK-274	467 (39800)	1.28	–1.01	13.42	749	0.77	7.69	[30]
JK-275	483 (56900)	1.16	–1.05	14.92	661	0.76	7.54	[30]
JK-276	485 (53100)	1.14	–1.06	15.50	727	0.75	8.40	[30]
JK-200	450 (23100)	0.95	–1.33	13.02	570	0.72	5.30	[31]
JK-201	481 (25000)	1.00	–1.23	13.81	590	0.68	5.65	[31]
JK-178	455 (32100)	1.03	–1.24	16.34	640	0.74	7.83	[31]
JK-179	476 (38400)	1.02	–1.22	15.22	580	0.70	6.21	[31]
JK-184	466 (45100)	0.99	–1.26	17.49	700	0.70	8.70	[31]
JK-185	484 (47800)	0.97	–1.24	15.94	660	0.67	7.04	[31]
JA1	492 (24100)	1.04	–1.01	9.69	664	0.70	4.65	[12]
JA2	513 (sh)	1.02	–1.04	11.71	709	0.71	5.80	[12]

Based on the literature survey, difluorenylamine have been found to serve as better donor due to the following reasons (1) bulky rigid conjugation with trigonal structure; (2) facile introduction of alkyl chains at C9-positions; (3) outstanding thermal stability and photo stability. By keeping all these points in mind, we haved designed a set of dyes (shown in Chart 4.3) by incorporating 2,7-disubstitued carbazole linker and difluorenylamine donor and cyanoacrylic acid acceptor. In addition, we also synthesized dyes containing fluorenylphenylamine donor to study the effect of fluorene unit. Also, the effect of symmetrical and unsymmetrical donor units on the efficiency was also studied. These bulky

and trigonal structural dyes are expected to improve the optical properties, inhibit the aggregation on TiO_2 surface, and retard the charge recombination which could essentially enhance the power conversion efficiencies in the DSSC.

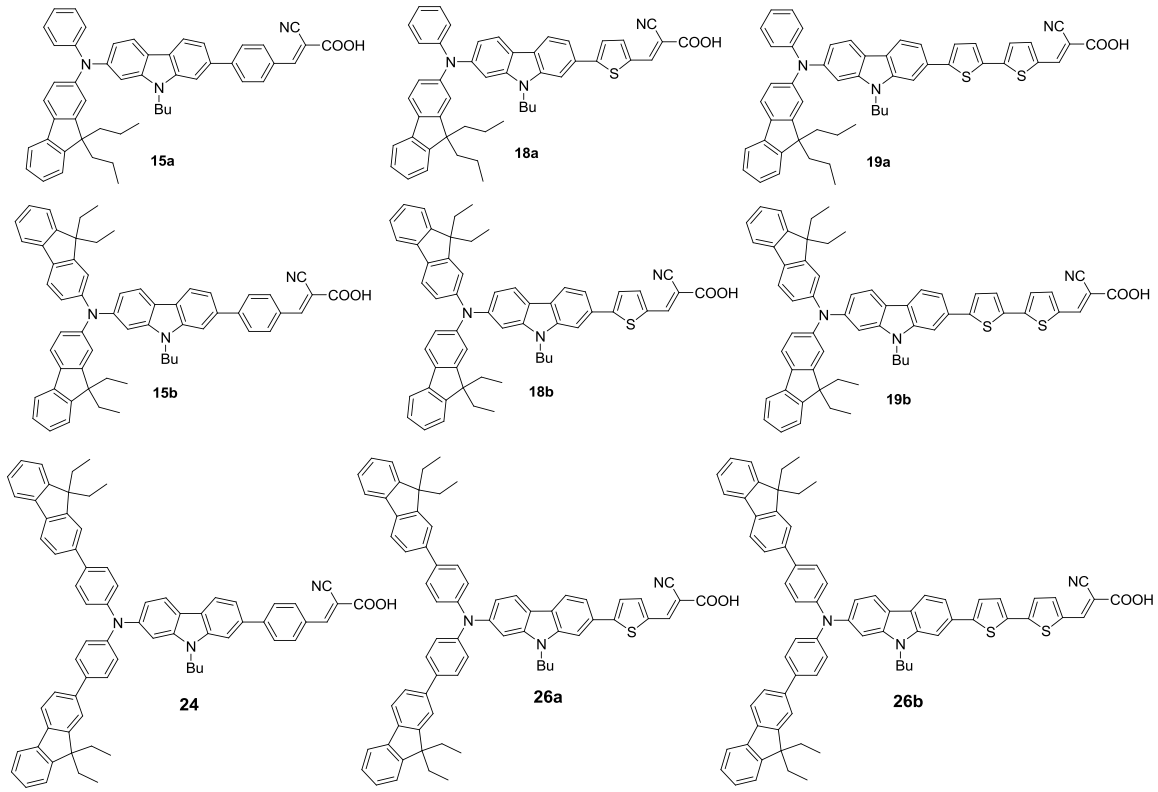

Chart 4.3 Structure of the carbazole dyes containing arylamine donor decorated with fluorene units.

4.2 Results and Discussion

4.2.1 Synthesis and Characterization

The structures of the dyes are displayed in Chart 4.3 and the synthetic pathway illustrated in Scheme 4.1. Secondary amines (**12a** and **12b**) were synthesized according to Buchwald-Hartwig C-N coupling [32] from bromoaromatics and arylamines in moderate yields. The slight excess of 2,7-dibromo-9-butyl-9*H*-carbazole (**1**) [33, 34] was treated with aromatic secondary amines (**12a** and **12b**) *via* the Hartwig's palladium catalyzed C-N coupling protocol [32] to give the precursor containing bromo aromatics (**13a** and **13b**) in good yield. The Suzuki coupling [35] of 4-formylphenylboronic acid with the bromo derivatives gave corresponding carbazole aryl carboxaldehydes (**14a** and **14b**) in excellent yields. The other heteroaromatic aldehydes (**16a**, **16b**, **17a** and **17b**) were prepared by Stille coupling reaction

[36] of bromo aromatics (**13a** and **13b)** with tin reagents of the suitably protected heteroaryl aldehydes in the presence of palladium catalyst and followed by acidic hydrolysis. The aldehyde derivatives were later converted to the corresponding cyanoacrylic acid derivatives (**18** and **19**) by Knoevenagel condensation with cyanoacetic acid [37].

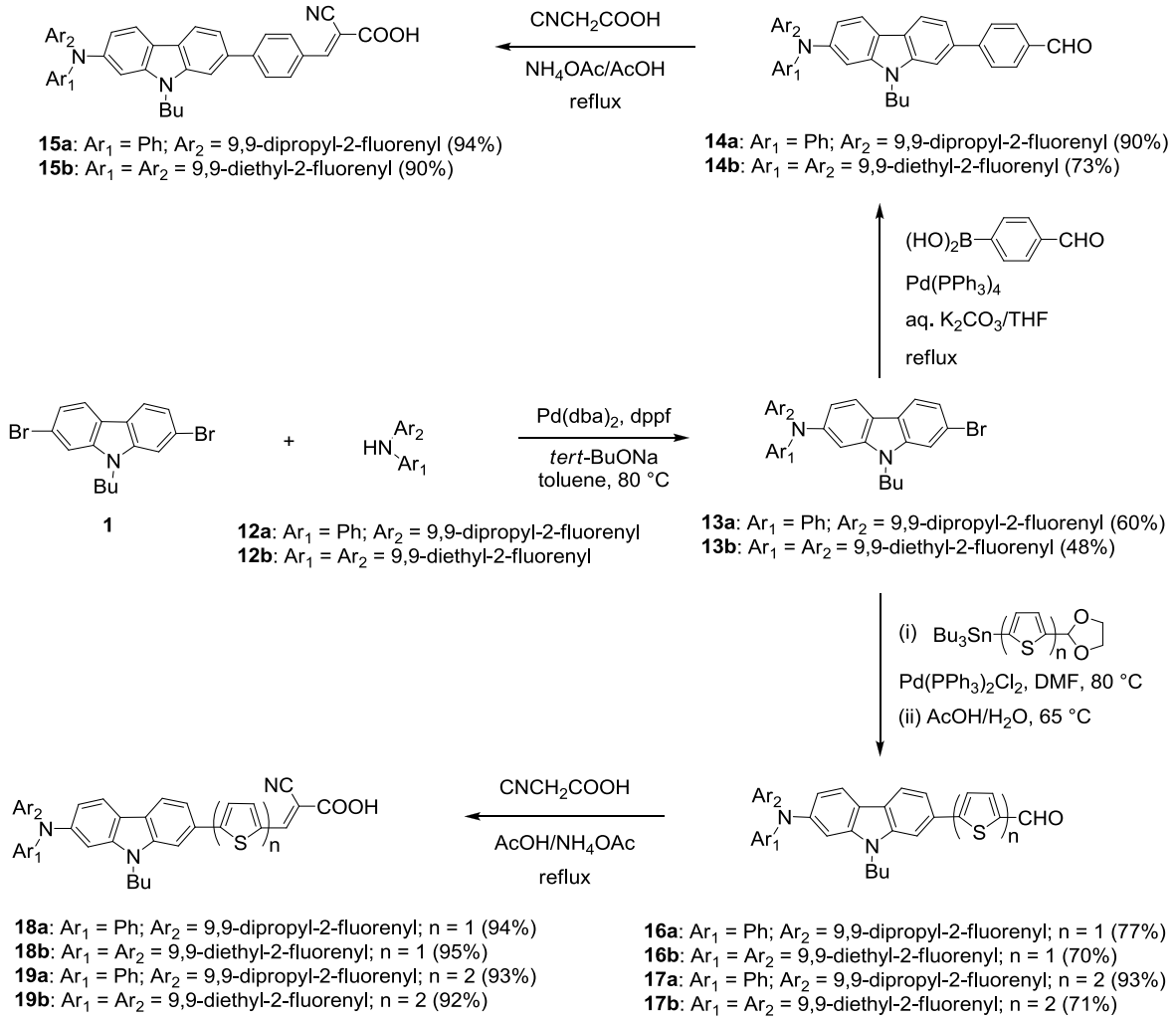

Scheme 4.1 Synthetic scheme for the preparation of 2,7-disubstituted carbazole dyes**.**

The synthesis of the dyes containing fluorene in periphery of the donor is shown in Scheme 4.2. The synthesis of secondary amine **21** was accomplished by Suzuki coupling [35] of bis(4-bromophenyl)amine (**20**) with 9,9-diethyl-9*H*-fluoren-2-ylboronic acid in moderate yield. The reaction of secondary amine, **21** with slight excess of 2,7-dibromo-9-butyl-9*H*-carbazole (**1**) by Hartwig-Buchwald C-N coupling protocol [32] gave 7-bromo-9-butyl-***N***,***N***-bis(2',4'-dimethoxybiphenyl-4-yl)-9*H*-carbazol-2-amine **22** in moderate yield. Again, the Suzuki coupling [35] of **22** with 4-formylphenylboronic acid gave aldehyde derivative of carbazole (**23**). The Stille coupling reaction [36] of bromo derivative of carbazole (**22**) with suitable tin reagents of protected heteroaromatic aldehydes and followed by acidic hydrolysis

gave the carbazole containing oligothiophene aldehydes (**25a**, **25b**). The target dyes (**24**, **26a** and **26b**) were synthesized from corresponding carbazole aldehyde derivatives (**23**, **25a** and **25b**) by Knoevenagel condensation [37] with cyanoacetic acid in presence of ammonium acetate as a catalyst. All the compounds were thoroughly characterized by IR, NMR (^{1}H and ^{13}C) and HR mass spectral methods.

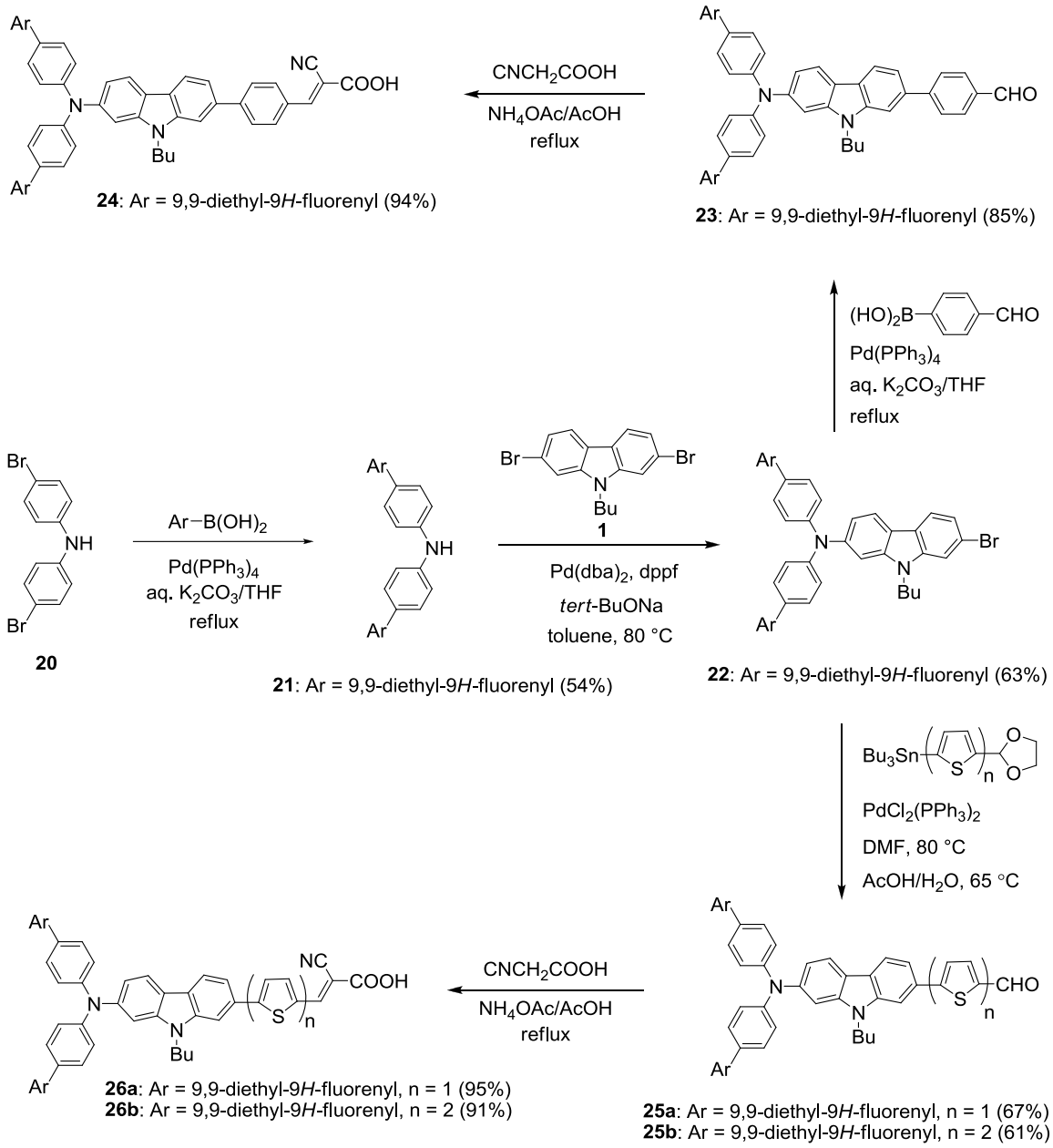

Scheme 4.2 Synthetic scheme to prepare target dyes.

4.2.2 Photophysical Properties

The absorption spectra of the dyes measured in dichloromehtane are displayed in Figure 4.1 and the relevant data compiled in Table 4.2. For comparison absorption spectra of bromo and

aldehyde analouges were recorded in dichloromethane (Figure 4.2) and data is presented in Table 4.3.

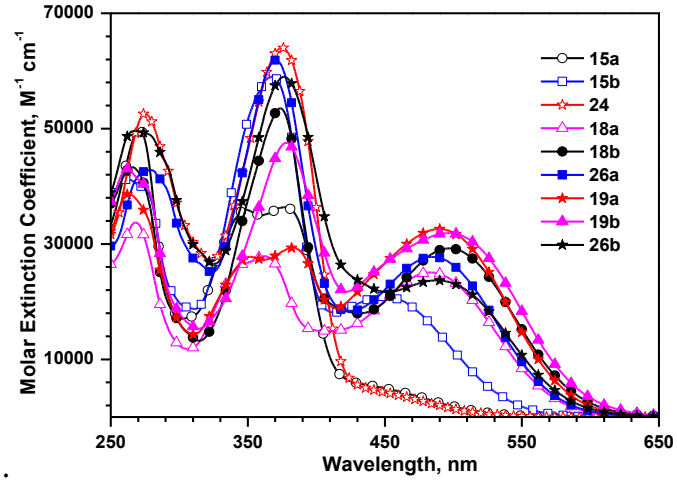

Figure 4.1 Absorption spectra of the dyes (**15, 18, 19, 23** and **26**) recorded in dichloromethane.

All the dyes showed three major distinguishable absorption peaks. The high energy peak around 265 nm is attributed to the π-π* transition localized on the diarylamine unit. The next absorption peak ranging from 310-410 nm is a π-π* transition originating from the conjugation pathway of the dyes and its molar extinction coefficient raised on fluorene incorporation. Longer wavelength absorption peak is due to the charge transfer transition from the amine donor to the cyanoacrylic acid acceptor. The overall trend observed for absorption maxima of all the dyes assumes an order: **15a** (449 nm) < **24** (454 nm) < **15b** (455 nm) < **18a** (483 nm) < **26a** (485 nm) < **26b** < (488 nm) < **19a** (490 nm) < **18b** (497 nm) < **19b** (498 nm). The dyes containing difluorenylamine showed red shifted absorption with high molar extinction coefficient owing to its strong donating strength which favors strong donor-acceptor interactions. Broader absorption of the dyes may facilitate the larger photocurrent generation in DSSC due to more capability to harvest photons [38]. Fluorenylphenylamine containing dyes showed red shifted absorption than fluorene unit decorated on *para* position of the phenyl unit. It indicates that direct incorporation of fluorene into amine unit has more impact on donor strength and absorption maxima of the dyes. For each individual donating unit, the order of absorption wavelength maxima for linkers follows the order: phenyl < thiophene < bithiophene. The shorter wavelength absorption of dyes corresponds to phenyl which is due to its twisting angle which weakens the donor-acceptor interaciton [39]. While

the dyes containing bithiophene showed red shifted absorption when compared to thiophene analogs owing to the elongation of conjugation and its electron richness [40, 41].

Table 4.2 Optical properties of the dyes recorded in dichloromethane

Dye	$\lambda_{abs,}$ nm ($\varepsilon_{max} \times 10^3$ M^{-1} cm^{-1})		
	DCM	DCM + TFA	DCM + TEA
15a	449 (sh), 377 (36.4), 348 (36.0), 271 (49.9)	457 (5.8), 377 (37.5), 349 (36.4)	382 (40.4), 349 (36.8)
15b	455 (20.8), 368 (59.0), 262 (41.2)	455 (20.0), 370 (59.8)	411 (38.1), 378 (49.0)
18a	483 (25.1), 363 (27.9), 268 (33.7)	493 (26.8), 364 (29.6), 268 (37.4)	434 (38.9), 350 (35.3)
18b	497 (29.2), 374 (53.5), 266 (43.3)	510 (27.9), 375 (53.7), 267 (44.8)	441 (36.8), 370 (47.9)
19a	490 (32.6), 383 (29.3), 352 (27.8), 263 (38.7)	503 (35.6), 385 (31.2), 351 (28.9), 264 (42.3)	448 (42.9), 353 (30.7)
19b	498 (31.9), 378 (47.5), 262 (43.0)	503 (31.5), 379 (44.6), 264 (42.7)	450 (42.3), 376 (48.6)
24	454 (sh), 375 (64.0), 275 (52.6)	467 (45.6), 374 (64.7), 276 (53.2)	377 (72.2)
26a	485 (27.7), 371 (61.9), 279 (42.8)	497 (25.9), 372 (60.1), 279 (44.8)	432 (45.1), 370 (71.1), 277 (55.8)
26b	488 (23.7), 376 (59.0), 267 (50.0)	500 (23.9), 375 (54.5), 270 (48.4)	431 (43.7), 375 (68.1)

It is intersting to compare the absorption properties of the dyes with the parent carbazole dyes (**7a** and **7b**) and the phenyl [11] and fluorene [12] linked dyes containing diflourenylamine donor. These new dyes are benefited in terms of optical properties when compared to the fluorene-based dyes (**FL1**-**FL5**) which contain different diarylamine unit [18, 19]. Particulary, these dyes possess longer wavelength absorption than the dyes **JA1** and **JA2** which contain fluorene linker [12]. The dyes showed red shifted absorption when comapred to the dyes (**JKBF1** and **JKBF1**) containing benzo[*b*]furan linker which indicates that the carbazole facilitates effective electronic communication between the donor and acceptor units [27]. Also, the new dyes showed longer wavelength absorption when compared to the dyes containing 4,4-dimethyl-4*H*-indeno[1,2-*b*]thiophene or 4,4-dimethyl-

4*H*-indeno[1,2-*b*]thienothiophene linker which further attest the beneficial role of carbazole linker [28, 30]. These fluorene incorporated dyes showed red shifted absorption than parent carbazole dyes (**7a** and **7b**). All these newly synthesized dyes possess significantly larger molar extinction coefficients (25100 M^{-1} cm^{-1} to 32600 M^{-1} cm^{-1}) for the CT transition than that of the Ru-based dyes (**N3** and **N719**) [42].

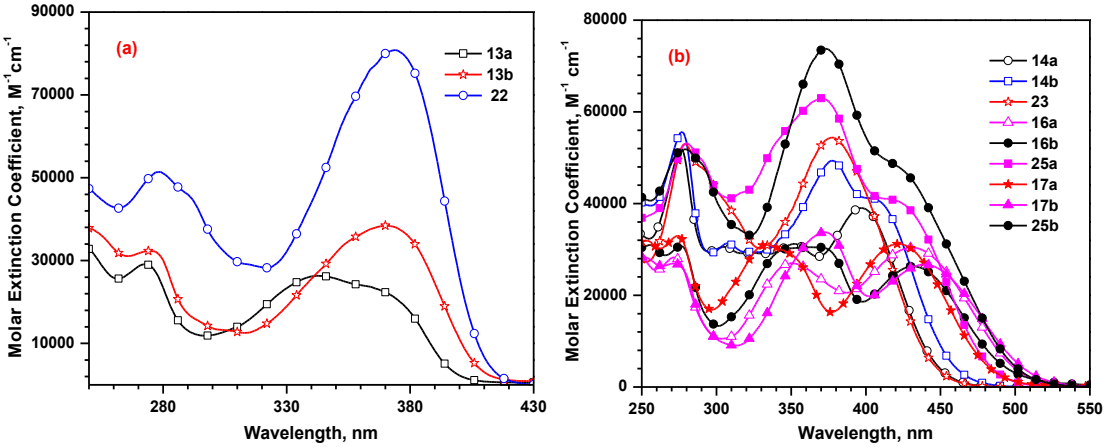

Figure 4.2 Absorption spectra of the bromo (a) and aldehyde (b) derivatives recorded in dichloromethane.

Table 4.3 Absorption and emission properties of bromo and aldehydes recorded in dichloromethane.

compd.	$\lambda_{abs,}$ nm (ε_{max} ×10^3 M^{-1} cm^{-1})	$\lambda_{em,}$ nm	Stokes shift, cm^{-1}
13a	342 (26.3), 273 (29.1)	412	4968
13b	370 (38.4), 275 (32.3)	423	3386
14a	397 (39.0), 352 (31.2), 307 (30.5), 276 (52.0)	565	7490
14b	409 (40.6), 377 (49.4), 308 (31.4), 277 (55.6)	568	6844
16a	431 (30.4), 350 (27.0), 271 (28.3)	496	3041
16b	432 (26.3), 368 (30.5), 276 (30.7), 255 (31.0)	579	5877
17a	422 (31.2), 333 (31.0), 274 (32.9), 253 (31.9)	575	6305
17b	439 (26.7), 372 (33.8), 272 (26.9)	515	3362
22	374 (80.8), 279 (51.4)	445	4266
23	378 (54.4), 279 (53.0)	567	8818
25a	424 (40.1), 370 (63.0), 280 (53.2)	574	6163
25b	425 (47.3), 373 (73.8), 279 (51.8)	503	3649

The origin of the longer wavelength absorption of the dyes is confirmed as the intramolecular charge transfer transition by the following studies. The dyes exhibited longer wavelength absorption when compared to the corresponding bromo- and aldehyde derivatives. The absorption wavelength assumes the order in accordance with the electron-withdrawing effect of the end group (Br < CHO < cyanoacrylic acid). Addition of trifluoroacetic acid (TFA) to dichloromethane solution of the dyes shows a bathochromic shift to the charge transfer absorption. But, addition of triethylamine (TEA) leads to a pronounced blue shift for this peak and they are displayed in Figures 4.3 and 4.4. Such observations have been earlier ascribed to the increment/decrement in acceptor strength on addition of TFA/TEA caused by protonation/deprotonation [43, 44].

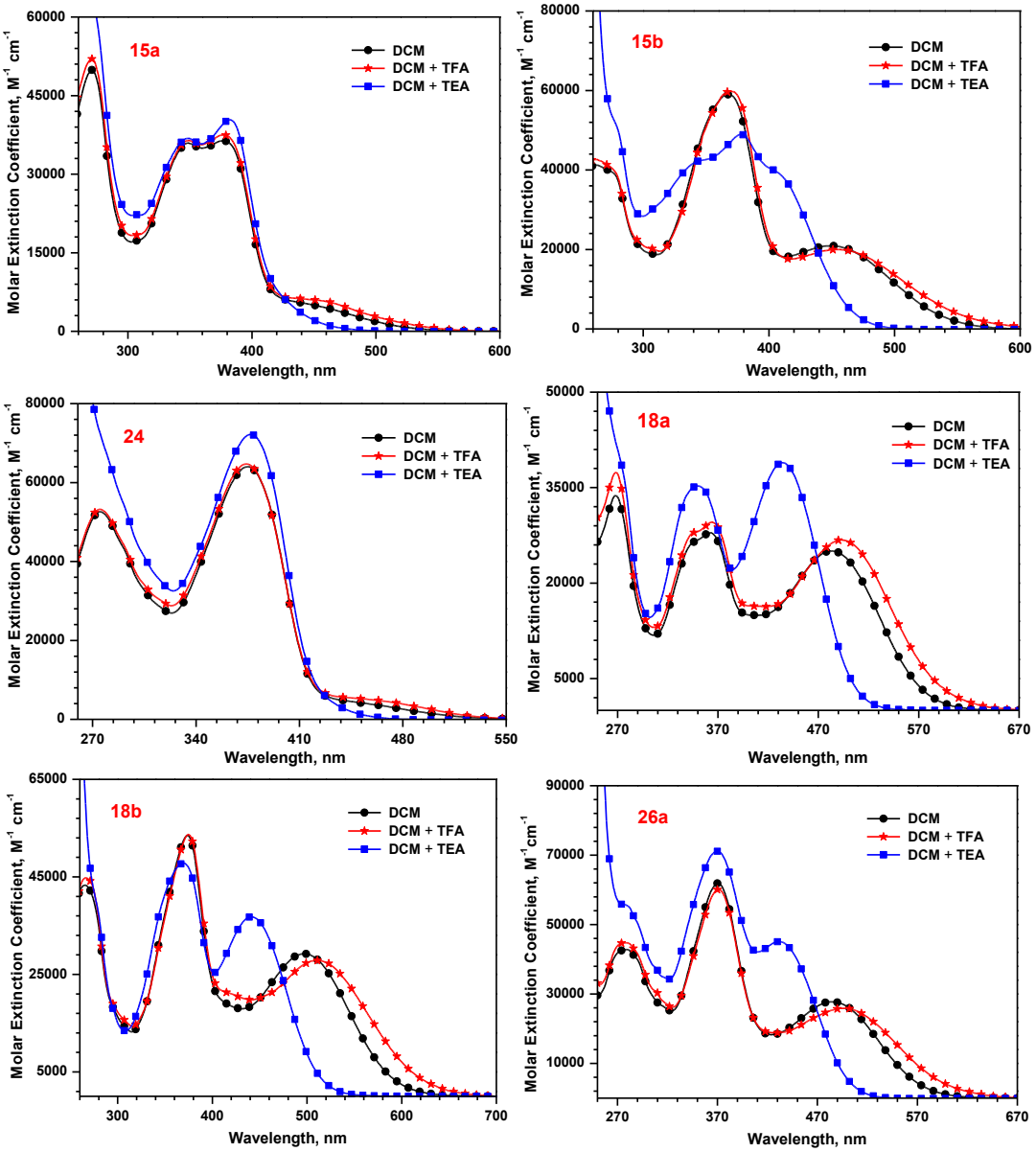

Figure 4.3 Absorption spectra of the dyes recorded in dichloromethane solution, after the addition of TEA or TFA.

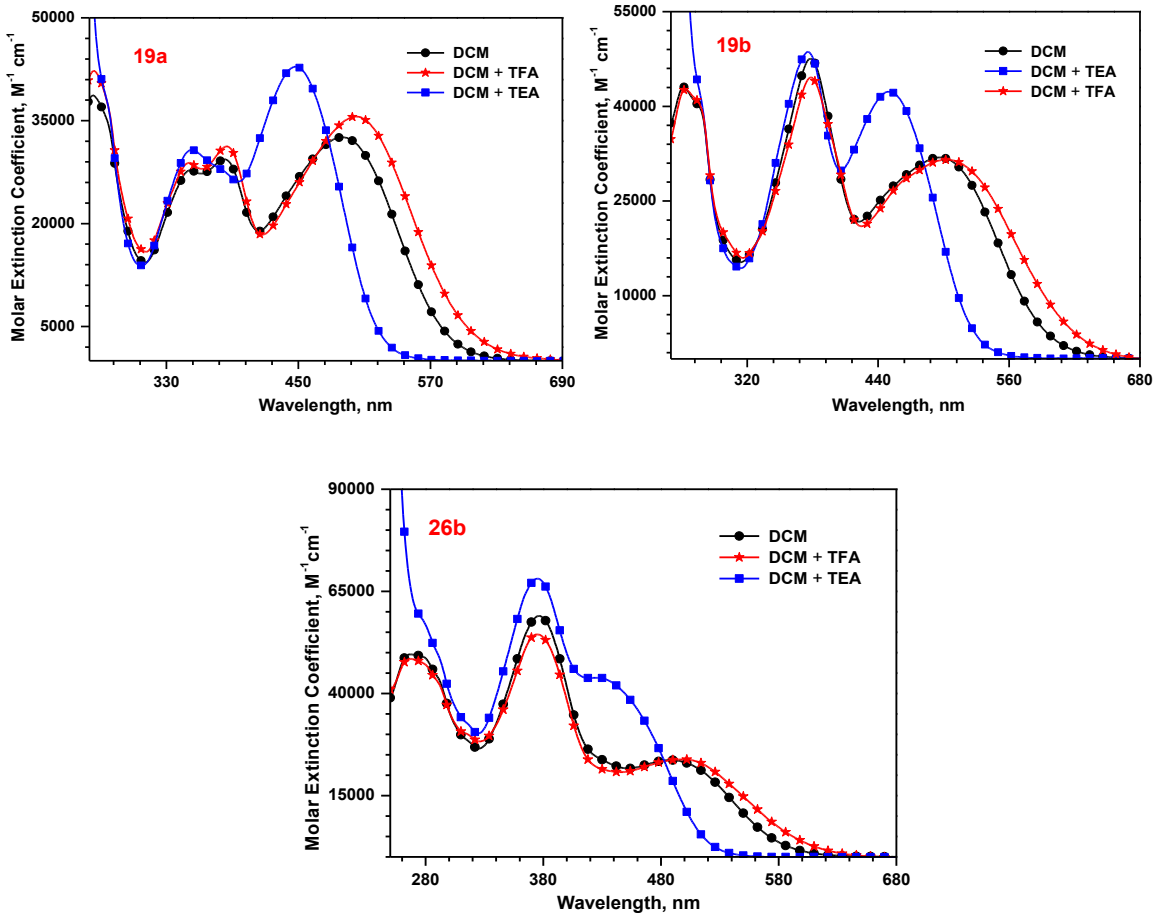

Figure 4.4 Absorption spectra of the dyes recorded in dichloromethane solution, after the addition of TEA or TFA.

All the dyes displayed a negative solvatochromism (Figures 4.5 and 4.6) in the absorption spectra. This clearly indicates that the longer absorption wavelength of the dyes is corresponding to the intramolecular charge transfer transition. The blue-shift observed on increasing the polarity of the solvent is attributed to the effective solvation of the dyes [45, 46]. However, a drastic blue shift witnessed for all dyes in DMF is probably due to the basic nature of the solvent which leads to the deprotonation of the dyes [13]. Also, the dyes showed blue shifted absorption in THF owing to its tendency of forming hydrogen bond with carboxylic acid and it might deprotonate the carboxylic acid resulting carboxylate ion which leads to poor donor-acceptor interactions and causes blue shifted absorption [13]. Similarly, a significant red-shift observed in chloro-solvents such as dichloromethane and chloroform arises due to the rapid relaxation of polarizable electrons in the excited state [47, 48].

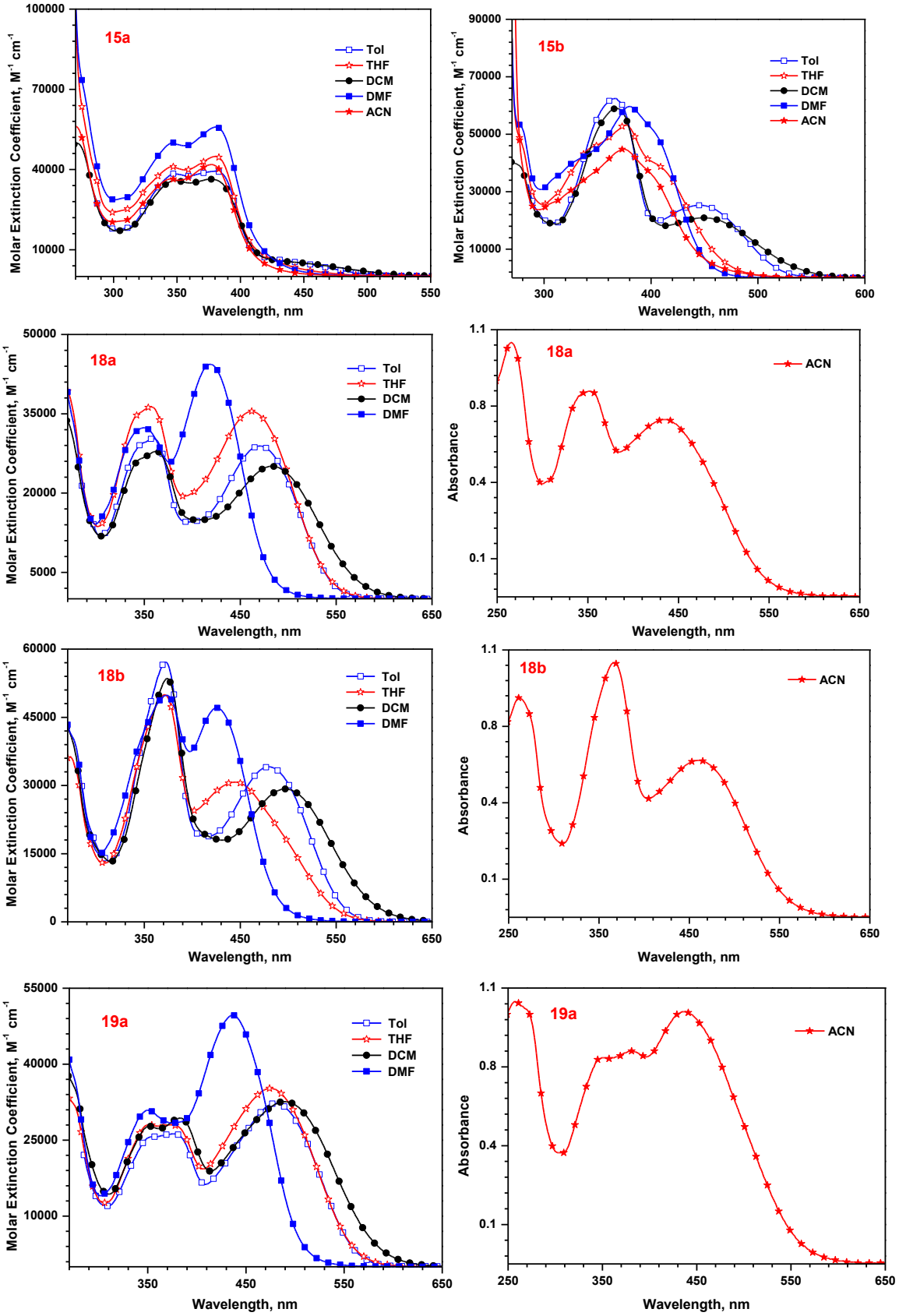

Figure 4.5 Absorption spectra of the dyes recorded in different solvents.

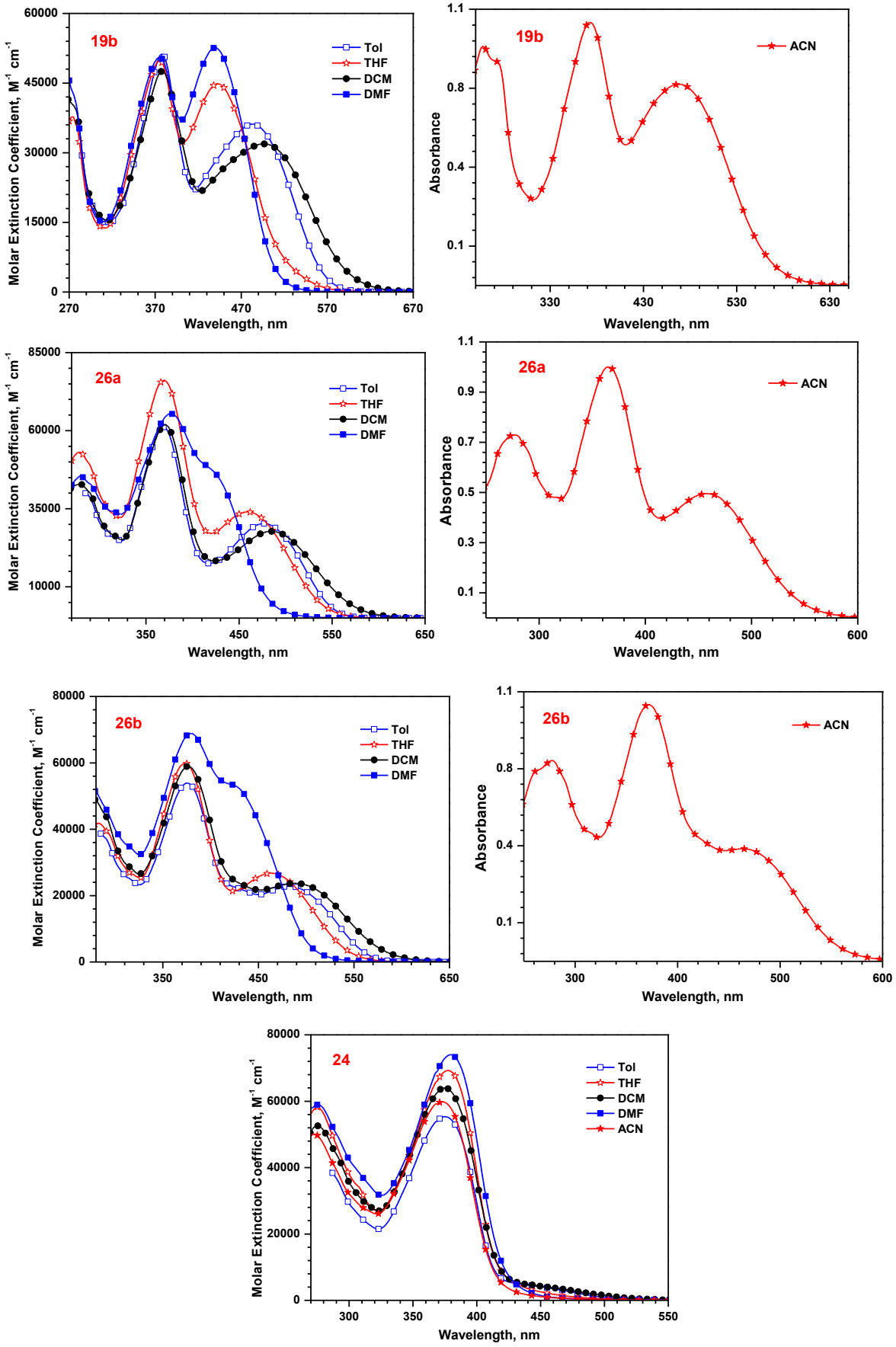

Figure 4.6 Absorption spectra of the dyes recorded in different solvents.

Table 4.4 Absorption properties of the dyes recorded in different solvents

Dye	$\lambda_{abs,}$ nm ($\varepsilon_{max} \times 10^3\ M^{-1}\ cm^{-1}$)				
	TiO_2 film	Tol	THF	DMF	ACN
15a	na	381 (39.4), 348 (38.5)	381 (44.9), 347 (41.0)	380 (55.9), 347 (50.0)	377 (41.9), 345 (36.5)
15b	na	446 (25.2), 366 (62.4)	411 (38.0), 376 (53.2), 279 (47.0)	406 (49.2), 379 (59.6), 279 (52.6)	375 (40.7)
18a	457	471 (28.9), 359 (30.3)	462 (34.9), 357 (35.8)	419 (44.4), 350 (32.4)	435, 352, 266
18b	472	480 (34.1), 372 (57.1)	445 (30.7), 371 (50.0)	426 (47.1), 324 (49.8)	460, 367, 262
19a	492	481 (32.3), 376 (26.2), 358 (25.6)	474 (35.2), 374 (28.0)	437 (49.7), 351 (30.9)	437, 381, 351, 257
19b	495	483 (36.1), 378 (51.2)	443 (44.9), 376 (49.9), 274 (37.8)	440 (52.6), 375 (50.5)	468, 373, 258
24	na	383 (36.2), 342 (40.8)	377 (69.2), 276 (58.2)	380 (59.7), 279 (52.6)	374 (44.8)
26a	475	477 (30.3), 369 (61.0)	459 (34.0), 369 (76.0), 283 (53.0)	426 (46.0), 378 (65.0), 280 (45.0)	457, 365, 276
26b	496	482 (22.8), 375 (53.9)	463 (23.7), 374 (60.0),	428 (52.7), 379 (68.8), 277 (51.6)	470, 373, 277

na = not measured

The solvatochromism data of the dyes were analyzed by correlating with $E_T(30)$ parameter [49] and plots are displayed in Figures 4.7 and 4.8. The dyes exhibited deviation from linearity for polar solvents such as dichloromethane solutions due to the effective solvent specific interaction which led to unusual red shift of these dyes. Similar behaviour has been

earlier observed for organic dyes and attributed to the instant stabilization due to a fast rearrangement of polarizable electrons during excitation [47, 48].

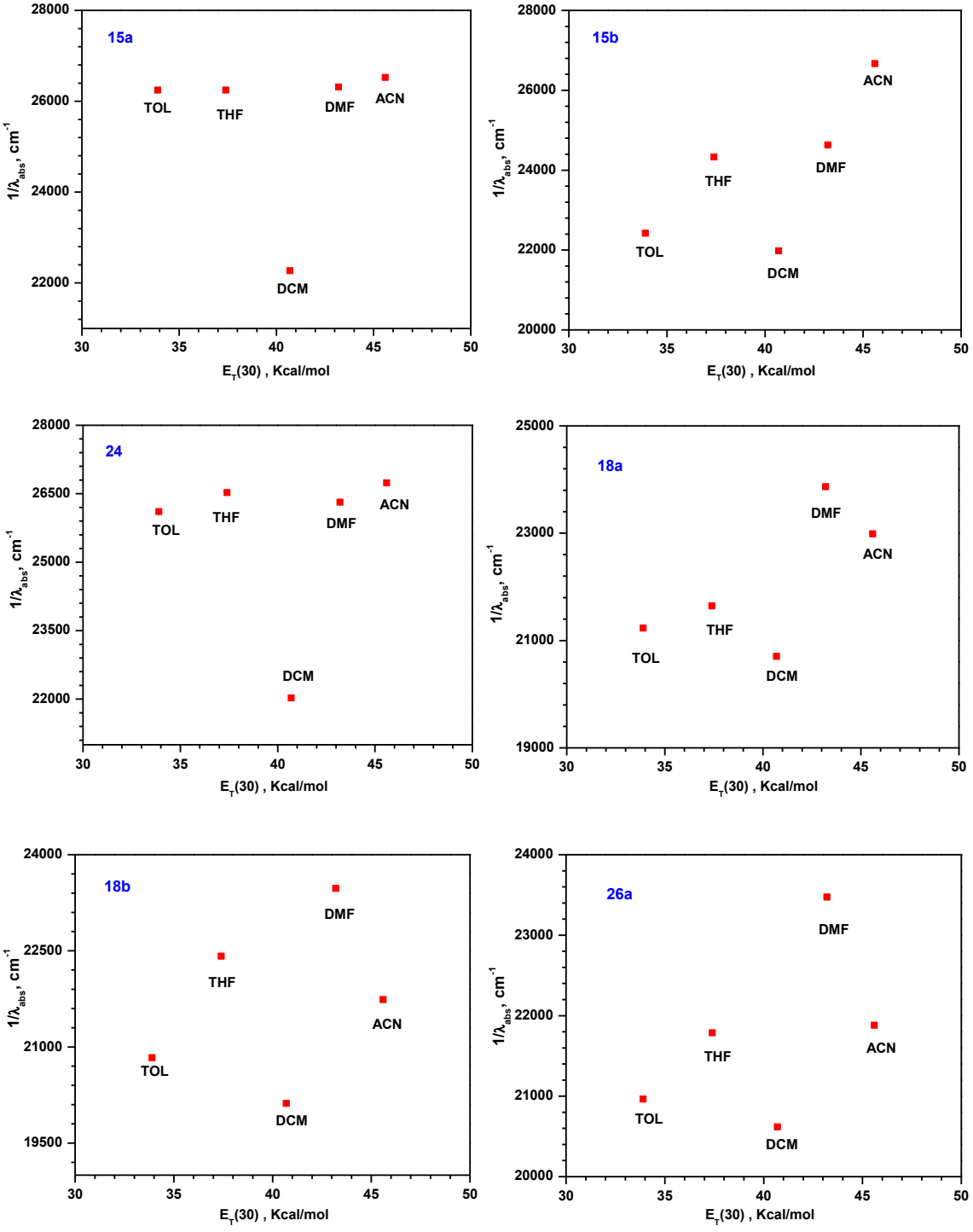

Figure 4.7 Variation of absorption (in cm^{-1}) with the solvents polarity parameter $E_T(30)$.

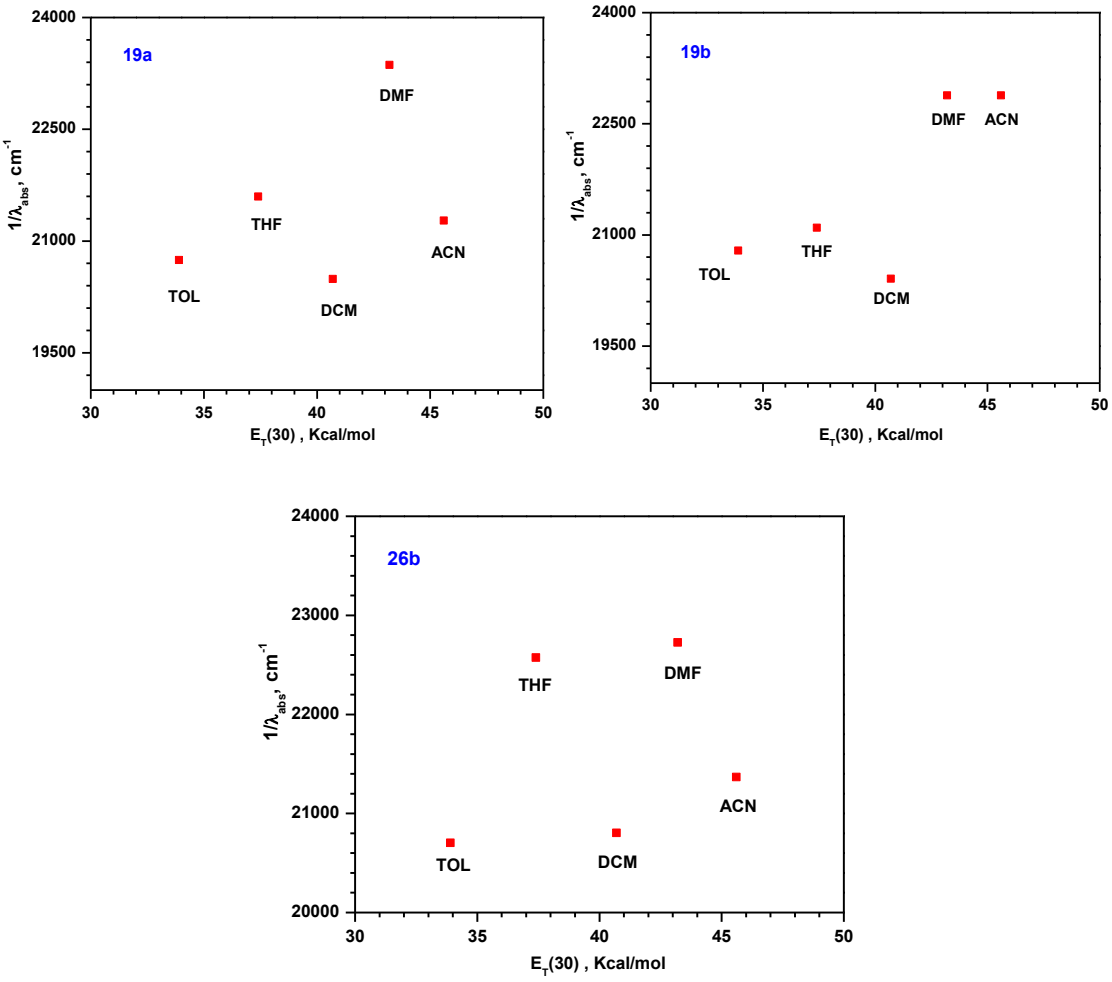

Figure 4.8 Variation of absorption (in cm^{-1}) with the solvents polarity parameter $E_T(30)$.

The emission spectra of the dyes recorded in dichloromethane are shown in Figure 4.9 and for comparison photoluminescence of precursors (bromo and aldehyde) also recorded under identical conditions (Figure 4.10). The dyes are weakly emissive in dichloromethane and the emission wavelength is not sensitive by changing the donor unit. Also the dyes showed red shifted emission when compared to their precursors. When we recorded the photoluminescence in dichloromethane solution, the emission of the dyes was quenched and feeble emission obtained. Since the excited state is charge transfer in nature most of the dyes exhibited poor emission in polar solvents. This might be due to the dipole-dipole interaction and the non-radiative relaxation of excited state by electron transfer mechanism [50, 51].

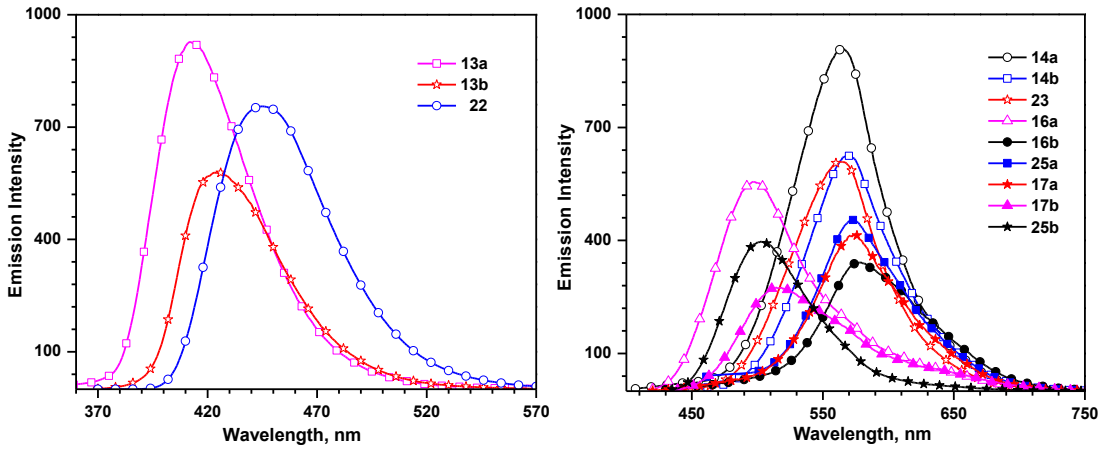

Figure 4.9 Normalized emission spectra of the bromo (a) and aldehyde (b) derivatives recorded in dichloromethane.

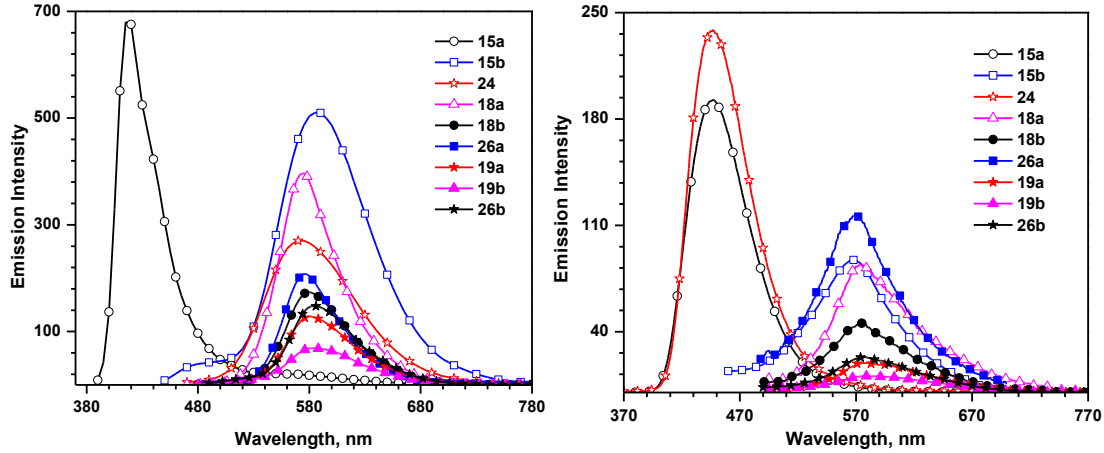

Figure 4.10 Emission spectra of the dyes (**15**, **18**, **19**, **24**, and **26b**) recorded in toluene (a) and dichloromethane (b).

Absorption spectra of the dyes anchored on transparent nanocrystalline anatase TiO_2 are displayed in Figure 4.11. The absorption of monothiophene containig dyes are blue shifted when compared with the solution spectra. This might be due to the deprotanation of the carboxylic acid on dye-TiO_2 interaction [52]. However, the bithiophene dyes exhibited severe aggregation (*J*-type) at TiO_2 surface as evidenced by broader and red-shifted absorption [53, 54]. Aggregation of the dyes may lead to self quenching excited state, which in turn might decrease the light harvesting ability of the dye.

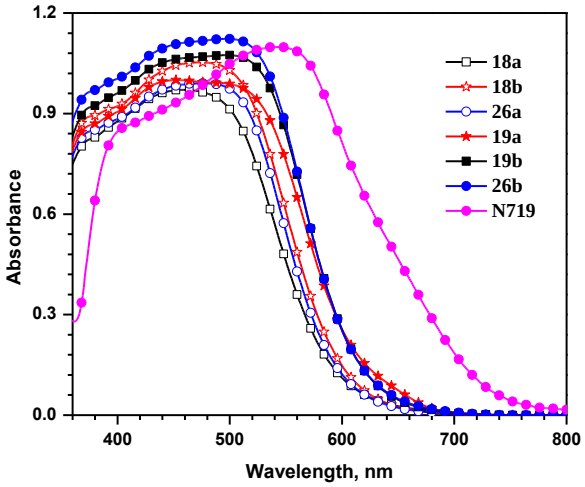

Figure 4.11 Absorption spectra of the dyes anchored on TiO_2 films.

4.2.3 Electrochemical Properties

The redox propensities of the dyes were estimated in dichloromethane by cyclic voltammetry and differential pulse voltammetry measurements. Cyclic voltammograms of the dyes are displayed in Figure 4.12 and the pertinent data displayed in Table 4.5.

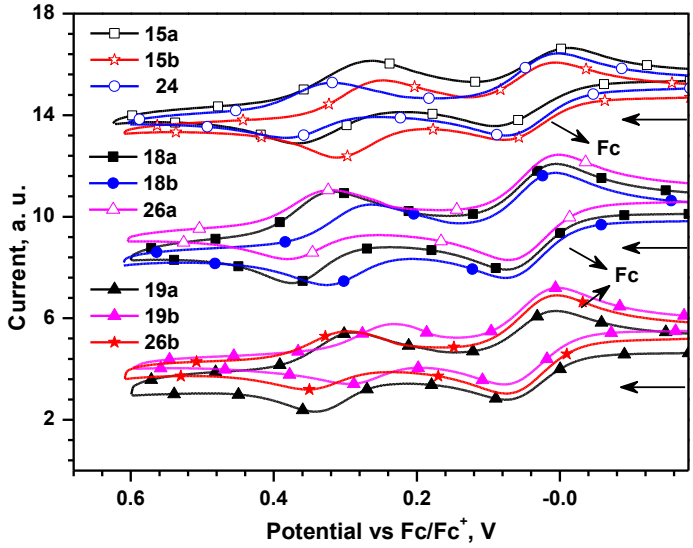

Figure 4.12 Cyclic voltammograms of the dyes (**15**, **18**, **19**, **24** and **26**) measured in dichloromethane.

All the dyes showed one quasi-reversible oxidation couple and one irreversible oxidation wave, corresponding to the removal of electron each from the amine unit and the conjugation pathway of the dyes, respectively. The order of oxidation potentials of the dyes is **19b** (0.22 V) < **15b** (0.24 V) < **18b** (0.26 V) < **15a** = **19a** = **26b** (0.28 V) < **24** (0.30 V) < **18a** (0.31 V) < **26a** (0.32 V). Difluroenylamine unit containing dyes showed easiest oxidation due to its

electron richness. The next easy oxidation is for the fluorenylphenylamine containing dyes. This indicates that the donor strength of amine segment is influenced by the incorporation of fluorene units. Higher electron richness of the system facilitates easy oxidation. The dyes which contain fluorene units on peripheral positions showed difficult oxidation when compared to other units owing to the absence of direct attachment of fluorene unit with the amine donor. The trend observed for various linkers is: bithiophene < phenyl < thiophene. The more electron richness of bithiophene is responsible for the easiest oxidation but the twisting of phenyl linker weakens the donor-acceptor interactions led to easy oxidation [5].

Table 4.5 Electrochemical data of the dyes and precursors measured in dichloromethane

compd.	E_{ox} (ΔE_P), V	HOMO, eV	LUMO, eV	$E_{0\text{-}0}$, eV	E_{ox}^*, V	ΔG_{inj}, V
13a	0.32 (68), 0.82	5.12	1.93	3.19	-2.10	1.60
13b	0.26 (69), 0.80	5.06	1.97	3.09	-2.06	1.56
22	0.32 (67), 0.83	5.12	2.08	3.04	-1.95	1.45
14a	0.30 (27), 0.77	5.10	2.50	2.60	-1.53	1.03
14b	0.24 (64), 0.77	5.04	2.53	2.51	-1.50	1.20
23	0.31 (64), 0.80	5.11	2.53	2.58	-1.50	1.20
16a	0.29 (63), 0.72	5.09	2.44	2.65	-1.59	1.09
16b	0.25 (60), 0.80	5.05	2.57	2.48	-1.46	0.96
25a	0.32 (65), 0.81	5.12	2.59	2.53	-1.44	0.94
17a	0.31 (69), 0.80	5.11	2.57	2.54	-1.46	0.96
17b	0.23 (64), 0.80	5.03	2.45	2.58	-1.58	1.08
25b	0.30 (67), 0.72	5.10	2.45	2.65	-1.58	1.08
15a	0.28 (76), 0.85	5.08	2.75	2.33	-1.28	0.78
15b	0.24 (65), 0.75	5.04	2.92	2.12	-1.11	0.61
24	0.30 (61), 0.79	5.10	2.80	2.30	-1.23	0.73
18a	0.31 (57), 0.78	5.11	2.78	2.30	-1.22	0.72
18b	0.26 (61), 0.77	5.06	2.75	2.31	-1.28	0.78
26a	0.32 (61), 0.80	5.12	2.73	2.39	-1.30	0.80
19a	0.28 (54), 0.71	5.08	2.81	2.27	-1.22	0.72
19b	0.22 (57), 0.71	5.03	2.75	2.28	-1.29	0.79
26b	0.28 (58), 0.69	5.08	2.74	2.34	-1.29	0.79

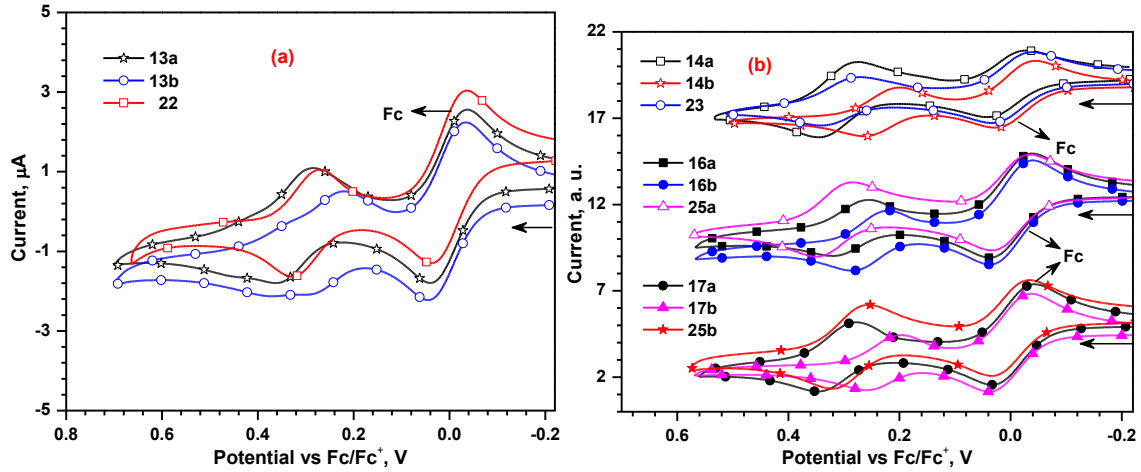

Figure 4.13 Cyclic voltammograms of the bromo (a) and aldehyde (b) derivatives recorded in dichloromethane.

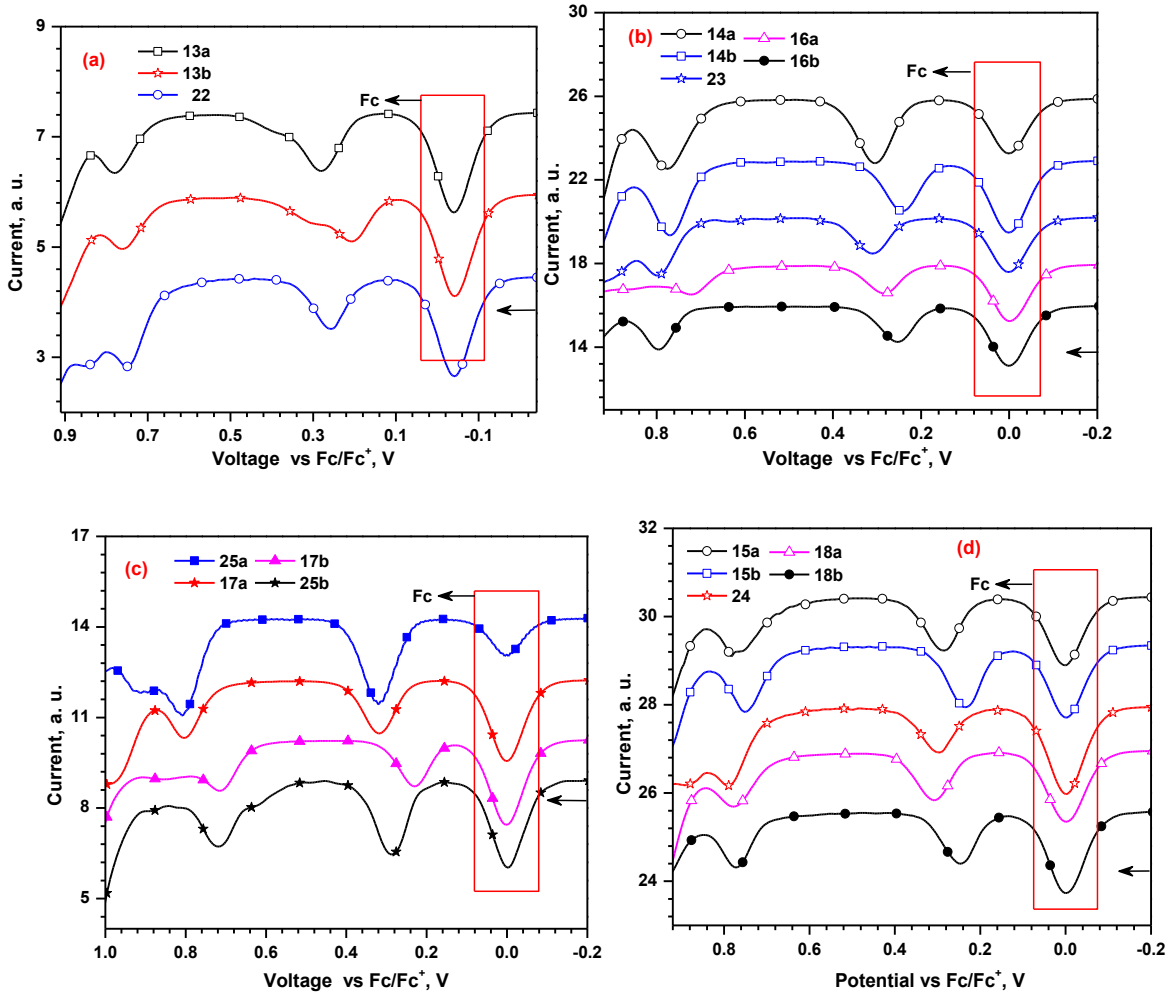

Figure 4.14 Differential pulse voltammograms of the (a) bromo (b and c) aldehyde and (d) dyes recorded in dichloromethane.

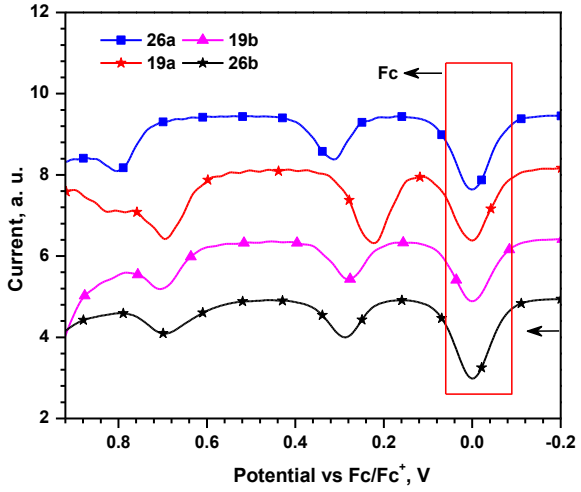

Figure 4.15 Differential pulse voltammograms of the dyes recorded in dichloromethane.

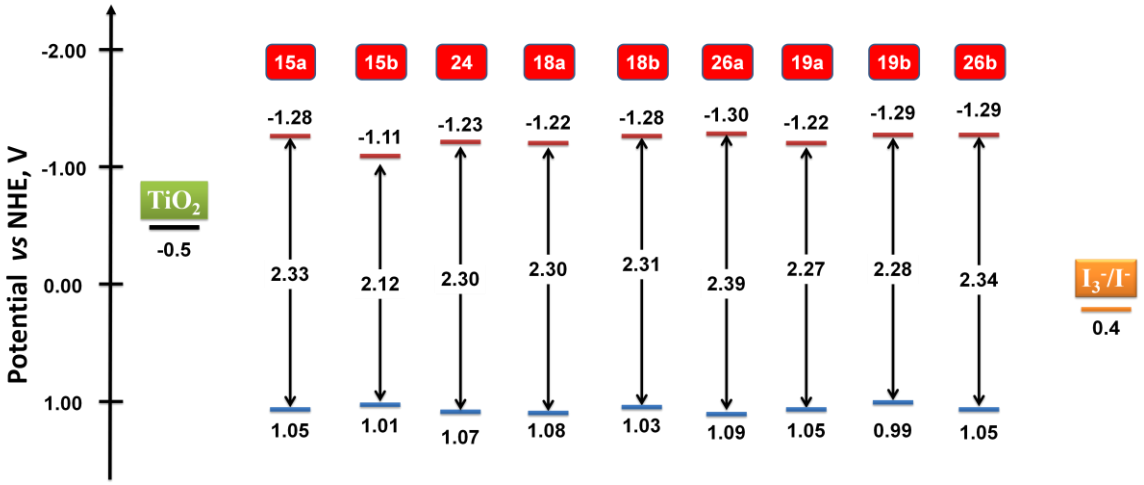

Figure 4.16 Comparison of the energy levels of the dyes (**15, 18, 19, 24** and **26**) in the ground and excited states.

The comparison of energy levelsof the dyes is presented in Figure 4.16. The simultaneous introduction of fluorene unit in donor raises the excited state potentials and also incorporation of fluorene at peripheral positions of donor lifted the LUMO more negative which are beneficial for thermodynamically favourable electron injection process [55]. The ground state oxidation potentials for these dyes are in the range of 0.99-1.09 V *vs* NHE, which are more positive than the redox potential of I^-/I_3^- redox couple, thus favors the efficient regeneration of the dyes from the oxidized form by the electrolyte [1]. The excited-state oxidation potentials (-1.11 V to -1.30 V) of the sensitizers are more negative than the conduction band of the TiO_2 which is suitable for electron injection from the excited state of the dye into the conduction band of the TiO_2 [1]. The calculated ΔG_{inj} of the dyes are in the following order:

15b (0.61 V) < **18a** = **19a** (0.72 V) < **24** (0.73 V) < **15a** = **18b** (0.78 V) < **19b** = **26b** (0.79 V) < **26a** (0.80 V). High ΔG_{inj} of the dyes favor thermodynamically favourable process and more charge injection from excited state of the dyes into the conduction band of TiO_2.

4.2.4 Theoretical Calculations

To gain further insight into the electronic structure of the compounds, density functional theory (DFT) calculations were performed by using the 6-31+G (d, p) basis set and two different correlation functionals (B3LYP [56] and MPW1K [57]). The geometry of compounds was first optimized in the ground state. The vertical energies were computed using the time dependent density functional theory in the same level using the ground state optimized structures. The vertical transitions and assignments are listed in Tables 4.6 and 4.7. The frontier molecular orbitals (HOMO and LUMO) of the dyes are displayed in Figure 4.17. The HOMO of the dyes is mainly located on diarylamine unit and carbazole while the LUMO of the dyes mainly distributed on cyanoacrylic acid and spread upto oligothiophene units.

The longer wavelength absorption corresponds to the electronic transition from HOMO to LUMO. In thiophene containing dyes (**18a** and **18b**), HOMO-1 is mainly located on the carbazole linker but for **26a** it is located on fluorene units decorated on diphenylamine unit. This clearly indicates that the carbazole acts as donating unit and it is origin of second oxidation in this dye. But, for bithiophene containing dyes (**19a**, **19b** and **26b**), HOMO-1 is spread over carbazole and oligothiophene conjugation pathway. The next absorption wavelength of the dyes corresponds to the electronic excitation of HOMO-2 to LUMO and/or HOMO-1 to LUMO. The peak position estimated by B3LYP calculations are over estimated but MPW1K gave more reliable results. For the dyes which contain fluorene decoration on the periphery of donor, HOMO of the dyes is mainly located on the triarylamine segment composed of diphenylamine and carbazole units and slightly diffused into the peripheral fluorene and thiophene units. The LUMO of the dyes is mainly contributed by the cyanoacrylic acid acceptor and the thiophene units.

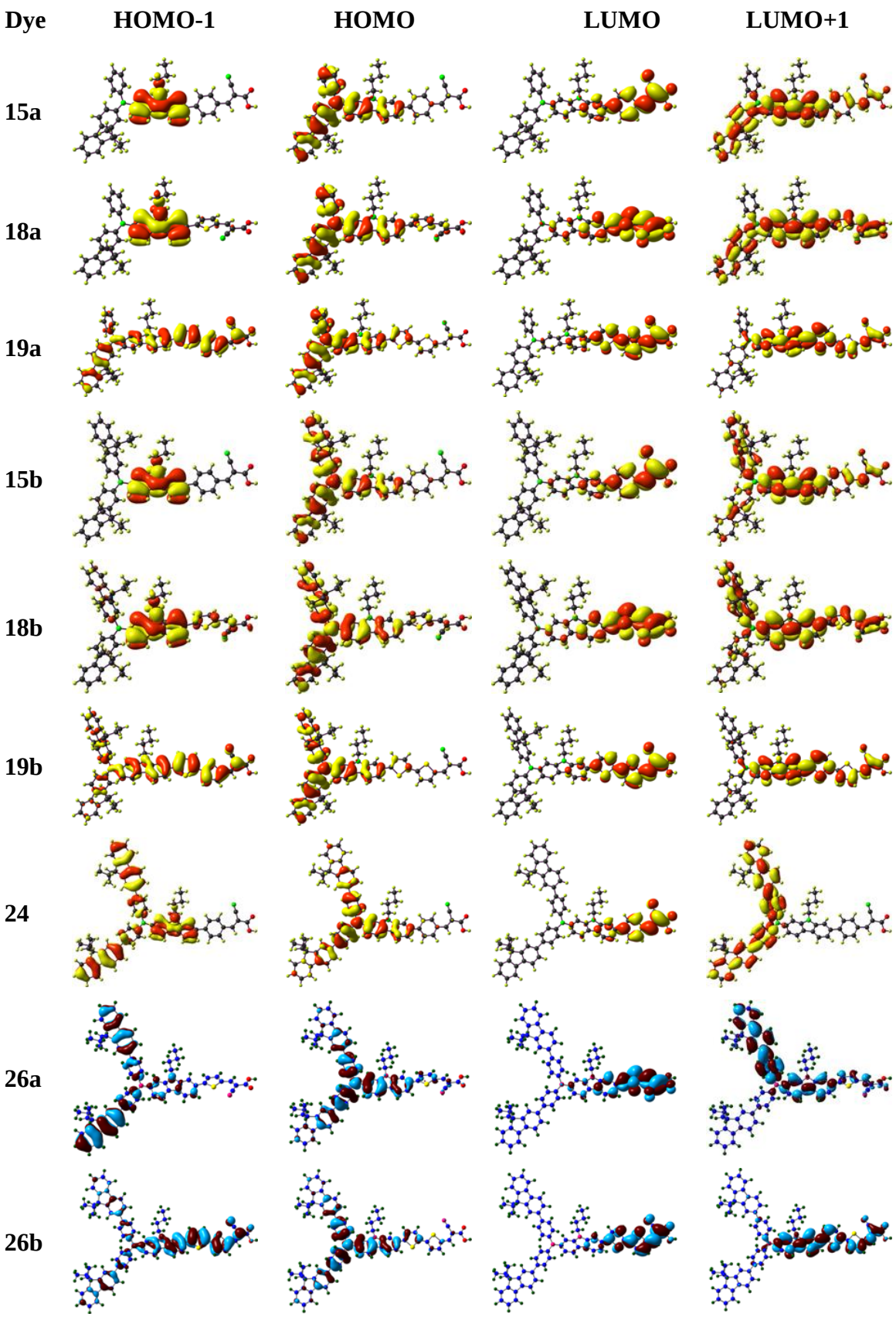

Figure 4.17 Frontier molecular orbitals of the dyes.

Table 4.6 Computed vertical transition energies and their oscillator strengths, assignments, dipole moments and band gaps for the dyes using B3LYP theory

Dye	λ	*f*	assignments	μ_g (D)	HOMO (eV)	LUMO (eV)	E_g (eV)
15a (vacuum)	586.8	0.32	HOMO → LUMO (100%)	6.11	-4.88	-2.54	2.34
	403.4	0.77	HOMO-2 → LUMO (93%)				
	374.6	0.47	HOMO → LUMO+1 (89%)				
	349.9	0.21	HOMO → LUM+2 (78%), HOMO-3 → LUMO (18%)				
	345.7	0.26	HOMO-3 → LUMO (78%)				
15a (THF)	616.7	0.38	HOMO → LUMO (99%)	7.10	-4.88	-2.63	2.25
	417.6	0.80	HOMO-2 → LUMO (94%)				
	379.8	0.62	HOMO → LUMO+1 (91%)				
	356.7	0.15	HOMO-3 → LUMO (69%), HOMO → LUMO+2 (28%)				
	352.3	0.34	HOMO → LUMO+2 (67%), HOMO-3 → LUMO (27%)				
15b (vacuum)	608.8	0.29	HOMO → LUMO (100%)	6.16	-4.80	-2.54	2.26
	408.0	0.93	HOMO-2 → LUMO (86%)				
	384.6	0.20	HOMO → LUMO+1 (82%)				
	379.1	0.67	HOMO → LUMO+2 (92%)				
	327.4	0.32	HOMO-4 → LUMO (93%)				
15b (THF)	638.7	0.34	HOMO → LUMO (99%)	7.12	-4.81	-2.63	2.18
	423.0	0.91	HOMO-2 → LUMO (93%)				
	388.8	0.35	HOMO → LUMO+1 (87%)				
	385.8	0.80	HOMO → LUMO+2 (94%)				
	336.3	0.31	HOMO-4 → LUMO (96%)				
24 (vacuum)	593.6	0.33	HOMO → LUMO (100%)	6.73	-4.85	-2.54	2.31
	418.3	0.62	HOMO-3 → LUMO (92%)				
	390.8	0.88	HOMO → LUMO+1 (94%)				
	385.7	0.78	HOMO → LUMO+2 (85%)				
	363.2	0.19	HOMO-4 → LUMO (92%)				
24 (THF)	613.8	0.38	HOMO → LUMO (99%)	7.71	-4.86	-2.65	2.21
	439.5	0.59	HOMO-2 → LUMO (96%)				
	395.5	0.83	HOMO → LUMO+1 (97%)				
	386.8	0.81	HOMO → LUMO+2 (89%)				
	363.4	0.17	HOMO-4 → LUMO (91%)				

Table 4.6 (cont.)

Dye	λ	*f*	assignments	μ_g (D)	HOMO (eV)	LUMO (eV)	E_g (eV)
18a (vacuum)	586.1	0.45	HOMO→LUMO (100%)	9.53	-4.91	-2.57	2.34
	349.3	0.28	HOMO→LUMO+2 (81%)				
	414.6	0.95	HOMO-2→LUMO (91%)				
	376.3	0.36	HOMO→LUMO+1 (84%)				
	356.4	0.11	HOMO-3→LUMO (79%)				
18a (THF)	634.8	0.5	HOMO→LUMO (100%)	12.51	-4.91	-2.70	2.20
	437.8	0.92	HOMO-2→LUMO (95%)				
	382.9	0.51	HOMO→LUMO+1 (82%)				
	354.5	0.35	HOMO→LUMO+2 (90%)				
18b (vacuum)	607.8	0.41	HOMO→LUMO (100%)	9.19	-4.84	-2.56	2.27
	419.6	1.07	HOMO-2→LUMO (79%)				
	385.b2	0.12	HOMO→LUMO+1 (62%), HOMO-3→LUMO (28%)				
	378.4	0.64	HOMO→LUMO+2 (90%)				
18b (THF)	657.5	0.51	HOMO→LUMO (99%)	11.85	-4.83	-2.70	2.13
	443.1	1.03	HOMO-2→LUMO (93%)				
	391.0	0.28	HOMO→LUMO+1 (89%)				
	384.8	0.80	HOMO→LUMO+2 (95%)				
	354.2	0.15	HOMO-4→LUMO (94%)				
26a (vacuum)	594.9	0.47	HOMO→LUMO (99%)	9.53	-4.91	-2.57	2.34
	428.4	0.48	HOMO-1→LUMO (60%), HOMO-2→LUMO (36%)				
	425.0	0.40	HOMO-2→LUMO (41%), HOMO-3→LUMO (32%), HOMO-1→LUMO (24%)				
	390.5	0.71	HOMO→LUMO+1 (86%)				
	386.6	0.84	HOMO→LUMO+2 (76%), HOMO-4→LUMO (19%)				
26a (THF)	639.4	0.56	HOMO→LUMO (99%)	12.51	-4.91	-2.70	2.20
	448.8	0.90	HOMO-3→LUMO (61%), HOMO-2→LUMO (33%) HOMO-2→LUMO (41%), HOMO-3→LUMO (32%)				
	396.9	0.95	HOMO→LUMO+1 (95%)				
	395.0	0.78	HOMO-4→LUMO (48%), HOMO→LUMO+2 (45%)				

Table 4.6 (cont.)

Dye	λ	*f*	assignments	μ_g (D)	HOMO (eV)	LUMO (eV)	E_g (eV)
19a (vacuum)	631.6	0.44	HOMO→LUMO (100%)	7.43	-4.87	-2.70	2.16
	472.4	0.89	HOMO-1→LUMO (74%), HOMO-2→LUMO (23%)				
	465.9	0.38	HOMO-2→LUMO (76%), HOMO-1→LUMO (22%)				
	408.1	0.39	HOMO→LUMO+1 (85%)				
	355.6	0.39	HOMO→LUMO+2 (92%)				
19a (THF)	680.3	0.55	HOMO→LUMO (99%)	9.11	-4.86	-2.82	2.04
	505.9	0.75	HOMO-1→LUMO (80%), HOMO-2→LUMO (18%)				
	494.6	0.49	HOMO-2→LUMO (81%), HOMO-1→LUMO (17%)				
	415.9	0.49	HOMO→LUMO+1(85%)				
	362.0	0.44	HOMO→LUMO+2 (91%)				
19b (vacuum)	659.3	0.35	HOMO→LUMO (100%)	7.10	-4.80	-2.72	2.08
	478.3	1.30	HOMO-1→LUMO (91%)				
	420.8	0.23	HOMO→LUMO+1 (88%)				
	379.0	0.65	HOMO→LUMO+2 (82%), HOMO-4→LUMO (15%)				
	377.7	0.21	HOMO-4→LUMO (74%), HOMO→LUMO+2 (16%)				
19b (THF)	705.4	0.45	HOMO→LUMO (99%)	8.70	-4.79	-2.83	1.97
	510.9	1.17	HOMO-1→LUMO (94%)				
	494.8	0.19	HOMO-2→LUMO (95%)				
	426.6	0.35	HOMO→LUMO+1 (90%)				
	386.0	0.83	HOMO→LUMO+2 (98%)				
	352.9	0.13	HOMO→LUMO+3 (87%)				
26b (vacuum)	636.5	0.46	HOMO→LUMO (99%)	7.44	-4.87	-2.71	2.16
	477.9	1.20	HOMO-1→LUMO (91%)				
	466.7	0.09	HOMO-3→LUMO (55%)				
	416.3	0.59	HOMO→LUMO+1 (58%), HOMO-4→LUMO (35%)				

Table 4.6 (cont.)

Dye	λ	*f*	assignments	μ_g (D)	HOMO (eV)	LUMO (eV)	E_g (eV)
26b (THF)	680.8	0.56	HOMO→LUMO (99%)	9.11	-4.86	-2.82	2.04
	509.2	1.03	HOMO-1→LUMO (90%)				
	495.1	0.23	HOMO-2→LUMO (84%)				
	424.5	0.54	HOMO-4→LUMO (62%), HOMO→LUMO+1 (33%)				
	414.8	0.16	HOMO→LUMO+1 (58%), HOMO-4→LUMO (37%)				

Table 4.7 Computed vertical transition energies and their oscillator strengths, assignments, dipole moments and band gaps for the dyes using MPW1K theory

Dye	λ	*f*	assignments	μ_g (D)	HOMO (eV)	LUMO (eV)	E_g (eV)
15a	412.9	0.89	HOMO → LUMO (87%)	6.12	-5.76	-2.06	3.70
(vacuum)	327.7	1.05	HOMO-2 → LUMO (75%)				
	317.5	0.22	HOMO → LUMO+1 (67%)				
	301.3	0.33	HOMO → LUMO+2 (77%)				
	285.5	0.04	HOMO → LUMO+3 (34%), HOMO → LUMO+4 (32%)				
	276.9	0.16	HOMO-3 → LUMO (22%), HOMO-1 → LUMO+1 (20%), HOMO-6 → LUMO (15%)				
15a	423.8	1.02	HOMO → LUMO (85%)	7.05	-5.81	-2.16	3.65
(THF)	334.9	0.89	HOMO-2 → LUMO (62%)				
	323.1	0.50	HOMO → LUMO+1 (76%)				
	304.2	0.40	HOMO → LUMO+2 (76%)				
15b	422.1	0.80	HOMO → LUMO (88%)	6.15	-5.66	-2.06	3.60
(vacuum)	334.1	1.06	HOMO-2 → LUMO (57%), HOMO → LUMO+1 (18%)				
	327.5	0.94	HOMO → LUMO+2 (88%)				
15b	432.0	0.92	HOMO → LUMO (86%)	7.05	-5.72	-2.16	3.55
(THF)	341.0	0.99	HOMO-2 → LUMO (67%)				
	332.2	1.07	HOMO → LUMO+2 (90%)				
	326.1	0.22	HOMO → LUMO+1 (878%)				

Table 4.7 (cont.)

Dye	λ	*f*	assignments	μ_g (D)	HOMO (eV)	LUMO (eV)	E_g (eV)
24 (vaccum)	414.4	0.97	HOMO → LUMO (85%)	6.71	-5.73	-2.06	3.66
	332.8	1.02	HOMO-3 → LUMO (27%), HOMO-4 → LUMO (18%), HOMO-2 → LUMO (17%)				
	331.4	1.18	HOMO → LUMO+1 (81%)				
	319.9	0.23	HOMO → LUMO+2 (67%)				
	289.1	0.18	HOMO → LUMO+3 (26%), HOMO → LUMO+4 (24%),				
	283.7	0.18	HOMO-4 → LUMO (42%), HOMO-3 → LUMO (15%)				
24 (THF)	426.3	1.03	HOMO → LUMO (85%)	7.17	-5.82	-2.17	3.65
	339.6	1.09	HOMO-2 → LUMO (91%)				
	331.4	1.48	HOMO → LUMO+1 (81%)				
	325.9	0.25	HOMO → LUMO+2 (67%)				
18a (vacuum)	418.3	1.08	HOMO → LUMO (83%)	9.12	-5.75	-2.00	3.75
	336.1	0.54	HOMO-2 → LUMO (73%),				
	314.9	0.49	HOMO → LUMO+1 (77%)				
	299.8	0.31	HOMO → LUMO+2 (76%)				
18a (THF)	440.7	1.24	HOMO → LUMO (81%)	11.82	-5.79	-2.15	3.64
	349.2	0.41	HOMO-2 → LUMO (69%), HOMO → LUMO (15%)				
	319.9	0.67	HOMO → LUMO+1 (75%)				
	302.9	0.36	HOMO → LUMO+2 (74%)				
18b (vacuum)	427.1	0.98	HOMO → LUMO (84%)	8.68	-5.66	-2.01	3.65
	345.3	0.12	HOMO-1→ LUMO (84%)				
	342.5	0.60	HOMO-2→ LUMO (75%)				
	324.8	0.74	HOMO → LUMO+2 (68%), HOMO → LUMO+1 (22%)				
	320.2	0.37	HOMO → LUMO+1 (60%), HOMO → LUMO+2 (24%)				
18b (THF)	448.0	1.14	HOMO → LUMO (82%)	11.10	-5.70	-2.15	3.54
	361.1	0.24	HOMO-1→LUMO (82%)				
	355.6	0.38	HOMO-2→LUMO (72%)				
	328.7	0.96	HOMO → LUMO+2 (80%)				
	324.4	0.44	HOMO → LUMO+1 (72%)				

Table 4.7 (cont.)

Dye	λ	*f*	assignments	μ_g (D)	HOMO (eV)	LUMO (eV)	E_g (eV)
19a (vacuum)	438.2	1.45	HOMO → LUMO (69%), HOMO-1→ LUMO (25%)	6.53	-5.71	-2.16	3.54
	371.2	0.41	HOMO-1 → LUMO (63%), HOMO → LUMO (27%)				
	303.7	0.45	HOMO → LUMO+2 (71%)				
19a (THF)	462.1	1.64	HOMO → LUMO (63%), HOMO-1→ LUMO (30%)	7.86	-5.74	-2.29	3.45
	386.0	0.27	HOMO-1→ LUMO (57%), HOMO → LUMO (33%)				
	335.9	0.72	HOMO → LUMO+1 (70%)				
	308.3	0.56	HOMO → LUMO+2 (68%)				
19b (vacuum)	443.2	1.32	HOMO → LUMO (71%), HOMO-1→ LUMO (22%)	6.41	-5.62	-2.17	3.45
	379.6	0.59	HOMO-1→ LUMO (65%), HOMO → LUMO (26%)				
	338.8	0.24	HOMO → LUMO+1 (44%), HOMO-2 → LUMO (32%)				
	336.9	0.18	HOMO-2 → LUMO (53%), HOMO → LUMO+1 (28%)				
	324.6	0.90	HOMO → LUMO+2 (89%)				
19b (THF)	464.8	1.54	HOMO → LUMO (64%), HOMO-1→ LUMO (29%)	7.65	-5.66	-2.29	3.37
	394.1	0.40	HOMO-1→ LUMO (58%), HOMO → LUMO (32%)				
	342.0	0.58	HOMO → LUMO+1 (71%)				
	329.8	1.05	HOMO → LUMO+2 (90%)				
26a (vacuum)	419.5	1.19	HOMO→LUMO (81%)	9.12	-5.75	-2.00	3.75
	339.8	0.58	HOMO-2→LUMO (44%), HOMO-4→LUMO (22%),				
	325.4	1.27	HOMO→LUMO+1 (62%), HOMO→LUMO+2 (21%)				
	317.2	0.55	HOMO→LUMO+2 (61%), HOMO→LUMO+1 (20%)				
26a (THF)	438.7	1.32	HOMO→LUMO (79%)	11.82	-5.77	-2.15	3.64
	359.9	0.13	HOMO-1→LUMO (37%), HOMO-2→LUMO (26%), HOMO-3→LUMO (25%)				
	352.4	0.38	HOMO-3→LUMO (35%), HOMO-2→LUMO (24%), HOMO-4→LUMO (20%)				
	330.9	1.48	HOMO→LUMO+1 (82%)				
	321.8	0.71	HOMO→LUMO+2 (81%)				

Table 4.7 (cont.)

Dye	λ	*f*	assignments	μ_g (D)	HOMO (eV)	LUMO (eV)	E_g (eV)
26b (vacuum)	454.7	1.70	HOMO→LUMO (60%), HOMO-1→LUMO (31%)	6.53	-5.72	-2.16	3.54
	383.8	0.26	HOMO-1→LUMO (50%), HOMO→LUMO (36%),				
	336.9	0.91	HOMO→LUMO+1 (71%)				
	330.1	1.45	HOMO→LUMO+2 (78%)				
26b (THF)	460.8	1.74	HOMO→LUMO (60%), HOMO-1→LUMO (31%)	7.86	-5.74	-2.29	3.45
	387.5	0.26	HOMO-1→LUMO (50%), HOMO→LUMO (36%),				
	338.1	0.90	HOMO→LUMO+1 (71%)				
	331.8	1.46	HOMO→LUMO+2 (79%)				

4.2.5 DSSC Characteristics

The photovoltaic performance of the dyes (**18a**-**18b**, **19a**-**19b** and **26a**-**26b**) was tested by using Grätzel photo electrochemical cells [58]. The IPCE spectra of DSSC based on these dyes are shown in Figure 4.18 and I-V curves displayed in Figure 4.19. All the dyes are showing 70% IPCE in the 350-550 nm region except the dye **18a** which may be due to poor injection. The dye **19a** has achieved reasonable efficiency of 6.10% with highest J_{SC} = 16.20 mA cm^{-2}, V_{OC} = 616 mV and *ff* = 0.61. But the dye **18b** exhibited highest conversion efficiency of 6.44% owing to its highest V_{OC} = 616 mV, J_{SC} = 16.20 mA cm^{-2} and *ff* = 0.61 among all other dyes. Broader IPCE spectra of **19a** and **18b** are responsible for higher power conversion efficiency of the devices. The inferior power conversion efficiency for **18a** might be due to the low molar extinction coefficient of the charge transfer transition which led to poor IPCE values and highest dark current of the device.

Table 4.8 Performance parameters of the DSSCs fabricated using the dyes

Dye	$J_{SC,}$ mA cm^{-2}	V_{OC}, mV	*ff*	η (%)	R_{ct2} (ohm)	τ_e (ms)	R_{rec} (ohm)
18a	8.25	562	0.64	2.98	29.29	1.16	14.71
18b	15.60	666	0.62	6.44	14.76	8.41	50.00
19a	16.20	616	0.61	6.10	13.33	3.80	22.35
19b	12.50	630	0.61	4.77	20.00	2.55	26.47
26a	14.60	634	0.62	5.76	20.50	8.41	23.53
26b	11.50	596	0.61	4.20	23.53	4.63	22.35
N719	17.80	744	0.69	9.12	12.13	12.50	84.71

Light harvesting efficiency affects the J_{SC} and the efficiency of the device. The increasing order of the J_{SC} assumes an order: **18a** < **26b** < **19b** < **26a** < **18b** < **19a**. The trend is consistent with the IPCE spectra of the devices and the larger photocurrent for the dyes **19a** and **18b** is due to the high response in the IPCE spectrum by the electron richness of the fluorene incorporation on amine-donor segment. More flat structure of the bithiophene is responsible for aggregation of the dye molecules on TiO_2 surface which caused low J_{SC} values [20]. However, for the fluorenephenylamine donor, bithiophene containing dye **19a** showing higher J_{SC} than the congener thiophene dye **18a.** This is attributed to the unsymmetrical fluorenylphenylamine donor, which allows systematic packing on TiO_2 in such a way that intermolecular interactions between the fluorene units are minimized [14]. The open circuit voltage for the devices by using the dyes follows an order: **18a** < **26b** < **19a** < **19b** < **26a** < **18b**. Four alkyl groups on the amine donor help to suppress the recombination and hence led to highest V_{OC} of 666 mV.

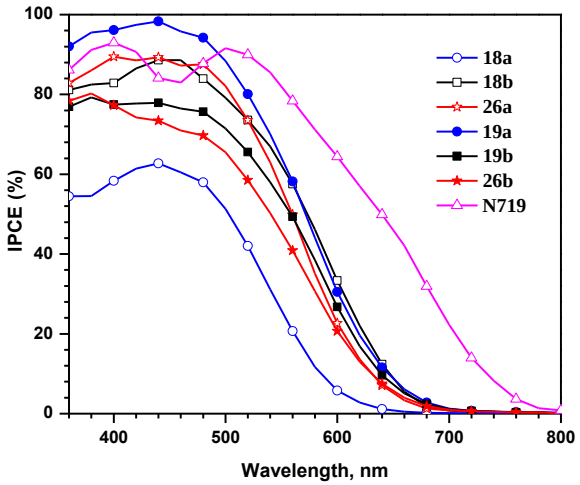

Figure 4.18 IPCE spectra of the devices fabricated using the dyes.

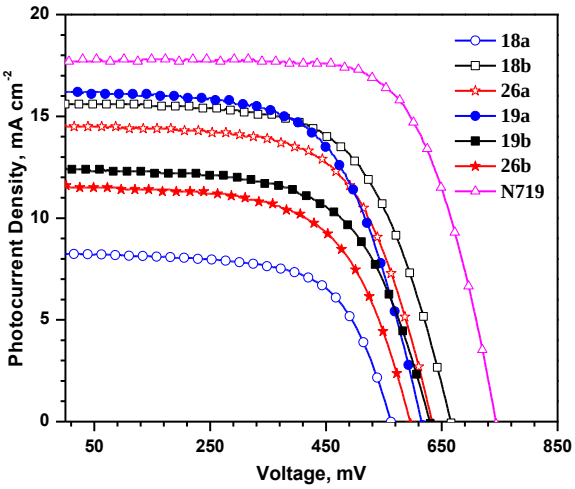

Figure 4.19 I-V Characteristics of the devices fabricated using the dyes.

The interfacial electron transport resistance, kinetics of the charge transfer and recombination in the devices were investigated by electrochemical impedance spectroscopy (EIS). Nyquist plots of the DSSCs in dark under forward bias are displayed in Figure 4.20. In this, second semicircle of each dye corresponds to the recombination resistance (R_{rec}) between the electrons on the conduction band of TiO_2 and oxidized electrolyte (I_3^-). The larger value of the R_{rec} indicates the slower recombination of electrons and it follows an order: **18a** < **19a** = **26b** < **26a** < **19b** < **18b.** This order is matching with the trend observed with observed V_{OC} of the devices except for **26a** due to its high electron life time when compared to **19b** [59, 60]. Incorporation of four alkyl

chains at C9 positions of the fluorene in donor part of the dye seems to be beneficial for dark current suppression [21]. In addition, elongation of the hydrophobic π-bridge is useful to reduce charge recombination [61]. The bithiophene dyes possess better recombination resistance when compared to the thiophene dyes. Due to this reason the difluorenylamine donor containing dyes exhibit higher recombination resistance.

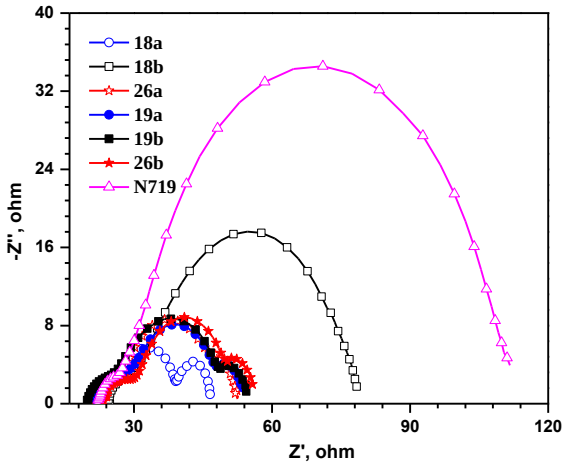

Figure 4.20 Nyquist plots observed for the DSSCs measured under dark.

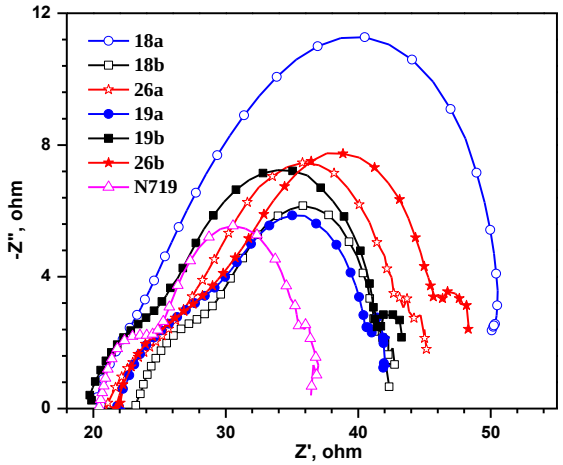

Figure 4.21 Nyquist plots observed for the DSSCs measured under illumination.

Nyquist plots of the dyes under illumination at open circuit voltage conditions are displayed in Figure 4.21 and intermediate semicircle represents the charge transport resistance (R_{ct2}) at the TiO_2/dye/electrolyte interface and it follows the increasing order: **19a** < **18b** < **19b** < **26a** < **26b** < **18a**. The smaller value of R_{ct2} represents the low electron transport resistance. The higher value of R_{ct2} confirms the low J_{SC} of the device for the dyes (**18a** and **26b**) due to the less electron collection from the excited state of the dyes in to conduction band of the TiO_2. These results from the EIS spectra are consistent with the aforementioned trend observed for V_{OC} of the devices.

Bode-phase plots are shown in Figure 4.22. The electron life time (τ) extracted from the angular frequency (ω_{min}) at the mid frequency in the Bode phase plot using τ_e = 1/ ω_{min}, [62] assumes order **18a** < **19b** < **19a** < **26b** < **18b** = **26a**. The significantly increased electron lifetime of the dyes because of the suppression of the recombination of electrons from the TiO_2 to the I_3^- ions in the electrolyte and this can be due to the introduction of difluorenylamine segment. Efficiency of the devices is mainly influenced by the electron recombination and aggregation of the dyes. These processes control the J_{SC} and V_{OC} of the devices, respectively. The dye **18b** achieved higher power conversion efficiency

owing to the highest J_{SC} and V_{OC} due to the higher recombination resistance and electron lifetime of the device.

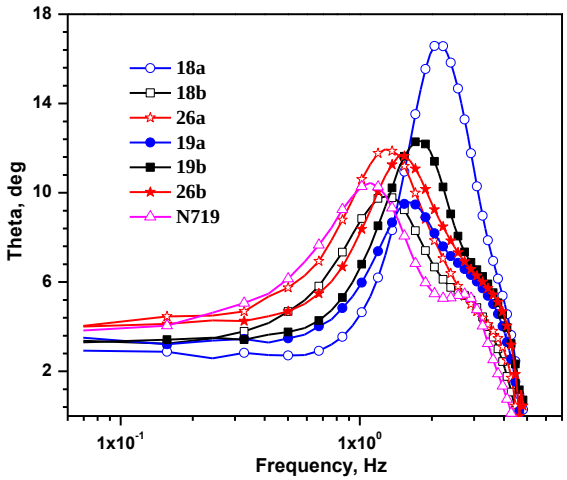

Figure 4.22 Bode-phase plots observed for the DSSCs measured under illumination.

4.3 Conclusions

In this chapter, we have successfully synthesized and thoroughly characterized a set of dyes containing fluorene incorporated/decorated diarylamine as donor, carbazole linking at 2,7 positions and cyanoacrylic acid as an acceptor. We have observed the electron rich donor enhances the optical properties and it helps the dye to achieve high lying HOMO for better regeneration of the dye, low lying LUMO for thermodynamically favourable injection of the electron from the dye into the conduction band of the TiO_2. Highest power conversion efficiency (6.44%) observed for the dye **18b** due to highest photo response in the IPCE curve and its highest HOMO facilitate the faster dye regeneration and suppress the back electron transfer helps to achieve high V_{OC}. In addition, the strong donor shows the trivial effect on the donor-acceptor interactions and shows the superior photo current density. The interfacial electron transfer properties of the dyes were analyzed by electrochemical impedance spectroscopy and dark current studies. The current study proves the efficiency of the dyes can be effectively increased by structural variation in the donor part of the dye.

4.4 Experimental Section

4.4.1 General Experimental Methods

Computational methods, device fabrication and characterization are similar to the procedure described in chapter 3.

4.4.2 Synthesis

2,7-Dibromo-9-butyl-9*H*-carbazole (**1**) [63, 64], bis(4-bromophenyl)amine [65] and 9,9-diethyl-9*H*-fluoren-2-ylboronic acid [66] prepared according to literature procedure.

***N*-Phenyl-9,9-dipropyl-9*H*-fluoren-2-amine, 12a.** A mixture of 2-bromo-9,9-diethyl-9*H*-fluorene (3.29 g, 10 mmol), aniline (1.12 g, 12 mmol), pd(dba)$_2$ (0.06 g, 0.20 mmol), dppf (0.05 g, 0.20 mmol), sodium *tert*-butoxide (2.40 g, 25 mmol), and toluene (25 mL) taken in a pressure tube was heated at 80 °C for 48 h under N_2 atmosphere. After completion of the reaction, the volatiles were removed under vacuum, and the resulting solution was extracted with dichloromethane (3 × 60 mL). The combined organic extract washed with brine solution, dried over Na_2SO_4, and concentrated to leave yellow solid. Further the crude product was purified by column chromatography on silica gel by using hexane/dichloromethane mixture (2:1) as an eluant. White solid; Yield 2.37 g (70%); mp 79 °C; ^{1}H NMR ($CDCl_3$, 500.13 MHz) δ 7.57-7.61 (m, 2H), 7.27-7.31 (m, 4H), 7.22 (td, *J* = 7.5 Hz, 1.5 Hz, 1H), 7.06-7.10 (m, 3H), 7.05 (dd, *J* = 7.5 Hz, 2.0 Hz, 1H), 6.93 (tt, *J* = 6.5 Hz, 1.0 Hz, 1H), 5.82 (s, 1H), 1.86-1.93 (m, 4H), 0.64-0.73 (m, 10H); ^{13}C NMR ($CDCl_3$, 125.77 MHz) δ 152.48, 150.26, 143.68, 142.25, 141.25, 134.90, 129.49, 126.82, 125.99, 122.79, 120.74, 120.50, 118.85, 117.39, 117.18, 116.85, 113.05, 52.25, 43.19, 42.95, 32.54, 17.32, 14.61; HRMS calcd for $C_{25}H_{27}N$ $[M]^+$ *m/z* 341.2138, found 341.2123.

Bis(9,9-diethyl-9*H*-fluoren-2-yl)amine, 12b. It was prepared from 2-bromo-9,9-diethyl-9*H*-fluorene (3.01 g, 10 mmol) and 9,9-diethyl-9*H*-fluoren-2-amine (2.84 g, 12 mmol) by following a procedure described above for **12a**. White powder; Yield 2.92 g (64%); mp 160 °C; ^{1}H NMR (DMSO-d_6, 500.13 MHz) δ 8.45 (s, 1H), 7.40 (d, *J* = 8.0 Hz, 4H), 7.07 (q, *J* = 12.0 Hz, 7.5 Hz, 4H), 7.00 (t, *J* = 7.5 Hz, 2H), 6.96 (d, *J* = 1.5 Hz, 2H), 6.85 (dd, *J* = 7.5 Hz, 2.0 Hz, 2H), 1.73-1.84 (m, 8H), 0.13 (t, *J* = 2.0 Hz, 12H); ^{13}C NMR (DMSO-d_6, 125.77 MHz) δ 150.54, 148.60, 143.07, 141.27, 133.16, 126.82, 125.62, 122.57, 120.74, 118.55, 116.18, 111.07, 55.27, 31.99, 8.46; HRMS calcd for $C_{34}H_{35}N$ $[M]^+$ *m/z* 457.2764, found 457.2745.

7-Bromo-9-butyl-*N*-(9,9-dipropyl-9*H*-fluoren-2-yl)-*N*-phenyl-9*H*-carbazol-2-amine, 13a. A mixture of 2,7-dibromo-9-butyl-9*H*-carbazole (**1**, 3.81 g, 10 mmol) and *N*-phenyl-9,9-dipropyl-9*H*-fluoren-2-amine (1.70 g, 5 mmol), pd(dba)$_2$ (0.03 g, 0.10 mmol), dppf (0.03 g, 0.10 mmol), sodium *tert*-butoxide (1.20 g, 12.5 mmol), and toluene

(10 mL) taken in a pressure tube was heated at 80 °C for 48 h under N_2 atmosphere. After completion of the reaction, the volatiles were removed under vacuum, and the resulting solution was extracted with dichloromethane (3 × 50 mL). The combined organic extract washed with brine solution, dried over Na_2SO_4, and concentrated. Further the crude product was purified by column chromatography on silica gel by using hexane/dichloromethane mixture (5:1) as an eluant. White solid; Yield 1.92 g (60%); mp 145 °C; ^{1}H NMR ($CDCl_3$, 500.13 MHz) δ 7.88 (d, *J* = 8.5 Hz, 1H), 7.83 (d, *J* = 8.0 Hz, 1H), 7.61 (d, *J* = 7.5 Hz, 1H), 7.57 (d, *J* = 8.0 Hz, 1H), 7.46 (d, *J* = 0.5 Hz, 1H), 7.28-7.31 (m, 4H), 7.24 (s, 2H), 7.18 (s, 3H), 7.02-7.10 (m, 4H), 4.06 (t, *J* = 7.5 Hz, 2H), 1.85-1.91 (m, 2H), 1.78-1.83 (m, 2H), 1.68-1.75 (m, 2H), 1.25-1.32 (m, 2H), 0.85-0.88 (m, 3H), 0.71-0.77 (m, 12H); ^{13}C NMR ($CDCl_3$, 125.77 MHz) δ 152.12, 150.60, 148.40, 147.40, 146.90, 141.76, 141.68, 140.93, 136.32, 129.16, 126.83, 126.33, 123.70, 123.55, 122.78, 122.43, 122.07, 120.81, 120.33, 119.29, 119.12, 118.31, 117.81, 117.04, 111.60, 104.35, 55.25, 42.80, 42.64, 30.94, 20.45, 17.34, 14.56, 13.83; HRMS calcd for $C_{41}H_{41}BrN_2$ $[M]^+$ *m/z* 640.2448, found 640.2456.

7-Bromo-9-butyl-*N*,*N*-bis(9,9-diethyl-9*H*-fluoren-2-yl)-9*H*-carbazol-2-amine, 13b. It was prepared from **1** (3.81 g, 10 mmol) and *N*-phenyl-9,9-dipropyl-9*H*-fluoren-2-amine (1.81 g, 5 mmol) by following a procedure described above for 1**3a**. White solid; Yield 2.37 g (48%); mp 159 °C; ^{1}H NMR ($CDCl_3$, 500.13 MHz) δ 7.82-7.93 (m, 2H), 7.58-7.66 (m, 4H), 7.47 (d, *J* = 10.0 Hz, 1H), 7.24-7.32 (m, 7H), 7.20 (d, *J* = 9.0 Hz, 2H), 7.12 (d, *J* = 5.0 Hz, 2H), 7.07 (t, *J* = 8.5 Hz, 2H), 4.04 (t, *J* = 7.0 Hz, 2H), 1.85-1.97 (m, 8H), 1.71 (t, *J* = 7.0 Hz, 2H), 1.25-1.30 (m, 2H), 0.85 (sextet, *J* = 3.5 Hz, 2H), 0.37 (t, *J* = 7.0 Hz, 3H); ^{13}C NMR ($CDCl_3$, 125.77 MHz) δ 151.26, 149.69, 147.70, 147.20, 141.75, 141.42, 136.58, 126.90, 126.32, 123.28, 122.79, 122.08, 121.97, 120.84, 120.77, 120.31, 119.07, 118.85, 118.27, 117.68, 116.93, 111.59, 104.08, 56.13, 42.86, 32.77, 30.92, 20.45, 13.76, 8.64; HRMS calcd for $C_{50}H_{49}BrN_2Na$ $[M + Na]^+$ *m/z* 779.2971, found 779.2971.

4-(9-Butyl-7-((9,9-dipropyl-9*H*-fluoren-2-yl)(phenyl)amino)-9*H*-carbazol-2-yl)benzaldehyde, 14a. A two neck RB flask charged with a mixture of **13a** (0.64 g, 1 mmol), 4-formylphenylboronic acid (0.18 g, 1.2 mmol), anhydrous K_2CO_3 (0.48 g, 3.5 mmol) and $Pd(PPh_3)_4$ (0.04 g, 0.03 mmol) were dissolved in mixture of THF/H_2O (3:1). The reaction mixture was degassed with N_2 and refluxed for 12 h under nitrogen atmosphere. After cooling to room temperature, the organic layer extracted with dichloromethane and dried with sodium sulfate. The crude product was purified by

column chromatography on silica gel by using a hexane/dichloromethane mixture (2:1) as eluant. Yellow solid; Yield 0.60 g (90%); mp 180-182 °C; IR (KBr, cm^{-1}) 1692 ($\nu_{C=O}$); ^1H NMR ($CDCl_3$, 500.13 MHz) δ 10.06 (s, 1H), 8.08 (d, *J* = 8.0 Hz, 1H), 7.99 (d, *J* = 8.0 Hz, 2H), 7.95 (d, *J* = 7.5 Hz, 1H), 7.88 (d, *J* = 8.0 Hz, 2H), 7.62-7.64 (m, 1H), 7.56-7.59 (m, 2H), 7.50 (dd, *J* = 8.5 Hz, 3.5 Hz, 1H), 7.30-7.32 (m, 2H), 7.27-7.28 (m, 2H), 7.20-7.21 (m, 2H), 7.14 (d, *J* = 1.5 Hz, 1H), 7.10 (dd, *J* = 8.5 Hz, 2.0 Hz, 1H), 7.05-7.06 (m, 2H), 4.18 (t, *J* = 7.0 Hz, 2H), 1.76-1.92 (m, 6H), 1.29-1.37 (m, 2H), 0.88 (t, *J* = 7.0 Hz, 3H), 0.75-0.77 (m, 10H); ^{13}C NMR ($CDCl_3$, 125.77 MHz) δ 191.96, 152.13, 150.60, 148.42, 148.39, 147.42, 147.01, 142.38, 141.35, 140.93, 136.41, 136.35, 134.89, 130.31, 129.14, 127.96, 126.81, 126.32, 123.74, 123.61, 123.31, 122.77, 122.44, 121.05, 120.31, 120.15, 119.37, 119.11, 118.73, 117.90, 116.90, 107.27, 104.24, 55.24, 42.63, 31.09, 20.48, 17.33, 14.54, 13.84; HRMS calcd for $C_{48}H_{46}N_2ONa$ $[M + Na]^+$ *m/z* 689.3502, found 689.3520.

4-(7-(Bis(9,9-diethyl-9*H*-fluoren-2-yl)amino)-9-butyl-9*H*-carbazol-2-yl)benzaldehyde, 14b. Compound **14b** was synthesized from **13b** (0.76 g, 1 mmol) and by following a procedure similar to that described above for 1**4a**. Yellow solid; Yield 0.57 g (73%); mp 158 °C; IR (KBr, cm^{-1}) 1693 ($\nu_{C=O}$); ^1H NMR ($CDCl_3$, 500.13 MHz) δ 10.08 (s, 1H), 8.08 (d, *J* = 8.5 Hz, 1H), 7.96-8.00 (m, 3H), 7.89 (d, *J* = 8.0 Hz, 2H), 7.64 (d, *J* = 7.5 Hz, 2H), 7.61 (d, *J* = 8.0 Hz, 2H), 7.57 (s, 1H), 7.50 (d, *J* = 3.0 Hz, 1H), 7.27-7.34 (m, 6H), 7.23 (s, 2H), 7.15 (d, *J* = 8.0 Hz, 3H), 7.08 (d, *J* = 8.0 Hz, 1H), 4.17 (t, *J* = 7.0 Hz, 3H), 1.94-2.00 (m, 4H), 1.85-1.92 (m, 4H), 1.75-1.79 (m, 2H), 1.29-1.34 (m, 2H), 0.86 (t, *J* = 7.0 Hz, 3H), 0.39 (t, *J* = 7.5 Hz, 12H); ^{13}C NMR ($CDCl_3$, 125.77 MHz) δ 191.92, 151.22, 149.66, 148.35, 147.67, 147.26, 142.33, 141.38, 136.56, 136.34, 134.84, 130.28, 127.91, 126.86, 126.28, 123.29, 122.74, 121.03, 120.26, 120.09, 119.02, 118.86, 118.71, 117.73, 116.76, 107.22, 103.94, 56.09, 42.71, 32.72, 31.05, 20.46, 13.77, 8.60; HRMS calcd for $C_{57}H_{54}N_2O$ $[M]^+$ *m/z* 782.4231, found 782.4228.

5-(9-Butyl-7-((9,9-dipropyl-9*H*-fluoren-2-yl)(phenyl)amino)-9*H*-carbazol-2-yl)thiophene-2-carbaldehyde, 16a. A mixture of **13a** (0.64 g, 1 mmol) and (5-(1,3-dioxolan-2-yl)thiophen-2-yl)tributylstannane (0.49 g, 1.1 mmol) was dissolved in dry DMF (5 mL) and degassed with nitrogen, and add $Pd(PPh_3)_2Cl_2$ (0.01 g, 0.01 mmol). The reaction mixture was heated at 80 ℃ for 15 h. After cooling the reaction mixture poured into water. The organic compound extracted with dichloromethane (3 × 40 mL). The combined organic extract washed with brine solution, dried over Na_2SO_4, and

concentrated to leave yellow solid. The yellow solid dissolved in 5 mL of acetic acid and heated at 65 °C for 2 h. Added 5 mL of water and continued the heating for 2 h. Extracted the organic layer with dichloromethane and dried over Na_2SO_4. Further the crude product was purified by column chromatography on silica gel by using hexane/dichloromethane mixture (1:1) as an eluent: Yellow solid; Yield 0.52 g (77%); mp 142 °C; IR (KBr, cm^{-1}) 1663 ($\nu_{C=O}$); ^{1}H NMR ($CDCl_3$, 500.13 MHz) δ 9.90 (s, 1H), 8.01 (d, *J* = 8.0 Hz, 1H), 7.92 (d, *J* = 8.5 Hz, 1H), 7.77 (d, *J* = 4.0 Hz, 1H), 7.62 (d, *J* = 8.0 Hz, 1H), 7.59 (d, *J* = 5.0 Hz, 1H), 7.58 (s, 2H), 7.54 (dd, *J* = 8.0 Hz, 1.5 Hz, 1H), 7.50 (d, *J* = 4.0 Hz, 1H), 7.30-7.31 (m, 3H), 7.28 (s, 1H), 7.19-7.20 (m, 3H), 7.08-7.11 (m, 2H), 7.02-7.04 (m, 2H), 4.45 (t, *J* = 7.0 Hz, 2H), 1.83-1.89 (m, 2H), 1.76-1.78 (m, 4H), 1.33 (quintet, *J* = 7.5 Hz, 2H), 0.89 (q, *J* = 7.0 Hz, 3H), 0.68-0.76 (m, 10H); ^{13}C NMR ($CDCl_3$, 125.77 MHz) δ 182.76, 156.13, 152.16, 150.61, 148.32, 147.33, 147.31, 142.60, 141.79, 141.09, 140.89, 137.71, 136.48, 129.47, 129.19, 126.84, 126.38, 124.22, 123.89, 123.73, 122.79, 122.61, 121.13, 120.37, 120.23, 119.46, 119.15, 117.82, 117.75, 116.94, 106.37, 103.99, 55.26, 42.70, 42.64, 31.06, 20.47, 17.35, 14.57, 13.85; HRMS calcd for $C_{46}H_{44}N_2OSNa$ $[M + Na]^+$ *m/z* 695.3067, found 695.3062.

5-(7-(Bis(9,9-diethyl-9*H*-fluoren-2-yl)amino)-9-butyl-9*H*-carbazol-2-yl)thiophene-2-carbaldehyde, 16b. Compound **16b** synthesized from **13b** (0.76 g, 1 mmol) and (5-(1,3-dioxolan-2-yl)thiophen-2-yl)tributylstannane (0.49 g, 1.1 mmol) mixture by following a procedure similar to that described above for **16a.** Yellow solid; Yield 0.42 g (70%); mp 106 °C; IR (KBr, cm^{-1}) 1662 ($\nu_{C=O}$); ^{1}H NMR ($CDCl_3$, 500.13 MHz) δ 9.90 (s, 1H), 8.00 (d, *J* = 8.0 Hz, 1H), 7.93 (d, *J* = 8.5 Hz, 1H), 7.77 (d, *J* = 4.5 Hz, 1H), 7.65 (d, *J* = 7.0 Hz, 2H), 7.60-7.61 (m, 3H), 7.54 (dd, *J* = 8.0 Hz, 2.0 Hz, 1H), 7.49 (d, *J* = 3.5 Hz, 1H), 7.25-7.34 (m, 6H), 7.21 (d, *J* = 5.0 Hz, 2H), 7.13-7.15 (m, 3H), 7.07 (dd, *J* = 7.5 Hz, 2.0 Hz, 1H), 4.13 (t, *J* = 7.0 Hz, 2H), 1.97 (septet, *J* = 7.5 Hz, 4H), 1.88 (septet, *J* = 1.5 Hz, 4H), 1.75 (t, *J* = 12.5 Hz, 2H), 1.30 (septet, *J* = 6.5 Hz, 3H), 0.38 (t, *J* = 7.5 Hz, 12H); ^{13}C NMR ($CDCl_3$, 125.77 MHz) δ 182.71, 156.14, 151.29, 149.70, 147.61, 147.58, 142.57, 141.79, 141.37, 141.13, 137.65, 136.73, 129.43, 126.90, 126.36, 124.24, 123.69, 123.42, 122.79, 121.12, 120.31, 120.17, 119.08, 119.01, 117.81, 117.61, 116.82, 106.35, 103.70, 56.13, 42.76, 32.76, 31.04, 20.47, 13.78, 8.63; HRMS calcd for $C_{55}H_{52}N_2OSNa$ $[M + Na]^+$ *m/z* 811.3693, found 811.3677.

5-(5-(9-Butyl-7-((9,9-dipropyl-9*H*-fluoren-2-yl)(phenyl)amino)-9*H*-carbazol-2-yl)thiophen-2-yl)thiophene-2-carbaldehyde, 17a. Compound **17a** obtained from **3b**

(0.64 g, 1 mmol) and (5-(5-(1,3-dioxolan-2-yl)thiophen-2-yl)thiophen-2-yl)tributylstannane (0.58 g, 1.1 mmol) mixture by following a procedure similar to that described above for 1**6a.** Orange solid; Yield 0.70 g (93%); mp 130 °C; IR (KBr, cm^{-1}) 1661 ($\nu_{C=O}$); ^{1}H NMR ($CDCl_3$, 500.13 MHz) δ 9.87 (s, 1H), 7.99 (d, *J* = 8.0 Hz, 1H), 7.92 (d, *J* = 8.5 Hz, 1H), 7.69 (d, *J* = 8.0 Hz, 1H), 7.62-7.63 (m, 1H), 7.58 (d, *J* = 8.0 HZ, 1H), 7.53 (d, *J* = 1.0 Hz, 1H), 7.48 (dd, *J* = 8.0 Hz, 1.5 Hz, 1H), 7.37 (dd, *J* = 11.5 Hz, 4.0 Hz, 2H), 7.28-7.32 (m, 5H), 7.19-7.20 (m, 3H), 7.08-7.12 (m, 2H), 7.02-7.03 (m, 2H), 4.16 (t, *J* = 7.5 Hz, 2H), 1.75-1.92 (m, 6H), 1.31-1.35 (m, 2H), 0.89 (t, *J* = 7.5 Hz, 3H), 0.67-0.68 (m, 10H); ^{13}C NMR ($CDCl_3$, 125.77 MHz) δ 182.44, 152.13, 150.61, 148.39, 147.82, 147.39, 146.96, 142.39, 141.36, 141.21, 140.93, 137.49, 136.36, 134.51, 130.09, 129.15, 127.27, 126.82, 126.33, 123.89, 123.81, 123.77, 123.61, 123.26, 122.77, 122.46, 120.91, 120.32, 120.17, 119.35, 119.11, 118.03, 117.48, 116.93, 105.66, 104.20, 55.25, 42.63, 31.06, 26.93, 20.47, 17.34, 14.55, 13.85; HRMS calcd for $C_{50}H_{46}N_2OS_2Na$ $[M + Na]^+$ *m/z* 777.2944, found 777.2952.

5-(5-(7-(Bis(9,9-diethyl-9*H*-fluoren-2-yl)amino)-9-butyl-9*H*-carbazol-2-yl)thiophen-2-yl)thiophene-2-carbaldehyde, 17b. Compound 1**7b** synthesized from **13b** (0.76 g, 1.1 mmol) and (5-(5-(1,3-dioxolan-2-yl)thiophen-2-yl)thiophen-2-yl)tributylstannane (0.58 g, 1.1 mmol) mixture by following a procedure similar to that described above for 1**6a.** Orange solid; Yield 0.62 g (71%); mp 166 °C; IR (KBr, cm^{-1}) 1656 ($\nu_{C=O}$); ^{1}H NMR ($CDCl_3$, 500.13 MHz) δ 9.87 (s, 1H), 7.99 (d, *J* = 8.0 Hz, 1H), 7.92 (d, *J* = 8.5 Hz, 1H), 7.69 (d, *J* = 11.5 Hz, 1H), 7.64 (d, *J* = 7.5 Hz, 2H), 7.60 (d, *J* = 8.0 Hz, 2H), 7.53 (s, 1H), 7.48 (dd, *J* = 8.0 Hz, 1.0 Hz, 1H), 7.36 (dd, *J* = 10.0 Hz, 4.0 Hz, 2H), 7.27-7.33 (m, 7H), 7.21 (d, *J* = 2.0 Hz, 2H), 7.13-7.15 (m, 3H), 7.06 (dd, *J* = 8.5 Hz, 1.5 Hz, 1H), 4.14 (t, *J* = 7.0 Hz, 2H), 1.94-1.99 (m, 2H), 1.87-1.91 (m, 2H), 1.75-1.78 (m, 2H), 1.30-1.34 (m, 2H), 0.87 (t, *J* = 7.5 Hz, 3H), 0.38 (t, *J* = 7.5 Hz, 12H); ^{13}C NMR ($CDCl_3$, 125.77 MHz) δ 182.44, 151.25, 149.68, 147.85, 147.67, 147.48, 147.24, 142.37, 141.40, 141.36, 141.24, 137.48, 136.59, 134.50, 130.04, 127.27, 126.88, 126.31, 123.86, 123.81, 123.32, 122.77, 120.92, 120.28, 120.12, 119.05, 118.89, 117.88, 117.48, 116.82, 105.65, 103.92, 56.12, 42.72, 32.76, 31.05, 20.48, 13.79, 8.63; HRMS calcd for $C_{59}H_{54}N_2OS_2$ $[M]^+$ *m/z* 870.3672, found 870.3658.

(*E*)-3-(4-(9-Butyl-7-((9,9-dipropyl-9*H*-fluoren-2-yl)(phenyl)amino)-9*H*-carbazol-2-yl)phenyl)-2-cyanoacrylic acid, 15a. The aldehyde (0.20 g, 0.33 mmol) and 2-cyanoacetic acid (0.04 g, 0.5 mmol), ammonium acetate (0.04 g, 0.25 mmol), and acetic

acid (5 mL) were mixed and refluxed for 24 h. The resulting red precipitate was filtered and washed several times with water and dried. It was crystallized from dichloromethane/hexane mixture to obtain the analytically pure sample. Yellow solid; Yield 0.23 g (94%); mp 135-136 °C; IR (KBr, cm^{-1}) 2230 ($\nu_{C\equiv N}$); ^{1}H NMR ($CDCl_3$, 500.13 MHz) δ 8.17 (t, *J* = 10.0 Hz, 1H), 8.07-8.14 (m, 2H), 7.86 (d, *J* = 8.0 Hz, 2H), 7.72-7.77 (m, 3H), 7.54 (t, *J* = 9.5 Hz, 2H), 7.41 (d, *J* = 7.5 Hz, 2H), 7.28-7.34 (m, 4H), 7.18 (d, *J* = 4.5 Hz, 1H), 7.16 (s, 1H), 7.08-7.10 (m, 2H), 7.00-7.03 (m, 2H), 6.90-6.92 (m, 1H), 4.28 (m, 2H), 1.75-1.92 (m, 4H), 1.64-1.67 (m, 2H), 1.19-1.24 (m, 2H), 0.78 (t, *J* = 7.0 Hz, 3H), 0.56-0.67 (m, 10H); ^{13}C NMR ($CDCl_3$, 125.77 MHz) δ 173.94, 158.55, 154.84, 154.38, 152.06, 150.53, 148.38, 147.46, 142.12, 141.62, 140.76, 140.74, 137.14, 137.13, 136.34, 136.32, 131.83, 129.77, 128.42, 128.01, 127.84, 127.38, 126.96, 123.81, 123.51, 123.19, 122.92, 121.65, 121.26, 121.24, 120.59, 120.58, 119.72, 119.70, 119.44, 119.10, 118.19, 116.60, 108.55, 55.19, 42.20, 31.01, 23.25, 20.16, 17.44, 14.75, 14.02; HRMS calcd for $C_{51}H_{48}N_3O_2$ $[M + H]^+$ *m/z* 734.3741, found 734.3749.

(*E*)-3-(4-(7-(Bis(9,9-diethyl-9*H*-fluoren-2-yl)amino)-9-butyl-9*H*-carbazol-2-yl)phenyl)-2-cyanoacrylic acid, 15b. It was prepared form **14b** (0.26 g, 0.33 mmol) and 2-cyanoacetic acid (0.04 g, 0.5 mmol) by following a procedure described above for **15a**. Red solid; Yield 0.25 g (90%); mp 235-238 °C; IR (KBr, cm^{-1}) 2217; ^{1}H NMR ($CDCl_3$, 500.13 MHz) δ 8.01 (d, *J* = 8.5 Hz, 1H), 7.93 (d, *J* = 8.5 Hz, 1H), 7.79 (s, 1H), 7.64 (d, *J* = 6.5 Hz, 2H), 7.60-7.62 (m, 3H), 7.53-7.56 (m, 2H), 7.27-7.34 (m, 9H), 7.21 (d, *J* = 2.0 Hz, 2H), 7.14 (dd, *J* = 8.0 Hz, 3.0 Hz, 2H), 7.12 (s, 1H), 7.07 (d, *J* = 8.5 Hz, 1H), 4.15 (t, *J* = 7.5 Hz, 2H), 1.94-2.01 (m, 4H), 1.85-1.90 (m, 4H), 1.73-1.78 (m, 2H), 1.28-1.34 (m, 2H), 0.86 (t, *J* = 7.5 Hz, 3H), 0.38 (t, *J* = 7.5 Hz, 12H); ^{13}C NMR ($CDCl_3$, 125.77 MHz) δ 172.50, 163.95, 154.25, 151.11, 149.56, 147.65, 146.95, 145.89, 142.32, 141.61, 141.19, 136.57, 135.65, 131.88, 130.50, 127.96, 127.41, 126.91, 123.46, 123.10, 123.04, 121.87, 121.19, 120.67, 119.65, 118.79, 118.62, 117.87, 116.88, 116.52, 107.94, 104.30, 103.12, 56.0, 42.26, 32.35, 31.05, 20.18, 13.96, 8.90; HRMS calcd for $C_{60}H_{55}N_3O_2$ $[M]^+$ *m/z* 849.4289, found 849.4284.

(*E*)-3-(5-(9-Butyl-7-((9,9-dipropyl-9*H*-fluoren-2-yl)(phenyl)amino)-9*H*-carbazol-2-yl)thiophen-2-yl)-2-cyanoacrylic acid, 18a. Compound **18a** was obtained from **16a** (0.34 g, 0.5 mmol) by following a procedure similar to that described above for 1**5a**. Brown solid; Yield 0.35 g (94%); mp 217 °C; IR (KBr, cm^{-1}) 2217 ($\nu_{C\equiv N}$); ^{1}H NMR ($CDCl_3$, 500.13 MHz) δ 8.37 (s, 1H), 8.02 (d, *J* = 8.0 Hz, 1H), 7.92 (d, *J* = 8.5 Hz, 1H),

7.82 (d, *J* = 4.0 Hz, 1H), 7.62 (d, *J* = 9.0 Hz, 2H), 7.58 (t, *J* = 10.0 Hz, 2H), 7.54 (d, *J* = 4.0 Hz, 1H), 7.32-7.30 (m, 3H), 7.28 (s, 1H), 7.27 (s, 1H), 7.20-7.21 (m, 3H), 7.08-7.10 (m, 2H), 7.05-7.07 (m, 2H), 4.17 (t, *J* = 7.5 Hz, 2H), 1.74-1.91 (m, 4H), 1.29-1.34 (m, 2H), 0.88 (t, *J* = 7.0 Hz, 4H), 0.68-0.70 (m, 10H); ^{13}C NMR ($CDCl_3$, 125.77 MHz) δ 152.16, 150.60, 148.24, 147.49, 147.24, 142.73, 140.87, 136.53, 134.24, 129.19, 128.96, 126.83, 126.39, 124.27, 123.97, 123.76, 122.78, 122.69, 121.18, 120.37, 119.50, 119.15, 118.04, 117.62, 106.39, 103.85, 55.26, 42.63, 31.08, 20.44, 17.33, 14.56, 13.85; HRMS calcd for $C_{49}H_{45}N_3O_2S$ $[M]^+$ *m/z* 739.3227, found 739.3223.

(*E*)-3-(5-(7-(Bis(9,9-diethyl-9*H*-fluoren-2-yl)amino)-9-butyl-9*H*-carbazol-2-yl)thiophen-2-yl)-2-cyanoacrylic acid, 18b. Compound **18b** was obtained from **16b** (0.39 g, 0.5 mmol) by following a procedure similar to that described above for 1**5a**. Grey solid; Yield 0.41 g (95%); mp 225 °C; IR (KBr, cm^{-1}) 2208 ($\nu_{C\equiv N}$); ^{1}H NMR ($CDCl_3$, 500.13 MHz) δ 8.36 (s, 1H), 8.02 (d, *J* = 8.0 Hz, 1H), 7.93 (d, *J* = 8.0 Hz, 1H), 7.82 (d, *J* = 4.5 Hz, 1H), 7.65 (d, *J* = 7.5 Hz, 2H), 7.61 (d, *J* = 8.0 Hz, 3H), 7.57 (q, *J* = 8.5 Hz, 1H), 7.54 (d, *J* = 4.0 Hz, 1H), 7.28-7.34 (m, 6H), 7.22 (d, *J* = 2.5 Hz, 2H), 7.12-7.15 (m, 3H), 7.07-7.09 (m, 1H), 4.16 (t, *J* = 6.5 Hz, 2H), 1.97 (septet, *J* = 7.0 Hz, 4H), 1.88 (septet, *J* = 3.0 Hz, 4H), 1.75 (q, *J* = 7.5 Hz, 2H), 1.28-1.33 (m, 2H), 0.86 (t, *J* = 7.5 Hz, 3H), 0.38 (t, *J* = 7.5 Hz, 12H); ^{13}C NMR ($CDCl_3$, 125.77 MHz) δ 158.17, 151.31, 149.71, 148.04, 147.83, 147.52, 142.77, 141.36, 141.13, 140.53, 136.82, 134.18, 128.88, 126.91, 124.73, 124.31, 123.50, 122.79, 121.21, 120.33, 120.25, 119.10, 118.09, 117.51, 116.83, 115.88, 106.39, 103.62, 56.14, 42.74, 32.76, 31.06, 20.44, 13.78, 8.63; HRMS calcd for $C_{58}H_{53}N_3O_2SNa$ $[M + Na]^+$ *m/z* 878.3751, found 878.3748.

(*E*)-3-(5-(5-(9-Butyl-7-((9,9-dipropyl-9*H*-fluoren-2-yl)(phenyl)amino)-9*H*-carbazol-2-yl)thiophen-2-yl)thiophen-2-yl)-2-cyanoacrylic acid, 19a. Compound **19a** was obtained from **17a** (0.38 g, 0.5 mmol) by following a procedure similar to that described above for 1**5a**. Violet solid; Yield 0.38 g (93%); mp 258 °C; IR (KBr, cm^{-1}) 2213 ($\nu_{C\equiv N}$); ^{1}H NMR ($CDCl_3$, 500.13 MHz) δ 8.32 (s, 1H), 8.00 (d, *J* = 3.0 Hz, 1H), 7.91 (d, *J* = 8.5 Hz, 1H), 7.72 (d, *J* = 4.0 Hz, 1H), 7.62-7.63 (m, 1H), 7.58 (d, *J* = 8.5 Hz, 1H), 7.54 (s, 1H), 7.48 (dd, *J* = 8.0 Hz, 1.5 Hz, 1H), 7.45 (d, *J* = 4.0 Hz, 1H), 7.39 (d, *J* = 4.0 Hz, 1H), 7.28-7.33 (m, 5H), 7.25 (s, 1H), 7.19-7.20 (m, 3H), 7.11 (d, *J* = 2.0 Hz, 1H), 7.09 (dd, *J* = 8.0 Hz, 2.0 Hz, 1H), 7.01-7.05 (m, 2H), 4.16 (m, 2H), 1.77-1.89 (m, 6H), 1.33-1.34 (m, 2H), 0.89 (t, *J* = 7.0 Hz, 3H), 0.667-0.673 (m, 10H); ^{13}C NMR ($CDCl_3$, 125.77 MHz) δ 152.12, 150.60, 148.38, 147.81, 147.49, 147.38, 146.95, 142.38, 141.33,

141.20, 140.92, 137.55, 136.34, 134.50, 130.08, 129.15, 127.28, 126.82, 126.33, 123.89, 123.82, 123.77, 123.59, 123.24, 122.77, 122.46, 120.92, 120.32, 120.17, 119.33, 119.11, 118.01, 117.47, 116.93, 105.66, 104.19, 55.25, 42.63, 31.07, 26.88, 17.55, 17.33, 20.48, 14.56, 13.86; HRMS calcd for $C_{53}H_{47}N_3O_2S_2$ $[M]^+$ *m/z* 821.3104, found 821.3103.

(*E*)-3-(5-(5-(7-(Bis(9,9-diethyl-9*H*-fluoren-2-yl)amino)-9-butyl-9*H*-carbazol-2-yl)thiophen-2-yl)thiophen-2-yl)-2-cyanoacrylic acid, 19b. Compound **19b** was obtained from **17b** (0.44 g, 0.5 mmol) by following a procedure similar to that described above for 1**5a**. Violet solid; Yield 0.43 g (92%); mp 231 °C; IR (KBr, cm^{-1}) 2215 ($\nu_{C\equiv N}$); ^{1}H NMR ($CDCl_3$, 500.13 MHz) δ 8.49 (s, 1H), 7.92-8.08 (m, 4H), 7.70-7.76 (m, 6H), 7.63 (s, 1H), 7.54 (d, *J* = 7.0 Hz, 1H), 7.38 (d, *J* = 5.1 Hz, 2H), 7.28-7.32 (m, 4H), 7.17-7.21 (m, 3H), 7.07 (d, *J* = 7.5 Hz, 2H), 6.97 (d, *J* = 8.0 Hz, 1H), 4.26 (m, 2H), 1.86-1.95 (m, 8H), 1.63-1.65 (m, 2H), 1.20 (t, *J* = 6.5 Hz, 2H), 0.73-0.76 (m, 3H), 0.26-0.29 (m, 12H); ^{13}C NMR (DMSO-d_6, 125.77 MHz) δ 166.01, 162.83, 152.56, 152.21, 150.65, 149.12, 147.30, 147.16, 146.83, 146.45, 141.83, 141.31, 140.93, 140.73, 136.10, 133.81, 133.52, 129.51, 128.29, 126.97, 126.47, 125.19, 124.67, 122.99, 122.67, 122.41, 120.76, 120.32, 119.20, 118.34, 117.48, 117.08, 116.13, 106.98, 105.79, 103.90, 55.56, 41.76, 31.87, 30.53, 19.67, 13.49, 8.43; HRMS calcd for $C_{62}H_{55}N_3O_2S_2Na$ $[M + Na]^+$ *m/z* 960.3628, found 960.3618.

Bis(4-(9,9-diethyl-9*H*-fluoren-2-yl)phenyl)amine, 21. A two neck RB flask charged with a mixture of **20** (1.30 g, 4 mmol), 9,9-diethyl-9*H*-fluoren-2-ylboronic acid (0.87 g, 8.8 mmol), anhydrous K_2CO_3 (3.86 g, 28 mmol) and $Pd(PPh_3)_4$ (0.27 g, 0.24 mmol) were dissolved in mixture of THF/H_2O (3:1). The reaction mixture was degassed with N_2 and refluxed for 12 h under nitrogen atmosphere. After cooling to room temperature, the organic layer extracted with dichloromethane and dried with sodium sulfate. The crude product was purified by column chromatography on silica gel by using a hexane/dichloromethane mixture (2:1) as eluant. Pale yellow solid; Yield 1.31 g (54%); mp 184-186 °C; ^{1}H NMR (DMSO-d_6, 500.13 MHz) δ 8.55 (s, 1H), 7.86 (d, *J* = 8.0 Hz, 2H), 7.83 (d, *J* = 7.0 Hz, 2H), 7.70-7.72 (m, 2H), 7.64 (d, *J* = 8.0 Hz, 2H), 7.44 (d, *J* = 7.0 Hz, 2H), 7.33-7.38 (m, 4H), 7.25 (d, *J* = 8.5 Hz, 4H), 2.02-2.16 (m, 8H), 0.28 (t, *J* = 7.0 Hz, 12H); ^{13}C NMR (DMSO-d_6, 125.77 MHz) δ 150.10, 149.50, 142.53, 140.71, 139.39, 139.02, 131.71, 127.47, 126.97, 126.93, 124.70, 122.83, 120.16, 120.07, 119.68, 117.09, 55.65, 31.81, 8.47; HRMS calcd for $C_{46}H_{44}N$ $[M + H]^+$ *m/z* 609.3390, found 609.3363.

7-Bromo-9-butyl-*N*,*N*-bis(4-(9,9-diethyl-9*H*-fluoren-2-yl)phenyl)-9*H*-carbazol-2-amine, 22. A mixture of **1** (1.52 g, 4 mmol) and **21** (1.22 g, 2 mmol), $Pd(dba)_2$ (0.01 g, 0.01 mmol), dppf (0.01 g, 0.01 mmol), sodium *tert*-butoxide (0.43 g, 5.0 mmol), and toluene taken in a pressure tube and heated at 80 °C for 48 h. After completion of the reaction, the volatiles were removed under vacuum, and the resulting solution was extracted with dichloromethane (3 × 50 mL). The combined organic extracts washed with brine solution, dried over Na_2SO_4, and concentrated. Further the crude product was purified by column chromatography on silica gel by using hexane/dichloromethane mixture (5:1) as an eluant. White solid; Yield 1.14 g (63%); mp 138 °C; ^{1}H NMR ($CDCl_3$, 500.13 MHz) δ 7.94 (d, *J* = 8.5 Hz, 1H), 7.87 (d, *J* = 8.0 Hz, 1H), 7.76 (d, *J* = 7.5 Hz, 2H), 7.72-7.73 (m, 2H), 7.61 (d, *J* = 8.5 Hz, 5H), 7.58 (d, *J* = 1.5 Hz, 1H), 7.56 (s, 2H), 7.50 (d, *J* = 1.5 Hz, 1H), 7.28-7.36 (m, 11H), 7.20 (s, 1H), 7.09 (m, 1H), 4.14 (t, *J* = 7.0 Hz, 2H), 2.05-2.10 (m, 8H), 1.77 (t, *J* = 7.5 Hz, 2H), 1.32-1.34 (m, 2H), 0.91 (t, *J* = 7.0 Hz, 3H), 0.37 (t, *J* = 7.5 Hz, 12H); ^{13}C NMR ($CDCl_3$, 125.77 MHz) δ 150.62, 150.13, 147.19, 141.81, 141.24, 140.54, 139.45, 135.80, 127.83, 126.99, 125.52, 124.18, 122.93, 122.16, 120.98, 119.95, 119.66, 118.53, 117.60, 111.70, 105.21, 56.19, 32.85, 31.02, 20.51, 13.90, 8.61; HRMS calcd for $C_{17}H_{17}BrNO$ $[M + H]^+$ *m/z* 330.0488, found 330.0487.

4-(7-(Bis(4-(9,9-diethyl-9*H*-fluoren-2-yl)phenyl)amino)-9-butyl-9*H*-carbazol-2-yl)benzaldehyde, 23. Compound **23** was synthesized from **22** (0.46 g, 0.5 mmol) by following a procedure similar to that described above for **14a**. Yellow solid; Yield 0.40 g (85%); mp 165 °C; IR (KBr, cm^{-1}) 1683 ($\nu_{C=O}$); ^{1}H NMR ($CDCl_3$, 500.13 MHz) δ 10.09 (s, 1H), 8.11 (d, *J* = 8.5 Hz, 1H), 8.00-8.03 (m, 3H), 7.90 (d, *J* = 8.5 Hz, 2H), 7.72-7.77 (m, 4H), 7.57-7.63 (m, 9H), 7.52 (d, *J* = 8.0 Hz, 1H), 7.30-7.37 (m, 10H), 7.24 (s, 1H), 7.11 (dd, *J* = 8.5 Hz, 1.0 Hz, 1H), 4.26 (t, *J* = 7.0 Hz, 2H), 2.06-2.10 (m, 8H), 1.80-1.86 (m, 2H), 1.34-1.42 (m, 2H), 0.92 (t, *J* = 7.5 Hz, 3H), 0.37 (t, *J* = 7.5 Hz, 12H); ^{13}C NMR ($CDCl_3$, 125.77 MHz) δ 191.97, 150.63, 150.13, 148.35, 147.22, 146.45, 142.43, 141.42, 141.25, 140.55, 139.46, 136.62, 135.83, 134.93, 130.34, 128.00, 127.84, 126.99, 126.90, 125.53, 124.24, 123.28, 122.93, 121.29, 120.99, 120.30, 119.996, 119.67, 118.82, 118.45, 117.44, 107.37, 105.09, 56.19, 42.80, 32.85, 31.19, 20.56, 13.94, 8.61; HRMS calcd for $C_{69}H_{63}N_2O$ $[M + 1]^+$ *m/z* 935.4935, found 935.4907.

5-(7-(Bis(4-(9,9-diethyl-9*H*-fluoren-2-yl)phenyl)amino)-9-butyl-9*H*-carbazol-2-yl)thiophene-2-carbaldehyde, 25a. It was synthesized from **22** (0.46 g, 0.5 mmol) and

((5-(1,3-dioxolan-2-yl)thiophen-2-yl)tributylstannane (0.24 g, 0.55 mmol) by following a procedure similar to that described above for **16a**. Yellow solid; Yield 0.32 g (67%); mp 160 °C; IR (KBr, cm^{-1}) 1669 ($\nu_{C=O}$); ^1H NMR ($CDCl_3$, 500.13 MHz) δ 9.91 (s, 1H), 8.04 (d, *J* = 8.0 Hz, 1H), 7.98 (d, *J* = 8.5 Hz, 1H), 7.73-7.79 (m, 5H), 7.56-7.69 (m, 10H), 7.51 (d, *J* = 3.5 Hz, 1H), 7.30-7.44 (m, 10H), 7.23-7.26 (m, 1H), 7.11 (d, *J* = 8.5 Hz, 1H), 4.23 (t, *J* = 6.5 Hz, 2H), 1.79-1.85 (m, 8H), 1.79-1.85 (m, 2H), 1.34-1.39 (m, 2H), 0.86-0.95 (m, 3H), 0.38 (t, *J* = 7.0 Hz, 12H); ^{13}C NMR ($CDCl_3$, 125.77 MHz) δ 182.77, 160.07, 157.44, 156.18, 147.06, 146.37, 142.63, 141.76, 141.08, 137.72, 136.98, 132.56, 131.05, 130.10, 129.45, 126.51, 124.26, 123.72, 123.56, 123.07, 121.19, 120.27, 117.99, 117.76, 117.72, 106.38, 104.84, 104.64, 99.01, 55.55, 55.45, 42.74, 31.12, 20.49, 13.94 8.61; HRMS calcd for $C_{67}H_{61}N_2OS$ $[M + H]^+$ *m/z* 330.0488, found 330.0487.

5'-(7-(Bis(4-(9,9-diethyl-9*H*-fluoren-2-yl)phenyl)amino)-9-butyl-9*H*-carbazol-2-yl)-[2,2'-bithiophene]-5-carbaldehyde, 25b. It was obtained from **22** (0.46 g, 0.5 mmol) and (5-(5-(1,3-dioxolan-2-yl)thiophen-2-yl)thiophen-2-yl)tributylstannane (0.30 g, 0.55 mmol) by following a procedure similar to that described above for 1**6a**. Yellow solid; Yield 0.31 g (61%); mp 178 °C; IR (KBr, cm^{-1}) 1661 ($\nu_{C=O}$); ^1H NMR ($CDCl_3$, 500.13 MHz) δ 9.88 (s, 1H), 8.01 (d, *J* = 8.0 Hz, 1H), 7.97 (d, *J* = 8.5 Hz, 1H), 7.75 (d, *J* = 8.0 Hz, 2H), 7.72-7.73 (m, 2H), 7.67 (d, *J* = 9.0 Hz, 1H), 7.60-7.63 (m, 5H), 7.56-7.59 (m, 4H), 7.49 (dd, *J* = 8.0 Hz, 1.5 Hz, 1H), 7.37-7.40 (m, 2H), 7.34-7.37 (m, 4H), 7.32 (d, *J* = 1.5 Hz, 1H), 7.29-7.30 (m, 6H), 7.22 (d, *J* = 1.5 Hz, 1H), 7.09-7.11 (m, 1H), 4.23 (t, *J* = 7.0 Hz, 2H), 2.04-2.10 (m, 8H), 1.79-1.85 (m, 2H), 1.33-1.40 (m, 2H), 0.93 (t, *J* = 7.5 Hz, 3H), 0.38 (t, *J* = 7.5 Hz, 12H); ^{13}C NMR ($CDCl_3$, 125.77 MHz) δ 182.59, 150.76, 150.25, 147.87, 147.55, 147.31, 146.52, 142.57, 141.48, 141.41, 141.37, 140.67, 139.57, 137.66, 135.95, 134.70, 130.41, 127.98, 127.43, 127.14, 127.05, 125.67, 124.40, 124.10, 123.97, 123.34, 123.07, 121.30, 121.10, 120.47, 120.12, 119.82, 118.70, 117.69, 117.59, 105.86, 105.16, 56.32, 42.89, 32.99, 31.30, 20.69, 14.10, 8.77; HRMS calcd for $C_{71}H_{62}N_2OS_2$ $[M]^+$ *m/z* 1022.4298, found 1022.4278.

(*E*)-3-(4-(7-(Bis(4-(9,9-diethyl-9*H*-fluoren-2-yl)phenyl)amino)-9-butyl-9*H*-carbazol-2-yl)phenyl)-2-cyanoacrylic acid, 24. It was prepared form **23** (0.31 g, 0.33 mmol) and 2-cyano acetic acid (0.04 g, 0.5 mmol) by following a procedure described above for **15a**. Brown solid; Yield 0.31 g (94%); mp 160 °C; IR (KBr, cm^{-1}) 2222 ($\nu_{C\equiv N}$); ^1H NMR ($CDCl_3$, 500.13 MHz) δ 8.36 (s, 1H), 8.14-8.19 (m, 2H), 8.10 (d, *J* = 7.5 Hz, 1H), 7.89 (d, *J* = 8.0 Hz, 3H), 7.84 (d, *J* = 7.0 Hz, 2H), 7.73-7.77 (m, 8H), 7.68 (d, *J* = 7.0

Hz, 3H), 7.54-7.57 (m, 2H), 7.45 (d, *J* = 6.5 Hz, 2H), 7.34-7.38 (m, 6H), 7.23 (d, *J* = 8.0 Hz, 4H), 7.00 (d, *J* = 8.0 Hz, 1H), 4.24 (t, *J* = 6.5 Hz, 2H), 2.04-2.15 (m, 8H), 1.65 (t, *J* = 7.5 Hz, 2H), 1.25-1.29 (m, 2H), 0.84 (t, *J* = 7.5 Hz, 3H), 0.27 (t, *J* = 7.5 Hz, 12H); ^{13}C NMR ($CDCl_3$, 125.77 MHz) δ 167.44, 150.64, 150.05, 148.81, 147.25, 147.20, 147.18, 141.10, 139.06, 135.29, 134.97, 131.99, 129.13, 127.61, 127.44, 125.57, 124.16, 123.35, 120.95, 120.73, 120.30, 118.01, 117.38, 117.32, 108.20, 106.00, 105.98, 56.20, 41.26, 32.30, 31.16, 20.27, 14.14, 8.94; HRMS calcd for $C_{76}H_{64}N_3O_2$ $[M + H]^+$ *m/z* 1002.4993, found 1002.4962.

(*E*)-3-(5-(7-(Bis(4-(9,9-diethyl-9*H*-fluoren-2-yl)phenyl)amino)-9-butyl-9*H*-carbazol-2-yl)thiophen-2-yl)-2-cyanoacrylic acid, 26a. It was prepared form **25a** (0.34 g, 0.33 mmol) and 2-cyano acetic acid (0.04 g, 0.5 mmol) by following a procedure described above for **15a**. Red solid; Yield 0.32 g (95%); mp 220 °C; IR (KBr, cm^{-1}) 2215 ($\nu_{C\equiv N}$); ^{1}H NMR ($CDCl_3$, 500.13 MHz) δ 8.27 (s, 1H), 7.99 (d, *J* = 8.0 Hz, 1H), 7.92 (d, *J* = 8.5 Hz, 1H), 7.77 (s, 1H), 7.64 (d, *J* = 6.5 Hz, 3H), 7.60 (d, *J* = 3.0 Hz, 2H), 7.53 (s, 2H), 7.47-7.50 (m, 2H), 7.41 (d, *J* = 4.0 Hz, 2H), 7.28-7.34 (m, 10H), 7.21 (s, 2H), 7.13 (d, *J* = 8.5 Hz, 3H), 7.06 (d, *J* = 8.0 Hz, 1H), 4.14 (t, *J* = 6.5 Hz, 2H), 1.94-2.01 (m, 8H), 1.73-1.79 (m, 2H), 1.29-1.34 (m, 2H), 0.86 (t, *J* = 7.0 Hz, 3H), 0.37 (t, *J* = 7.0 Hz, 12H); ^{13}C NMR ($CDCl_3$, 125.77 MHz) δ 172.58, 164.21, 155.04, 150.60, 150.01, 146.99, 146.52, 142.64, 141.76, 141.28, 141.25, 140.99, 140.39, 138.89, 135.25, 134.54, 129.47, 128.05, 127.99, 127.58, 127.56, 127.48, 127.37, 125.50, 125.43, 124.51, 124.43, 123.91, 123.28, 121.06, 121.04, 120.81, 120.72, 120.68, 120.61, 120.18, 118.23, 117.13, 117.11, 117.02, 105.15, 56.10, 42.23, 32.27, 31.02, 20.15, 13.94, 8.85; HRMS calcd for $C_{70}H_{62}N_3O_2S$ $[M + H]^+$ *m/z* 1008.4563, found 1008.4587.

(*E*)-3-(5'-(7-(Bis(4-(9,9-diethyl-9*H*-fluoren-2-yl)phenyl)amino)-9-butyl-9*H*-carbazol-2-yl)-[2,2'-bithiophen]-5-yl)-2-cyanoacrylic acid, 26b. It was prepared form **25b** (0.34 g, 0.33 mmol) and 2-cyano acetic acid (0.04 g, 0.5 mmol) by following a procedure described above for **15a**. Red solid; Yield 0.33 g (91%); mp 239 °C; IR (KBr, cm^{-1}) 2213; ^{1}H NMR (DMSO-d_6, 500.13 MHz) δ 8.50 (s, 1H), 8.25 (d, *J* = 8.0 Hz, 1H), 8.13 (t, *J* = 7.5 Hz, 2H), 8.00 (s, 1H), 7.87 (d, *J* = 8.0 Hz, 2H), 7.23 (d, *J* = 6.5 Hz, 2H), 7.70-7.78 (m, 4H), 7.65 (d, *J* = 8.0 Hz, 3H), 7.57 (d, *J* = 8.0 Hz, 1H), 7.44 (d, *J* = 7.0 Hz, 2H), 7.33-7.38 (m, 4H), 7.31 (s, 1H), 7.23 (d, *J* = 10.0 Hz, 4H), 6.99 (d, *J* = 8.5 Hz, 1H), 4.36 (t, *J* = 7.5 Hz, 3H), 2.04-2.14 (m, 8H), 1.68-1.71 (m, 2H), 1.25 (t, *J* = 6.0 Hz, 2H), 0.84 (t, *J* = 4.0 Hz, 3H), 0.27 (t, *J* = 7.5 Hz, 12H); ^{13}C NMR (DMSO-d_6, 125.77 MHz) δ

164.10, 150.60, 150.01, 147.32, 147.05, 146.18, 146.11, 142.39, 141.75, 141.40, 141.00, 140.37, 138.91, 135.76, 135.11, 134.05, 130.32, 127.98, 127.57, 127.38, 125.50, 125.09, 124.37, 123.75, 123.28, 122.89, 121.81, 120.80, 120.62, 120.18, 118.50, 117.17, 105.40, 56.10, 42.26, 32.27, 31.07, 20.18, 13.99, 8.85; HRMS calcd for $C_{74}H_{64}N_3O_2S_2$ $[M + H]^+$ *m/z* 1089.4362, found 1089.4373.

4.5 References

[1] A. Hagfeldt, G. Boschloo, L. Sun, L. Kloo and H. Pettersson, Dye-sensitized solar cells. *Chem. Rev.,* **2010**, *110,* 6595-6663.

[2] A. Mishra, M. K. R. Fischer and P. Bäuerle, Metal-Free organic dyes for dye-sensitized solar cells: From structure: Property relationships to design rules. *Angew. Chem. Int. Ed.,* **2009**, *48*, 2474-2499.

[3] Y. Wu and W. Zhu, Organic sensitizers from D-[π]-A to D-A-[π]-A: Effect of the internal electron-withdrawing units on molecular absorption, energy levels and photovoltaic performances. *Chem. Soc. Rev.,* **2013**, *42*, 2039-2058.

[4] N. Koumura, Z.-S. Wang, S. Mori, M. Miyashita, E. Suzuki and K. Hara, Alkyl-functionalized organic dyes for efficient molecular photovoltaics. *J. Am. Chem. Soc.,* **2006**, *128,* 14256-14257.

[5] Y. J. Chang and T. J. Chow, Dye-sensitized solar cell utilizing organic dyads containing triarylene conjugates. *Tetrahedron,* **2009**, *65,* 4726-4734.

[6] K. Sayama, S. Tsukagoshi, K. Hara, Y. Ohga, A. Shinpou, Y. Abe, S. Suga and H. Arakawa, Photoelectrochemical properties of J-aggregates of benzothiazole merocyanine dyes, on a nanostructured TiO_2 film. *J. Phys. Chem. B*, **2002**, *106*, 1363-1371.

[7] K. Hara, Z.-S. Wang, T. Sato, A. Furube, R. Katoh, H. Sugihara, Y. Dan-oh, C. Kasada, A. Shinpo and S. Suga, Oligothiophene containing coumarin dyes for efficient dye-sensitized solar cells. *J. Phys. Chem. B*, **2005**, *109,* 15476-15482.

[8] M. Liang and J. Chen, Arylamine organic dyes for dye-sensitized solar cells. *Chem. Soc. Rev,* **2013**, *42*, 3453-3488.

[9] Z. Ning and H. Tian, Triarylamine: A promising core unit for efficient photovoltaic materials. *Chem. Commun.,* **2009**, 5483-5495.

[10] D. P. Hagberg, T. Marinado, K. M. Karlsson, K. Nonomura, P. Qin, G. Boschloo, T. Brinck, A. Hagfeldt and L. Sun, Tuning the HOMO and LUMO energy levels of

organic chromophores for dye sensitized solar cells. *J. Org. Chem.*, **2007**, *72*, 9550-9556.

[11] S. Kim, J. W. Lee, S. O. Kang, J. Ko, J.-H. Yum, S. Fantacci, F. D. Angellis, D. D. Censo, M. K. Nazeeruddin and M. Grätzel, Molecular engineering of organic sensitizers for solar cell applications. *J. Am. Chem. Soc.*, ***2006***, *128*, 16701-16707.

[12] A. Baheti, S. R. Gajjela, P. Balaya and K. R. J. Thomas, Synthesis, optical, electrochemical and photovoltaic properties of organic dyes containing trifluorenylamine donors. *Dyes Pigm.*, **2015**, *113*, 78-86.

[13] A. Baheti, P. Tyagi, K. R. J. Thomas, Y.-C. Hsu and J. T. Lin, Simple triarylamine-based dyes containing fluorene and biphenyl linkers for efficient dye-sensitized solar cells. *J. Phys. Chem. Lett*., **2009**, *113*, 8541-8547.

[14] Q. Chai, W. Li, S. Zhu, Q. Zhang and W. Zhu, Influence of donor configurations on photophysical, electrochemical, and photovoltaic performances in D-π-A organic sensitizers. *ACS Sustainable Chem. Eng.*, **2014**, *2*, 239-247.

[15] A. Yella, R. Humphry-Baker, B. F. E. Curchod, N. S. Astani, J. Teuscher, L. E. Polander, S. Mathew, J.-E. Moser, I. Tavernelli, U. Rothlisherger, M. Grätzel, M. K. Nazeeruddin and J. Frey, Molecular engineering of a fluorene donor for dye-sensitized solar cells. *Chem. Mater.*, **2013**, *25*, 2733-2739.

[16] L. Zhou, C. Jia, Z. Wan, X. Chen and X. Yao, Effect of imidazole derivatives in triphenylamine-based organic dyes for dye-sensitized solar cells. *Org. Electron.*, **2013**, *14*, 1755-1762.

[17] D. P. Hagberg, X. Jiang, E. Gabrielsson, M. Linder, T. Marinado, T. Brinck, A. Hagfeldt and L. Sun, Symmetric and unsymmetric donor functionalization. comparing structural and spectral benefits of chromophores for dye-sensitized solar cells. *J. Mater. Chem.*, **2009**, *19*, 7232-7238.

[18] R. Y.-Y. Lin, Y.-S. Yen, Y.-T. Cheng, C.-P. Lee, Y.-C. Hsu, H.-H. Chou, C.-Y. Hsu, Y.-C. Chen, J. T. Lin, K.-C. Ho and C. Tsai, Dihydrophenanthrene-based metal-free dyes for highly efficient co-sensitized solar cells. *Org. Lett.*, **2012**, *14*, 3612-3615.

[19] K. R. J. Thomas, J. T. Lin, Y.-C. Hsu and K.-C. Ho, Organic dyes containing thienylfluorene conjugation for solar cells. *Chem. Commun.*, **2005**, 4098-4100.

[20] A. Baheti, K. R. J. Thomas, C.-P. Lee, C.-T. Li and K.-C. Ho, Organic dyes containingfluoren-9-ylidene chromophores for efficient dye-sensitized solar cells. *J. Mater. Chem. A*, **2014**, *2*, 5766-5779.

[21] B. Liu, Q. Liu, D. You, X. Li, Y. Naruta and W. Zhu, Molecular engineering of indoline based organic sensitizers for highly efficient dye-sensitized solar cells. *J. Mater. Chem.*, **2012**, *22*, 13348-13356.

[22] B. Liu, B. Wang, R. Wang, L. Gao, S. Huo, Q. Liu, X. Li and W. Zhu, Influence of conjugated π-linker in D-D-π-A indoline dyes: Towards long-term stable and efficient dye-sensitized solar cells with high photovoltage. *J. Mater. Chem. A*, **2014**, *2*, 804-812.

[23] G. Zhou, N. Pschirer, J. C. Schöneboom, F. Eickemeyer, M. Baumgarten and K. Müllen, Ladder-type pentaphenylene dyes for dye-sensitized solar cells. *Chem. Mater.*, **2008**, *20*, 1808-1815.

[24] M. Wang, M. Xu, D. Shi, R. Li, F. Gao, G. Zhang, Z. Yi, R. Humphry-Baker, P. Wang, S. M. Zakeeruddin and M. Grätzel, High-performance liquid and solid dye-sensitized solar cells based on a novel metal-free organic sensitizer. *Adv. Mater*., **2008**, *20*, 4460-4463.

[25] H. Qin, S. Wenger, M. Xu, F. Gao, X. Jing, P. Wang, S. M. Zakeeruddin and M. Grätzel, An organic sensitizer with a fused dithienothiophene unit for efficient and stable dye-sensitized solar cells. *J. Am. Chem. Soc.*, **2008**, *130*, 9202-9203.

[26] M. Xu, S. Wenger, H. Bala, D. Shi, R. Li, Y. Zhou, S. M. Zakeeruddin, M. Grätzel and P. Wang, Tuning the energy level of organic sensitizers for high-performance dye-sensitized solar cells. *J. Phys. Chem. C*, **2009**, *113*, 2966-2973.

[27] I. Jung, J. K. Lee, K. H. Song, K. Song, S. O. Kang and J. Ko, Synthesis and photovoltaic properties of efficient organic dyes containing the benzo[*b*]furan moiety for solar cells. *J. Org. Chem.*, **2007**, *72*, 3652-3658.

[28] K. Lim, C. Kim, J. Song, T. Yu, W. Lim, K. Song, P. Wang, N. Zu and J. Ko, Enhancing the performance of organic dye-sensitized solar cells via a slight structure modification. *J. Phys. Chem. C*, **2011**, *115*, 22640-22646.

[29] S. Ko, H. Choi, M.-S. Kang, H. Hwang, H. Ji, J. Kim, J. Ko and Y. Kang, Silole-spaced triarylamine derivatives as highly efficient organic sensitizers in dye-sensitized solar cells (DSSCs). *J. Mater. Chem*., **2010**, *20*, 2391-2399.

[30] H. Choi, S. Paek, K. Lim, C. Kim, M.-S. Kang, K. Song and J. Ko, Molecular engineering of organic sensitizers for highly efficient gel-state dye-sensitized solar cells. *J. Mater. Chem. A*, **2013**, *1*, 8226-8233.

[31] S. Paek, H. Choi, H. Choi, C.-W. Lee, M.-S. Kang, K. Song, M. K. Nazeeruddin and J. Ko, Molecular engineering of efficient organic sensitizers incorporating a

binary π-conjugated linker unit for dye-sensitized solar cell.s, *J. Phys. Chem. C,* **2010**, *114*, 14646-14653.

[32] J. F. Hartwig, Transition metal catalyzed synthesis of arylamines and aryl ethers from aryl halides and triflates: Scope and mechanism. *Angew. Chem. Int. Ed.,* **1998**, *37*, 2047-2067.

[33] A. W. Freeman, M. Urvoy and M. E. Criswell, Triphenylphosphine-mediated reductive cyclization of 2-nitrobiphenyls: A practical and convenient synthesis of carbazoles. *J. Org. Chem.,* **2005**, *70*, 5014-5019.

[34] Y. Che, D. E. Gross, H. Huang, D. Yang, X. Yang, E. Discekici, Z. Xue, H. Zhao, J. S. Moore and L. Zang, Diffusion-controlled detection of trinitrotoluene: Interior nanoporous structure and low highest occupied molecular orbital level of building blocks enhance selectivity and sensitivity. *J. Am. Chem. Soc.,* **2012**, *134*, 4978-4982.

[35] N. Miyaura and A. Suzuki, Palladium-catalyzed cross-coupling reactions of organoboron compounds. *Chem. Rev.,* **1995**, *95*, 2457-2483.

[36] J. K. Stille, The Palladium-catalyzed cross-coupling reactions of organotin reagents with organic electrophiles. *Angew. Chem. Int. Ed.,* **1986**, *25*, 508-524.

[37] E. Knoevenagel, Ueber eine darstellungsweise des benzylidenacetessigesters. *Chem. Ber.,* **1896**, *29*, 172-174.

[38] C.-J. Yang, Y. J. Chang, M. Watanabe, Y.-S. Hon and T. J. Chow, Phenothiazine derivatives as organic sensitizers for highly efficient dye-sensitized solar cells. *J. Mater. Chem.,* **2012**, *22*, 4040-4049.

[39] X. Qian, Y.-Z. Zhu, J. Song, X.-P. Gao and J.-Y. Zheng, New donor-π-acceptor type triazatruxene derivatives for highly efficient dye-sensitized solar cells. *Org. Lett.,* **2013**, *15*, 6034-6037.

[40] A. Mishra, N. Pootrakulchote, M. Wang, S.-J. Moon, S. M. Zakeeruddin, M. Grätzel and P. Bäuerle, A thiophene-based anchoring ligand and its heteroleptic Ru(II)-Complex for efficient thin-film dye-sensitized solar cells. *Adv. Funct. Mater.,* **2011**, *21*, 963-970.

[41] K. R. J. Thomas, Y.-C. Hsu, J. T. Lin, K.-M. Lee, K.-C. Ho, C.-H. Lai, Y.-M. Cheng and P.-T. Chou, 2,3-Disubstituted thiophene based organic dyes for solar cells. *Chem. Mater.,* **2008**, *20*, 1830-1840.

[42] M. K. Nazeeruddin, A. Kay, I. Rodicio, R. Humphry-Baker, E. Müller, P. Liska, N. Vlachopoulos and M. Grätzel, Conversion of light to electricity by cis-X2bis(2,2′-

bipyridyl-4,4′-dicarboxylate)-ruthenium(II) charge-transfer sensitizers (X = Cl^-, Br^-, I^-, CN^-, and SCN^-) on nanocrystalline titanium dioxide electrodes. *J. Am. Chem. Soc.*, **1993**, *115*, 6382-6390.

[43] M. K. Nazeeruddin, P. Péchy, T. Renouard, S. M. Zakeeruddin, R. Humphry-Baker, P. Comte, P. Liska, L. Cevey, E. Costa, V. Shklover, L. Spiccia, G. B. Deacon, C. A. Bignozzi and M. Grätzel, Engineering of efficient panchromatic sensitizers for nanocrystalline TiO_2-based solar cells. *J. Am. Chem. Soc.*, **2001**, *123*, 1613-1624.

[44] M. K. Nazeeruddin, S. M. Zakeeruddin, R. Humphry-Baker, M. Jirousek, P. Liska, N. Vlachopoulos, V. hklover, C. H. Fisher and M. Grätzel, Acid-base equilibria of (2,2‘-bipyridyl-4,4‘-dicarboxylic acid)ruthenium(II) complexes and the effect of protonation on charge-transfer sensitization of nanocrystalline titania. *Inorg. Chem.*, **1999**, *38*, 6298-6305.

[45] Z.-S. Wang, F.-Y. Li and C.-H. Huang, photocurrent enhancement of hemicyanine dyes containing RSO_3-group through treating TiO_2 films with hydrochloric acid. *J. Phys. Chem. B*, **2001**, *105*, 9210-9217.

[46] P. Singh, A. Baheti and K. R. J. Thomas, Synthesis and optical properties of acidochromic amine-substituted benzo[*a*]phenazines. *J. Org. Chem.*, **2011**, *76*, 6134-6145.

[47] O.van den Berg, W. F. Jager and S. J. Picken, 7-Dialkylamino-1-alkylquinolinium Salts: Highly versatile and stable fluorescent probes. *J. Org. Chem.*, **2006**, *71*, 2666-2676.

[48] A. Granzhan, H. Ihmels and G. Viola, 9-Donor-substituted acridizinium salts: Versatile environment-sensitive fluorophores for the detection of biomacromolecules. *J. Am. Chem. Soc*., **2007**, *129*, 1254-1267.

[49] C. Reichardt, Solvatochromic Dyes as solvent polarity indicators. *Chem. Rev*., **1994**, *94*, 2319-2358.

[50] K. Rurack, J. L. Bricks, G. Reck, R. Radeglia and U. Resch-Genger, Chalcone-analogue dyes emitting in the near-infrared (NIR): Influence of donor-acceptor substitution and cation complexation on their spectroscopic properties and X-ray structure. *J. Phys. Chem. A*, **2000**, *104*, 3087-3109.

[51] J. A. Pollard, D. Zhang, J. A. Downing, F. J. Knorr and J. L. McHale, Solvent effects on interfacial electron transfer from Ru(4,4′-dicarboxylic acid-2,2′-

bipyridine)$_2$(NCS)$_2$ to nanoparticulate TiO_2: Spectroscopy and solar photoconversion. *J. Phys. Chem. A*, **2005**, *109*, 11443-11452.

[52] W. Kylberg, Y. Zhang, A. Aebersold, F. A. D. Castro, T. Geiger, J. Heier, S. Kuster, C.-Q. Ma, P. Bäuerle, F. Nüesch, J.-N. Tisserant and R. Hany, Oligothiophene dendron-decorated squaraine dyes: Synthesis, thin film formation, and performance in organic solar cells. *Org. Electron.*, **2012**, *13*, 1204-1212.

[53] K. Sayama, S. Tsukagoshi, K. Hara, Y. Ohga, A. Shinpou, Y. Abe, S. Suga and H. Arakawa, Photoelectrochemical properties of J aggregates of benzothiazole merocyanine dyes on a nanostructured TiO_2 film. *J. Phys. Chem. B*, **2002**, *106*, 1363-1371.

[54] C. Teng, X. Yang, C. Yang, H. Tian, S. Li, X. Wang, A. Hagfeldt and L. Sun, Influence of triple bonds as π-Spacer units in metal-free organic dyes for dye-sensitized solar cells. *J. Phys. Chem. C*, **2010**, *114*, 11305-11313.

[55] M. Grätzel, Photoelectrochemical cells. *Nature*, **2001**, *414*, 338-344.

[56] R. G. Parr and W. Yang, Density-functional theory of the electronic structure of molecules. *Annu. Rev. Phys. Chem.*, **1995**, *46*, 701-728.

[57] B. J. Lynch, P. L. Fast, M. Harris and D. G. Truhlar, Adiabatic connection for kinetics. *J. Phys. Chem. A*, **2000**, *104*, 4811-4815.

[58] K. Pei, Y. Wu, A. Islam, Q. Zhang, L. Han, H. Tian and W. Zhu, Constructing high-efficiency D-A-π-A-featured solar cell sensitizers: a promising building block of 2,3-diphenylquinoxaline for anti aggregation and photostability. *ACS Appl. Mater. Interfaces*, **2013**, *5*, 4986-4995.

[59] Q. Chai, W. Li, Y. Wu, K. Pei, J. Liu, Z. Geng, H. Tian and W. Zhu, Effect of a long alkyl group on cyclopentadithiophene as a conjugated bridge for D-A-π-A organic sensitizers: IPCE, electron diffusion length, and charge recombination. *ACS Appl. Mater. Interfaces*, **2014**, *6*, 14621-14630.

[60] B. O'Regan and M. Grätzel, A low-cost, high-efficiency solar cell based on dye-sensitized colloidal TiO_2 films. *Nature*, **1991**, *353*, 737-740.

[61] K. Guo, K. Yan, X. Lu, Y. Qiu, Z. Liu, J. Sun, F. Yan, W. Guo and S. Yang, Dithiafulvenyl unit as a new donor for high-efficiency dye-sensitized solar cells: synthesis and demonstration of a family of metal-free organic sensitizers. *Org. Lett.*, **2012**, *14*, 2214-2217.

[62] J. van de Lagemaat, N.-G. Park and A. J. Frank, Influence of electrical potential distribution, charge transport, and recombination on the photopotential and

photocurrent conversion efficiency of dye-sensitized nanocrystalline TiO_2 solar cells: A study by electrical impedance and optical modulation techniques. *J. Phys. Chem. B*, **2000**, *104*, 2044-2052.

[63] A. W. Freeman, M. Urvoy and M. E. Criswell, Triphenylphosphine-mediated reductive cyclization of 2-nitrobiphenyls: A practical and convenient synthesis of carbazoles. *J. Org. Chem.*, **2005**, *70*, 5014-5019.

[64] Y. Che, D. E. Gross, H. Huang, D. Yang, X. Yang, E. Discekici, Z. Xue, H. Zhao, J. S. Moore and L. Zang, Diffusion-controlled detection of trinitrotoluene: Interior nanoporous structure and low highest occupied molecular orbital level of building blocks enhance selectivity and sensitivity. *J. Am. Chem. Soc.*, **2012**, *134*, 4978-4982.

[65] E. Ishow, A. Brosseau, G. Clavier, K. Nakatani, R. B. P., J.-J. Vachon, P. Tauc, D. Chauvat, C. R. Mendoncüa and E. Piovesan, Two-photon fluorescent holographic rewritable micropatterning. *J. Am. Chem. Soc.*, **2007**, *129*, 8970-8971.

[66] M. Holzapfel and C. Lambert, Photoinduced charge separation and recombination in acridine-triarylamine-based redox cascades. *J. Phys. Chem. C*, **2008**, *112*, 1227-1243.

CHAPTER 5

Effect of Auxiliary Chromophores on the Optical, Electrochemical and Photovoltaic Properties of Carbazole-Based Dyes

5.1 Introduction

Triarylamine-based dyes display relatively red-shifted absorption with high molar extinction coefficient owing to the strong donor strength [1-3]. Also, the trigonal structural arrangement of the triarylamine segment inhibits the aggregation of the dyes at the surface of TiO_2 [4-6]. Attachment of additional chromophores to the triarylamine core have been demonstrated as a way to fine tune the HOMO and LUMO energies of the dyes which assist either to regenerate the dyes by the redox couple in the electrolyte or to inject the electron into the conduction band of TiO_2 [7-9]. With subtle modifications, organic dyes displaying high efficiency in DSSC, challenging the Ru-based dyes have been discovered. Fused aromatic heterocyclic building blocks such as dithieno[3,2-*b* : 2′,3′-*d*]pyrrole (DTP) [10, 11] and cyclopenta[2,1-*b* : 3,4-*b*]dithiophene (CPDT) [12,13] have been exemplified as efficient mediators for the donor-acceptor interactions in the organic dyes. However, owing to their electron-richness, these dyes suffered from regeneration ability with the iodine/iodide redox electrolyte system because of the high lying HOMO. Fine tuning of the HOMO and LUMO energies of the organic dyes requires careful molecular engineering with judicious choice of structural elements in the donor and π-linker segments [14]. Introduction of auxiliary electron donating groups on the donor unit red shift the absorption spectrum and raises the HOMO and LUMO levels effectively [14]. In such a scenario, though the LUMO values are positioned well to facilitate the electron injection into the conduction band of TiO_2, the high HOMO values mismatch with the electrolyte redox potential and affect the dye regeneration [7, 8]. However, the presence of electron-rich units in the π-linker and moderate acceptors/delocalizing units in the donor segment have been found to be beneficial for fine-tuning the HOMO and LUMO energies suitably [15-17]. The efficiency of the DSSC is also reduced due to the dye aggregation induced recombination processes. However, these pathways can be inhibited by the use of bulky donor units or long alkyl chains either on the donor or linker part of the sensitizer [4, 5].

The effect of carbazole as auxiliary donor on simple triphenylamine-based metal free organic dyes was studied by Wang and co-workers. They have prepared three new dyes (**AD1**-**AD3** shown in Chart 5.1) based on triphenylamine framework and featuring one or two carbazole or acceptor units in a dye [18]. The dyes (**AD1**-**AD3**) displayed red-shifted (15-24 nm) absorption when compared to the parent dyes [19] which established the conjugating effect of carbazole segment. Moreover, introduction of two carbazole units in a dye (**AD3**)

benefits the absorption significantly than the dye (**AD2**) containing two acceptor units. Probably, in the former dye due to the presence of two carbazole auxiliary donors, the donor-acceptor interaction is enhanced, while in the later dye, it is bifurcated between the two acceptors. Finally, **AD3** displayed higher power conversion efficiency (4.63%) due to larger photocurrents (J_{SC} = 12.70 mA cm^{-2}) when compared to **AD1** and **AD2**. Tian and co-workers [3] incorporated the triphenylamine/carbazole auxiliary donor on triphenylamine and formed new dyes (**AD34** and **AC25-AC27**). The absorption spectra of diphenylamine auxiliary chromophore containing dyes (**AC25-AC27**) are red shifted when compared to carbazole containing dye **AD34**. However, carbazole incorporation fine tuned the HOMO and LUMO energy levels of the dyes and better charge injection led to better conversion efficiency of 6.02% (**AD34**) than the tiphenylamine auxiliary donor containing dye (**AC26**; 2.87%).

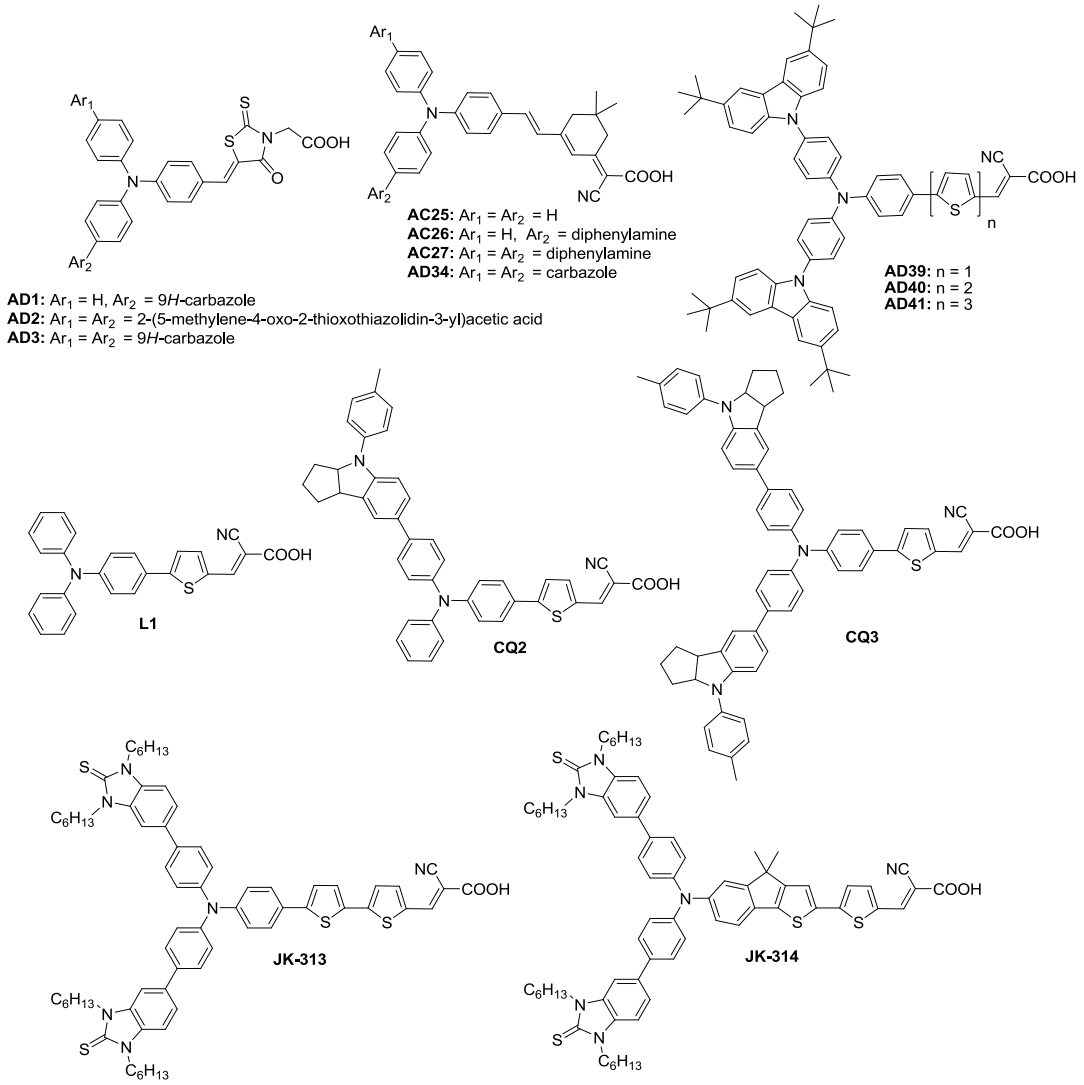

Chart 5.1 Structures of the dyes containing auxiliary donors.

Promarak and co-workers reported three dyes **AD39**–**AD41** (Chart 5.1) containing 3,6-di-*tert*-butylcarbazole as auxiliary donor [20]. In these dyes, the conjugation extension with thiophene red-shifted the absorption maximum and absorption coefficient increased when compared to the dyes without carbazole auxiliary donors. They exhibited efficiencies in the range of 3.70-4.62%. Zhu and co-workers [21] incorporated one or two indoline units on periphery of triphenylamine to obtain the dyes (**L1**, **CQ2** and **CQ3**) whcih showed improved visible light-harvesting capability and strong intramolecular chargetransfer (ICT) process, as well as positive shifting of the HOMO energy level. The efficiency of the dyes are effected by the addition of CDCA co-adsorbent and **CQ2** containing one indoline unit shows the highest conversion efficiency of 4.44% which increased to 6.38% after the addition of CDCA. The inferior efficiency of **CQ3** (2.08%) is attributed to the deteriorating intermolecular interactions between crowded donor units. Ko and co-workers [22] designed axiliary donor containing dyes (**JK-313** and **JK-314**) by incorporation of bulky cyclic thiourea functionalized triphenylamine. They showed intense charge transfer transition with longer wavelength peak and exhibited good power conversion efficiencies (**JK-313;**7.51% and **JK-314**; 8.61%).

Jia and co-workers [23] incorporated benzimidazole auxiliary donor in the triphenylamine and synthesized new dyes (**TPA-B1** and **TPA-B2** shown in Chart 5.2). The incorporation of benzimidazole units increased the molar extinction coefficient which led to larger photocurrent of the devices. The dyes **TPA-B1** and **TPA-B2** exhibited higher efficiencies of 2.43% and 2.65% than the un-substituted triphenylamine dye (η = 1.23%). Later, they incorporated imidazole units on triphenylamine unit (**CD4** and **CD6**) [16] and found that molar extinction coefficient increased along with device performance. The dye **CD-4** performed effectively to give higher efficiency of 4.11% than that of **CD-6** (1.51%) due to better molar extinction coefficient. They incorporated fused imidazole to obtain the dyes **TPA-B5** and **TPA-B6** [17]. They found that the the planar imidazole formed aggregates on the TiO_2 surface and led to blue shifted absorption. However, nonplanar imidazole improved the molar extinction coefficient and resulted broadening of the IPCE spectra and power conversion efficiency of 2.23% and 5.38% respectively. Zani and co-workers [24] synthesized unsymmetrical thiazolo[5,4-*d*]thiazole based dye (**TZ1**) which possess high molar extinction coefficient (40000 M^{-1} cm^{-1}). The device based on this dye showed an average efficiency of 2.55% with J_{SC} of 7.00 mA cm^{-2} and V_{OC} of 712 mV.

Thomas and co-workers [15] incorporated weak acceptors or π-delocalizing groups in the donor segment of **FL1** and **FL2** resulting **FL6**-**FL9** dyes. They found this strategy is helpful to fine-tune the HOMO and LUMO energies favourably. The incorporation of fluorenylidene unit broadens the optical properties when compared with dicyanovinyl unit. Finally, fluorenylidene containing dyes achieved higher efficiencies than parent dyes and the dye **FL8** exhibited higher power conversion efficiency of 6.13% with J_{SC} = 14.80 mA cm^{-2}, V_{OC} = 650 mV and *ff* = 0.64.

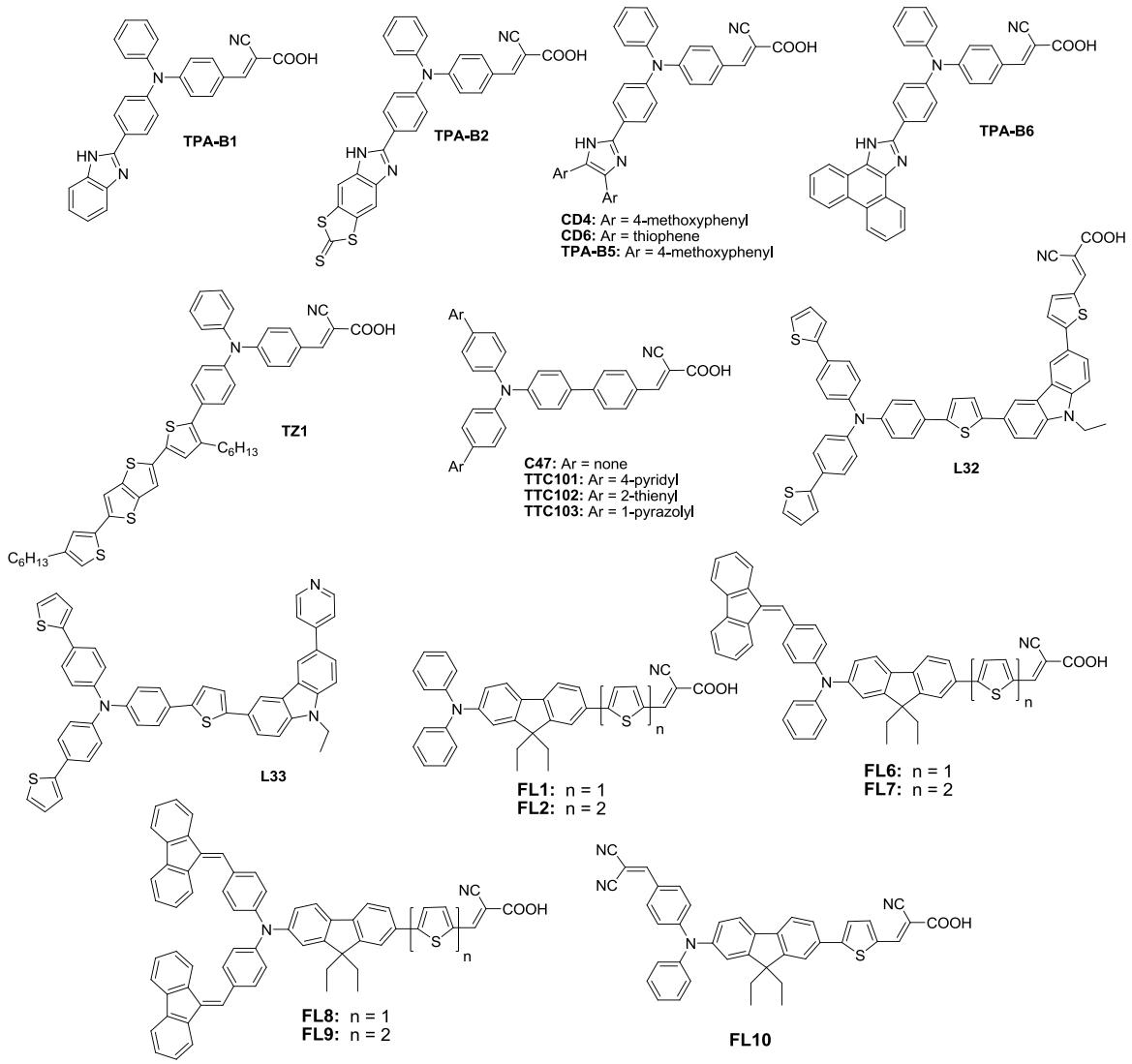

Chart 5.2 Structures of the dyes containing auxiliary chromophores on donor unit.

Zhou and co-workers designed and synthesized a set of dyes (**C47**, **TTC102-TTC103**, **L32** and **L33** shown in Chart 5.2) by incorporating heterocylic units (pyridine, thiophene, pyrazolyl) on triphenylamine and with carbazole linker [25]. They found that the thiophene and pyrazole units red shifted the absorption and help the delocalization of positive charge on

these units after photooxidation. The power conversion efficiencies of **TTC102** and **TTC103** are 4.92% and 5.21% respectively. The dyes featured different anchoring units such as cyanoacrylic acid (**L32**) and pyridine (**L33**) [26]. Compared to **C47** (η = 5.24%) where biphenyl bridging unit was there in place of carbazole, **L32** showed higher J_{SC} (14.12 mA cm^{-2}) and better conversion efficiency (6.37%). Pyridine-based dye, **L33** displayed significantly low conversion efficiency (η = 1.88%) due to less dye loading, huge dark current and pronounced charge recombination.

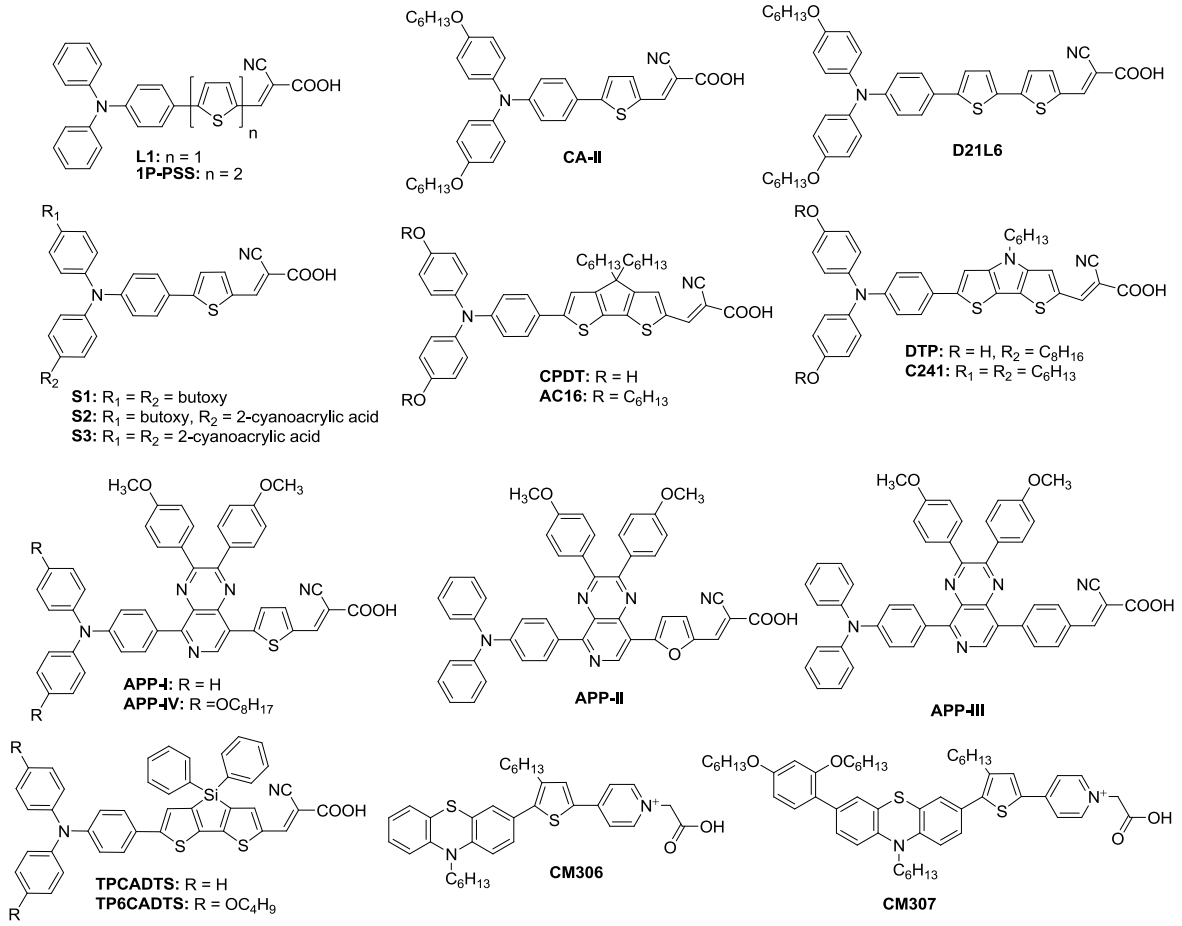

Chart 5.3 Structures of the dyes containing auxiliary chromophores on donor unit.

Tian and coworkers [27] synthesized **CA-II** by using butoxy group on the peripheral position of the triphenylamine based dye **L1** [28]. The new dye **CA-II** showed red shifted absorption of 74 nm due to enhanced donor strength. This dye **CA-II** achieved higher efficiency of 6.39% than **L1** (2.75%) due to longer absorption which led to longer J_{SC} of 11.34 mA cm^{-2} and butoxy groups prevented aggregation caused high V_{OC} of 804 mV. Kim and co-workers [29] synthesized **D2L16** and showed red shifted absorption when compared to **TT** dye [30] attributable to the electron rich triarylamine containing butxoy groups.

Zhan and co-workers [31] designed organic sensitizers (**S1**-**S3**) which contain different number of cyanoacrylic acid/butoxy groups on the periphery of the diphenylamine donor. The increasing ratio of anchoring groups/butoxy groups leads to decreasing V_{OC} due to positive shift of the conduction band of TiO_2 and more recombination which deters the efficiency of the dyes. The dyes **S1** (two butoxy and one anchoring), **S2** (one butoxy and two anchoring) and **S3** (three anchoring) showed efficiency of 6.65%, 5.49% and 5.34% with V_{OC} of 630 mV, 570 mV and 565 mV, respectively. Wang and co-workers [32] synthesized **AC16** dye by incorporating hexyloxy group on the peripheral position of the donor of **CPDT** dye [33]. The **AC16** dye showed red shifted absorption with high molar extinction coefficient due to the electron rich butoxy group which resulted in strong donor-acceptor interactions and exhibited an efficiency of 8.95% than **CPDT** dye which a moderate efficiency 5.80%. They incorporated the hexyloxy groups on donor of the **DTP** dye [34] to obtain **C241** dye [35] and it showed red shifted (22 nm) absorption. The dye **C241** achieved higher efficiency of 7.50% than **DTP** which showed efficiency of 6.10% attributable to higher J_{SC} (12.53 mA cm^{-2}) for the dye **C241**.

Grätzel and co-workers [36] designed and synthesized octyloxy substituted pyrido[3,4-*b*]pyrazine-based dyes and effectively used for DSSC. They showed red shifted absorption and its HOMO was raised due to the presence of octyloxy group. Methoxyphenyl-substituted pyrido[3,4-*b*]pyrazine unit improved the J_{SC} and V_{OC} and the use of phenyl π-spacers rather than thiophene or furan moieties results mainly in an increased V_{OC}. The electron lifetime and charge recombination resistance of these dyes are increased due to the introduction of octyloxy chains on the donor unit, resulting in the high photo voltage (691 mV). Highest power conversion efficiency (PCE) of 7.12% was achieved for **APP-IV** dye.

Wu and co-workers [37] incorporated hexyloxy unit on periphery of the dithienosilole based dyes and found that 2,4-dihexyloxy phenyl unit is beneficial for the suppression of the electronic coupling and charge recombination which resulted in high V_{OC} when compared to the parent dye. The dye **TP6CADTS** achieved higher efficiency of 7.60% than the parent dye **TPCADTS** which showed efficiency of 6.65%. Sun and co-workers [38] synthesized a series of phenothiazine based cationic dyes (**CM306** and **CM307**) by using butoxy and 2,4-dibutoxyphenyl units as auxiliary donor. These chromophores shift the HOMO and LUMO negetively, broaden the IPCE spectra and lower electron recombination of electrons which yielded high J_{SC}, V_{OC} and efficiecny of the devices. The dye **CM306** achieved higher

efficiency of 7.10% than **CM305** with efficiency of 6.90% attributable to the benfit of 2,4-dihexyloxy phenyl unit in **CM306** dye.

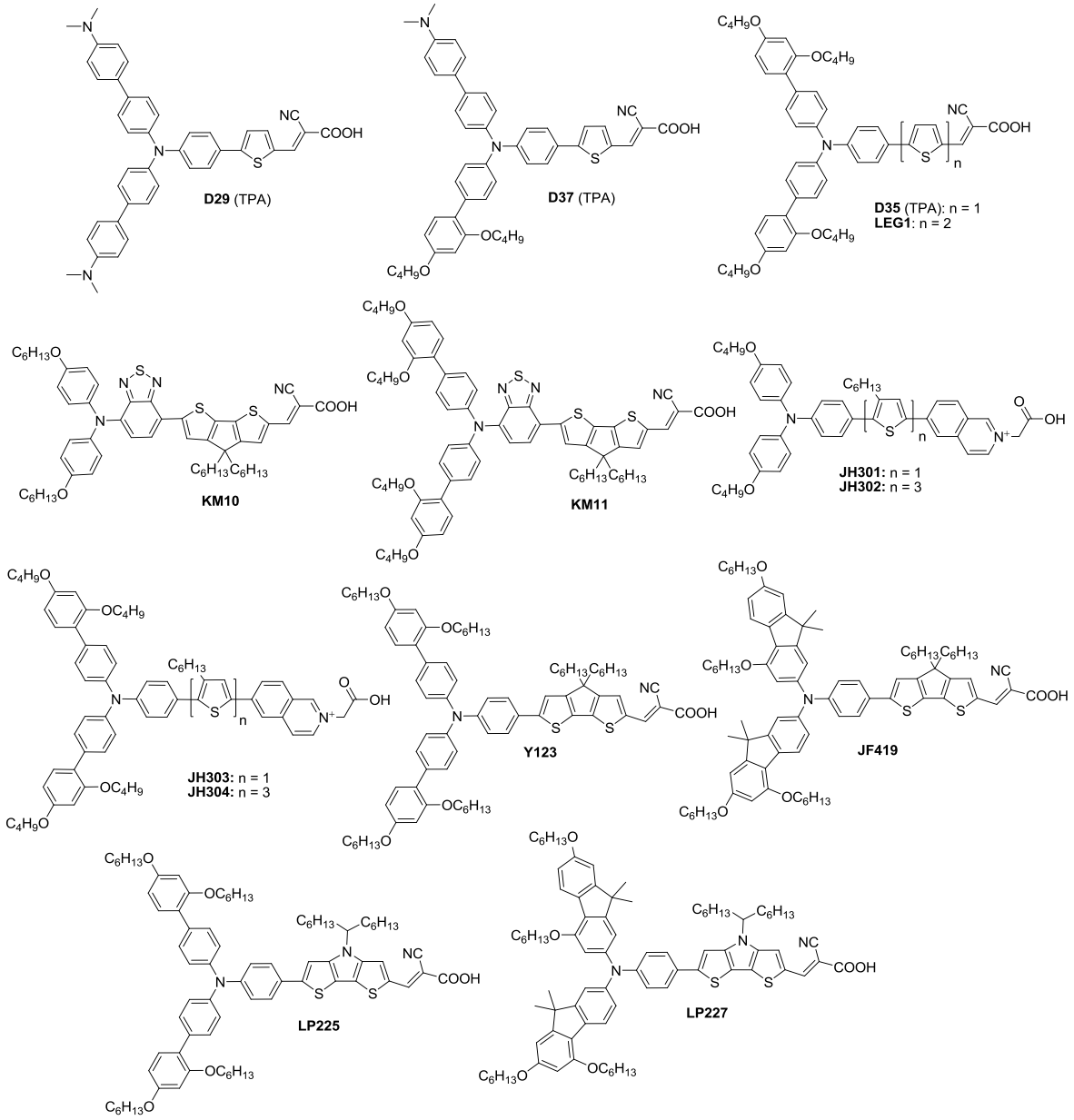

Chart 5.4 Structures of the organic dyes containing alkoxy units on donor unit.

Sun and co-workers [6] investigated the effect of symmetrical and asymmetrical auxiliary donor such as 2,4-dimethoxyphenyl and *N*,*N*-dimethylaniline based triphenylamine dyes (**D29**, **D35** and **D37** shown in Chart 5.4). They found that incorporation of 2,4-dibutoxyphenyl unit on the periphery of triphenylamine donor decreases the electron recombination with the redox species in the electrolyte and led to huge increment in V_{OC}. Among the dyes, **D35** exhibited higher efficiency of 6.00% with J_{SC} of 12.96 mA cm^{-2}, V_{OC} of 750 mV and *ff* of 0.61 attributable to the structural benefit of 2,4-dimethoxyphenyl unit.

They extended the conjugation of **D35** by thiophene to form a dye **LEG1** [12] which showed red shifted absorption and achieved efficiency of 4.26% with J_{SC} of 7.77 mA cm^{-2} and V_{OC} of 870 mV. Grätzel and co-workers [39] synthesized two dyes **KM-10** and **KM-11** (Chart 5.4) which contain butoxy and 2,4-dibutoxyphenyl on peripheral position of the donor. They showed longer wavelength absorption at 600 nm due to strong donor-acceptor interactions and exhibited efficiency of 7.10% for **KM-10** and 8.00% for **KM-11**. The higher efficiency of **KM-11** is due to the larger V_{OC} is originating due to the presence of bulky 2,4-dibutoxyphenyl unit which reduces the intermolecular interactions and aggregation.

Sun and co-workers [40] designed and synthesized a set of dyes (**JH-301**-**JH-304**) containing alkoxy substituted donor based on iso-quinoline cation. These dyes containing butoxy and 2,4-dibutoxyphenyl auxiliary chromophores displayed high efficiency and 2,4-dibutoxyphenyl containing dyes showed high V_{OC} due to minimization of intermolecular interactions. The dye **JH-304** exhibited higher efficiency of 7.30% with J_{SC} of 14.40 mA cm^{-2} and V_{OC} of 684 mV. Frey and co-workers reported a set of dyes (**LP225**, **LP227**, **Y123** and **JF419**) by the use of alkoxy-substituted fluorene-based amine donors and achieved good efficiency in the DSSC [41]. However the dithienopyrrole dyes showed better performance due to red shifted absorption and **LP227** ranked top with power conversion efficiency of 10.3% arising from J_{SC} of 16.20 mA cm^{-2} and V_{OC} of 840 mV. However, alkoxy-containing dyes showed poor dye-regeneration capacity due to the reduced thermodynamic driving force for the dye-regeneration by the redox shuttle caused by the high-lying HOMO of the dye.

Table 5.1 Optical, electrochemical and photovoltaic performance parameters of dyes

Dye	$\lambda_{max,}$ nm (ε_{max}, M^{-1} cm^{-1})	E_{ox}, V (*vs* NHE)	E_{ox}^{*}, V (*vs* NHE)	J_{SC} (mA cm^{-2})	V_{OC} (mV)	*ff*	η (%)	*Ref*
AD1	470 (35564)	0.85	−1.27	10.60	579	0.58	3.54	[18]
AD2	491 (28702)	0.88	−1.08	12.70	598	0.61	4.63	[18]
AD3	477 (20170)	0.97	−1.04	5.06	561	0.59	1.67	[18]
AD34	480 (25000)	1.68	−0.49	13.80	630	0.69	6.02	[3]
AC25	487 (8850)	1.29	−0.87	13.60	615	0.69	5.77	[3]
AC27	508 (33300)	0.91	−1.26	8.02	543	0.64	2.79	[3]
AC26	522 (19800)	0.68	−1.23	9.05	567	0.56	2.87	[3]
AD39	458 (25225)	1.65	−0.60	7.53	720	0.69	3.70	[20]

Table 5.1 (cont.)

Dye	$\lambda_{max,}$ nm (ε_{max}, M^{-1} cm^{-1})	E_{ox} , V (*vs* NHE)	E_{ox}^{*}, V (*vs* NHE)	J_{SC} (mA cm^{-2})	V_{OC} (mV)	*ff*	η (%)	*Ref*
AD40	455 (29322)	1.60	−0.61	9.02	710	0.68	4.34	[20]
AD41	464 (33926)	1.55	−0.58	9.98	700	0.67	4.62	[20]
L1	442 (13700)	1.16	−1.11	8.73	761	0.68	4.50	[21]
CQ2	458 (19800)	0.76	−1.36	8.91	753	0.66	4.44	[21]
CQ3	479 (21800)	0.74	−1.32	4.26	739	0.66	2.08	[21]
JK-313	460 (20600)	1.26	−1.01	13.66	719	0.76	7.51	[22]
JK-314	482 (40300)	1.10	−1.12	15.56	725	0.76	8.61	[22]
TPA-B1	421 (48000)	1.27	−0.81	5.12	659	0.72	2.43	[23]
TPA-B2	410 (74900)	1.32	−0.70	6.12	679	0.64	2.65	[23]
CD-4	405 (28979)	1.08	−1.47	8.60	630	0.75	4.11	[16]
CD-6	411 (24873)	1.15	−1.31	5.33	510	0.55	1.51	[16]
TPA-B5	405 (28600)	1.34	−0.77	7.13	646	0.68	3.13	[17]
TPA-B6	397 (6400)	1.36	−0.78	3.04	603	0.66	1.21	[17]
TZ1	438 (40000)	1.28	−1.89	7.00	712	0.67	2.55	[24]
TTC101	368 (31100)	1.19	−1.18	7.02	701	0.60	2.99	[25]
TTC102	425 (27100)	1.17	−1.02	11.61	766	0.58	5.21	[25]
TTC103	440 (28400)	1.20	−1.04	11.71	709	0.59	4.92	[25]
L32	379 (50800)	1.22	−1.14	14.12	774	0.58	6.37	[26]
C47	425 (27100)	1.22	−1.19	12.00	776	0.56	5.24	[26]
L33	372 (30000)	1.21	−1.57	4.20	674	0.67	1.88	[26]
FL 1	469 (34900)	1.17	−0.97	10.56	690	0.65	4.70	[13]
FL 2	487 (40500)	1.08	−1.00	7.52	618	0.65	3.01	[13]
FL6	464 (35500)	1.19	−1.00	14.10	642	0.66	5.98	[13]
FL7	470 (38800)	1.14	−0.99	14.80	650	0.64	6.13	[13]
FL8	439 (51500)	1.17	−0.97	13.70	650	0.65	5.82	[13]
FL9	437 (60300)	1.15	−1.02	13.20	640	0.64	5.38	[13]
FL10	460 (34700)	1.35	−0.87	10.30	586	0.67	4.01	[13]
L1	404 (25000)	1.21	−1.43	5.42	735	0.69	2.75	[28]
1P-PSS	473 (43500)	1.26	−0.94	16.00	630	0.61	6.15	[30]
CA-II	477 (23600)	0.74	−1.23	11.34	804	0.70	6.39	[27]

Table 5.1 (cont.)

Dye	$\lambda_{max,}$ nm (ε_{max}, M^{-1} cm^{-1})	E_{ox} , V (*vs* NHE)	E_{ox}^{*}, V (*vs* NHE)	J_{SC} (mA cm^{-2})	V_{OC} (mV)	*ff*	η (%)	*Ref*
D21L6	486 (27700)	0.97	−1.30	13.50	670	0.72	6.67	[29]
S1	510 (33000)	0.93	−1.15	16.80	630	0.63	6.65	[31]
S2	506 (46000)	1.08	−1.04	16.53	570	0.58	5.49	[31]
S3	484 (84000)	1.13	−1.11	16.77	565	0.53	5.34	[31]
CPDT	491(36000)	0.91	−1.34	14.40	601	0.67	5.80	[33]
AC16	555 (62700)	na	na	11.14	799	0.71	6.28	[32]
DTP	479 (48080)	0.70	−1.33	10.60	762	0.75	6.10	[34]
C241	511 (65000)	na	na	12.53	820	0.73	7.50	[35]
APP-I	497 (16800)	1.12	−0.95	12.11	671	0.76	6.14	[36]
APP-II	506 (11500)	1.11	−0.97	8.37	631	0.73	3.93	[36]
APP-III	461 (13500)	1.13	−1.12	8.20	694	0.76	4.35	[36]
APP-IV	524 (23300)	0.85	−1.10	13.56	691	0.76	7.12	[36]
TPCADTS	495 (44500)	1.07	−0.89	12.70	760	0.69	6.65	[37]
TP6CADTS	511(36900)	0.88	−0.99	13.39	810	0.70	7.60	[37]
CM305	506 (24100)	0.82	−1.19	13.10	702	0.75	6.90	[38]
CM306	520 (24000)	0.76	−1.24	13.60	710	0.74	7.10	[38]
D29 (TPA)	482 (70200)	0.84	−1.47	12.00	670	0.60	4.83	[6]
D35 (TPA)	445 (70100)	1.04	−1.37	12.96	750	0.61	6.00	[6]
D37 (TPA)	459 (37200)	0.81	−1.60	12.50	710	0.59	5.24	[6]
LEG1	515 (33000)	0.93	−1.17	7.77	870	0.63	4.26	[12]
KM-10	600 (20706)	1.00	−0.90	14.50	653	0.74	7.10	[39]
KM-11	598 (21200)	1.07	−0.83	16.00	678	0.73	8.00	[39]
JH301	479 (29830)	0.66	−1.59	12.50	670	0.73	6.10	[40]
JH302	493 (18657)	0.62	−1.41	14.30	671	0.72	7.00	[40]
JH303	474 (26951)	0.77	−1.51	12.80	680	0.74	6.50	[40]
JH304	485 (14445)	0.80	−1.27	14.40	684	0.74	7.30	[40]
Y123	526 (57700)	0.99	−1.23	13.40	901	0.74	8.86	[41]
JF419	541 (52600)	0.84	−1.31	14.10	811	0.77	8.72	[41]
LP225	542 (50500)	1.01	−1.16	14.10	876	0.78	9.77	[41]
LP227	548 (47500)	0.85	−1.25	16.20	840	0.76	10.30	[41]

na = not available

By keeping all these points, we have synthesized a set of carbazole based dyes (shown in Chart 5.5) linking at 2 and 7 positions, incorporating butoxy/2,4-dimethoxyphenyl units on the periphery of the donor unit. These groups are used to minimize intermolecular interactions and aggregation at the surface of TiO_2. The strong donating ability and extension of conjugation with donor led to longer wavelength absorption which helps to improve the photovoltaic parameters. As we expected, the absorption spectra of dyes anchored on TiO_2 match with absorption spectra of the dyes in solution which indicated absence of significant dye aggregation at TiO_2 surface.

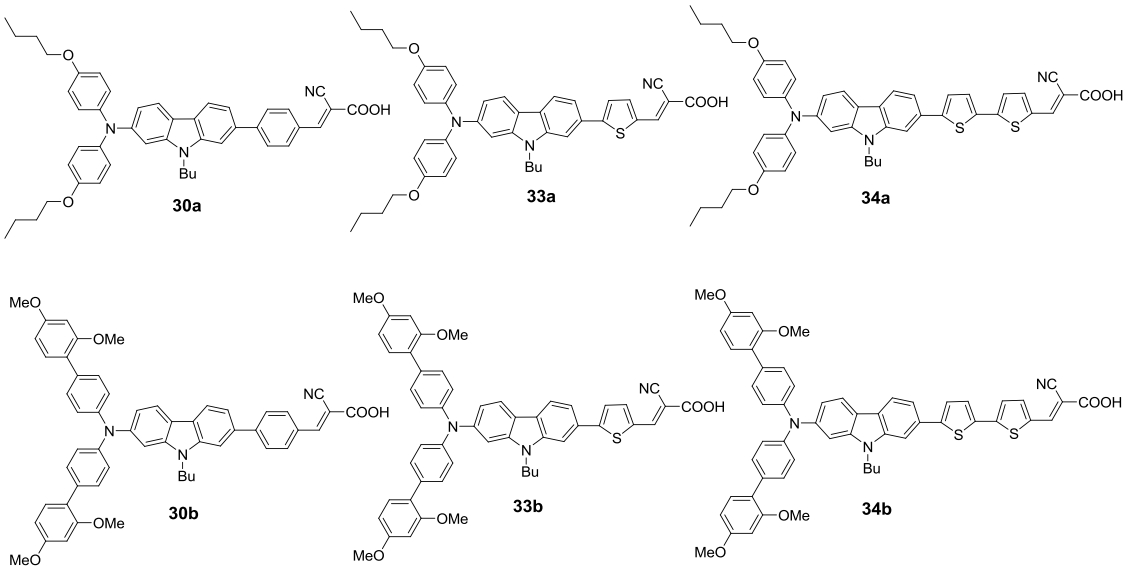

Chart 5.5 Structures of the alkoxy donor containing carbazole based dyes.

5.2 Results and Discussions

5.2.1 Synthesis and Characterization

The syntheses of the dyes were accomplished as shown in Scheme 5.1. The pathways for the dyes involved palladium-catalyzed protocols such as Hartwig-Buchwald C-N coupling [42], Suzuki [43] and Stille [44] C-C coupling, and copper catalyzed C-O coupling [45] reactions. In the first step, the butoxy or 2,4-dimethoxyphenyl functionalized diphenylamine (**2**) was prepared by either copper-catalyzed C-O coupling [45] with butanol or palladium catalyzed C-C coupling [43] with 2,4-dimethoxyphenylboronic acid [46]. Further, the secondary amines, **27a** and **27b** were converted to the triarylamines **28a** and **28b** by treatment with 2,7-dibromo-9-butyl-9*H*-carbazole (**1**) [47, 48] under the Hartwig-Buchwald C-N coupling conditions [42]. Suzuki coupling of **28a** and **28b** with 4-formylphenylboronic acid gave carbazole aldehyde derivatives (**29a** and **29b**). Then the Stille coupling reaction [44] of **28a**

and **28b** with the appropriate tin reagents derived from thiophene or bithiophene aldehydes followed by acidic hydrolysis generated the required aldehydes, **31a, 31b, 32a** and **32b**. Finally, the target dyes **30**, **33,** and **34** were synthesized by Knoevenagel condensation [49] of the aldehydes **29, 31,** and **32** with cyanoacetic acid in the presence of ammonium acetate.

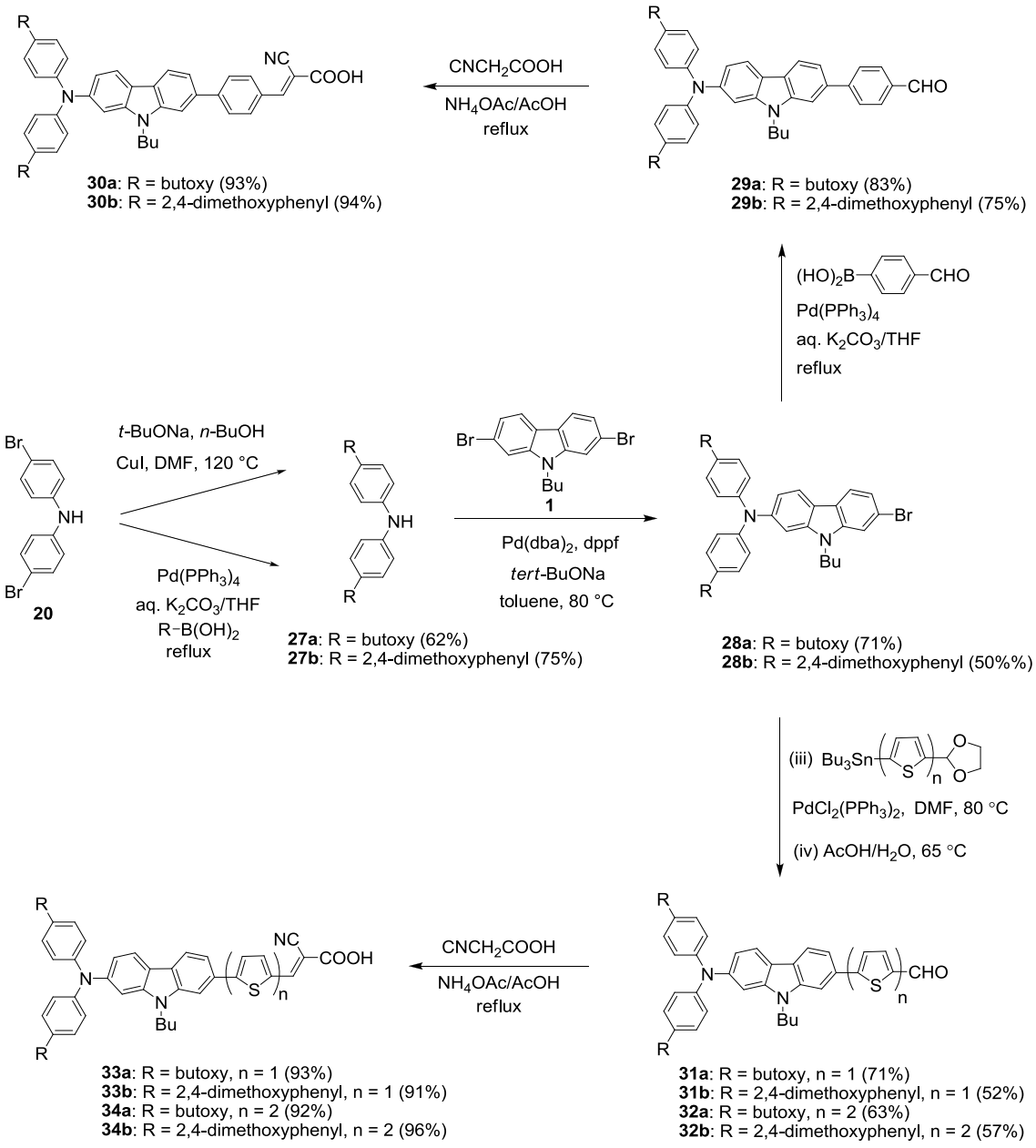

Scheme 5.1 Synthetic scheme to prepare target dyes.

All the new compounds were thoroughly characterized by IR, NMR (^{1}H and ^{13}C) and mass spectral measurements. The proposed structures are consistent with the spectral data. The dyes are generally dark red in color and dissolved completely in common organic solvents such as dichloromethane, tetrahydrofuran, dimethyl sulfoxide, dimethylformamide etc.

5.2.2 Photophysical Properties

The UV-visible absorption spectra of the dyes (**30**, **33** and **34**) were recorded in dichloromethane and the precursor bromo and aldehyde derivatives also measured comparison and for better understanding about the origin and nature of the absorption peaks. The absorption spectra of the dyes recorded in dichloromethane is displayed in Figure 5.1 and the pertinent data collected in Table 5.2.

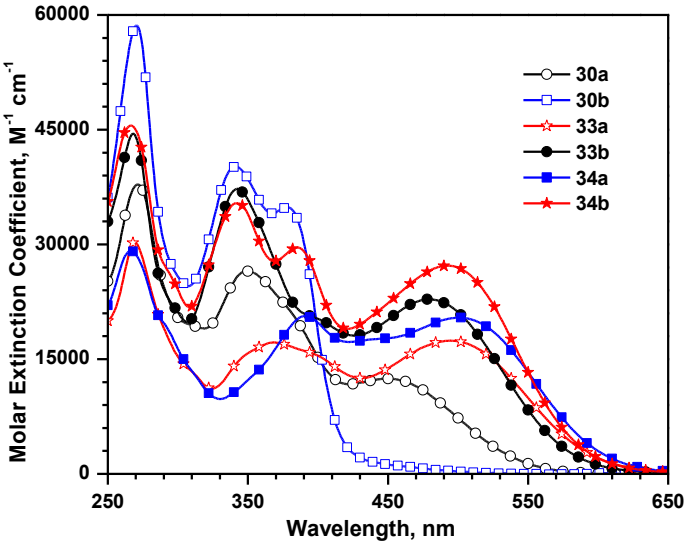

Figure 5.1 Absorption spectra of the dyes (**30, 33** and **34**) recorded in dichloromethane.

All the dyes showed three peaks. The lower energy absorption peak arises due to intramolecular charge transfer (ICT) transition from arylamine donor unit to the cyanoacryllic acid acceptor unit. The higher energy peaks probably originate from localized π-π* transitions of arylamine or entire conjugation pathway of the molecule. The absorption maxima of the dyes (**33a** and **34a**) which contain butoxy diphenylamine showed a red shift around 15 nm when compared to the 2,4-dimethoxyphenyl diphenylamine containing dyes (**33b** and **34b**). The alkoxy unit directly attached to amine donor has more impact on donating strength of donor when compared to alkoxyphenyl attached to amine donor [40]. This clearly indicates that the strong donating strength for butoxy diphenylamine unit than 2,4-dimethoxy phenyl diphenylamine [40]. The oligothiophene containing dyes (**33** and **34**) showed red shifted absorption maxima than phenyl containing dyes (**30**) due to the electron richness of former oligothiophene unit which facilitate the donor-acceptor interactions while phenyl linker caused twisted geometry which led to poor donor-acceptor interactions [30, 50]. Within the same class of oligothiophenes, bithiophene containing dyes showed red shifted

absorption than the mono thiophene containing dyes owing to the elongated conjugation and electron richness of additional thiophene unit.

Table 5.2 Optical data of the dyes recorded in dichloromethane and after the addition of TFA, TEA

Dye	$\lambda_{abs,}$ nm ($\varepsilon_{max} \times 10^3$ $M^{-1}cm^{-1}$)		
	DCM	DCM + TFA	DCM + TEA
30a	455 (12.4), 349 (26.5), 272 (37.8)	463 (13.4), 357 (29.6), 271 (41.0)	389 (27.0), 307 (28.9)
30b	379 (34.8), 342 (40.2), 271 (58.6)	379 (35.0), 340 (41.7), 271 (60.5)	377 (36.1), 340 (40.6)
33a	495 (17.4), 369 (17.2), 269 (30.3)	705 (1.0), 511 (19.3), 373 (19.4), 270 (34.6)	442 (23.4), 348 (16.7)
33b	480 (22.9), 343 (37.2), 268 (44.5)	488 (25.8), 342 (40.7), 268 (50.7)	430 (34.6), 341 (41.1)
34a	500 (20.5), 390 (20.6), 266 (29.2)	700 (1.6), 510 (23.8), 391 (23.0), 267 (33.4)	447 (28.1)
34b	493 (27.2), 385 (29.6), 343 (35.4), 266 (45.5)	503 (31.6), 386 (32.4), 341 (38.7), 267 (51.2)	443 (33.4), 343 (35.6)

It is interesting to compare the optical properties of the carbazole based dyes (**33a** and **34a**) with the reported phenyl linked dyes (**CA-II** [27] and **D21L6** [29]) which contain similar alkoxy substituted donor. The dyes (**33a** and **34a**) showed red shifted absorption spectra when compared to **CA-II** and **D21L6**. It is observed that the optical properties are benefited for these new carbazole containing dyes in terms of absorption maxima. The dyes **33** and **34** showed red shifted absorption when compared to the parent carbazole dyes **7a** and **7b** (Chapter 3). This clearly indicates that the introduction of alkoxy unit on donor unit causes strong donor-acceptor interactions which led to longer absorption wavelength. Compared to triphenylamine dye **D35** (TPA) which contain 2,4-dibutoxyphenyl diphenylamine, the absorption spectra of carbazole dye **33a** is red shifted due to the incorporation of carbazole unit [6]. The dyes show promisingly high molar extinction coefficients (22900 M^{-1} cm^{-1} to 27200 M^{-1} cm^{-1}) than Ru metal dye **N3** (16000 M^{-1} cm^{-1}) which is necessary factor for light harvesting property of the organic sensitizers [51]. All these observations can be rationalized as the incorporation of alkoxy groups containing amine

donor in carbazole dyes displayed good light harvesting properties which are suitable for the photovoltaic properties.

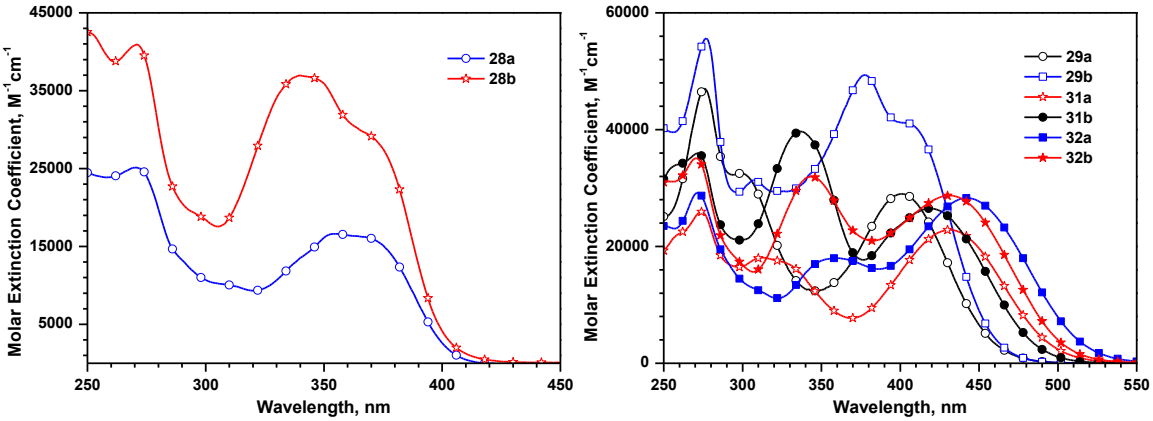

Figure 5.2 Absorption spectra of the bromo (a) and aldehyde (b) analogues recorded in dichloromethane.

Table 5.3 Optical data of the bromo and aldehyde analogues recorded in dichloromethane

compd.	$\lambda_{abs,}$ nm ($\varepsilon_{max} \times 10^3$ $M^{-1}cm^{-1}$)	$\lambda_{em,}$ nm	Stokes shift, cm^{-1}
28a	356 (16.6), 270 (25.1)	449	5818
28b	372 (28.6), 340 (36.9), 271 (50.0)	439	4102
29a	400 (29.0), 299 (32.5), 276 (47.0)	478	4079
29b	396 (35.4), 333 (44.4), 274 (55.8)	567	7616
31a	431 (22.9), 313(18.1), 274 (25.9)	515	3784
31b	419 (26.5), 337 (39.7), 271 (36.0)	572	6383
32a	443 (28.3), 360 (18.0), 272 (29.2)	557	4620
32b	431 (28.7), 343 (32.0), 271 (35.1)	513	3709

The nature of the charge transfer transition of the dyes is confirmed by the following studies. Addition of trifluoroacetic acid (TFA) to dichloromethane solution of the dyes shows a bathochromic shift to the charge transfer absorption. But, addition of triethylamine (TEA) leads to a pronounced blue shift for this peak and it is displayed in Figure 5.3. Such observations have been earlier ascribed to the increment/decrement in acceptor strength on addition of TFA/TEA caused by protonation/deprotonation [52, 53]. Also, the dyes exhibited longer wavelength absorption when compared to the corresponding bromo- and aldehyde derivatives (shown in Figure 5.2). The absorption wavelength assumes the order in

accordance with the electron-withdrawing effect of the end group (Br < CHO < cyanoacrylic acid).

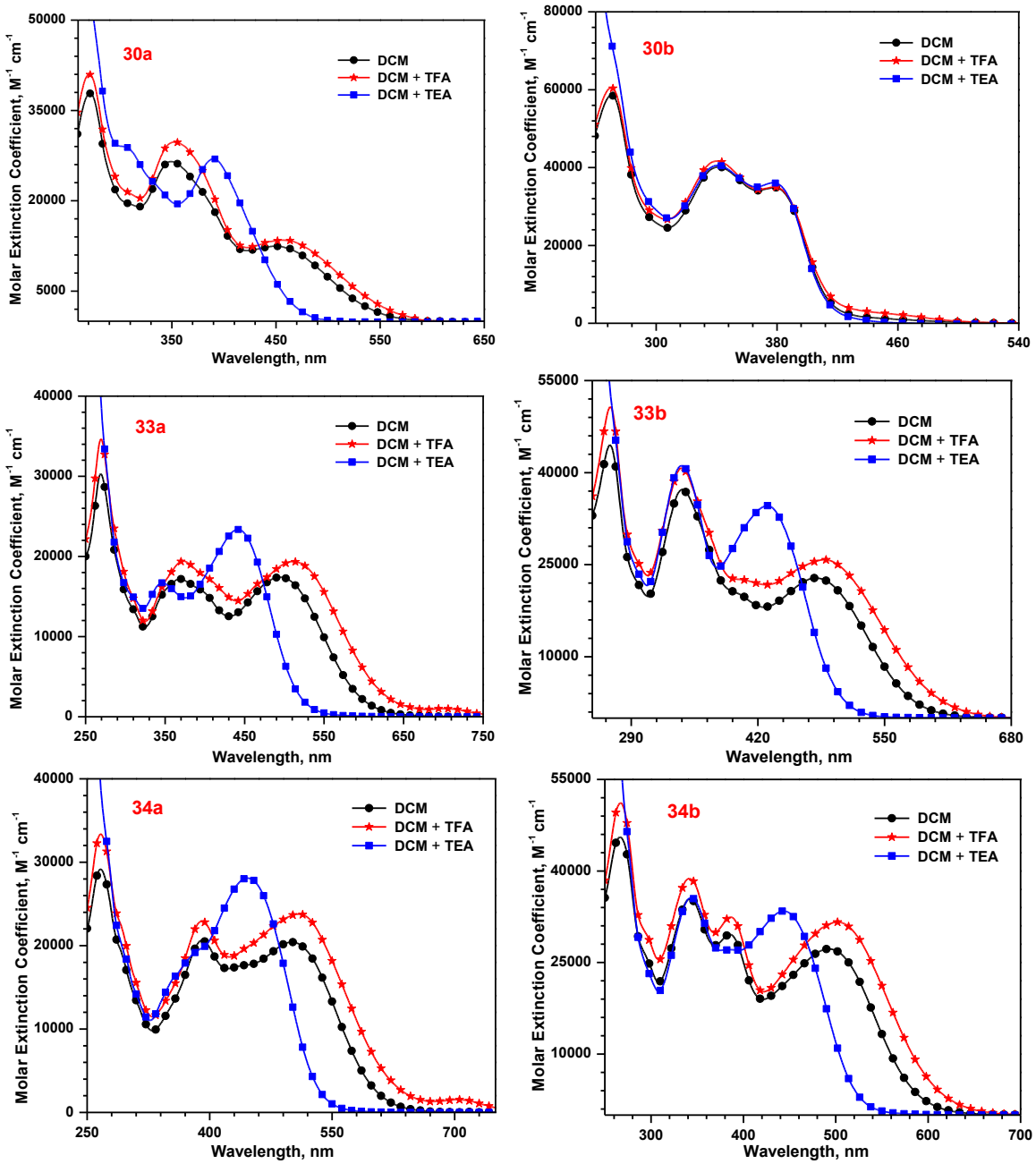

Figure 5.3 Absorption spectra of the dyes (**30a**, **30b**, **33a**, **33b**, **34a** and **34b**) recorded in dichloromethane and after the addition of TFA, TEA.

All the dyes displayed a negative solvatochromism in the absorption spectra as showed in Figures 5.4 and 5.5. The blue-shift observed on increasing the polarity of the solvent is attributed to the effective solvation of the dyes by the polar solvents [54, 55]. However, a drastic blue shift witnessed for all dyes in DMF is probably due to the basic nature of the solvent which leads to the deprotonation of the dyes [56]. Also the dyes showed blue shifted

absorption in THF owing to its tendency for forming hydrogen bond with carboxylic acid and it might deprotonate the carboxylic acid resulting carboxylate ion which results in poor donor-acceptor interactions and causes blue shifted absorption [56]. Similarly, the significant red-shift observed in chloro-solvents such as dichloromethane and chloroform arises due to the rapid relaxation of polarizable electrons in the excited state [57, 58].

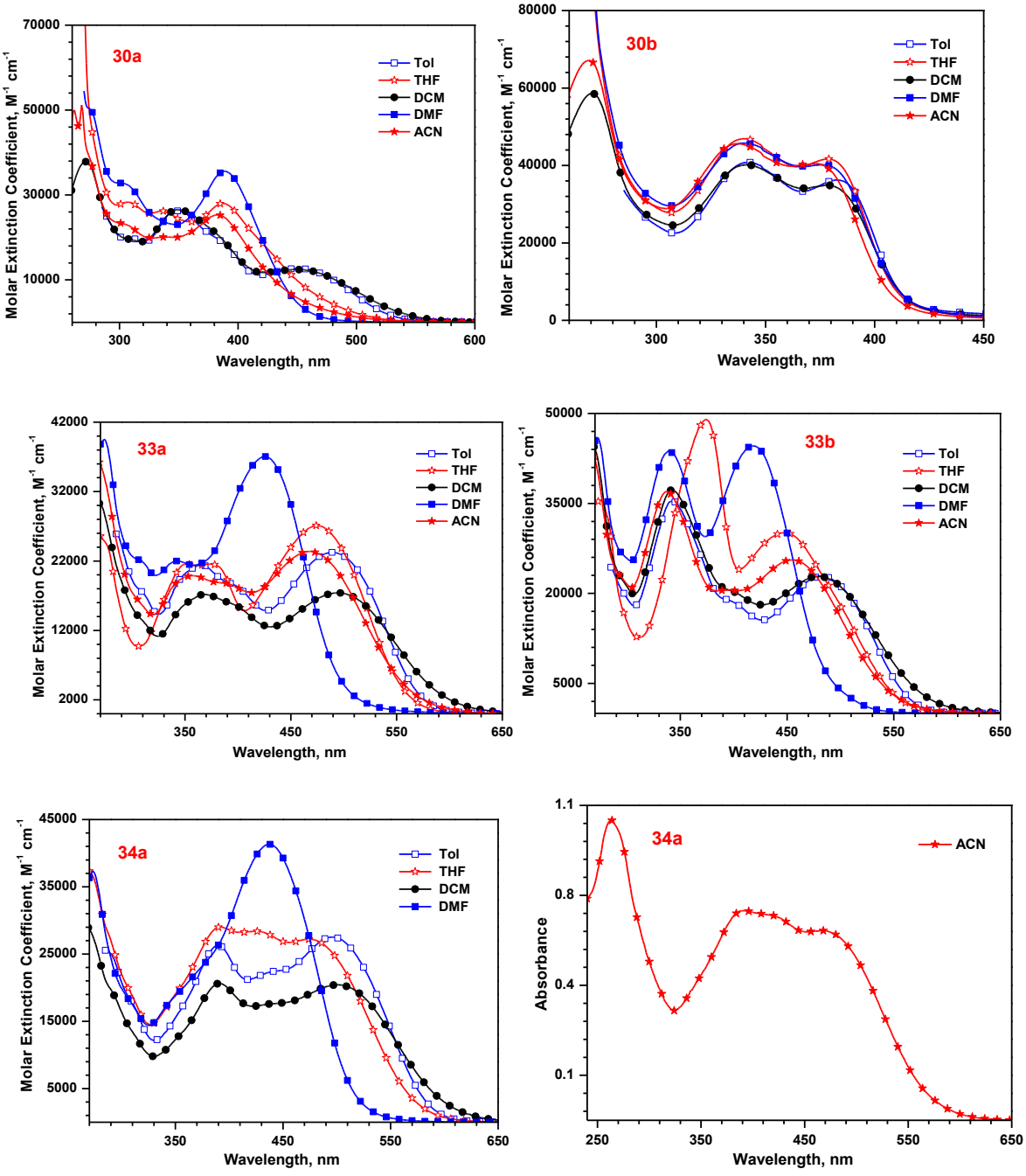

Figure 5.4 Absorption spectra of the dyes recorded in different solvents.

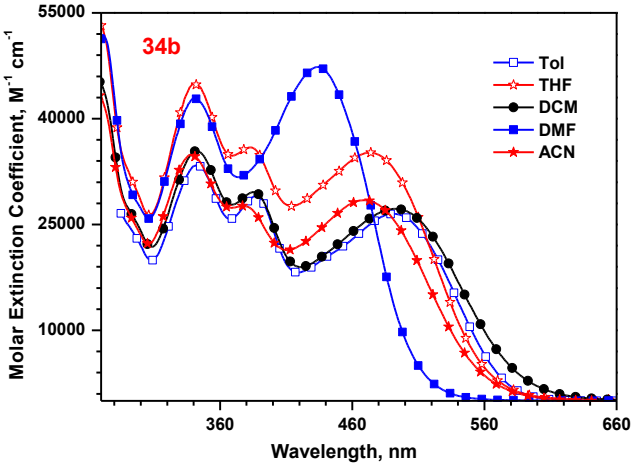

Figure 5.5 Absorption spectra of the dye (**34b**) recorded in different solvents.

Table 5.4 Optical properties of the dyes recorded in different solvents

Dye	$\lambda_{abs,}$ nm ($\varepsilon_{max} \times 10^3$ $M^{-1}cm^{-1}$)				
	TiO_2 film	Tol	THF	DMF	ACN
30a	na	451 (12.7), 348 (26.4)	388 (28.0), 336 (26.2)	389 (35.6), 307 (32,3)	383 (25.3)
30b	na	375 (55.3)	378 (69.3)	381 (73.9)	375 (59.7)
33a	496	489 (23.3), 365 (21.5)	475 (27.1), 375 (21.5), 352 (21.5)	426 (37.0), 343 (22.0), 308 (22.1), 274 (39.5)	468 (23.4), 357 (19.9), 266 (36.8)
33b	487	482 (22.8), 375 (53.9)	447 (30.1), 374 (49.0),	418 (44.5), 342 (43.4), 272 (46.0)	455 (25.6), 373 (55.7), 340 (36.9)
34a	498	496 (27.5), 390 (26.3)	475 (27.2), 426 (28.4), 391 (29.0)	438 (41.3)	470, 390, 263
34b	516	493 (27.2), 385 (29.6), 343 (35.4)	473 (35.2), 383 (35.9), 340 (45.0)	434 (47.3), 340 (42.9)	471 (28.4), 378 (27.6), 340 (34.9)

na = not measured

The solvatochromism data of the dyes are analyzed by correlating with $E_T(30)$ parameter [59] and plots are displayed in Figure 5.6. The dyes exhibited deviation for polar solvents such as dichloromethane and acetonitrile due to the effective solvation which led to unusual red-shift for these dyes. Similar behavior has been earlier observed for organic dyes and attributed to the instant stabilization due to a fast rearrangement of polarizable electrons during excitation [57, 58].

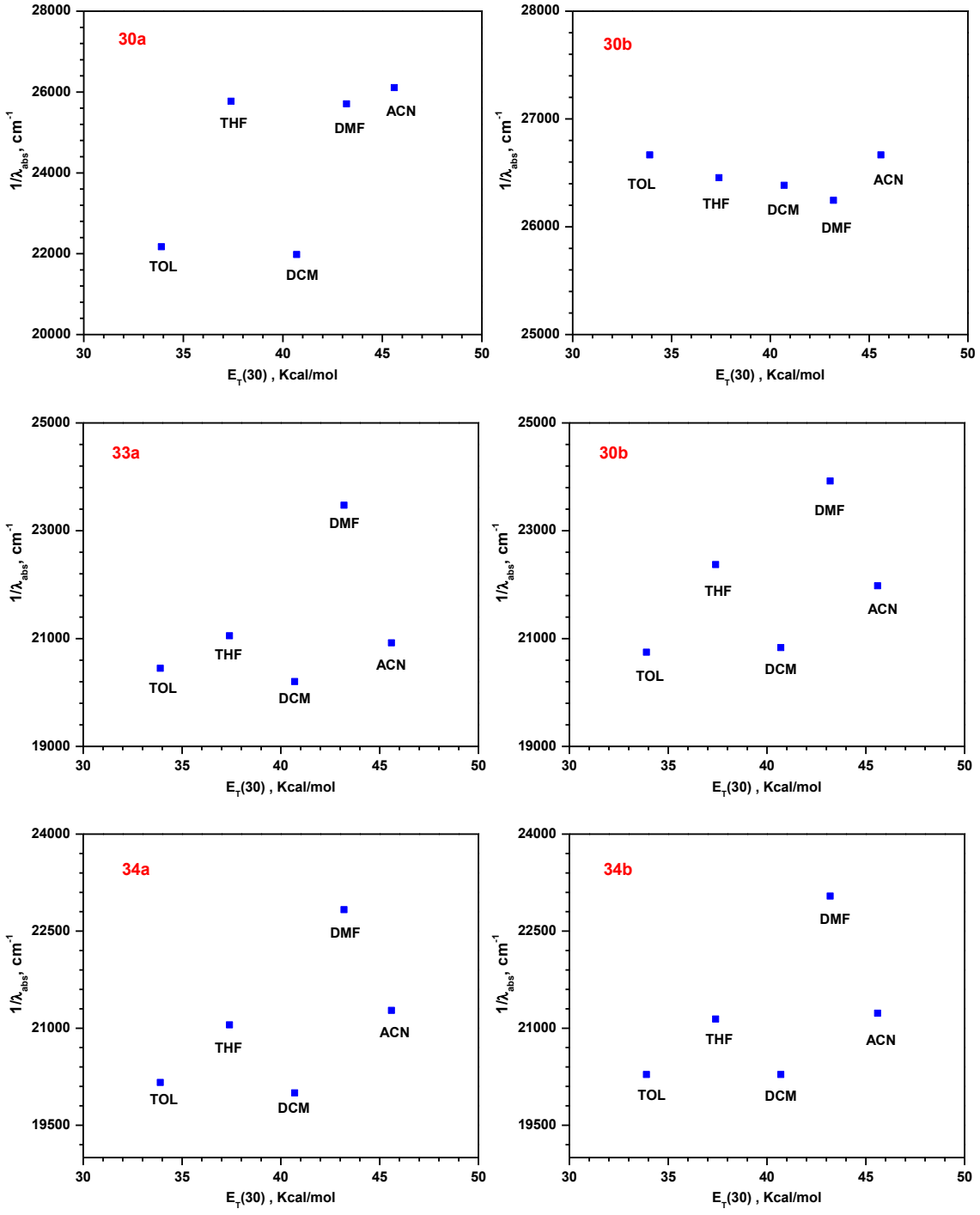

Figure 5.6 Variation of absorption (in cm^{-1}) with the solvents polarity parameter $E_T(30)$.

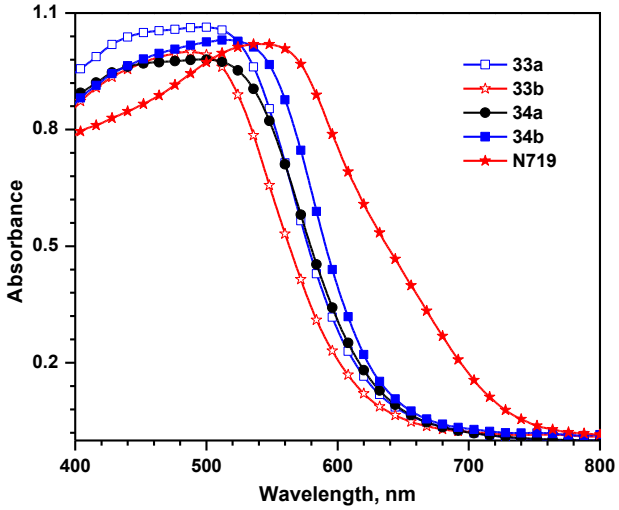

Figure 5.7 Absorption spectra of the dyes anchored on TiO_2 films.

Absorption spectra recorded for the dyes adsorbed on TiO_2 films are displayed in Figure 5.7. The dyes showed similar absorption maxima compared to the absorption spectra measured in solution except for the dye **34b** which showed red shifted abosrption spectra probably arising due to the stacking of the dye on TiO_2 surface which causes *J*-aggregates [60]. While the parent carbazole dyes (**7a** and **7b**) showed aggregation on TiO_2 film, the lack of aggregation for the present dyes indicates the beneficial role of peripheral alkoxy units in reducing the stacking interactions. However, the dye **34b** showed aggregation may be due to the planar configuration of the bithiophene unit.

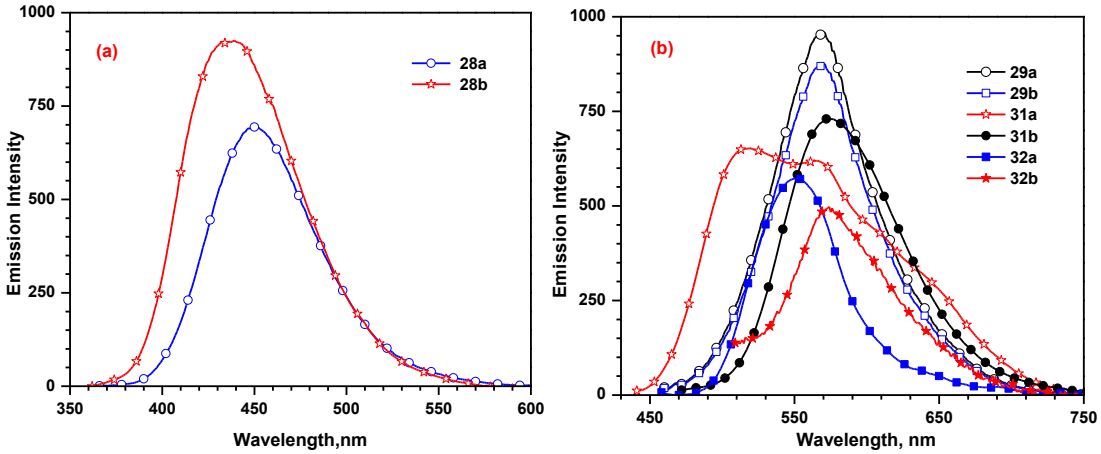

Figure 5.8 Emission spectra of the bromo (a) aldehyde (b) derivatives recorded in dichloromethane.

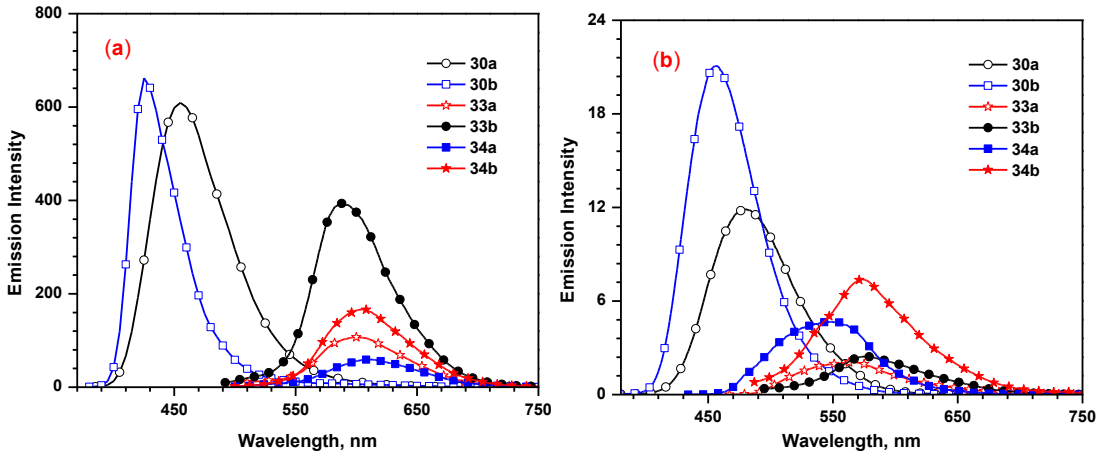

Figure 5.9 Emission spectra of the dyes (**30a, 30b, 33a**, **33b, 34a** and **34b**) recorded in (a) toluene and (b) dichloromethane.

All the dyes displayed moderate emission in toluene ranging from blue to yellow and the photoluminescence spectra is displayed in Figure 5.9 (a). For comparison, photoluminescence of bromo and aldehyde analogues (Figure 5.8) of the corresponding dyes were recorded in dichloromethane and they intensively emitted in blue to yellow region. In contrast, the dyes are weakly emitting in dichloromethane (Figure 5.9) and the emission intensity is quenched and they showed blue shift emission also. This indicated the excited state is more polar with noticeable dipole which might interact with solvent dipole and relax the excited state of the dye by electron transfer mechanism [61, 62]. The emission of dyes is red shifted with weak emission than the corresponding aldehydes also confirm the charge transfer peak corresponds to longer wavelength absorption maxima of the dyes.

5.2.3 Theoretical Calculations

To gain more insight into the geometry and nature of electronic transitions of the dyes we have performed the density functional theory calculations using Gaussian 09 program [63]. The geometry of the dyes was optimized with tight SCF convergence without any symmetry constraints. Frontier molecular orbitals of the dyes are displayed in Figure 5.10. The vertical electronic excitation energies computed by B3LYP [64] and MPW1K [65] and frontier molecular orbitals listed in Tables 5.5 and 5.6.

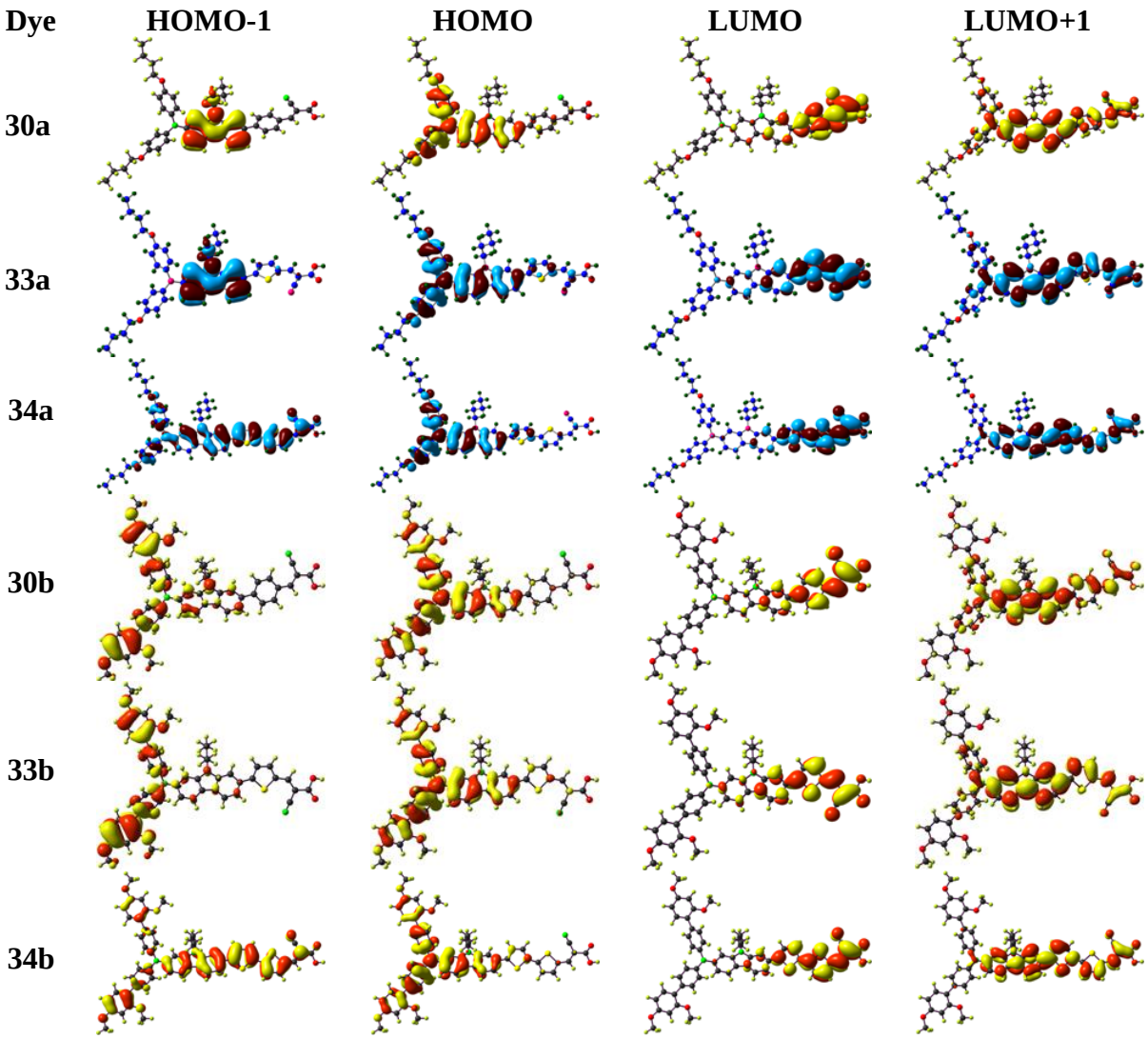

Figure 5.10 Frontier molecular orbitals of the dyes.

The HOMO of the dyes is mainly localized on bulky arylamine donor and carbazole which confirms the auxochrome 2,4-dimethoxy phenyl unit participating in HOMO. LUMO of the dyes is mainly localized on the cyanoacrylic acid, phenyl/thiophene linkers and little contribution from carbazole. This clearly indicates enough charge separation from HOMO to LUMO. Thus electronic excitation from HOMO to LUMO occurring at the low energy electromagnetic radiation for the dyes **30b** and **33b** ensures better electron injection upon photo excitation. The HOMO-1 is mainly located on 2,4-dimethoxyphenyl unit and it establishes the auxiliary donation nature. Moreover, the HOMO-1 to LUMO electronic transition also helps to harvest photons. However, the incorporation of bithiophene in conjugation pathway shifts the HOMO-1 towards the conjugation pathway. So, it is reasonable to conclude that the electron richness of the 2,4-dimethoxyphenyl unit lies in between the thiophene and bithiophene units. The shorter wavelength absorption is assigned for π-π* transitions. The predicted dipole moment for **33** higher than the **34** indicates that the

dye containing butoxy unit caused more donor-acceptor interactions than compared to 2,4-dimethoxyphenyl unit.

Table 5.5 Computed vertical transition energies and their oscillator strengths, assignments, dipole moments and band gaps for the dyes using B3LYP theory

Dye	λ (nm)	*f*	assignments	μ_g (D)	HOMO (eV)	LUMO (eV)	$E_{0\text{-}0}$ (eV)
30a (vacuum)	625.3	0.34	HOMO → LUMO (100%)	9.45	-4.65	-2.44	2.20
	402.7	0.79	HOMO-2 → LUMO (94%)				
	370.8	0.34	HOMO → LUMO+1 (89%)				
	318.6	0.36	HOMO-4 → LUMO (88%)				
	306.3	0.23	HOMO → LUMO+4 (91%)				
30a (THF)	662.9	0.39	HOMO → LUMO (100%)	10.64	-4.71	-2.61	2.10
	418.6	0.82	HOMO-2 → LUMO (95%)				
	376.9	0.43	HOMO → LUMO+1 (92%)				
	327.7	0.34	HOMO-4 → LUMO (94%)				
30b (vacuum)	643.8	0.35	HOMO → LUMO (100%)	6.15	-4.62	-2.48	2.13
	436.2	0.49	HOMO → LUMO (91%)				
	387.9	0.72	HOMO → LUMO+1 (78%), HOMO-4→ LUMO (17%)				
	369.7	0.13	HOMO-4→ LUMO (81%), HOMO → LUMO+1(16%)				
	353.1	0.73	HOMO → LUMO+2 (98%)				
30b (THF)	652.1	0.36	HOMO → LUMO (100%)	6.93	-4.76	-2.63	2.13
	444.0	0.48	HOMO-3 → LUMO (94%)				
	387.3	0.90	HOMO →LUMO+1(100%), HOMO-4 → LUMO (28%),				
	358.1	0.85	HOMO → LUMO+2 (98%)				
33a (vacuum)	614.7	0.48	HOMO→LUMO (100%)	12.74	-4.69	-2.46	2.23
	412.9	0.95	HOMO-2→LUMO (91%)				
	372.7	0.25	HOMO→LUMO+1 (87%)				
	306.2	0.20	HOMO→LUMO+4 (75%)				
33a (THF)	670.9	0.61	HOMO→LUMO (100%)	16.18	-4.75	-2.67	2.08
	437.9	0.90	HOMO-2→LUMO (95%)				
	379.7	0.34	HOMO→LUMO+1 (89%)				
	346.6	0.13	HOMO-4→LUMO (89%)				

Table 5.5 (cont.)

Dye	λ (nm)	*f*	assignments	μ_g (D)	HOMO (eV)	LUMO (eV)	$E_{0\text{-}0}$ (eV)
33b (vacuum)	638.7	0.42	HOMO → LUMO (100%)	9.00	-4.66	-2.50	2.16
	438.7	0.58	HOMO-2 → LUMO (75%), HOMO-3 → LUMO (22%)				
	392.5	0.66	HOMO → LUMO+1 (60%), HOMO-4 → LUMO (36%)				
	352.3	0.73	HOMO → LUMO+2 (98%)				
33b (THF)	650.0	0.45	HOMO → LUMO (99%)	9.79	-4.76	-2.61	2.14
	458.7	0.56	HOMO-3 → LUMO (46%), HOMO-2 → LUMO (46%)				
	403.9	0.62	HOMO→ LUMO+1 (80%), HOMO-4 → LUMO (13%)				
	358.3	0.81	HOMO→ LUMO+2 (98%)				
34a (vacuum)	681.2	0.42	HOMO→LUMO (100%)	11.09	-4.65	-2.63	2.01
	484.5	0.26	HOMO-2→LUMO (60%), HOMO-1→LUMO (38%)				
	472.4	1.02	HOMO-1→LUMO (56%), HOMO-2→LUMO (38%)				
	415.1	0.29	HOMO→LUMO+1 (88%)				
	373.9	0.14	HOMO-3→LUMO (87%)				
	335.1	0.17	HOMO-1→LUMO+1 (57%)				
34a (THF)	734.8	0.53	HOMO→LUMO (100%)	13.30	-4.70	-2.80	1.90
	514.8	0.53	HOMO-1→LUMO (80%), HOMO-2→LUMO (19%)				
	499.4	0.74	HOMO-2→LUMO (79%), HOMO-1→LUMO (18%)				
	424.6	0.36	HOMO→LUMO+1 (90%)				
	388.3	0.09	HOMO-3→LUMO (86%)				
	338.6	0.18	HOMO-1→LUMO+1 (40%), HOMO-2→LUMO+1 (22%)				

Table 5.5 (cont.)

Dye	λ (nm)	*f*	assignments	μ_g (D)	HOMO (eV)	LUMO (eV)	$E_{0\text{-}0}$ (eV)
34b (vacuum)	701.6	0.36	HOMO→ LUMO (100%)	7.29	-4.62	-2.67	1.96
	492.1	0.97	HOMO-1→ LUMO (82%)				
	484.9	0.17	HOMO-3→ LUMO (55%), HOMO-2→ LUMO (30%), HOMO-1→ LUMO (15%)				
	432.0	0.53	HOMO→ LUMO+1 (55%), HOMO-4→ LUMO (40%)				
	363.0	0.14	HOMO-5→ LUMO (80%), HOMO-1→ LUMO+1(13%)				
	353.9	0.63	HOMO→ LUMO+3(77%), HOMO→ LUMO+2 (20%)				
	347.8	0.24	HOMO→ LUMO+2 (63%), HOMO→ LUMO+3 (18%)				
34b (THF)	715.0	0.46	HOMO→ LUMO (99%)	8.12	-4.74	-2.80	1.94
	513.9	0.97	HOMO-1→ LUMO (89%)				
	501.4	0.22	HOMO-3→ LUMO (58%), HOMO-2→ LUMO (33%)				
	435.1	0.47	HOMO-4→ LUMO (75%), HOMO→ LUMO+1 (21%)				
	420.6	0.12	HOMO→ LUMO+1 (72%), HOMO-4→ LUMO (24%)				
	358.9	0.80	HOMO→ LUMO+3 (85%), HOMO→ LUMO+2 (12%)				

Table 5.6 Computed vertical transition energies and their oscillator strengths, assignments, dipole moments and band gaps for the dyes using MPW1K theory

Dye	λ (nm)	*f*	assignments	μ_g (D)	HOMO (eV)	LUMO (eV)	$E_{0\text{-}0}$ (eV)
30a (vaccum)	430.3	0.83	HOMO → LUMO (91%)	9.11	-5.56	-1.98	3.58
	328.1	0.98	HOMO-2 → LUMO (70%)				
	311.5	0.16	HOMO → LUMO+1 (75%)				
	275.5	0.10	HOMO-1 → LUMO+1 (47%)				
	269.9	0.14	HOMO → LUMO+4 (60%), HOMO-4 → LUMO (23%)				
	269.1	0.34	HOMO-4 → LUMO (35%), HOMO → LUMO+4 (30%)				

Table 5.6 (cont.)

Dye	λ (nm)	*f*	assignments	μ_g (D)	HOMO (eV)	LUMO (eV)	$E_{0\text{-}0}$ (eV)
30a (vaccum)	430.3	0.83	HOMO → LUMO (91%)	9.11	-5.56	-1.98	3.58
	328.1	0.98	HOMO-2 → LUMO (70%)				
	311.5	0.16	HOMO → LUMO+1 (75%)				
	275.5	0.10	HOMO-1 → LUMO+1 (47%)				
	269.9	0.14	HOMO → LUMO+4 (60%), HOMO-4 → LUMO (23%)				
	269.1	0.34	HOMO-4 → LUMO (35%), HOMO → LUMO+4 (30%)				
30a (THF)	441.8	0.94	HOMO → LUMO (89%)	10.13	-5.67	-2.15	3.53
	336.2	0.91	HOMO-2 → LUMO (72%)				
	316.2	0.31	HOMO → LUMO+1 (81%)				
	271.0	0.41	HOMO → LUMO+4 (86%)				
30b (vacuum)	436.0	0.76	HOMO → LUMO (90%)	6.12	-5.51	-2.01	3.49
	338.5	1.01	HOMO-3 → LUMO (57%), HOMO-4 → LUMO (16%)				
	318.4	0.22	HOMO → LUMO+1 (73%), HOMO → LUMO (10%)				
	307.5	0.18	HOMO-1 → LUMO (56%), HOMO-2 → LUMO (28%)				
	305.4	0.80	HOMO → LUMO+2 (78%)				
	286.8	0.26	HOMO-4 → LUMO (37%), HOMO-3 → LUMO (18%), HOMO-9 → LUMO (15%)				
30b (THF)	435.6	0.95	HOMO→ LUMO (86%)	6.87	-5.70	-2.16	3.54
	341.6	0.89	HOMO-3 → LUMO (57%), HOMO-4 → LUMO (19%)				
	320.4	0.37	HOMO→ LUMO+1 (79%)				
	310.3	1.06	HOMO→ LUMO+2 (85%)				
	288.6	0.25	HOMO-4 → LUMO (32%), HOMO-3→ LUMO (24%), HOMO-9 → LUMO (15%)				

Table 5.6 (cont.)

33a (vacuum)	433.0	1.00	HOMO→LUMO (88%)	11.86	-5.55	-1.91	3.64
	336.7	0.60	HOMO-2→LUMO (80%)				
	310.0	0.28	HOMO→LUMO+1 (81%)				
	268.5	0.11	HOMO→LUMO+4 (29%), HOMO-1→LUMO+1 (27%)				
	266.5	0.23	HOMO→LUMO+4 (61%), HOMO-1→LUMO+1 (15%)				
33a (THF)	456.4	1.15	HOMO→LUMO (86%)	14.71	-5.65	-2.12	3.53
	349.5	0.48	HOMO-2→LUMO (77%)				
	313.7	0.40	HOMO→LUMO+1 (84%)				
	287.8	0.10	HOMO→LUMO+2 (81%)				
34a (vacuum)	454.9	1.23	HOMO→LUMO (79%), HOMO-1→LUMO (16%)	9.61	-5.50	-2.10	3.40
	378.2	0.62	HOMO-1→LUMO (71%), HOMO→LUMO (19%)				
	330.7	0.47	HOMO→LUMO+1 (75%)				
	268.2	0.24	HOMO→LUMO+4 (69%)				
34a (THF)	476.3	1.45	HOMO→LUMO (73%), HOMO-1→LUMO (20%)	11.16	-5.60	-2.27	3.33
	392.5	0.45	HOMO→LUMO (73%), HOMO-1→LUMO (20%)				
	336.3	0.60	HOMO→LUMO+1 (75%)				
	268.4	0.34	HOMO→LUMO+4 (74%)				
33b (vacuum)	456.2	1.06	HOMO → LUMO (86%)	8.87	-5.54	-2.09	3.45
	359.5	0.56	HOMO-1 → LUMO (29%), HOMO-2 → LUMO (24%), HOMO-3 → LUMO (18%), HOMO-4 → LUMO (15%)				
	320.8	0.30	HOMO → LUMO+1(85%)				
	305.2	0.96	HOMO → LUMO+2(87%)				
33b (THF)	468.0	1.25	HOMO → LUMO (82%), HOMO-2→LUMO+2(10%)	10.87	-5.71	-2.28	3.44
	375.2	0.14	HOMO-1 → LUMO (37%), HOMO-3 → LUMO (34%), HOMO-2 → LUMO (18%)				
	367.4	0.39	HOMO-2 → LUMO (35%), HOMO-3 → LUMO (31%), HOMO-4 → LUMO (17%)				
	322.7	0.42	HOMO → LUMO+1(79%)				
	309.2	1.04	HOMO → LUMO+2(86%)				

Table 5.6 (cont.)

Dye	λ (nm)	*f*	assignments	μ_g (D)	HOMO (eV)	LUMO (eV)	$E_{0\text{-}0}$ (eV)
34b (vacuum)	482.1	1.33	HOMO → LUMO (76%), HOMO-1 → LUMO (18%)	6.89	-5.50	-2.28	3.22
	402.9	0.63	HOMO-1 → LUMO (65%), HOMO → LUMO (21%)				
	343.2	0.47	HOMO → LUMO+1 (73%)				
	306.0	0.95	HOMO → LUMO+3 (84%)				
34b (THF)	493.1	1.65	HOMO → LUMO (65%), HOMO-1 → LUMO (28%)	7.67	-5.67	-2.43	3.25
	409.0	0.34	HOMO-1 → LUMO (55%), HOMO → LUMO (31%)				
	344.6	0.63	HOMO → LUMO+1 (71%)				
	310.4	1.07	HOMO → LUMO+2(62%), HOMO → LUMO+3 (25%)				

5.2.4 Electrochemical Properties

The electrochemical propensity of the dyes was scrutinized by cyclic voltammetry and differential pulse voltammetry measurements in dichloromethane. Cyclic voltammograms of the dyes are showed in Figure 5.11.

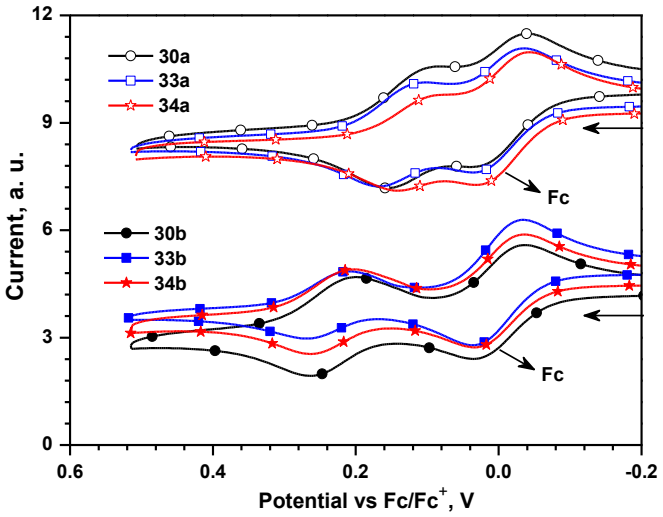

Figure 5.11 Cyclic voltammograms of the carbazole dyes (**30, 33** and **34)** recorded in dichloromethane.

All the dyes exhibited one quasi-reversible oxidation wave and one irreversible oxidation wave which originate from the removal of an electron cloud from the amine donor unit and

conjugation pathway of the dye, respectively. The first oxidation potential of the dyes assumes an order: **30a** (0.12 V) = **34a** (0.12 V) < **33a** (0.13 V) < **30b** (0.23 V) = **34b** (0.23 V) < **33b** (0.26 V). The dyes which contain butoxy unit possess cathodically shifted oxidation potential when compared to that of 2,4-dimethoxyphenyl containing dyes owing to the more electron richness of the former unit [40]. Within the same class of dyes the order of linker is phenyl < bithiophene < thiophene. The phenyl showed easy oxidation even with less electron richness when compared to thiophene units due to its twisted structure which break the effective conjugation and results weak donor-acceptor interactions. Bithiophene containing dyes showed cathodic shift due to more electron richness when compared to thiophene containing dyes. The oxidation potential of dyes **33b** and **34b** cathodically shifted when compared to the parent dyes **7a** and **7b** (0.38 V and 0.33 V). This clearly indicates the introduction of alkoxy units at *para* position of the diphenylamine unit enhancing the electron richness.

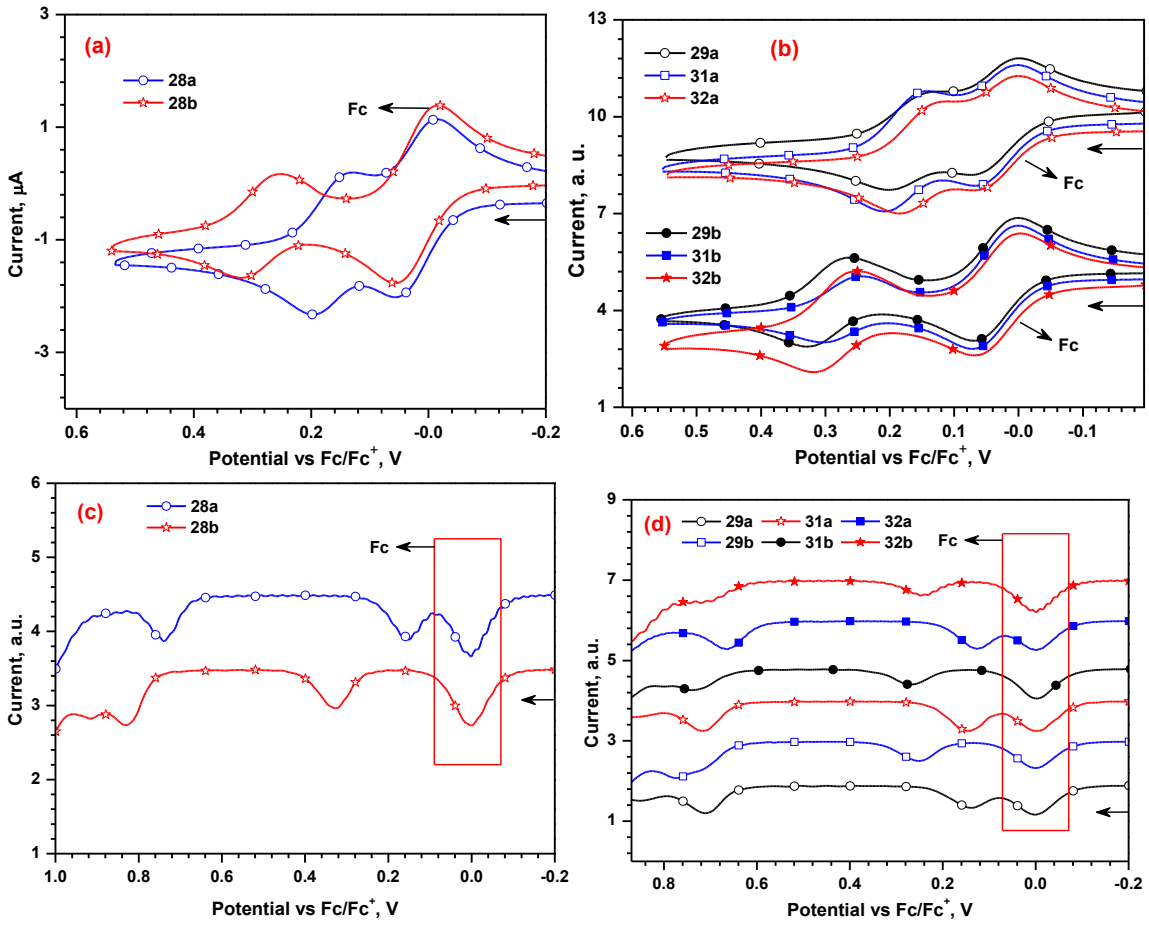

Figure 5.12 Cyclic voltammograms and differential pulse voltammograms of the (a and c) bromo and (b and d) aldehyde derivatives recorded in dichloromethane.

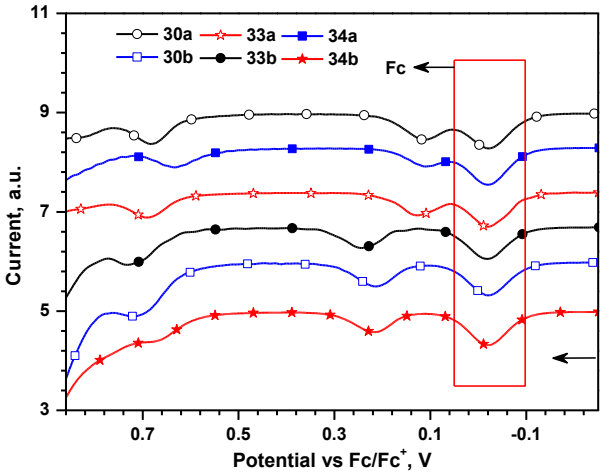

Figure 5.13 Differential pulse voltammograms of dyes recorded in dichloromethane.

Table 5.7 Electrochemical data of precursors and the dyes recorded in dichloromethane

compd.	E_{ox}, V	HOMO, eV	LUMO, eV	$E_{0\text{-}0}$, eV	E_{ox}^{*}, V	ΔG_{inj}, V
2a	0.14 (65), 0.74	4.94	1.88	3.06	-2.15	1.65
28b	0.26 (67), 0.74	5.06	1.92	3.14	-2.11	1.61
29a	0.13 (77), 0.71	4.93	2.43	2.50	-1.60	1.10
29b	0.25 (65), 0.77	5.05	2.49	2.56	-1.54	1.04
31a	0.14 (68), 0.72	4.94	2.62	2.32	-1.41	0.91
31b	0.26 (65), 0.74	5.06	2.57	2.49	-1.46	0.96
32a	0.12 (70), 0.66	4.92	2.66	2.26	-1.37	0.87
32b	0.26 (59), 0.72	5.06	2.64	2.42	-1.39	0.89
30a	0.12 (70), 0.70	4.92	2.76	2.16	-1.27	0.77
30b	0.23 (67), 0.74	5.03	2.52	2.51	-1.51	1.01
33a	0.13 (68), 0.71	4.93	3.10	1.85	-0.95	0.45
33b	0.26 (62), 0.72	5.06	2.98	2.08	-1.05	0.55
34a	0.12 (52), 0.65	4.92	3.12	1.83	-0.94	0.44
34b	0.23 (62), 0.70	5.03	2.98	2.05	-1.05	0.55

Figure 5.14 displays the energy levels of the dyes in ground and excited states along with the energy levels of the conduction band of TiO_2 and redox potential of the electrolyte (I^-/I_3^-). The positive ground state oxidation potentials of the dyes (0.89 V to 1.03 V *vs* NHE) when compared to redox potential of the electrolyte (0.4 V *vs* NHE) ensure the effective regeneration of the dyes[66]. The negative excited state oxidation potential of the dyes (-0.94 V to -1.51 V *vs* NHE) when compared to the conduction band of TiO_2 (-0.50 V *vs* NHE) are

thermodynamically favorable to inject the electrons into conduction band of TiO_2 [67]. The excited state potential of the 2,4-dimethoxyphenyl containing dyes (**33b** and **34b**) are more negative when compared to butoxy containing dyes (**33a** and **34a**) which indicates the electron injection of former dyes are more favorable which help to obtain high photocurrent density. However, the dyes are possessing low lying LUMO when compared to parent carbazole dyes **7a** and **7b** (-1.17 V and -1.18 V) which suggests the thermodynamic driving force for electron injection for the current dyes are relatively less favorable. The order of ΔG_{inj} of the dyes is in the following order: **34a** (0.44 V) < **33a** (0.45 V) < **33b** = **34b** (0.55 V) < **30a** (0.77 V) < **30b** (1.01 V). Higher ΔG_{inj} of the dyes, is favorable for attain charge injection from excited state of dyes into the conduction band of TiO_2. The dyes (**33b** and **34b**) containing 2,4-dimethoxyphenyl unit possessed higher LUMO favorable for efficient electron injection and led to higher J_{SC} of the device based on these dyes than butoxy containing dyes (**33a** and **34a**).

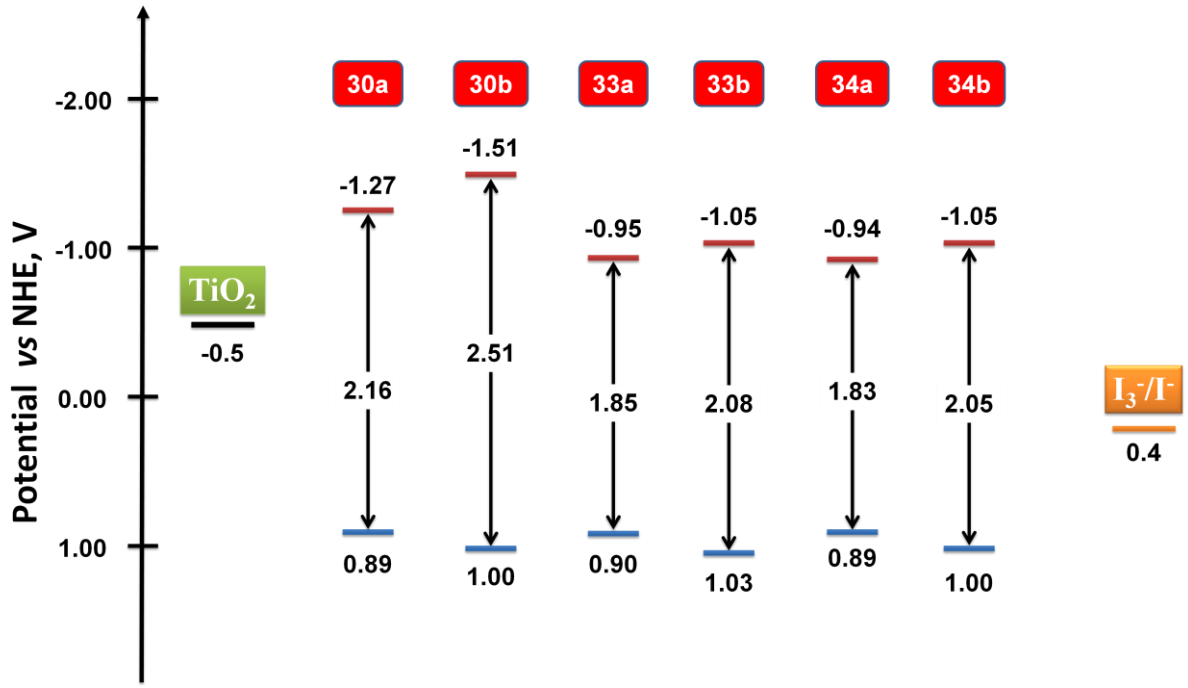

Figure 5.14 Comparison of the oxidation potentials of the carbazole dyes (**30, 33** and **34**) in the ground and excited states.

5.2.5 DSSC Characteristics

The photovoltaic performance of the dyes was evaluated using the dyes as sensitizers in Grätzel solar cells under 1.5 AM illumination [68]. The solar cells were fabricated with an effective area of 0.25 cm^2 and the electrolyte composed of 0.1 M LiI/0.6 M DMPII/0.05 M

I_2/0.5 M *tert*-butyl pyridine in ACN/*t*-BuOH/DMSO (3.5:3.5:3, *v/v*) dye bath. The fabrication of the cell for these dyes made with a thickness of 15 μm TiO_2 photoanode which consists of transparent layer of 11 μm of 13 nm TiO_2 layer and scattering layer of 4 μm of 20 nm TiO_2 layer.

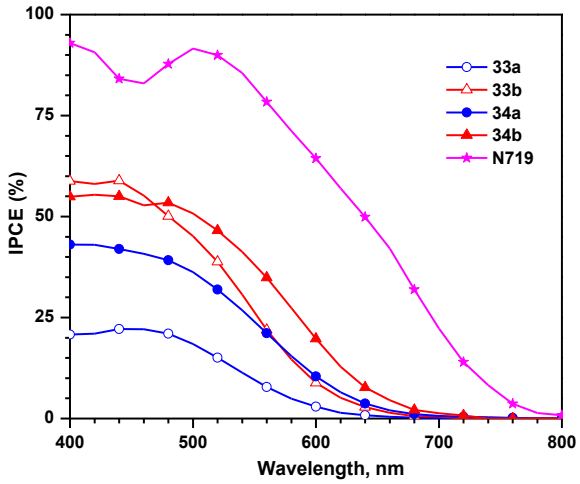

Figure 5.15 IPCE spectra of the devices fabricated using the dyes.

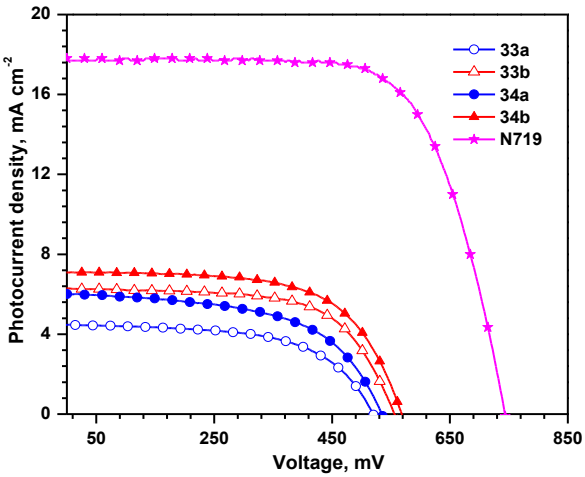

Figure 5.16 IV-Characteristics of the devices fabricated using the dyes.

IPCE action spectra of the devices made from the dyes are shown in Figure 5.15. The IPCE of the dyes covered the region from 400 nm to 600 nm and peak tailing up to 750 nm. Higher the IPCE spectra of the devices indicate more number of photons are converting in to electrons which helpful to increase the efficiency of the device. The dyes are showing inferior IPCE values when compared to the parent dyes (**7a** and **7b**) due to low lying LUMO levels which decreas the driving force to inject the electrons into the conduction band of TiO_2 from excited state of the dye. Among them, the dye with 2,4-dimethoxyphenyl unit and bithiophene conjugation (**34b**) showed broad IPCE spectra and this broadening of IPCE spectra is beneficial for larger photocurrent (J_{SC}).

I-V characteristics of the devices by using the dyes are shown in Figure 5.16 and J_{SC} follow an increasing order: **33a** < **34a** < **33b** < **34b**. As has been observed that, the trend of J_{SC} for the devices follows the absorption spectra features of the dyes in solution spectra. The dye **34b** claimed higher efficiency of 2.53% with high J_{SC} of 7.09 mA cm^{-2} when compared to other dyes. The lower molar extinction coefficient of dye **33a** is responsible for poor IPCE with a lowest efficiency of 1.36%. In general, the devices based on the dyes containing 2,4-dimethoxyphenyl unit (**34a** and **34b**) showed better photovoltaic performance than the dyes containing butoxy units (**33a** and **33b**). This can be attributed to two factors: (a) significant

high molar extinction coefficient led to larger photocurrent (b) efficient electron injection in to the conduction band of TiO_2 facilitated by high lying LUMO of the 2,4-dimethoxyphenyl containing dyes when compared to butoxy containing dyes [14].

Table 5.8 Performance parameters of the DSSCs fabricated using the dyes

Dye	J_{SC}, mA cm^{-2}	V_{OC}, mV	*ff*	η (%)	R_{ct2}, Ω	τ_e, ms	R_{rec}, Ω
33a	4.47	520	0.58	1.36	81.18	1.12	16.50
33b	6.29	555	0.64	2.22	40.57	1.41	40.57
34a	6.02	536	5.53	1.78	48.24	0.95	17.65
34b	7.09	567	0.63	2.53	36.40	1.72	36.40
N719	17.80	744	0.69	9.12	12.13	12.50	84.71

The increasing order of V_{OC} for the dyes assumes: **33a** < **34a** < **33b** < **34b**. The dyes (**33b** and **34b**) exhibited higher V_{OC} owing to the insulating 2,4-dimethoxybiphenyl unit decrease the recombination of electrons from conduction band of TiO_2 with the redox shuttle due to bulky donor which keep away the redox shuttle constituents from photoanode [40]. The bulky nature of 2,4-dimethoxyphenyl unit prevent recombination of electrons more when compared to butoxy unit [40]. The hydrophobic nature of the alkoxy unit proved as a good strategy to increase the V_{OC} of the device.

To rationalize the effect of electron transfer resistance and photovoltaic parameters, electrochemical impedance spectroscopy (EIS) was measured under forward bias with a frequency range from 10 mHz to 65 KHz and amplitude of 10 mV. Interfacial charge transfer resistance at the surface of the electrodes mainly influenced the efficiency of the device. The typical configuration for DSSC is FTO/TiO_2/dye/electrolyte/Pt and it shows three semicircles in the frequency range of 10 mHz to 130 KHz. In Nyquist plot, the first small semicircle is due to the charge transfer resistance from the counter electrode (R_{ct1}) to the oxidized species in the electrolyte and the second large semicircle correspond to the resistance at TiO_2/dye/electrolyte interface (R_{ct2}) and the third small semicircle corresponds to the Warburg diffusion of I^-/I_3^- interface. Figure 5.17 (a) displayed Nyquist plots under dark condition and **33b** showed larger semicircle. The increasing order of radius of semicircle follows as **33a** < **34a** < **34b** < **33b**. But, **34b** has higher V_{OC} owing to higher electron life time due to the suppression of more dark current from conduction band of TiO_2 to redox shuttle.

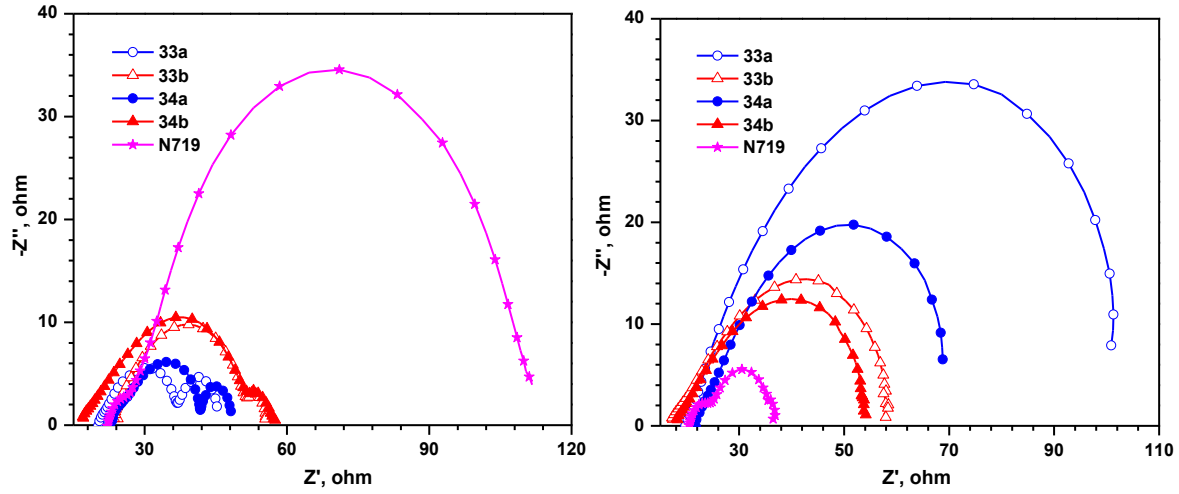

Figure 5.17 Nyquist plots observed for the DSSCs measured under dark (a) and under illumination (b) conditions.

Nyquist plots under the illumination for the devices by using the dyes are displayed in Figure 5.17 (b). The radius of the intermediate frequency semicircle (R_{ct2}) corresponds to charge transport resistance and follows an order: **34b < 33b < 34a < 33a**. The device with low electron transport resistance will assist the electron collection at the conduction band of the TiO_2 and thereby increment of efficiency of the device. The dye **33a** has more R_{ct2} and this reflect in poor injection efficiency and poor J_{SC} values compared to other dyes. Over all the R_{ct2} for butoxy containing dyes is higher than 2,4-dimethoxy phenyl containing dyes.

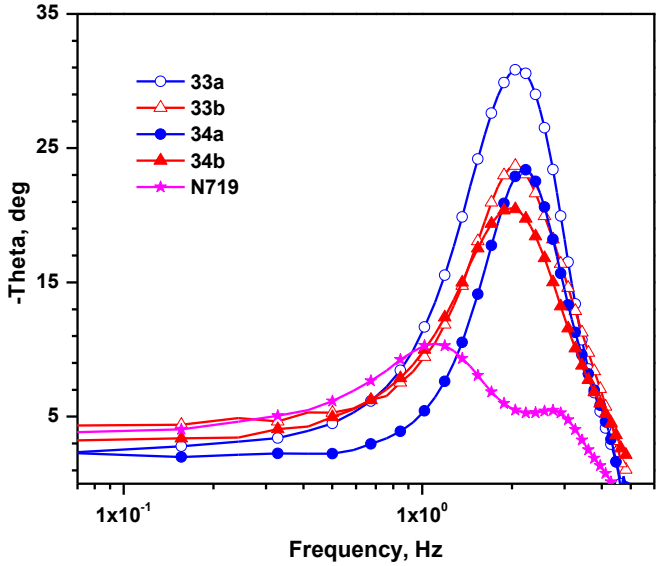

Figure 5.18 Bode phase plots observed for the DSSCs measured under illumination.

Bode phase plots are shown in Figure 5.18 and the small semicircle in the Nyquist plot corresponds to the high frequency peak in the Bode phase plots. The electron life time (τ) extracted from the angular frequency (ω_{min}) at the mid frequency in the Bode phase plot using $\tau_e = 1/\omega_{min}$ [69]. The order of life time for the devices constructed for the dyes follows as **6b < 7a < 34a < 33a < 33b < 34b**. The significantly high electron lifetime for the dye **34b** is due to the suppression of the recombination of electrons from the TiO_2 to the I_3^- ions in the electrolyte. Thus, higher V_{OC} observed for 2,4-dimethoxyphenyl containing dyes may be attributed to the bulky structure which retard the recombination led to high electron collection efficiency at the conduction band of TiO_2.

5.3 Conclusions

In conclusion, we have synthesized a set of dyes which contain 2,4-dimethoxyphenyl and butoxy units as auxiliary chromophores incorporated at the para position of diphenylamine donor of the parent dyes (**7a** and **7b**). All the dyes showed red-shifted absorption owing to the introduction of peripheral units which increases the donor strength and donor-acceptor interaction. The oxidation potentials of the dyes are reflective of the electron releasing effect of the peripheral units (4-butoxy > 2,4-dimethoxyphenyl). Both the auxiliary chromophore units retard the intermolecular interactions by providing hydrophobic environment on the donor side when compared to the parent dyes (**7a** and **7b**). However, the introduction of alkoxy units raised the HOMO and lowered the LUMO. This resulted in the poor dye regeneration and low electron injection efficiency which results inferior power conversion efficiency. Among this class of dyes, a dye with 2,4-dimethoxyphenyl peripheral unit and bithiophene in conjugation (**34b**) showed relatively high power conversion efficiency attributable to the favorable LUMO and facile the electron injection from the excited dye into the conduction band of TiO_2.

5.4 Experimental Section

Computational methods, device fabrication and characterization: Similar to the procedures described in Chapter 3.

5.4.1 Synthesis

2,7-Dibromo-9-butyl-9*H*-carbazole (**1**) [47, 48], bis(4-bromophenyl)amine [70] and 2,4-dimethoxyphenylboronic acid [46] prepared according to literature procedure.

Bis(4-butoxyphenyl)amine, 27a. In a two neck RB flask a mixture of Sodium (1.70 g, 73.9 mmol) was dissolved in dry 1-Butanol (20 mL) and bis(4-bromophenyl)amine (**20**, 1.21 g, 3.69 mmol), copper-(I)-iodide (2.96 g, 15.5 mmol) and dry DMF (40 mL) were added and heated under reflux for 6 h. After the reaction ethyl acetate (160 mL) was added, the mixture was filtered over celite and washed with brine (3 x 75 mL). Removal of volatiles by rotary evaporation produced a solid residue. Further the crude product was purified by column chromatography on silica gel by using hexane/dichloromethane mixture (3:1) as an eluant. White solid; Yield (1.94 g, 62%); mp 78-80 °C; ^{1}H NMR ($CDCl_3$, 500.13 MHz) δ 7.52 (s, 1H), 6.90 (d, *J* = 9.0 Hz, 4H), 6.80 (d, *J* = 9.0 Hz, 4H), 3.90 (t, *J* = 6.5 Hz, 4H), 1.65-1.69 (m, 4H), 1.41-1.46 (m, 4H), 0.93 (t, *J* = 7.5 Hz, 6H); ^{13}C NMR ($CDCl_3$, 125.77 MHz) δ 157.42, 143.08, 123.20, 120.36, 72.57, 36.14, 24.01, 23.87, 18.94; HRMS calcd for $C_{17}H_{17}BrNO$ $[M + H]^+$ *m/z* 314.2114, found 314.2099.

Bis(2',4'-dimethoxy-[1,1'-biphenyl]-4-yl)amine, 27b. A two neck RB flask charged with a mixture of **20** (1.30 g, 4 mmol), 2,4-dimethoxyphenylboronic acid (1.74 g, 4.8 mmol), anhydrous K_2CO_3 (3.86 g, 28 mmol) and $Pd(PPh_3)_4$ (0.27 g, 0.24 mmol) were dissolved in mixture of THF/H_2O (3:1). The reaction mixture was degassed with N_2 and refluxed for 12 h under nitrogen atmosphere. After cooling to room temperature, the organic layer extracted with dichloromethane and dried with sodium sulfate. The crude product was purified by column chromatography on silica gel by using a hexane/dichloromethane mixture (2:1) as eluant. White solid; Yield 1.32 g (75%); mp 195 °C; ^{1}H NMR ($CDCl_3$, 500.13 MHz) δ 7.42 (d, *J* = 8.0 Hz, 4H), 7.24 (s, 2H), 7.14 (d, *J* = 6.5 Hz, 4H), 6.55-6.58 (m, 4H), 5.80 (s, 1H), 3.85 (s, 6H), 3.82 (s, 6H); ^{13}C NMR ($CDCl_3$, 125.77 MHz) δ 159.90, 157.41, 141.65, 130.91, 130.81, 130.32, 123.36, 117.30, 104.51, 98.97, 55.56, 55.45; HRMS calcd for $C_{28}H_{27}NO_4Na$ $[M + Na]^+$ *m/z* 464.1836, found 464.1836.

7-Bromo-*N*,*N*-bis(4-butoxyphenyl)-9-butyl-9*H*-carbazol-2-amine, 28a. A mixture of **1** (1.96 g, 6 mmol), **27a** (0.94 g, 3 mmol), $pd(dba)_2$ (17 mg, 0.02 mmol), dppf (17 mg, 0.02 mmol), sodium *tert*-butoxide (0.72 g, 7.5 mmol), and toluene taken in a pressure tube and heated at 80 °C for 48 h. After completion of the reaction, the volatiles were removed under vacuum, and the resulting solution was extracted with dichloromethane (3 × 50 mL). The combined organic extracts washed with brine solution, dried over Na_2SO_4, and concentrated. Further the crude product was purified by column chromatography on silica gel by using hexane/dichloromethane mixture (5:1) as an eluant. White solid; Yield 1.30 g (71%); mp 60-62 °C; ^{1}H NMR ($CDCl_3$, 500.13 MHz) δ 7.91 (d, *J* = 8.0 Hz, 2H), 7.75 (d, *J* = 1.0 Hz, 1H),

7.25 (dd, *J* = 13.5 Hz, 1.5 Hz, 1H), 7.00 (d, *J* = 9.0 Hz, 4H), 6.86-6.88 (m, 5H), 6.69 (d, *J* = 8.5 Hz, 1H), 1.65-1.71 (m, 4H), 1.54-1.60 (m, 2H), 1.40-1.47 (m, 4H), 1.12-1.19 (m, 2H), 0.94 (t, *J* = 7.5 Hz, 6H), 0.78 (t, *J* = 8.0 Hz, 3H); ^{13}C NMR ($CDCl_3$, 125.77 MHz) δ 155.18, 147.91, 141.81, 141.47, 141.29, 126.16, 122.09, 121.78, 120.53, 120.38, 117.66, 116.26, 115.14, 114.79, 111.33, 101.35, 67.89, 42.57, 31.40, 30.86, 20.37, 19.25, 13.86, 13.81; HRMS calcd for $C_{36}H_{41}BrN_2O_2$ $[M]^+$ *m/z* 612.2345, found 612.2321.

7-Bromo-9-butyl-*N*,*N*-bis(2',4'-dimethoxy-[1,1'-biphenyl]-4-yl)-9*H*-carbazol-2-amine, 28b. It was obtained from **1** (1.52 g, 4 mmol) and **27b** (0.88 g, 2 mmol) by following a procedure similar to that described above for **16a**. Pale yellow solid; Yield 0.74 g (50%); mp 78-80 °C; ^{1}H NMR ($CDCl_3$, 500.13 MHz) δ 7.90 (d, *J* = 5.5 Hz, 1H), 7.83 (d, *J* = 8.0 Hz, 1H), 7.47 (d, *J* = 1.0 Hz, 1H), 7.41-7.45 (m, 4H), 7.29 (d, *J* = 1.5 Hz, 2H), 7.27 (s, 1H), 7.24 (s, 1H), 7.20-7.21 (m, 3H), 7.18 (d, *J* = 3.5 Hz, 1H), 7.07 (dd, *J* = 8.5 Hz, 1.5 Hz, 1H), 6.56-6.58 (m, 4H), 4.11 (t, *J* = 7.0 Hz, 2H), 3.84 (s, 6H), 3.81 (s, 6H), 1.73-1.77 (m, 2H), 1.29-1.35 (m, 2H), 0.89 (t, *J* = 7.5 Hz, 3H); ^{13}C NMR ($CDCl_3$, 125.77 MHz) δ 160.04, 157.43, 146.59, 146.45, 141.79, 141.68, 132.35, 131.04, 130.07, 123.35, 123.09, 122.01, 121.97, 120.91, 120.86, 118.32, 118.08, 117,88, 111.61, 105.26, 104.61, 55.55, 55.45, 42.84, 31.00, 20.47, 13.94; HRMS calcd for $C_{44}H_{41}BrN_2O_4$ $[M]^+$ *m/z* 740.2244, found 740.2215.

4-(7-(Bis(4-butoxyphenyl)amino)-9-butyl-9*H*-carbazol-2-yl)benzaldehyde, 29a. A two neck RB flask charged with a mixture of **28a** (0.61 g, 1 mmol), 4-formylphenylboronic acid (0.18 g, 1.2 mmol), anhydrous K_2CO_3 (0.48 g, 3.5 mmol) and $Pd(PPh_3)_4$ (0.35 g, 0.03 mmol) were dissolved in mixture of THF/H_2O (3:1). The reaction mixture was degassed with N_2 and refluxed for 12 h under nitrogen atmosphere. After cooling to room temperature, the organic layer extracted with dichloromethane and dried with sodium sulfate. The crude product was purified by column chromatography on silica gel by using a hexane/dichloromethane mixture (2:1) as eluant. Orange solid; Yield 0.53 g (83%); mp 98 °C; IR (KBr, cm^{-1}) 1698 ($\nu_{C=O}$); ^{1}H NMR ($CDCl_3$, 500.13 MHz) δ 10.07 (s, 1H), 8.01 (d, *J* = 8.0 Hz, 1H), 7.97 (d, *J* = 8.5 Hz, 2H), 7.86 (t, *J* = 8.0 Hz, 3H), 7.53 (s, 1H), 7.46 (d, *J* = 8.0 Hz, 1H), 7.10 (d, *J* = 9.0 Hz, 4H), 6.93 (d, *J* = 1.0 Hz, 1H), 6.83-6.88 (m, 5H), 4.16 (t, *J* = 7.0 Hz, 2H), 3.96 (t, *J* = 6.5 Hz, 4H), 1.73-1.80 (m, 6H), 1.47-1.55 (m, 4H), 1.25-1.34 (m, 2H), 1.25-1.34 (m, 6H), 0.96-1.00 (m, 3H); ^{13}C NMR (C DCl_3, 125.77 MHz) δ 192.02, 155.26, 148.48, 148.11, 142.52, 141.38, 141.19, 135.80, 134.75, 130.32, 127.89, 126.30, 123.56, 120.85, 119.82, 118.56, 116.38, 115.22, 114.69, 107.10, 105.16, 104.36, 101.23, 101.18, 67.98, 42.56, 31.47, 31.11, 20.51, 19.33, 13.94; HRMS calcd for $C_{43}H_{46}N_2O_3$ $[M]^+$ *m/z* 638.3503, found 638.3490.

4-(7-(Bis(2',4'-dimethoxybiphenyl-4-yl)amino)-9-butyl-9*H*-carbazol-2-yl)benzaldehyde, 29b. Compound **29b** was synthesized from **28b** (0.37 g, 0.5 mmol) by following a procedure similar to that described above for **29a**. Yellow solid; Yield 0.29 g (75%); mp 118 °C; IR (KBr, cm^{-1}) 1695 ($\nu_{C=O}$); ^{1}H NMR ($CDCl_3$, 500.13 MHz) δ 10.08 (s, 1H), 8.07 (d, *J* = 8.0 Hz, 2H), 7.97-8.00 (m, 3H), 7.88-7.92 (m, 2H), 7.58 (s, 1H), 7.49 (dd, *J* = 8.0 Hz, 1.5 Hz, 1H), 7.43 (d, *J* = 9.0 Hz, 4H), 7.28-7.29 (m, 3H), 7.21-7.25 (m, 5H), 7.10 (dd, *J* = 8.5 Hz, 1.0 Hz , 1H), 6.57-6.59 (m, 4H), 4.25 (t, *J* = 7.0 Hz, 2H), 3.87 (s, 6H), 3.83 (s, 6H), 1.78-1.83 (m, 2H), 1.33 (m, 2H), 0.90 (t, *J* = 7.5 Hz, 3H); ^{13}C NMR ($CDCl_3$, 125.77 MHz) δ 192.05, 166.27, 160.04, 157.43, 146.46, 142.41, 136.38, 134.84, 132.38, 131.03, 130.33, 130.06, 127.98, 123.40, 123.11, 121.16, 120.20, 118.67, 117.70, 107.29, 105.12, 104.62, 100.47, 55.55, 55.45, 42.73, 31.16, 20.51, 13.96; HRMS calcd for $C_{51}H_{46}N_2O_5Na$ $[M + Na]^+$ *m/z* 789.3299, found 789.3296.

5-(7-(Bis(4-butoxyphenyl)amino)-9-butyl-9*H*-carbazol-2-yl)thiophene-2-carbaldehyde, 31a. A mixture of **28a** (0.61 g, 1 mmol), (5-(1,3-dioxolan-2-yl)thiophen-2-yl)tributylstannane (0.49 g, 1.1 mmol) and dry DMF (5 mL) was maintained under nitrogen atmosphere and $Pd(PPh_3)_2Cl_2$ (0.01 g, 0.01 mmol) added to it. The resulting reaction mixture was heated at 80 °C for 15 h. After completion of the reaction, the reaction mixture was poured into cold water and extracted with dichloromethane (3 × 40 mL). Removal of volatiles from the dichloromethane extract by rotary evaporation produced a solid residue. It was dissolved in glacial acetic acid (4 mL) and heated at 60 °C for 1 h to form a clear solution. After the addition of water (3 mL) the reaction mixture was maintained at 60 °C for additional 1 h. Finally, it was extracted with dichloromethane (3 × 40 mL). The dichloromethane extract was washed thoroughly with brain solution and dried over anhydrous sodium sulfate. The solid residue obtained on evaporation of the dichloromethane extract was purified by column chromatography on silica gel by using hexane/dichloromethane mixture (2:1) as an eluant. Yellow solid; Yield 0.46 g (71 %); mp 104 °C; IR (KBr, cm^{-1}) 1662 ($\nu_{C=O}$); ^{1}H NMR ($CDCl_3$, 500.13 MHz) δ 9.88 (s, 1H), 7.94 (d, *J* = 8.0 Hz, 1H), 7.82 (d, *J* = 8.5 Hz, 1H), 7.74 (d, *J* = 4.0 Hz, 1H), 7.57 (s, 1H), 7.49-7.51 (m, 1H), 7.46-7.47 (d, *J* = 4.0 Hz, 1H), 7.11 (d, *J* = 8.5 Hz, 4H), 6.91 (d, *J* = 1.5 Hz, 1H), 6.84-6.89 (m, 5H), 4.13 (t, *J* = 7.0 Hz, 2H), 3.97 (t, *J* = 6.5 Hz, 4H), 1.73-1.82 (m, 6H), 1.49-1.56 (m, 4H), 1.30-1.36 (m, 2H), 1.00 (t, *J* = 2.5 Hz, 6H), 0.90 (t, *J* = 7.0 Hz, 3H); ^{13}C NMR ($CDCl_3$, 125.77 MHz) δ 182.48, 156.15, 155.24, 148.29, 142.60, 141.46, 141.07, 140.77, 137.47, 128.76, 126.26, 124.34, 123.35, 120.74, 119.66, 117.49, 116.11, 115.11, 114.54,

106.02, 100.77, 67.84, 42.40, 31.29, 30.87, 20.28, 19.14, 13.73, 13.70; HRMS calcd for $C_{41}H_{44}N_2O_3S$ $[M]^+$ *m/z* 644.3067, found 644.3067.

5-(7-(Bis(2',4'-dimethoxy-[1,1'-biphenyl]-4-yl)amino)-9-butyl-9*H*-carbazol-2-yl)thiophene-2-carbaldehyde, 31b. It was synthesized from **28b** (0.37 g, 0.5 mmol) and ((5-(1,3-dioxolan-2-yl)thiophen-2-yl)tributylstannane (0.24 g, 1.1 mmol) by following a procedure similar to that described above for **31a**. Orange solid**;** Yield 0.20 g (52%); mp 134-136 °C; IR (KBr, cm^{-1}) ($\nu_{C=O}$) 1661; ^{1}H NMR ($CDCl_3$, 500.13 MHz) δ 9.90 (s, 1H), 8.01 (d, *J* = 8.0 Hz, 1H), 7.94 (d, *J* = 8.5 Hz, 1H), 7.77 (d, *J* = 3.5 Hz, 1H), 7.61 (s, 1H), 7.51 (dd, *J* = 15.0 Hz, 3.5 Hz, 2H), 7.44 (d, *J* = 8.5 Hz, 4H), 7.28 (d, *J* = 8.5 Hz, 2H), 7.22 (d, *J* = 8.5 Hz, 4H), 7.09 (d, *J* = 8.0 Hz, 1H), 6.57 (d, *J* = 7.0 Hz, 4H), 4.21 (t, *J* = 6.5 Hz, 2H), 3.85 (s, 6H), 3.83 (s, 6H), 1.78-1.80 (m, 2H), 1.32-1.37 (m, 2H), 0.91 (t, *J* = 12.5 Hz, 3H); ^{13}C NMR ($CDCl_3$, 125.77 MHz) δ 182.77, 160.07, 157.44, 156.18, 147.06, 146.37, 142.63, 141.76, 141.08, 137.72, 136.98, 132.56, 131.05, 130.10, 129.45, 126.51, 124.26, 123.72, 123.56, 123.07, 121.19, 120.27, 117.99, 117.76, 117.72, 106.38, 104.84, 104.64, 99.01, 55.55, 55.45, 42.74, 31.12, 20.49, 13.94; HRMS calcd for $C_{49}H_{44}N_2O_5SNa$ $[M + Na]^+$ *m/z* 795.2863, found 795.2861.

5-(5-(7-(Bis(4-butoxyphenyl)amino)-9-butyl-9*H*-carbazol-2-yl)thiophen-2-yl)thiophene-2-carbaldehyde, 32a. It was obtained from **28a** (0.61 g, 1 mmol) and (5-(5-(1,3-dioxolan-2-yl)thiophen-2-yl)thiophen-2-yl)tributylstannane (0.58 g, 1.1 mmol) by following a procedure similar to that described above for **31a**. Red solid; Yield 0.36 g (50%); mp 142-144 °C; IR (KBr, cm^{-1}) 1660 ($\nu_{C=O}$); ^{1}H NMR ($CDCl_3$, 500.13 MHz) δ 9.85 (s, 1H), 7.91 (d, *J* = 8.0 Hz, 1H), 7.82 (d, *J* = 8.5 Hz, 1H), 7.65 (d, *J* = 2.5 Hz, 1H), 7.50 (s, 1H), 7.43 (d, *J* = 8.0 Hz, 1H), 7.34 (d, *J* = 10.0 Hz, 2H), 7.11 (d, *J* = 8.5 Hz, 5H), 6.92 (s, 1H), 6.83-6.88 (m, 5H), 4.13 (t, *J* = 6.0 Hz, 2H), 3.96 (t, *J* = 6.0 Hz, 4H), 1.79 (t, *J* = 7.5 Hz, 6H), 1.50-1.54 (m, 4H), 1.27-1.34 (m, 2H), 1.00 (t, *J* = 2.5 Hz, 6H), 0.90 (t, *J* = 7.0 Hz, 3H); ^{13}C NMR ($CDCl_3$, 125.77 MHz) δ 182.42, 155.30, 148.09, 148.02, 147.54, 142.55, 141.36, 141.26, 141.05, 137.51, 134.31, 129.55, 127.27, 126.31, 123.74, 123.70, 123.53, 120.71, 119.81, 117.31, 116.55, 115.24, 114.73, 105.51, 101.22, 68.00, 42.54, 31.48, 31.07, 20.48, 19.33, 13.92; HRMS calcd for $C_{45}H_{46}N_2O_3S_2$ $[M]^+$ *m/z* 726.2944, found 726.2942.

5'-(7-(Bis(2',4'-dimethoxy-[1,1'-biphenyl]-4-yl)amino)-9-butyl-9*H*-carbazol-2-yl)-[2,2'-bithiophene]-5-carbaldehyde, 32b. It was synthesized from **28b** (0.37 g, 0.5 mmol) and (5-(5-(1,3-dioxolan-2-yl)thiophen-2-yl)thiophen-2-yl)tributylstannane (0.29 g, 0.55

mmol) by following a procedure similar to that described above for **31a**. Red solid; Yield 0.24 g (57%); mp 154 °C; IR (KBr, cm^{-1}) 1659 ($\nu_{C=O}$); ^{1}H NMR ($CDCl_3$, 500.13 MHz) δ 9.87 (s, 1H), 7.99 (d, *J* = 8.5 Hz, 1H), 7.94 (s, 1H), 7.70 (d, *J* = 4.0 Hz, 1H), 7.54 (s, 1H), 7.47 (d, *J* = 8.5 Hz, 1H), 7.43 (d, *J* = 8.5 Hz, 4H), 7.36-7.40 (m, 2H), 7.27-7.30 (m, 4H), 7.22 (d, *J* = 8.5 Hz, 4H), 7.08 (d, *J* = 8.0 Hz, 1H), 6.57-6.58 (d, *J* = 7.0 Hz, 4H), 4.22 (t, *J* = 7.0 Hz, 2H), 3.86 (s, 6H), 3.83 (s, 6H), 1.77-1.83 (m, 2H), 1.31-1.38 (m, 2H), 0.91-0.94 (m, 3H); ^{13}C NMR ($CDCl_3$, 125.77 MHz) δ 182.49, 160.05, 157.45, 147.87, 147.51, 146.67,146.45, 142.43, 141.32, 141.20, 137.55, 134.48, 132.41, 131.04, 130.08, 127.29, 123.89, 123.82, 123.43, 123.29, 123.11, 121.00, 120.22, 118.28, 117.75, 117.43, 105.68, 105.08, 104.63, 99.02, 55.55, 55.45, 42.70, 31.13, 20.50, 13.97; HRMS calcd for $C_{53}H_{46}N_2O_5S_2$ $[M]^+$ *m/z* 854.2843, found 854.2846.

(*E*)-3-(4-(7-(Bis(4-butoxyphenyl)amino)-9-butyl-9*H*-carbazol-2-yl)phenyl)-2-cyanoacrylic acid, 30a. The aldehyde **29a** (0.21 g, 0.33 mmol), 2-cyanoacetic acid (0.04 g, 0.5 mmol), ammonium acetate (0.04 g, 0.25 mmol), and acetic acid (5 mL) were mixed and refluxed for 24 h. The resulting red precipitate was filtered and washed several times with water and dried. It was crystallized from dichloromethane/hexane mixture to obtain the analytically pure sample. Red solid; Yield 0.22 g (93%); mp 110 °C; IR (KBr, cm^{-1}) ($\nu_{C\equiv N}$); ^{1}H NMR ($CDCl_3$, 500.13 MHz) δ 8.31 (s, 1H), 7.93 (d, *J* = 8.0 Hz, 1H), 7.82 (d, *J* = 8.5 Hz, 1H), 7.50 (s, 1H), 7.44-7.46 (m, 2H), 7.39 (d, *J* = 3.5 Hz, 1H), 7.31 (d, *J* = 4.0 Hz, 2H), 7.10 (d, *J* = 8.5 Hz, 4H), 6.90 (s, 1H), 6.83-6.87 (m, 5H), 4.14 (t, *J* = 6.5 Hz, 2H), 3.95 (t, *J* = 6.5 Hz, 2H), 1.75-1.79 (m, 6H), 1.48-1.53 (m, 4H), 1.29-1.33 (m, 2H), 0.99 (t, *J* = 7.0 Hz, 6H), 0.89 (t, *J* = 7.0 Hz, 3H); ^{13}C NMR ($CDCl_3$, 125.77 MHz) δ 158.99, 155.53, 155.24, 155.21, 150.47, 148.83, 147.93, 147.40, 143.05, 142.41, 141.41, 141.36, 141.32, 141.02, 140.87, 140.47, 133.49, 132.41, 129.78, 129.48, 127.88, 126.48, 126.31, 126.26, 125.29, 124.11, 123.22, 122.86, 121.07, 120.65, 119.94, 119.82, 119.76, 117.95, 117.38, 116.59, 115.97, 115.27, 115.20, 114.75, 114.64, 113.75, 112.02, 106.27, 105.61, 42.55, 31.45, 31.05, 20.43, 19.31, 13.91, 13.89; HRMS calcd for $C_{46}H_{47}N_3O_4$ $[M]^+$ *m/z* 705.3561, found 705.3568.

(*E*)-3-(4-(7-(Bis(2',4'-dimethoxybiphenyl-4-yl)amino)-9-butyl-9*H*-carbazol-2-yl)phenyl)-2-cyanoacrylic acid, 30b. It was prepared form **29b** (0.25 g, 0.33 mmol) and 2-cyano acetic acid (0.04 g, 0.5 mmol) by following a procedure described above for **18a**. Orange solid; Yield 0.26 g (94%); mp 153-155 °C; IR (KBr, cm^{-1}) 2191 ($\nu_{C\equiv N}$); ^{1}H NMR ($CDCl_3$, 500.13 MHz) δ 8.11-8.17 (m, 2H), 7.97-8.01 (m, 1H), 7.85-7.89 (m, 2H), 7.80 (d, *J* = 8.5 Hz, 1H), 7.55 (t, *J* = 8.5 Hz, 2H), 7.42 (d, *J* = 8.0 Hz, 5H), 7.30 (s, 1H), 7.26 (d, *J* = 8.0

Hz, 4H), 6.96 (d, *J* = 8.5 Hz, 1H), 6.67 (d, *J* = 2.0 Hz, 2H), 6.62 (dd, *J* = 8.5 Hz, *J* = 2.0 Hz, 2H), 4.37 (t, *J* = 6.0 Hz, 3H), 3.82 (s, 6H), 3.80 (s, 6H), 1.70-1.77 (m, 2H), 1.25-1.28 (m, 2H), 0.84 (t, *J* = 7.5 Hz, 3H); ^{13}C NMR ($CDCl_3$, 125.77 MHz) δ 160.01, 157.43, 146.52, 146.37, 142.97, 142.22, 142.18, 141.37, 137.00, 136.36, 132.24, 131.03, 130.03, 128.49, 128.14, 127.49, 127.12, 123.28, 123.14, 122.64, 120.99, 120.10, 118.47, 118.37, 117.71, 116.96, 107.06, 105.31, 55.54, 55.44, 42.72, 31.14, 20.51, 13.96; HRMS calcd for $C_{54}H_{47}N_3O_6Na$ $[M + Na]^+$ *m/z* 856.3357, found 856.3358.

(*E*)-3-(5-(7-(Bis(4-butoxyphenyl)amino)-9-butyl-9*H*-carbazol-2-yl)thiophen-2-yl)-2-cyanoacrylic acid, 33a. It was prepared form **31a** (0.21 g, 0.33 mmol) and 2-cyano acetic acid (0.04 g, 0.5 mmol) by following a procedure described above for **30a**. Brick red solid; Yield 0.22 g (93%); mp 135-137 °C; IR 2221 ($\nu_{C\equiv N}$); ^{1}H NMR ($CDCl_3$, 500.13 MHz) δ 8.33 (s, 1H), 7.88 (s, 1H), 7.78-7.82 (m, 2H), 7.44-7.53 (m, 3H), 7.09 (d, *J* = 8.5 Hz, 4H), 6.82-6.91 (m, 6H), 4.12 (t, *J* = 6.0 Hz, 2H), 3.95 (t, *J* = 8.5 Hz, 4H), 1.73-1.80 (m, 6H), 1.47-1.52 (m, 4H), 1.25-1.29 (m, 2H), 0.99 (t, *J* = 7.0 Hz, 6H), 0.88 (t, *J* = 5.0 Hz, 3H); ^{13}C NMR ($CDCl_3$, 125.77 MHz) δ 164.21, 155.50, 155.30, 154.91, 148.46, 146.43, 142.72, 141.35, 140.97, 140.72, 134.36, 128.70, 126.90, 126.59, 125.00, 124.19, 121.56, 120.38, 118.68, 117.93, 117.37, 115.86, 115.71, 113.75, 106.54, 67.73, 42.01, 31.20, 30.78, 20.06, 19.17, 14.05, 13.86; HRMS calcd for $C_{44}H_{46}N_3O_4S$ $[M + 1]^+$ *m/z* 734.3022, found 734.3016.

(*E*)-3-(5-(5-(7-(Bis(4-butoxyphenyl)amino)-9-butyl-9*H*-carbazol-2-yl)thiophen-2-yl)thiophen-2-yl)-2-cyanoacrylic acid, 34a. It was prepared form **32a** (0.24 g, 0.33 mmol) and 2-cyano acetic acid (0.04 g, 0.5 mmol) by following a procedure described above for **30a**. Black solid; Yield 0.11 g (92%); mp 200-202 °C; IR (KBr, cm^{-1}) 2213 ($\nu_{C\equiv N}$); ^{1}H NMR ($CDCl_3$, 500.13 MHz) δ 8.31 (s, 1H), 7.94 (d, *J* = 8.0 Hz, 1H), 7.81 (d, *J* = 8.0 Hz, 1H), 7.68 (d, *J* = 4.5 Hz, 1H), 7.61 (d, *J* = 4.0 Hz, 1H), 7.49 (s, 1H), 7.42-7.44 (m, 2H), 7.36 (d, *J* = 4.0 Hz, 1H), 7.30 (s, 1H), 7.27-7.28 (m, 2H), 7.09 (d, *J* = 8.5 Hz, 4H), 6.83 (d, *J* = 8.5 Hz, 4H), 4.14 (t, *J* = 6.0 Hz, 2H), 3.95 (t, *J* = 6.5 Hz, 4H), 1.74-1.80 (m, 6H), 1.5-1.54 (m, 4H), 1.31-1.34 (m, 2H), 1.04 (t, *J* = 7.5 Hz, 6H), 0.89 (t, *J* = 7.5 Hz, 3H); ^{13}C NMR ($CDCl_3$, 125.77 MHz) δ 164.06, 155.41, 148.12, 147.38, 145.77, 142.49, 141.27, 141.10, 140.93, 134.27, 133.83, 129.40, 128.57, 126.76, 125.30, 124.98, 123.16, 121.38, 120.31, 117.36, 116.18, 115.78, 113.89, 105.92, 67.78, 42.01, 31.22, 30.86, 20.12, 19.19, 14.10, 13.96; HRMS calcd for $C_{48}H_{47}N_3O_4S_2Na$ $[M + Na]^+$ *m/z* 816.2900, found 816.2877.

(*E*)-3-(5-(7-(Bis(2',4'-dimethoxy-[1,1'-biphenyl]-4-yl)amino)-9-butyl-9*H*-carbazol-2-yl)thiophen-2-yl)-2-cyanoacrylic acid, 33b. It was prepared form **31b** (0.25 g, 0.33 mmol) and 2-cyano acetic acid (0.04 g, 0.5 mmol) by following a procedure described above for **30a**. Red solid; Yield 0.14 g (91%); mp 165 °C; IR (KBr, cm^{-1}) 2208 ($\nu_{C\equiv N}$); ^{1}H NMR ($CDCl_3$, 500.13 MHz) δ 8.44 (s, 1H), 8.00 (d, *J* = 8.0 Hz, 1H), 7.93 (d, *J* = 8.5 Hz, 1H), 7.77 (d, *J* = 4.5 Hz, 1H), 7.65 (d, *J* = 7.0 Hz, 2H), 7.60-7.61 (m, 3H), 7.54 (q, *J* = 8.0 Hz, 2.0 Hz, 1H), 7.29-7.34 (m, 5H), 7.27 (s, 1H), 7.21 (d, *J* = 5.0 Hz, 2H), 7.07 (q, *J* = 7.5 Hz, 2.0 Hz, 1H), 6.56 (d, *J* = 7.0 Hz, 4H), 4.13 (t, *J* = 7.0 Hz, 2H), 3.87 (s, 6H), 3.83 (s, 6H), 1.72-1.78 (m, 2H), 1.28-1.33 (m, 2H), 0.87 (t, *J* = 7.5 Hz, 3H); ^{13}C NMR ($CDCl_3$, 125.77 MHz) δ 164.20, 160.30, 157.56, 156.69, 154.57, 146.83, 146.16, 142.68, 141.27, 134.76, 132.95, 131.11, 130.51, 129.49, 125.41, 123.85, 123.62, 122.32, 122.14, 118.15, 118.06, 117.43, 117.40, 117.36, 113.82, 113.23, 107.67, 107.05, 105.75, 55.96, 55.71, 42.24, 31.08, 20.18, 14.11; HRMS calcd for $C_{17}H_{17}BrNO$ $[M + H]^+$ *m/z* 330.0488, found 330.0487.

(*E*)-3-(5'-(7-(Bis(2',4'-dimethoxy-[1,1'-biphenyl]-4-yl)amino)-9-butyl-9*H*-carbazol-2-yl)-[2,2'-bithiophen]-5-yl)-2-cyanoacrylic acid, 34b. It was prepared form **32b** (0.28 g, 0.33 mmol) and 2-cyano acetic acid (0.04 g, 0.5 mmol) by following a procedure described above for **30a**. Red solid; Yield 0.15 g (96%); mp 180 °C; IR (KBr, cm^{-1}) 2215 ($\nu_{C\equiv N}$); ^{1}H NMR ($CDCl_3$, 500.13 MHz) δ 8.45 (s, 1H), 7.99 (d, *J* = 8.0 Hz, 1H), 7.92 (d, *J* = 8.5 Hz, 1H), 7.69 (d, *J* = 11.5 Hz, 2H), 7.64 (d, *J* = 7.5 Hz, 2H), 7.60 (d, *J* = 8.0 Hz, 2H), 7.48 (dd, *J* = 8.0 Hz, 1.0 Hz, 1H), 7.36 (dd, *J* = 10.0 Hz, 4.0 Hz, 2H), 7.27-7.33 (m, 6H), 7.21 (d, *J* = 2.0 Hz, 2H), 7.06 (dd, *J* = 8.5 Hz, 1.5 Hz, 1H), 6.57 (d, *J* = 7.0 Hz, 4H), 4.14 (t, *J* = 7.0 Hz, 2H), 3.87 (s, 6H), 3.84 (s, 6H), 1.75-1.78 (m, 2H), 1.30-1.34 (m, 2H), 0.87 (t, *J* = 7.5 Hz, 3H); ^{13}C NMR ($CDCl_3$, 125.77 MHz) δ 172.47, 164.16, 162.78, 160.29, 157.57, 147.32, 146.46, 146.22, 146.02, 142.46, 141.56, 141.38, 134.31, 134.07, 132.85, 131.07, 130.44, 130.07, 128.67, 125.60, 125.08, 123.52, 123.33, 122.93, 122.39, 121.80, 120.81, 118.29, 117.53, 117.28, 106.28, 105.75, 105.31, 55.94, 55.68, 42.21, 31.09, 20.18, 14.09; HRMS calcd for $C_{52}H_{45}N_3O_6SNa$ $[M + Na]^+$ *m/z* 862.2921, found 862.2912.

5.5 References

[1] M. Liang and J. Chen, Arylamine organic dyes for dye-sensitized solar cells. *Chem. Soc. Rev.*, **2013**, *42*, 3453-3488.

[2] Z. Ning and H. Tian, Triarylamine: A promising core unit for efficient photovoltaic materials. *Chem. Commun.*, **2009**, 5483-5495.

[3] Z. Ning, Q. Zhang, W. Wu, H. Pei, B. Liu and H. Tian, Starburst triarylamine based dyes for efficient dye-sensitized solar cells. *J. Org. Chem.*, **2008**, *73*, 3791-3797.

[4] S. Kim, J. W. Lee, S. O. Kang, J. Ko, J.-H. Yum, S. Fantacci, F. D. Angellis, D. D. Censo, M. K. Nazeeruddin and M. Grätzel, Molecular engineering of organic sensitizers for solar cell applications. *J. Am. Chem. Soc.*, **2006**, *128*, 16701-16707.

[5] M. Lu, M. Liang, H.-Y. Han, Z. Sun and S. Xue, Organic dyes incorporating bis-hexapropyltruxeneamino moiety for efficient dye-sensitized solar cells. *J. Phys. Chem. C*, **2011**, *115*, 274-281.

[6] D. P. Hagberg, X. Jiang, E. Gabrielsson, M. Linder, T. Marinado, T. Brinck, A. Hagfeldt and L. Sun, Symmetric and unsymmetric donor functionalization. comparing structural and spectral benefits of chromophores for dye-sensitized solar cells. *J. Mater. Chem.*, **2009**, *19*, 7232-7238.

[7] J. Tang, J. Hua, W. Wu, J. Li, Z. Jin, Y. Long and H. Tian, New starburst sensitizer with carbazole antennas for efficient and stable dye-sensitized solar cells. *Energy Environ. Sci.*, **2010**, *3*, 1736-1745.

[8] Z. Wan, C. Jia, Y. Duan, L. Zhou, J. Zhang, Y. Lin and Y. Shi, Influence of the antennas in starburst triphenylamine-based organic dye sensitized solar cells: phenothiazine versus carbazole. *RSC Adv.*, **2012**, *2*, 4507-4514.

[9] M.-D. Zhang, H. Pan, X.-H. Ju, Y.-J. Ji, L. Qin, H.-G. Zheng and X.-F. Zhou, Improvement of dye-sensitized solar cells' performance through introducing suitable heterocyclic groups to triarylamine dyes. *Phys. Chem. Chem. Phys.*, **2012**, *14*, 2809-2815.

[10] Z. Wang, M. Liang, L. Wang, Y. Hao, C. Wang, Z. Sun and S. Xue, New triphenylamine organic dyes containing dithieno[3,2-*b*:2',3'-*d*]pyrrole (DTP) units for iodine-free dye-sensitized solar cells. *Chem. Commun.*, **2013**, *49*, 5748-5750.

[11] A. Yella, R. Humphry-Baker, B. F. E. Curchod, N. A. Astani, J. Teuscher, L. E. Polander, S. Mathew, J.-E. Moser, I. Tavernelli, U. Rothlisberger, M. Grätzel, M. K. Nazeeruddin and J. Frey, Molecular engineering of a fluorene donor for dye-sensitized solar cells. *Chem. Mater.*, **2013**, *25*, 2733-2739.

[12] E. Gabrielsson, H. Ellis, S. Feldt, H. Tian, G. Boschloo, A. Hagfeldt and L. Sun, Convergent/divergent synthesis of a linker-varied series of dyes for dye-sensitized solar cells based on the **D35** donor. *Adv. Energy Mater.*, **2013**, *3*, 1647-1656.

[13] D.-Y. Chen, Y.-Y. Hsu, H.-C. Hsu, B.-S. Chen, Y.-T. Lee, H. Fu, M.-W. Chung, S.-H. Liu, H.-C. Chen, Y. Chi and P.-T. Chou, Organic dyes with remarkably high

absorptivity; all solid-state dye sensitized solar cell and role of fluorine substitution. *Chem. Commun.*, **2010**, *46*, 5256-5258.

[14] A. Mishra, M. K. R. Fischer and P. Bäuerle, Metal-Free organic dyes for dye-sensitized solar cells: From structure: Property relationships to design rules. *Angew. Chem. Int. Ed.*, **2009**, *48*, 2474-2499.

[15] A. Baheti, K. R. J. Thomas, C.-P. Lee, C.-T. Li and K.-C. Ho, Organic dyes containingfluoren-9-ylidene chromophores for efficient dye-sensitized solar cells. *J. Mater. Chem. A*, **2014**, *2*, 5766-5779.

[16] X. Chen, C. Jia, Z. Wan and X. Yao, Organic dyes with imidazole derivatives as auxiliary donors for dye-sensitized solar cells: Experimental and theoretical investigation. *Dyes Pigm.*, **2014**, *104*, 48-56.

[17] L. Zhou, C. Jia, Z. Wan, X. Chen and X. Yao, Effect of imidazole derivatives in triphenylamine-based organic dyes for dye-sensitized solar cells. *Org. Electron.*, **2013**, *14*, 1755-1762.

[18] C.-H. Yang, S.-H. Liao, Y.-K. Sun, Y.-Y. Chuang, T.-L. Wang, Y.-T. Shieh and W.-C. Lin, Optimization of multiple electron donor and acceptor in carbazole-triphenylamine-based molecules for application of dye-sensitized solar cells. *J. Phys. Chem. C*, **2010**, *114*, 21786-21794.

[19] C.-H. Yang, H.-L. Chen, Y.-Y. Chuang, C.-G. Wu, C.-P. Chen, S.-H. Liao and T.-L. Wang, Characteristics of triphenylamine-based dyes with multiple acceptors in application of dye-sensitized solar cells. *J. Power Sources*, **2009**, *188*, 627-634.

[20] T. Khanasa, N. Jantasing, S. Morada, N. Leesakul, R. Tarsang, S. Namuangruk, T. Kaewin, S. Jungsuttiwong, T. Sudyoadsuk and V. Promarak, Synthesis and characterization of D-D-π-A-type organic dyes bearing bis(3,6-di-*tert*-butylcarbazol-9-ylphenyl)aniline as donor moiety for dye-sensitized solar cells. *Eur. J. Org. Chem.*, **2013**, 2608-2620.

[21] Q. Chai, W. Li, S. Zhu, Q. Zhang and W. Zhu, Influence of Donor Configurations on Photophysical, Electrochemical, and photovoltaic performances in D-π-A organic sensitizers, *ACS Sustainable Chem. Eng.*, **2014**, *2*, 239-247.

[22] H. Choi, M. Shin, K. Song, M.-S. Kang, Y. Kang and J. Ko, The impact of an indeno[1,2-*b*]thiophene spacer on dye-sensitized solar cell performances of cyclic thiourea functionalized organic sensitizers. *J. Mater. Chem. A*, **2014**, *2*, 12931-12939.

[23] L. Zhou, C. Jia, Z. Wan, Z. Li, J. Bai, L. Zhang, J. Zhang and X. Yao, Triphenylamine-based organic dyes containing benzimidazole derivatives for dye-sensitized solar cells. *Dyes Pigm.*, **2012**, *95*, 743-750.

[24] L. Zani, G. Reginato, A. Mordini, M. Calamante, M. Peruzzini, M. Taddeib, A. Sinicropi, M. L. Parisi, F. F. de Biani, R. Basosi, A. Cavallaro and M. Bruzz, An unusual thiazolo[5,4-*d*]thiazole sensitizer for dye-sensitized solar cells. *Tetrahedron Lett.*, **2013**, *54*, 3944-3948.

[25] M.-D. Zhang, H. Pan, X.-H. Ju, Y.-J. Ji, L. Qin, H.-G. Zheng and X.-F. Zhou, Improvement of dye-sensitized solar cells' performance through introducing suitable heterocyclic groups to triarylamine dyes. *Phys. Chem. Chem. Phys.*, **2012**, *14*, 2809-2815.

[26] M.-D. Zhang, H.-X. Xie, X.-H. Ju, L. Qin, Q.-X. Yang, H.-G. Zheng and X.-F. Zhou, D-D-π-A organic dyes containing 4,4'-di(2-thienyl)-triphenylamine moiety for efficient dye-sensitized solar cells. *Phys. Chem. Chem. Phys.*, **2013**, *15*, 634-641.

[27] J. Mao, N. He, Z. Ning, Q. Zhang, F. Guo, L. Chen, W. Wu, J. Hua and H. Tian, Stable dyes containing double acceptors without cooh as anchors for highly efficient dye-sensitized solar cells. *Angew. Chem. Int. Ed.*, **2012**, *51*, 9873-9876.

[28] D. P. Hagberg, T. Marinado, K. M. Karlsson, K. Nonomura, P. Qin, G. Boschloo, T. Brinck, A. Hagfeldt and L. Sun, Tuning the HOMO and LUMO energy levels of organic chromophores for dye sensitized solar cells. *J. Org. Chem.*, **2007**, *72*, 9550-9556.

[29] K. D. Seo, B. S. You, I. T. Choi, M. J. Ju, M. You, H. S. Kang and H. K. Kim, Dye-sensitized solar cells based on organic dual-channel anchorable dyes with well-defined core bridge structures. *ChemSusChem*, **2013**, *6*, 2069-2073.

[30] K. R. J. Thomas, Y.-C. Hsu, J. T. Lin, K.-M. Lee, K.-C. Ho, C.-H. Lai, Y.-M. Cheng and P.-T. Chou, 2,3-Disubstituted thiophene based organic dyes for solar cells. *Chem. Mater.*, **2008**, *20*, 1830-1840.

[31] H. Shang, Y. Luo, X. Guo, X. Huang, X. Zhan, K. Jiang and Q. Meng, The effect of anchoring group number on the performance of dye-sensitized solar cells. *Dyes Pigm.*, **2010**, *87*, 249-256.

[32] R. Li, J. Liu, N. Cai, M. Zhang and P. Wang, Synchronously reduced surface states, charge recombination, and light absorption length for high-performance organic dye-sensitized solar cells. *J. Phys. Chem. B*, **2010**, *114*, 4461-4464.

[33] X. Cheng, S. Sun, M. Liang, Y. Shi, Z. Sun and S. Xue, Organic dyes incorporating the cyclopentadithiophene moiety for efficient dye-sensitized solar cells. *Dyes Pigm.*, **2012**, *92*, 1292-1299.

[34] A. Gupta, M. M. A. Kelson, V. Armel, A. Bilic and S. V. Bhosale, N-Alkyl- and N-aryl-dithieno[3,2-*b*:2',3'-*d*]pyrrole-containing organic dyes for efficient dye-sensitized solar cells. *Tetrahedron*, **2014**, *70*, 2141-2150.

[35] N. Cai, J. Zhang, M. Xu, M. Zhang and P. Wang, Improving the photovoltage of dithienopyrrole dyesensitized solar cells via attaching the bulky bis(octyloxy) biphenyl moiety to the conjugated π-linker. *Adv. Funct. Mater.*, **2013**, *23*, 3539-3547.

[36] W. Ying, J. Yang, M. Wielopolski, T. Moehl, J.-E. Moser, P. Comte, J. Hua, S. M. Zakeeruddin, H. Tian and M. Grätzel, New pyrido[3,4-*b*]pyrazine-based sensitizers for efficient and stable dye-sensitized solar cells. *Chem. Sci.*, **2014**, *5*, 206-214.

[37] L.-Y. Lin, C.-H. Tsai, K.-T. Wong, T.-W. Huang, L. Hsieh, S.-H. Liu, H.-W. Lin, C.-C. Wu, S.-H. Chou, S.-H. Chen and A.-I Tsai, Organic dyes containing coplanar diphenyl-substituted dithienosilole core for efficient dye-sensitized solar cells. *J. Org. Chem.*, **2010**, *75*, 4778-4785.

[38] M. Cheng, X. Yang, F. Zhang, J. Zhao and L. Sun, Tuning the HOMO and LUMO energy levels of organic dyes with N‑Carboxomethylpyridinium as acceptor to optimize the efficiency of dye-sensitized solar cells. *J. Phys. Chem. C*, **2013**, *117*, 9076-9083.

[39] M. Katono, M. Wielopolski, M. Marszalek, T. Bessho, J.-E. Moser, R. Humphry-Baker, S. M. Zakeeruddin and M. Grätzel, Effect of extended π-conjugation of the donor structure of organic D-A-π-A dyes on the photovoltaic performance of dye-sensitized solar cells. *J. Phys. Chem. C*, **2014**, *118*, 16486-16493.

[40] J. Zhao, X. Yang, M. Cheng, S. Li, X. Wang and L. Sun, Highly efficient iso-quinoline cationic organic dyes without vinyl groups for dye-sensitized solar cells. *J. Mater. Chem. A*, **2013**, *1*, 2441-2446.

[41] L. E. Polander, A. Yella, J. Teuscher, R. Humphry-Baker, B. F. E. Curchod, N. A. Astani, P. Gao, J.-E. Moser, I. Tavernelli, U. Rothlisberger, M. Grätzel, M. Khaja Nazeeruddin and J. Frey, Unravelling the potential for dithienopyrrole sensitizers in dyesensitized solar cells. *Chem. Mater.*, **2013**, *25*, 2642-2648.

[42] J. F. Hartwig, Transition metal catalyzed synthesis of arylamines and aryl ethers from aryl halides and triflates: Scope and mechanism. *Angew. Chem., Int. Ed.*, **1998**, *37*, 2046-2067.

[43] N. Miyaura and A. Suzuki, Palladium-catalyzed cross-coupling reactions of organoboron compounds. *Chem. Rev.*, **1995**, *95*, 2457.

[44] J. K. Stille, The palladium-catalyzed cross-coupling reactions of organotin reagents with organic electrophiles. *Angew. Chem. Int. Ed.*, **1986**, *25*, 508-524.

[45] G. Evano, N. Blanchard and M. Toumi, Copper-mediated coupling reactions and their applications in natural products and designed biomolecules synthesis. *Chem. Rev.*, **2008**, *108*, 3054-3131.

[46] M. Holzapfel and C. Lambert, Photoinduced charge separation and recombination in acridine-triarylamine-based redox cascades. *J. Phys. Chem. C*, **2008**, *112*, 1227-1243.

[47] A. W. Freeman, M. Urvoy and M. E. Criswell, Triphenylphosphine-mediated reductive cyclization of 2-nitrobiphenyls: A practical and convenient synthesis of carbazoles. *J. Org. Chem.*, **2005**, *70*, 5014-5019.

[48] Y. Che, D. E. Gross, H. Huang, D. Yang, X. Yang, E. Discekici, Z. Xue, H. Zhao, J. S. Moore and L. Zang, Diffusion-controlled detection of trinitrotoluene: Interior nanoporous structure and low highest occupied molecular orbital level of building blocks enhance selectivity and sensitivity. *J. Am. Chem. Soc.*, **2012**, *134*, 4978-4982.

[49] E. Knoevenagel, Ueber eine darstellungsweise des benzylidenacetessigesters. *Chem. Ber.*, **1896**, *29*, 172-174.

[50] A. Mishra, N. Pootrakulchote, M. Wang, S.-J. Moon, S. M. Zakeeruddin, M. Grätzel and P. Bäuerle, A thiophene-based anchoring ligand and its heteroleptic Ru(II)-complex for efficient thin-film dye-sensitized solar cells. *Adv. Funct. Mater.*, **2011**, *21*, 963-970.

[51] M. K. Nazeeruddin, A. Kay, I. Rodicio, R. Humphry-Baker, E. Müller, P. Liska, N. Vlachopoulos and M. Grätzel, Conversion of light to electricity by cis-X2bis(2,2′-bipyridyl-4,4′-dicarboxylate)-ruthenium(II) charge-transfer sensitizers (X = Cl^-, Br^-, I^-, CN^-, and SCN^-) on nanocrystalline titanium dioxide electrodes. *J. Am. Chem. Soc.*, **1993**, *115*, 6382-6390.

[52] M. K. Nazeeruddin, P. Péchy, T. Renouard, S. M. Zakeeruddin, R. Humphry-Baker, P. Comte, P. Liska, L. Cevey, E. Costa, V. Shklover, L. Spiccia, G. B. Deacon, C. A. Bignozzi and M. Grätzel, Engineering of efficient panchromatic sensitizers for nanocrystalline TiO_2-based solar cells. *J. Am. Chem. Soc.*, **2001**, *123*, 1613-1624.

[53] M. K. Nazeeruddin, S. M. Zakeeruddin, R. Humphry-Baker, M. Jirousek, P. Liska, N. Vlachopoulos, V. hklover, C. H. Fisher and M. Grätzel, Acid-base equilibria of (2,2‘-bipyridyl-4,4‘-dicarboxylic acid)ruthenium(II) complexes and the effect of protonation on charge-transfer sensitization of nanocrystalline titania. *Inorg. Chem.*, **1999**, *38*, 6298-6305.

[54] Z.-S. Wang, F.-Y. Li and C.-H. Huang, photocurrent enhancement of hemicyanine dyes containing RSO_3-group through treating TiO_2 films with hydrochloric acid. *J. Phys. Chem. B*, **2001**, *105*, 9210-9217.

[55] P. Singh, A. Baheti and K. R. J. Thomas, Synthesis and optical properties of acidochromic amine-substituted benzo[*a*]phenazines. *J. Org. Chem.*, **2011**, *76*, 6134-6145.

[56] A. Baheti, P. Tyagi, K. R. J. Thomas, Y.-C. Hsu and J. T. Lin, Simple triarylamine-based dyes containing fluorene and biphenyl linkers for efficient dye-sensitized solar cells. *J. Phys. Chem. Lett*., **2009**, *113*, 8541-8547.

[57] O. van den Berg, W. F. Jager and S. J. Picken, 7-Dialkylamino-1-alkylquinolinium Salts: Highly versatile and stable fluorescent probes. *J. Org. Chem.*, **2006**, *71*, 2666-2676.

[58] A. Granzhan, H. Ihmels and G. Viola, 9-Donor-substituted acridizinium salts: Versatile environment-sensitive fluorophores for the detection of biomacromolecules. *J. Am. Chem. Soc*., **2007**, *129*, 1254-1267.

[59] C. Reichardt, Solvatochromic dyes as solvent polarity indicators. *Chem. Rev.*, **1994**, *94*, 2319.

[60] K. Sayama, S. Tsukagoshi, K. Hara, Y. Ohga, A. Shinpou, Y. Abe, S. Suga and H. Arakawa, Photoelectrochemical properties of J aggregates of benzothiazole merocyanine dyes on a nanostructured TiO_2 film. *J. Phys. Chem. B*, **2002**, *106*, 1363-1371.

[61] K. Rurack, J. L. Bricks, G. Reck, R. Radeglia and U. Resch-Genger, Chalcone-analogue dyes emitting in the near-infrared (NIR): Influence of donor-acceptor substitution and cation complexation on their spectroscopic properties and X-ray structure. *J. Phys. Chem. A*, **2000**, *104*, 3087-3109.

[62] J. A. Pollard, D. Zhang, J. A. Downing, F. J. Knorr and J. L. McHale, Solvent effects on interfacial electron transfer from Ru(4,4′-dicarboxylic acid-2,2′-bipyridine)$_2$(NCS)$_2$ to nanoparticulate TiO_2: Spectroscopy and solar photoconversion. *J. Phys. Chem. A*, **2005**, *109*, 11443-11452.

[63] M. J. Frisch, G. W. Trucks, H. B. Schlegel, G. E. Scuseria, M. A. Robb, J. R. Cheeseman, G. Scalmani, V. Barone, B. Mennucci, G. A. Petersson, H. Nakatsuji, M. Caricato, X. Li, H. P. Hratchian, A. F. Izmaylov, J. Bloino, G. Zheng, J. L. Sonnenberg, M. Hada, M. Ehara, K. Toyota, R. Fukuda, J. Hasegawa, M. Ishida, T. Nakajima, Y. Honda, O. Kitao, H. Nakai, T. Vreven, J. A. Montgomery, J. E. Peralta, F. Ogliaro, M. Bearpark, J. J. Heyd, E. Brothers, K. N. Kudin, V. N. Staroverov, R. Kobayashi, J. Normand, K. Raghavachari, A. Rendell, J. C. Burant, S. S. Iyengar, J. Tomasi, M. Cossi, N. Rega, N. J. Millam, M. Klene, J. E. Knox, J. B. Cross, V. Bakken, C. Adamo, J. Jaramillo, R. Gomperts, R. E. Stratmann, O. Yazyev, A. J. Austin, R. Cammi, C. Pomelli, J. W. Ochterski, R. L. Martin, K. Morokuma, V. G. Zakrzewski, G. A. Voth, P. Salvador, J. J. Dannenberg, S. Dapprich, A. D. Daniels, O. Farkas, J. B. Foresman, J. V. Ortiz, J. Cioslowski and D. J. Fox, Gaussian 09, Revision A.02, Gaussian, Inc.: Wallingford, CT, **2009**.

[64] R. G. Parr and W. Yang, Density-functional theory of the electronic structure of molecules. *Annu. Rev. Phys. Chem.*, **1995**, *46*, 701-728.

[65] B. J. Lynch, P. L. Fast, M. Harris and D. G. Truhlar, Adiabatic connection for kinetics. *J. Phys. Chem. A*, **2000**, *104*, 4811-4815.

[66] M. Grätzel, Photoelectrochemical cells. *Nature*, **2001**, *414*, 338-344.

[67] A. Hagfeldt, G. Boschloo, L. Sun, L. Kloo and H. Pettersson, Dye-sensitized solar cells. *Chem. Rev.*, **2010**, *110*, 6595-6663.

[68] B. O'Regan and M. Grätzel, A low-cost, high-efficiency solar cell based on dye-sensitized colloidal TiO_2 films. *Nature*, **1991**, *353*, 737-740.

[69] J. van de Lagemaat, N.-G. Park and A. J. Frank, Influence of electrical potential distribution, charge transport, and recombination on the photopotential and photocurrent conversion efficiency of dye-sensitized nanocrystalline TiO_2 solar cells: A study by electrical impedance and optical modulation techniques. *J. Phys. Chem. B*, **2000**, *104*, 2044-2052.

[70] E. Ishow, A. Brosseau, G. Clavier, K. Nakatani, R. B. P., J.-J. Vachon, P. Tauc, D. Chauvat, C. R. Mendoncüa, and E. Piovesan, Two-photon fluorescent holographic rewritable micropatterning. *J. Am. Chem. Soc.*, **2007**, *129*, 8970-8971.

CHAPTER 6

Organic Dyes Containing Carbazole as Donor and π-Linker: Optical, Electrochemical, and Photovoltaic Properties

6.1 Introduction

Recombination of injected electrons with the oxidized dye or the triiodide ions (I_3^-) in electrolyte severely diminishes the photocurrent density and photo voltage in DSSC [1]. Aggregation of the dyes on the surface of the TiO_2 film is one of the main drawbacks of the organic dyes used as sensitizer in DSSC. This causes self-quenching of the excited electron resulting in the decrement of J_{SC} and recombination of the electrons which lowers V_{OC} [2-5]. The aggregation of the dyes can be minimized by incorporating bulky donor groups or hydrophobic groups such as alkyl groups on either donor [6-8] or linker [9-11] of the dye. Several organic dyes were designed to minimize aggregation and recombination of the electrons in DSSC. The promising methods to alleviate the dye aggregation on the TiO_2 film and charge recombination in the DSSC by designing star burst triarylamine based dyes and incorporation of the alkyl groups on the donor/linker part of the dye sensitizer.

Hara and co-workers [9] developed alkyl functionalized thiophene containing carbazole based dyes (**D20**-**D22**) to suppress the aggregation of the dyes on TiO_2 surface and enhance the electron life time by preventing the approach of I_3^- towards the TiO_2 layer. The hexyl functionalized dyes **D21** and **D22** showed high open circuit voltage of 750 mV and 690 mV, respectively than the parent dye **D20** (V_{OC} = 670 mV). This is attributed to the effective blocking of TiO_2 layer from I_3^- ions. Zhu and co-workers [12] also demonstrated that dyes contain hexyl groups on thiophene linker effectively suppressed the charge recombination, resulting in a decreased dark current and enhanced open-circuit voltage. The enhanced V_{OC} of the dyes **WS-6** (V_{OC} = 639 mV) and **WS-11** (V_{OC} = 629 mV) originating from hexyl group incorporated on the thiophene is effectively suppressing the charge recombination of electrons when compared to the parent dye **WS-2** (V_{OC} = 589 mV). Also, they specifically focused on critical effect of length of the alkyl group linked to the bridging carbon atoms of 4*H*-cyclopenta[2,1-*b*:3,4-*b*′]dithiophene (CPDT) on the photovoltaic performances [13]. Octyl-substituted **WS-39** showed a broader IPCE onset with an enhanced V_{OC} of 65 mV and exhibited an efficiency of 7.42% than the analogue **WS-5** (η = 5.23%, V_{OC} = 589 mV)**.** But, contrarily methyl substituted **WS-43** showed relatively low power conversion efficiency along with low photocurrent density due to short electron diffusion length with significant electron loss during the electron transport. The octyl unit of the **WS-39** dye exhibited dual role. It increased the propensity to prevent electron

recombination and efficiently retarded the charge recombination. Despite the high V_{OC} and efficiencies the stability of the dyes are lowered due to the degradation of hexyl unit on thiophene moiety.

Grätzel and co-workers [4] investigated the influence of phenyl incorporation in between the donor and acceptor. Though the absorption spectra of the phenyl incorporated dye, **BTP1**, is blue shifted, it inhibits the electron transfer and slows down recombination by 5 times when compared to the parent dye **BT1.** The phenyl incorporated dye **BTP1** effectively increased the V_{OC} by 151 mV and achieved an efficiency of 8.21% when compared to **BT1** (η = 5.23%). This indicates that the **BTP1** produced stable radical cation and the interruption of donor-acceptor interaction by phenyl unit inhibits the back electron transfer.

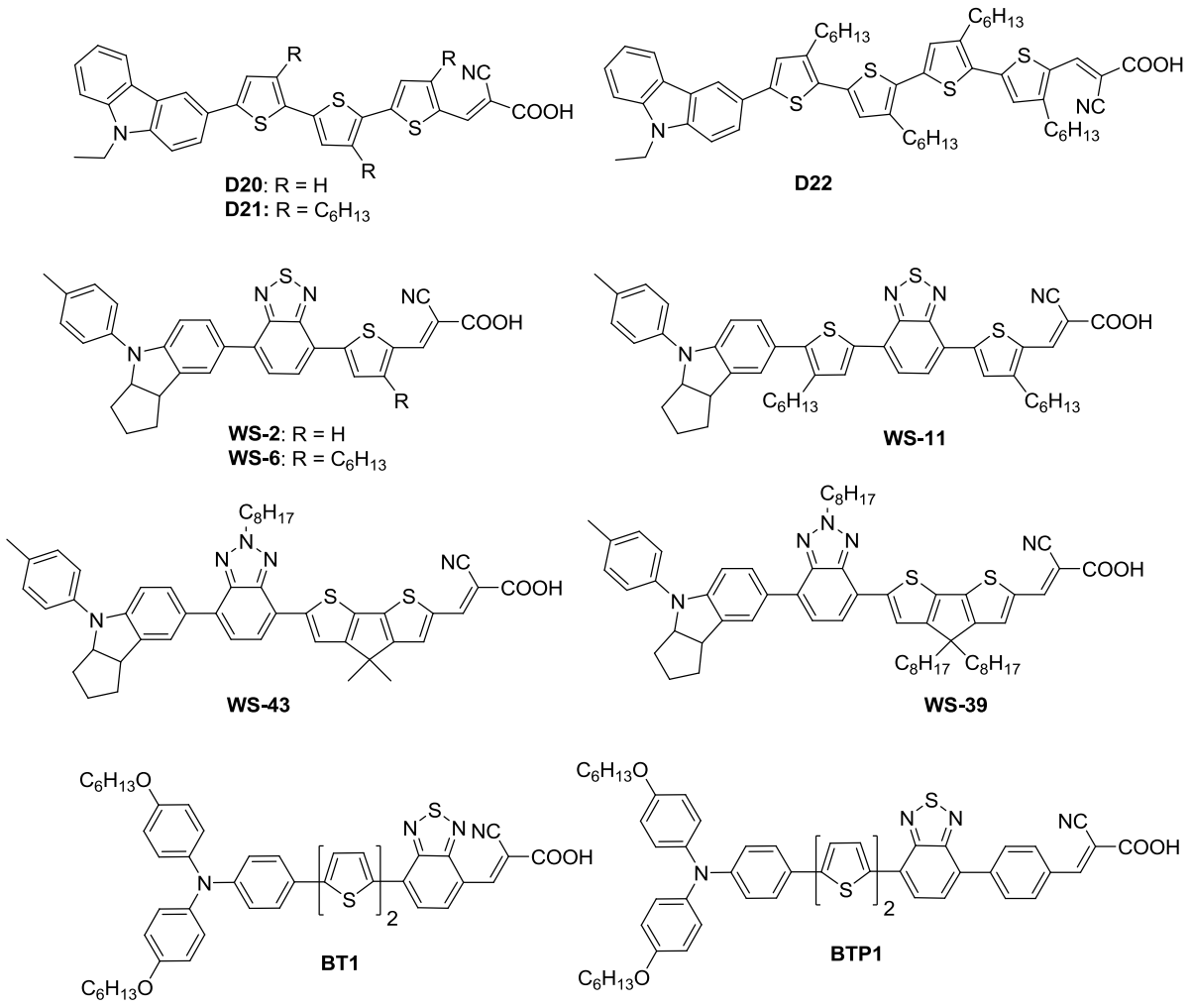

Chart 6.1 Structure of the dyes containing alkyl chains on linker to impede aggregation or to retard the recombination of electrons from TiO_2 to the redox electrolyte.

Ko and co-workers [14] developed novel organic sensitizers (**JK-72**, **JK-97** and **JK-98**) by incorporating a planar amine unit with long alkyl chains. The alkyl units on the donor enhanced the electron lifetime and effective spatial charge separation led to retardation of charge recombination. The long alkyl group present on the dye **JK-98** achieved higher efficiency of 8.71% than the parent dye **JK-72** (η = 7.87%, V_{OC} = 720 mV) due to higher V_{OC} (750 mV).

Table 6.1 Optical, electrochemical and photovoltaic performance parameters of known dyes

Dye	$\lambda_{max,}$ nm (ε_{max}, M^{-1} cm^{-1})	E_{ox}, V (*vs* NHE)	E_{ox}^{*}, V (*vs* NHE)	J_{SC} (mA cm^{-2})	V_{OC} (mV)	*ff*	η (%)	*Ref*
D19	485 (40100)	0.99	−0.78	10.56	670	0.63	4.46	[9]
D20	480 (38800)	1.07	−0.83	9.90	750	0.67	4.97	[9]
D21	480 (38400)	0.96	−0.89	10.67	690	0.68	5.01	[9]

Zhu and co-workers [15] developed indoline based dyes (**AD10** and **AC9**) containing alkyl functionalized carbazole and fluorene. The alkyl groups present on the carbazole and fluorene effectively prevent the molecular π-aggregation on the TiO_2 surface and led to improved electron life time and V_{OC} for the devices. Thus, the dyes **AD10** and **AC9** achieved power conversion efficiencies of 5.87% and 5.09% with high open circuit voltages of 628 mV and 614 mV, respectively.

Chow and co-workers [16] developed a series of dyes (**D15** and **C2-C6**) composed of 4-*tert*-butylphenyl group on carbazole donor. The *tert*-butylphenyl group increased the donor strength and also effectively suppressed the aggregation of the dyes. All the dyes exhibited V_{OC} in the range of 570 mV to 685 mV and a dye containing a bulky *tert*-butylphenylene-substituted carbazole donor achieved highest efficiency of 6.70%. In order to suppress the intermolecular aggregations, Chen and co-workers [17] developed dyes (**D13** and **D14**) containing newly designed *tert*-butyl phenyl attached at *N*-position of *tert*-butyl carbazole as donor. The *tert*-butyl groups present on the donor unit effectively impede the aggregation and dye **D14** achieved higher efficiency of 3.75% with V_{OC} of 660 mV.

Promarak and co-workers [18, 19] developed a series of dyes (**AD30-AD32** and **AD39-AD41**) by using 3,6-di(*tert*-butyl)carbazole as auxiliary donor and demonstrated that *tert*-butyl groups on the carbazole effectively suppress the intermolecular interactions and enhanced donating

strength of the carbazole. All the dyes showed high V_{OC} in the range of 700 mV to 830 mV and power conversion efficiencies are in the range of 3.52% to 5.12%. The impressive power conversion of the dyes by using the 3,6-di(*tert*-butyl)carbazole stands as good donor and effectively controlling the dye aggregation on the TiO_2 surface.

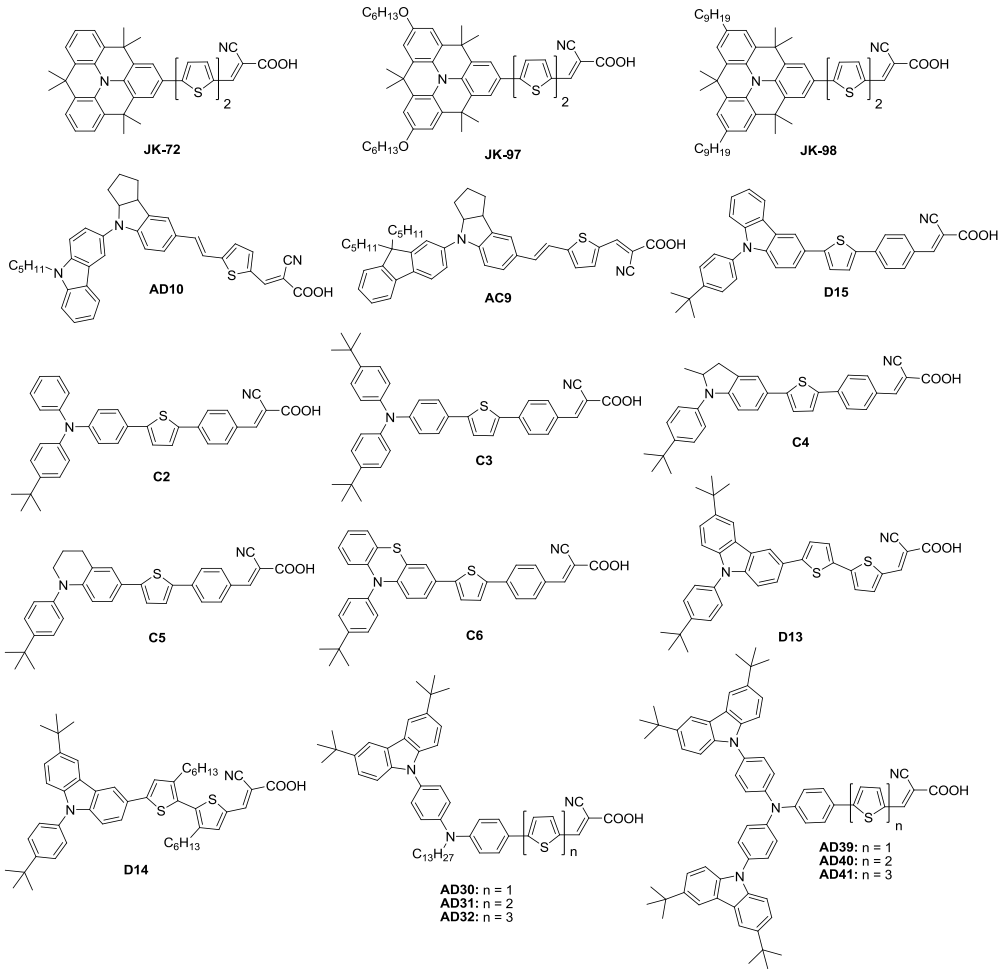

Chart 6.2 Structure of the reported dyes containing alkyl chains on donor unit to impede aggregation or retard the recombination of electrons from TiO_2 to the redox electrolyte.

Table 6.2 Optical, electrochemical and photovoltaic performance parameters of known dyes

Dye	$\lambda_{max,}$ nm (ε_{max}, M^{-1} cm^{-1})	E_{ox}, V (*vs* NHE)	E_{ox}^{*}, V (*vs* NHE)	J_{SC} (mA cm^{-2})	V_{OC} (mV)	*ff*	*η* (%)	*Ref*
WS-2	546 (20400)	0.67	−1.33	11.8	589	0.73	5.07	[12]
WS-6	547 (23500)	0.67	−1.39	14.3	639	0.75	6.85	[12]

Table 6.2 (cont.)

Dye	$\lambda_{max,}$ nm (ε_{max}, M^{-1} cm^{-1})	E_{ox}, V (*vs* NHE)	E_{ox}^{*}, V (*vs* NHE)	J_{SC} (mA cm^{-2})	V_{OC} (mV)	*ff*	η (%)	*Ref*
WS-11	557 (27500)	0.57	−1.28	10.4	629	0.71	4.64	[12]
WS-39	514 (40300)	0.74	−1.28	13.71	795	0.68	7.42	[13]
WS-43	514 (42600)	0.76	−1.21	11.38	730	0.63	5.23	[13]
BT1	570 (18900)	0.97	−0.63	3.40	489	0.74	1.24	[4]
BTP1	515 (29400)	0.88	−0.79	18.47	640	0.69	8.21	[4]
JK-72	455 (20369)	1.07	−1.25	15.20	0.72	0.72	7.87	[14]
JK-97	444 (20289)	1.00	−1.43	16.30	0.73	0.70	8.28	[14]
JK-98	463 (12614)	1.01	−1.28	16.80	0.75	0.70	8.71	[14]
AD10	523 (27900)	0.83	−1.11	14.16	628	0.66	5.87	[15]
AC9	504 (27200)	0.98	−1.05	12.28	614	0.68	5.09	[15]
D13	428 (40000)	0.91	−1.55	14.63	685	0.67	6.70	[16]
C2	433 (32600)	0.73	−1.76	13.32	660	0.61	5.43	[16]
C3	439 (34000)	0.69	−1.77	13.96	670	0.66	6.14	[16]
C4	460 (28900)	0.51	−1.77	12.60	630	0.61	4.87	[16]
C5	454 (26400)	0.54	−1.72	8.48	570	0.65	3.14	[16]
C6	446 (33900)	0.56	−1.83	14.12	680	0.64	6.32	[16]
D14	465 (47900)	1.33	−0.74	10.02	570	0.64	3.62	[17]
D15	417 (18500)	1.35	−0.77	9.44	660	0.63	3.75	[17]
AD15	457 (25174)	1.07	−1.24	7.19	730	0.67	3.52	[18]
AD16	463 (27460)	1.03	−1.23	8.88	700	0.66	4.10	[18]
AD17	472 (30102)	0.98	−1.26	10.89	700	0.67	5.12	[18]
AD25	458 (25225)	1.65	−0.60	7.53	720	0.69	3.70	[19]
AD26	455 (29322)	1.60	−0.61	9.02	710	0.68	4.34	[19]
AD27	464 (33926)	1.55	−0.58	9.98	700	0.67	4.62	[19]

na = not available

Carbazole is an efficient donor for dyes used in DSSC due to its electron rich functionality which can be further enhanced by substitution of alkyl or aryl groups at C3 and C4 positions [20, 21]. Particularly, in the dyes serving as sensitizers in DSSCs, carbazole has been either used as a

donor or as a π-linker [6, 22-24]. Also, the 3,6 di-substitution of carbazole inhibit the molecular aggregation on TiO_2 film due to its hydrophobic alkyl chains, bulky nature and twisted geometry [19, 27]. Suitable configuration of the dyes with 3,6-di-substituted carbazole as a donor serve as better candidates for DSSC application.

Sun and coworkers [28] designed and synthesized a set of dyes based on carbazole as donor at *N*-9 position and compared the optoelectronic properties with the dyes which contain triphenylamine as donor by using Br^-/Br_3^- as redox couple. Even though the absorption of **D68** is inferior compared to **C27**, the former dye showed higher conversion efficiency of 3.68% compared to **C27** dye (2.65%) due to the higher V_{OC} originating due to the minimized intermolecular interactions attributable to the carbazole donor [20]. However, the incorporation of *tert*-butyl groups on 3 and 6 positions of carbazole on **D68** resulted in dye **D69,** which achieved higher efficiency of 4.05% due to better light absorption ensured by electron richness of the carbazole donor. Zafer and coworkers [22] introduced oligothiophene units as π-linker in **D69** to obtain dye **D70** and **D71** and they generated in DSSC larger J_{SC} when compared to parent dye **D69**. This observation speculated that the oligothiophenes are necessary for good light harvesting properties in carbazole-based dyes. Su and coworkers [29] incorporated thiophene units and synthesized dyes (**D94**-**D96**), and later used a dendritic donor containing peripheral and bridging carbazole by incorporation of carbazole on 3 and 6 position of carbazole to obtain a dye **D97**. The introduction of oligothiophenes increased the absorption properties while the dendritic donor increased the molar extinction coefficients and suppressed the intermolecular interactions resulting in high J_{SC} and V_{OC} led to reasonable power conversion efficiency of 4.86%.

Promarak and coworkers [27] introduced carbazole as π-linker substituted at 3 and 6 positions instead of phenyl linker and 3,6-di-*tert*-butyl-carbazole as donor and synthesized dyes **DL13**-**DL15** and **DL17**. These dyes possess red shifted absorption when compared to the phenyl linked dyes (**D70** and **D71**) and resulted in higher light harvesting parameters. The dye **DL15** has achieved higher conversion efficiency of 5.69% due to larger J_{SC} value (11.31 mA cm^{-2}). All the dyes showed impressive V_{OC} values > 700 mV due to the presence of bulky 3,6-di-*tert*-butyl-carbazole and hydrophobic *tert*-butyl groups on carbazole minimized the intermolecular interactions. These observations suggested that the carbazole served as efficient π-linker and donor.

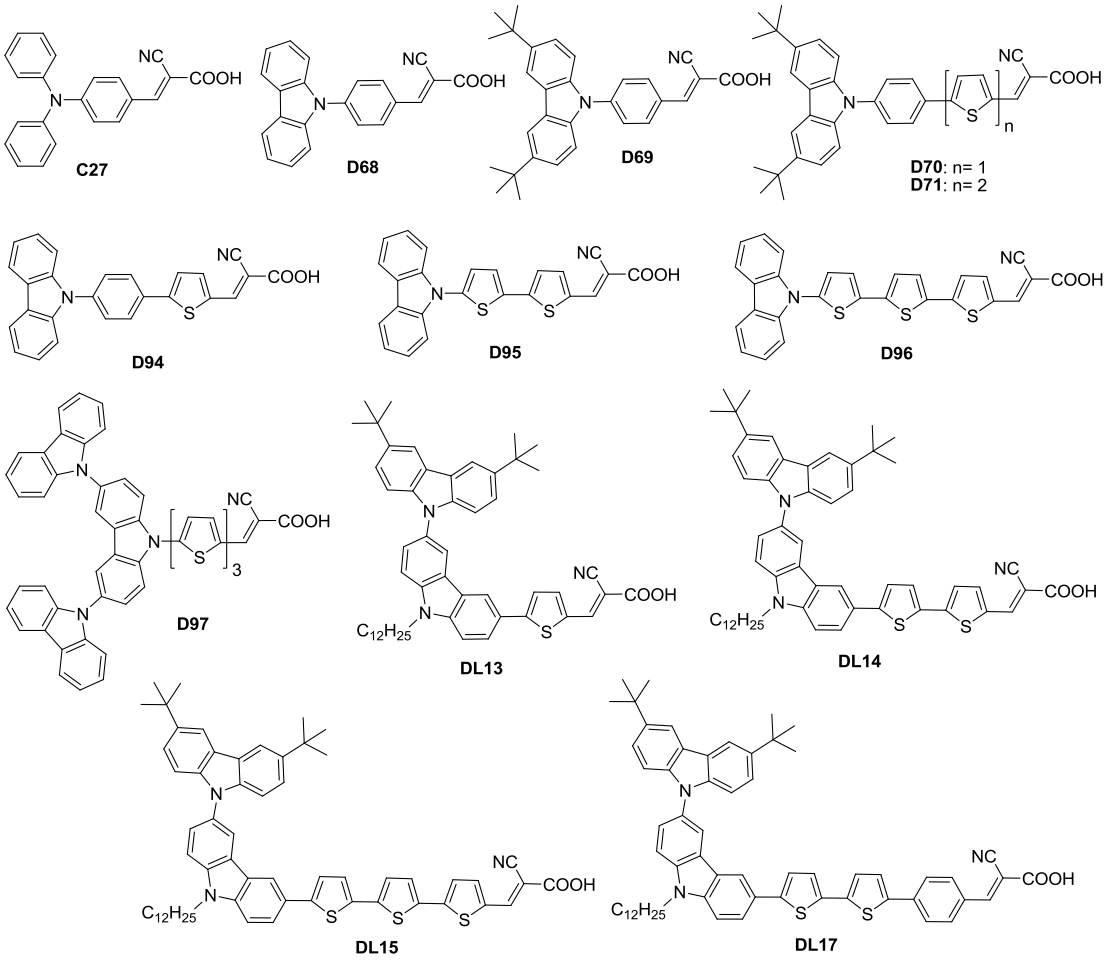

Chart 6.3 Structure of the reported dyes containing carbazole as donor and/or π-linker.

Table 6.3 Optical, electrochemical and photovoltaic performance parameters of dyes known in literature

Dye	$\lambda_{max,}$ nm (ε_{max}, M^{-1} cm^{-1})	E_{ox}, V (*vs* NHE)	E_{ox}^{*}, V (*vs* NHE)	J_{SC} (mA cm^{-2})	V_{OC} (mV)	*ff*	η (%)	*Ref*
C27	381 (10700)	1.33	−1.30	3.73	946	0.75	2.65	[12]
D68	374 (12300)	1.59	−1.09	4.00	1156	0.80	3.68	[21]
D69	381 (7800)	1.46	−1.35	4.71	1091	0.79	4.05	[21]
D70	438 (71000)	1.55	−0.89	8.47	470	0.60	2.39	[14]

Table 6.4 Optical, electrochemical and photovoltaic performance parameters of dyes known in literature

Dye	$\lambda_{max,}$ nm (ε_{max}, M^{-1} cm^{-1})	E_{ox}, V (*vs* NHE)	E_{ox}^{*}, V (*vs* NHE)	J_{SC} (mA cm^{-2})	V_{OC} (mV)	*ff*	η (%)	*Ref*
D71	468 (73200)	1.55	−0.78	10.90	400	0.57	2.48	[14]
D94	416 (8700)	0.74	−1.82	6.17	601	0.74	2.74	[22]
D95	440 (8700)	0.80	−1.58	6.70	589	0.74	2.94	[22]
D96	467 (17300)	0.65	−1.64	9.98	586	0.74	4.30	[22]
D97	465 (34600)	0.67	−1.63	10.65	643	0.71	4.86	[22]
DL13	433 (21952)	0.99	−1.42	7.35	740	0.67	3.64	[20]
DL14	457 (23492)	0.95	−1.27	9.70	730	0.68	4.80	[20]
DL15	443 (27938)	0.85	−1.30	11.31	710	0.71	5.69	[20]
DL17	487 (21037)	0.88	−0.92	9.98	700	0.67	4.62	[20]

Keeping all this in mind, we have designed and synthesized a series of metal free organic dyes (Chart 6.4) containing carbazole as a donor and π-linker due to the excellent optical properties offered by carbazole-based dyes. Introduction of carbazole/3,6-di-*tert*-butyl-carbazole instead of diphenylamine as a donor raise the LUMO level of the dyes which is essential for increasing the thermodynamic driving force for injection of electron into the conduction band of the TiO_2. Bulky 3,6-di-*tert*-butyl-carbazole end groups retard the π-π stacking interaction of the molecules and improve the V_{OC} of the DSSC based on these dyes. We have studied the effect of substituent variation on the carbazole nucleus as well as the nature of the conjugation bridge on the optical and electrochemical properties. We found that, despite the presence of two carbazole units, additional phenyl/electron-rich thiophene groups were necessary to enhance the functional properties such as optical absorption and redox potentials of this class of dyes. Introduction of electron-rich segments in the conjugation pathway raises the HOMO and LUMO energy and facilitate the regeneration of the dye and electron-injection from the photo-excited dye into the conduction band of TiO_2 [30].

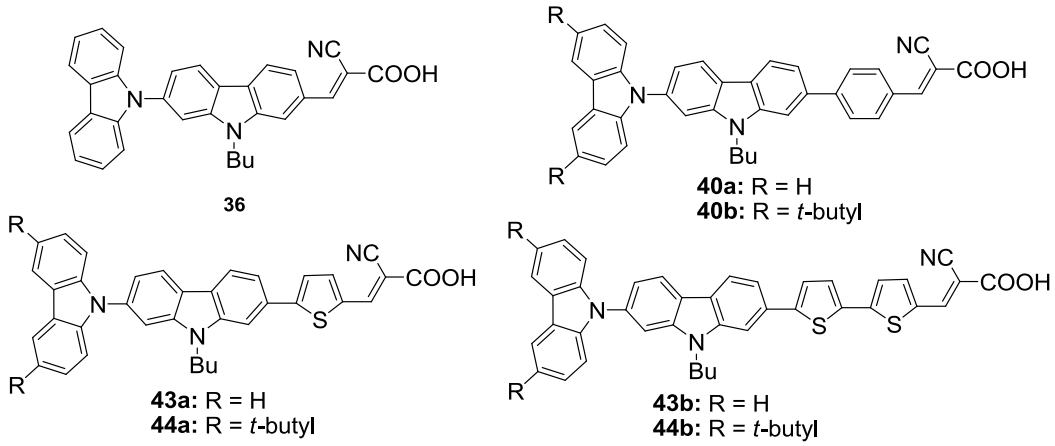

Chart 6.4 Structure of the newly developed organic dyes based on carbazole donor and π-linker.

6.2 Results and Discussion

6.2.1 Synthesis and Characterization

The synthetic approach used to prepare the new carbazole-containing dyes is outlined in Scheme 6.1. The compounds **38a** and **38b** were synthesized by an Ullmann-type coupling [31] of 9*H*-carbazole (**37a**) or 3,6-di-*tert*-butyl-9*H*-carbazole [32] (**37b**) with 2,7-dibromo-9-butyl-9*H*-carbazole [33, 34] (**1**) in DMF in the presence of CuI, 1,10-phenanthroline and K_2CO_3. Suzuki coupling [35] of resulting bromo derivatives (**38a** and **38b)** with 4-formylphenylboronic acid gave carbazole substituted aryl aldehydes (**39a**-**39b**) in good yields. Another set of aldehyde precursors (**41a-41b** and **42a-42b**) were prepared in moderate yield by Stille coupling reaction [36] between the bromo derivatives (**38a** and **38b**) and the tin reagents of the suitably protected heteoaryl aldehydes and followed by acidic hydrolysis. The dye **36** was prepared by a three step reaction pathway. The required aldehyde, 7-bromo-9-butyl-9*H*-carbazole-2-carbaldehyde (**8**) was prepared from **1** by lithiation with *n*-butyl lithium followed by quenching with DMF and subsequent acidic hydrolysis. The aldehyde **35** was synthesized by Ullmann-type reaction [31] of **8** with 9*H*-carbazole (**37a**). Finally, the aldehydes (**35, 39**, **41** and **42**) were converted to the corresponding dyes (**36, 40**, **43** and **44**) in good yields by Knoevenagel condensation reaction [37] with cyanoacetic acid in acetic acid. The dyes are red in color and moderately soluble in DCM, $CHCl_3$, TOL, THF, DMF and ACN. The dyes were thoroughly characterized by IR, NMR and mass spectral methods and the observed parameters are consistent with the proposed structures.

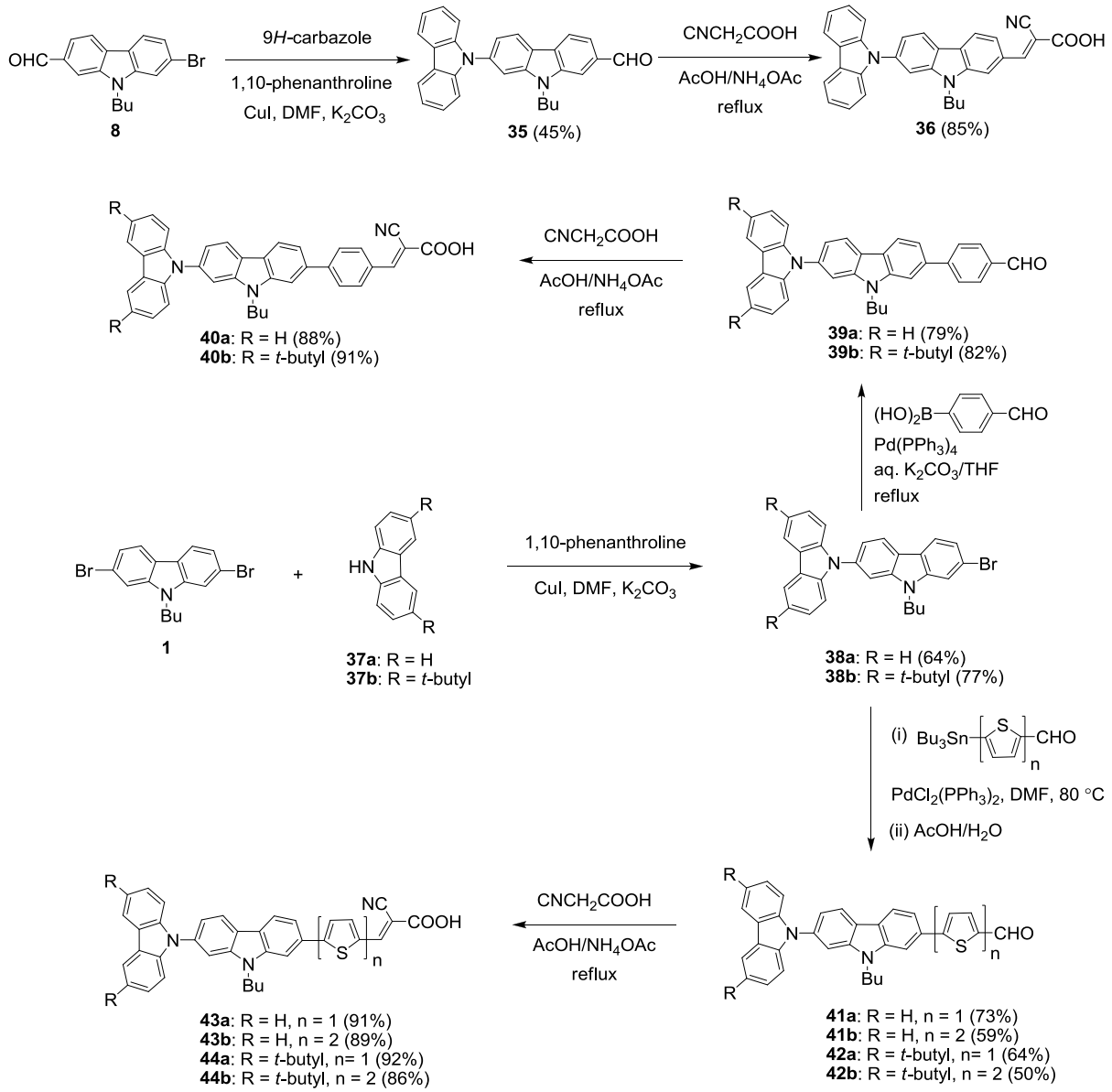

Scheme 6.1 Synthetic route to organic dyes based on carbazole as donor and π-linker.

6.2.2 X-ray Crystallographic Characterization

The crystals of the compound **41a** were obtained from toluene/chloroform mixture at room temperature by allowing for slow evaporation. The structure of the aldehyde **41a** was confirmed by single crystal X-ray diffraction studies. The ORTEP plot of **41a** is shown in Figure 6.1.

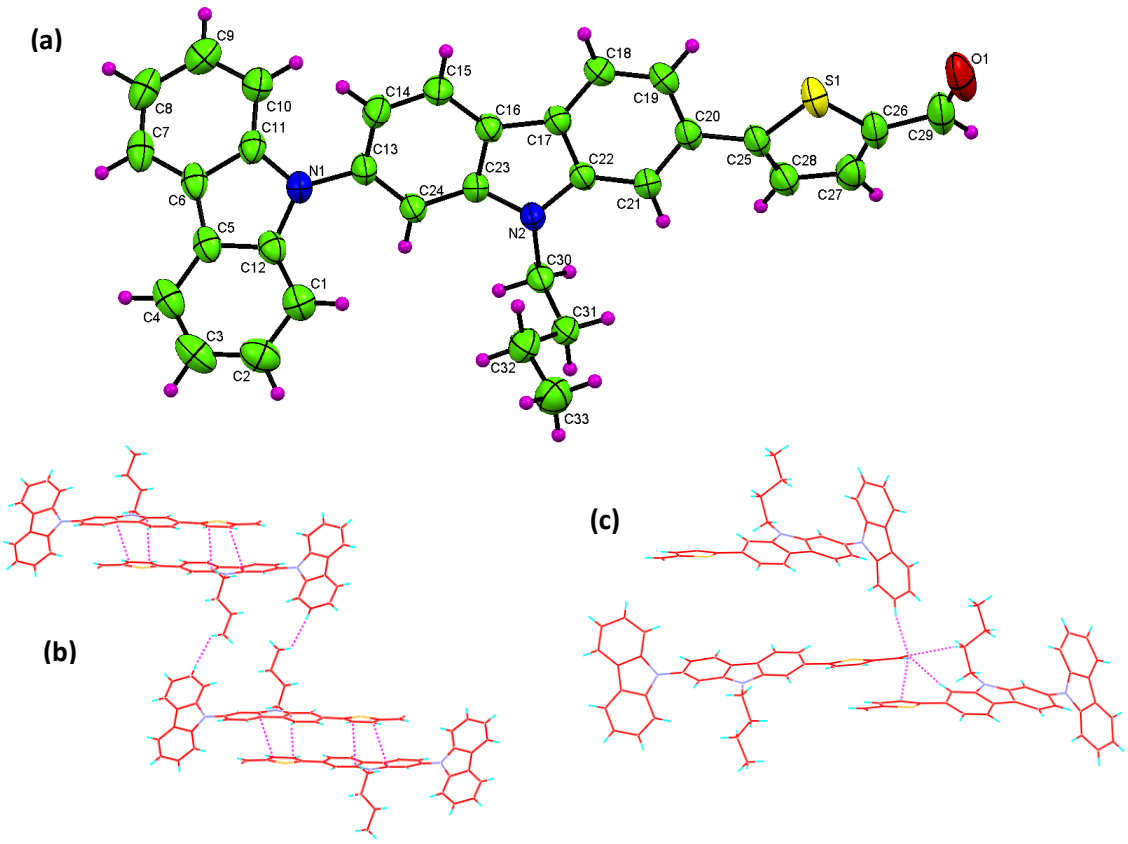

Figure 6.1 ORTEP plot (50% thermal ellipsoids) of the compound **41a.**

The compound **41a** crystallizes in the monoclinic crystal system with P-2_1/c space group. The molecule adopts a non-coplanar geometry in such a way the carbazole and thiophene units are twisted from one another with wide torsion angles. The terminal and bridging carbazole units are tilted from one another with an inter-planar angle of 47.49°. The bridging carbazole and thiophene units also deviated from planarity albeit with a smaller inter-planar angle of 22.13°. This non-planar structural arrangement of aromatic π-systems in the conjugation pathway of the dye may be beneficial for the effective charge separation in the excited state [38] and to prevent the aggregation of the dyes at the surface of TiO_2 due to the overall twisted molecular structure [9]. Organic dyes with tilted π-linkers generally displayed enhanced efficiency in the DSSC despite possessing shorter wavelength absorption [40]. There are different types of interactions observed as shown in Figure 6.1. The electron cloud of carbazole interacts with thiophene unit of other molecule (Figure 6.1 (b)) and resulted in head to tail dimer arrangement.

Table 6.5 Crystal data and structure refinement parameters for **41a**

Identification code	**41a**
Empirical formula	C_{33} H_{26} N_2 O S
Formula weight	498.62
Temperature	298(2) K
Wavelength	0.71073 Å
Crystal system, space group	Monoclinic, P2(1)/c
Unit cell dimensions	a = 16.9193(8) Å alpha = 90 deg. b = 10.2687(5) Å beta = 90.055(2) deg. c = 14.6199(6) Å gamma = 90 deg.
Volume	2540.0(2) $Å^3$
Z, Calculated density	4, 1.304 Mg/m^3
Absorption coefficient	0.157 mm^{-1}
F(000)	1048
Crystal size	0.35 x 0.22 x 0.15 mm
Theta range for data collection	1.20 to 28.35 deg.
Limiting indices	-22<=h<=21, -10<=k<=13, -19<=l<=14
Reflections collected / unique	18066 / 6153 [R(int) = 0.0218]
Completeness to theta	25.00 98.9 %
Absorption correction	Multi-scan
Max. and min. transmission	0.9768 and 0.9470
Refinement method	Full-matrix least-squares on F^2
Data / restraints / parameters	6153 / 0 / 335
Goodness-of-fit on F^2	1.031
Final R indices [I>2sigma(I)]	R_1 = 0.0448, wR_2 = 0.1200
R indices (all data)	R_1 = 0.0762, wR_2 = 0.1441
Largest diff. peak and hole	0.285 and -0.343 e.$Å^{-3}$

Table 6.6 Atomic coordinates (x 10^4) and equivalent isotropic displacement parameters (A^2 x 10^3) for **41a**. U(eq) is defined as one third of the trace of the orthogonalized Uij tensor.

Atom	x	y	z	U(eq)
C(1)	5338(1)	10989(2)	7971(1)	54(1)
C(2)	4629(1)	11654(2)	8004(2)	62(1)
C(3)	4333(1)	12151(2)	8816(2)	65(1)
C(4)	4742(1)	12011(2)	9618(2)	55(1)
C(5)	5472(1)	11375(2)	9606(1)	45(1)
C(6)	6044(1)	11086(2)	10304(1)	45(1)
C(7)	6097(1)	11364(2)	11236(1)	55(1)
C(8)	6752(1)	10980(2)	11715(1)	60(1)
C(9)	7366(1)	10320(2)	11279(1)	61(1)
C(10)	7335(1)	10034(2)	10359(1)	54(1)
C(11)	6664(1)	10406(2)	9878(1)	44(1)
C(12)	5755(1)	10868(2)	8779(1)	44(1)
C(13)	6965(1)	9600(2)	8300(1)	43(1)
C(14)	7268(1)	8366(2)	8516(1)	50(1)
C(15)	7775(1)	7729(2)	7933(1)	47(1)
C(16)	7971(1)	8315(2)	7101(1)	38(1)
C(17)	8494(1)	7979(2)	6356(1)	39(1)
C(18)	9029(1)	6973(2)	6200(1)	47(1)
C(19)	9482(1)	6995(2)	5417(1)	48(1)
C(20)	9421(1)	8009(2)	4775(1)	42(1)
C(21)	8882(1)	9014(2)	4919(1)	41(1)
C(22)	8432(1)	8995(2)	5712(1)	39(1)
C(23)	7633(1)	9531(2)	6873(1)	38(1)
C(24)	7138(1)	10191(2)	7477(1)	41(1)
C(25)	9929(1)	8068(2)	3959(1)	43(1)
C(26)	10830(1)	7582(2)	2677(1)	52(1)
C(27)	10651(1)	8873(2)	2742(1)	56(1)
C(28)	10138(1)	9153(2)	3465(1)	51(1)
C(29)	11329(1)	6966(3)	2000(1)	65(1)
C(30)	7717(1)	11136(2)	5550(1)	44(1)
C(31)	7176(1)	10945(2)	4738(1)	49(1)
C(32)	6388(1)	10344(2)	4959(1)	55(1)
C(33)	5890(1)	10101(2)	4116(1)	68(1)
N(1)	6483(1)	10254(2)	8951(1)	46(1)
N(2)	7906(1)	9921(1)	6024(1)	40(1)
O(1)	11458(1)	5810(2)	1945(1)	81(1)
S(1)	10366(1)	6692(1)	3515(1)	56(1)

6.2.4 Photophysical Properties

The photophysical behavior of the organic dyes (**36**, **40**, **43**, and **44**) was analyzed by recording absorption and fluorescence spectra in five different solvents, e.g., DCM, Tol, THF, $CHCl_3$, DMF and ACN. The pertinent data are compiled in Tables 6.7 and 6.10 and the absorption spectra recorded for DCM solutions are displayed in Figure 6.2. In order to understand the origin of absorption in these dyes, the absorption spectra of the precursor compounds were also measured.

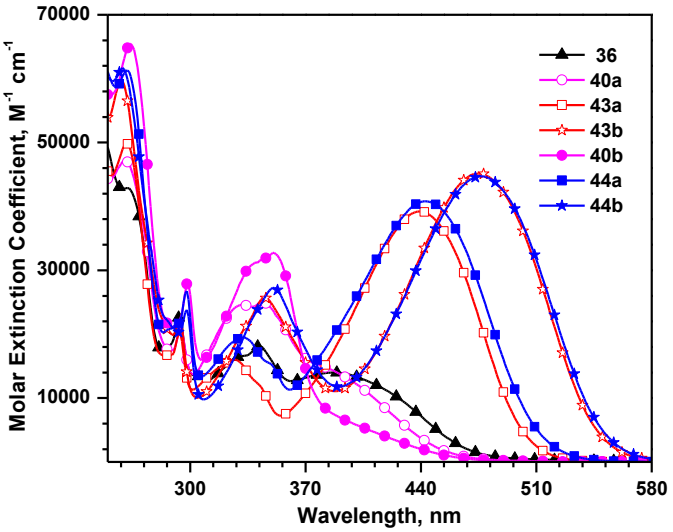

Figure 6.2 Absorption spectra of the dyes recorded in DCM.

All the dyes show four prominent absorption peaks in the range from 250-550 nm (Figure 6.2). The absorption peaks appearing below 360 nm are either originating from localized π-π* transitions or n-π* transitions. The lower energy transition showing absorption maximum above 380 nm corresponds to the charge transfer from the carbazole donor to the cyanoacrylic acid acceptor unit. This band progressively shifted to the longer wavelength region and exhibited enhancement in the molar extinction coefficient on introduction of additional thiophene units in the conjugation pathway. This probably suggests that the charge transfer from carbazole donor to cyanoacrylic acid acceptor is weak due to the poor electron releasing nature of carbazole and incorporation of thiophene units increase the electron-richness of the donor segment due to the delocalization of the contributing molecular orbital. Extension of conjugation by oligothiophene units has been found to render a planar bridge between the donor and acceptor and facilitate the donor-acceptor interactions in dipolar compounds [14, 33]. The absorption maxima of the dyes

are following the order of **40b** (351 nm) < **36** (387 nm) < **40a** (394 nm) < **43a** (440 nm) < **44a** (443 nm) < **43b** (476 nm) < **44b** (478 nm). The shorter absorption maxima of the phenyl containing dyes (**40a** and **40b**) owing to the weak donor acceptor interactions due to twisting of phenyl unit with the carbazole linker.

Table 6.7 Optical data of the dyes recorded in DCM

Dye	$\lambda_{abs,}$ nm ($\varepsilon_{max} \times 10^3$ M^{-1} cm^{-1})		
	DCM	DCM + TFA	DCM + TEA
36	387 (14.0), 342 (18.2), 293 (22.6), 261 (42.9)	389 (13.9), 342 (17.6), 293 (22.4)	343 (24.6), 293 (23.1)
40a	394 (13.3), 344 (25.2), 332 (24.6), 260 (47.2)	395 (14.2), 344 (24.2), 330 (24.9), 295 (21.3)	346 (35.6), 294 (27.7)
40b	351 (32.7), 298 (27.9), 264 (65.4)	418 (54.2), 350 (33.2), 298 (29.3), 264 (68.9)	350 (37.8), 299 (34.2),
43a	440 (39.2), 327 (16.0), 293 (20.2), 262 (49.8)	445 (42.4), 328 (17.9), 293 (22.2)	398 (43.7), 294 (21.3)
43b	476 (45.1), 345 (25.7), 294 (22.2), 262 (61.3)	481 (45.3), 345 (26.5), 294 (22.7)	431 (48.5), 345 (20.8), 294 (21.6)
44a	443 (40.8), 332 (19.5), 298 (26.7), 259 (61.7)	454 (40.7), 333 (20.1), 298 (26.4), 262 (61.4)	403 (51.3), 298 (29.5)
44b	478 (44.7), 351 (27.3), 298 (23.8), 258 (59.7)	484 (44.3), 351 (28.0), 298 (24.1)	431 (48.5), 345 (20.9), 294 (21.7)

It is interesting to compare the absorption spectral features of these dyes with the closely related dyes possessing phenyl linkages instead of carbazole. Generally, the absorption maxima of the present dyes are red-shifted when compared to the known dyes **D68**-**D71**, [22, 28] **D94**-**D97** [29] **DL** dyes [27] (Chart 6.1). The incorporation of 2,7-disbstituted carbazole linker (**43a)** showed red shifted absorption (62 nm) with high molar extinction coefficient (39200 $M^{-1}cm^{-1}$) when compared to dye **D94** which contain phenyl linker. Also, similar red shift observed for **44a** and **44b** when compared to **D70** and **D71**, respectively. It clearly indicates the incorporation of carbazole extending the conjugation pathway. Thisled to a red shift in absorption and contributed to its good photovoltaic performance. Particularly, the longer wavelength absorption realized for the dyes **43b** and **44b** when compared to the analogous dyes **DL13** and **DL14** respectively

possessing 3,6-disubstituted carbazole as a π-bridge highlights the effective conjugation pathway rendered by the 2,7-disubstituted carbazole. Also, the new dyes developed by us showed larger molar extinction coefficient when compared to these dyes. All these observations can be attributed to the electron-richness of the carbazole linker and the facile electronic communication *via* the 2,7-disubstituion in carbazole.

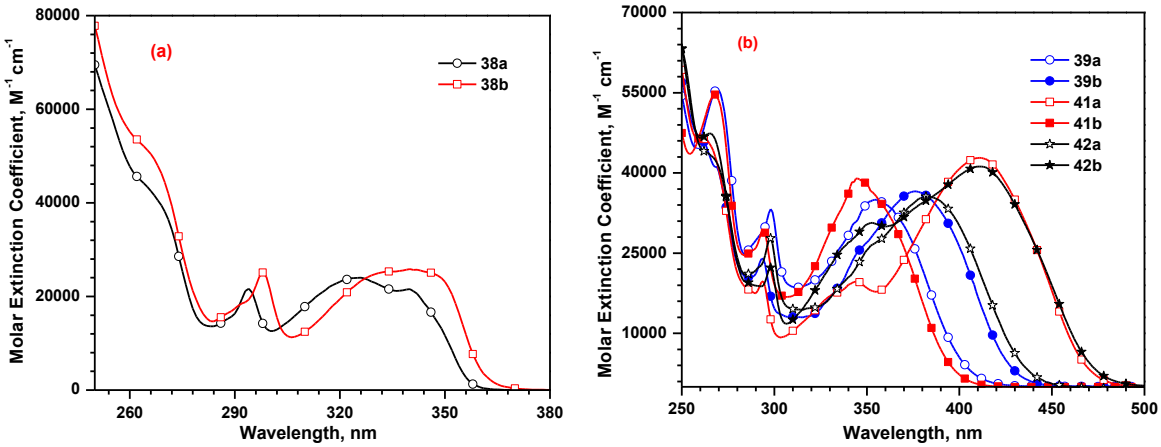

Figure 6.3 Absorption spectra of bromo (a) and aldehyde (b) derivatives recorded in DCM.

Table 6.8 Optical data of the bromo and aldehyde derivatives recorded in DCM

Dye	$\lambda_{abs,}$ nm ($\varepsilon_{max} \times 10^3$ M^{-1} cm^{-1})	$\lambda_{em,}$ nm	Stokes shift, cm^{-1}
38a	340 (21.6), 326 (24.0), 294 (21.7)	372, 357	1400
38b	342 (25.7), 298 (25.1), 267 (49.3)	381, 374, 367	1992
39a	355 (35.0), 298 (33.2), 269 (55.5)	486	7592
39b	345 (39.0), 294 (29.5), 268 (54.6)	511	9416
41a	376 (36.6), 294 (24.0)	503	6715
42a	383 (35.6), 298 (27.8)	531	7277
41b	411 (42.8), 345 (19.7), 294 (19.8)	521	5137
42b	340 (21.6), 326 (24.0), 294 (21.7)	538	10824

The nature of the charge transfer transition was confirmed by the following studies. (1) Addition of trifluoroacetic acid (TFA) to DCM solution of the dyes shows a bathochromic shift to the charge transfer absorption. But addition of triethylamine (TEA) leads to a pronounced blue shift for this peak and they are displayed in Figures 6.4 and 6.5. Such observations have been earlier ascribed to the increment/decrement in acceptor strength on addition of TFA/TEA caused

by protonation/deprotonation [41, 42]. (2) Also the dyes exhibited longer wavelength absorption when compared to the corresponding bromo- and aldehyde derivatives. The absorption wavelength assumes the order in accordance with the electron-withdrawing effect of the end group (Br < CHO < cyanoacrylic acid). (3) Additionally, all the dyes displayed a negative solvatochromism (shown in Table 6.9) in the absorption spectra. The blue-shift observed on increasing the polarity of the solvent is attributed to the effective solvation of the dyes [43, 44]. However, a drastic blue shift witnessed for all dyes in DMF is probably due to the basic nature of the solvent which leads to the deprotonation of the dyes [45]. Similarly, the significant red-shift observed in chloro-solvents such as DCM and chloroform arises due to the rapid relaxation of polarizable electrons in the excited state [46, 47].

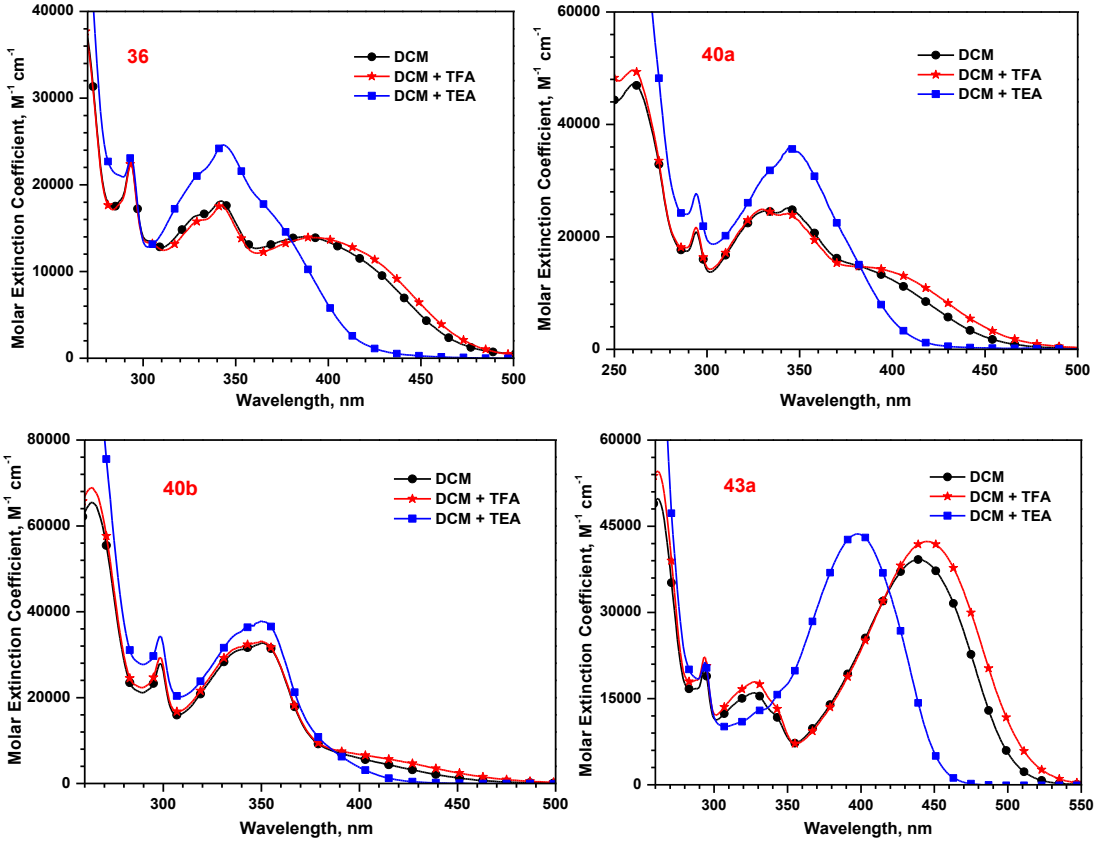

Figure 6.4 Absorption spectra of the dyes (**36, 40a, 40b** and **43a**) recorded in DCM, after the addition of TFA and TEA.

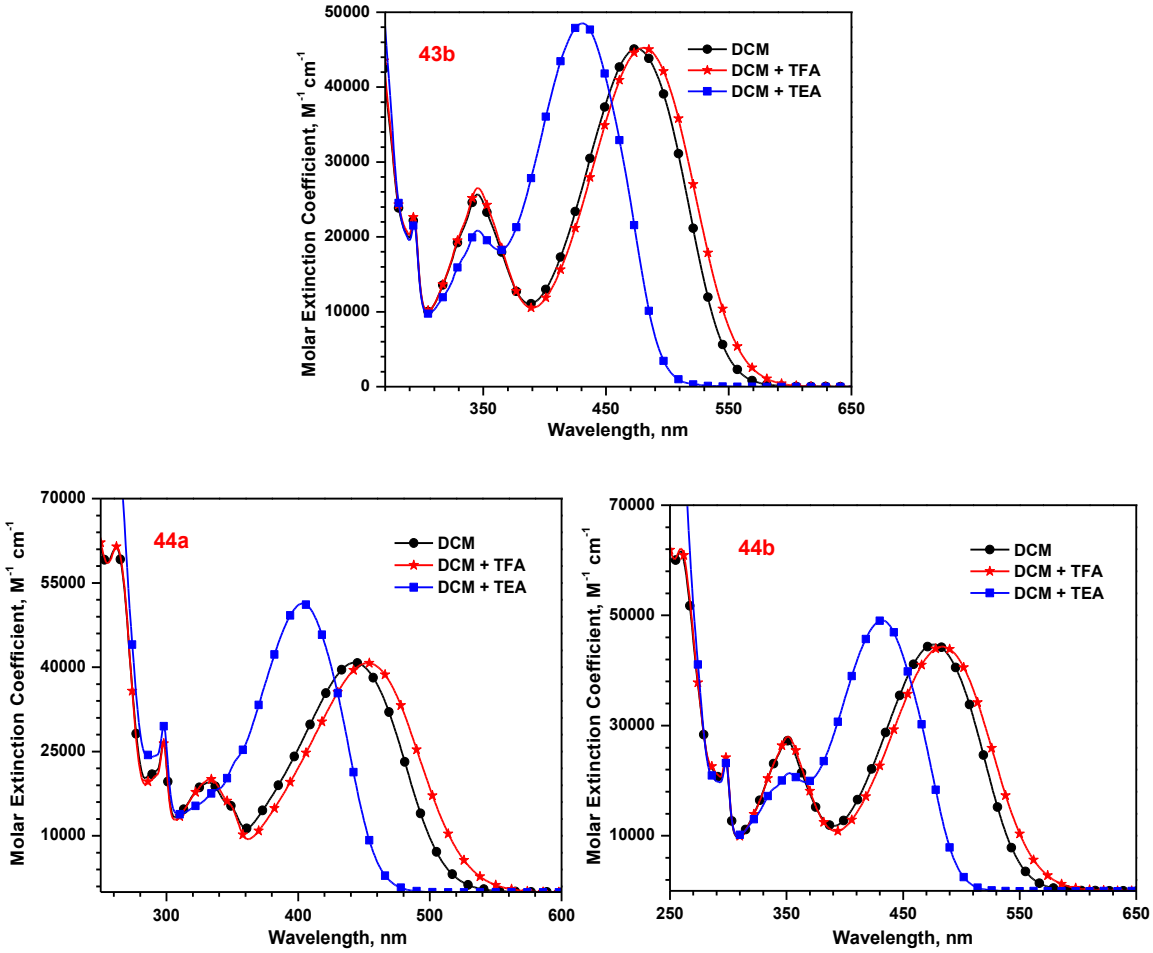

Figure 6.5 Absorption spectra of the dyes (**43b, 44a** and **44b)** recorded in DCM, after the addition of TFA and TEA.

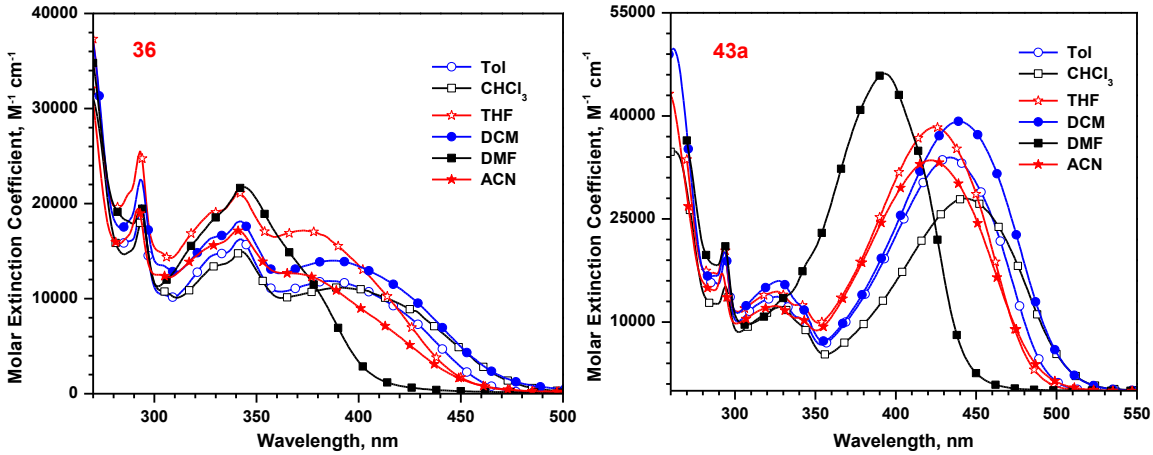

Figure 6.6 Absorption spectra of the dye (**36** and **43a**) recorded in different solvents.

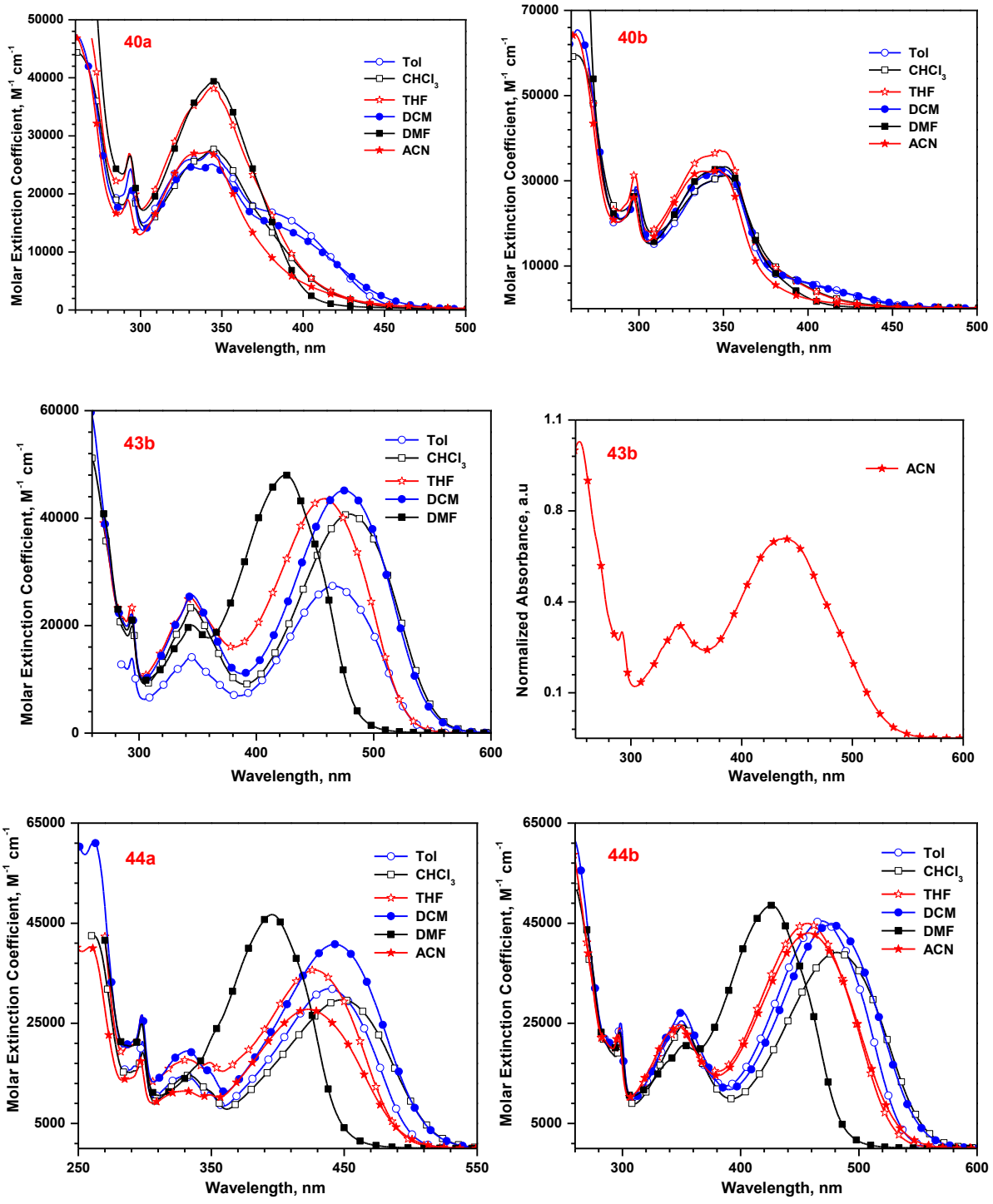

Figure 6.7 Absorption spectra of the dyes (**40, 43** and **44**) recorded in different solvents.

Table 6.9 Absorption data of the dyes recorded in different solvents

Dye	$\lambda_{abs,}$ nm ($\varepsilon_{max} \times 10^3$ M^{-1} cm^{-1})					
	TiO_2 film	Tol	$CHCl_3$	THF	DMF	ACN
36	460	386 (11.9), 342 (16.3), 294 (19.9)	401 (11.0), 343 (15.0), 294 (18.3)	373 (17.2), 342 (21.1), 293 (25.6)	344 (21.8), 293 (19.6),	369 (12.7), 340 (17.2), 292 (19.5), 261 (37.0)
40a	na	388 (16.1), 344 (27.2), 330 (25.9), 294 (24.4)	345 (27.7), 293 (20.3), 262 (44.8)	344 (38.2), 293 (27.0)	345 (39.4), 294 (26.6)	341 (27.3), 292 (19.1)
40b	na	351 (31.6), 298 (28.7)	351 (31.2), 298 (27.9)	348 (37.3), 298 (31.5)	351 (33.3), 297 (26.3)	348 (32.6), 338 (32.2), 297 (26.0)
43a	510	434 (34.0), 326 (13.7), 293 (18.9)	442 (28.0), 328 (12.2), 294 (15.2)	424 (38.4), 340 (12.6), 326 (14.4), 293 (21.1)	393 (46.2), 294 (21.0)	422 (33.6), 325 (12.4), 292 (17.1), 259 (43.2)
43b	547	466, 344, 294	480 (40.8), 345 (23.5), 294 (20.0)	458 (43.6), 344 (25.2), 293 (23.9)	426 (48.0), 345 (20.0), 292 (20.3)	439, 342, 292, 254
44a	507	439 (31.9), 331 (14.4), 298 (21.4)	449 (29.7), 333 (14.6), 298 (19.2)	428 (35.7), 348 (17.2), 333 (17.7)	396 (46.7), 298 (24.9)	422 (27.8), 331 (11.5), 297 (17.4), 259 (40.3)
44b	533	468 (45.5), 350 (25.5), 298 (25.0)	481 (39.2), 352 (24.6), 299 (21.1)	457 (45.0), 349 (24.2), 299 (22.4)	426 (48.6), 352 (20.6), 297 (24.1)	457 (43.1), 349 (24.7), 297 (22.7), 254 (61.2)

na = not measured

The solvatochromism data of the dyes were analyzed by correlating with $E_T(30)$ parameter [48] and the correlation plots displayed in Figures 6.8 and 6.9. The dyes exhibited deviation for polar solvents such as chloro-solvents and ACN due to the specific solvation effects which led to unusual red shift in absorption. This is attributed to the instant stabilization due to a fast rearrangement of polarizable electrons during excitation [46, 47].

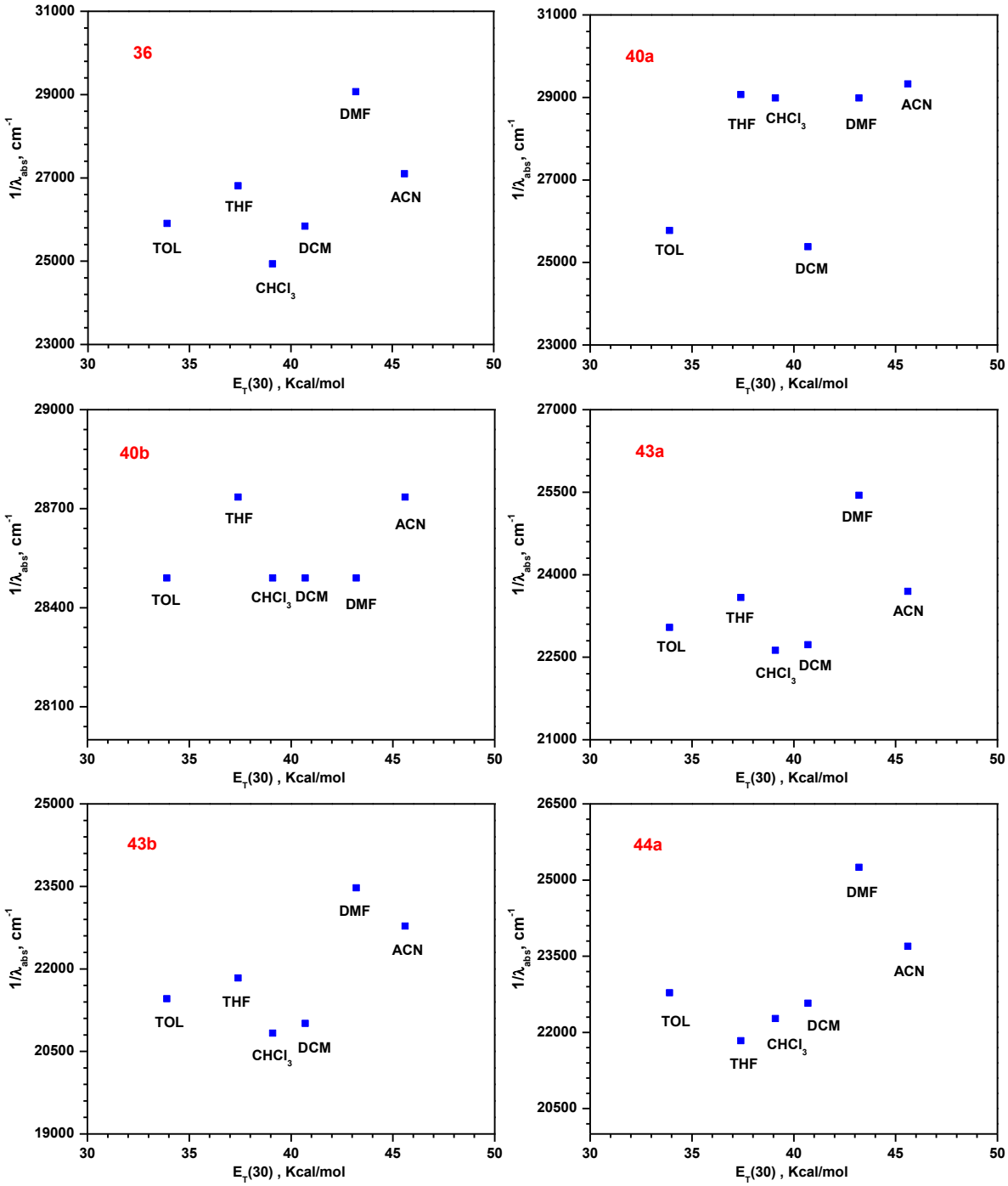

Figure 6.8 Variation of absorption (in cm^{-1}) with the solvents polarity parameter $E_T(30)$.

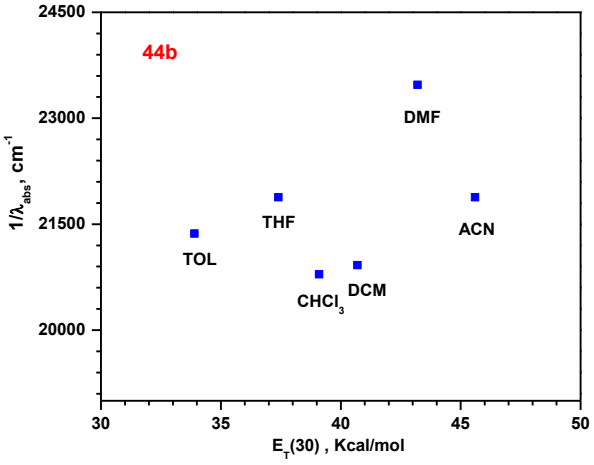

Figure 6.9 Variation of absorption wavelength (in cm^{-1}) with the solvents polarity parameter $E_T(30)$.

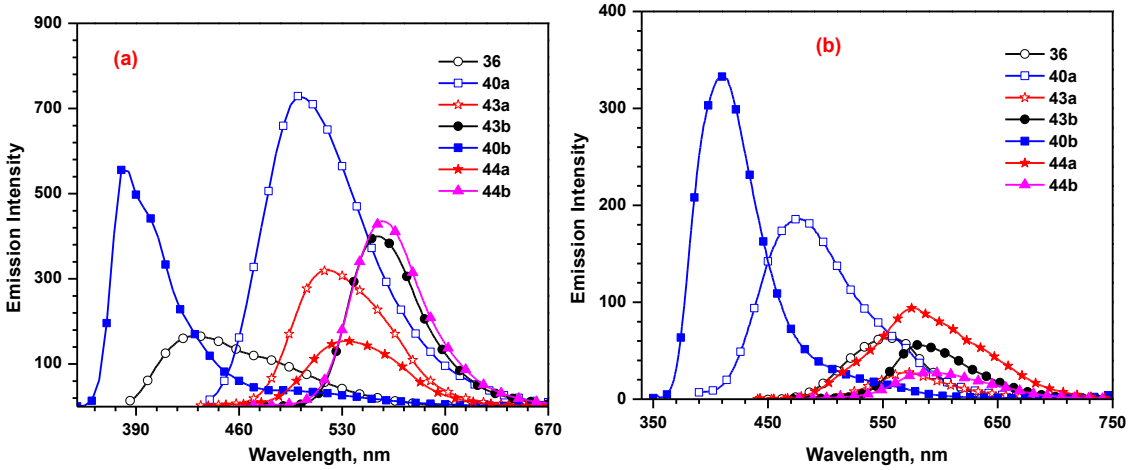

Figure 6.10 Emission spectra of the dyes recorded in (a) toluene and (b) DCM.

All the dyes displayed moderate emission in toluene ranging from blue to yellow and photoluminescence spectra shown in Figure 6.10 (a). The emission spectra of the dyes recorded in DCM solutions are shown in Figure 6.8. The emission maxima of the dyes are following order of **40b** (411 nm) < **40a** (479 nm) < **44a** (531 nm) < **36** (557 nm) < **43a** (572 nm) < **43b** (575 nm) < **44b** (588 nm). The trend is similar to the order observed for the absorption maxima. The dye **38** undergoes dipole-dipole relaxation led to blue shift in the emission spectra of the dyes even though it showed lower wavelength in absorption spectra. In contrast the dyes are weakly emitting in DCM because the emission intensity is quenched and they showed blue shift emission also. This indicated the excited state is more polar with noticeable dipole which might interact with solvent dipole and relax the excited state of the

dye by electron transfer mechanism [48, 49]. The emission of dyes is red shifted with weak emission than the corresponding aldehydes also confirm the charge transfer peak corresponds to higher absorption maxima of the dyes.

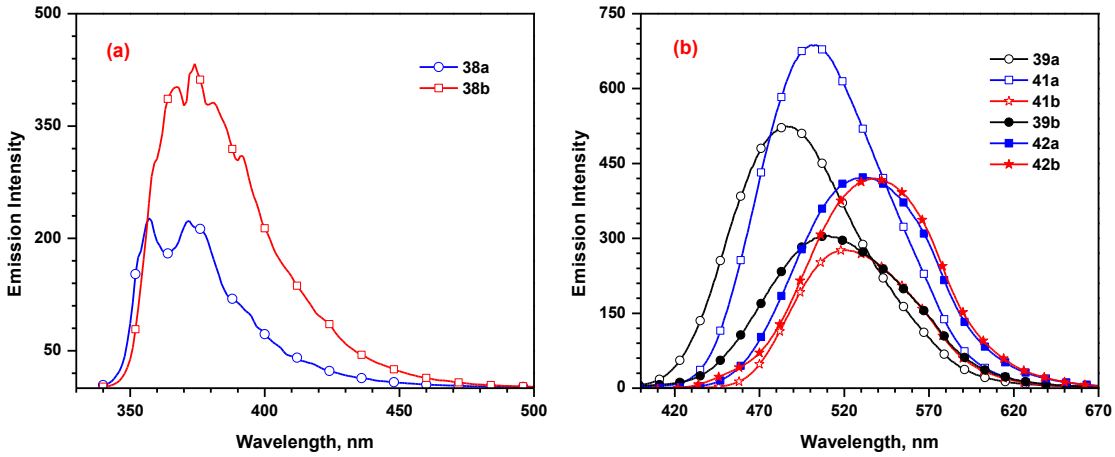

Figure 6.11 Emission spectra of the bromo (a) and aldehyde (b) derivatives recorded in DCM.

Though the dyes containing *tert*-butyl groups (**44a** and **44b**) displayed a slightly red-shifted absorption in solution, the absorption spectra of the dyes anchored on TiO_2 displayed (Figure 6.12) a reverse trend. Aggregation at the surface of TiO_2 may produce either blue-shift or red-shift depending on the nature of aggregate formation. Generally, the *J*-aggregates shift the absorption to the longer wavelength region while the H-aggregates produce blue-shifted absorption [51-54]. A drastic red-shift in the absorption for the dye **43b** (Figure 6.12) points the formation of *J*-aggregates at the surface of TiO_2 probably due to the extended conjugation of bithiophene segment. Aggregation behavior of the dye **43b** was also probed by monitoring the changes in the emission spectra on addition of water to the THF solution (Figure 6.13). No precipitation was observed by naked eye during the addition of water. The dye exhibited a blue shift up to 20% of water then the spectra progressively shifted to longer wavelength region on increasing the water concentration to 90%. The initial blue-shift may be attributed to the hydrogen bonding leading to deprotonation of the carboxylic acid unit [55]. However; the longer wavelength emission observed with 90% water is a clear indication of *J*-aggregate formation. Moreover, the hike in emission intensity at high water concentrations suggests the minimization of non-radiative pathway for the aggregated species which may be beneficial for light harvesting.

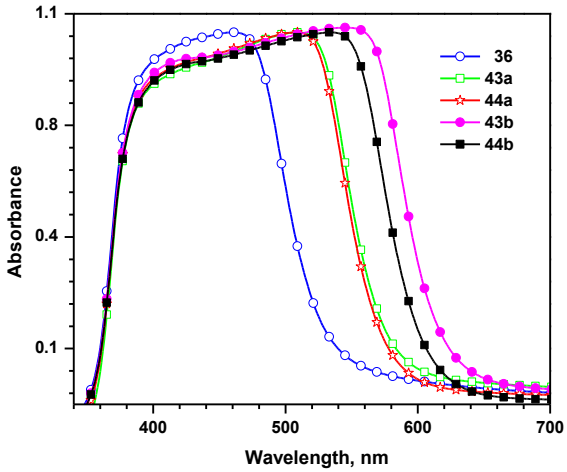

Figure 6.12 Absorption spectra of the dyes anchored on nanocrystalline TiO_2.

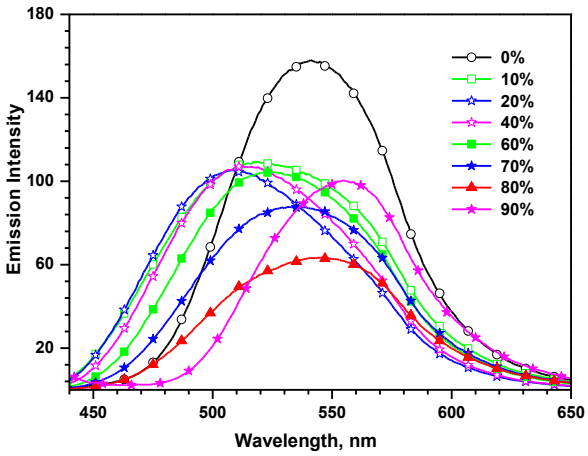

Figure 6.13 Changes in the emission spectra of the dye (**43b)** in THF on addition of water.

6.2.4 Theoretical Calculations

To gain further insight into the electronic structure of the dyes, we have optimized the geometry of the dyes by density functional theory (DFT) [56] at the level B3LYP/6-31G (d, p) [56] and computed the vertical excitation energies using B3LYP/6-31G (d, p). Also computed with MPW1K/6-31G (d, p) [57] because this theoretical treatment gave reliable estimate on the absorption parameters for the donor-acceptor compounds, particularly the organic sensitizers possessing D-π-A molecular configuration. The computed parameters are listed in Tables 6.10 and 6.11 and the electronic distribution observed for the frontier molecular orbitals are also shown in Figure 6.15. The HOMOs of the dyes are mainly contributed by the carbazole fragments (donor and linker) and it is spread up to one of the thiophenes in the dyes containing bithiophene unit in the conjugation pathway (Figure 6.14). But for the dyes (**40a** and **40b**) HOMO mainly located on carbazole fragments without contribution from phenyl due to the twisting with carbazole linker.

However, the LUMO is precisely located on the thiophene cyanoacrylic acid segment for the dyes possessing thiophene units in the conjugation pathway and phenyl cyanoacrylic acid segment for the dyes containing phenyl unit in the conjugation pathway. The carbazole linker also contributed to the LUMO of the dye **36**. The HOMO and LUMO of the dyes were well separated in the dyes (**43** and **44)** which favor a facile charge migration from the donor to acceptor on irradiation at the charge transfer transition. However, for the dye **36**, the HOMO and LUMO are overlapping significantly and suggest a poor charge transfer propensity. Due

to this the dye **36** exhibited poor performance in the DSSC (*vide supra*). The orbital of HOMO-1 mainly located on donor unit of carbazole fragment and LUMO+1 located on carbazole and little contribution from thiophene/phenyl cyanoacrylic acid. The transitions contributed for higher energy corresponds to HOMO-1 to LUMO+1 also useful to inject the electron and favorable for overlap of sensitizer orbitals and TiO_2. MPW1K theory reveals that these transitions are contributed in higher absorption transition, particularly for the bithiophene containing dyes with reasonable oscillator strength. The dipole moment of dyes pointed towards cyanoacrylic acid from donor and bithiophene containing dyes showed higher dipole moment than other thiophene/phenyl containing dyes due to the more polarization which leads to better photo induced electron injection.

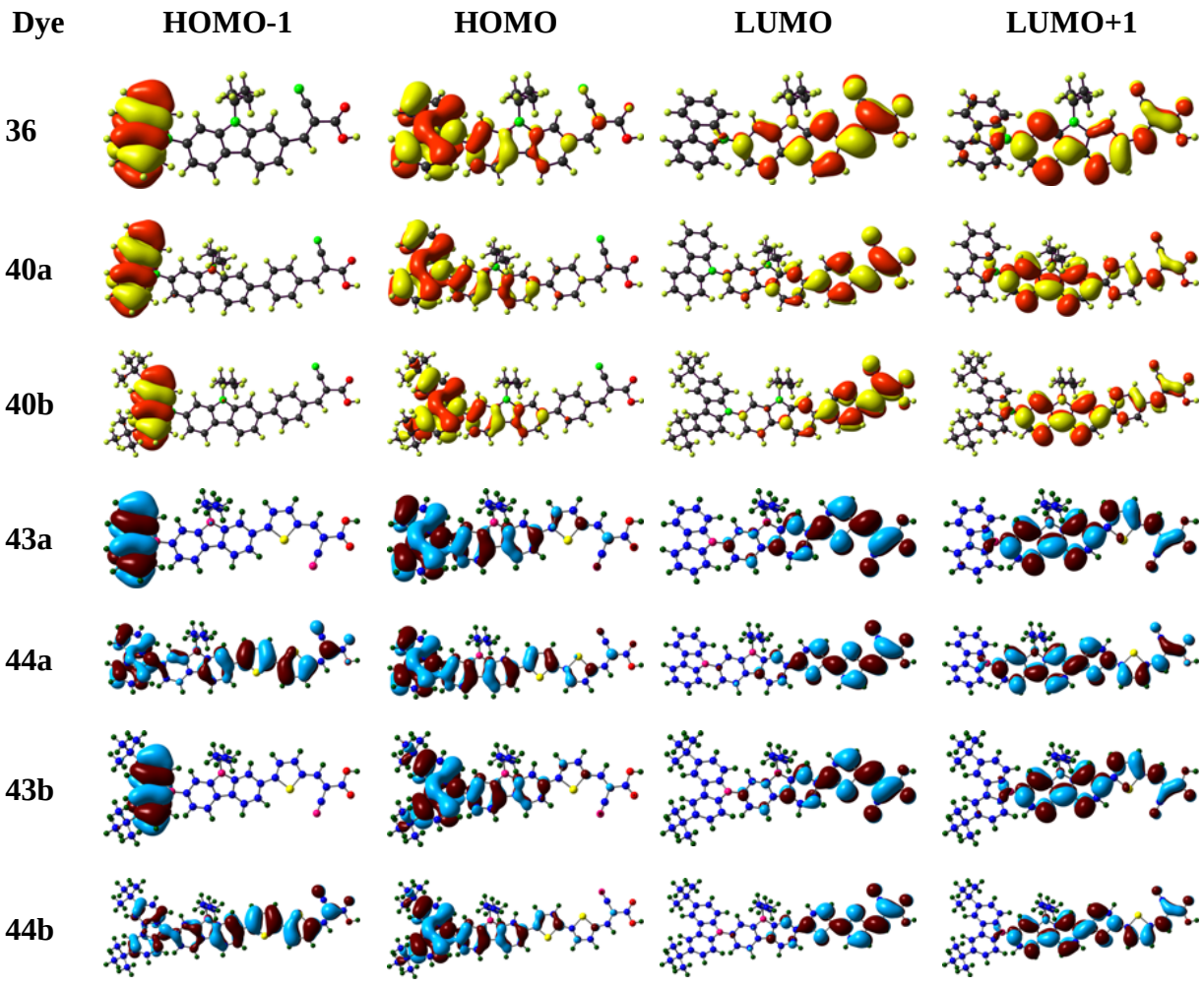

Figure 6.14 Frontier molecular orbitals of the carbazole dyes.

Table 6.10 Computed vertical transition energies and their oscillator strengths, assignments, dipole moments and band gaps for the dyes using B3LYP theory

Dye	λ, nm	*f*	assignments	μ_g (D)	HOMO (eV)	LUMO (eV)	$E_{0\text{-}0}$ (eV)
36 (vacuum)	492.6	0.27	HOMO→LUMO (99%)	4.29	-5.43	-2.61	2.82
	356.3	0.78	HOMO-3→LUMO (97%)				
	272.3	0.11	HOMO-1→LUMO+2 (51%), HOMO→LUMO+4 (23%)				
36 (THF)	492.5	0.38	HOMO→LUMO (99%)	5.76	-5.48	-2.63	2.84
	368.4	0.85	HOMO-3→LUMO (98%)				
	274.8	0.11	HOMO-2→LUMO+1 (54%), HOMO→LUMO+4 (20%) HOMO-1→LUMO+1 (17%)				
	274.1	0.16	HOMO-6→LUMO (83%)				
	257.7	0.17	HOMO-3→LUMO+2 (44%), HOMO-1→LUMO+3 (42%)				
40a (vacuum)	502.3	0.23	HOMO → LUMO (99%)	5.23	-5.35	-2.64	2.71
	392.2	0.78	HOMO-3 → LUMO (98%)				
	344.8	0.26	HOMO → LUMO+1 (95%)				
	305.3	0.40	HOMO-5 → LUMO (76%)				
40a (THF)	500.2	0.37	HOMO → LUMO (99%)	6.33	-5.40	-2.66	2.74
	404.2	0.74	HOMO-3 → LUMO (98%)				
	336.1	0.43	HOMO → LUMO+1 (93%)				
	311.1	0.28	HOMO-4 → LUMO (77%)				
40b (vacuum)	535.5	0.20	HOMO → LUMO (100%)	5.43	-5.17	-2.62	2.55
	397.7	0.85	HOMO-3 → LUMO (98%)				
	357.0	0.24	HOMO → LUMO+1 (96%)				
	306.8	0.38	HOMO-5 → LUMO (63%), HOMO-1 → LUMO+1 (23%)				
40b (THF)	533.4	0.29	HOMO → LUMO (99%)	6.53	-5.22	-2.66	2.57
	411.5	0.84	HOMO-3 → LUMO (99%)				
	348.7	0.37	HOMO → LUMO+1 (95%)				
	318.6	0.11	HOMO-1 → LUMO+1 (82%)				
	312.8	0.37	HOMO-5 → LUMO (81%)				

Table 6.10 (cont.)

Dye	λ, nm	*f*	assignments	μ_g (D)	HOMO (eV)	LUMO (eV)	$E_{0\text{-}0}$ (eV)
43a (vacuum)	508.9	0.34	HOMO→LUMO (99%)	7.80	-5.37	-2.68	2.68
	407.6	0.92	HOMO-3→LUMO (74%), HOMO-2→LUMO (24%)				
	348.1	0.22	HOMO→LUMO+1 (91%)				
43a (THF)	518.7	0.54	HOMO→LUMO (99%)	10.45	-5.41	-2.75	2.66
	427.9	0.84	HOMO-3→LUMO (97%)				
	342.2	0.33	HOMO→LUMO+1 (79%), HOMO-4→LUMO (18%)				
44a (vacuum)	541.6	0.29	HOMO→LUMO (99%)	8.12	-5.20	-2.67	2.53
	412.8	1.03	HOMO-3→LUMO (49%), HOMO-2→LUMO (49%)				
	360.1	0.19	HOMO→LUMO+1 (94%)				
44a (THF)	553.2	0.41	HOMO→LUMO (99%)	10.89	-5.24	-2.74	2.50
	353.9	0.27	HOMO→LUMO+1 (92%)				
	331.6	0.11	HOMO-5→LUMO (83%)				
43b (vacuum)	535.8	0.55	HOMO→LUMO (99%)	5.55	-5.31	-2.79	2.52
	462.2	0.95	HOMO-1→LUMO (96%)				
	377.9	0.40	HOMO→LUMO+1 (70%), HOMO-4→LUMO (26%)				
43b (THF)	553.9	1.02	HOMO→LUMO (98%)	7.24	-5.33	-2.85	2.49
	484.9	0.33	HOMO-1→LUMO (70%), HOMO-2→LUMO (29%)				
	475.9	0.31	HOMO-2→LUMO (70%), HOMO-1→LUMO (28%)				
	380.4	0.39	HOMO-4→LUMO (65%), HOMO→LUMO+1 (32%)				
44b (vacuum)	569.3	0.37	HOMO→LUMO (99%)	5.95	-5.16	-2.78	2.38
	470.8	1.19	HOMO-1→LUMO (97%)				
	389.3	0.34	HOMO→LUMO+1 (86%)				
	365.9	0.11	HOMO-4→LUMO (73%)				
44b (THF)	582.0	0.65	HOMO→LUMO (98%)	7.74	-5.20	-2.84	2.36
	498.5	0.95	HOMO-1→LUMO (96%)				
	386.5	0.46	HOMO→LUMO+1 (55%), HOMO-4→LUMO (40%)				

Table 6.11 Computed vertical transition energies and their oscillator strengths, assignments, dipole moments and band gaps for the dyes using MPW1K theory

Dye	λ, nm	*f*	assignments	μ_g (D)	HOMO (eV)	LUMO (eV)	$E_{0\text{-}0}$ (eV)
36 (vacuum)	368.0	0.69	HOMO→LUMO (80%)	4.41	-6.36	-2.04	4.32
	306.6	0.42	HOMO-3→LUMO (82%)				
	251.1	0.14	HOMO-1→LUMO+2 (74%), HOMO→LUMO+4 (15%)				
	236.1	0.15	HOMO-4→LUMO (57%), HOMO-6→LUMO (18%)				
	234.0	0.16	HOMO-4→LUMO (28%), HOMO-6→LUMO (27%) HOMO-2→LUMO+3 (17%)				
36 (THF)	373.6	0.61	HOMO→LUMO (44%), HOMO-1→LUMO (41%)	5.82	-6.44	-2.07	4.37
	366.9	0.42	HOMO-1→LUMO (51%), HOMO→LUMO (37%)				
	310.0	0.35	HOMO-3→LUMO (81%)				
	253.0	0.22	HOMO-2→LUMO+1 (77%)				
	249.1	0.10	HOMO→LUMO+2 (72%)				
	237.0	0.35	HOMO-6→LUMO (47%), HOMO-1→LUMO+3 (31%)				
40a (vacuum)	318.3	0.46	HOMO-3 → LUMO (68%), HOMO → LUMO (22%)	5.42	-6.28	-2.15	4.13
	286.1	0.25	HOMO → LUMO+1 (82%)				
	266.1	0.14	HOMO-5 → LUMO (73%)				
	255.1	0.16	HOMO-1 → LUMO+2 (78%), HOMO → LUMO+6 (15%)				
40a (THF)	375.2	1.38	HOMO → LUMO (65%), HOMO-3 → LUMO (27%)	6.51	-6.37	-2.18	4.18
	317.4	0.28	HOMO-3 → LUMO (59%), HOMO → LUMO (29%)				
	284.5	0.38	HOMO → LUMO+1 (59%), HOMO → LUMO+2 (21%)				
	269.6	0.15	HOMO-4 → LUMO (72%)				
	256.8	0.24	HOMO-2 → LUMO+2 (81%)				

Table 6.11 (cont.)

Dye	λ, nm	*f*	assignments	μ_g (D)	HOMO (eV)	LUMO (eV)	$E_{0\text{-}0}$ (eV)
40b (vacuum)	379.7	0.91	HOMO → LUMO (79%), HOMO-3 → LUMO (15%)	5.60	-6.09	-2.13	3.95
	326.8	0.70	HOMO-3 → LUMO (74%), HOMO → LUMO (17%)				
	293.7	0.25	HOMO → LUMO+1 (84%)				
	267.3	0.15	HOMO-5 → LUMO (71%)				
	258.5	0.15	HOMO-1 → LUMO+2 (77%), HOMO → LUMO+6 (16%)				
40b (THF)	383.5	1.23	HOMO → LUMO (77%), HOMO-3 → LUMO (24%)	6.67	-6.19	-2.18	4.01
	328.6	0.46	HOMO-3 → LUMO (63%), HOMO → LUMO (26%)				
	291.6	0.36	HOMO → LUMO+2 (43%), HOMO → LUMO+1 (41%)				
	271.1	0.14	HOMO-5 → LUMO (71%)				
	259.5	0.24	HOMO-2 → LUMO+2 (80%)				
43a (vacuum)	378.1	1.27	HOMO→LUMO (64%), HOMO-3→LUMO (26%)	7.72	-6.29	-2.11	4.18
	325.1	0.18	HOMO-3→LUMO (56%), HOMO→LUMO (30%)				
	283.5	0.23	HOMO→LUMO+1 (80%)				
	251.3	0.15	HOMO-1→LUMO+2 (76%), HOMO→LUMO+5 (15%)				
43a (THF)	394.8	1.49	HOMO→LUMO (60%), HOMO-3→LUMO (34%)	10.27	-6.36	-2.18	4.17
	277.3	0.13	HOMO-4→LUMO (33%), HOMO-1→LUMO+1 (26%), HOMO-4→LUMO+1 (20%)				
	264.4	0.11	HOMO-7→LUMO (67%), HOMO-4→LUMO (21%)				
	253.1	0.24	HOMO-2→LUMO+2 (80%)				

Table 6.11 (cont.)

Dye	λ, nm	*f*	assignments	μ_g (D)	HOMO (eV)	LUMO (eV)	$E_{0\text{-}0}$ (eV)
44a (vacuum)	386.8	1.15	HOMO→LUMO (69%), HOMO-2→LUMO (17%)	7.96	-6.09	-2.09	4.00
	335.8	0.33	HOMO-3→LUMO (37%), HOMO-2→LUMO (32%), HOMO→LUMO (24%)				
	290.9	0.24	HOMO→LUMO+1 (82%)				
	254.8	0.15	HOMO-1→LUMO+2 (76%), HOMO→LUMO+5 (16%)				
44a (THF)	401.5	1.44	HOMO→LUMO (59%), HOMO-3→LUMO (33%)	10.62	-6.17	-2.18	3.99
	341.2	0.17	HOMO-3→LUMO (56%), HOMO→LUMO (35%)				
	288.6	0.36	HOMO→LUMO+1 (69%)				
	256.2	0.24	HOMO-2→LUMO+2 (76%)				
43b (vacuum)	411.5	1.68	HOMO→LUMO (53%), HOMO-1→LUMO (40%)	5.20	-6.22	-2.24	3.98
	377.9	0.95	HOMO-1→LUMO (50%), HOMO→LUMO (41%)				
	303.2	0.42	HOMO→LUMO+1 (75%)				
	290.1	0.47	HOMO-4→LUMO (78%)				
43b (THF)	436.1	1.79	HOMO→LUMO (63%), HOMO-1→LUMO (29%)	6.68	-6.26	-2.30	3.96
	305.8	0.47	HOMO→LUMO+1 (71%)				
	294.9	0.11	HOMO-4→LUMO (69%)				
44b (vacuum)	415.7	1.68	HOMO-1→LUMO (49%), HOMO→LUMO (44%)	5.50	-6.04	-2.22	3.82
	355.9	0.10	HOMO→LUMO (51%), HOMO-1→LUMO (42%)				
	309.2	0.44	HOMO→LUMO+1 (73%)				
44b (THF)	438.2	1.80	HOMO-1→LUMO (47%), HOMO→LUMO (45%)	6.95	-6.12	-2.30	3.82
	310.2	0.52	HOMO→LUMO+1 (65%)				
	298.5	0.11	HOMO-4→LUMO (72%)				

6.2.5 Electrochemical Properties

Redox properties of the dyes were estimated by measuring oxidation potentials using cyclic voltammetry in DCM solutions. By comparing the redox potentials of the dyes with oxidation potential of ferrocene measured under same condition we have deduced the energies of the HOMO and LUMO levels of the dyes. From these values the thermodynamic driving force for electron injection into the conduction band of TiO_2 and regeneration feasibility of the oxidized dyes by electrolyte can be evaluated. The dyes (**44a**, **44b**) possessing *tert*-butyl substituents exhibited reversible oxidation couple (Figure 6.15) while the remaining dyes showed irreversible oxidation peaks. The redox potentials of the later dyes were estimated from differential pulse voltammetric studies. The reversibility observed for the dyes **40b**, **44a** and **44b** may be ascribed to the hindrance for dimerization of cation radicals formed on oxidation. Unsubstituted carbazoles undergo facile dimerization at C-3 and C-6 positions [58]. The presence of *tert*-butyl groups at C-3,C-6 positions in the present dyes suppress the dimerization of the radical cations formed on oxidation [59]. Also the facile oxidation of **40b**, **44a** and **44b** when compared to the rest may be attributed to the electron-releasing propensity of *tert*-butyl groups [20].

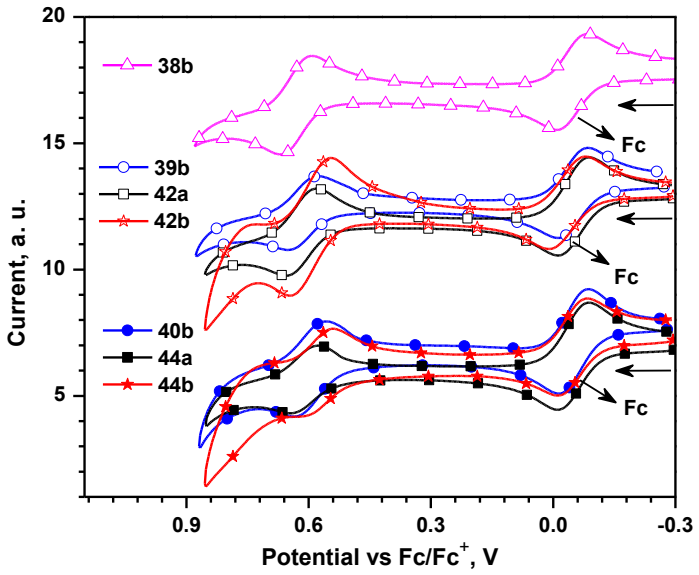

Figure 6.15 Cyclic voltammograms of the dyes recorded in DCM.

Table 6.12 Electrochemical data of the dyes and related compounds measured in DCM

Dye	E_{ox}, V	HOMO, eV	LUMO, eV	$E_{0\text{-}0}$, eV	E_{ox}^{*}, V	ΔG_{inj}, V
D62 [a]	0.90	5.70	2.88	2.82	-1.23	0.73
D63 [a]	0.77	5.57	2.89	2.68	-1.09	0.59
D64 [a]	0.86, 1.35	5.66	3.22	2.44	-0.89	0.39
D65 [a]	0.86, 1.07	5.66	3.33	2.33	-0.78	0.28
38a	0.80, 1.09	5.60	2.05	3.55	-1.98	1.48
38b	0.68 (100)	5.48	1.97	3.51	-2.06	1.56
39a	0.56	5.36	2.37	2.99	-1.66	1.16
39b	0.66 (73), 0.66	5.46	2.55	2.91	-1.48	0.98
41a	0.79, 1.00	5.59	2.72	2.87	-1.31	0.81
41b	0.67 (71), 0.83	5.47	2.80	2.67	-1.23	0.73
42a	0.67, 1.06	5.47	2.67	2.80	-1.36	0.86
42b	0.63 (99), 0.84	5.43	2.75	2.68	-1.61	1.11
36	0.82, 1.09	5.62	3.16	2.46	-0.87	0.37
40a	0.77	5.57	3.05	2.52	-0.98	0.48
40b	0.65 (81), 0.65	5.45	2.98	2.47	-1.05	0.55
43a	0.77	5.57	2.95	2.62	-1.08	0.58
43b	0.67, 0.78	5.47	3.17	2.30	-0.86	0.36
44a	0.66 (68), 1.04	5.46	2.98	2.48	-1.05	0.55
44b	0.62 (73), 0.82	5.42	3.12	2.30	-0.91	0.41

[a] Recorded in ACN.

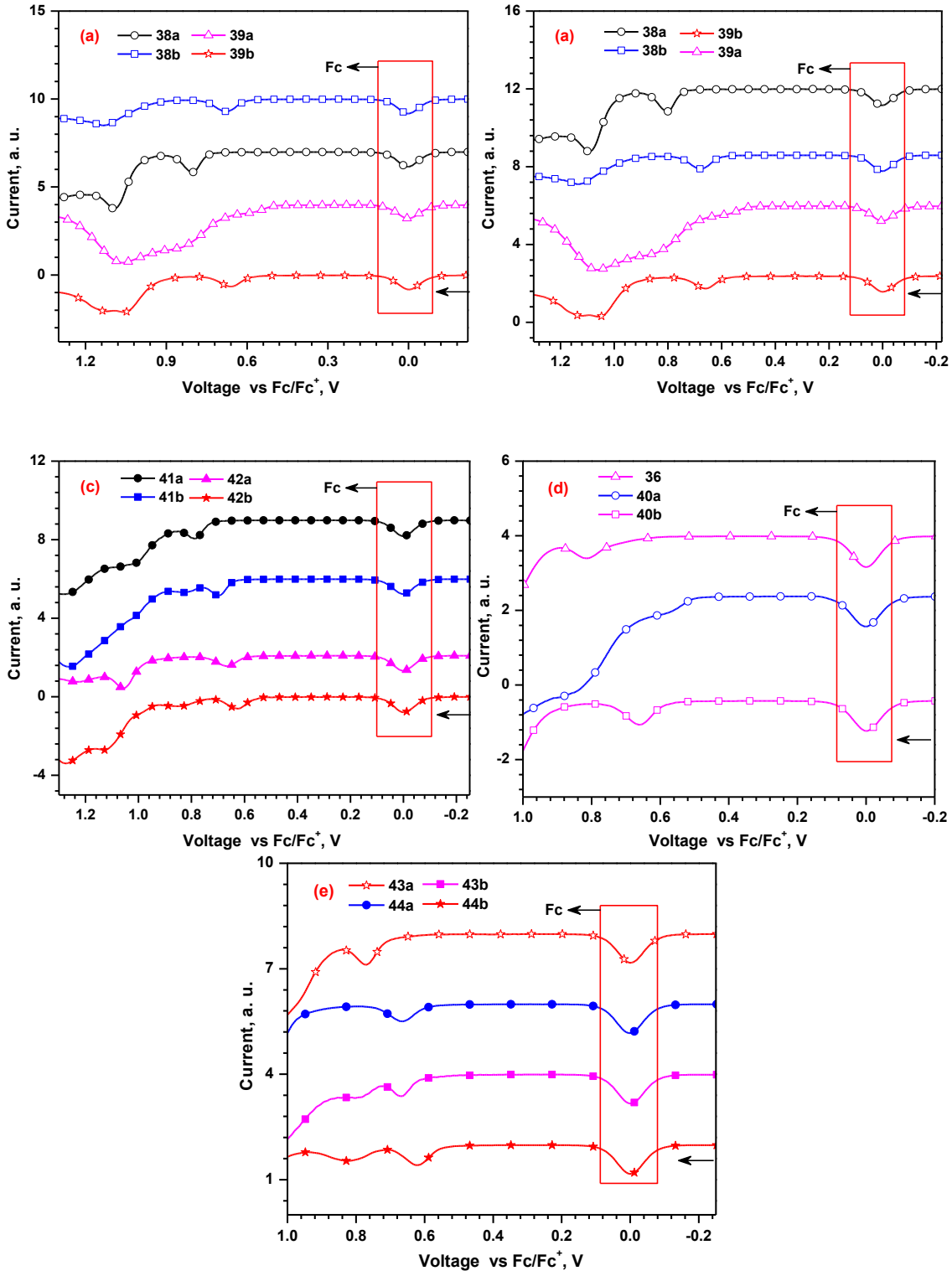

Figure 6.16 Differential pulse voltammograms of the bromo, aldehyde derivatives (a-c) and dyes (d and e) recorded in DCM.

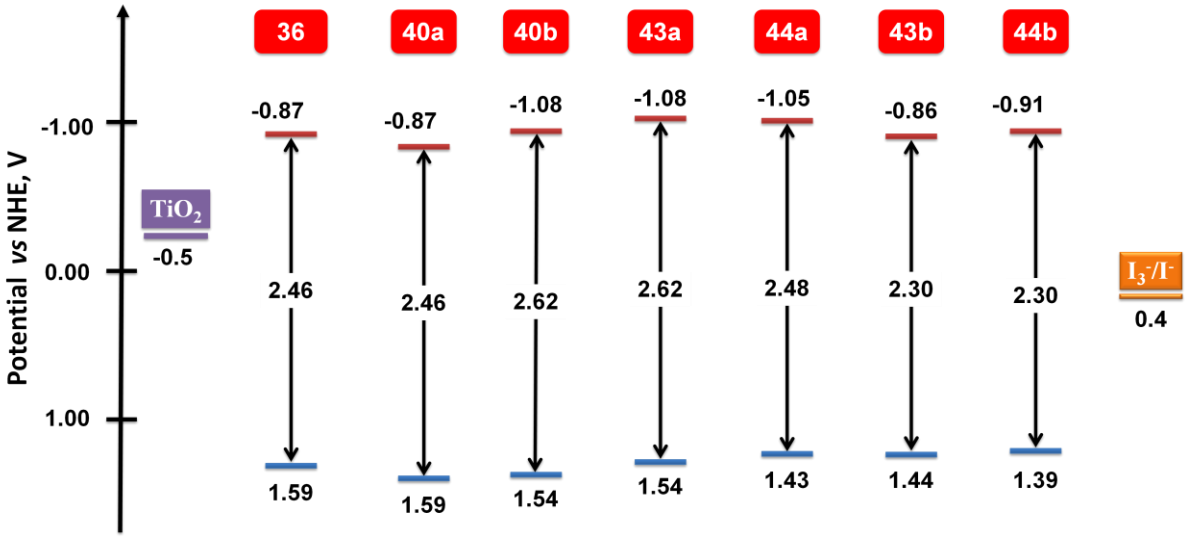

Figure 6.17 Comparison of the energy levels of the dyes (**36**, **40, 43** and **44**) in the ground and excited states.

It is interesting that the HOMO and LUMO energies of these dyes can be fine-tuned by changing the substituents on the donor carbazole and nature of the linker (Figure 6.17). The ground state oxidation potentials of the dyes are in the range of 1.39-1.59 V *vs* NHE. The oxidation potentials of the dyes were raised on elongation of the conjugation by thiophene and bithiophene insertion and donor strength by introduction of *tert*-butyl groups on carbazole. The order of ΔG_{inj} of the dyes is in the following order: **43b** (0.36 V) < **36** (0.37 V) < 4**4b** (0.41 V) < **40a** (0.48 V) < **40b** = **44a** (0.55 V) < **43a** (0.58 V). Carbazole donor containing dyes posses higher ΔG_{inj} and favorable for better electron injection from excited state of the dye led to higher J_{SC} than 3,6-di-*tert*-butyl-carbazole donor containing dyes. Moreover the dyes possess oxidation potential more positive than redox potential of the iodine/iodide electrolyte (0.4 V *vs* NHE) commonly employed in DSSC fabrication. This suggests that the dyes can be easily regenerated by the electrolyte. The first excited state oxidation potential of the dyes is located in the range -0.86 to -1.08 V. These values are more negative than the conduction band edge of TiO_2 (-0.5 V *vs* NHE) [60]. There exists at least 0.36 V differences which is sufficient to provide the required thermodynamic driving force for the injection of the photogenerated electrons from the dye into the conduction band of TiO_2 [61]. Since the dyes possess desired ground and excited state potentials, they are expected to serve as efficient sensitizers in nanocrystalline TiO_2-based dye-sensitized solar

cells. Particularly the dyes **43a** and **44a** are expected to show enhanced electron injection rate. However the longer wavelength intense absorption observed for the dyes **43b** and **44b** may be beneficial to generate more photocurrent.

6.2.6 DSSC Characteristics

Since the organic dyes showed interesting absorption and electrochemical properties suitable to perform as sensitizers in TiO_2-based dye-sensitized solar cells, we have tested their response in the DSSC by using photo anodes derived from the dyes. Photovoltaic performances of the DSSCs are tabulated in Table 6.13.

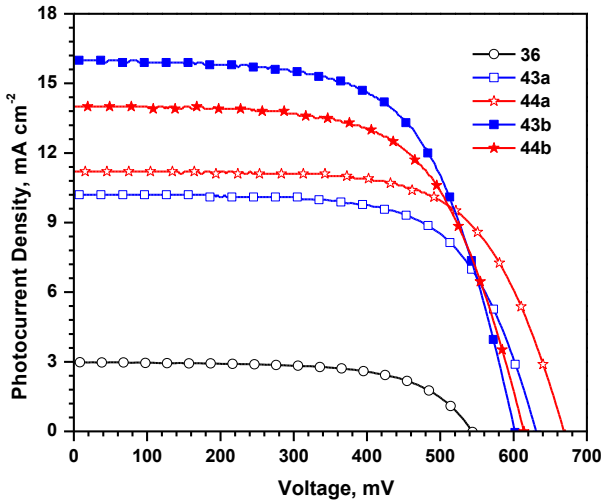

Figure 6.18 I-V characteristics of the DSSCs fabricated using the dyes.

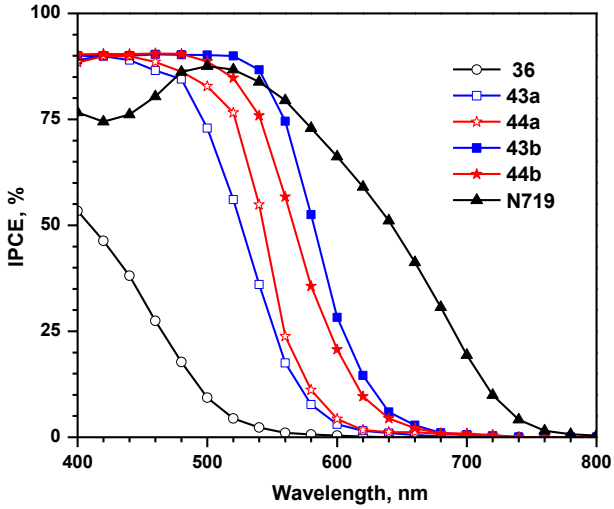

Figure 6.19 IPCE plots of the DSSCs fabricated using the dyes.

I-V characteristics observed for the devices under simulated solar light irradiation is displayed in Figure 6.18. The DSSC based on dye **43b** exhibited high photocurrent while that of the dye **44a** displayed high V_{OC} in the series. However, the dye **36** showed low J_{SC} and V_{OC} in DSSC. The poor performance of **36** in DSSC is attributed to the weak charge transfer transition appearing below 400 nm which probably reduces the electron generation propensity of the dye. Also, it possesses relatively small thermodynamic driving force for electron injection into the conduction band of TiO_2. Consequently, less electron generation and less favorable electron injection reduce the electron density in the conduction band of TiO_2. In general, V_{OC} of the thiophene derivatives **43a** and **44a** are larger than the analogous bithiophene counterparts **43b** and **44b**. This is again rationalized as originating from the

favorable electron injection possible for these dyes due to the more positive LUMO. There is also some interesting outcome due to the structural modification on carbazole donor. The dyes **44a** and **44b** containing *tert*-butyl substituents displayed larger V_{OC} when compared to the corresponding unsubstituted dyes **43a** and **43b**. This probably is due to the slightly enhanced light-harvesting property of the former dyes when compared to the later and the *tert*-butyl groups retarding the recombination of TiO_2 conduction band electrons with the triiodide ions (I_3^-) in electrolyte by rendering hydrophobic environment which prevent the approach of the triiodide ions to TiO_2.

Table 6.13 Performance parameters of the DSSCs fabricated using the dyes

Dye	J_{SC}, mAcm^{-2}	V_{OC}, mV	*ff*	η (%)	R_{rec}, Ω	R_{ct2}, Ω	f_{max}, Hz	τ_e, ms
36	2.79	555	0.64	0.99	26.62	70.35	93.3	1.7
43a	9.98	635	0.66	4.22	43.73	26.12	46.5	3.4
44a	11.22	666	0.66	4.95	47.11	25.55	26.5	6.2
43b	15.78	601	0.64	6.04	36.59	20.93	107.2	1.5
44b	14.00	612	0.64	5.48	42.10	23.03	70.5	2.3
N719	17.60	724	0.66	8.44	-	-	-	-

Incident photon to current conversion efficiency (IPCE) measured against the wavelength of irradiation for the DSSCs are displayed in Figure 6.19. All the dyes exhibited exceptional photon-to-electron conversion efficiency in the wavelength region from 400 nm to 600 nm. The action spectra are largely in accordance with the absorption band profile observed for the dyes in the solid state (Figure 6.12). The present dyes showed very high IPCE in the 400-500 nm region which is complimentary to the ruthenium-based organometallic dyes such as **N719** **[**62] and ascribed to the high molar extinction coefficients observed for the dyes in that region. The power conversion efficiencies of all the compounds are higher than 4% except the dye **38**. The device based on the dye **43b** exhibited a short circuit current density (J_{SC}) of 15.78 mA cm^{-2}, open circuit voltage (V_{OC}) of 601 mV, fill factor (*ff*) of 0.64 and power conversion efficiency of 6.04%. The J_{SC} of the dyes follows the order **36** < **43a** < **44a** < **44b** < **43b** consistent with the absorption spectra observed for the dyes anchored on TiO_2 (*vide supra*). The larger photocurrent observed for the DSSC based on the dye **43b** may be attributed to the longer wavelength light harvesting ability arising from the aggregated

species (*vide supra*) and the retardation of electron recombination with the electrolyte. However, for the dye **44b** though the conjugation segment is very similar to that in **10a**, the aggregation and electron recombination are retarded by the bulky *tert*-butyl groups. Similarly, the V_{OC} for the devices show the order: **36** < **43b** < **44b** < **43a** < **44a**. It is interesting that the dyes possessing bithiophene in the conjugation (**43b** and **44b**) possessed less V_{OC} than the corresponding dyes with short conjugation (**43a** and **44a**). It is well documented in the literature that organic dyes possessing extended conjugation normally show enhanced photocurrent at the expense of photovoltage attributable to the reduction in the electron density in the conduction band of TiO_2 [22].

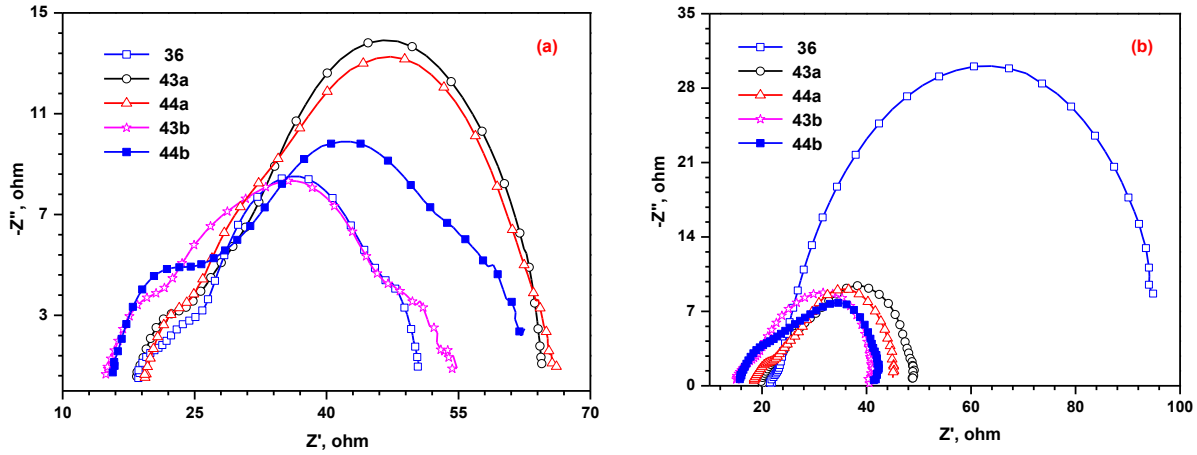

Figure 6.20 Nyquist plots observed for the DSSCs measured under (a) dark and (b) illumination conditions.

To understand the fate of the photogenerated electrons a detailed electrochemical impedance spectroscopy was performed on the DSSCs fabricated using the dyes. Nyquist plots of the DSSCs measured under dark and illumination conditions are displayed in Figure 6.20. Figure 6.20(a) corresponds to dark condition, displays three semicircles for all DSSCs and each semicircle corresponds to the resistance experienced at a particular interface of the components present in the DSSC device. The larger semicircle corresponds to the recombination resistance at TiO_2/dye/interface and the radius of this semicircle follows the order **44b < 43b < 44a < 43a < 36**. Smaller R_{rec} value is indicative of faster electron recombination and may result in a comparatively small open-circuit voltage [63, 64]. The R_{rec} for the devices follow the order, **36** < **43b** < **44b** < **43a** < **44a**. On this basis **36** is expected to

display small V_{OC} while **44a** may produce high V_{OC}. The oxidation potential of the dye and the charge-recombination resistance can alter the electron density in TiO_2. [65] Dyes that undergo oxidation more easily may increase the polarizability of the molecule and enhance the electron density on TiO_2. Relatively low oxidation potentials observed for the dyes **44a**, **43b**, and **44b** suggest favorable interfacial interaction between TiO_2 and dye. In accordance with this hypothesis, the electron transport resistance (R_{ct2}) estimated from the Nyquist plots recorded under illumination conditions (Figure 6.20 (b)) were relatively low for them (**36** > **43a** > **44a** > **44b** > **43b**).

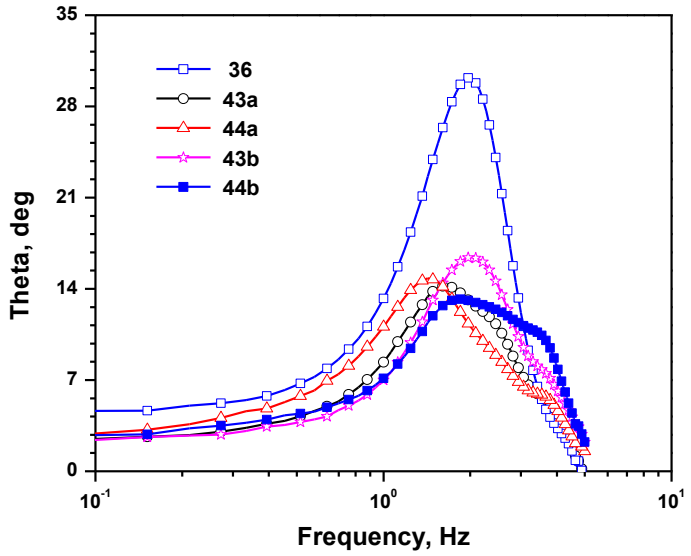

Figure 6.21 Bode-phase plots observed for the DSSCs measured under illumination.

The electron lifetime ($\tau_e = 1/\omega_{min} = 1/2\pi f_{max}$, where f_{max} is the maximum frequency of the low-frequency peak) in the Bode phase plot is highest for **44a** (**43b** < **36** < **44b** < **43a** < **44a**). The highest τ_e observed for **44a** is suggestive of effective suppression of back reaction of injected electrons with I_3^- ions in the electrolyte. Thus, the comparatively high V_{OC} observed for the thiophene conjugated dyes **43a** and **44a** may be attributed to the electron collection efficiency in their DSSCs due to the retardation of recombination of electron.

6.3 Conclusions

We have successfully synthesized a series of new organic dyes featuring carbazole/3,6-di(*tert*-butyl) carbazole donor, 2,7-carbazole linker and cyanoacrylic acid acceptor. Dyes containing phenyl or oligothiophene in the conjugation pathway in addition to carbazole were

also synthesized. All these dyes displayed high molar extinction coefficients for the charge-transfer transition and suitable LUMO and HOMO energy levels which facilitate the transfer of electron from the excited state of the dye into the conduction band of TiO_2 and the regeneration of the oxidized dyes by electrolyte. The dyes showed improved light-harvesting properties when compared to the analogous dyes possessing 3,6-carbazole (**DL7** and **DL8**) or phenyl (**D64** and **D65**) linker. This establishes the supremacy of the 2,7-carbazole as an effective π-conjugation pathway when compared to the similar chromophores. The DSSC based on a dye **43b** exhibited J_{SC} = 15.78 mA cm^{-2}, V_{OC} = 601 mV, *ff* = 0.64 and overall power conversion efficiency of 6.04% owing to the balance in the absorption properties and electron collection efficiency.

3.4 Experimental Section

General experimental methods, Computational methods and Device fabrication and Characterization are same as described in Chapter 3.

3.4.1 Crystal Structure Determination

Crystals of the compounds **41a** suitable for X-ray data collection were grown from DCM/hexane mixture. X-ray data of was collected on a CCD diffractometer using Mo Kα (λ=0.71073). The data were corrected for Lorentz and polarization effects. A total of 18066 reflections were measured out of which 6153 were independent and 4133 were observed [I>2 σ(I)] for maximum theta 27.47° at room temperature The structures were solved by direct methods using SHELXS-97 [66] and refined by full-matrix least squares refinement methods based on F^2, using SHELXL-97 [67]. All non-hydrogen atoms were refined anisotropically. All hydrogen atoms were fixed geometrically with their U_{iso} values 1.2 times of the phenylene and methylene carbons and 1.5 times of the methyl carbons. All calculations were performed using WinGX package [68]. A final refinement of 335 parameters gave R_1 = 0.0448, wR_2 = 0.1200 for the observed data and R_1 = 0.0762, wR_2 = 0.1441 for all data.

3.4.2 Synthesis

2,7-Dibromo-9-butyl-9*H*-carbazole (**1**) [33, 34] and 3, 6-di-*tert*-butyl-9*H*-carbazole [32] synthesized according to literature procedure.

3,6-Di-*tert*-butyl-9*H*-carbazole, **37b.** 9-*H*-carbazole (1.65 g, 10 mmol), 50 ml of nitromethane, and $ZnCl_2$ (4.05 g, 30 mmol) were added to a two-neck RB flask under a nitrogen atmosphere. *tert*-BuCl (3.3 ml, 30 mmol) was added dropwise under stirring. The resulting mixture was stirred for 24 h at room temperature and poured into water. The organic soluble content was extracted with DCM, dried over anhydrous sodium sulfate and evaporated to yield the crude product. Evaporate the solvent to yield the crude product, recrystalization from methanol to obtain white powder. White solid; Yield 2.34 g (84%); mp 232-234 °C; ^{1}H NMR ($CDCl_3$, 500.13 MHz) δ 8.09 (d, *J* = 2.0 Hz, 2H), 7.83 (s, 1H), 7.47 (dd, *J* = 8.5 Hz, 2.0 Hz, 2H), 7.33 (d, *J* = 8.5 Hz, 2H), 1.47 (s, 18H); HRMS calcd for $C_{20}H_{20}N_5$ $[M]^+$ *m/z* 279.4186, found 279.4185.

9-Butyl-7-(9*H*-carbazol-9-yl)-9*H*-carbazole-2-carbaldehyde, 35. A mixture of 9*H*-carbazole (**37a**, 0.19 g, 1.12 mmol), CuI (0.03 g, 15 mol%), 1,10-phenanthroline dihydrate (0.04 g, 20 mol%), anhydrous K_2CO_3 (0.41 g, 3 mmol), 7-bromo-9-butyl-9*H*-carbazole-2-carbaldehyde (**8**, 0.38 g, 1 mmol) and DMF (10 mL) was refluxed for 24 h under nitrogen atmosphere. On completion of the reaction, the reaction mixture was extracted with DCM, washed with brine solution and dried over anhydrous sodium sulfate. On evaporation of the DCM solution a tan yellow residue was obtained. It was purified by column chromatography on silica gel using hexane/DCM (2:3) as an eluant. Light yellow solid; Yield 0.19 g (45%); mp 122-124 °C; IR (KBr, cm^{-1}) 1693 ($\nu_{C=O}$); ^{1}H NMR ($CDCl_3$, 500.13 MHz) δ 10.20 (s, 1H), 8.34 (d, *J* = 8.5 Hz, 1H), 8.28 (d, *J* = 8.0 Hz, 1H), 8.18 (d, *J* = 3.0 Hz, 2H), 8.02 (s, 1H), 7.82 (d, *J* = 8.0 Hz, 1H), 7.64 (s, 1H),7.48 (t, *J* = 7.5 Hz, 3H), 7.44 (t, *J* = 8.5 Hz, 2H), 7.32 (t, *J* = 7.0 Hz, 2H), 4.38 (t, *J* = 7.5 Hz, 2H), 1.86-1.90 (m, 2H), 1.40-1.44 (m, 2H), 0.93-0.97 (m, 2H); ^{13}C NMR ($CDCl_3$, 125.77 MHz) δ 192.46, 143.00, 141.18, 140.89, 137.17, 134.11, 127.77, 123.49, 122.92, 122.67, 122.57, 121.85, 121.13, 120.73, 120.62, 118.91, 109.83, 109.79, 107.86, 43.33, 31.09, 20.56, 13.88; HRMS calcd for $C_{29}H_{24}N_2ONa$ $[M + Na]^+$ *m/z* 439.1780, found 439.1797.

(*E*)-3-(9-Butyl-7-(9*H*-carbazol-9-yl)-9*H*-carbazol-2-yl)-2-cyanoacrylic acid, 36. The aldehyde **35** (0.14 g, 0.33 mmol), 2-cyanoacetic acid (0.04 g, 0.5 mmol), ammonium acetate (0.04 g, 0.25 mmol), and acetic acid (5 mL) were mixed and refluxed for 24 h. The resulting red precipitate was filtered and washed several times with water and dried. It was crystallized from DCM/hexane mixture to obtain the analytically pure sample. Yellow solid; Yield: 0.14

g (85%); mp 155 °C; IR (KBr, cm^{-1}) 1600 ($\nu_{C\equiv N}$); ^{1}H NMR ($CDCl_3$, 500.13 MHz) δ 8.50 (s, 1H), 8.24 (m, 1H), 8.14-8.20 (m, 3H), 7.58 (d, *J* = 9.5 Hz, 1H), 7.37-7.49 (m, 5H), 7.30-7.34 (m, 2H), 4.31-4.33 (m, 2H), 1.85-1.88 (m, 2H), 1.39-1.44 (m, 2H), 0.92-0.97 (m, 3H); ^{13}C NMR ($CDCl_3$, 125.77 MHz) δ 142.89, 141.26, 141.22, 140.92, 137.19, 125.94, 125.89, 125.86, 123.41, 123.26, 122.40, 120.67, 120.32, 120.27, 120.04, 119.82, 119.79, 118.71, 109.68, 107.58, 43.11, 31.50, 20.46, 13.75; HRMS calcd for $C_{32}H_{25}N_3O_2$ $[M]^+$ *m/z* 483.1941, found 483.1972.

2-Bromo-9-butyl-7-(9*H*-carbazol-9-yl)-9*H*-carbazole, **38a.** It was prepared from **1** (7.56 g, 20 mmol) and **37b** (1.67 g, 10 mmol) by following a procedure described above for **35**. White solid; Yield 3.18 g (64%); mp 182-184 °C; ^{1}H NMR ($CDCl_3$, 500.13 MHz) δ 8.23 (d, *J* = 8.0 Hz, 1H), 8.18 (d, *J* = 7.5 Hz, 1H), 8.00 (d, *J* = 8.0 Hz, 1H), 7.59 (d, *J* = 1.5 Hz, 1H), 7.56 (d, *J* = 1.5 Hz, 1H), 7.46 (d, *J* = 8.0 Hz, 2H), 7.39-7.48 (m, 4H), 7.31-7.33 (m, 2H), 4.25 (t, *J* = 7.0 Hz, 2H), 1.82-1.85 (m, 2H), 1.37-1.42 (m, 2H), 0.92-0.95 (m, 3H); ^{13}C NMR ($CDCl_3$, 125.77 MHz) δ 141.33, 125.99, 123.35, 122.58, 121.64, 121.48, 120.39, 119.92, 118.69, 112.05, 109.87, 107.77, 43.28, 31.07, 20.58, 13.91; HRMS calcd for $C_{28}H_{24}BrN_2$ $[M + H]^+$ *m/z* 467.1117, found 467.1110.

9-(7-Bromo-9-butyl-9*H*-carbazol-2-yl)-3,6-di-*tert*-butyl-9*H*-carbazole, 38b. It was prepared from 3,6-di-*tert*-butyl-9*H*-carbazole (**37b**, 1.68 g, 6 mmol) and **1** (4.54 g, 12 mmol) by following a procedure described above for **38a**. White solid; Yield 2.68 g (77%); mp 102-104 °C; ^{1}H NMR ($CDCl_3$, 500.13 MHz) δ 8.19-8.22 (m, 3H), 8.00 (d, *J* = 8.0 Hz, 1H), 7.58 (d, *J* = 15.0 Hz, 2H), 7.49 (d, *J* = 8.5 Hz, 2H), 7.39-7.43 (m, 4H), 4.26 (t, *J* = 6.5 Hz, 2H), 1.84 (t, *J* = 7.0 Hz, 2H), 1.49 (s, 18H), 1.39-1.41 (m, 2H), 0.95 (t, *J* = 7.0 Hz, 3H); ^{13}C NMR ($CDCl_3$, 125.77 MHz) δ 142.84, 141.94, 141.37, 139.67, 136.25, 123.64, 123.34, 122.49, 121.58, 121.55, 121.36, 121.25, 119.54, 118.48, 116.32, 119.54, 109.25, 107.39 43.27, 34.79, 32.07, 31.08, 20.59, 13.92; HRMS calcd for $C_{36}H_{39}BrN_2$ $[M]^+$ *m/z* 578.2291, found 578.2292.

4-(9-Butyl-7-(9*H*-carbazol-9-yl)-9*H*-carbazol-2-yl)benzaldehyde, 39a. A two neck RB flask charged with a mixture of **38a** (0.47 g, 1 mmol), 4-formylphenylboronic acid (0.18 g, 1.2 mmol), anhydrous K_2CO_3 (0.48 g, 3.5 mmol) and $Pd(PPh_3)_4$ (0.35 g, 0.03 mmol) were dissolved in mixture of THF/H_2O (3:1). The reaction mixture was degassed with N_2 and

refluxed for 12 h under nitrogen atmosphere. After cooling to room temperature, the organic layer extracted with DCM and dried with sodium sulfate. The crude product was purified by column chromatography on silica gel by using a hexane/DCM mixture (2:1) as eluant. Yellow solid; Yield 0.39 g (79%); mp 162 °C; IR (KBr, cm^{-1}) 1693 ($\nu_{C=O}$); ^1H NMR ($CDCl_3$, 500.13 MHz) δ 10.11 (s, 1H), 8.31 (d, *J* = 8.0 Hz, 1H), 8.25 (d, *J* = 8.0 Hz, 1H), 8.20 (d, *J* = 7.5 Hz, 2H), 8.03 (d, *J* = 8.0 Hz, 2H), 7.93 (d, *J* = 9.0 Hz, 2H), 7.69 (s, 1H), 7.59-7.62 (m, 2H), 7.51 (d, *J* = 8.0 Hz, 2H), 7.43-7.46 (m, 3H), 7.33 (t, *J* = 7.0 Hz, 2H), 7.39 (t, *J* = 7.0 Hz, 3H), 1.90-1.93 (m, 2H), 1.43-1.47 (m, 2H), 0.89-0.97 (m, 3H); ^{13}C NMR ($CDCl_3$, 125.77 MHz) δ 191.81, 147.97, 141.49, 141.19, 137.63, 135.59, 134.94, 130.20, 127.98, 125.81, 123.20, 122.62, 121.52, 120.83, 120.21, 119.74, 118.98, 118.36,109.73, 107.53, 77.11, 76.86, 76.60, 43.00, 31.06, 20.46, 13.76; HRMS calcd for $C_{35}H_{28}N_2O$ $[M]^+$ *m/z* 492.2202, found 492.2208.

4-(9-Butyl-7-(3,6-di-*tert*-butyl-9*H*-carbazol-9-yl)-9*H*-carbazol-2-yl)benzaldehyde, 39b. Compound **39b** was synthesized from **38b** (0.58 g, 1 mmol) and by following a procedure similar to that described above for **39a**. Yellow Solid; Yield 0.50 g (82%); mp 160 °C; IR (KBr, cm^{-1}) 1700 ($\nu_{C=O}$); ^1H NMR ($CDCl_3$, 500.13 MHz) δ 10.10 (s, 1H), 8.28 (d, *J* = 8.0 Hz, 1H), 8.19-8.24 (m, 3H), 8.02 (d, *J* = 8.0 Hz, 2H), 7.92 (d, *J* = 8.0 Hz, 2H), 7.68 (s, 1H), 7.57-7.61 (m, 2H), 7.43-7.51 (m, 5H), 4.37 (t, *J* = 7.0 Hz, 2H), 1.87-1.93 (m, 2H), 1.50 (s, 18H), 1.42-1.46 (m, 2H), 0.96 (t, *J* = 7.5 Hz, 3H); ^{13}C NMR ($CDCl_3$, 125.77 MHz) δ 191.98, 148.20, 142.84, 141.95, 141.62, 139.70, 137.63, 135.09, 130.36, 128.14, 123.63, 123.36, 121.57, 121.34, 120.91, 119.09, 118.33, 116.31, 109.29, 107.66, 107.32, 43.16, 34.79, 32.07, 31.24, 20.64, 13.95; HRMS calcd for $C_{43}H_{45}N_2O$ $[M + H]^+$ *m/z* 605.3526, found.

5-(9-Butyl-7-(9*H*-carbazol-9-yl)-9*H*-carbazol-2-yl)thiophene-2-carbaldehyde, 41a. A mixture of (5-(1,3-dioxolan-2-yl)thiophen-2-yl)tributylstannane (0.49 g, 1.1 mmol), **38a** (0.47 g, 1 mmol) and dry DMF (5 mL) was maintained under nitrogen atmosphere and $Pd(PPh_3)_2Cl_2$ (0.01 g, 0.01 mmol) added to it. The resulting reaction mixture was heated at 80 °C for 15 h. After the completion of the reaction, the reaction mixture was poured into cold water and extracted with DCM (3 × 40 mL). Removal of volatiles from the DCM extract by rotary evaporation produced a solid residue. It was dissolved in glacial acetic acid (4 mL) and heated at 60 °C for 1 h to form a clear solution. After the addition of water (3 mL) the

reaction mixture was maintained at 60 °C for additional 1 h. Finally, it was extracted with DCM (3 × 40 mL). The DCM extract was washed thoroughly with brine solution and dried over anhydrous sodium sulfate. The solid residue obtained on evaporation of the DCM extract was purified by column chromatography on silica gel by using hexane /DCM mixture (1:1) as an eluant. Yellow solid; Yield 0.36 g (73%); mp 120-122 °C; IR (KBr, cm^{-1}) 1656 ($\nu_{C=O}$); ^{1}H NMR ($CDCl_3$, 500.13 MHz) δ 9.93 (s, 1H) 8.28 (d, *J* = 8.0 Hz, 1H), 8.18-8.20 (m, 2H), 7.80 (d, *J* = 4.0 Hz, 1H), 7.73 (d, *J* = 1.0 Hz, 1H), 7.63 (dd, *J* = 8.5 Hz, 1.5 Hz, 1H), 7.60 (d, *J* = 1.5 Hz, 1H), 7.55 (d, *J* = 4.0 Hz, 1H), 7.50 (d, *J* = 8.0 Hz, 2H), 7.42-7.46 (m, 2H), 7.31-7.34 (m, 2H), 4.36 (t, *J* = 7.0 Hz, 2H), 1.87-1.92 (m, 2H), 1.40-1.47 (m, 2H), 0.96 (t, *J* = 7.5 Hz, 3H); ^{13}C NMR ($CDCl_3$, 125.77 MHz) δ 182.74, 155.55, 142.28, 142.13, 141.45, 141.32, 137.50, 136.10, 130.85, 125.99, 124.15, 123.66, 123.41, 121.76, 121.66, 121.14, 120.38, 119.96, 118.74, 118.20, 109.87, 107.76, 106.79, 43.20, 31.18, 20.59, 13.88; HRMS calcd for $C_{33}H_{26}N_2OSNa$ $[M + Na]^+$ *m/z* 521.1658, found 521.1658.

5-(5-(9-Butyl-7-(9*H*-carbazol-9-yl)-9*H*-carbazol-2-yl)thiophen-2-yl)thiophene-2-carbaldehyde, 41b. Compound **41b** was synthesized in from **38a** (0.47 g, 1 mmol) and (5-(5-(1,3-dioxolan-2-yl)thiophen-2-yl)thiophen-2-yl)tributylstannane (0.58 g, 1.1 mmol) by following a procedure similar to that described above for **41a**. Yellow solid; Yield 0.34 g (59%); mp158-160 °C; IR (KBr, cm^{-1}) 1651 ($\nu_{C=O}$); ^{1}H NMR ($CDCl_3$, 500.13 MHz) δ 9.88 (s, 1H), 8.26 (d, *J* = 8.0 Hz, 1H), 8.19 (d, *J* = 7.5 Hz, 2H), 8.16 (d, *J* = 8.5 Hz, 1H), 7.70 (d, *J* = 4.0 Hz, 1H), 7.65 (s, 1H), 7.56-7.58 (m, 2H), 7.46 (d, *J* = 8.0 Hz, 2H), 7.40-7.45 (m, 5H), 7.30-7.33 (m, 3H), 4.35 (t, *J* = 7.0 Hz, 2H), 1.89 (quin, *J* = 7.5 Hz, 2H), 1.41-1.46 (m, 2H), 0.96 (t, *J* = 7.0 Hz, 3H); ^{13}C NMR ($CDCl_3$, 125.77 MHz) δ 181.54, 146.36, 146.33, 140.99, 140.60, 140.55, 140.39, 136.55, 134.75, 134.02, 130.44, 126.33, 125.05, 123.38, 123.02, 122.43, 121.76, 120.87, 120.59, 120.11, 119.45, 118.98, 117.62, 116.91, 108.96, 106.71, 105.06, 42.19, 30.25, 19.67, 13.00; HRMS calcd for $C_{37}H_{28}N_2OS_2$ $[M]^+$ *m/z* 580.1637, found 580.1637.

5-(9-Butyl-7-(3,6-di-*tert*-butyl-9*H*-carbazol-9-yl)-9*H*-carbazol-2-yl)thiophene-2-carbaldehyde, 42a. It was obtained from **38b** (0.58 g, 1 mmol) and ((5-(1,3-dioxolan-2-yl)thiophen-2-yl)tributylstannane (0.49 g, 1.1 mmol) by following a procedure similar to that described above for **41a**. Yellow solid; Yield 0.39 g (64%); mp 137-138 °C; IR (KBr, cm^{-1}) 1660 ($\nu_{C=O}$); ^{1}H NMR ($CDCl_3$, 500.13 MHz) δ 9.93 (s, 1H), 8.25 (s, 1H), 8.17-8.19 (m, 3H),

7.81 (d, *J* = 3.5 Hz, 1H), 7.72 (s, 1H), 7.62 (dd, *J* = 8.0 Hz, 1.5 Hz, 1H), 7.59 (d, *J* = 1.5 Hz, 1H), 7.55 (d, *J* = 4.0 Hz, 1H), 7.49 (d, *J* = 8.5 Hz, 2H), 7.43-7.45 (m, 3H), 4.35 (t, *J* = 7.5 Hz, 3H), 1.85-1.91 (m, 2H), 1.49 (s, 18H), 1.41-1.44 (m, 2H), 0.94-0.97 (m, 3H); ^{13}C NMR ($CDCl_3$, 125.77 MHz) δ 182.80, 155.64, 142.92, 142.18, 142.14, 141.39, 139.63, 137.63, 136.63, 130.66, 124.12, 123.74, 123.68, 123.41, 121.68, 121.26, 121.07, 118.50, 118.13, 116.35, 109.29, 107.34, 106.74, 43.19, 34.81, 32.09, 31.22, 20.63, 13.96; HRMS calcd for $C_{41}H_{42}N_2OS$ $[M]^+$ *m/z* 610.3012, found 610.3004.

5-(5-(9-Butyl-7-(3,6-di-*tert*-butyl-9*H*-carbazol-9-yl)-9*H*-carbazol-2-yl)thiophen-2-yl)thiophene-2-carbaldehyde, 42b. It was obtained from **38b** (0.58 g, 1 mmol) and (5-(5-(1,3-dioxolan-2-yl)thiophen-2-yl)thiophen-2-yl)tributylstannane (0.58 g, 1.1 mmol) by following a procedure similar to that described above for **41a**. Yellow solid; Yield 0.35 g (50%); mp 166-168 °C; IR (KBr, cm^{-1}) 1653 ($\nu_{C=O}$); ^{1}H NMR ($CDCl_3$, 500.13 MHz) δ 10.05 (s, 1H), 8.38-8.40 (m, 2H), 8.32 (s, 1H), 7.83-7.87 (m, 2H), 7.76 (s, 1H), 7.58-7.63 (m, 8H), 7.43-7.49 (m, 2H), 4.50-4.52 (m, 2H), 2.06-2.07 (m, 2H), 1.68 (s, 18H), 1.60-1.62 (m, 2H), 1.14-1.15 (m, 3H); ^{13}C NMR ($CDCl_3$, 125.77 MHz) δ 182.48, 147.41, 147.32, 142.85, 141.96, 141.51, 141.49, 139.68, 137.35, 137.35, 136.26, 134.92, 131.23, 129.10, 128.39, 127.29, 127.12, 126.19, 125.85, 124.28, 124.23, 123.95, 123.65, 123.36, 122.80, 121.44, 120.97, 118.37, 117.80, 116.32, 109.30, 107.29, 105.98, 43.14, 34.79, 32.08, 31.22, 20.63, 13.97; HRMS calcd for $C_{45}H_{45}N_2OS_2$ $[M + H]^+$ *m/z* 693.2967, found 693.2967.

(*E*)-3-(4-(9-Butyl-7-(9*H*-carbazol-9-yl)-9*H*-carbazol-2-yl)phenyl)-2-cyanoacrylic acid, 29a. It was prepared form **28a** (0.16 g, 0.33 mmol) and 2-cyano acetic acid (0.04 g, 0.5 mmol) by following a procedure described above for **36.** Brown solid; Yield (0.16 g, 88%); mp 170-172 °C; IR (KBr, cm^{-1}) 2219 ($\nu_{C\equiv N}$); ^{1}H NMR ($CDCl_3$, 500.13 MHz) δ 8.43 (s, 1H), 8.32 (d, *J* = 7.5 Hz, 1H), 8.23 (d, *J* = 4.5 Hz, 1H), 7.99 (d, *J* = 3.5 Hz, 1H), 7.95 (d, *J* = 9.0 Hz, 2H), 7.91 (d, *J* = 8.5 Hz, 1H), 7.54-7.56 (m, 2H), 7.52 (dd, *J* = 8.0 Hz, 1.5 Hz, 1H), 7.45 (d, *J* = 4.0 Hz, 1H), 7.27-7.30 (m, 3H), 7.25 (s, 1H), 7.16 (d, *J* = 7.5 Hz, 4H), 4.19 (t, *J* = 7.0 Hz, 2H), 1.76-1.79 (m, 2H), 1.30-1.35 (m, 2H), 0.90 (t, *J* = 7.0 Hz, 3H); ^{13}C NMR ($CDCl_3$, 125.77 MHz) δ 159.95, 148.50, 147.15, 146.94, 142.62, 141.52, 140.56, 136.38, 131.88, 131.48, 130.82, 130.55, 129.52, 129.16, 127.54, 125.80, 124.36, 124.33, 123.29, 122.92, 121.27, 120.50, 118.62, 117.75, 117.58, 113.94, 112.86, 105.92, 105.14, 42.98, 31.41, 20.80, 14.22; HRMS calcd for $C_{38}H_{29}N_3O_2$ $[M + Na]^+$ *m/z* 582.2151, found 582.2163.

(*E*)-3-(4-(9-Butyl-7-(3,6-di-*tert*-butyl-9*H*-carbazol-9-yl)-9*H*-carbazol-2-yl)phenyl)-2-cyanoacrylic acid, 40b. It was prepared form **39b** (0.20 g, 0.33 mmol) and 2-cyano acetic acid (0.04 g, 0.5 mmol) by following a procedure described above for **36**. Brown solid; Yield 0.20 g (91%); mp 178-180 °C; IR (KBr, cm^{-1}) 2216 ($\nu_{C\equiv N}$); ^{1}H NMR ($CDCl_3$, 500.13 MHz) δ 8.38-8.41 (m, 1H), 8.30-8.34 (m, 3H), 8.06-8.13 (m, 1H), 7.96 (s, 1H), 7.85-7.89 (m, 2H), 7.80 (t, *J* = 1.0 Hz, 1H), 7.56 (d, *J* = 7.5 Hz, 1H), 7.48 (d, *J* = 9.0 Hz, 3H), 7.36-7.41 (m, 3H), 4.52 (m, 2H), 1.79 (m, 2H), 1.42 (s, 18H), 1.30-1.38 (m, 2H), 0.87 (t, *J* = 7.5 Hz, 3H); ^{13}C NMR ($CDCl_3$, 125.77 MHz) δ 167.85, 157.08, 150.20, 142.81, 142.76, 141.79, 141.67, 139.75, 139.48, 138.17, 136.66, 136.04, 128.60, 128.23, 127.96, 127.59, 127.22, 123.64, 123.33, 122.25, 121.49, 121.42, 120.80, 118.91, 118.89, 118.21, 118.18, 116.97, 116.30, 109.33, 107.40, 107.28, 43.14, 34.79, 32.08, 31.10, 20.64, 13.96; HRMS calcd for $C_{46}H_{46}N_3O_2$ $[M + H]^+$ *m/z* 672.3584, found 672.3586.

(*E*)-3-(5-(9-Butyl-7-(9*H*-carbazol-9-yl)-9*H*-carbazol-2-yl)thiophen-2-yl)-2-cyanoacrylic acid, 43a. It was prepared form **41a** (0.16 g, 0.33 mmol) and 2-cyano acetic acid (0.04 g, 0.5 mmol) by following a procedure described above for **38**. Red solid; Yield 0.17 g (91%); mp 214 °C; IR (KBr, cm^{-1}) 2216 ($\nu_{C\equiv N}$); ^{1}H NMR (DMSO-d_6, 500.13 MHz) δ 8.42 (d, *J* = 8.5 Hz, 1H), 8.29-8.32 (m, 3H), 8.25 (s, 1H), 8.07 (s, 1H), 7.92 (s, 1H), 7.86-7.88 (m, 2H), 7.62 (d, *J* = 7.0 Hz, 1H), 7.40-7.47 (m, 5H), 7.31-7.33 (m, 2H), 4.53 (m, 2H), 2.52 (m, 2H), 1.31-1.36 (m, 2H), 0.85-0.90 (m, 3H); ^{13}C NMR (DMSO-d_6, 125.77 MHz) δ 141.67, 141.16, 140.53, 136.96, 135.81, 134.95, 130.62, 126.21, 124.88, 122.66, 122.35, 121.92, 121.39, 121.01, 120.48, 120.48, 119.96, 117.87, 117.70, 109.78, 108.03, 106.59, 42.10, 30.78, 19.73, 13.73; HRMS calcd for $C_{36}H_{28}N_3O_2S$ $[M + H]^+$ *m/z* 566.1896, found 566.1893.

(*E*)-3-(5-(5-(9-Butyl-7-(9*H*-carbazol-9-yl)-9*H*-carbazol-2-yl)thiophen-2-yl)thiophen-2-yl)-2-cyanoacrylic acid, 43b. It was obtained from **41b** (0.15 g, 0.25 mmol**)** by following a procedure similar to that described above for **36**. Red solid; Yield 0.15 g (92%); mp 210 °C; IR (KBr, cm^{-1}) 2220 ($\nu_{C\equiv N}$); ^{1}H NMR (DMSO-d_6, 500.13 MHz) δ 8.51 (t, *J* = 12.0 Hz, 1H), 8.40 (q, *J* = 12.0 Hz, 1H), 8.25-8.31 (m, 3H), 7.97-8.06 (m, 2H), 7.90 (t, *J* = 11.5 Hz, 1H), 7.78-7.83 (m, 1H), 7.81 (dt, *J* = 12.0 Hz, 3.5 Hz, 1H), 7.59-7.67 (m, 2H), 7.37-7.51 (m, 5H), 7.27-7.35 (m, 2H), 4.52 (m, 2H), 1.77-1.80 (m, 2H), 1.33-1.37 (m, 2H), 0.87-0.92 (m, 2H); ^{13}C NMR (DMSO-d_6, 125.77 MHz) δ 163.64, 146.58, 146.33, 145.76, 141.60, 141.22, 140.55, 134.80, 133.88, 133.79, 130.65, 128.38, 126.20, 125.63, 124.80, 122.66, 121.97,

121.79, 121.29, 121.10, 120.48, 119.93, 117.79, 117.31, 116.62, 109.79, 109.79, 106.23, 42.09, 30.84, 19.75, 13.78; HRMS calcd for $C_{40}H_{29}N_3O_2S_2$ $[M]^+$ *m/z* 647.1695, found 647.1694.

(*E*)-3-(5-(9-Butyl-7-(3,6-di-*tert*-butyl-9*H*-carbazol-9-yl)-9*H*-carbazol-2-yl)thiophen-2-yl)-2-cyanoacrylic acid, **44a.** It was synthesized from **42a** (0.15 g, 0.25 mmol) by following a procedure similar to that described above for **36**. Orange solid; Yield 0.15 g (89%); mp 224-226 °C; IR (KBr, cm^{-1}) 2219 ($\nu_{C\equiv N}$); ^{1}H NMR ($CDCl_3$, 500.13 MHz) δ 8.32 (s, 1H), 8.22 (d, *J* = 8.0 Hz, 1H), 8.19 (s, 2H), 8.12 (d, *J* = 8.0 Hz, 1.0 H), 7.79 (s, 1H), 7.71 (s, 1H), 7.59-7.61 (m, 2H), 7.55 (d, *J* = 3.0 Hz, 1H), 7.42-7.50 (m, 5H), 4.35 (m, 2H), 1.86-1.89 (m, 2H), 1.49 (s, 18H), 1.42-1.46 (m, 2H), 0.96 (t, *J* = 7.5 Hz, 3H); ^{13}C NMR ($CDCl_3$, 125.77 MHz) δ 157.54, 148.02, 142.94, 142.27, 141.35, 140.55, 139.53, 136.80, 134.50, 130.07, 124.67, 124.15, 123.69, 123.42, 121.74, 121.12, 118.49, 118.33, 116.34, 109.30, 107.30, 106.74, 43.17, 34.79, 32.06, 31.24, 20.60, 13.96; HRMS calcd for $C_{44}H_{43}N_3O_2S$ $[M]^+$ *m/z* 677.3070, found 677.3043.

(*E*)-3-(5-(5-(9-Butyl-7-(3,6-di-*tert*-butyl-9*H*-carbazol-9-yl)-9*H*-carbazol-2-yl)thiophen-2-yl)thiophen-2-yl)-2-cyanoacrylic acid, 44b. It was prepared from **42b** (0.17 g, 0.25 mmol) by following a procedure similar to that described above for **36**. Red solid; Yield 0.16 g (86%); mp 170 °C; IR (KBr, cm^{-1}) 2216 ($\nu_{C\equiv N}$); ^{1}H NMR (DMSO-d_6, 500.13 MHz) δ 8.32 (s, 1H), 8.22 (d, *J* = 8.0 Hz, 1H), 8.19 (s, 2H), 8.13 (d, *J* = 8.0 Hz, 1H), 7.79 (s, 1H), 7.71 (s, 1H), 7.60 (d, *J* = 9.0 Hz, 2H), 7.55 (d. *J* = 3.0 Hz, 1H), 7.42-7.50 (m, 5H), 4.33-4.34 (m, 2H), 1.88 (t, *J* = 7.5 Hz, 2H), 1.49 (s, 18H), 1.42-1.46 (m, 2H), 0.96 (t, *J* = 7.5 Hz, 3H); ^{13}C NMR (DMSO-d_6, 125.77 MHz) δ 172.03, 163.65, 146.60, 146.23, 145.70, 142.34, 141.59, 141.53, 141.17, 138.88, 135.34, 133.83, 133.79, 130.50, 128.34, 125.54, 124.75, 123.64, 122.74, 122.01, 121.66, 121.15, 120.72, 117.51, 117.25, 116.65, 116.58, 109.20, 107.47, 106.16, 98.03, 79.2, 42.07, 34.47, 31.82, 30.86, 19.75, 13.80; HRMS calcd for $C_{48}H_{45}N_3O_2S_2Na$ $[M + Na]^+$ *m/z* 782.2845, found 782.2825.

6.5 References

1. E. M. Barea and J. Bisquert, Properties of chromophores determining recombination at the TiO_2-dye-electrolyte interface. *Langmuir,* **2013**, *29*, 8773-8781.

2. A. Mishra, M. K. R. Fischer and P. Bäuerle, Metal-free organic dyes for dye-sensitized solar cells: From structure: Property relationships to design rules. *Angew. Chem. Int. Ed.*, **2009**, *48*, 2474-2499.
3. B.-G. Kim, K. Chung and J. Kim, Molecular design principle of all organic dyes for dye-sensitized solar cells. *Chem.–Eur. J.*, **2013**, *19*, 5220-5230.
4. S. Haid, M. Marszalek, A. Mishra, M. Wielopolski, T. Joël, J.-E. Moser, R. Humphry-Baker, S. M. Zakeeruddin, M. Grätzel and P. Bäuerle, Significant improvement of dye-sensitized solar cell performance by small structural modification in π-conjugated donor-acceptor dyes. *Adv. Funct. Mater.*, **2012**, *22*, 1291-1302.
5. Y.-S. Yen, H.-H. Chou, Y.-C. Chen, C.-Y. Hsu and J. T. Lin, Recent developments in molecule-based organic materials for dye sensitized solar cells. *J. Mater. Chem.*, **2012**, *22*, 8734-8747.
6. N. Koumura, Z.-S. Wang, S. Mori, M. Miyashita, E. Suzuki and K. Hara, Alkyl-functionalized organic dyes for efficient molecular photovoltaics. *J. Am. Chem. Soc.*, **2006**, *128*, 14256-14257.
7. H. Choi, J.-J. Kim, K. Song, J. Ko, M. K. Nazeeruddin and M. Grätzel, Molecular engineering of panchromatic unsymmetrical squaraines for dye-sensitized solar cell applications. *J. Mater. Chem.*, **2010**, *20*, 3280-3286.
8. Y. Hao, X. C. Yang, M. Z. Zhou, J. Y. Cong, X. N. Wang, A. Hagfeldt and L. Sun, Molecular design to improve the performance of donor–π acceptor Near-IR organic dye-sensitized solar cells. *ChemSusChem*, **2011**, *4*, 1601-1605.
9. Z.-S. Wang, N. Koumura, Y. Cui, M. Takahashi, H. Sekiguchi, A. Mori, T. Kubo, A. Furube and K. Hara, Hexylthiophene functionalized carbazole dyes for efficient molecular photovoltaics: Tuning of solar-cell performance by structural modification. *Chem. Mater.*, **2008**, *20*, 3993-4003.
10. X. Hu, S. Cai, G. Tian, X. Li, J. Su and J. Li, Rigid triarylamine based D-A-π-A structural organic sensitizers for solar cells: The significant enhancement of open-circuit photovoltage with a long alkyl group. *RSC Adv.*, **2013**, *3*, 22544-22553.
11. Y. Cui, Y. Wu, X. Lu, X. Zhang, G. Zhou, F. B. Miapeh, W. Zhu and Z.-S. Wang, Incorporating benzotriazole moiety to construct D-A-π-A organic sensitizers for solar

cells: Significant enhancement of open-circuit photovoltage with long alkyl group. *Chem. Mater.*, **2011**, *23*, 4394-4401.

12. Y. Wu, X. Zhang, W. Li, Z.-S. Wang, H. Tian and W. Zhu, Hexylthiophene-featured D-A-π-A structural indoline chromophores for coadsorbent-free and panchromatic dye-sensitized solar cells. *Adv. Energy Mater.*, **2012**, *2*, 149-156.
13. Q. Chai, W. Li, Y. Wu, K. Pei, J. Liu, Z. Geng, H. Tian and W. Zhu, Effect of a long alkyl group on cyclopentadithiophene as a conjugated bridge for D-A-π-A organic sensitizers: IPCE, electron diffusion length, and charge recombination. *ACS Appl. Mater. Interfaces*, **2014**, *6*, 14621-14630.
14. K. Do, D. Kim, N. Cho, S. Paek, K. Song and J. Ko, New type of organic sensitizers with a planar amine unit for efficient dyesensitized solar cells. *Org. Lett.*, **2012**, *14*, 222-225.
15. B. Liu, Q. Liu, D. You, X. Li, Y. Naruta and W. Zhu, Molecular engineering of indoline based organic sensitizers for highly efficient dye-sensitized solar cells. *J. Mater. Chem.*, **2012**, *22*, 13348-13356.
16. Y. J. Chang, P.-T. Chou, S.-Y. Lin, M. Watanabe, Z.-Q. Liu, J.-L. Lin, K.-Y. Chen, S.-S. Sun, C.-Y. Liu and T. J. Chow, High-Performance organic materials for dye-sensitized solar cells: Triarylene-linked dyads with a 4-*tert*-butylphenylamine donor. *Chem. - Asian J.*, **2012**, *7*, 572-581.
17. T. Duan, K. Fan, C. Zhong, T. Peng, J. Qin and X. Chen, New organic dyes containing *tert*-Butyl-capped *N*-Arylcarbazole moiety for dye-sensitized solar cells. *RSC Adv.*, **2012**, *2*, 7081-7086.
18. S. Namuangruk, R. Fukuda, M. Ehara, J. Meeprasert, T. Khanasa, S. Morada, T. Kaewin, S. Jungsuttiwong, T. Sudyoadsuk and V. Promarak, D-D-π-A-Type organic dyes for dye-sensitized solar cells with a potential for direct electron injection and a high extinction coefficient: Synthesis, characterization, and theoretical investigation. *J. Phys. Chem. C*, **2012**, *116*, 25653-25663.
19. T. Khanasa, N. Jantasing, S. Morada, N. Leesakul, R. Tarsang, S. Namuangruk, T. Kaewin, S. Jungsuttiwong, T. Sudyoadsuk and V. Promarak, Synthesis and characterization of D-D-π-A-type organic dyes bearing bis(3,6-di-*tert*-butylcarbazol-9-

ylphenyl)aniline as donor moiety for dye-sensitized solar cells. *Eur. J. Org. Chem.*, **2013**, 2608-2620.

20. C. Teng, X. Yang, S. Li, M. Cheng, A. Hagfeldt, L. Wu and L. Sun, Tuning the HOMO energy levels of organic dyes for dye sensitized solar cells based on Br^-/Br_3^- electrolytes. *Chem.–Eur. J.*, **2010**, *16*, 13127-13138.
21. W. Lee, N. Cho, J. Kwon, J. Ko and J.-I. Hong, New organic dye based on a 3,6-disubstituted carbazole donor for efficient dye sensitized solar cells. *Chem.–Asian J.*, **2012**, *7*, 343-350.
22. E. M. Barea, C. Zafer, B. Gultekin, B. Aydin, S. Koyuncu, S. Icli, F. F. Santiago and J. Bisquert, Quantification of the effects of recombination and injection in the performance of dye-sensitized solar cells based on N-Substituted carbazole dyes. *J. Phys. Chem. C*, **2010**, *114*, 19840-19848.
23. L.-L. Tan, J.-F. Huang, Y. Shen, L.-M. Xiao, J.-M. Liu, D.-B. Kuang and C.-Y. Su, Highly efficient and stable organic sensitizers with duplex starburst triphenylamine and carbazole donors for liquid and quasi-solid-state dye-sensitized solar cells. *J. Mater. Chem. A*, **2014**, *2*, 8988-8994.
24. A. Baheti, K. R. J. Thomas, C.-P. Lee and K.-C. Ho, Fine tuning the performance of dsscs by variation of the π-spacers in organic dyes that contain a 2,7-diaminofluorene donor. *Chem. Asian J.*, **2012**, *7*, 2942-2954.
25. K. S. V. Gupta, T. Suresh, S. P. Singh, A. Islam, L. Han and M. Chandrasekharam, Carbazole based A-π-D-π-A dyes with double electron acceptor for dye-sensitized solar cell. *Org. Electron.*, **2014**, *15*, 266-275.
26. M.-D. Zhang, H.-X. Xie, X.-H. Ju, L. Qin, Q.-X. Yang, H.-G. Zheng and X.-F. Zhou, D-D-π-A organic dyes containing 4,4′-di(2-thienyl)-triphenylamine moiety for efficient dye-sensitized solar cells. *Phys. Chem. Chem. Phys.*, **2013**, *15*, 634-641.
27. T. Sudyoadsuk, S. Pansay, S. Morada, R. Rattanawan, S. Namuangruk, T. Kaewin, S. Jungsuttiwong and V. Promarak, Synthesis and characterization of D–D–π–A-type organic dyes bearing carbazole–carbazole as a donor moiety (D–D) for efficient dye-sensitized solar cells. *Eur. J. Org. Chem.*, **2013**, 5051-5063.

28. C. Teng, X. Yang, C. Yuan, C. Li, R. Chen, H. Tian, S. Li, A. Hagfeldt and L. Sun, Two novel carbazole dyes for dye-sensitized solar cells with open-circuit voltages up to 1 V based on Br^-/Br_3^- electrolytes. *Org. Lett.*, **2009**, *11*, 5542-5545.
29. L.-L. Tan, L.-J. Xie, Y. Shen, J.-M. Liu, L.-M. Xiao, D.-B. Kuang and C.-Y. Su, Novel organic dyes incorporating a carbazole or dendritic 3,6-diiodocarbazole unit for efficient dye-sensitized solar cells. *Dyes Pigm.*, **2014**, *100*, 269-277.
30. A. Yella, R. Humphry-Baker, B. F. E. Curchod, N. S. Astani, J. Teuscher, L. E. Polander, S. Mathew, J.-E. Moser, I. Tavernelli, U. Rothlisherger, M. Grätzel, M. K. Nazeeruddin, and J. Frey, Molecular engineering of a fluorene donor for dye-sensitized solar cells. *Chem. Mater.*, **2013**, *25*, 2733-2739.
31. F. Monnier and M. Taillefer, Catalytic C-C, C-N, and C-O Ullmann-type coupling reactions. *Angew. Chem., Int. Ed.*, **2009**, *48*, 6954-6971.
32. Y. Liu, M. Nishiura, Y. Wang and Z. Hou, π-Conjugated aromatic enynes as a single-emitting component for white electroluminescence. *J. Am. Chem. Soc.*, **2006**, *128*, 5592-5593.
33. A. W. Freeman, M. Urvoy and M. E. Criswell, Triphenylphosphine-mediated reductive cyclization of 2-nitrobiphenyls: A practical and convenient synthesis of carbazoles. *J. Org. Chem.*, **2005**, *70*, 5014-5019.
34. Y. Che, D. E. Gross, H. Huang, D. Yang, X. Yang, E. Discekici, Z. Xue, H. Zhao, J. S. Moore and L. Zang, Diffusion-controlled detection of trinitrotoluene: Interior nanoporous structure and low highest occupied molecular orbital level of building blocks enhance selectivity and sensitivity. *J. Am. Chem. Soc.*, **2012**, *134*, 4978-4982.
35. N. Miyaura and A. Suzuki, Palladium-catalyzed cross-coupling reactions of organoboron compounds. *Chem. Rev.*, **1995**, *95*, 2457-2483.
36. J. K. Stille, The palladium-catalyzed cross-coupling reactions of organotin reagents with organic electrophiles. *Angew. Chem. Int. Ed.*, **1986**, *25*, 508-524.
37. E. Knoevenagel, Ueber eine darstellungsweise des benzylidenacetessigesters. *Chem. Ber.* **1896**, *29*, 172-174.
38. W. Zhu, Y. Wu, S. Wang, W. Li, X. Li, J. Chen, Z.-S. Wang and H. Tian, Organic D-A-π-A solar cell sensitizers with improved stability and spectral response. *Adv. Funct. Mater.*, **2011**, *21*, 756-763.

39. J.-J. Kim, H. Choi, J.-W. Lee, M.-S. Kang, K. Song, S. O. Kang and J. Ko, A polymer gel electrolyte to achieve ≥ 6% power conversion efficiency with a novel organic dye incorporating a lowband-gap chromophore. *J. Mater. Chem*., **2008**, *18*, 5223-5229.
40. A. Mishra, N. Pootrakulchote, M. Wang, S.-J. Moon, S. M. Zakeeruddin, M. Grätzel and P. Bäuerle, A thiophene-based anchoring ligand and its heteroleptic Ru(II)-Complex for efficient thin-film dye-sensitized solar cells. *Adv. Funct. Mater.*, **2011**, *21*, 963-970.
41. M. K. Nazeeruddin, P. Péchy, T. Renouard, S. M. Zakeeruddin, R. Humphry-Baker, P. Comte, P. Liska, L. Cevey, E. Costa, V. Shklover, L. Spiccia, G. B. Deacon, C. A. Bignozzi and M. Grätzel, Engineering of efficient panchromatic sensitizers for nanocrystalline TiO_2-based solar cells. *J. Am. Chem. Soc.*, **2001**, *123*, 1613-1624.
42. M. K. Nazeeruddin, S. M. Zakeeruddin, R. Humphry-Baker, M. Jirousek, P. Liska, N. Vlachopoulos, V. hklover, C. H. Fisher and M. Grätzel, Acid-base equilibria of (2,2‘-bipyridyl-4,4‘-dicarboxylic acid)ruthenium(II) complexes and the effect of protonation on charge-transfer sensitization of nanocrystalline titania. *Inorg. Chem.*, **1999**, *38*, 6298-6305.
43. Z.-S. Wang, F.-Y. Li and C.-H. Huang, photocurrent enhancement of hemicyanine dyes containing RSO3-group through treating TiO_2 films with hydrochloric acid. *J. Phys. Chem. B*, **2001**, *105*, 9210-9217.
44. P. Singh, A. Baheti and K. R. J. Thomas, Synthesis and optical properties of acidochromic amine-substituted benzo[*a*]phenazines. *J. Org. Chem*., **2011**, *76*, 6134-6145.
45. A. Baheti, P. Tyagi, K. R. J. Thomas, Y.-C. Hsu and J. T. Lin, Simple triarylamine-based dyes containing fluorene and biphenyl linkers for efficient dye-sensitized solar cells. *J. Phys. Chem. Lett*., **2009**, *113*, 8541-8547.
46. O.van den Berg, W. F. Jager and S. J. Picken, 7-Dialkylamino-1-alkylquinolinium Salts: Highly versatile and stable fluorescent probes. *J. Org. Chem.*, **2006**, *71*, 2666-2676.
47. A. Granzhan, H. Ihmels and G. Viola, 9-Donor-substituted acridizinium salts: Versatile environment-sensitive fluorophores for the detection of biomacromolecules. *J. Am. Chem. Soc*., **2007**, *129*, 1254-1267.
48. K. Rurack, J. L. Bricks, G. Reck, R. Radeglia and U. Resch-Genger, Chalcone-analogue dyes emitting in the near-infrared (NIR): Influence of donor-acceptor substitution and

cation complexation on their spectroscopic properties and X-ray structure *J. Phys. Chem. A*, **2000**, *104*, 3087-3109.

49. C. Reichardt, Solvatochromic dyes as solvent polarity indicators. *Chem. Rev.*, **1994**, *94*, 2319-23.
50. J. A. Pollard, D. Zhang, J. A. Downing, F. J. Knorr and J. L. McHale, Solvent effects on interfacial electron transfer from Ru(4,4′-dicarboxylic acid-2,2′-bipyridine)$_2$(NCS)$_2$ to nanoparticulate TiO_2: Spectroscopy and solar photoconversion. *J. Phys. Chem. A*, **2005**, *109*, 11443-11452.58.
51. K. Sayama, S. Tsukagoshi, K. Hara, Y. Ohga, A. Shinpou, Y. Abe, S. Suga and H. Arakawa, Photoelectrochemical properties of J aggregates of benzothiazole merocyanine dyes on a nanostructured TiO_2 film. *J. Phys. Chem. B*, **2002**, *106*, 1363-1371.
52. C. Teng, X. Yang, C. Yang, H. Tian, S. Li, X. Wang, A. Hagfeldt and L. Sun, Influence of triple bonds as π-Spacer units in metal-free organic dyes for dye-sensitized solar cells. *J. Phys. Chem. C*, **2010**, *114*, 11305-11313.
53. M. d. P. Carreón-Castro, M. Gutiérrez-Nava, O. G. Morales-Saavedra, J. M. Reyna-González and E. Rivera, Optical properties and aggregation of 1-N-methylamino-4'-nitroazobenzene in various environments. *Rev. mex. físic.*, **2008,** *54*, 229-235.
54. K. R. Mulhern, A. Orchard, D. F. Watson and M. R. Detty, Influence of surface-attachment functionality on the aggregation, persistence, and electron-transfer reactivity of chalcogenorhodamine dyes on TiO_2**.** *Langmuir*, **2012**, *28*, 7071-7082**.**
55. K. R. J. Thomas, Y.-C. Hsu, J. T. Lin, K.-M. Lee, K.-C. Ho, C.-H. Lai, Y.-M. Cheng and P.-T. Chou, 2,3-Disubstituted thiophene based organic dyes for solar cells. *Chem. Mater.*, **2008**, *20*, 1830-1840.
56. R. G. Parr and W. Yang, Density-functional theory of the electronic structure of molecules. *Annu. Rev. Phys. Chem.*, **1995**, *46*, 701-728.
57. B. J. Lynch, P. L. Fast, M. Harris and D. G. Truhlar, Adiabatic connection for kinetics. *J. Phys. Chem. A*, **2000**, *104*, 4811-4815.
58. J.-F. Morin, M. Leclerc, D. Adès and A. Siove, Polycarbazoles: 25 Years of progress. *Macromol. Rapid Commun.*, **2005**, *26*, 761-778.

59. S. Kato, H. Noguchi, A. Kobayashi, T. Yoshihara, S. Tobita and Y. Nakamura, Bicarbazoles: Systematic structure-property investigations on a series of conjugated carbazole dimers. *J. Org. Chem.*, **2012**, *77*, 9120-9133.
60. M. Grätzel, Photoelectrochemical cells. *Nature*, **2001**, *414*, 338-344.
61. A. Hagfeldt, G. Boschloo, L. Sun, L. Kloo and H. Pettersson, Dye-Sensitized Solar Cells. *Chem. Rev.*, **2010**, *110*, 6595-6663.
62. M. K. Nazeeruddin, A. Kay, I. Rodicio, R. Humphry-Baker, E. Müller, P. Liska, N. Vlachopoulos and M. Grätzel, Conversion of light to electricity by cis-X2bis(2,2′-bipyridyl-4,4′-dicarboxylate)-ruthenium(II) charge-transfer sensitizers (X = Cl^-, Br^-, I^-, CN^-, and SCN^-) on nanocrystalline titanium dioxide electrodes. *J. Am. Chem. Soc.*, **1993**, *115*, 6382-6390.
63. S. R. Raga, E. M. Barea and F. Fabregat-Santiago, Analysis of the origin of open circuit voltage in dye solar cells. *J. Phys. Chem. Lett.*, **2012**, *3*, 1629-1634.
64. G. Li, M. Liang, H. Wang, Z. Sun, L. Wang, Z. Wang and S. Xue, Significant enhancement of open-circuit voltage in indoline-based dye-sensitized solar cells via retarding charge recombination. *Chem. Mater.*, **2013**, *25*, 1713-1722.
65. S. A. Haque, Y. Tachibana, R. L. Willis, J. E. Moser, M. Grätzel, D. R. Klug and J. R. Durrant, Parameters influencing charge recombination kinetics in dye-sensitized nanocrystalline titanium dioxide films. *J. Phys. Chem. B*, **2000**, *104*, 538-547.
66. G. M. Sheldrick, SHELXS-97: Program for crystal structure determination; University of Göttingen: Germany, **1997**.
67. G. M. Sheldrick, SHELXL-97: Program for the refinement of crystal structure; University of Göttingen: Germany, **1997**.
68. L. J. Farrugia, WinGX and ORTEP for Windows: an Update. *J. Appl. Crystallogr.*, **2012**, *45*, 849-854.

CHAPTER 7

Summary

In this thesis, we have designed and synthesized carbazole-based organic dyes and studied the optical, electrochemical and photovoltaic properties. We analyzed the results by performing computational calculations with two different theories (B3LYP and MPW1K). The nature of donor and linker played major role in tuning the HOMO and LUMO energy levels and donor-acceptor interactions which influenced the photovoltaic performance of the dyes. So, we systematically designed four classes of dyes by varying the π-linker, introducing fluorene in to arylamine donor, incorporating auxiliary chromophores such as alkoxy units and introduced carbazole as donor as well as linker. The detailed synthesis and characterization of the dyes are given in each chapter and confirmation of proposed structures of the dyes accomplished by detailed IR, NMR and mass spectral studies. We found that changing the nature of donor or acceptor alters the optical, electrochemical and photovoltaic properties. The choice of selecting 2, 7-di-substituted carbazole improved the photovoltaic performance when compared to phenyl and fluorene linked dyes. The salient features of the thesis are listed below.

Chapter 3

- 2, 7 Di-substituted carbazole-based dyes showed red shifted absorption when compared to the dyes containing phenyl, biphenyl and fluorene linker due to the electron rich carbazole which facilitates the effective donor-acceptor interactions.
- Incorporation of oligothiophene unit bathochromically shifted the absorption and displayed low oxidation potentials attributable to the electron richness of the thiophene unit.
- The DSSC fabricated using the dye containing bithiophene linker (**7b)** as sensitizer exhibited power conversion efficiency of 6.8% which increased to 7.2% when chenodexoycholic acid (CDCA) was used to impede dye aggregation.
- Elongation of conjugation by the insertion of 2,7-carbazole or 2,7-fluorene π-linkers led to hike in the molar extinction coefficients of the visible absorption and helped to raise the LUMO.
- The dye containing *para*-conjugated phenyl linker showed red shifted absorption when compared to *meta*-congener due to delinking of donor-acceptor interactions for the later.

- Though the dyes possessing different linkers showed similar ground state oxidation potentials, they displayed huge variations in the excited state redox potentials which reflected in the charge collection efficiency of the devices and overall performance.

Chapter 4

- The dyes containing fluorene incorporated donors showed red shifted absorption with high molar extinction coefficient when compared to dyes containing diphenylamine donor (**7a** and **7b**).
- Simultaneously, incorporation of fluorene led to easy oxidation attributable to the electron richness of fluorneamine donors.
- The introduction of fluorenylphenylamine and difluorenylamine raises the HOMO which helps to increase the open circuit voltage (V_{OC}) by shifting Fermi level of TiO_2 negatively due to more injection of electrons.
- The incorporation of fluorene in amine donor unit raises the LUMO which is favourable for the injection of electron from excited state of the dye into the conduction band of TiO_2.
- Theoretical calculations predicted that the HOMO of the dyes distributed on fluorenylphenylamine and difluorenylamine, but there is no contribution of fluorene incorporated on periphery of diphenylamine donor.
- The alkyl chains of fluorene in donor offered hydrophobic interactions and bulky structure of fluorenylphenylamine reduce the aggregation of the dyes on TiO_2 surface.
- Dye (**6b**) containing difluorenylamine donor exhibited a high power conversion efficiency of 6.4% with high short-circuit current density (J_{SC}) of 15.6 $mAcm^{-2}$.

Chapter 5

- Dyes which contain 2,4-dimethoxyphenyl and butoxy units as auxiliary chromophores showed red-shifted absorption when compared to parent dyes (**7a** and **7b**) owing to the increase in the donor strength and donor-acceptor interaction.
- The oxidation potentials of the dyes are reflective of the electron releasing effect of the peripheral units (4-butoxy > 2, 4-dimethoxyphenyl).

- The incorporation of peripheral butoxy and 2, 4-dimethoxyphenyl groups significantly raised the HOMO and lowered the LUMO of the dyes relative to the parent dyes (**7a** and **7b**).
- The dye (**34b**) with 2, 4-dimethoxyphenyl unit and bithiophene linker showed relatively high power conversion efficiency than butoxy dye attributable to the favorable LUMO and facile the electron injection from the excited dye into the conduction band of TiO_2.

Chapter 6

- The dyes containing carbazole/di(*tert*-butyl)carbazole donor showed improved light-harvesting properties when compared to the analogous dyes possessing 3,6-carbazole (**DL13** and **DL14**) or phenyl (**D70** and **D71**) linker.
- The donor property of the carbazole is substantially enhanced on introduction of *tert*-butyl groups at C-3 and C-6 positions.
- Selection of carbazole as donor raised the LUMO level of the dyes when compared to the dyes containing diarylamine unit which help the injection of electrons into the CB of TiO_2.
- The presence of *tert*-butyl groups on the carbazole nucleus minimized the intermolecular interactions which benefited the performance of DSSCs.
- Dye with carbazole donor functionalized with *tert*-butyl groups and thiophene linker exhibited higher V_{OC} of 666 mV.
- The best device efficiency (6.0%) was observed for a dye (**43b**) with di(*tert*-butyl)carbazole donor and bithiophene π-linker unit due to the high J_{SC} (15.78 mA cm^{-2}).

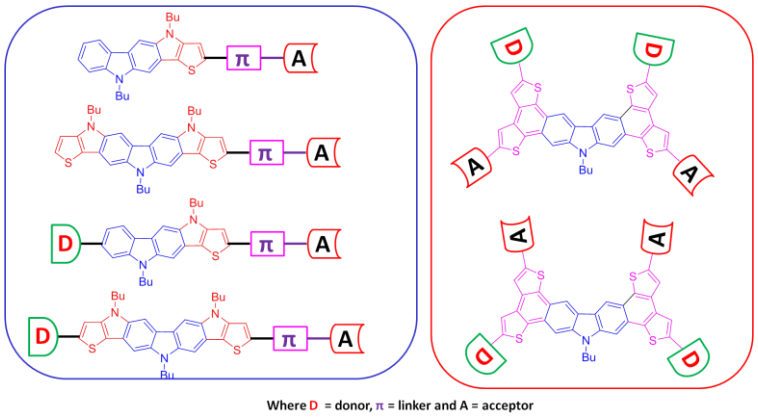

Figure 7.1 Thienopyrrole and dithienobenzene fused carbazole based dyes for DSSC.

In outlook, we believe that the promising absorption properties and impressive power conversion efficiencies of 2, 7 di-substituted carbazole offers further studies to achieve better dyes for DSSC. Since the electron rich carbazole as linker performed better photovoltaic properties, we can extend the journey to make promising sensitizers by using electron rich thienopyrrole fused carbazole and dithienobenzene fused carbazole units (Figure 7.1) for DSSC application.

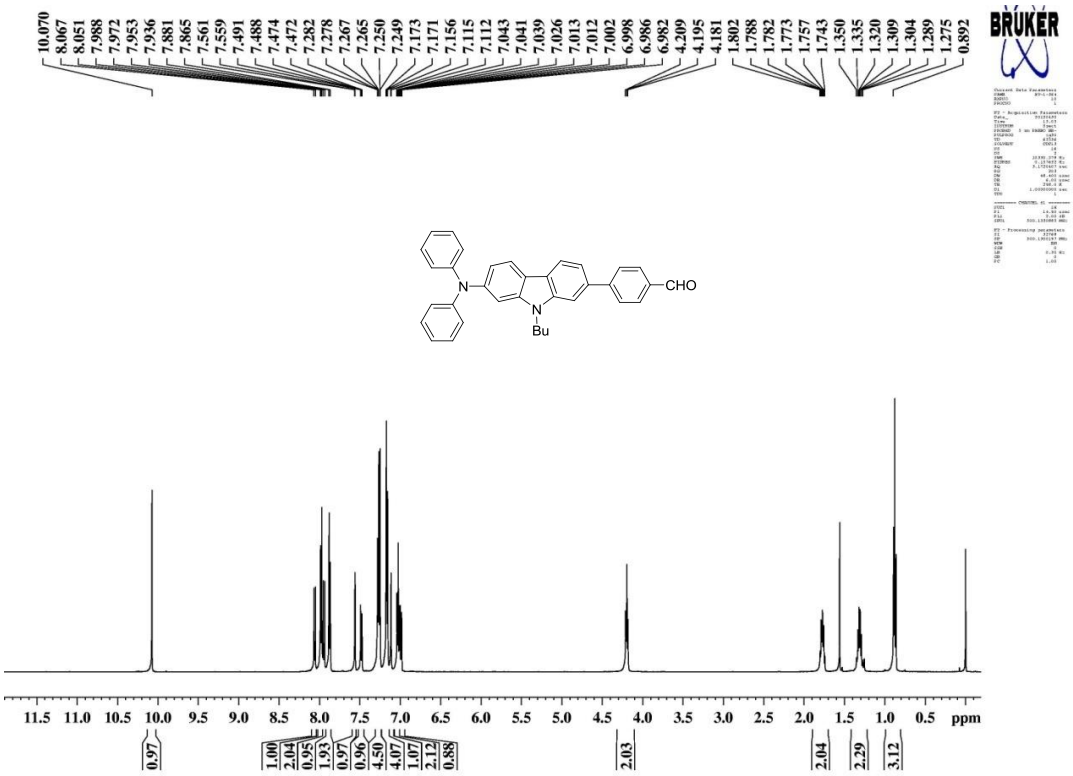

Figure S1 ^{1}H NMR spectrum of **4** recorded in $CDCl_3$.

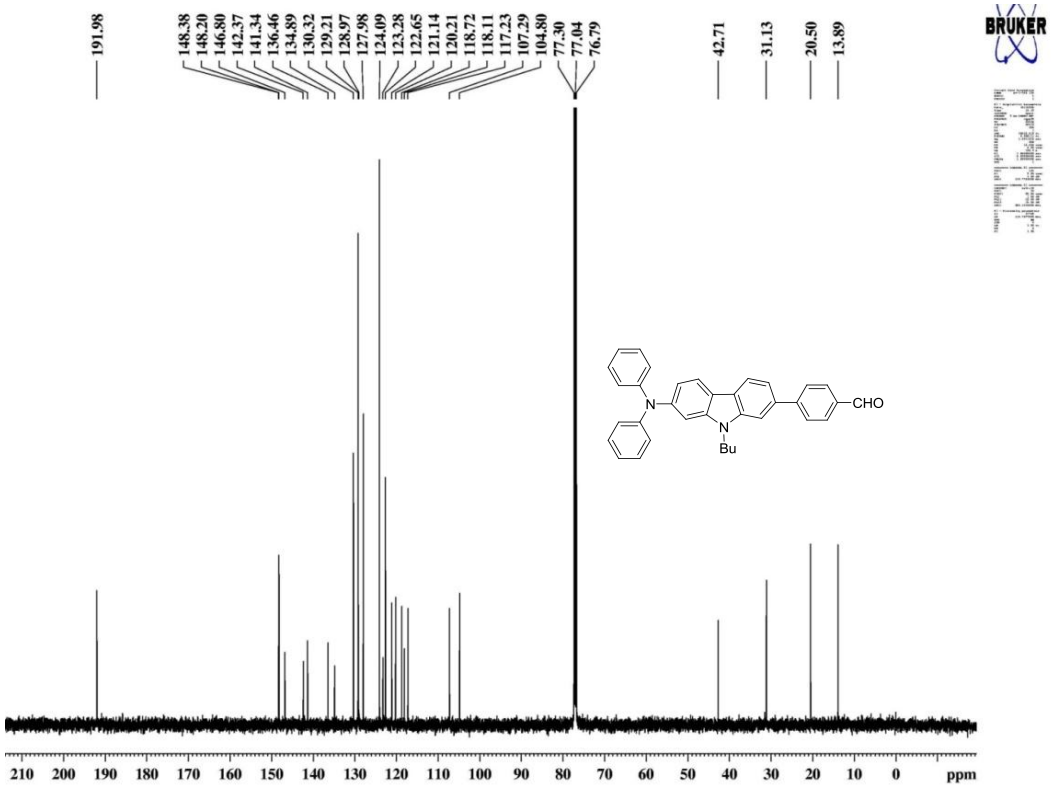

Figure S2 ^{13}C NMR spectrum of **4** recorded in $CDCl_3$.

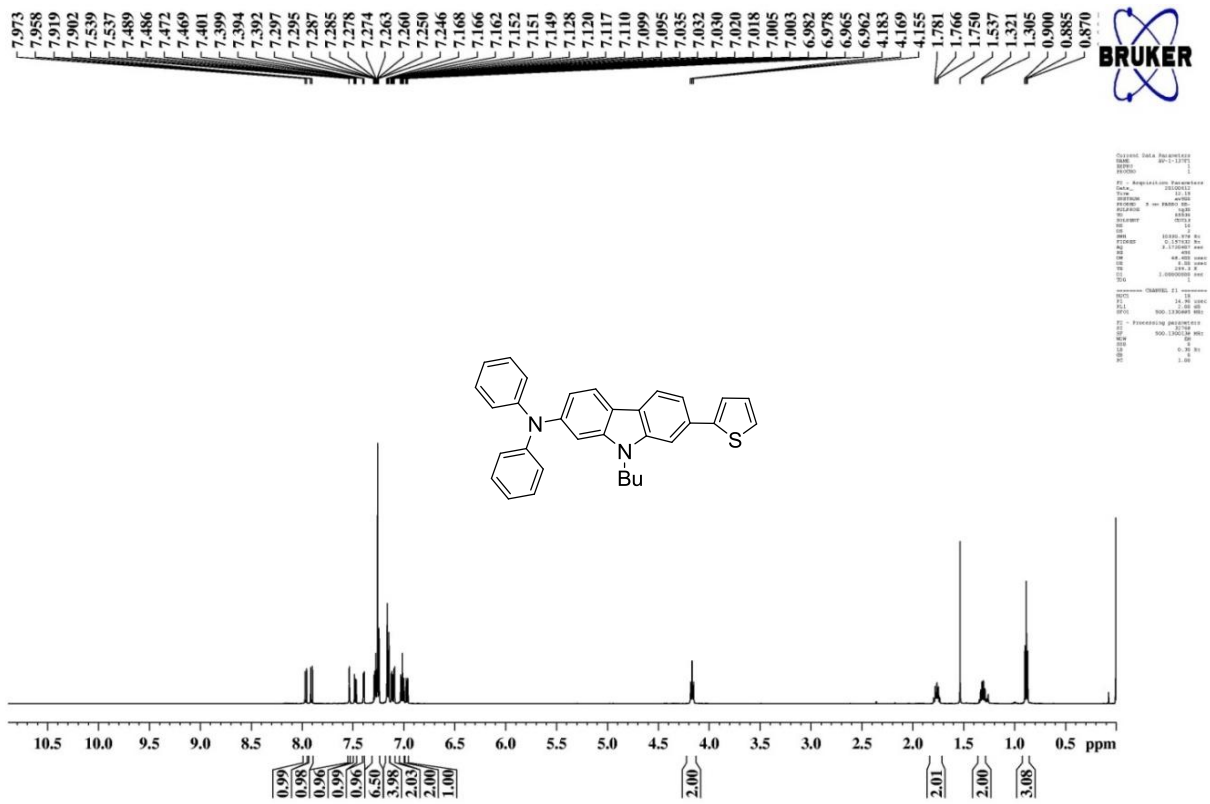

Figure S3 ^{1}H NMR spectrum of **9** recorded in $CDCl_3$.

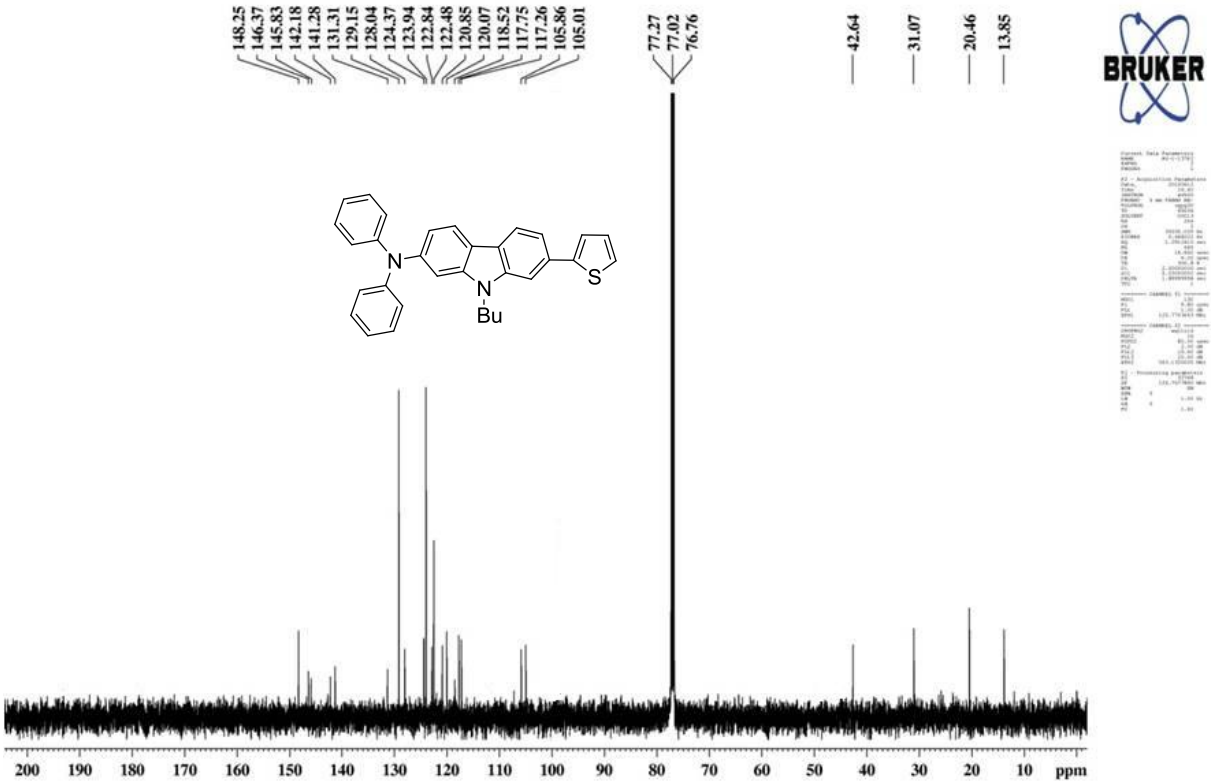

Figure S4 ^{13}C NMR spectrum of **9** recorded in $CDCl_3$.

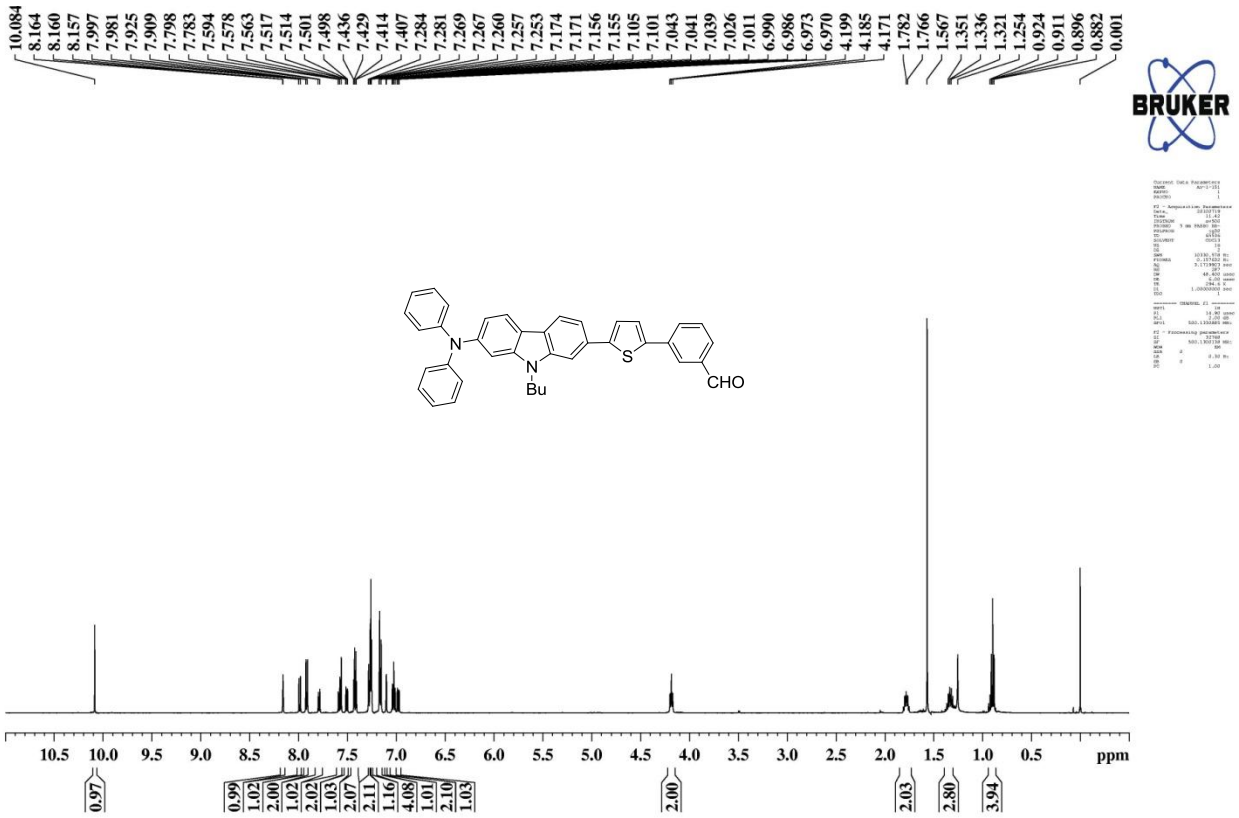

Figure S5 ^{1}H NMR spectrum of **10a** recorded in $CDCl_3$.

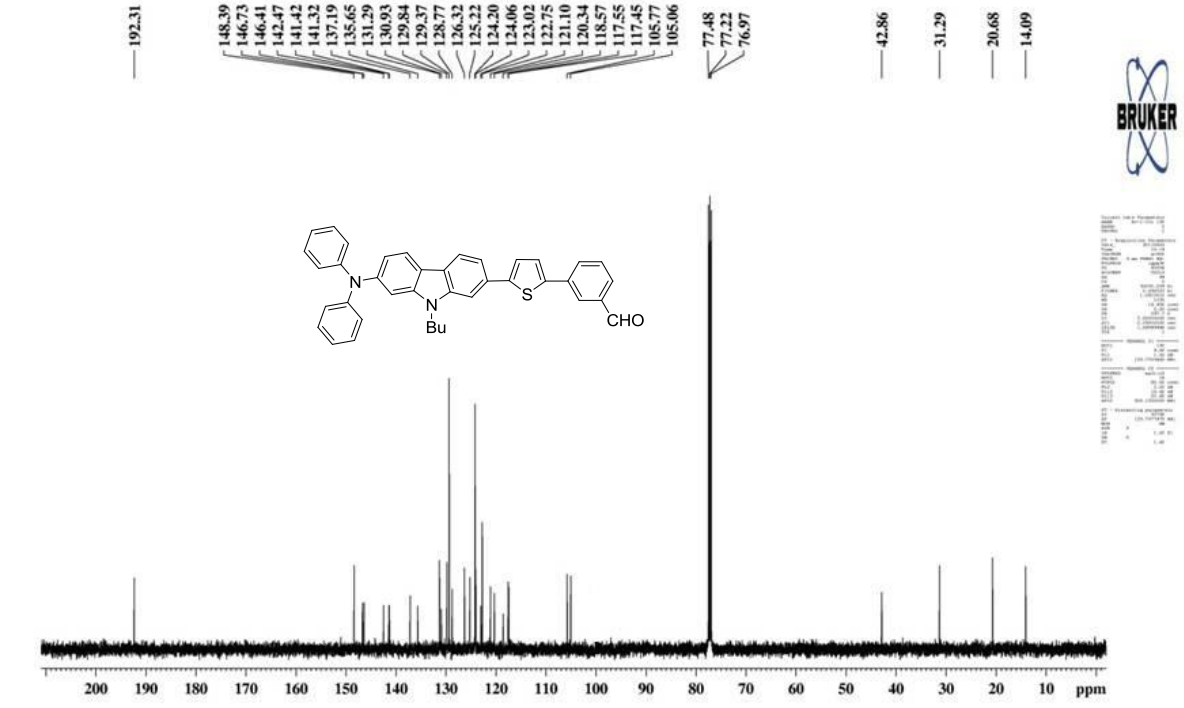

Figure S6 ^{13}C NMR spectrum of **10a** recorded in $CDCl_3$.

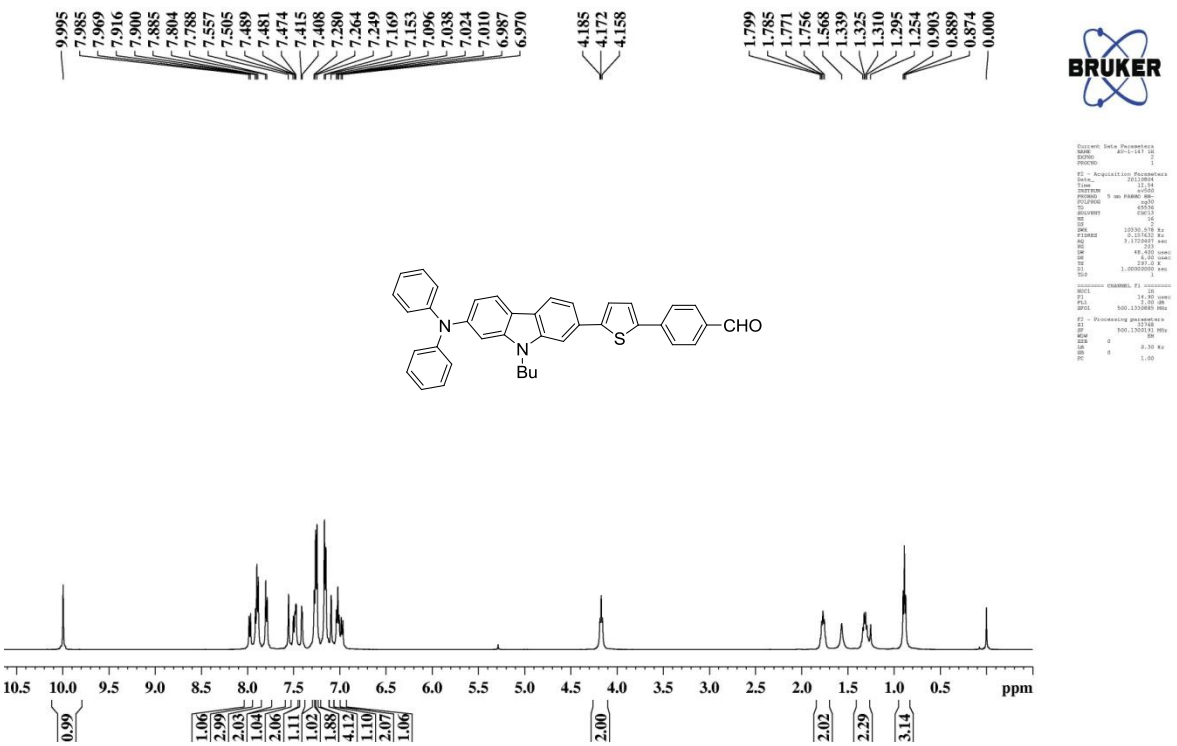

Figure S7 ^{1}H NMR spectrum of **10b** recorded in $CDCl_3$.

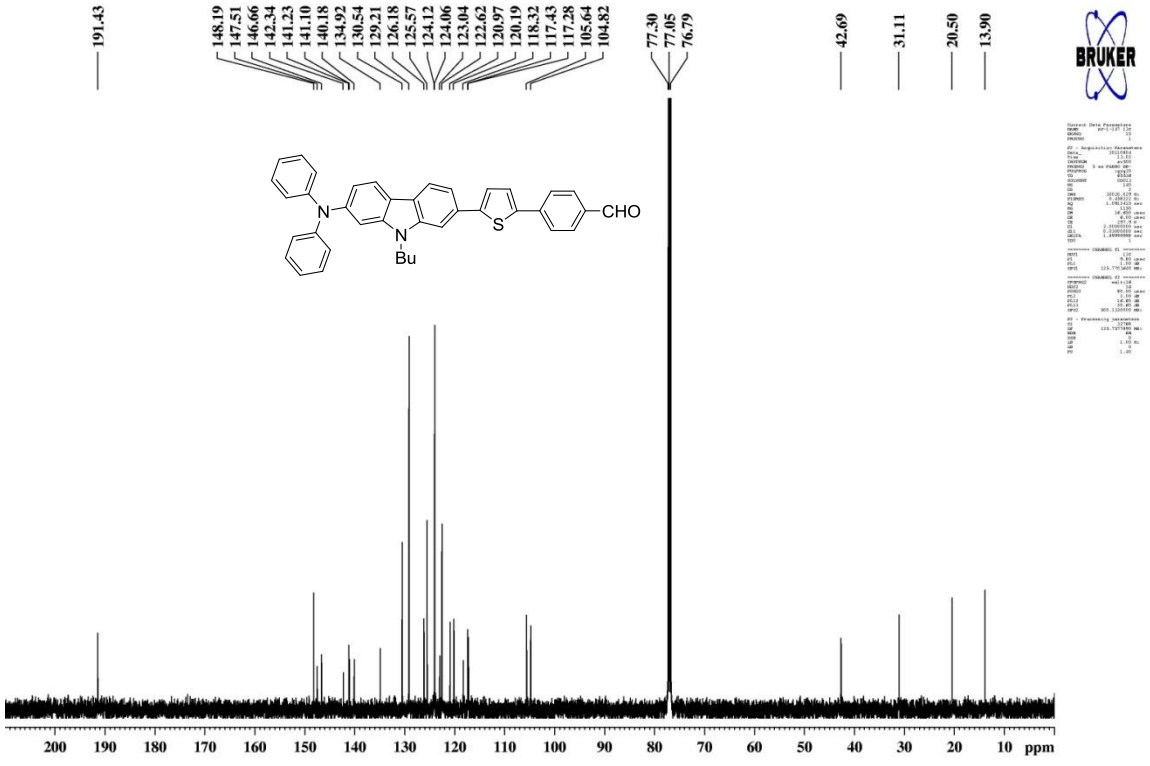

Figure S8 ^{13}C NMR spectrum of **10b** recorded in $CDCl_3$.

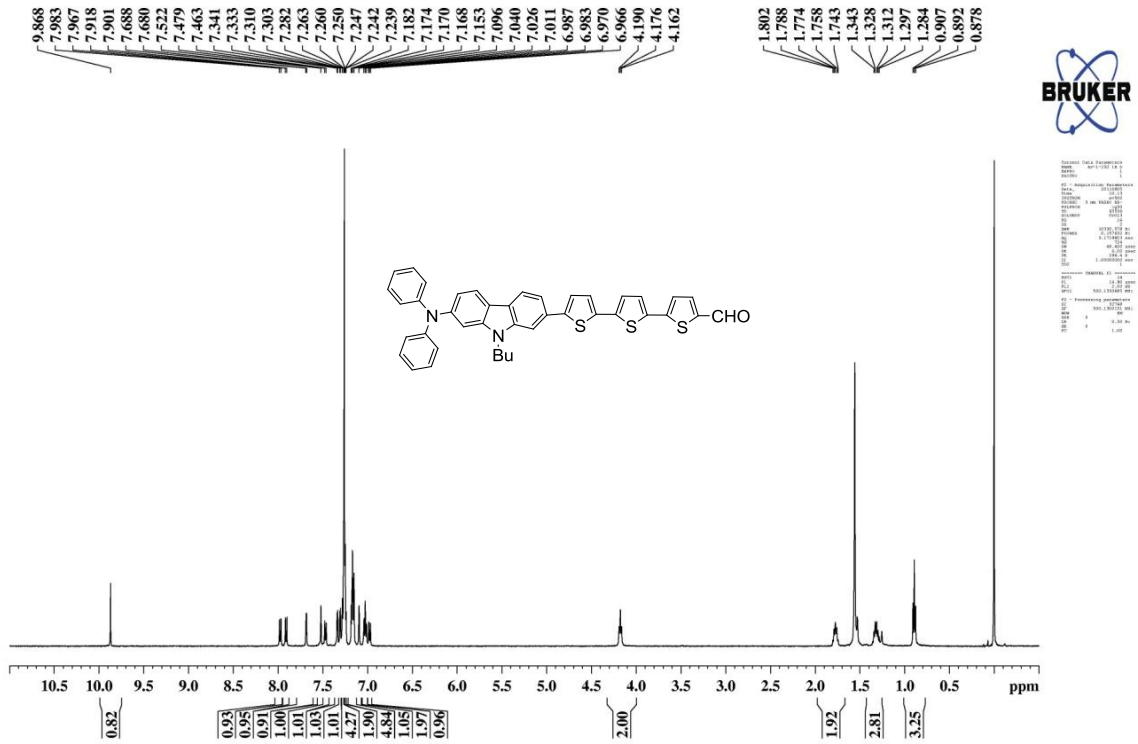

Figure S9 ^{1}H NMR spectrum of **10c** recorded in $CDCl_3$.

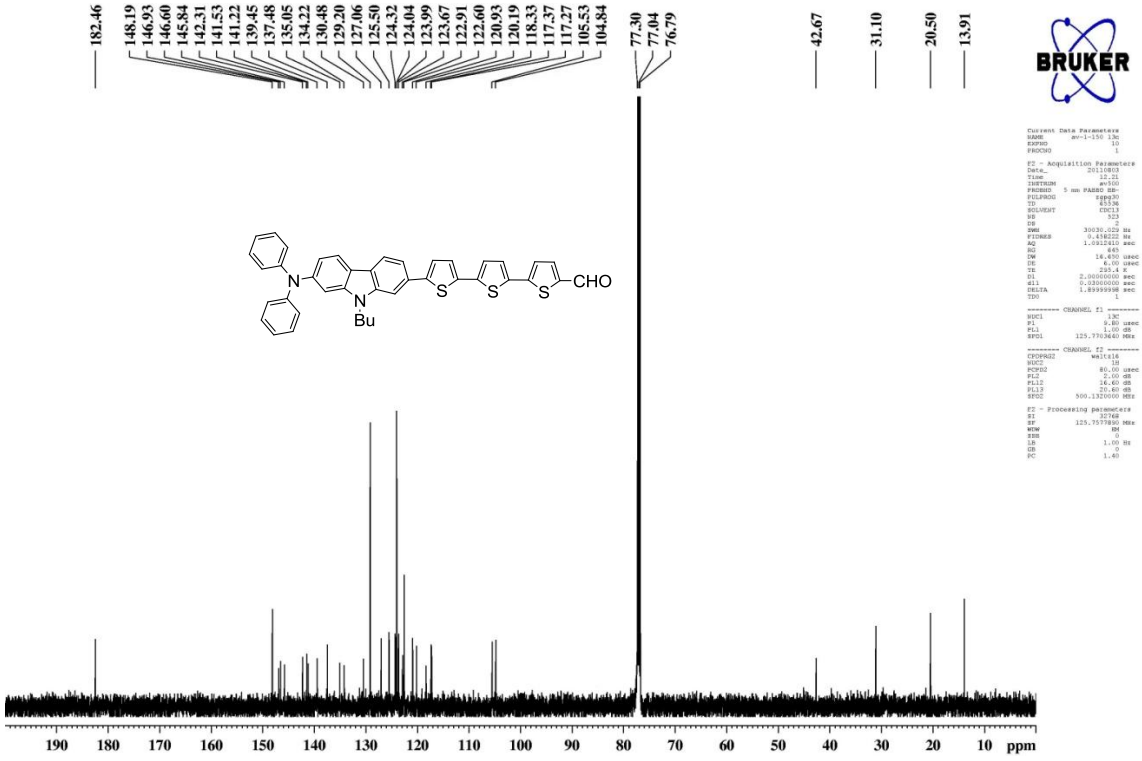

Figure S10 ^{13}C NMR spectrum of **10c** recorded in $CDCl_3$.

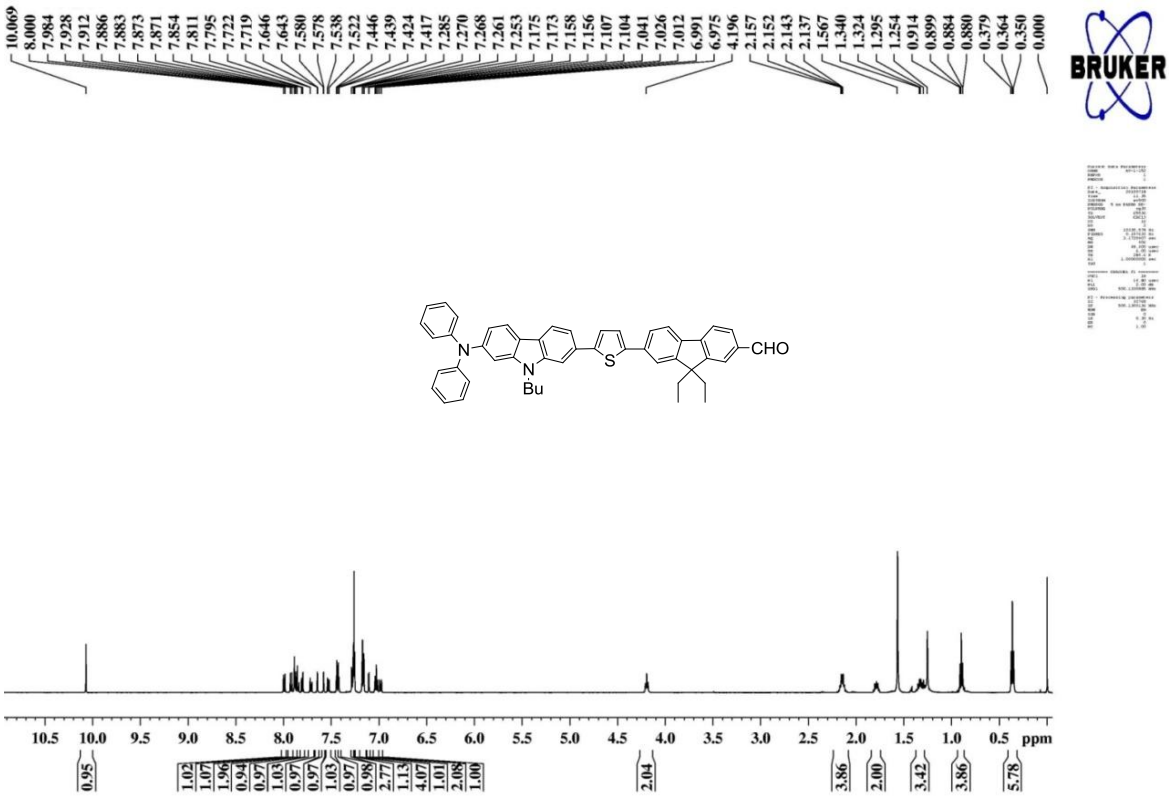

Figure S11 ^{1}H NMR spectrum of **10d** recorded in $CDCl_3$.

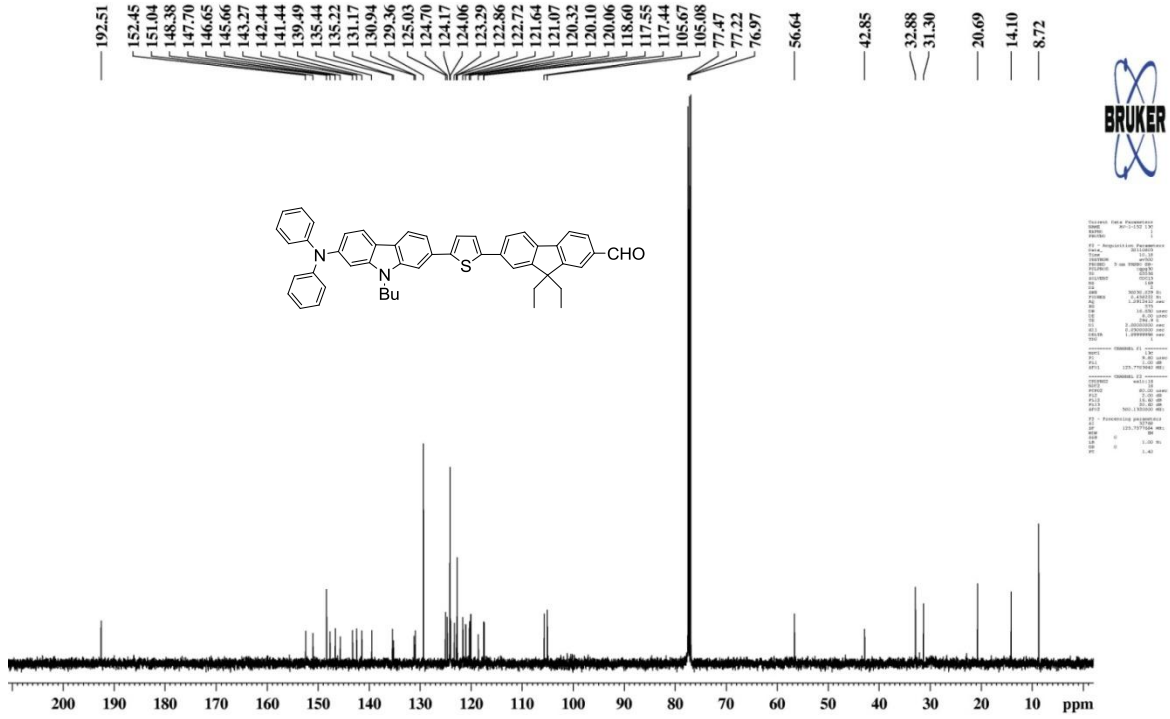

Figure S12 ^{13}C NMR spectrum of **10d** recorded in $CDCl_3$.

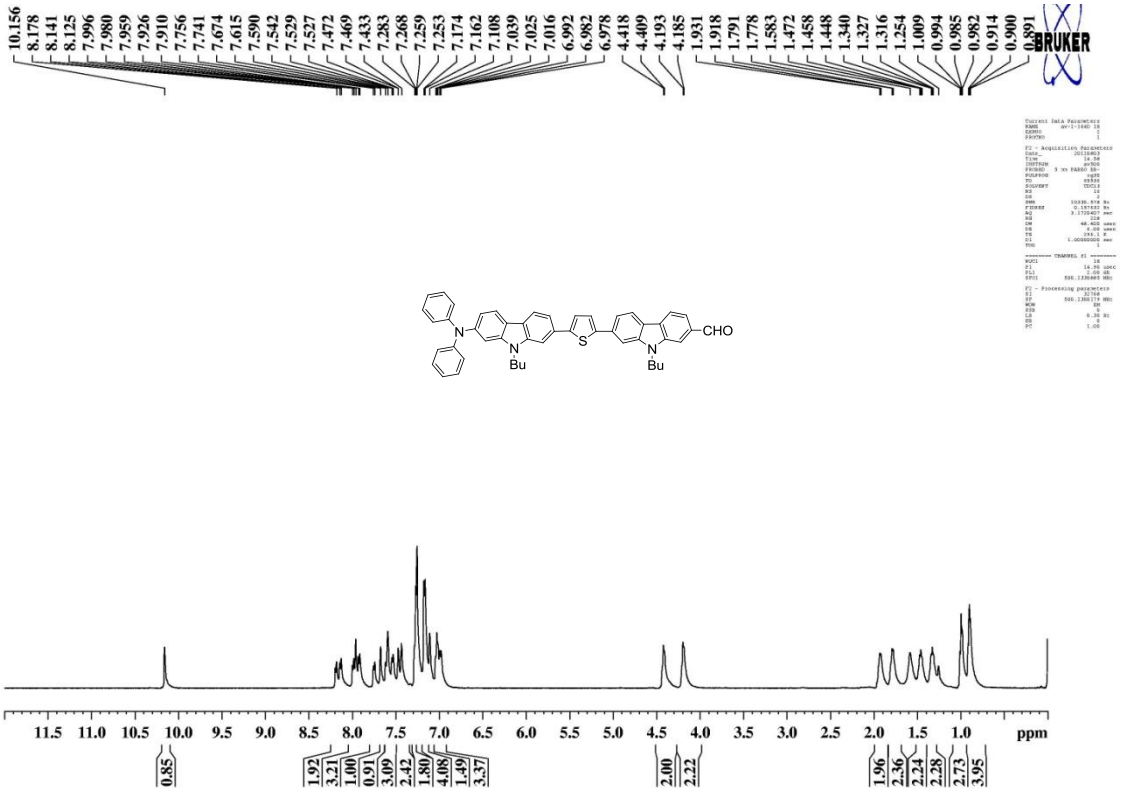

Figure S13 ^{1}H NMR spectrum of **10e** recorded in $CDCl_3$.

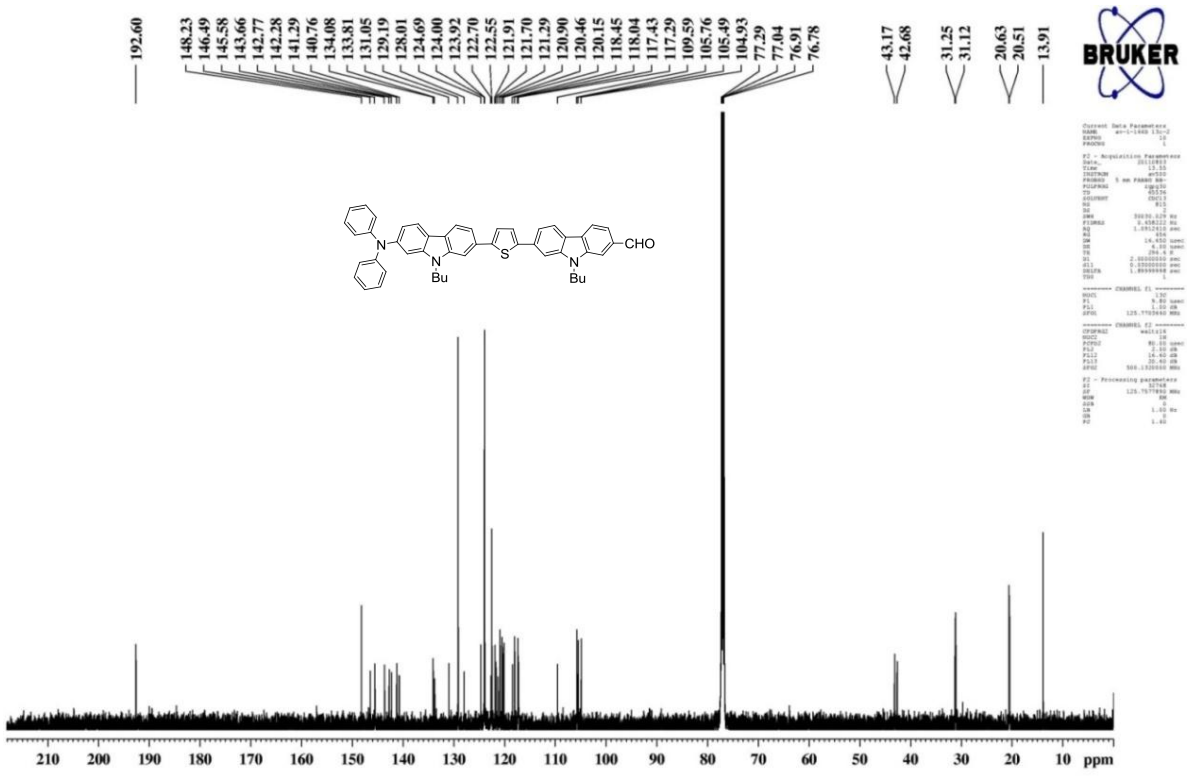

Figure S14 ^{13}C NMR spectrum of **10e** recorded in $CDCl_3$.

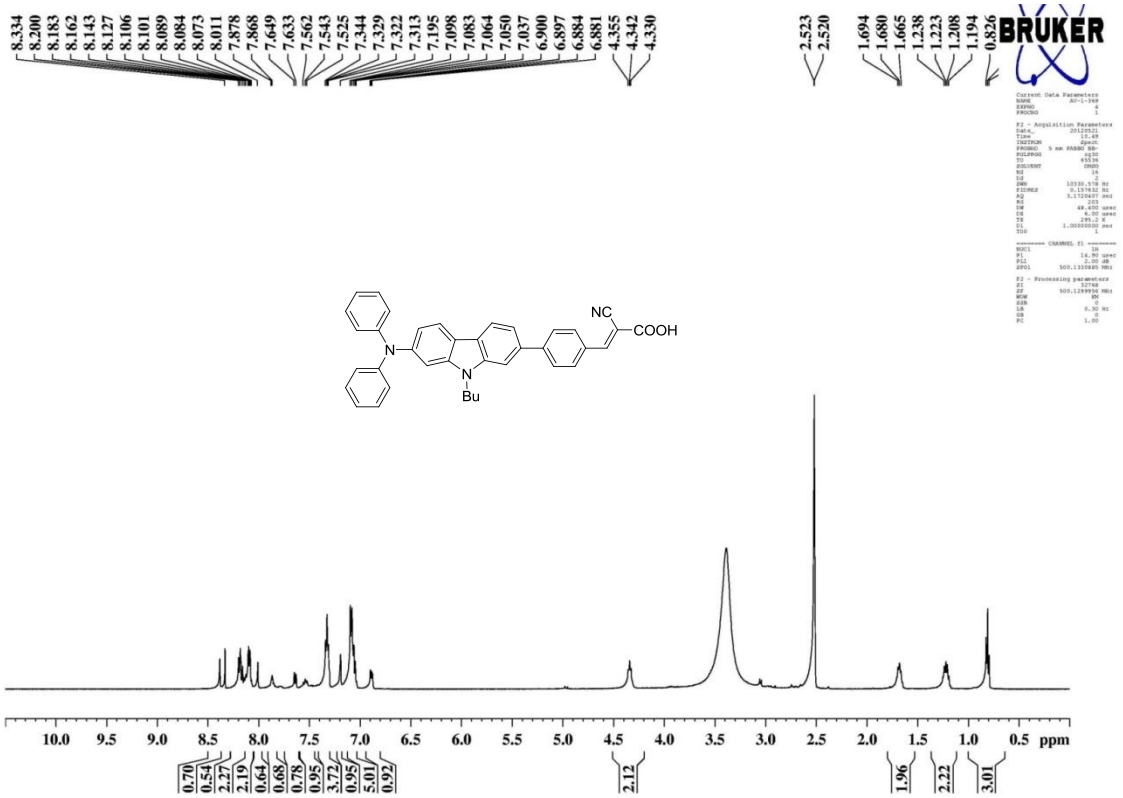

Figure S15 ^{1}H NMR spectrum of **5** recorded in DMSO-d_6.

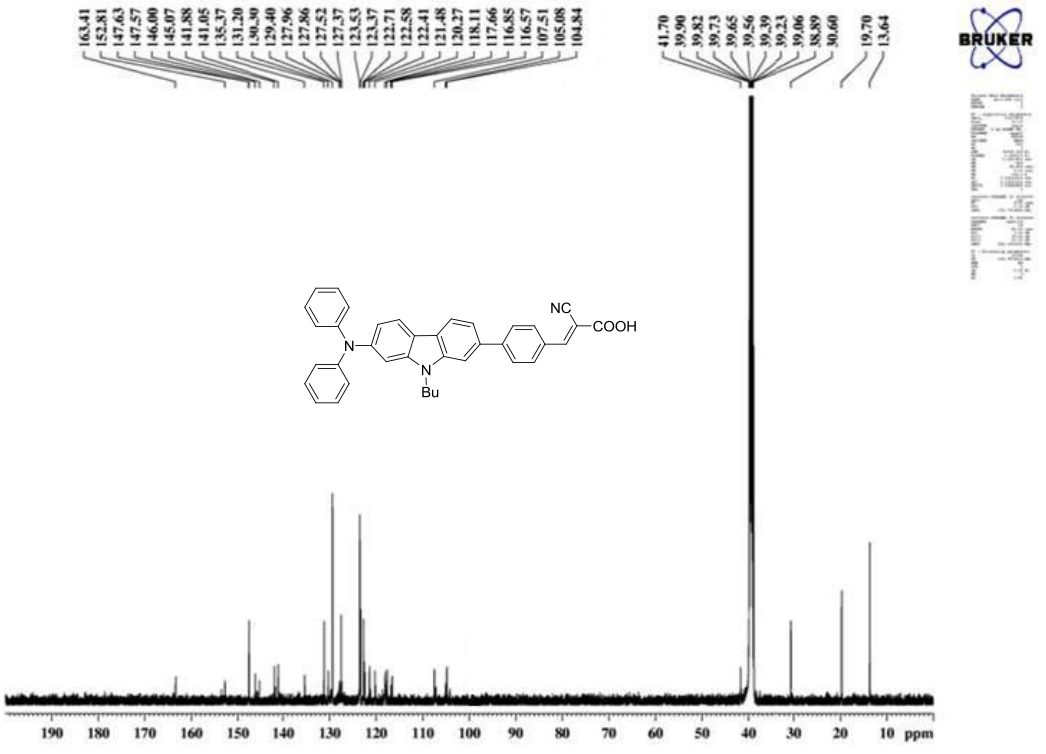

Figure S16 ^{13}C NMR spectrum of **5** recorded in DMSO-d_6.

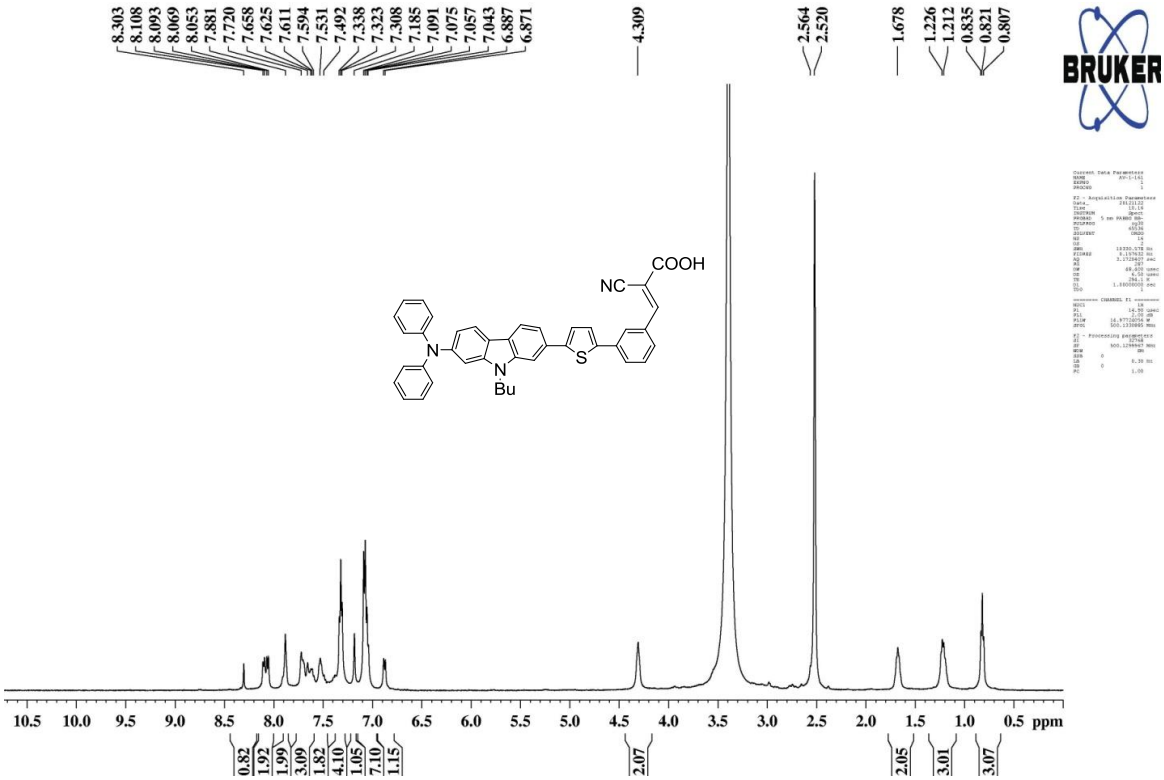

Figure S17 ^{1}H NMR spectrum of **11a** recorded in DMSO-d_6.

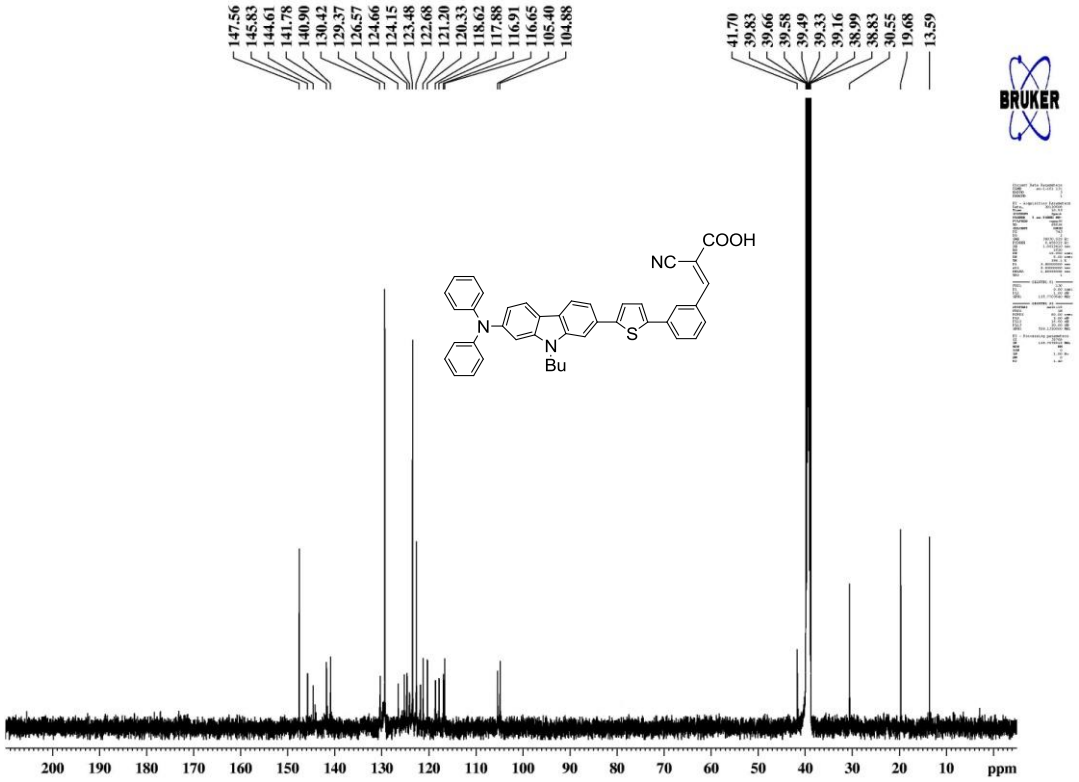

Figure S18 ^{13}C NMR spectrum of **11a** recorded in DMSO-d_6.

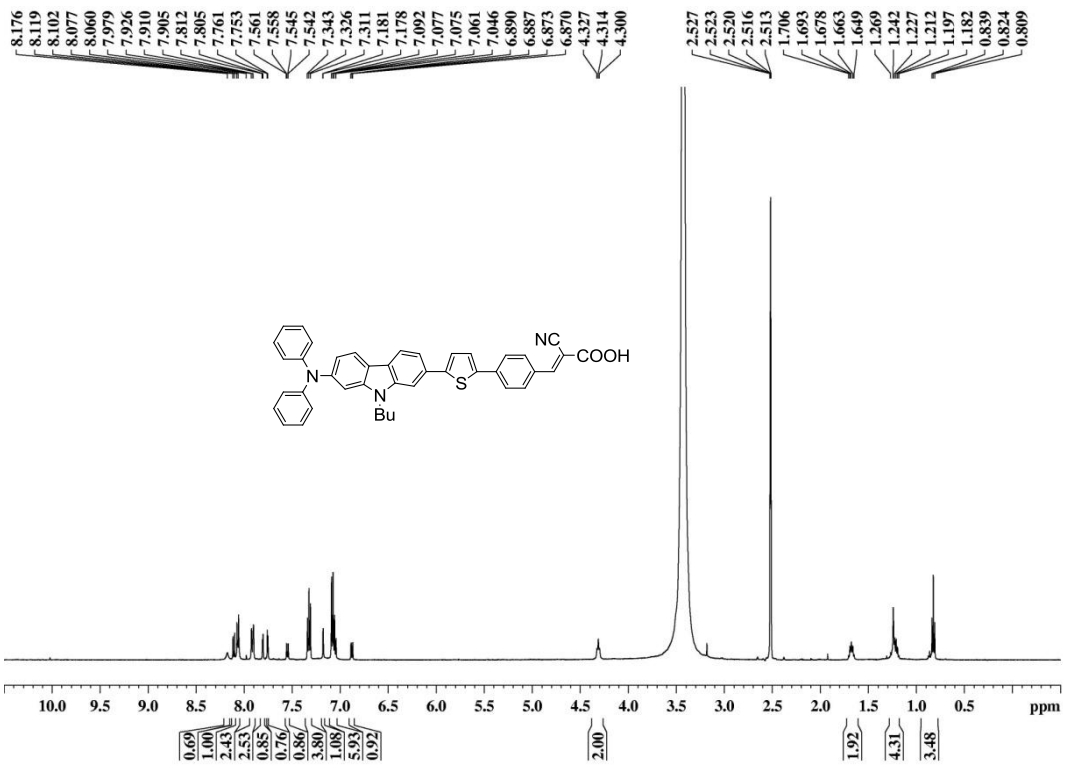

Figure S19 ^{1}H NMR spectrum of **11b** recorded in DMSO-d_6.

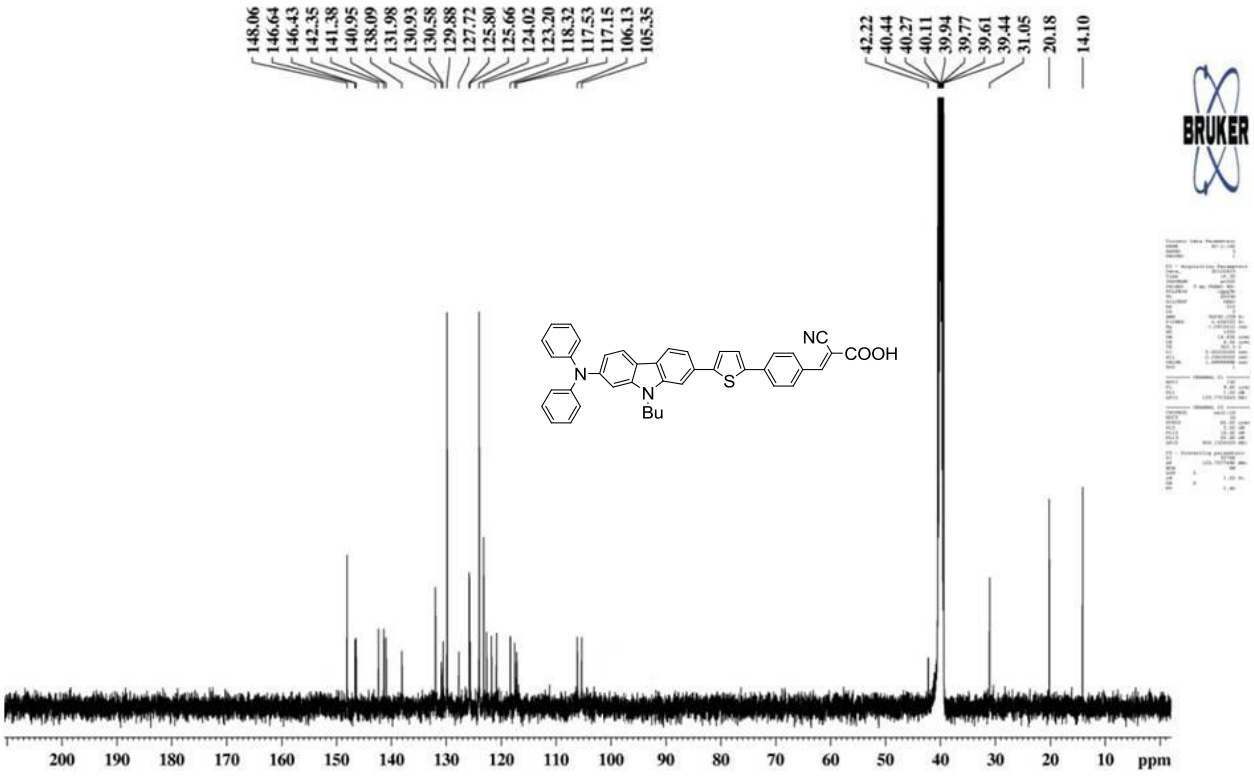

Figure S20 ^{13}C NMR spectrum of **11b** recorded in DMSO-d_6.

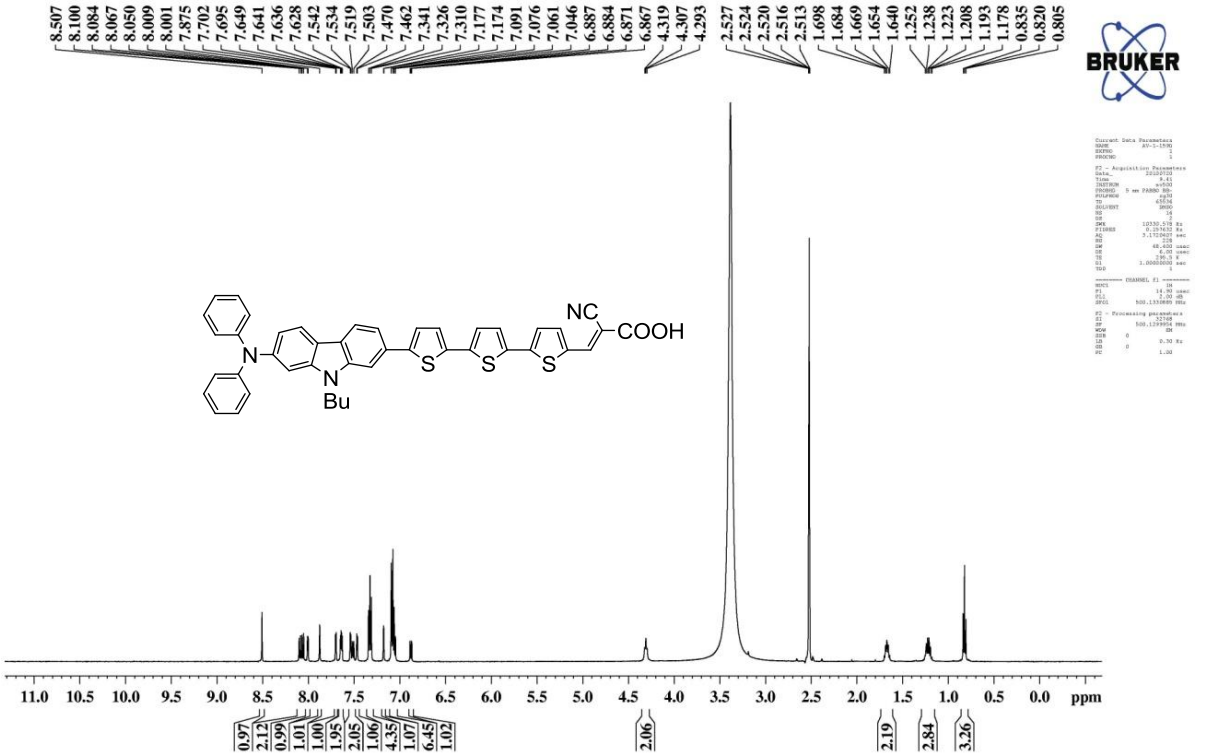

Figure S21 ^{1}H NMR spectrum of **11c** recorded in DMSO-d_6.

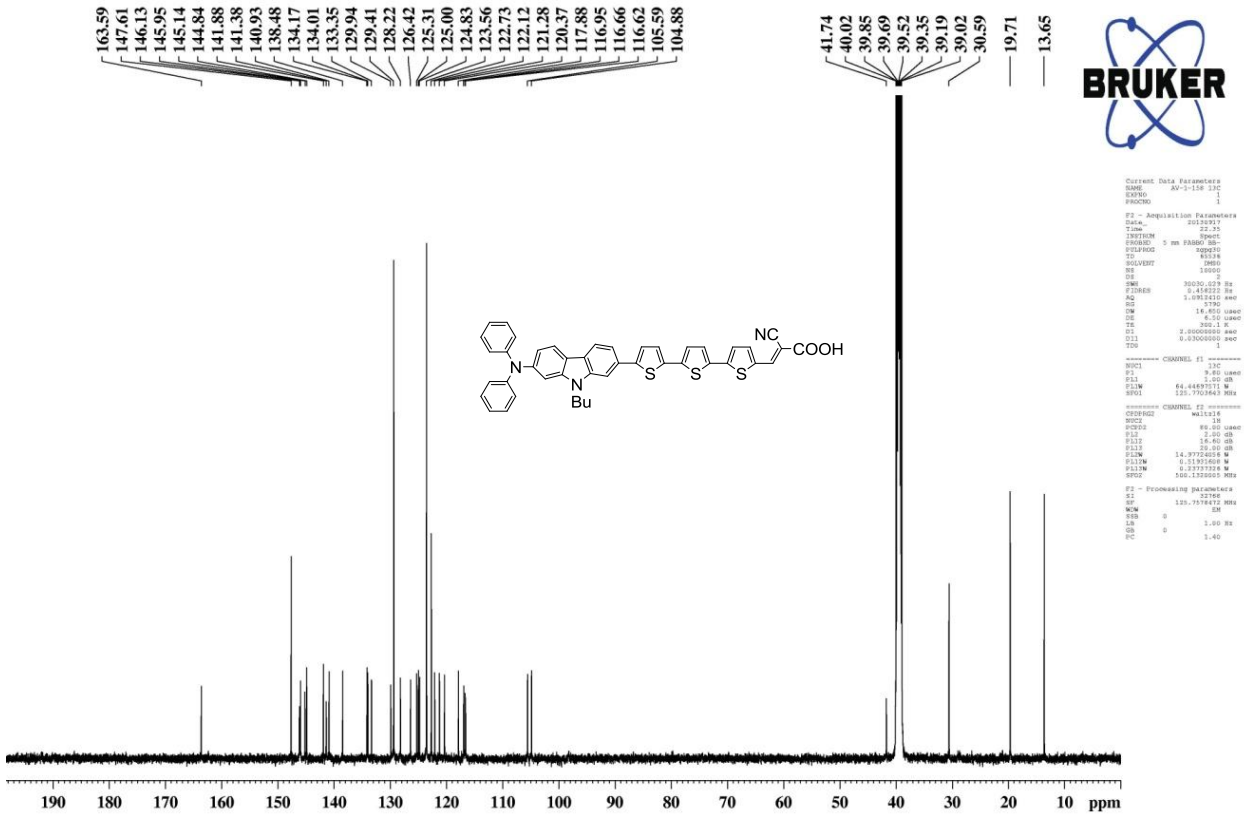

Figure S22 ^{13}C NMR spectrum of **11c** recorded in DMSO-d_6.

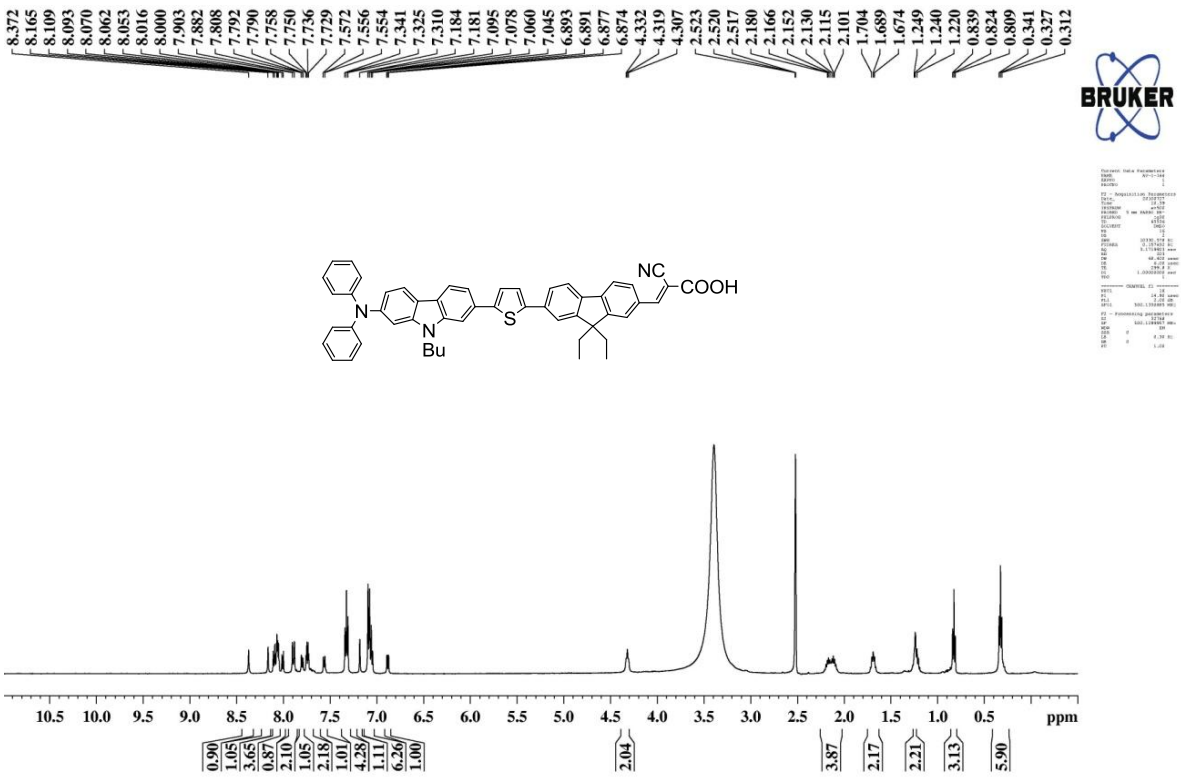

Figure S23 ^{1}H NMR spectrum of **11d** recorded in DMSO-d_6.

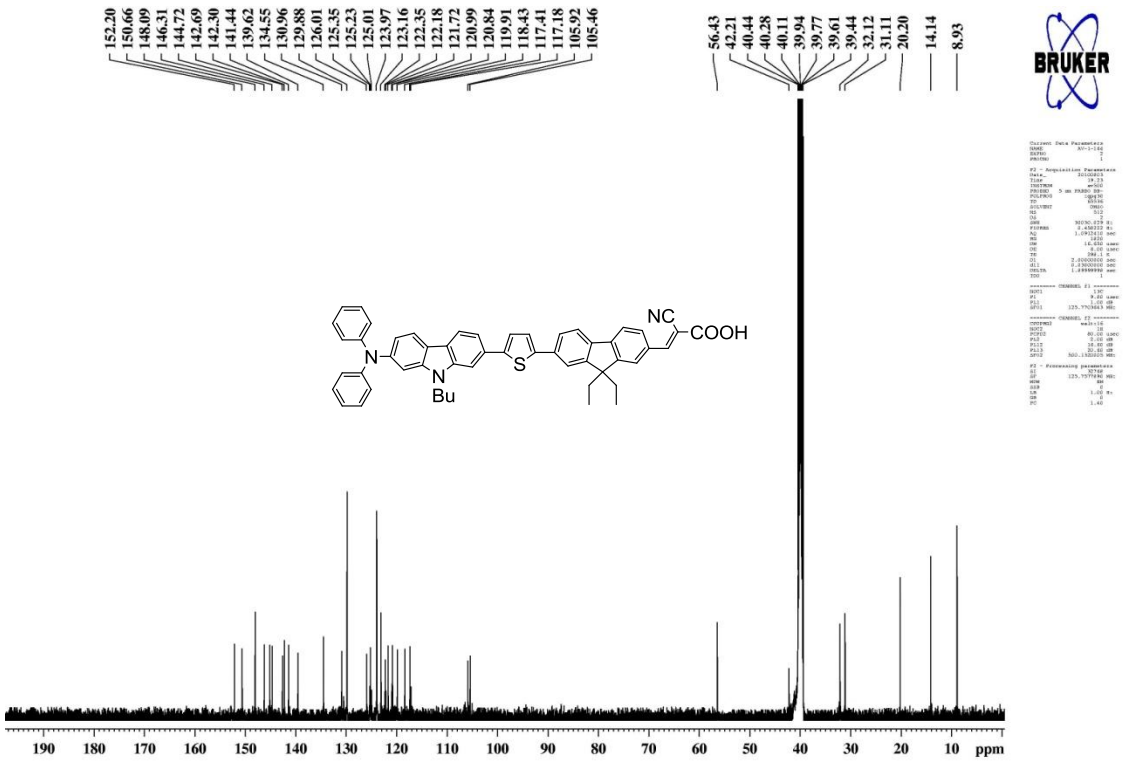

Figure S24 ^{13}C NMR spectrum of **11d** recorded in DMSO-d_6.

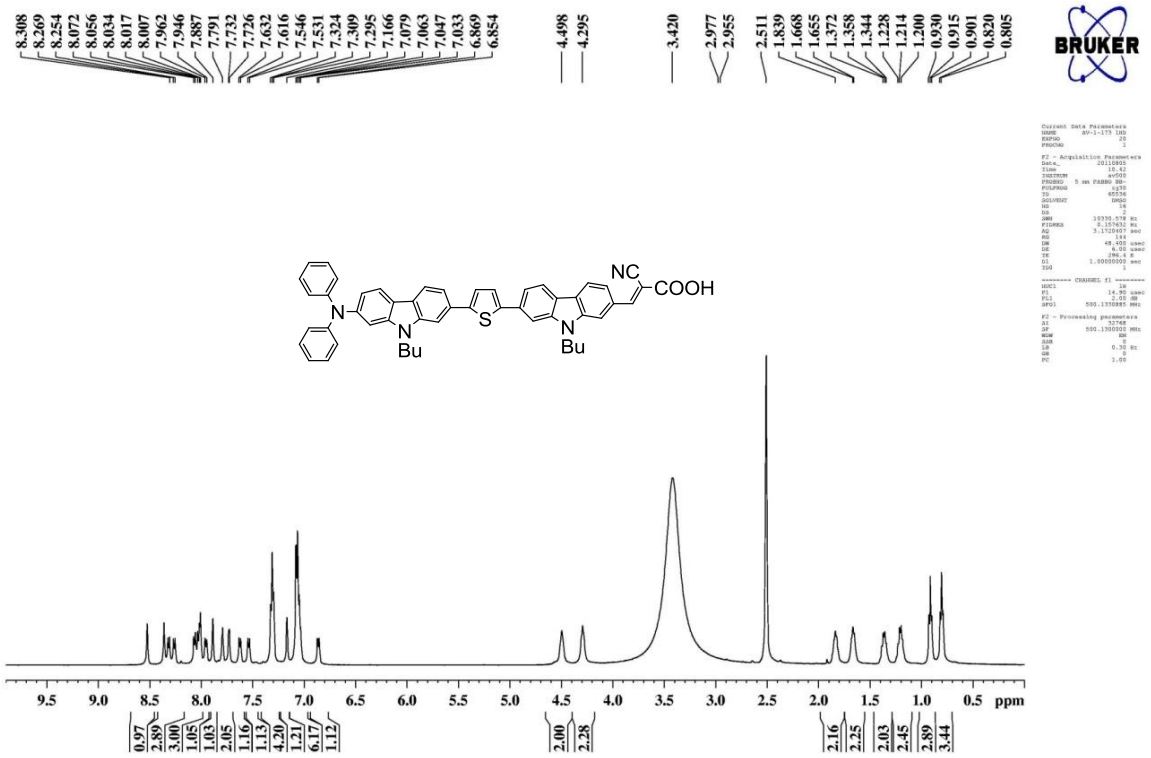

Figure S25 ^{1}H NMR spectrum of **11e** recorded in DMSO-d_6.

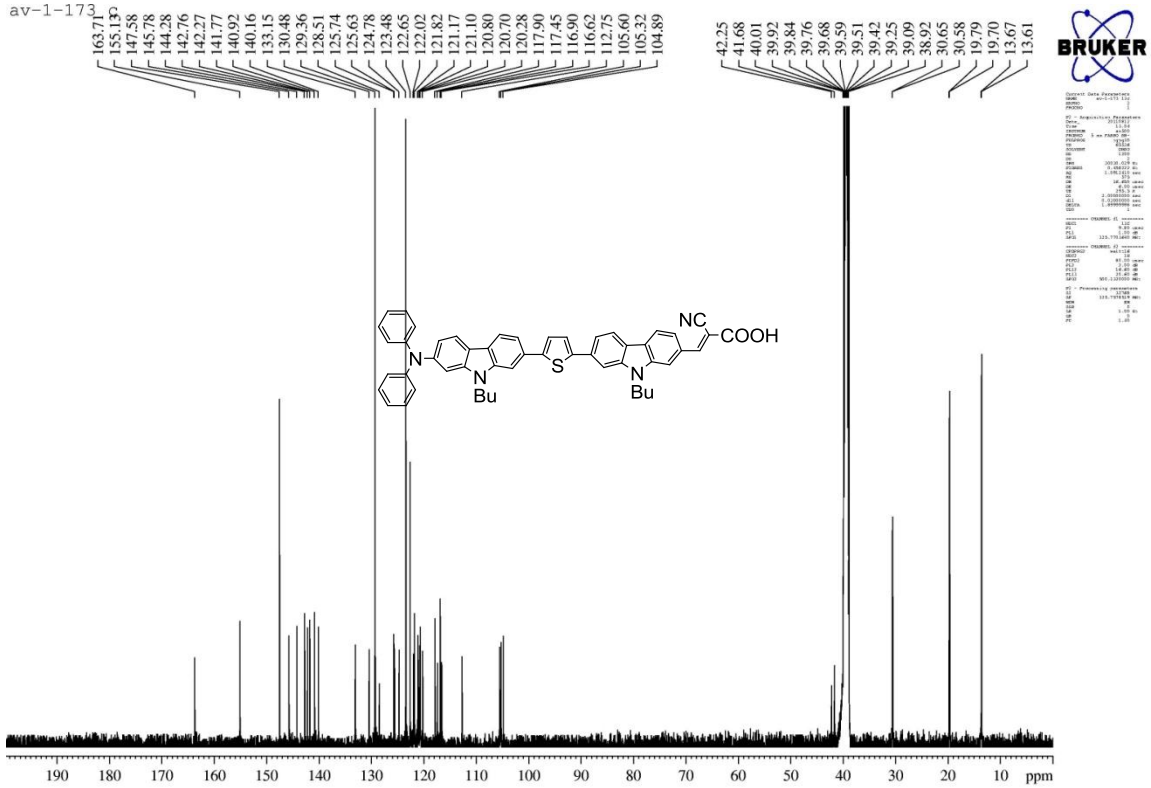

Figure S26^{13}C NMR spectrum of **11e** recorded in DMSO-d_6.

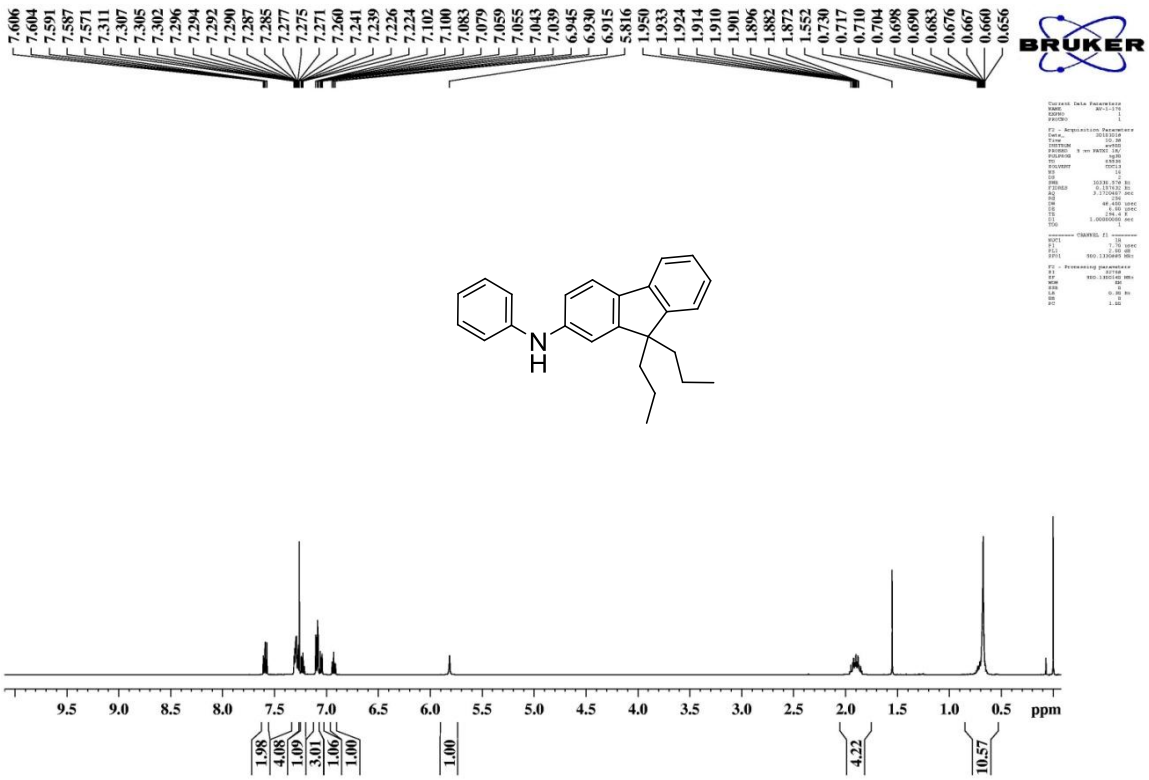

Figure S27 ^{1}H NMR spectrum of **12a** recorded in $CDCl_3$.

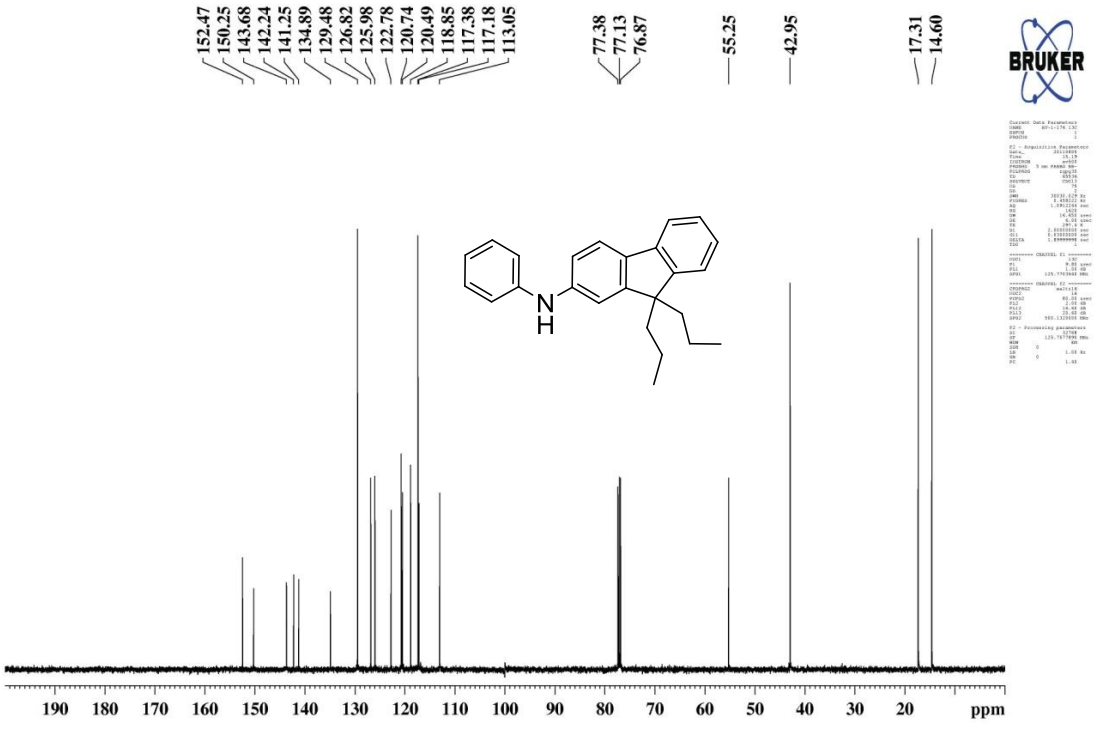

Figure S28 ^{13}C NMR spectrum of **12a** recorded in $CDCl_3$.

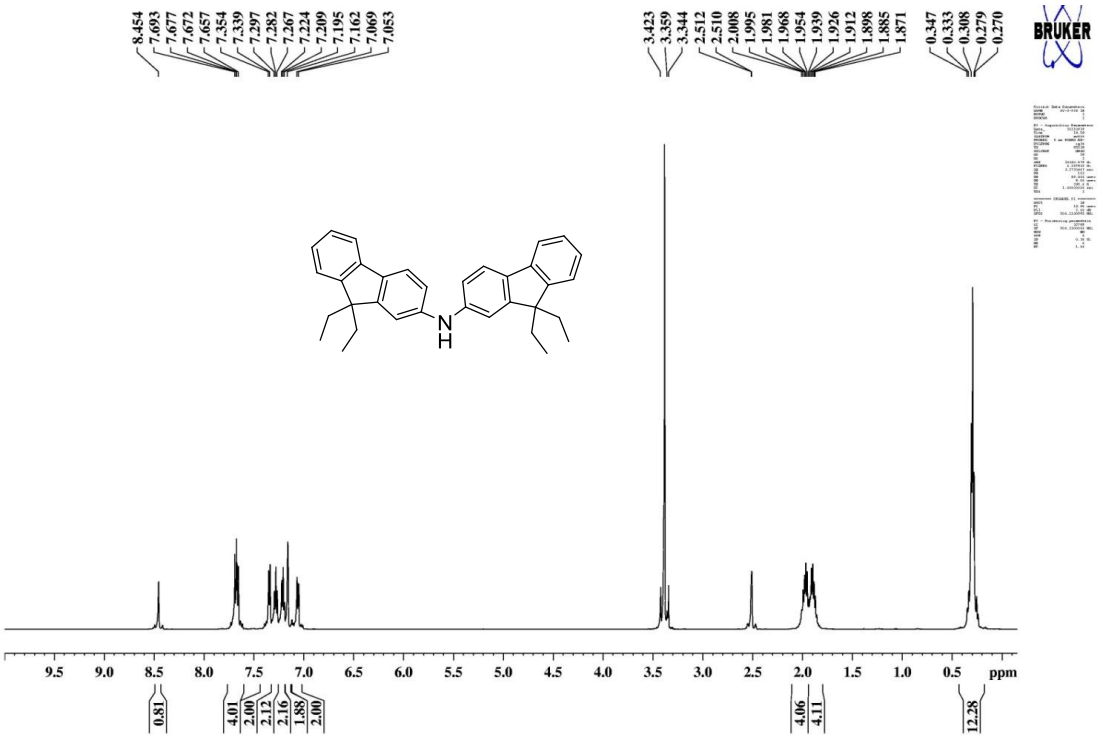

Figure S29 ^{1}H NMR spectrum of **12b** recorded in DMSO-d_6.

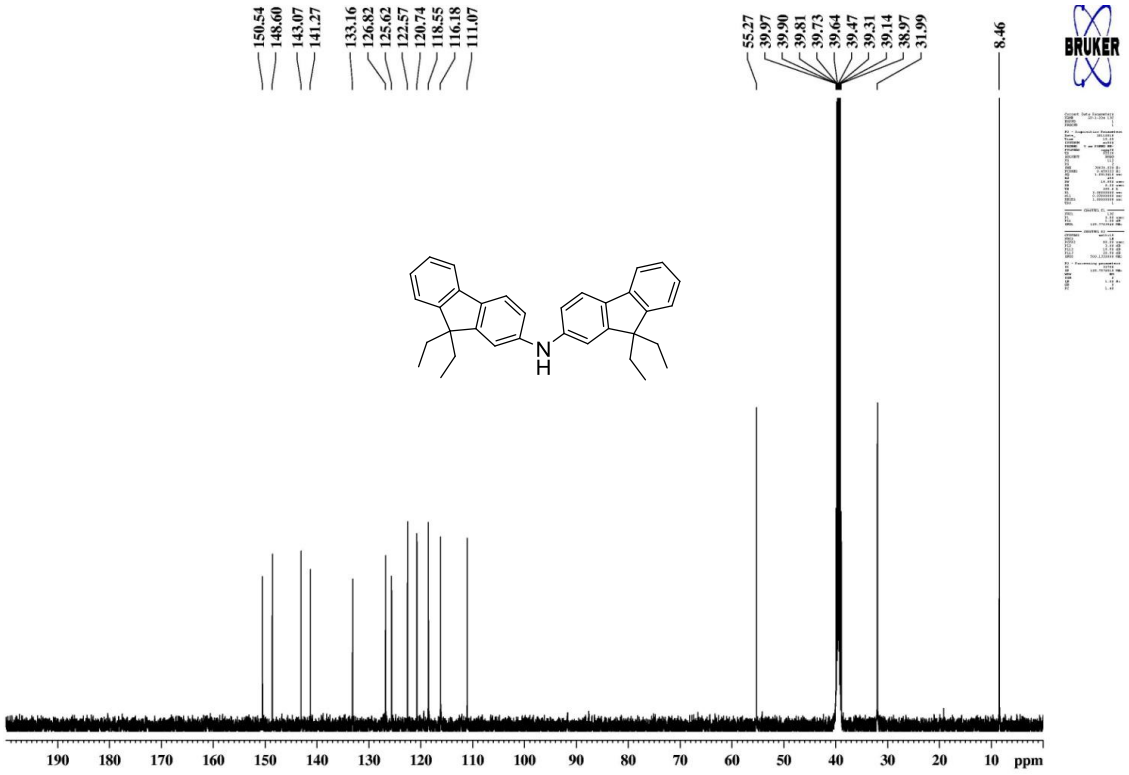

Figure S30 ^{13}C NMR spectrum of **12b** recorded in DMSO-d_6.

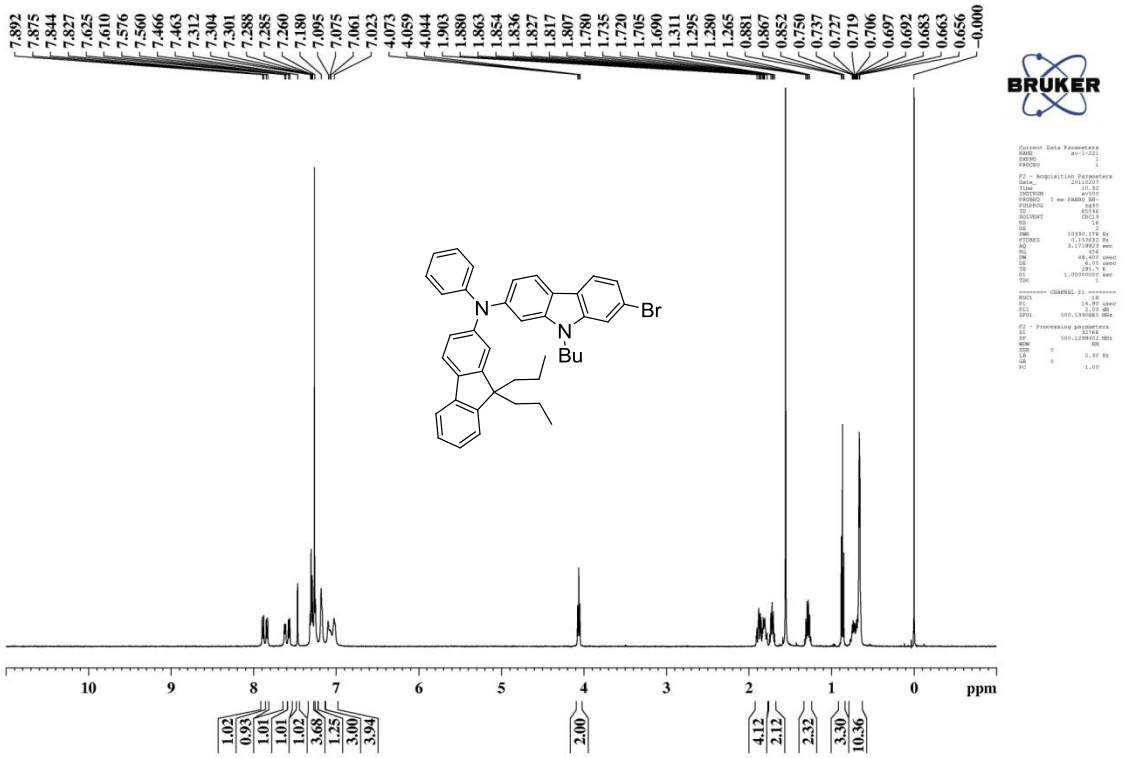

Figure S31 ^{1}H NMR spectrum of **13a** recorded in $CDCl_3$.

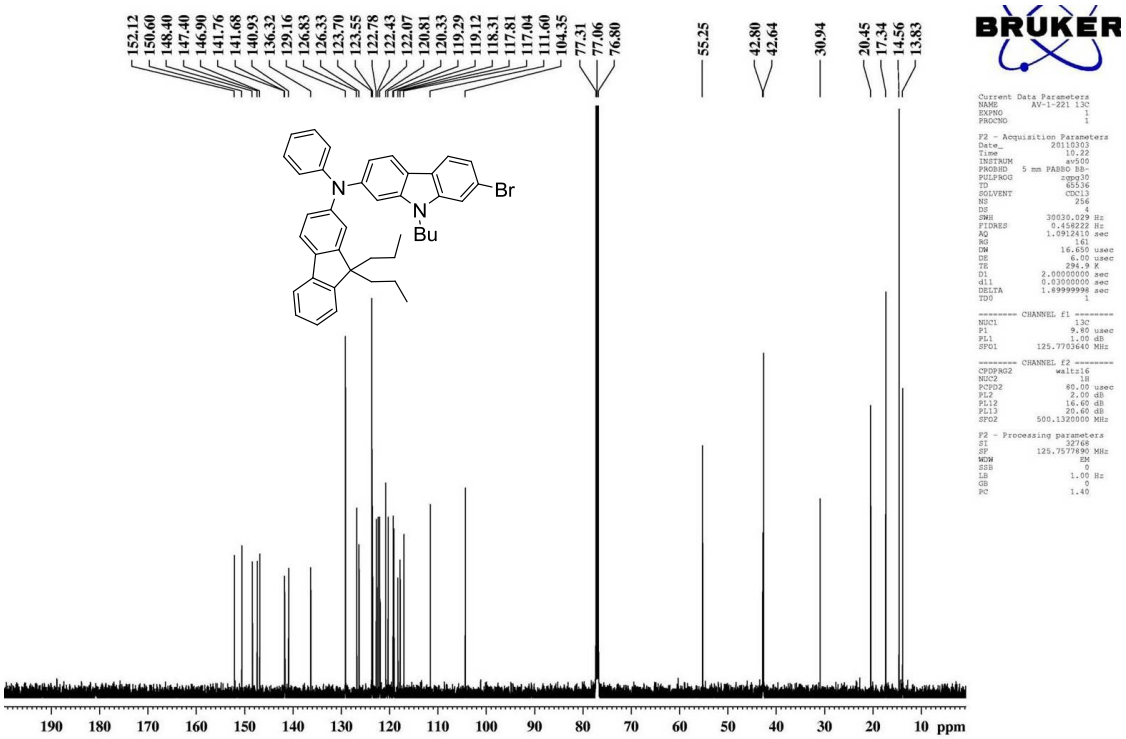

Figure S32 ^{13}C NMR spectrum of **13a** recorded in $CDCl_3$.

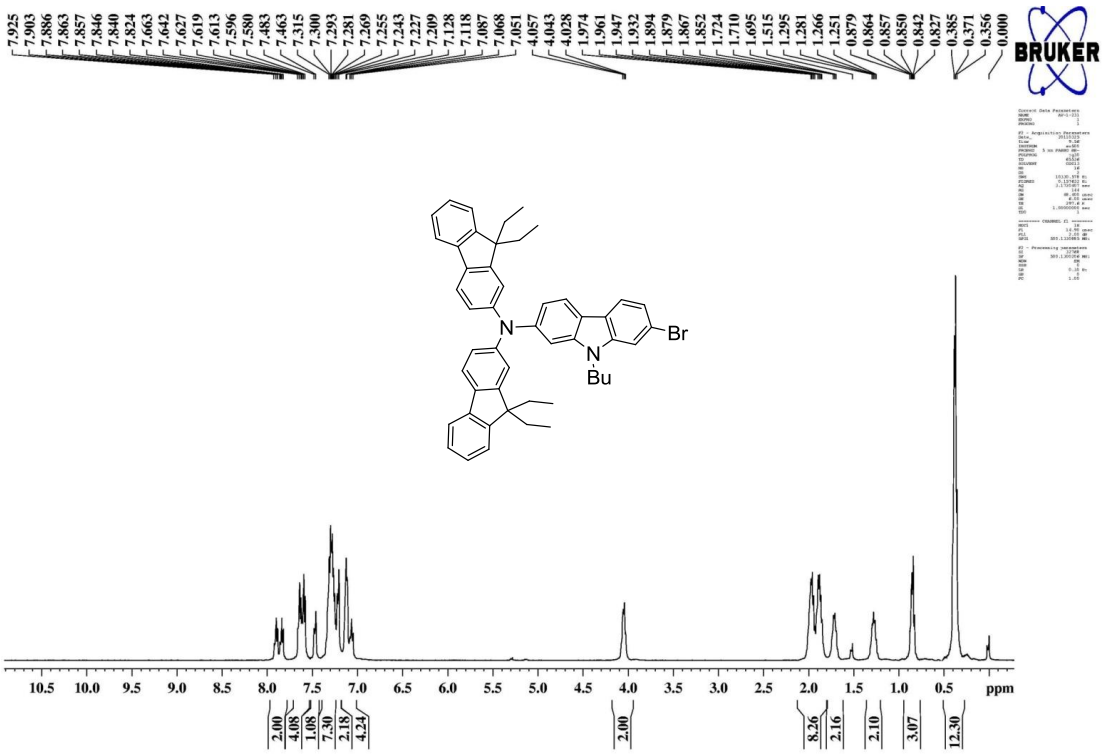

Figure S33 ^{1}H NMR spectrum of **13b** recorded in $CDCl_3$.

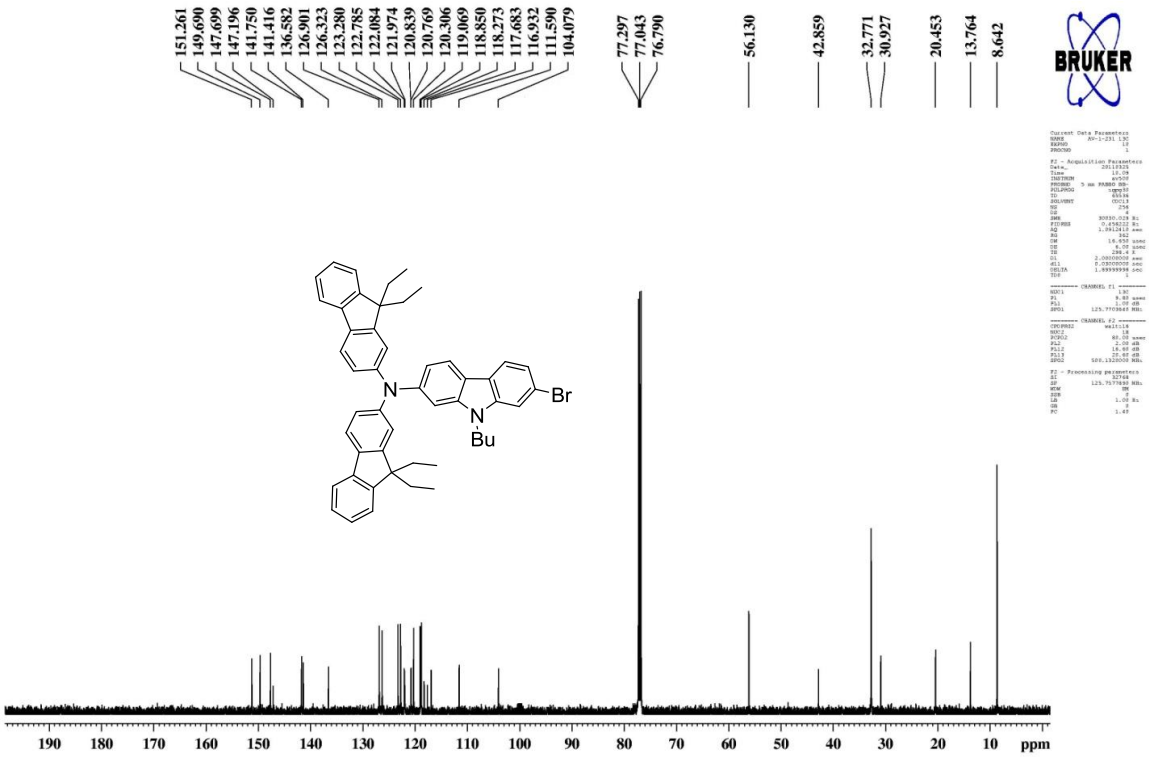

Figure S34 ^{13}C NMR spectrum of **13b** recorded in $CDCl_3$.

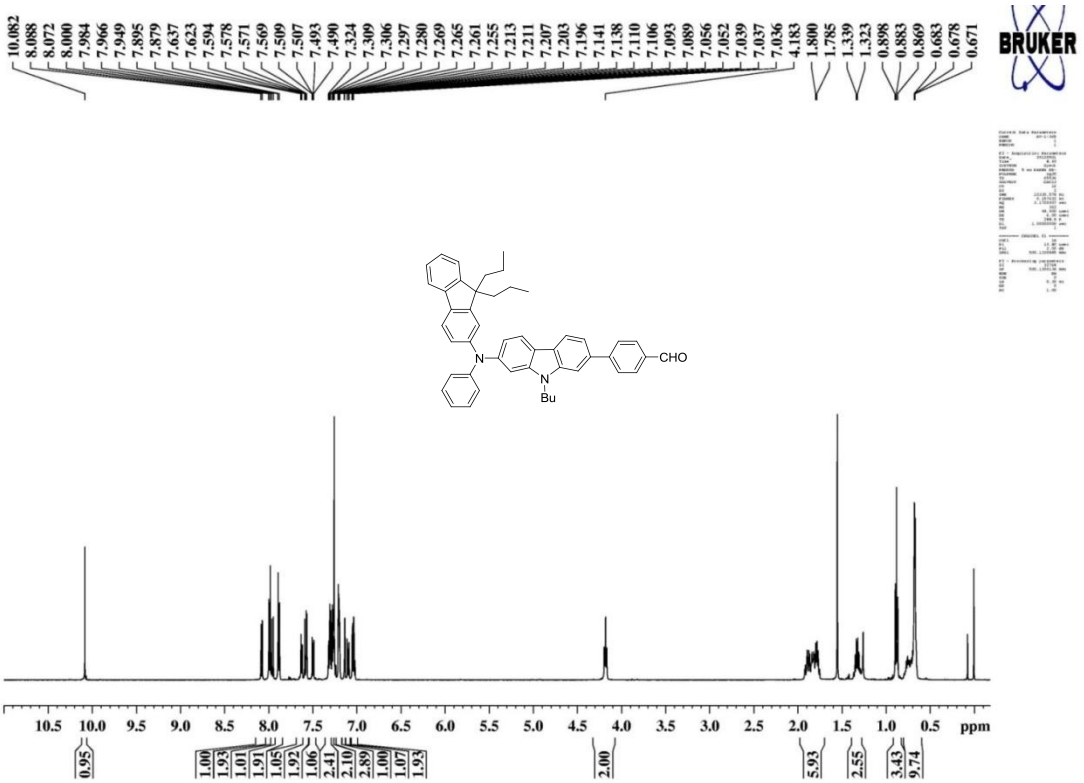

Figure S35 ^{1}H NMR spectrum of **14a** recorded in $CDCl_3$.

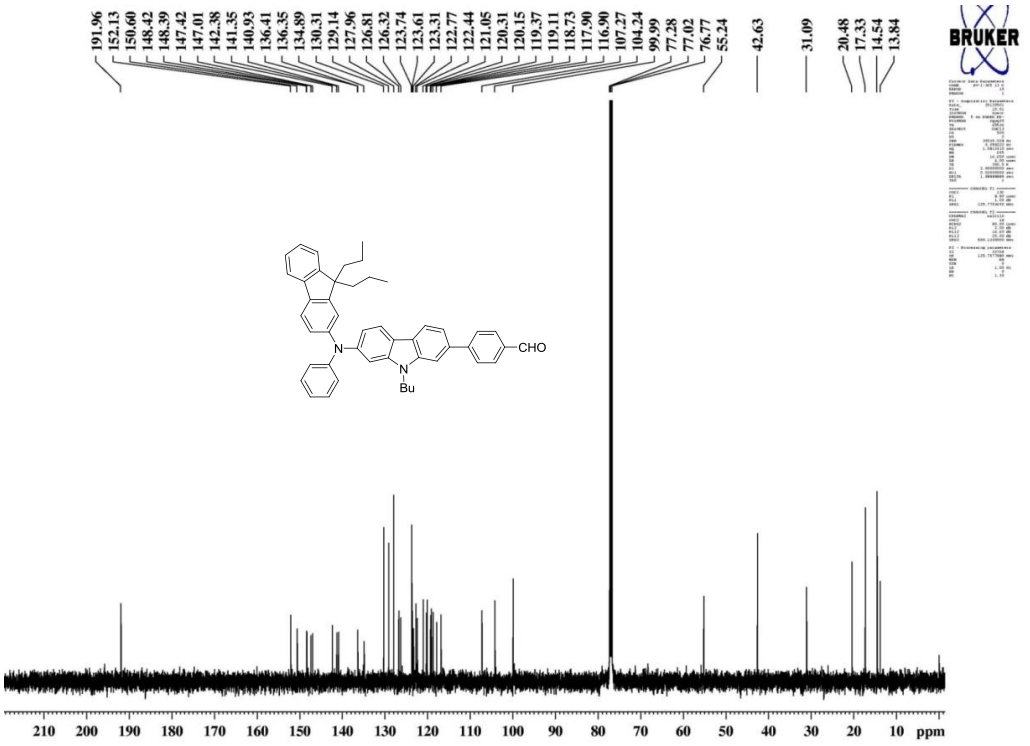

Figure S36 ^{13}C NMR spectrum of **14a** recorded in $CDCl_3$.

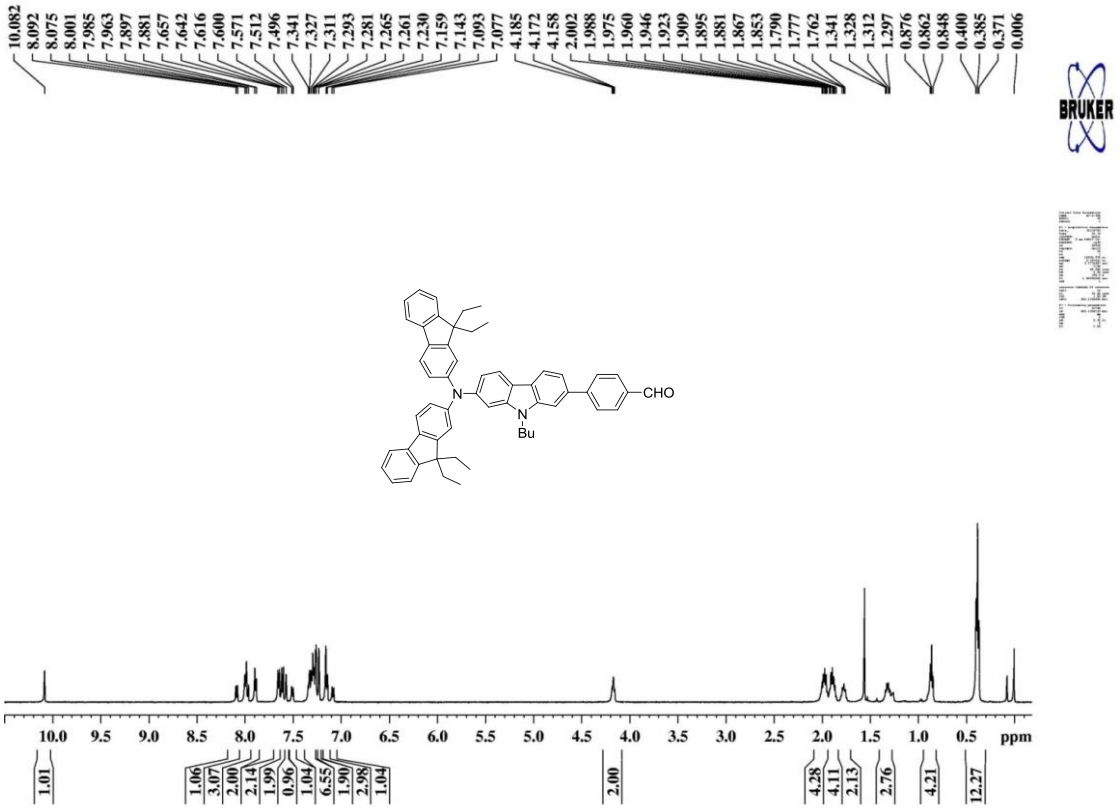

Figure S37 ^{1}H NMR spectrum of **14b** recorded in $CDCl_3$.

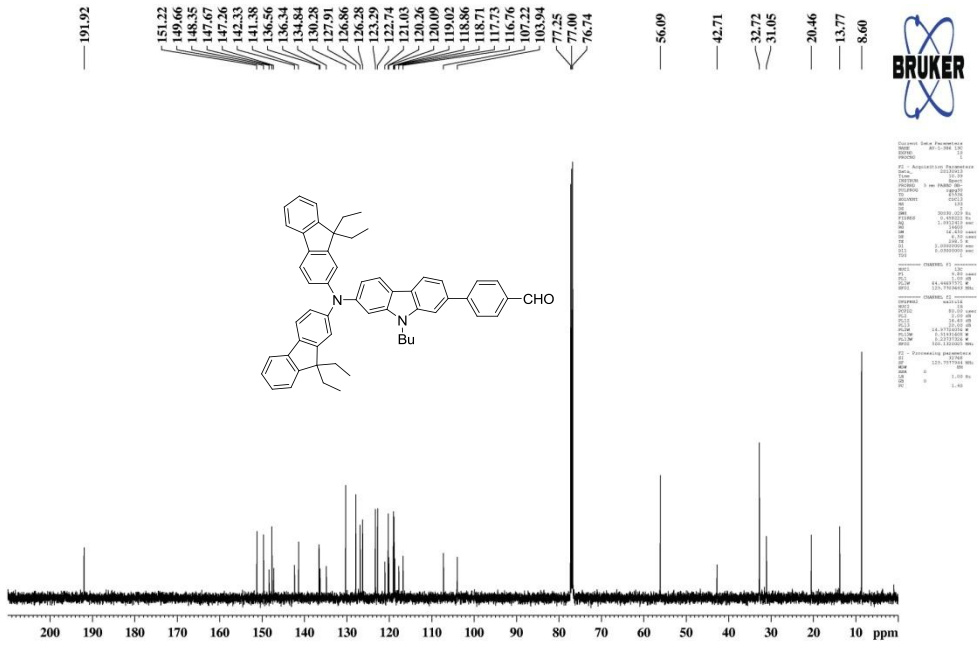

Figure S38 ^{13}C NMR spectrum of **14b** recorded in $CDCl_3$.

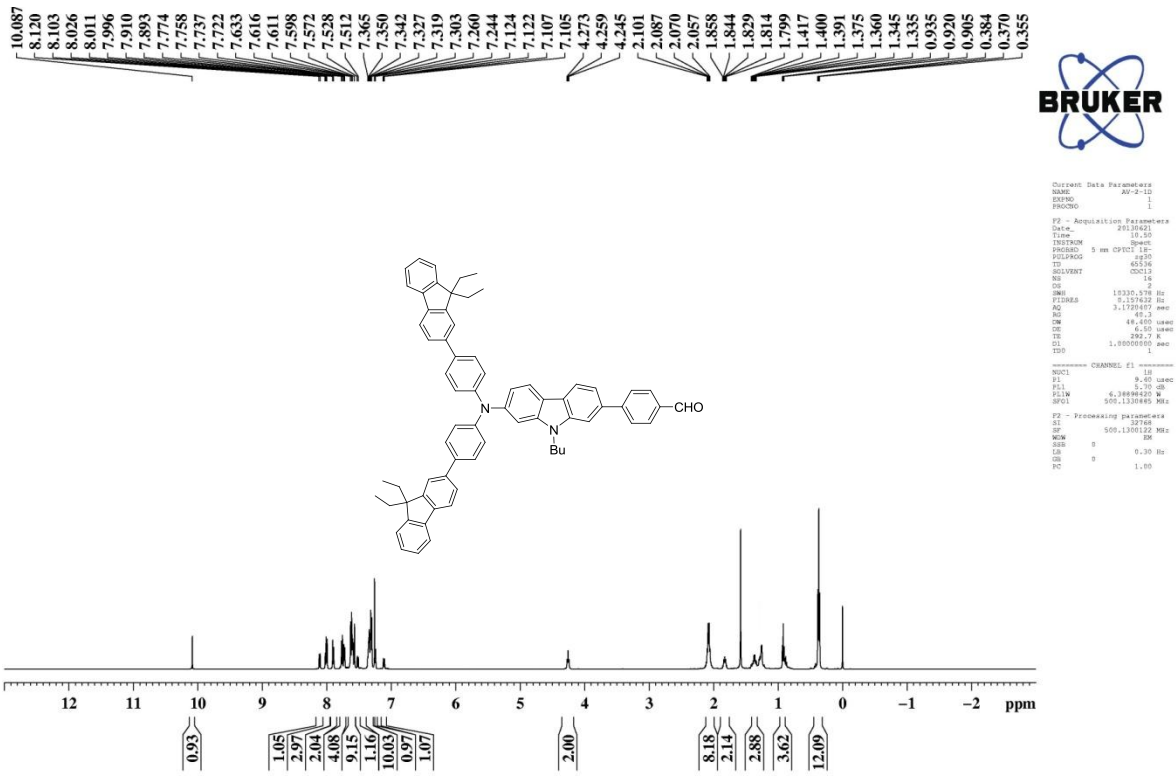

Figure S39 ^{1}H NMR spectrum of **23** recorded in $CDCl_3$.

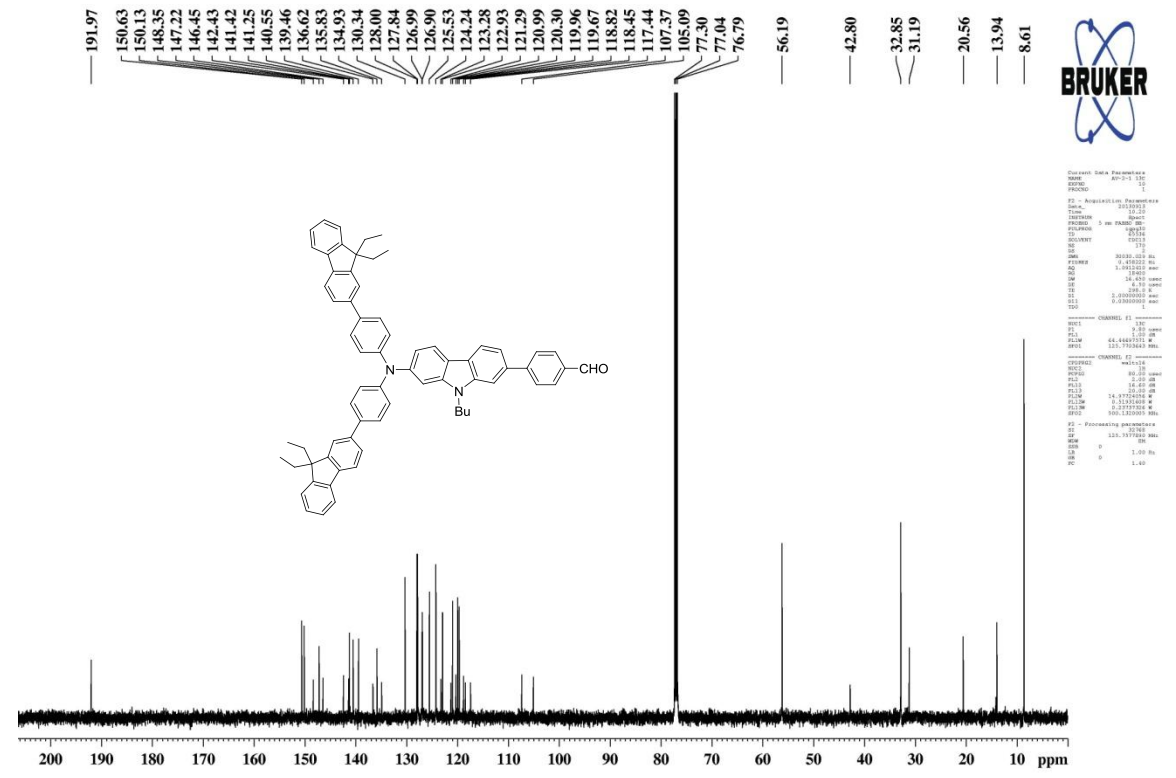

Figure S40 ^{13}C NMR spectrum of **23** recorded in $CDCl_3$.

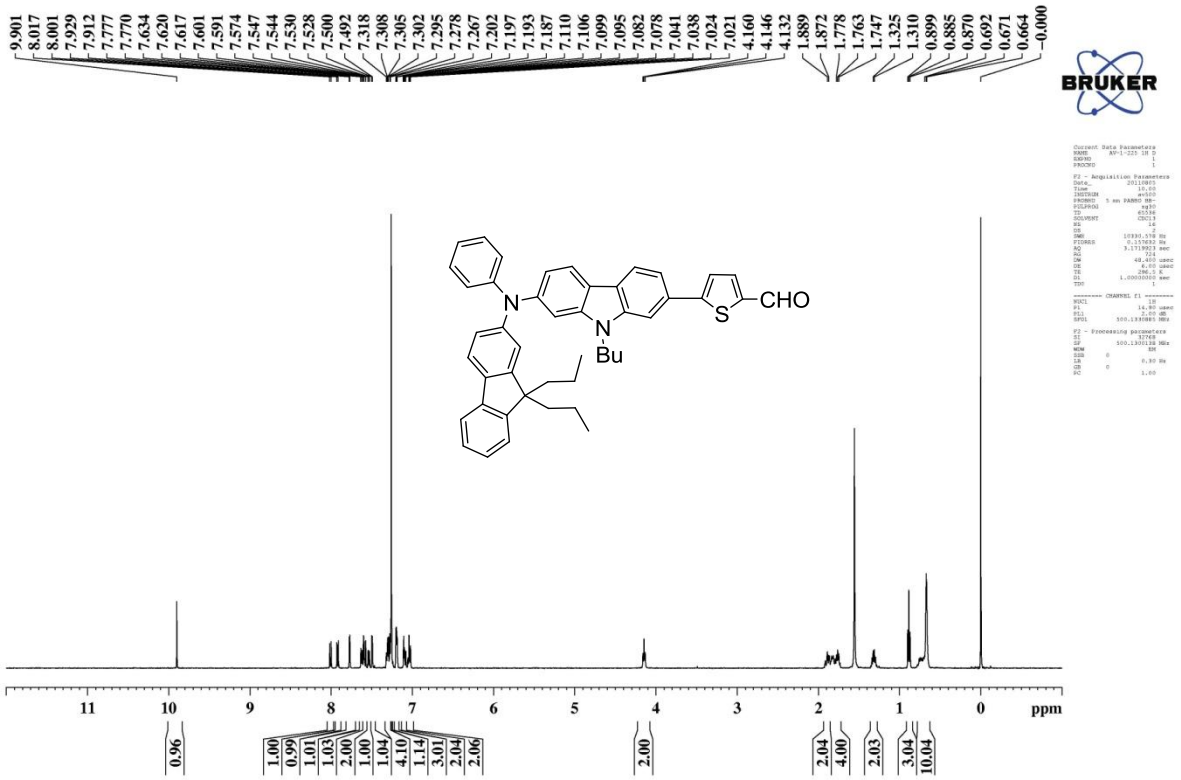

Figure S41 ^{1}H NMR spectrum of **16a** recorded in $CDCl_3$.

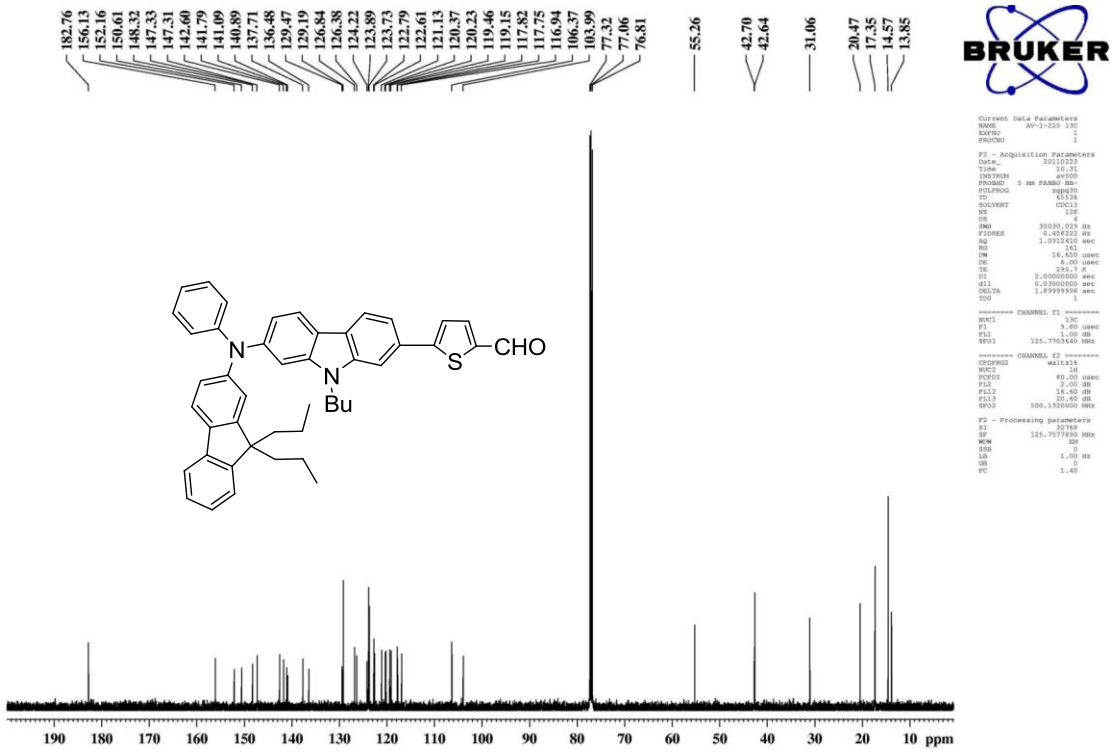

Figure S42 ^{13}C NMR spectrum of **16a** recorded in $CDCl_3$.

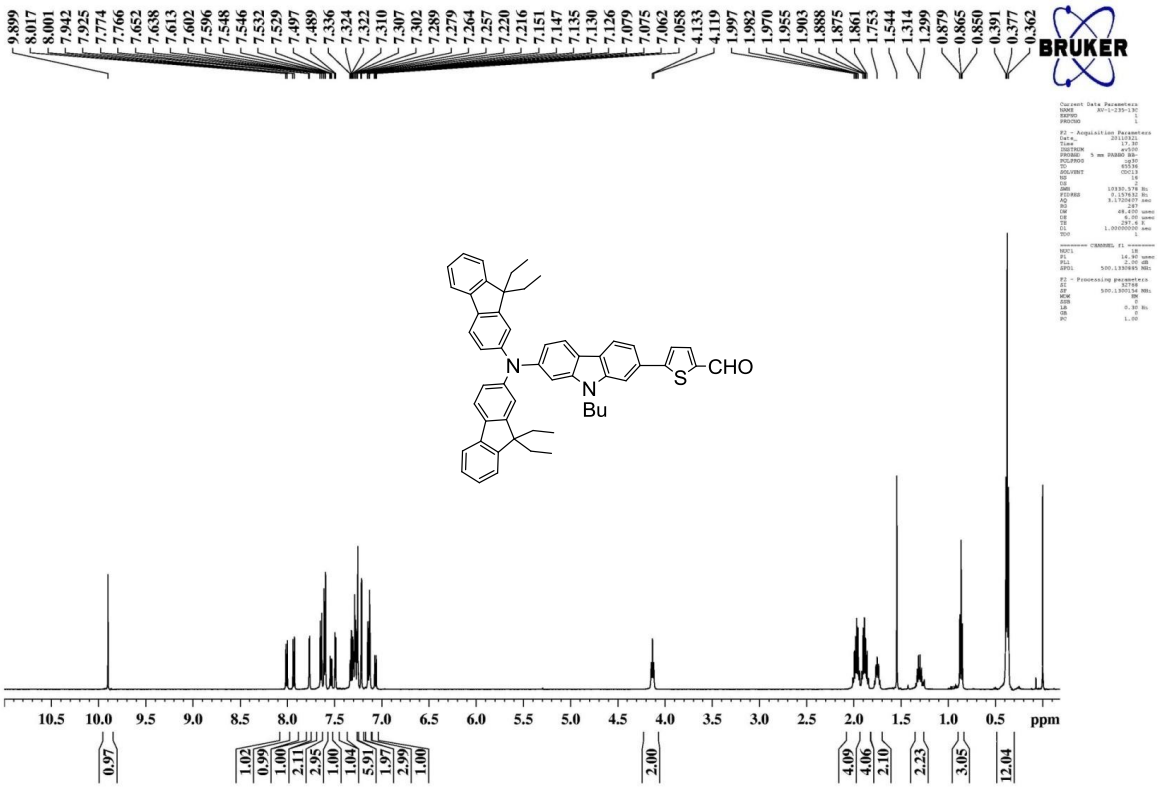

Figure S43 ^{1}H NMR spectrum of **16b** recorded in $CDCl_3$.

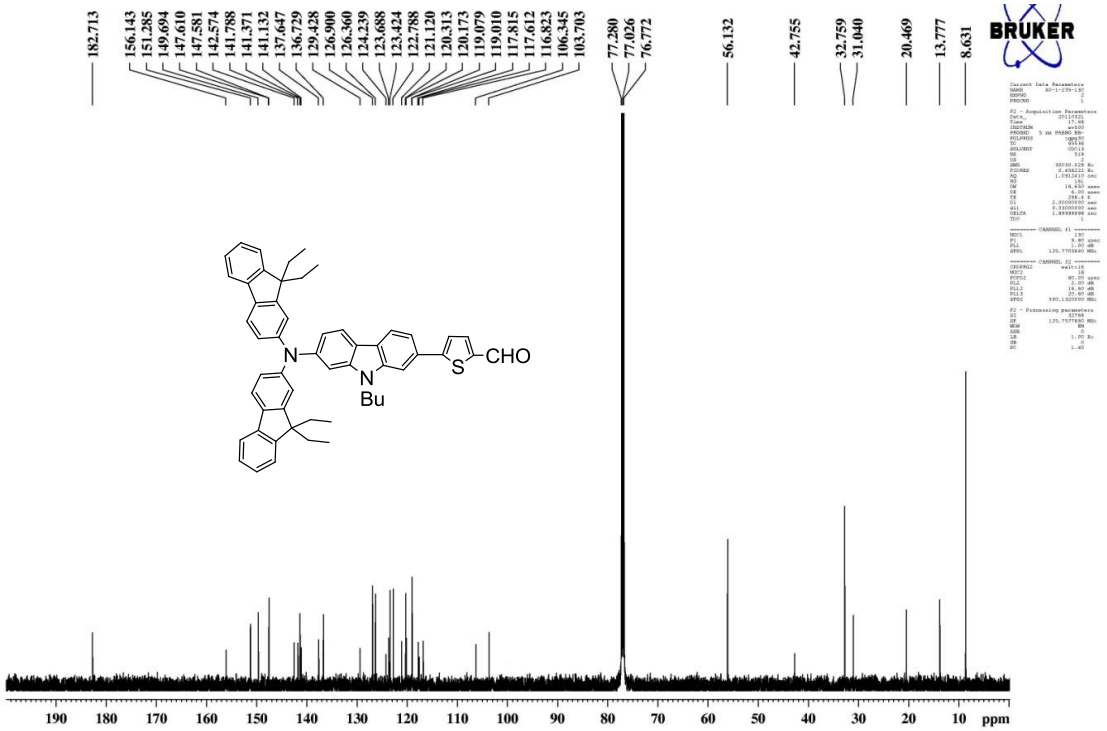

Figure S44 ^{13}C NMR spectrum of **16b** recorded in $CDCl_3$.

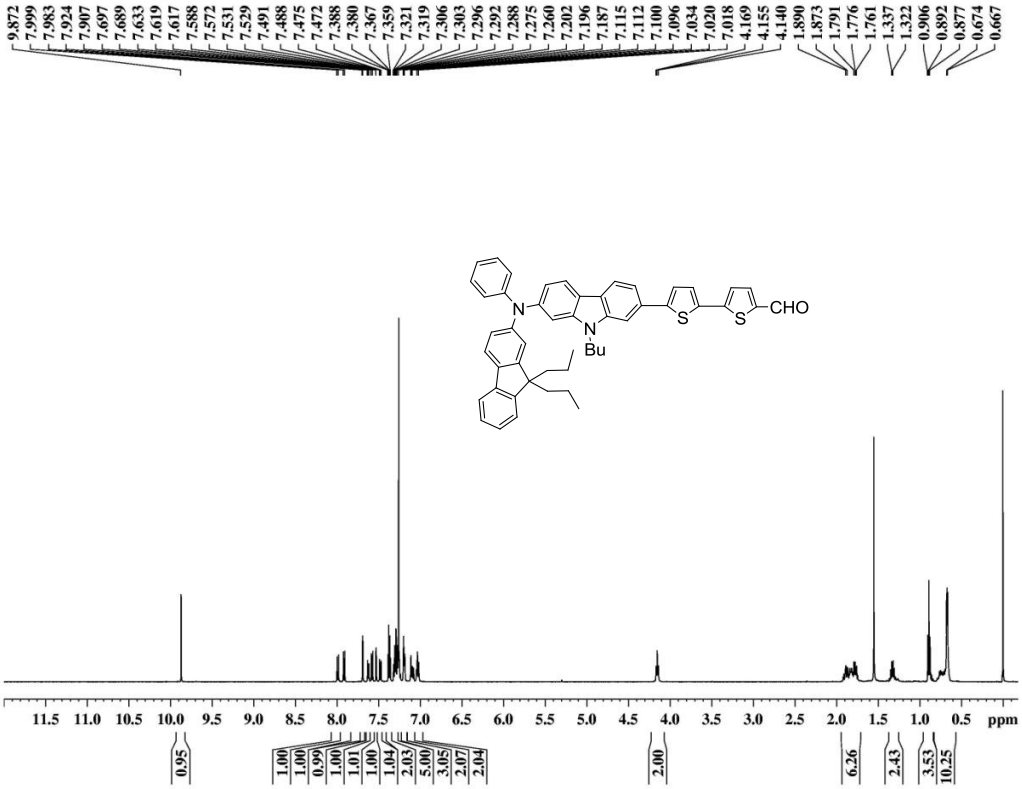

Figure S45 ^{1}H NMR spectrum of **17a** recorded in $CDCl_3$.

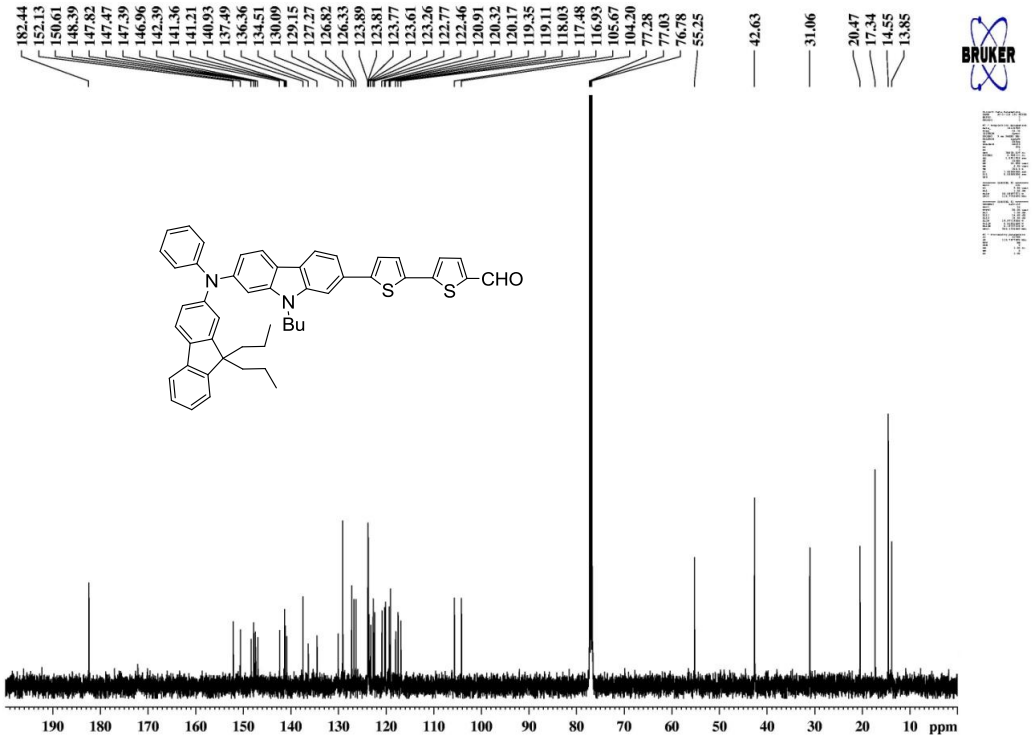

Figure S46 ^{13}C NMR spectrum of **17a** recorded in $CDCl_3$.

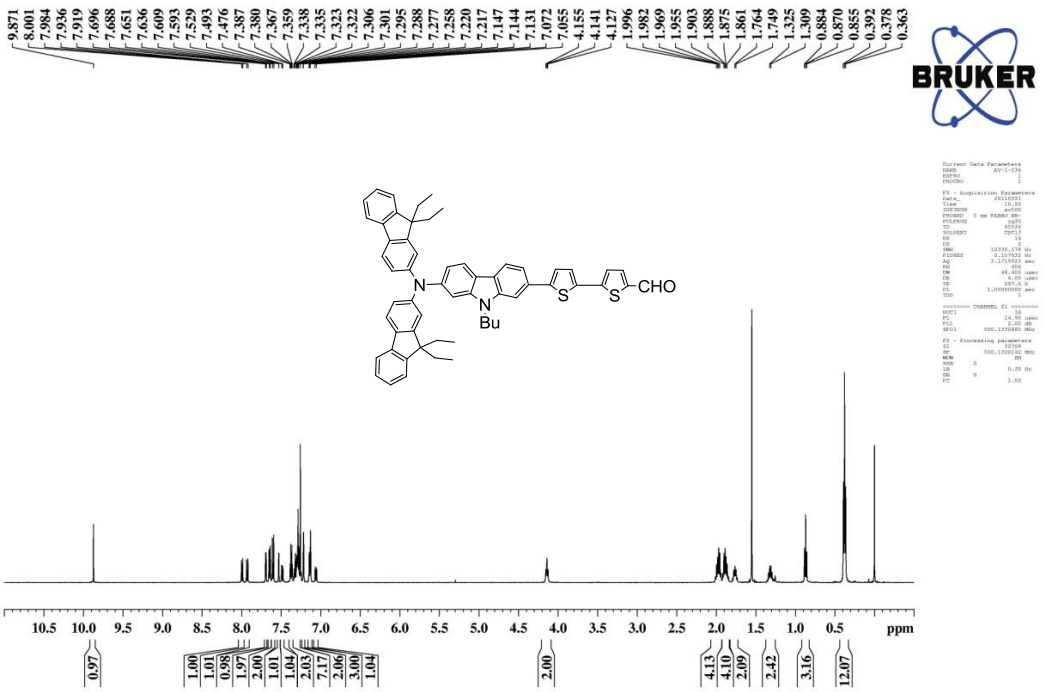

Figure S47 ^{13}C NMR spectrum of **17b** recorded in $CDCl_3$.

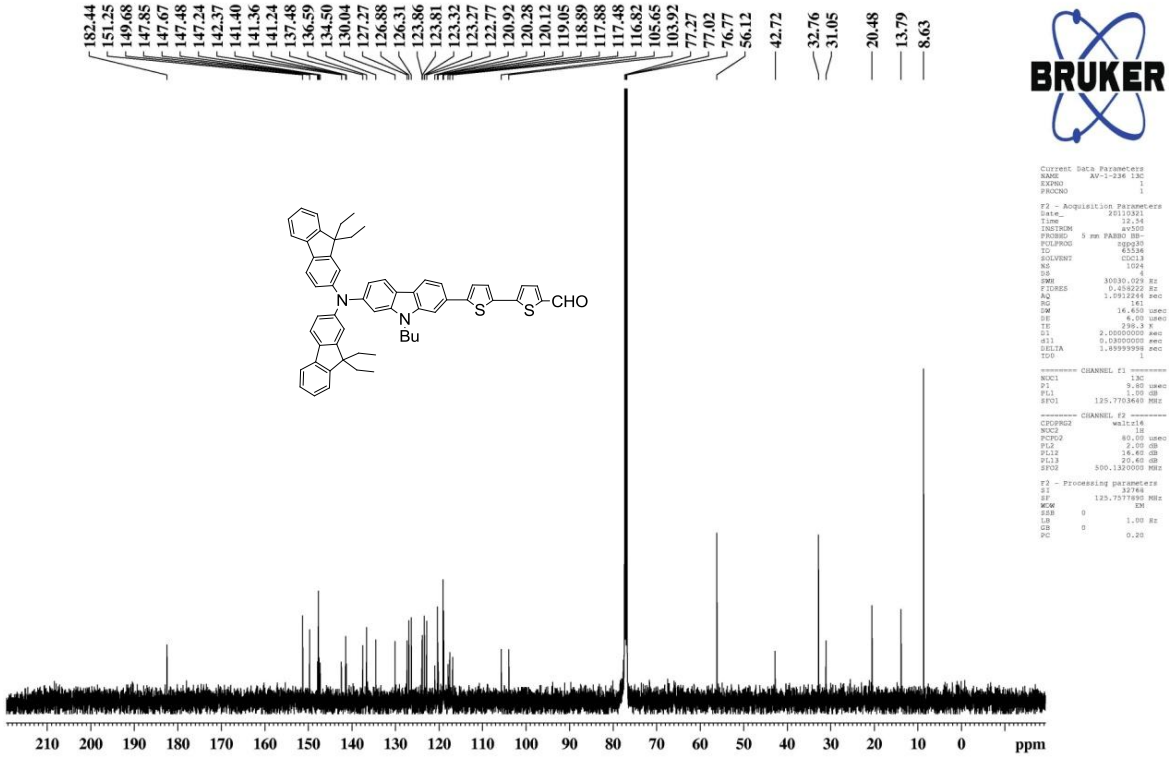

Figure S48 ^{13}C NMR spectrum of **17b** recorded in $CDCl_3$.

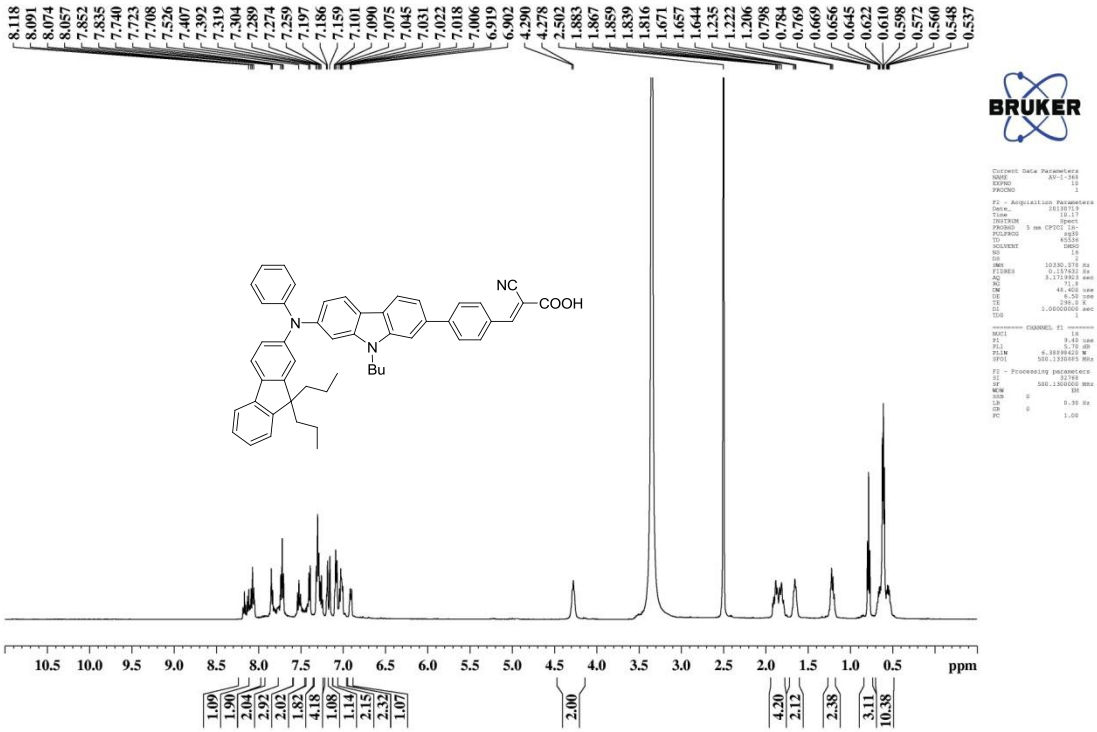

Figure S49 ^{1}H NMR spectrum of **15a** recorded in DMSO-d_6.

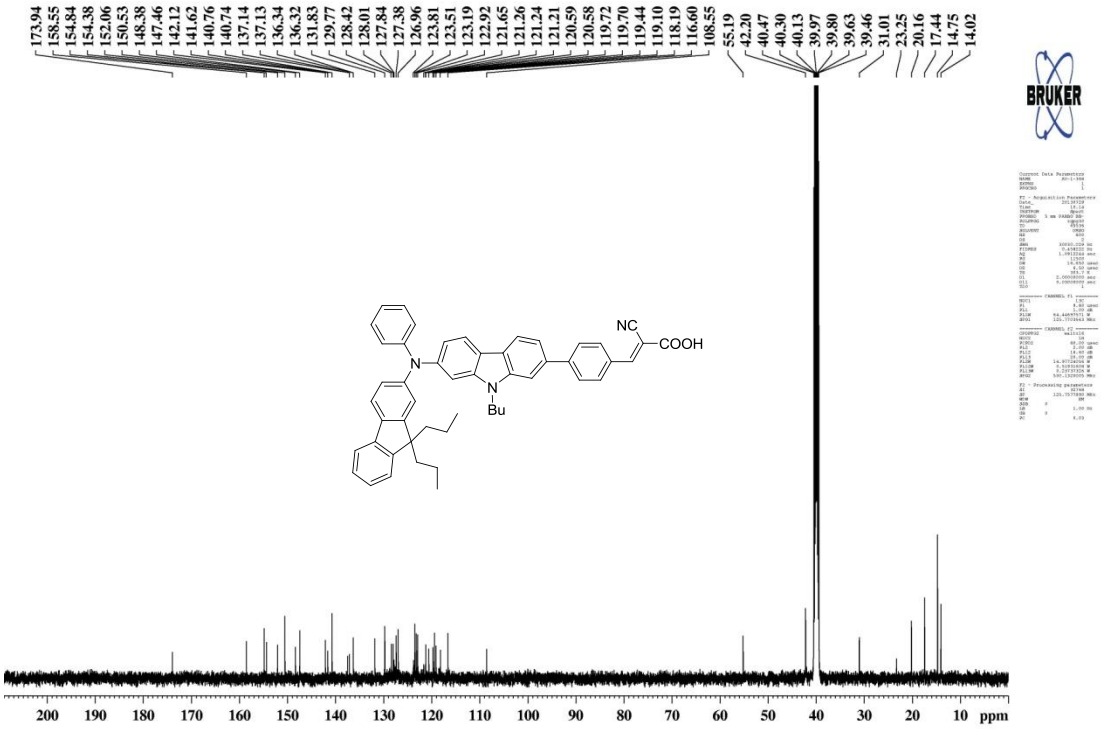

Figure S50 ^{13}C NMR spectrum of **15a** recorded in DMSO-d_6.

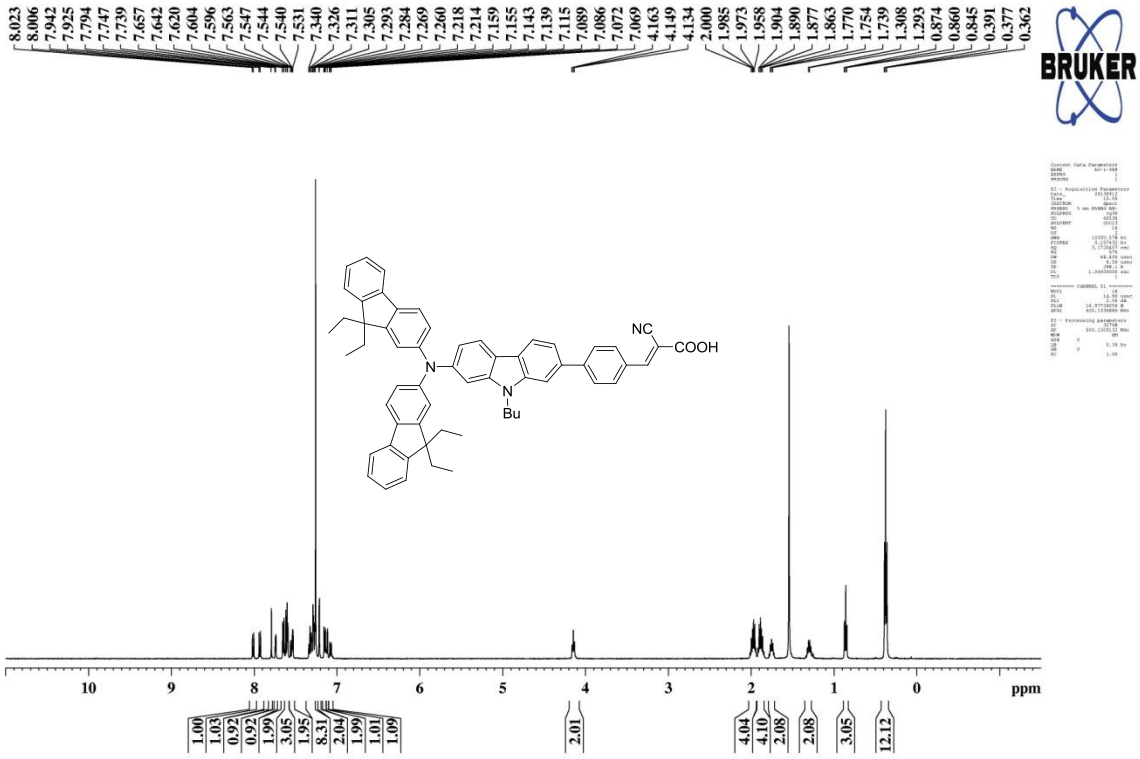

Figure S51 ^{1}H NMR spectrum of **15b** recorded in DMSO-d_6.

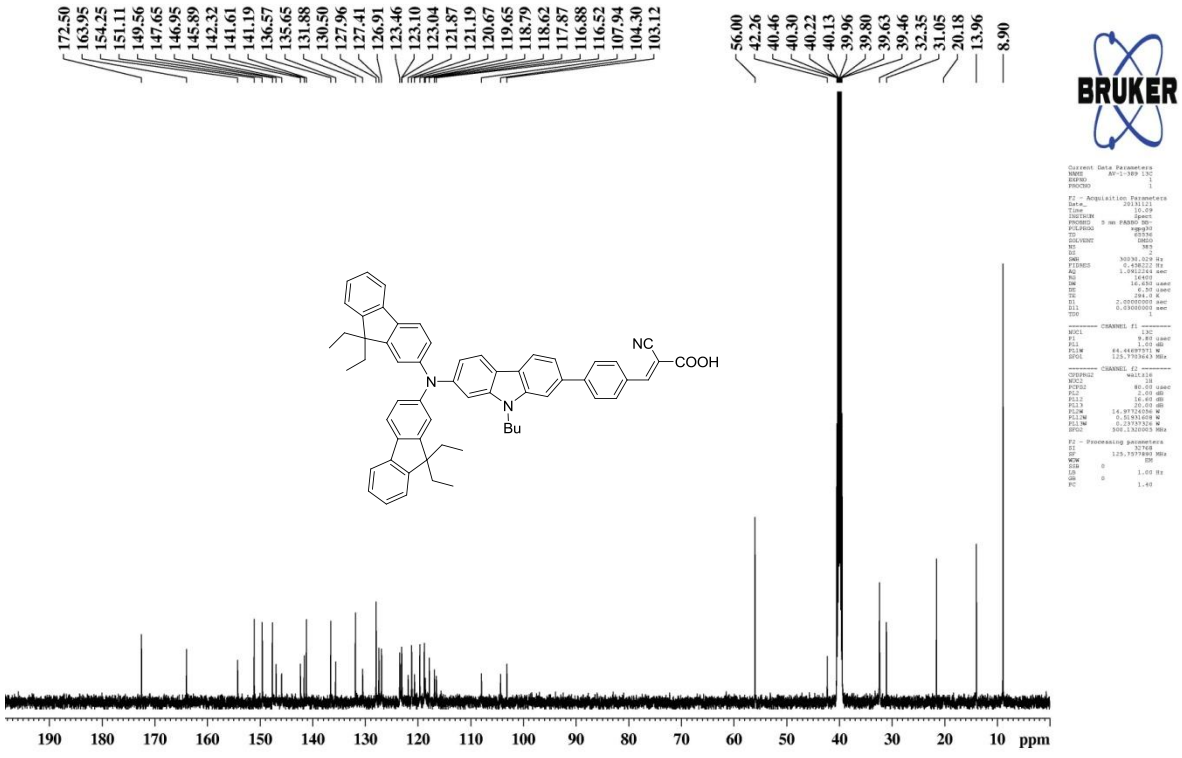

Figure S52 ^{13}C NMR spectrum of **15b** recorded in DMSO-d_6.

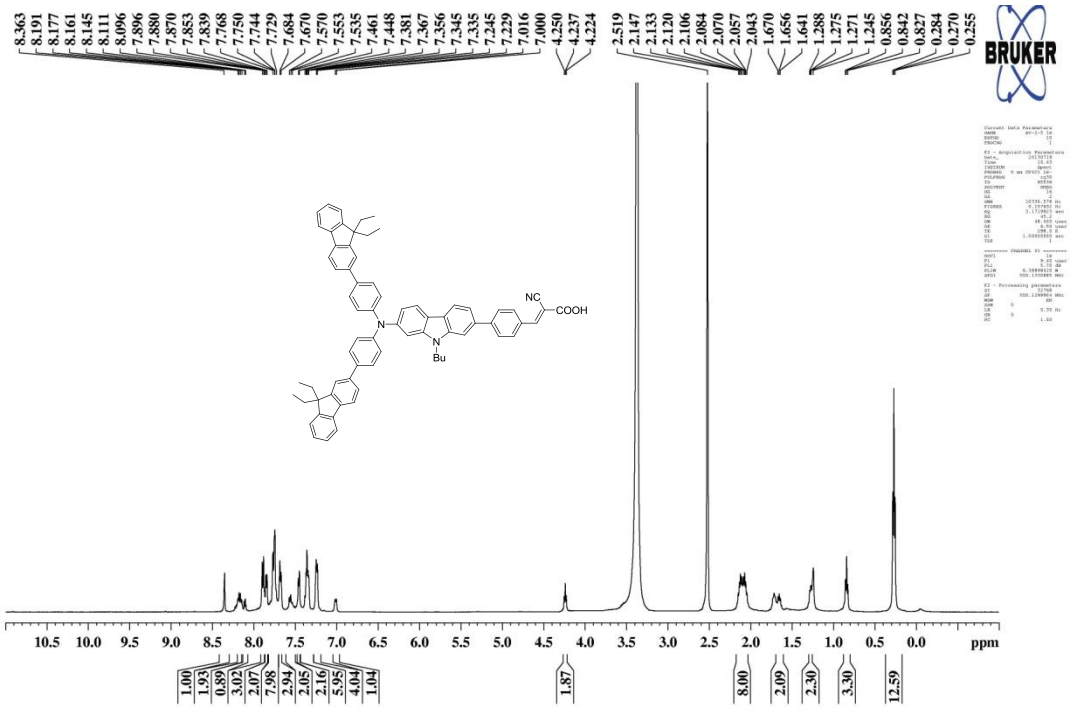

Figure S53 ^{1}H NMR spectrum of **24** recorded in DMSO-d_6.

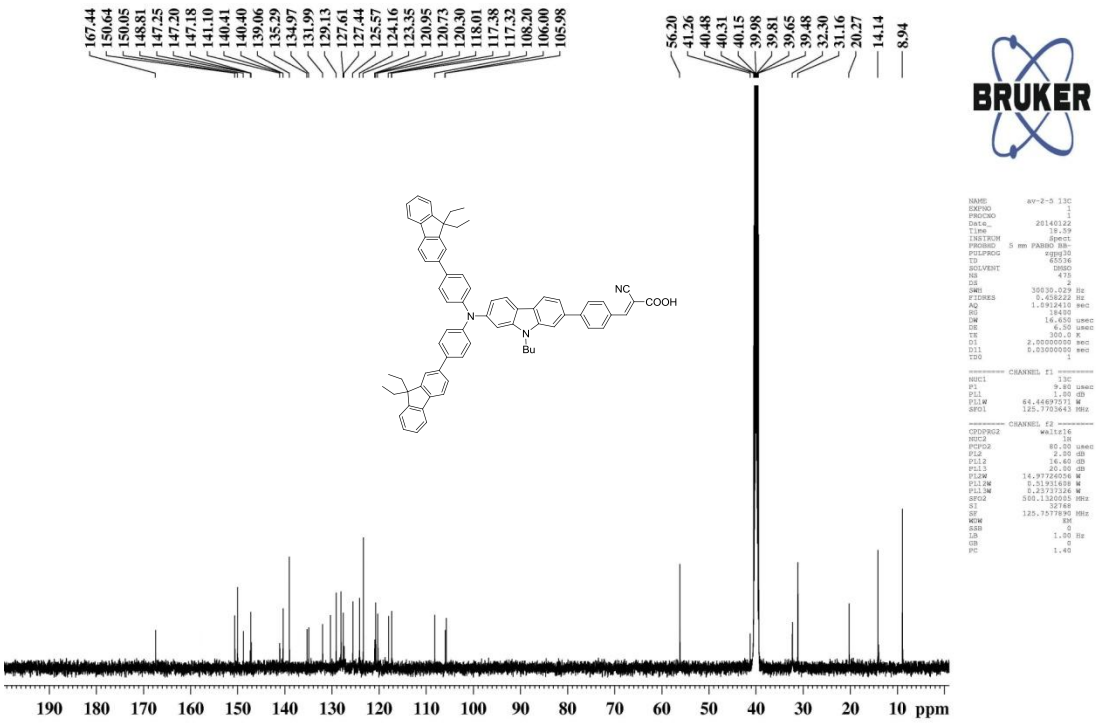

Figure S54 ^{13}C NMR spectrum of **24** recorded in DMSO-d_6.

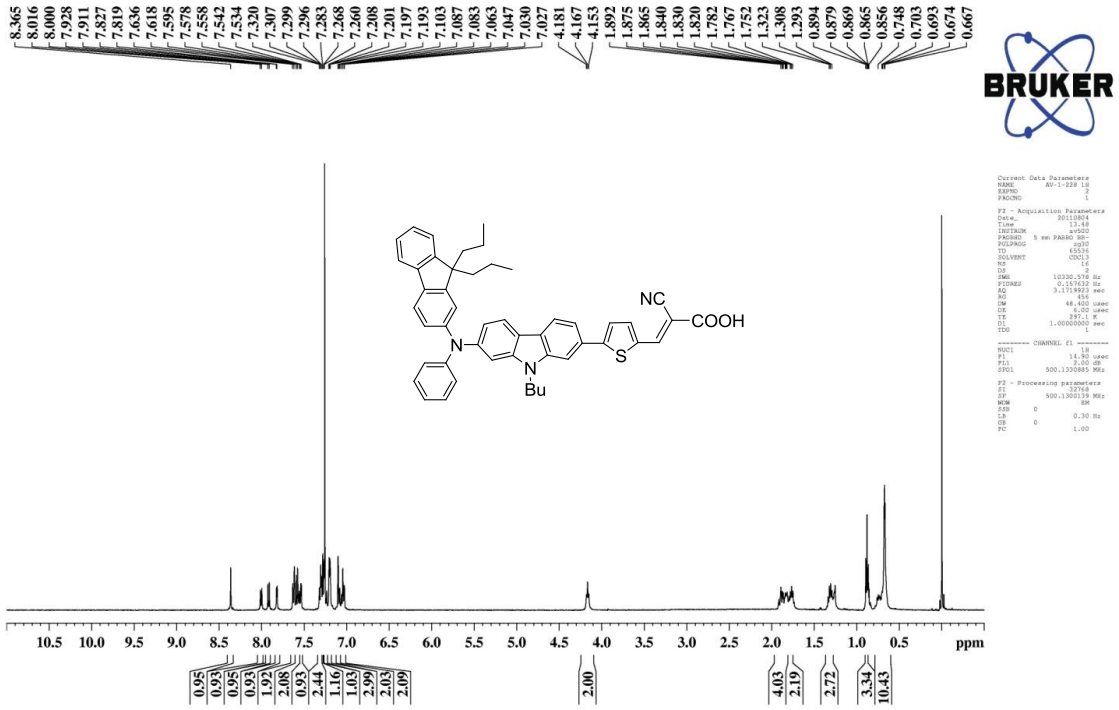

Figure S55 ^{1}H NMR spectrum of **18a** recorded in $CDCl_3$.

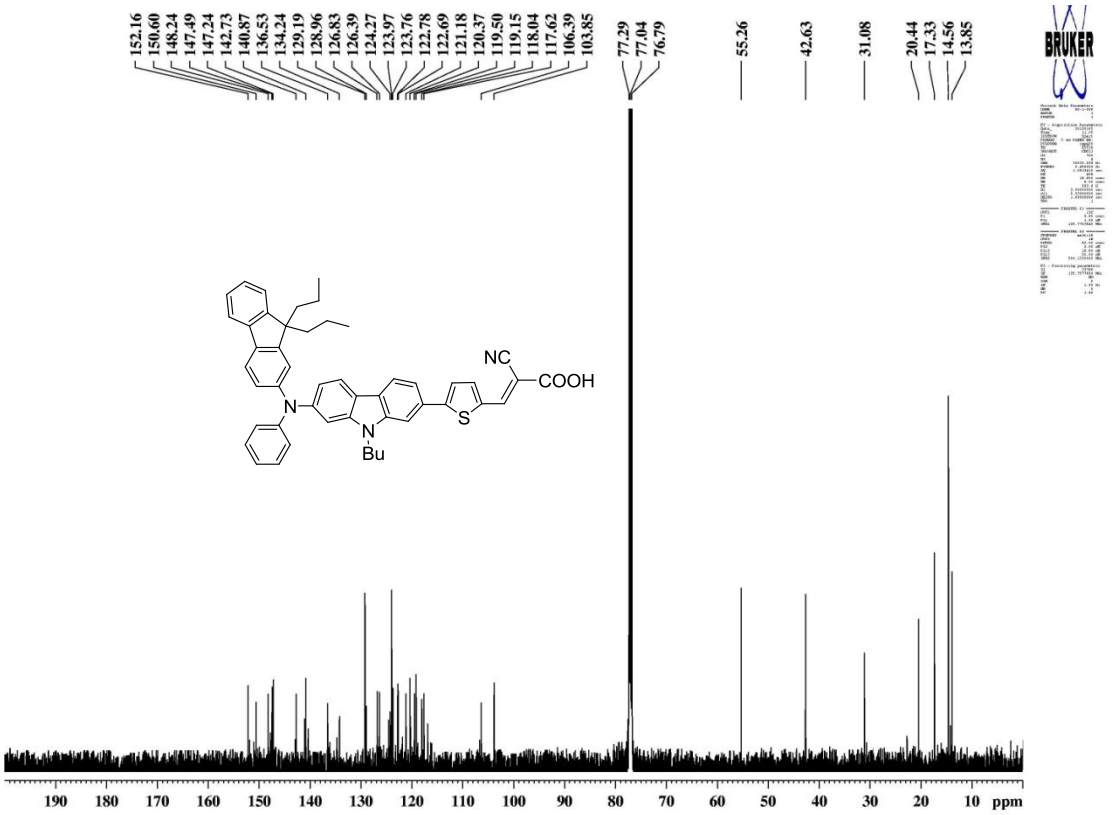

Figure S56 ^{13}C NMR spectrum of **18a** recorded in $CDCl_3$.

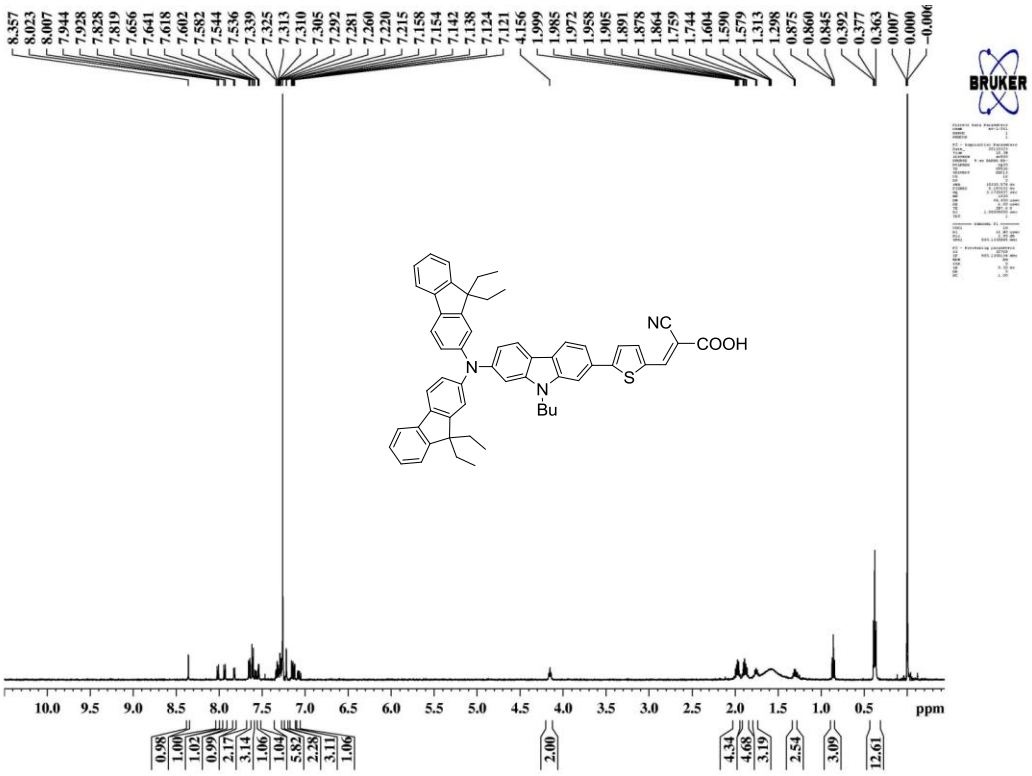

Figure S57 ^{1}H NMR spectrum of **18b** recorded in $CDCl_3$.

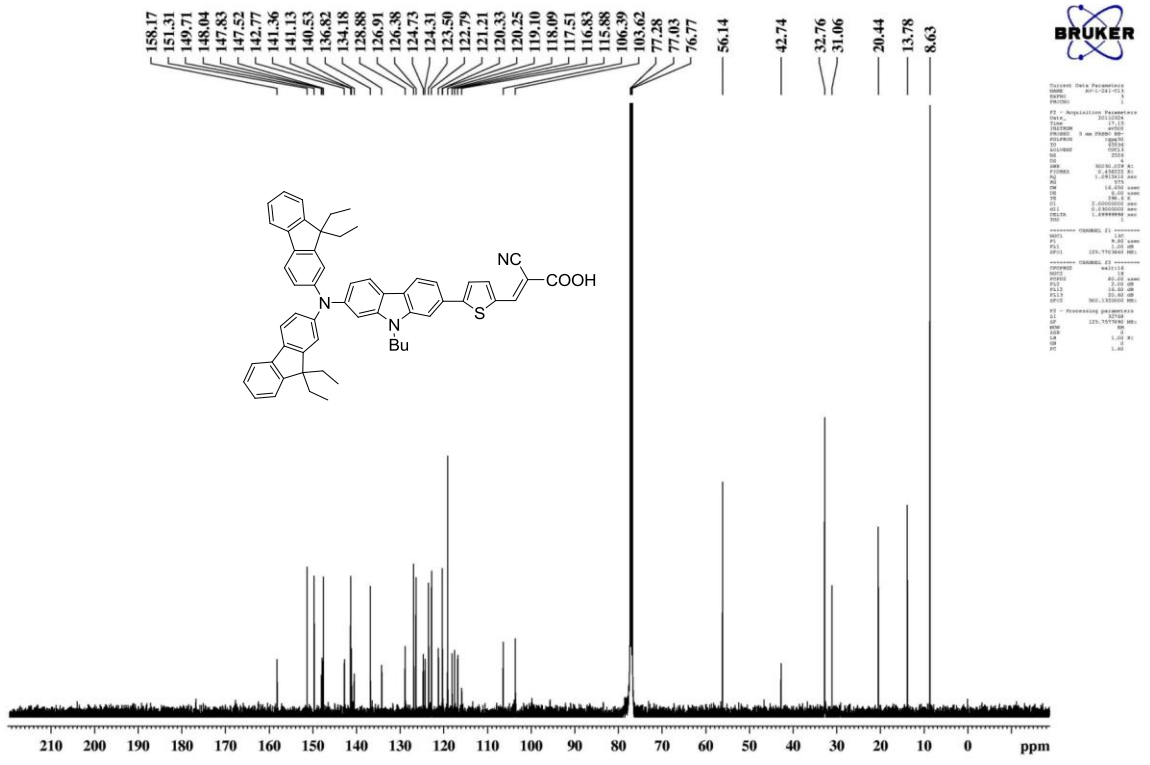

Figure S58 ^{13}C NMR spectrum of **18b** recorded in $CDCl_3$.

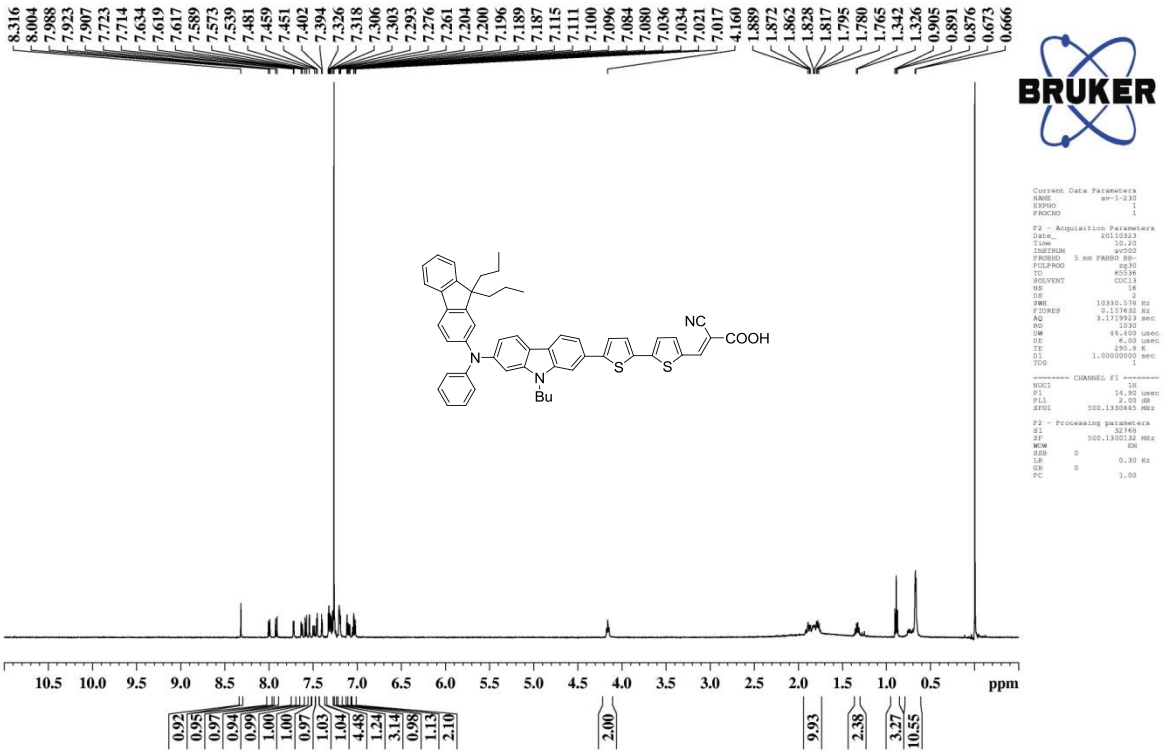

Figure S59 ^{1}H NMR spectrum of **19a** recorded in $CDCl_3$.

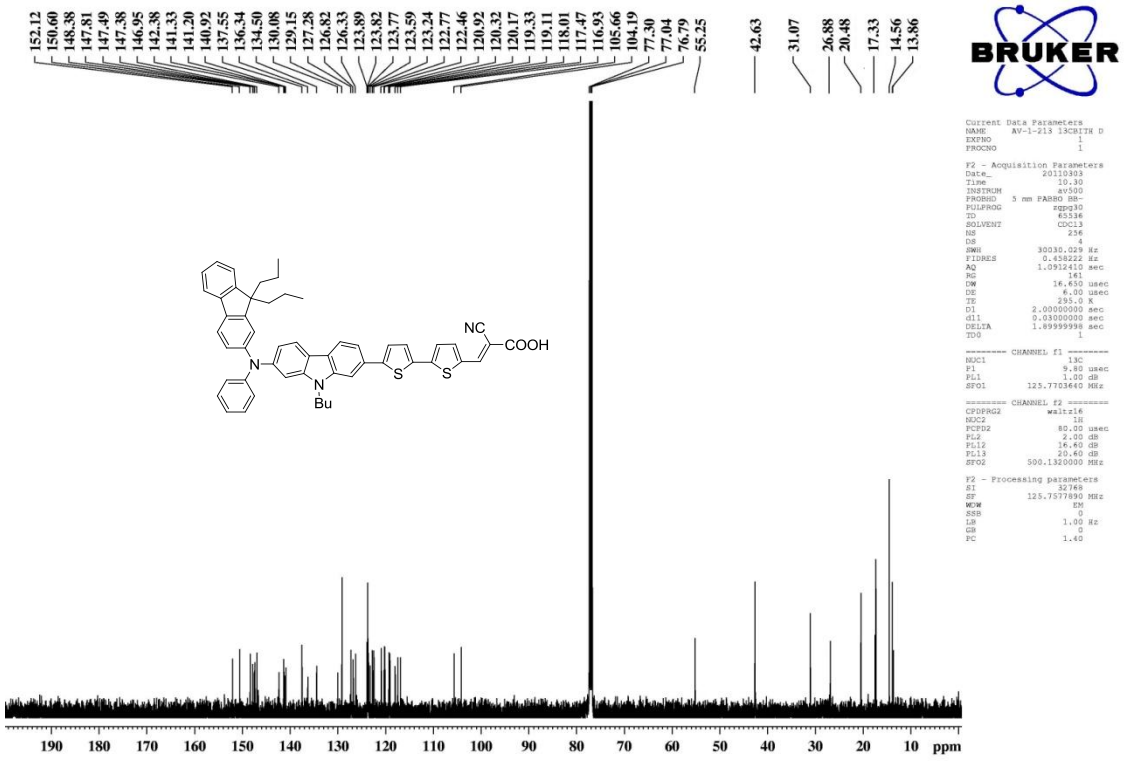

Figure S60 ^{13}C NMR spectrum of **19a** recorded in $CDCl_3$.

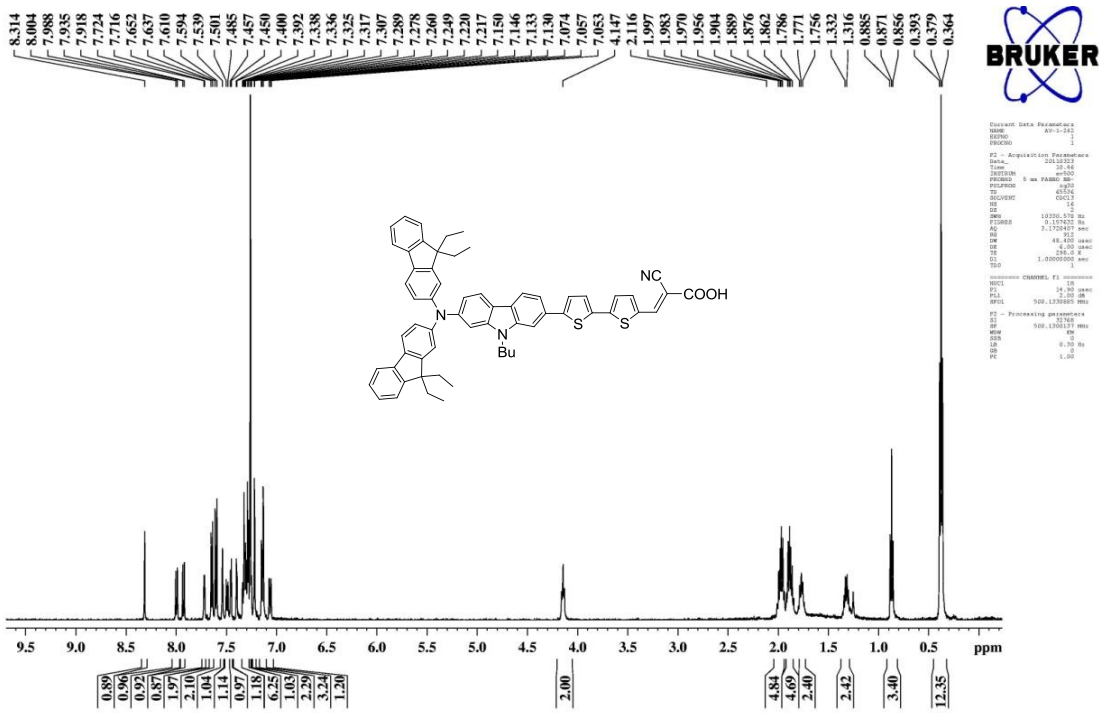

Figure S61 ^{1}H NMR spectrum of **19b** recorded in $CDCl_3$.

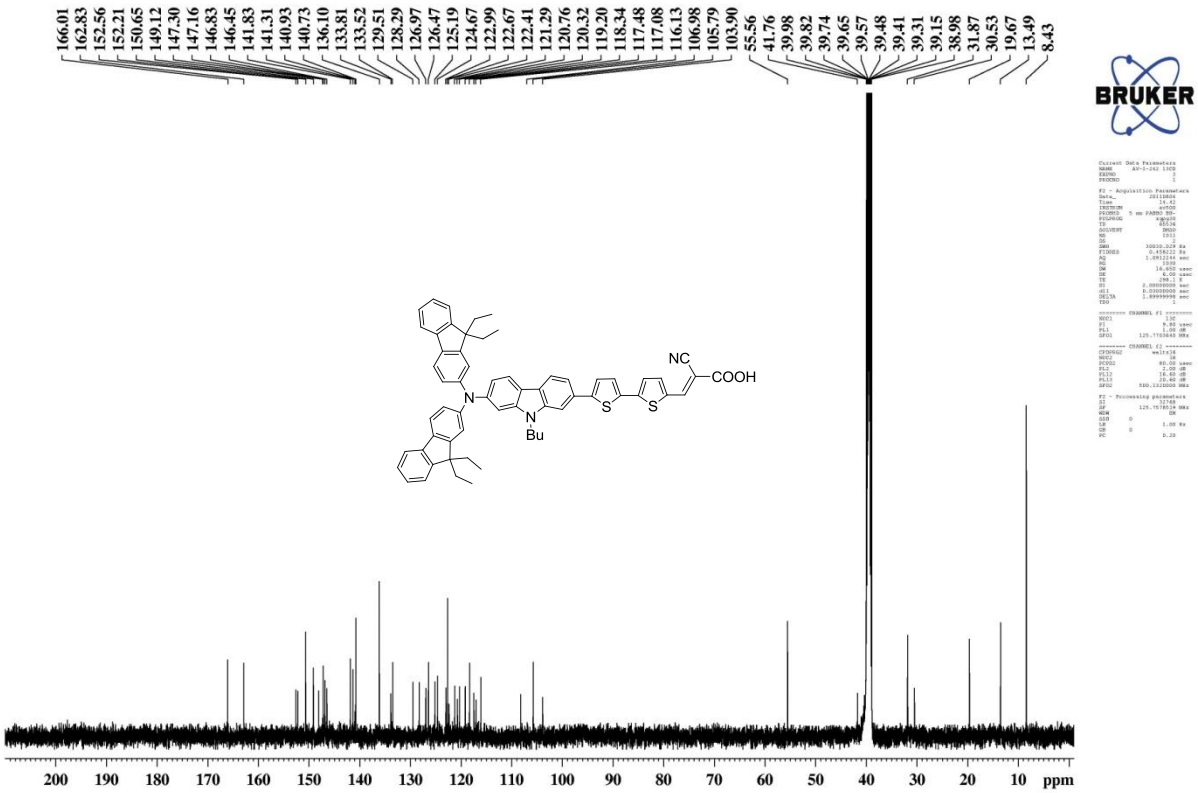

Figure S62 ^{13}C NMR spectrum of **19b** recorded in DMSO-d_6.

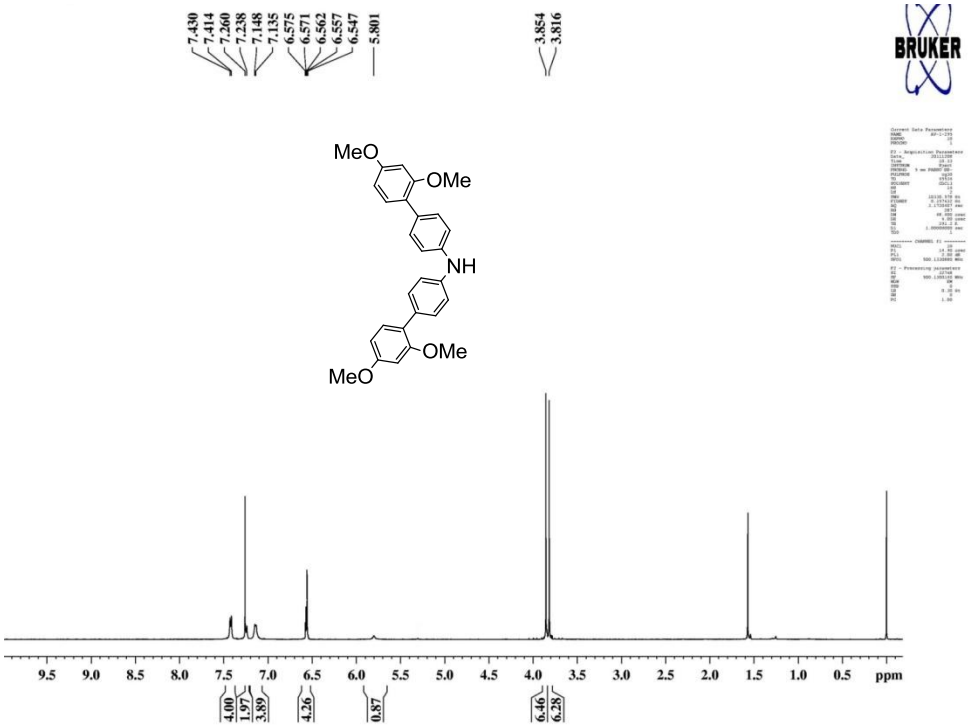

Figure S63 ^{1}H NMR spectrum of **27b** recorded in $CDCl_3$.

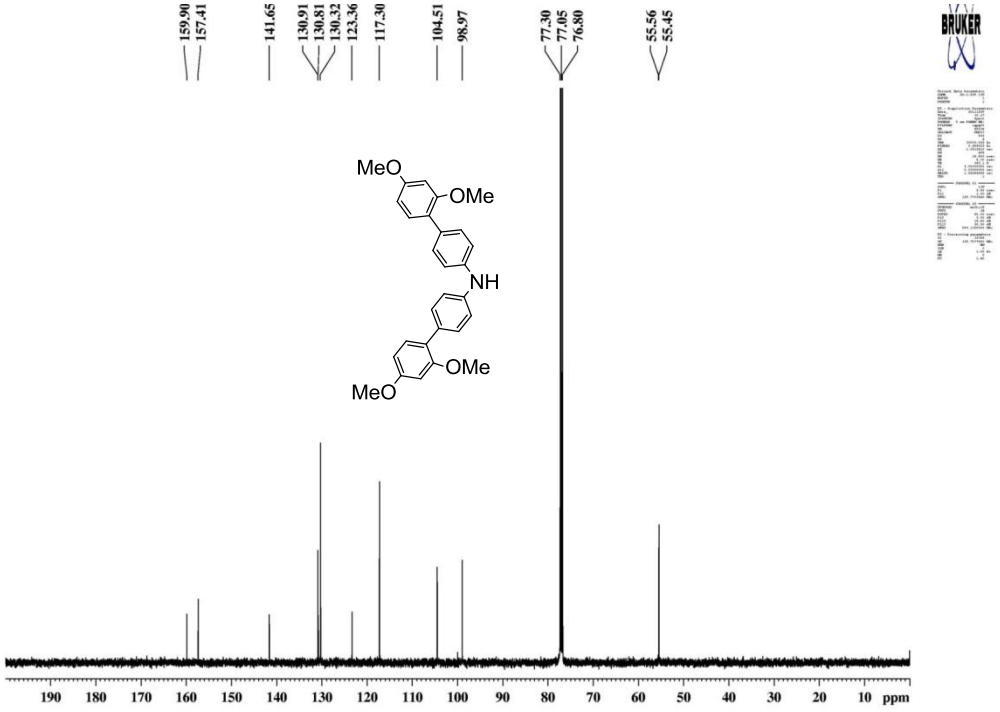

Figure S64 ^{13}C NMR spectrum of **27b** recorded in $CDCl_3$.

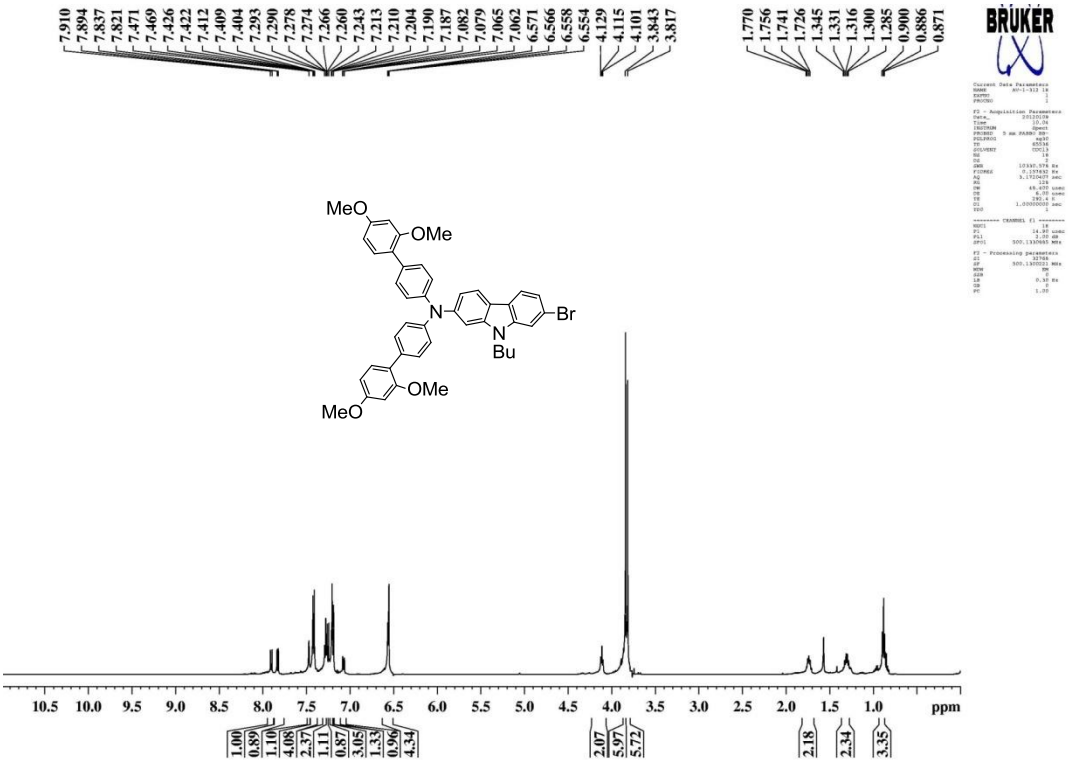

Figure S65 ^{1}H NMR spectrum of **28b** recorded in $CDCl_3$.

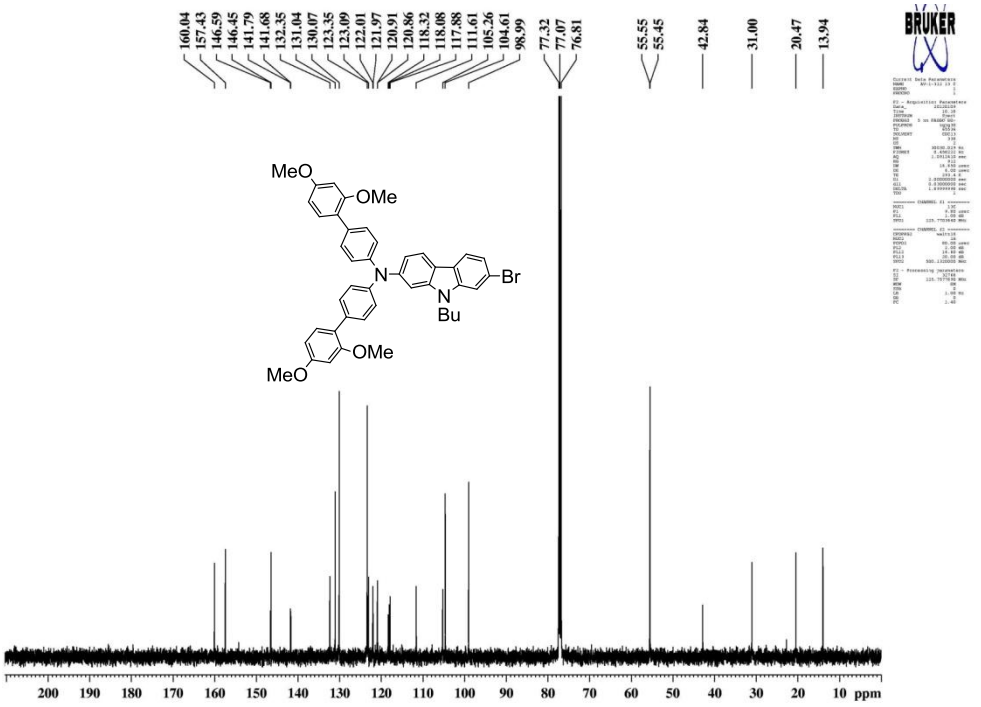

Figure S66 ^{13}C NMR spectrum of **28b** recorded in $CDCl_3$.

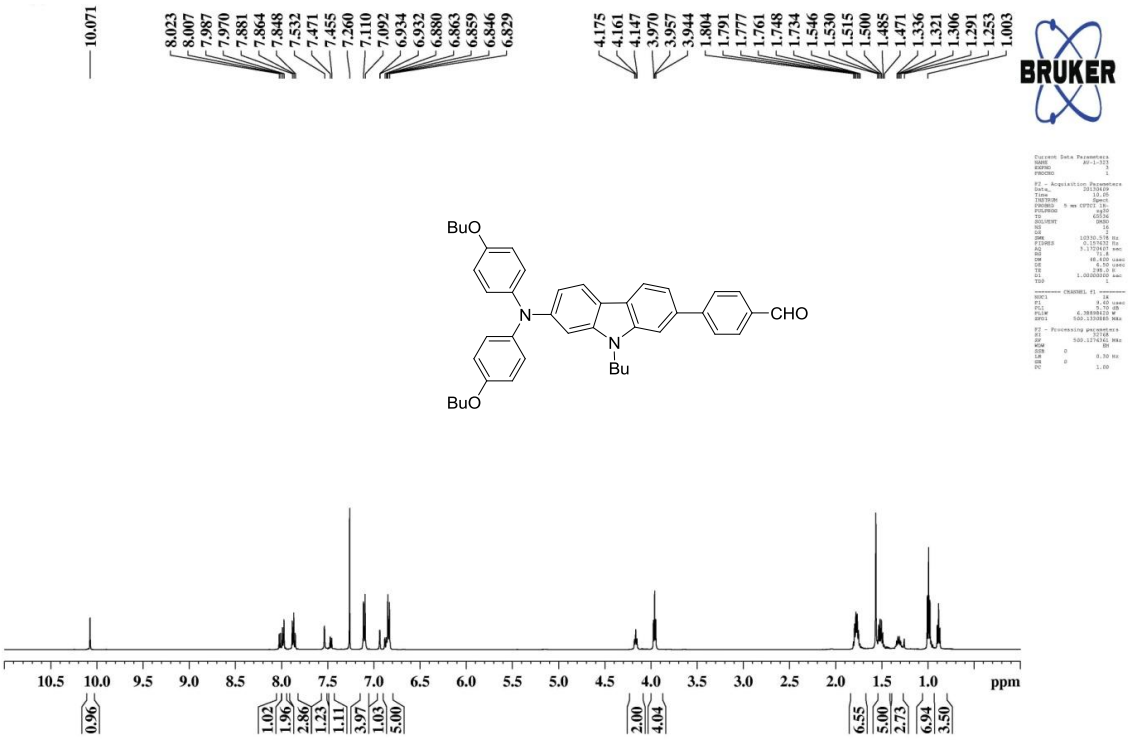

Figure S67 ^{1}H NMR spectrum of **29a** recorded in $CDCl_3$.

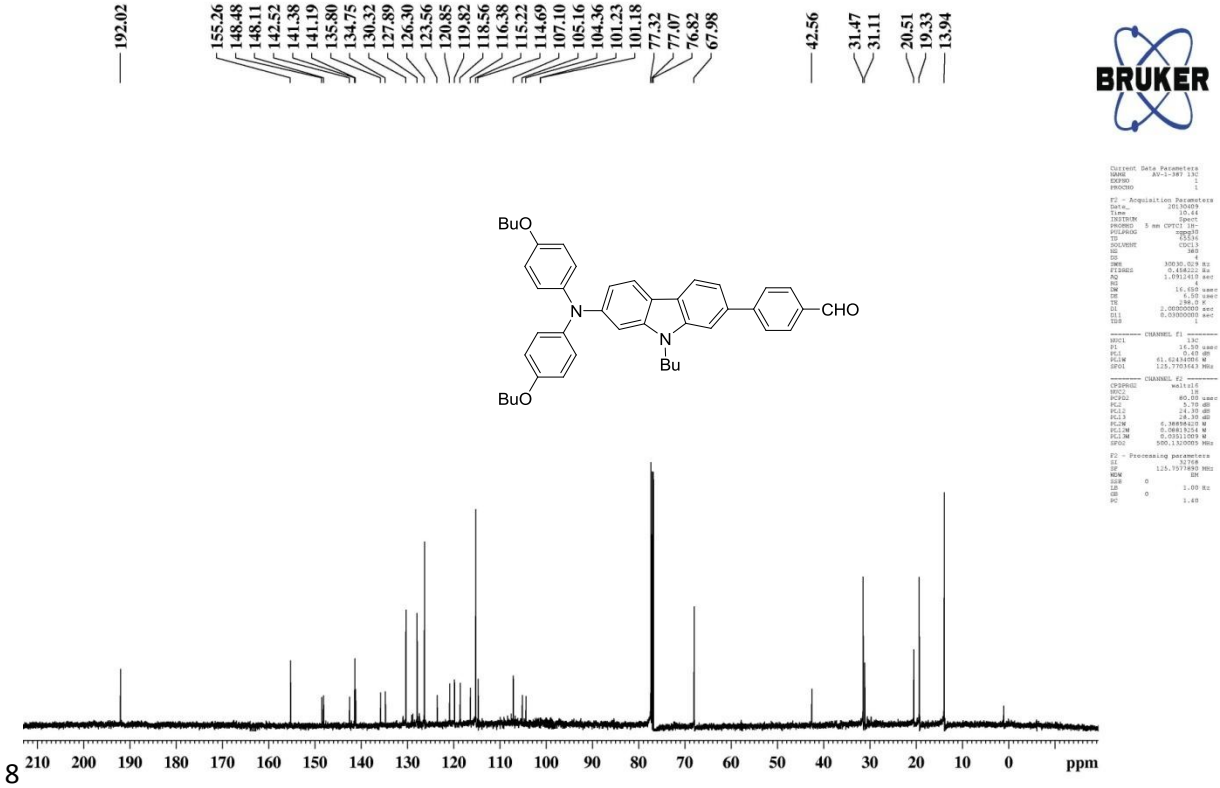

Figure S68 ^{13}C NMR spectrum of **29a** recorded in $CDCl_3$.

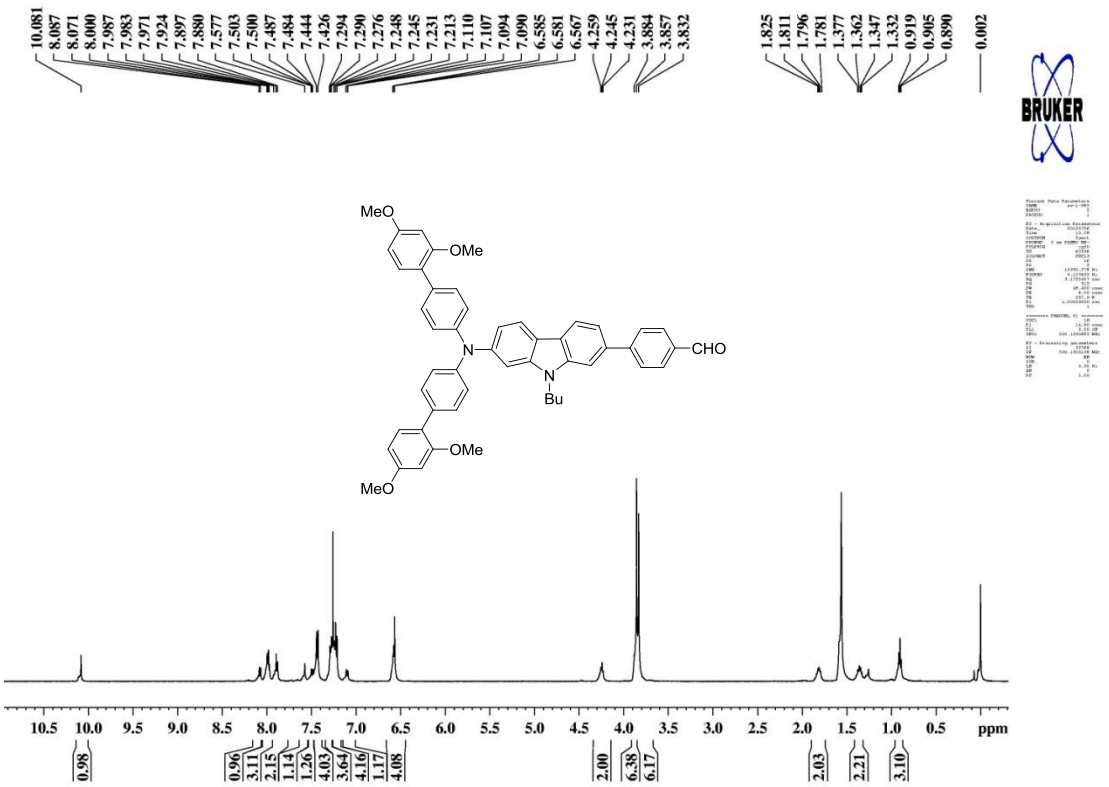

Figure S69 ^{1}H NMR spectrum of **29b** recorded in $CDCl_3$.

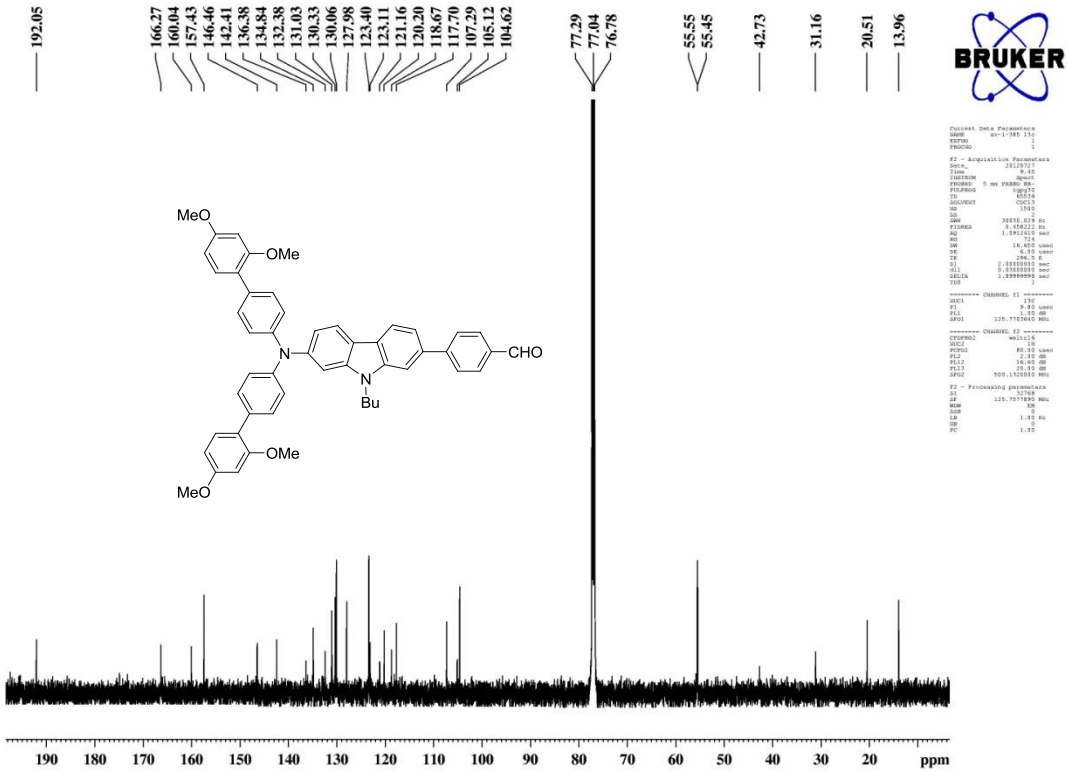

Figure S70 ^{13}C NMR spectrum of **29b** recorded in $CDCl_3$.

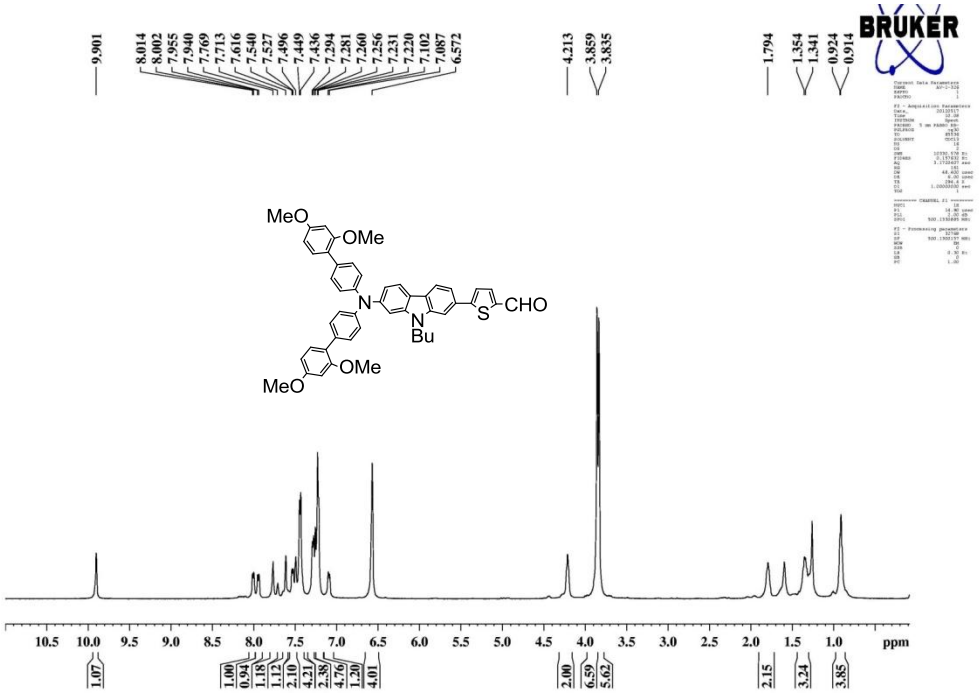

Figure S71 ^{1}H NMR spectrum of **31b** recorded in $CDCl_3$.

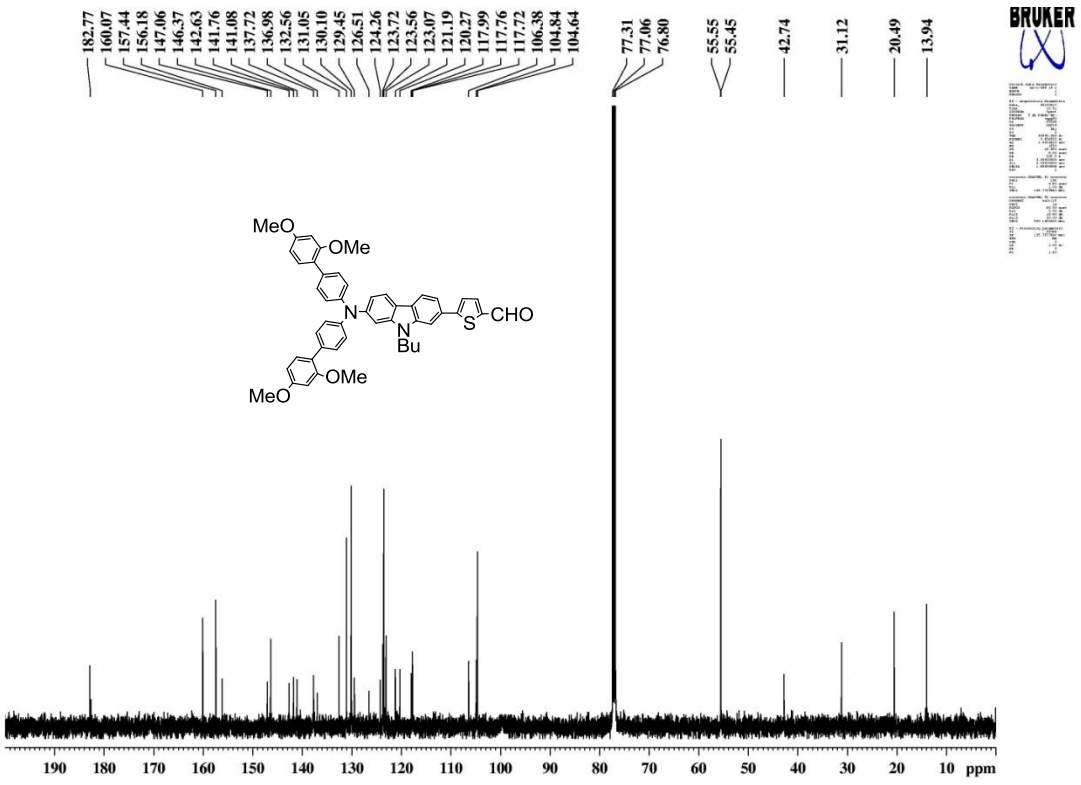

Figure S72 ^{13}C NMR spectrum of **31b** recorded in $CDCl_3$.

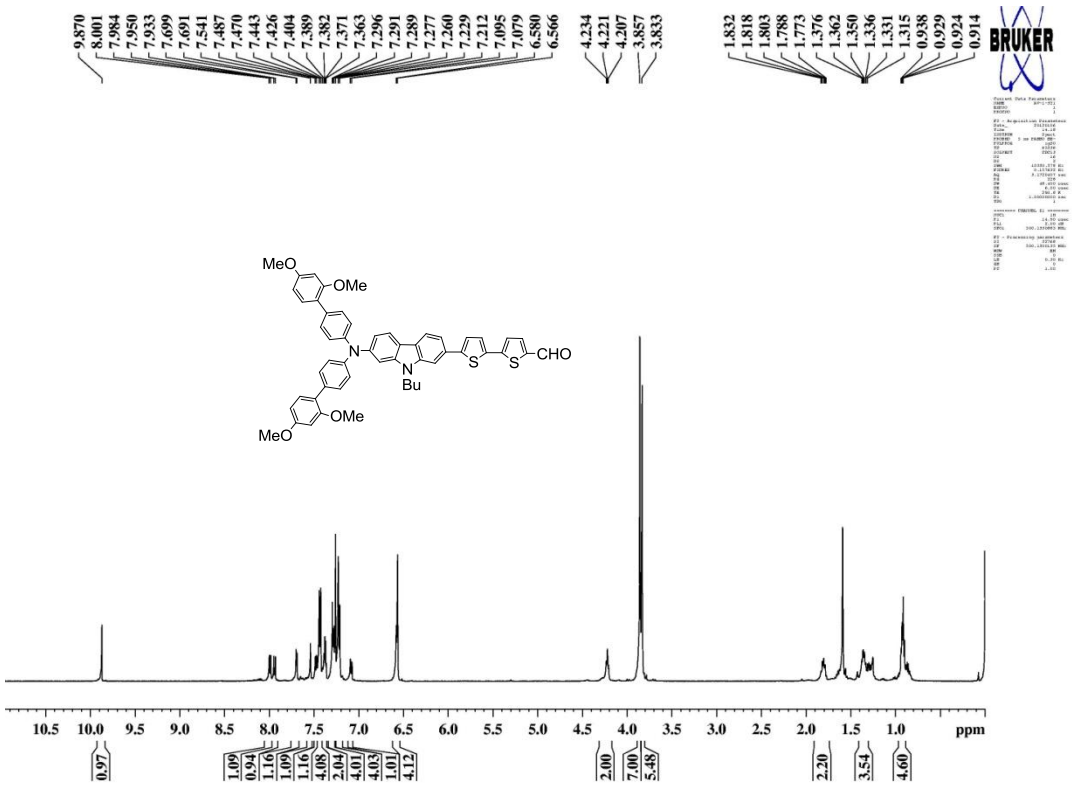

Figure S73 ^{1}H NMR spectrum of **32b** recorded in $CDCl_3$.

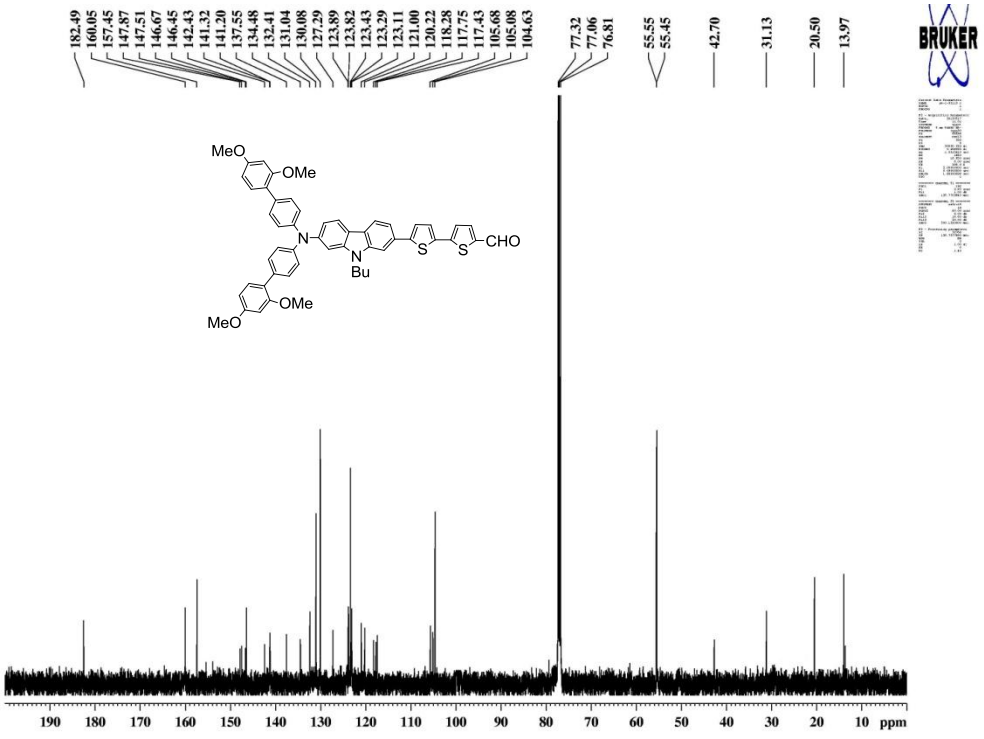

Figure S74 ^{13}C NMR spectrum of **32b** recorded in $CDCl_3$.

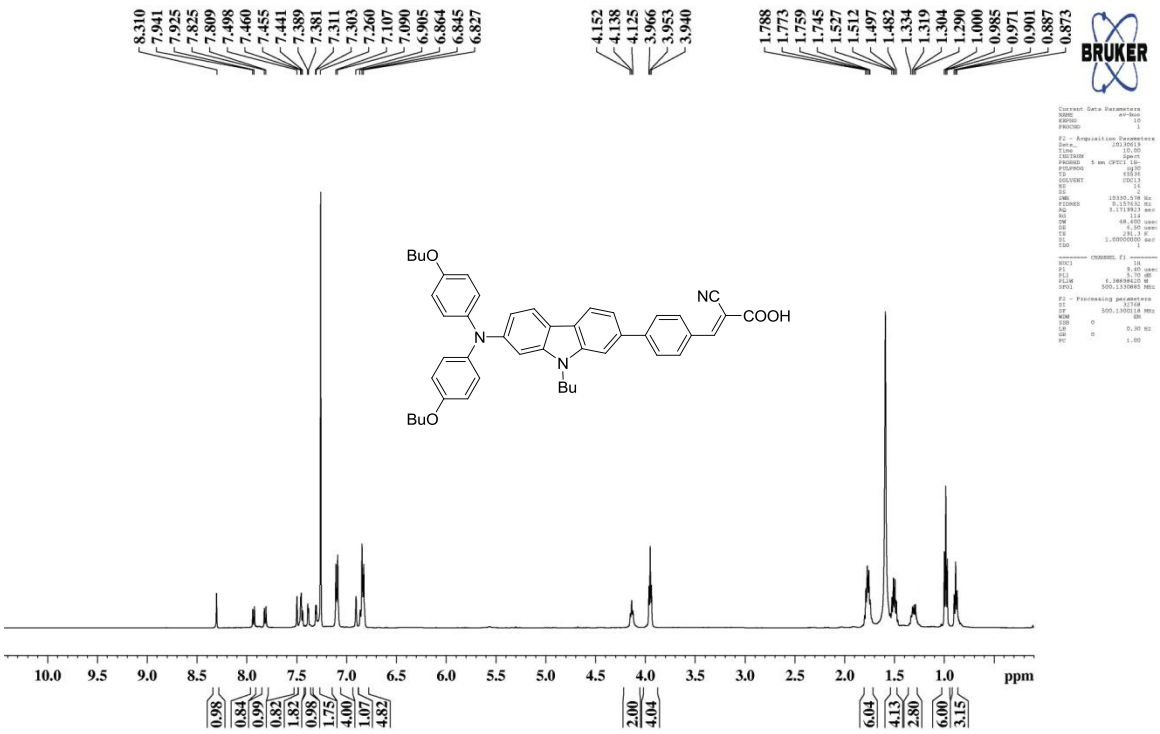

Figure S75 ^{1}H NMR spectrum of **30a** recorded in $CDCl_3$.

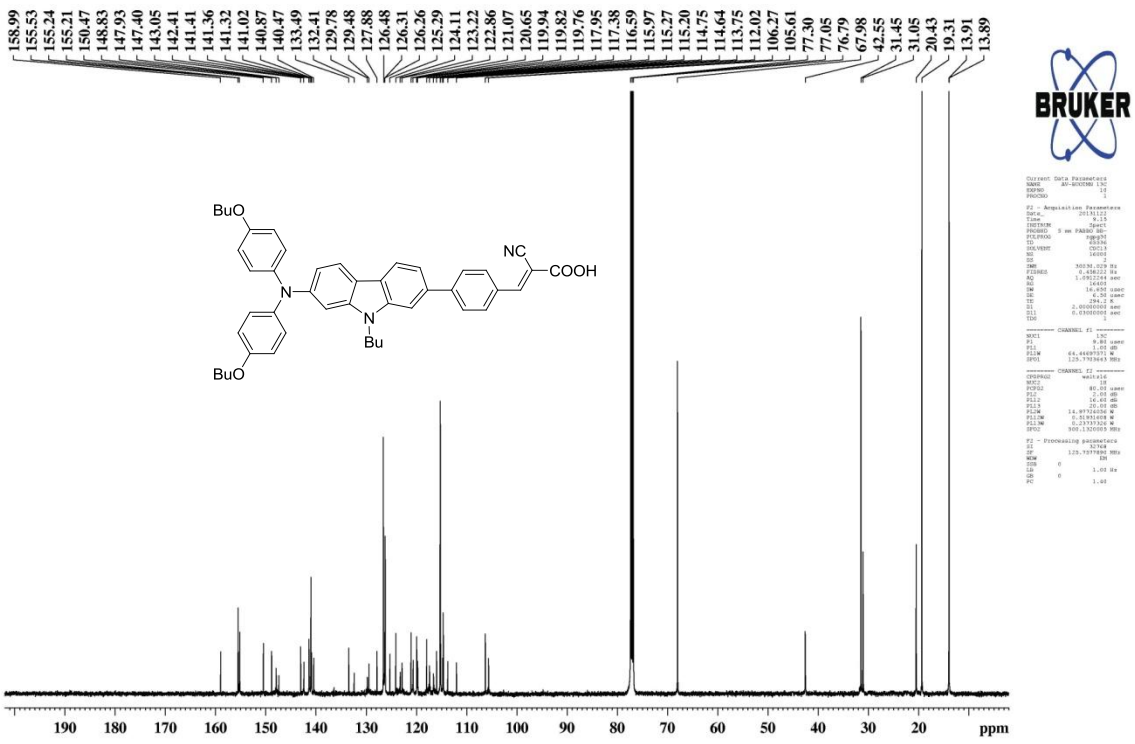

Figure S76 ^{13}C NMR spectrum of **30a** recorded in $CDCl_3$.

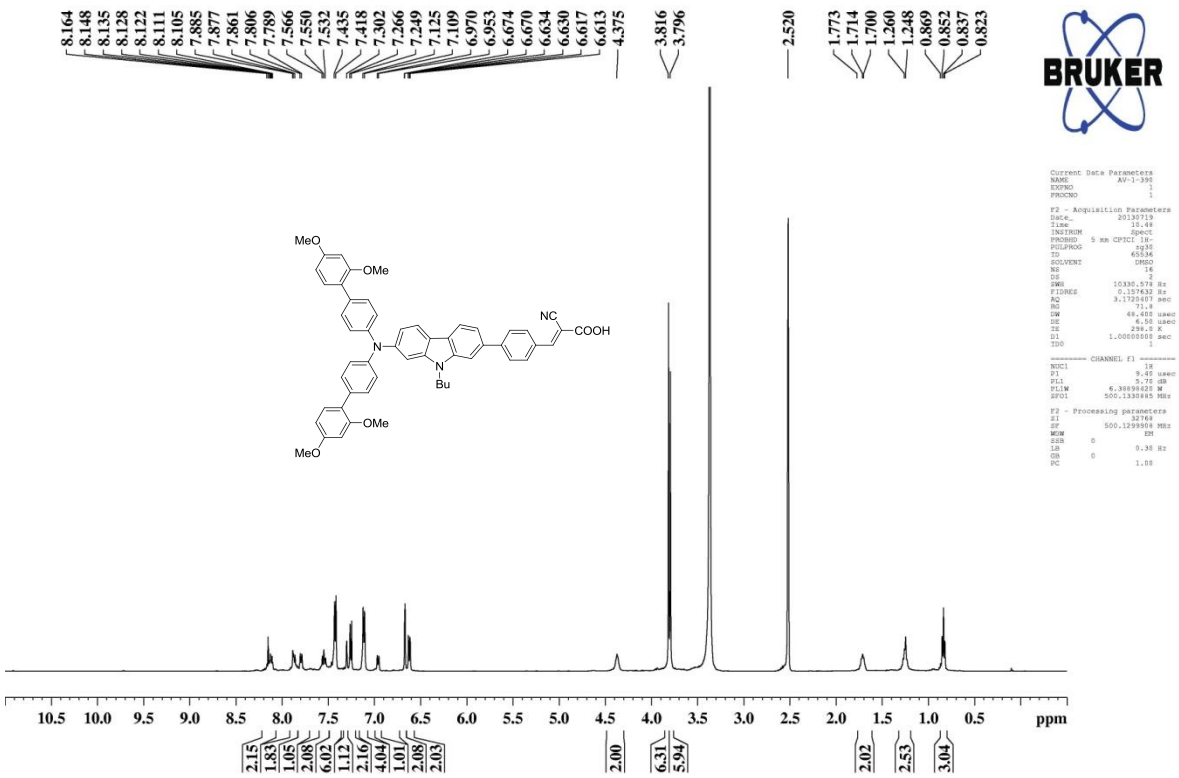

Figure S77 ^{1}H NMR spectrum of **30b** recorded in $CDCl_3$.

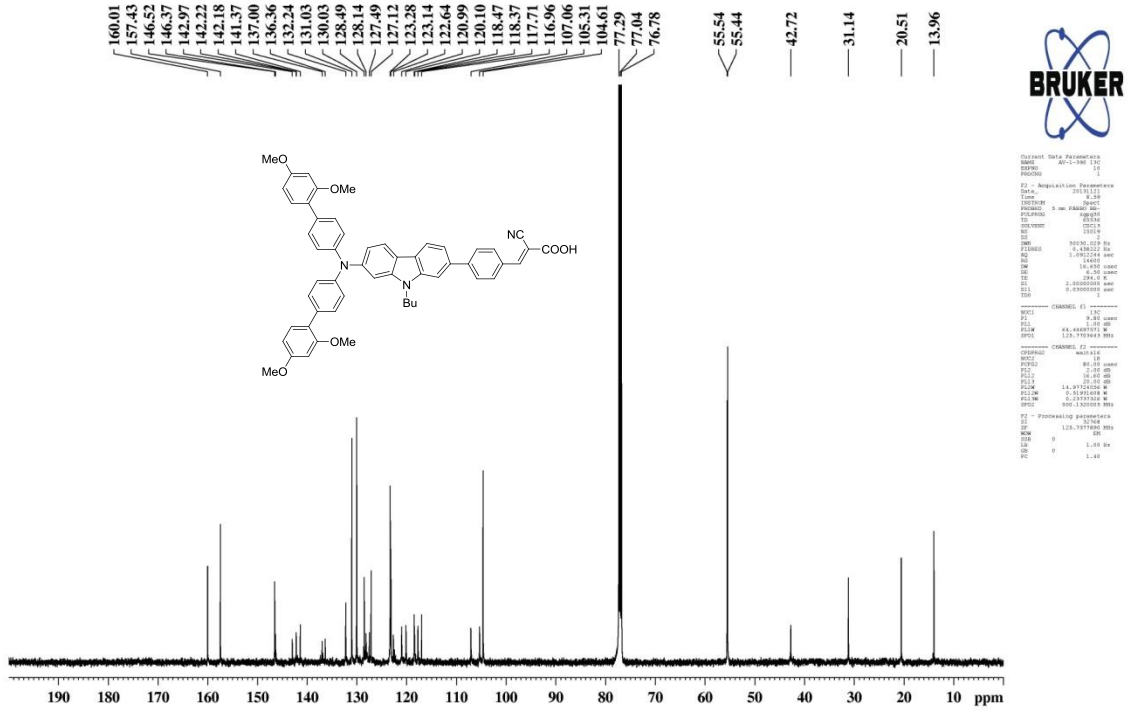

Figure S78 ^{13}C NMR spectrum of **30b** recorded in $CDCl_3$.

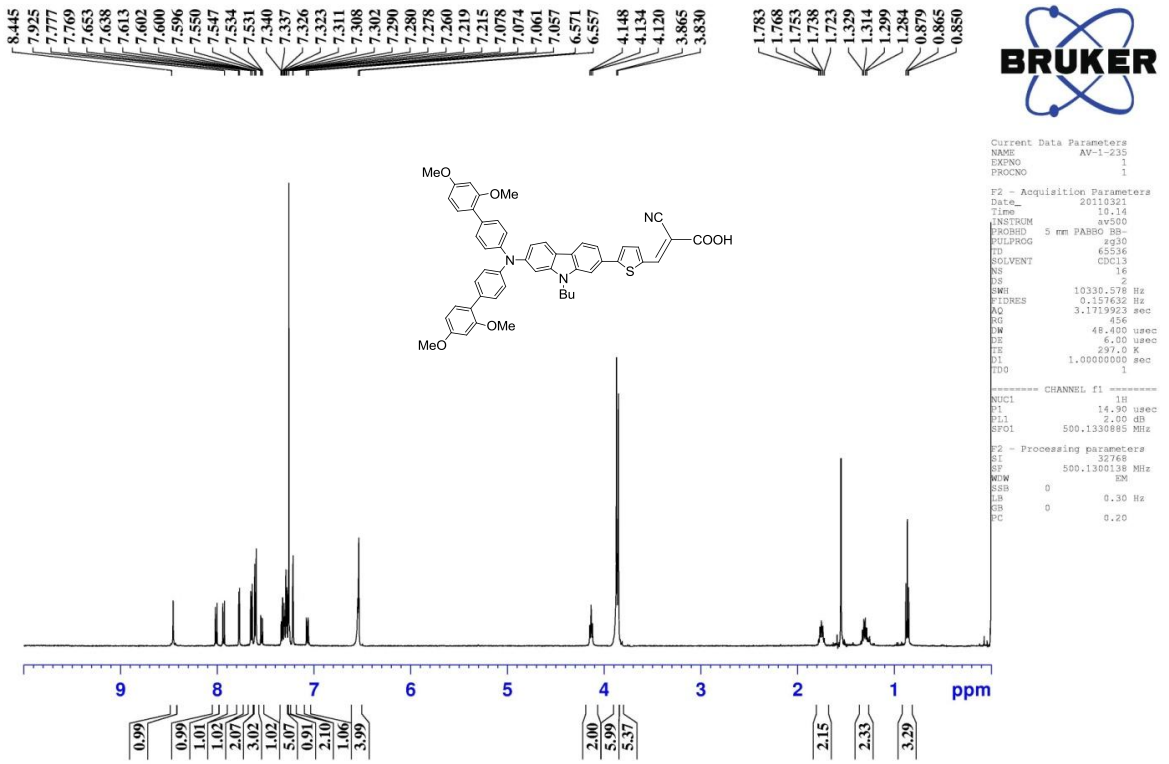

Figure S79 ^{1}H NMR spectrum of **33b** recorded in $CDCl_3$.

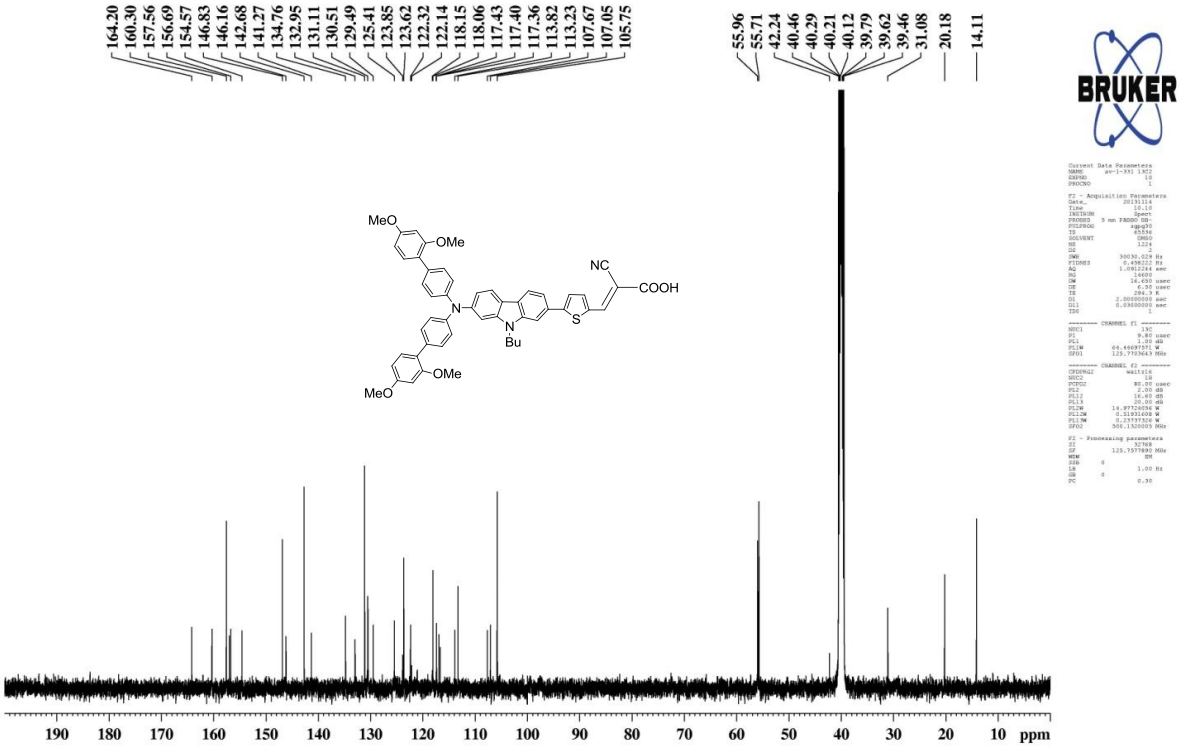

Figure S80 ^{13}C NMR spectrum of **33b** recorded in $CDCl_3$.

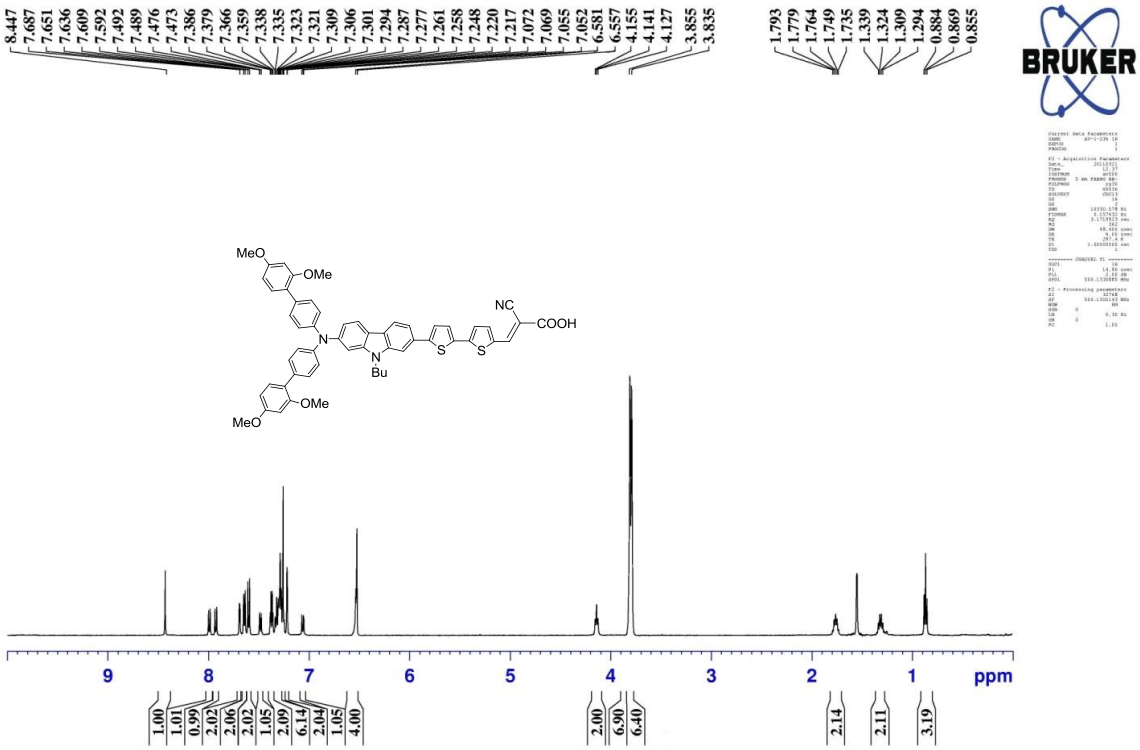

Figure S81 ^{1}H NMR spectrum of **34b** recorded in $CDCl_3$.

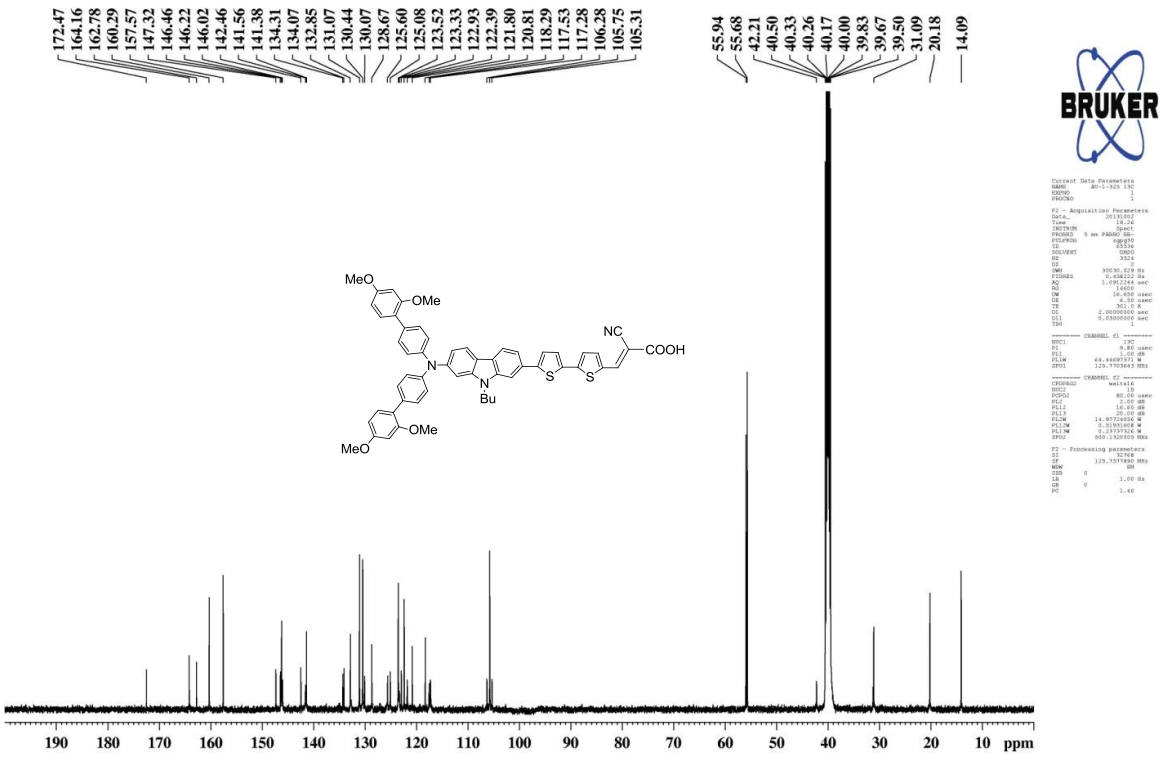

Figure S82 ^{13}C NMR spectrum of **34b** recorded in $CDCl_3$.

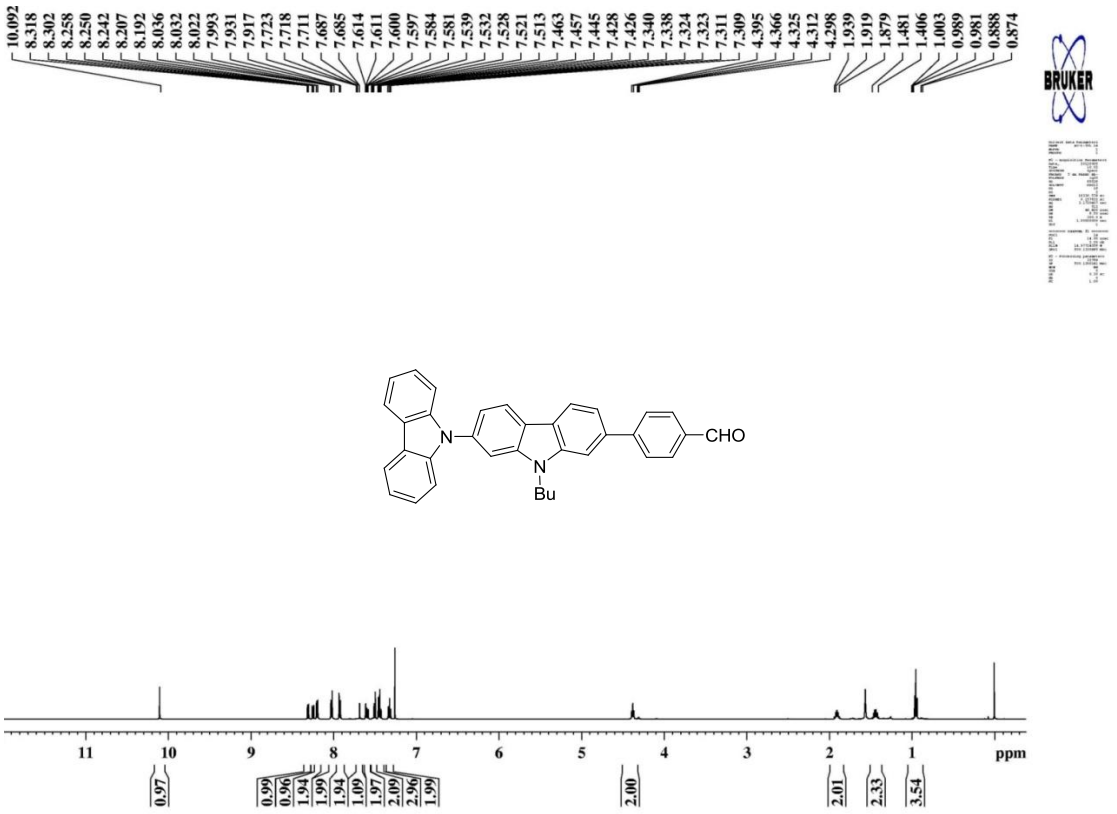

Figure S83 ^{1}H NMR spectrum of **39a** recorded in $CDCl_3$.

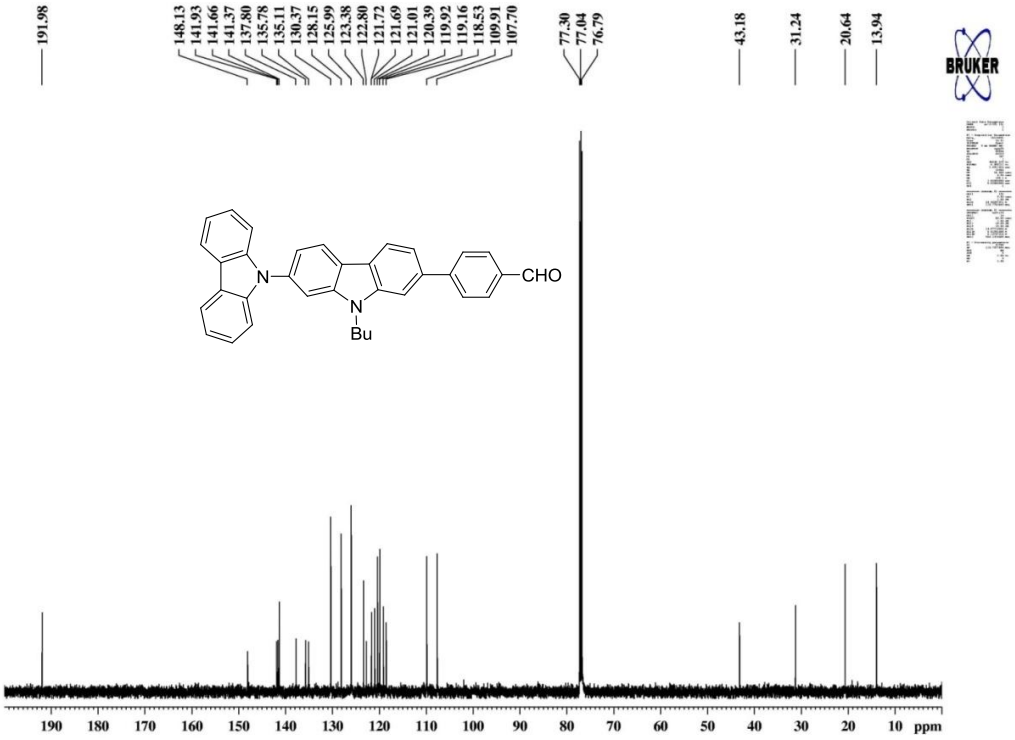

Figure S84 ^{13}C NMR spectrum of **39a** recorded in $CDCl_3$.

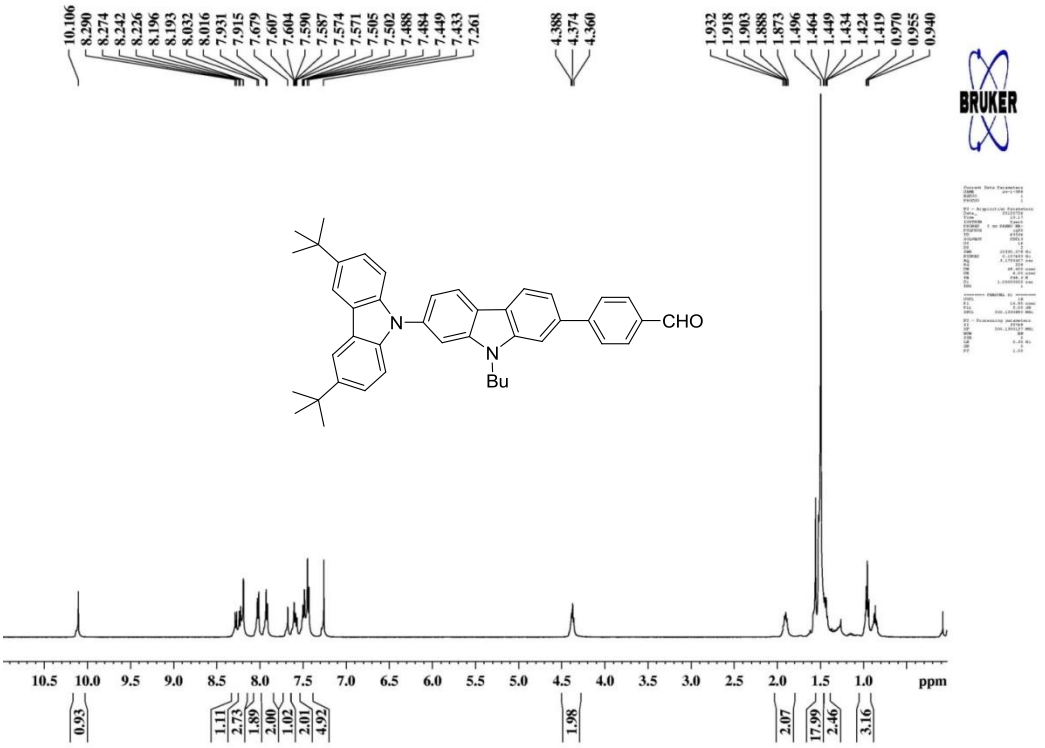

Figure S85 ^{1}H NMR spectrum of **39b** recorded in $CDCl_3$.

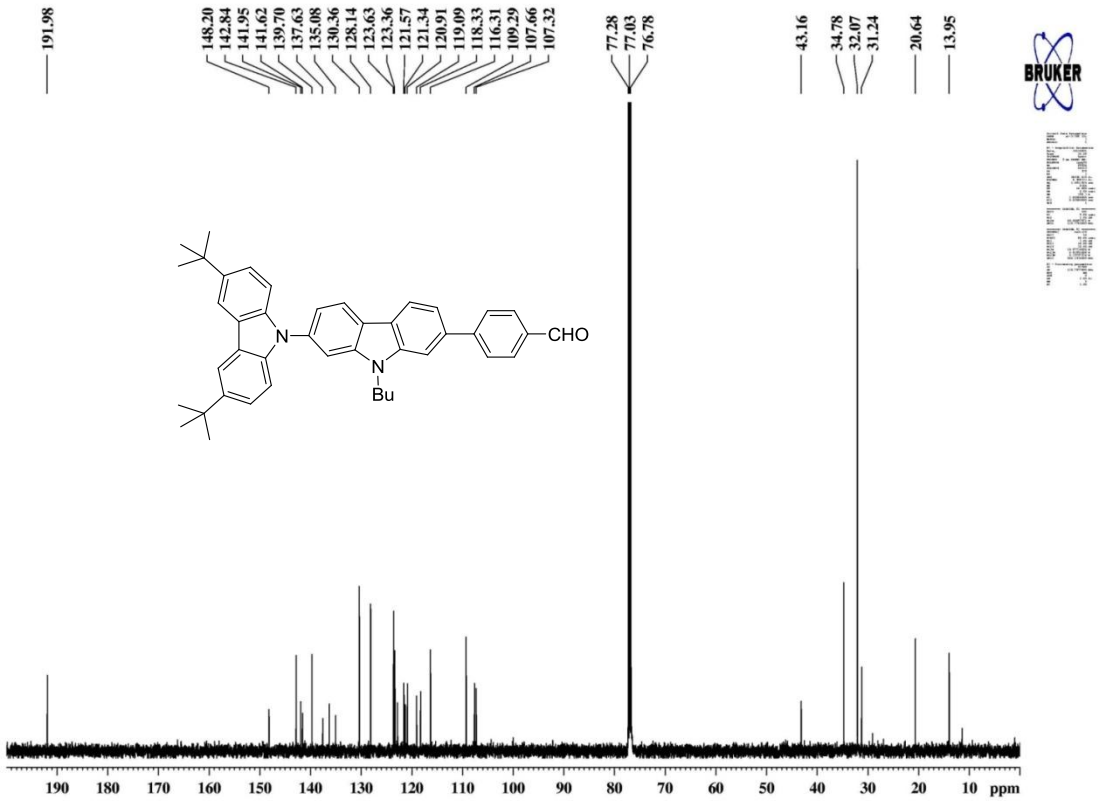

Figure S86 ^{13}C NMR spectrum of **39b** recorded in $CDCl_3$.

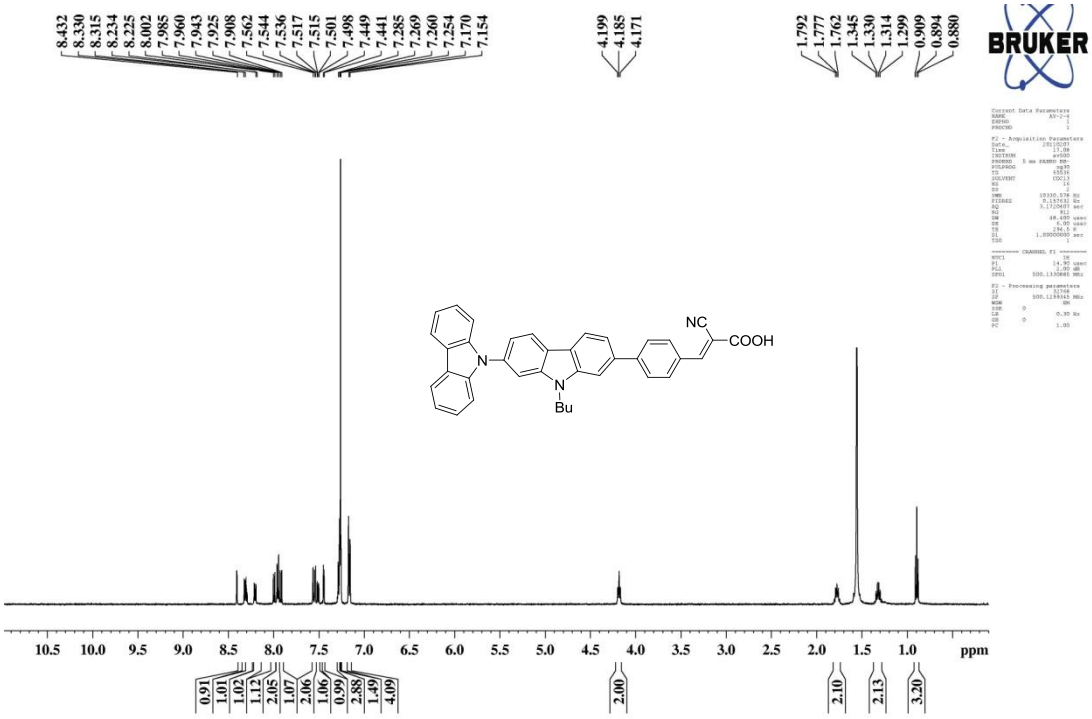

Figure S87 ^{1}H NMR spectrum of **40a** recorded in $CDCl_3$.

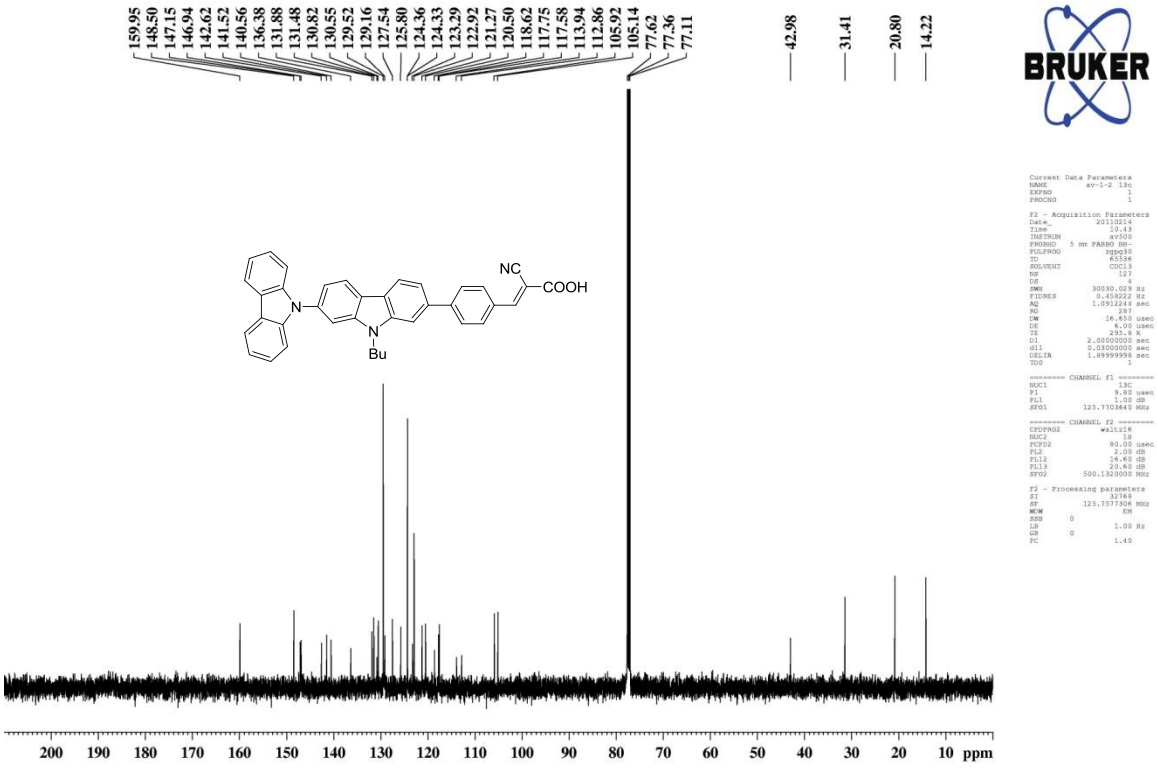

Figure S88 ^{13}C NMR spectrum of **40a** recorded in $CDCl_3$.

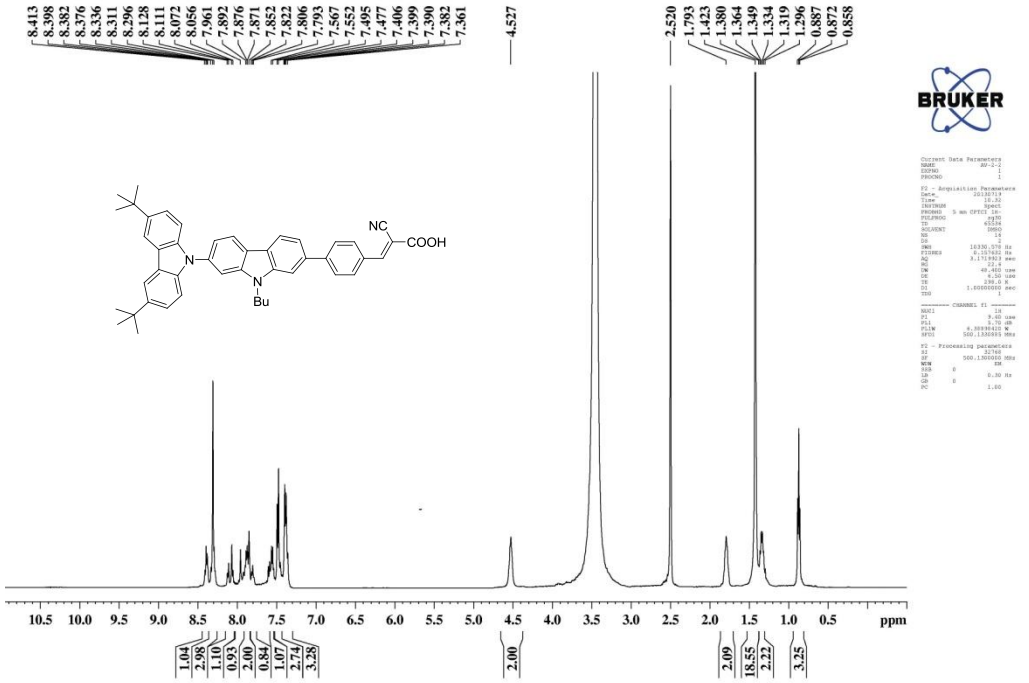

Figure S89 ^{1}H NMR spectrum of **40b** recorded in $CDCl_3$.

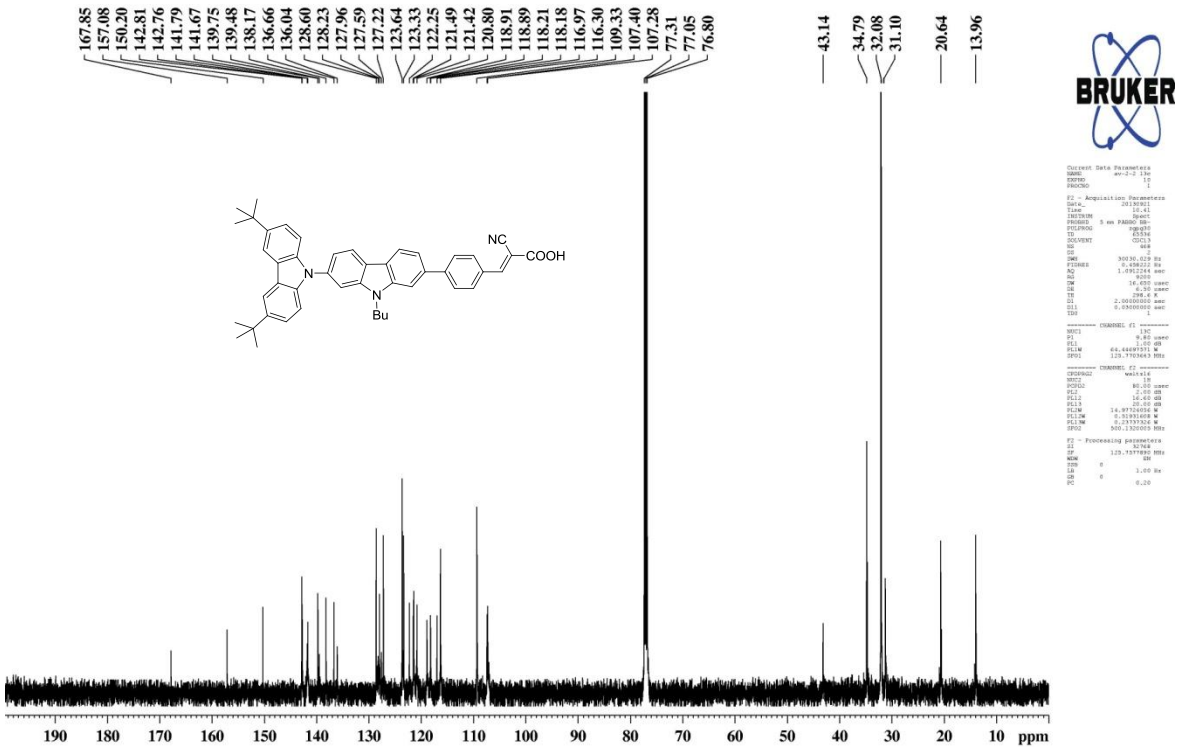

Figure S90 ^{13}C NMR spectrum of **40b** recorded in $CDCl_3$.